TECTONIC HISTORY OF THE NEPEWASSI DOMAIN, CENTRAL GNEISS BELT, GRENVILLE PROVINCE, ONTARIO: A LITHOLOGICAL, STRUCTURAL, METAMORPHIC AND GEOCHRONOLOGICAL STUDY

by

Samantha. R. Van De Kerckhove

Submitted in partial fulfilment of the requirements
for the degree of Master of Science

at

Dalhousie University
Halifax, Nova Scotia
December 2016

TABLE OF CONTENTS

List of Tables

List of Figures

ABSTRACT

The Nepewassi domain is a parautochthonous unit within the Central Gneiss Belt of the Grenville Province, Ontario. The Southern subdomain of the Nepewassi domain, the focus of this study, is composed of migmatitic quartz monzonite, the West Bay batholith, and three lithological associations: a tonalitic and granodioritic grey gneiss association, the bimodal West Phase association, and a thin, north-south trending supracrustal association that separates the West Phase association from the West Bay batholith. Supracrustal rocks coincide with an east-dipping ductile shear zone, the West Arm High strain zone (WAHSZ). Fold interference patterns east of the WAHSZ indicate that two phases of folding affected the Southern subdomain. Mineral assemblages indicate amphibolite facies metamorphism across the study area. Two pelites, one within the WAHSZ and one west of it, yielded P-T results of 6.8 ± 1 kbar - 632 ± 25°C and 7.3± 1 kbar - 656 ± 25°C respectively. A garnet amphibolite on the east edge of the WAHSZ yielded P-T conditions of 10.6 ± 0.5 kbar - 773 ± 25°C, consistent with the hypothesis that deeper rocks east of the WAHSZ were thrust over those to the west.

Igneous and detrital zircon U-Pb geochronology was completed using laser ablation – inductively coupled plasma – mass spectrometry. Tonalitic and granodioritic gneisses returned ages of 2673.2 ± 14 Ma and 2685.8 ± 4.8 Ma, similar to previously determined igneous ages in the Nepewassi domain and the cratonic foreland. Detrital zircons in four quartzite samples, three from metasupracrustal rocks within the WAHSZ and one at a higher structural level, were analyzed to determine provenance. All four samples have a detrital population peak at ca. 2.7 Ga. One quartzite within the WAHSZ yielded metamorphic ages of ca. 1.75 Ga, and the quartzite located structurally above the WAHSZ yielded a ca. 1.75 Ga detrital peak. Metamorphic monazite from a metapelite within the WAHSZ was analyzed *in situ* using U-Th-Pb geochronology. The age spectra show a large Grenvillian peak at 990 Ma and smaller Paleoproterozoic peaks with a dominant peak at ca.1760 Ma and a subsidiary peak at 1820 Ma.

The combination of igneous, detrital, and metamorphic ages provides significant insight into the tectonic history of the rocks of the Nepewassi domain. We can now infer that Laurentian (Superior Province) cratonic basement rocks were the source of detritus for metasedimentary rocks in the Nepewassi domain. Metamorphic and intrusive rocks formed ca. 1.75 Ga may have provided sediment for the structurally higher and younger quartzite. The ca. 2.7 Ga detrital zircon population in the Nepewassi quartzite samples closely resembles those from metasedimentary formations in the Huronian Supergroup, which were deposited on the Paleoproterozoic passive margin on the southern edge of the Laurentian craton. These data support the hypothesis that metasedimentary rocks in the Nepewassi domain were originally deposited on the passive margin of Laurentia after ca. 2.5 Ga and prior to ca. 1.75 Ga. The passive margin was inverted and imbricated at or before ca. 1.82 Ga and subsequently reworked during the Grenvillian orogeny.

List of Abbreviations Used

alt	alteration
amph	amphibole
BG	background
bio	biotite
BSE	backscattered electron
CAB	Composite Arc Belt
CABBZ	Composite Arc Belt boundary zone
CCMZ	Cartage-Colton shear zone
CGB	Central Gneiss Belt
DD	Dorval detachment
EDS	Energy Dispersive X-Ray Spectrometry
EMP	electron microprobe
FAB	Frontenac-Adirondack Belt
GASP	garnet-aluminosilicate-quartz-plagioclase
GB	garnet-biotite
GBPQ	garnet-biotite-plagioclase-quartz
GF	Grenville Front
GFTZ	Grenville Front Tectonic Zone
GH	garnet-hornblende
GPAO	Great Proterozoic Accretionary Orogen
GPHQ	garnet-plagioclase-hornblende-quartz
grt/gnt	garnet
HJSZ	Hart-Jaune shear zone
HREE	heavy rare earth elements
il	ilmenite
ky	kyanite
LA-ICP-MS	laser ablation-inductively coupled plasma-mass spectrometry
LESZ	Lac Émerillon shear zone
LPO	lattice preferred orientation
LSZ	Labelle shear zone
MF	Murray Fault
MJ	major
OGS	Ontario Geological Survey
plag	plagioclase
PPL	plane polarized light
P-T	pressure-temperature
qtz	quartz
REE	rare earth elements

RLSZ	Robertson Lake shear zone
rut	rutile
SCLSZ	St. Charles Lavigne straight zone
SEM	scanning election microscope
SHRIMP	sensitive high-resolution ion microprobe
sil	sillimanite
SPO	shape preferred orientation
TIMS	thermal ionization mass spectrometry
TS	tectonic schist
VAG	volcanic arc granites
WAHSZ	West Arm high strain zone
WDS	wavelength-dispersive spectroscopy
WPG	within plate granites
XPL	Cross-polarized light
ZAF	atomic number, absorption and fluorescence

ACKNOWLEDGMENTS

I am extremely grateful to my supervisor, Dr. Nicholas Culshaw, for being such an encouraging and inspiring mentor. Thanks for the stimulating conversations about geology, theology, and everything in between; I feel privileged to have worked with you.

Special thanks to Dr. Michael Easton and the Ontario Geological Survey, without whom, this project would not have been possible. The Ontario Geological Survey provided thin and polished sections, geochemical analysis, and logistical support for the 2014 field season - including my wonderful field assistant Chris Beckett-Brown. Mike Easton was an integral part of this project, providing insight and feedback throughout the entire process.

Dr. Rebecca Jamieson provided invaluable constructive feedback and was a fantastic teacher. This project would not have been possible without her knowledge and guidance about metamorphic petrology, thermobarometry and monazite U-Th-Pb geochronology

I would like to acknowledge several other people who helped me along the way. Dr. Trond Slagstad at the Norwegian Geological Survey provided crucial zircon LA-ICP-MS data and advice. The administrative and technical staff at the Department of Earth Sciences have been of great help, particularly Dan MacDonald in the microprobe lab and Gordon Brown in the thin section lab. The entire Department of Earth Sciences community, including undergraduate students, fellow graduate students, and professors, has made my experience at Dalhousie a positive one.

Thank you to Dr. Brendan Murphy and Dr. James Brenan for taking the time to read and critique this thesis.

Last but certainly not least, I would like to thank my friends and family for their support and encouragement. In particular, I'd like to thank Charlie Carlisle for his patience and for keeping my spirits up during this journey.

CHAPTER 1

INTRODUCTION

1.1 Background

1.1.1 The Grenville Province

The Grenville Province is a broad stretch of highly deformed, mid-crustal level rocks that crop out mostly across southeastern Canada from Labrador to central Ontario and in parts of northern New York; however, there are outliers throughout the continent, as far south as Texas and Mexico (Figure 1.1). The Grenville Province is a composite, Himalayan-scale orogen, resulting from the collision between Proterozoic Laurentia and a continent or continents to the southeast, likely Amazonia, during the mid- to late-Mesoproterozoic (Davidson 1998; Rivers et al. 2012). The Grenville Front (GF) marks the northernmost extent of the effects of the Grenvillian orogeny, from Georgian Bay to Labrador; it trends generally northeast – southwest and dips southeast (Figure 1.1).

Within the Grenville Province, a number of unresolved problems remain regarding the architecture and tectonic history of the province, including the extent of inherited pre-Grenvillian crust and its role in the subsequent development of the orogen. The main focus of this study is to investigate the role of inheritance in the Nepewassi domain. The Nepewassi domain was chosen because it is structurally distinct from surrounding domains, and has known Archean-aged rocks (Chen et al. 1995)

In Ontario, the Grenville Province can be divided into three belts: directly south of the GF is the Grenville Front Tectonic Zone (GFTZ), continuing south is the Central Gneiss Belt (CGB) and furthest south is the Central Metasedimentary Belt, which extends into New York (CMB) (Figure 1.2). Carr et al. (2000) divided the Central Metasedimentary Belt into the Composite Arc Belt (CAB) and northern portion of the Frontenac-Adirondack Belt (FAB). The Composite Arc Belt is made up predominantly of primitive volcanic and plutonic arcs and associated clastic and carbonate sedimentary rocks (Carr et al. 2000). The CAB is allochthonous, meaning it has been transported by tectonic processes from its original location, and monocyclic, meaning it has been affected by only one orogenic event. The Frontenac-Adirondack Belt to the south collided with the Composite Arc Belt ca. 1190 to 1140 Ma (Carr et al. 2000)(Figure 1.3). The Frontenac terrane,

which is the northern portion of the Frontenac-Adirondack Belt, is mostly comprised of metamorphosed supracrustal rocks, and the Adirondack Highlands are mainly metaplutonic rocks (McLelland et al. 1996).

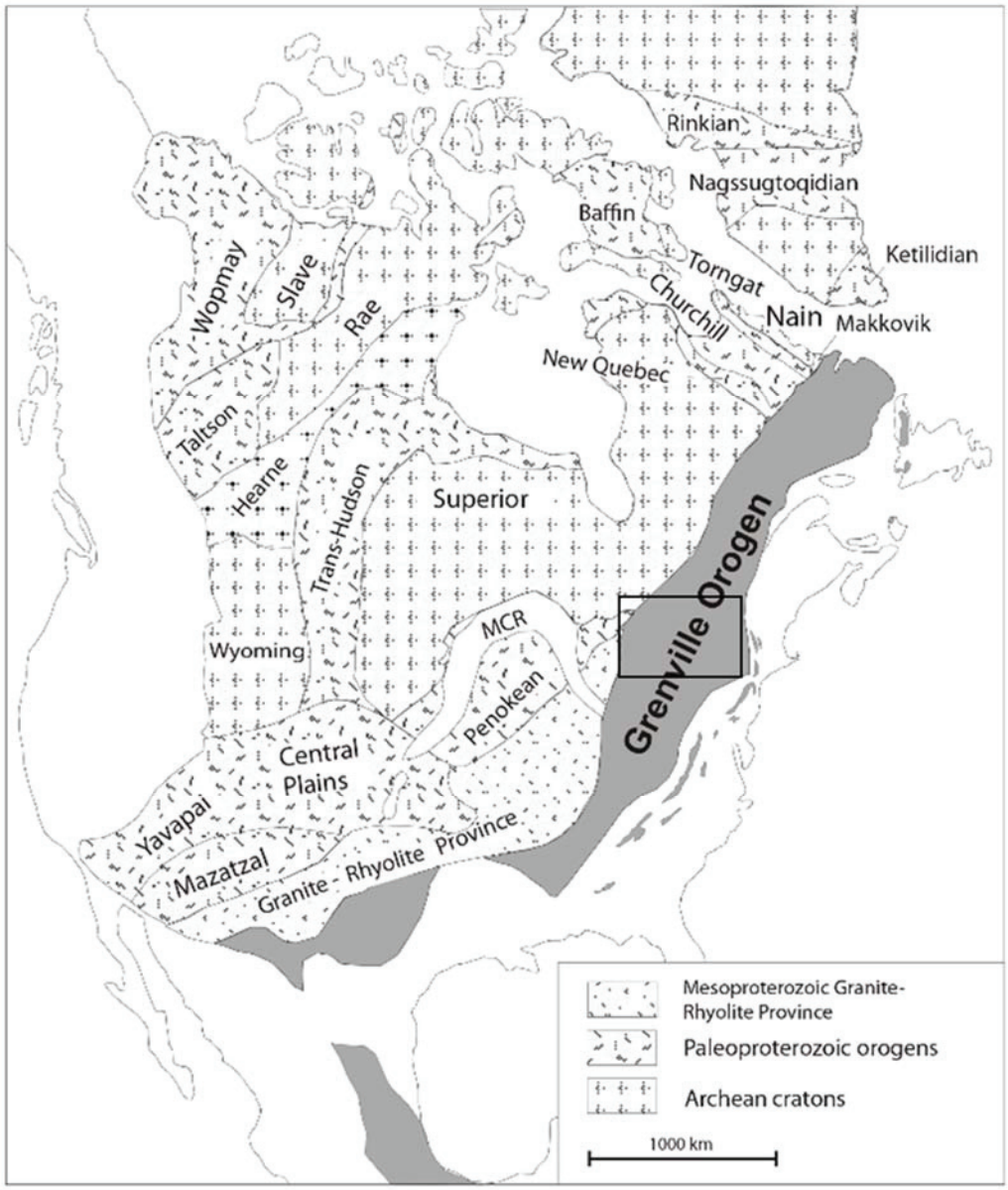

Figure 1.1: Generalized map showing the extent of the Grenville orogen in North America, including its subsurface extensions, exposed outliers in the Appalachians, and continuation into Texas and Mexico. Archean cratons and craton-forming orogens that make up North American are also shown. MCR = Mid-Continent Rift (modified from Tollo et al. 2004). Rectangle outlines Figure 1.2.

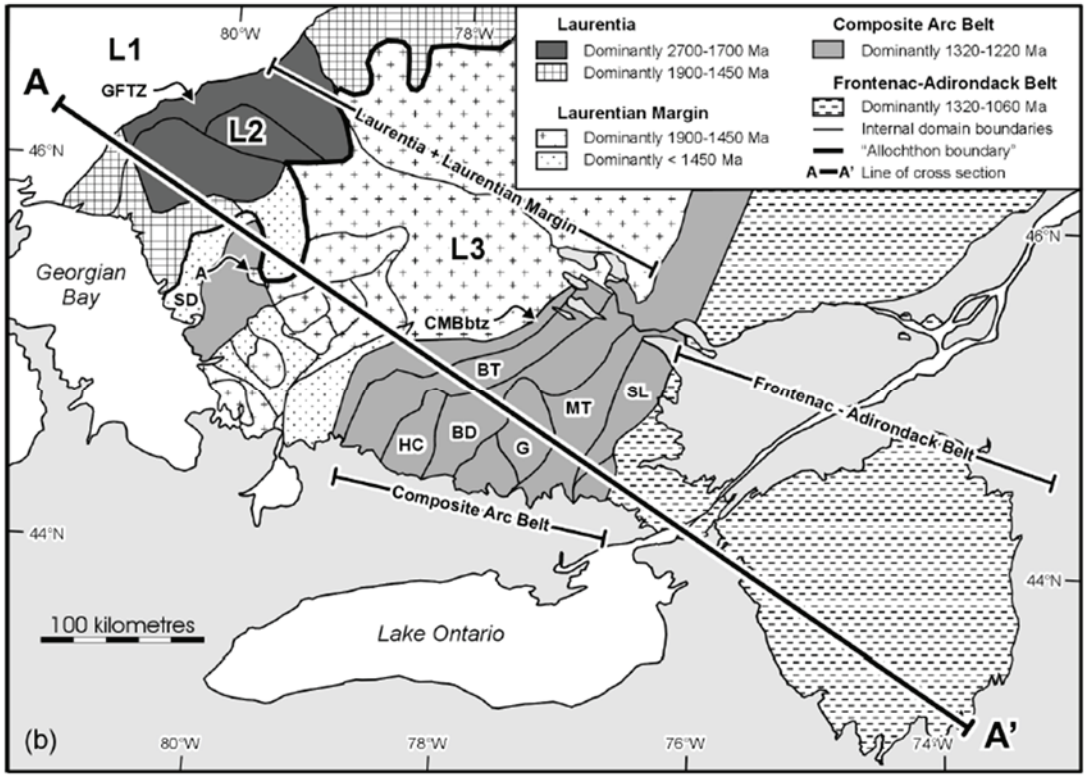

Figure 1.2: Divisions of the western Grenville Province proposed by Carr et al. (2000): Laurentia, Laurentian Margin, Composite Arc Belt and the Frontenack-Adirondack Belt. Cross-section line A-A' corresponds to Figure 1.3.

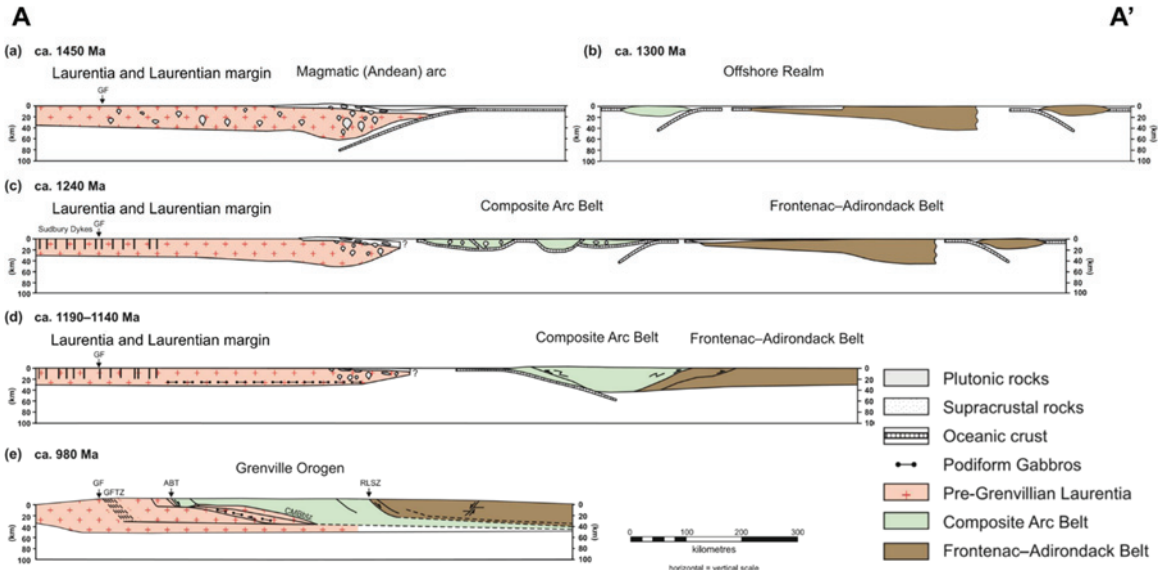

Figure 1.3: Series of schematic cross-sections illustrating orogenic evolution prior to, during, and after the Grenvillian orogeny, along line A-A' in Figure 1.2 (Carr et al., 2000).

The current architecture of the Grenville Province evolved from terrane accretion on the Laurentian margin, northwest-directed thrusting of accreted terranes and outer parts of the

margin toward Laurentian craton, widespread lateral ductile flow at mid-crustal levels, and late-orogenic extension and thrusting (Figure 1.3) (Jamieson et al. 1992; Culshaw et al. 1994, 1997; Carr et al. 2000; Rivers et al. 2012).

The term "Grenvillian orogeny" encompasses tectonic events that occurred from ca. 1.3 Ga to ca. 980 Ma (Davidson 1998; Gower and Krogh 2002), although the main continent-continent collision is believed to have occurred from 1090 to 980 Ma (Gower and Krogh 2002; Rivers 2012). Pre-Grenvillian orogenies that built up the Laurentian margin during the Paleoproterozoic and Mesoproterozoic eras include the Penokean orogeny (1.89 – 1.83 Ga), the Yavapai orogeny (1.75 – 1.70 Ga), the Mazatzal/Labradorian orogeny (1.65 – 1.60 Ga), the Pinwarian orogeny (1.52 – 1.45 Ga), and the Elzevirian orogeny (1.245 – 1.22 Ga). In addition, several phases of the Grenvillian orogeny have been recognized, including the Shawinigan orogenic pulse (ca. 1190 - 1140 Ma), the Ottawan orogenic pulse (phase) (ca. 1090-1020 Ma), and the Rigolet orogenic pulse (phase) (ca. 1005-980 Ma) (Culshaw et al. 1997, 2016; Rivers and Corrigan 2000; Hynes and Rivers 2010; Rivers et al. 2012; Craddock et al. 2013). A major episode of extension is documented between 1040 Ma and 990 Ma, in the Shawanaga Shear Zone and throughout the CGB, causing southeast transport of allochthonous rocks (Ketchum 1994; Culshaw et al. 1997; Ketchum et al. 1998; Jamieson et al. 2010).

Penokean, Yavapai, Mazatzal/Labradorian orogenies are collectively termed the Great Proterozoic Accretionary Orogen (GPAO)(Condie 2013). The GPAO contributed to the creation of the Nuna and Rodina continents, part of the Proterozoic Columbia supercontinent (Figure 1.4) (Meert 2012). For this study, the terms Laurentia, Laurentian craton and Laurentian margin will be used rather than Nuna, Columbia or Superior continent/craton.

In order to better understand the Grenville orogen, numerical models have been used to investigate the effects of convergence between continents using blocks of different composition, laterally and vertically across the crust (Jamieson et al. 2007, 2010). These models represent collision driven by simple suborogenic subduction and underthrusting by a strong craton (indentor). Results show that synconvergent ductile flow of melt-weakened middle crust, accompanied by underthrusting by a lower crustal indentor, caused detachment and exhumation of nappes toward the foreland, over the lower crustal indentor. Figure 1.5 displays a map and cross section from Culshaw et al. (1997) and Jamieson et al. (2007) which is used for comparison with the numerical model results in Figure 1.6.

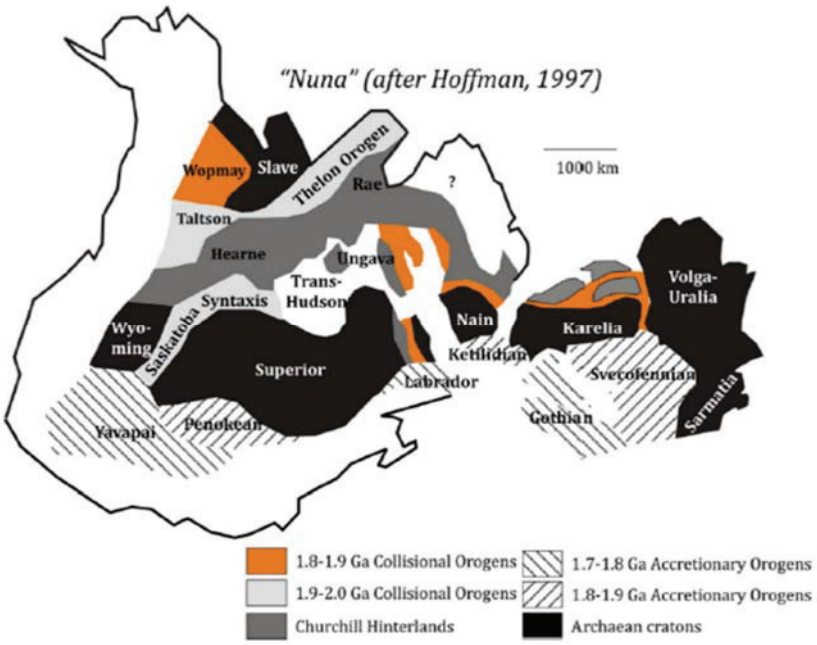

Figure 1.4: Components of Nuna, which made up part of the Columbia supercontinent. Image from Meert (2012) and Hoffman (1997).

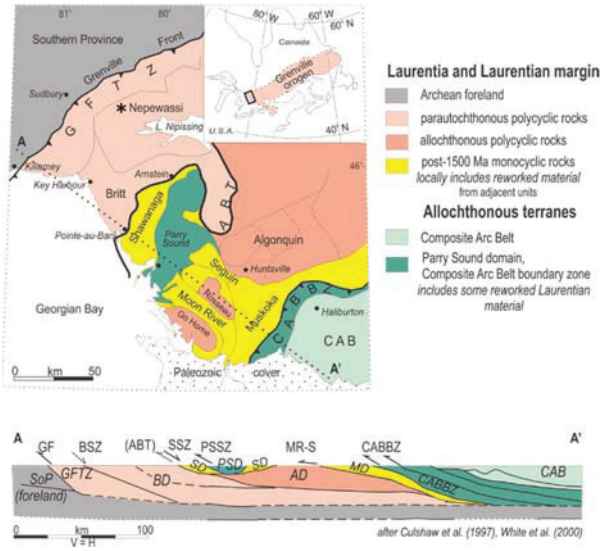

Figure 1.5: Georgian Bay crustal-scale cross-section and regional map of the Grenville Province in Ontario, showing stacking of lithotectonic domains resulting from northwest-directed thrusting. Modified from Jamieson et al. 2007. Cross-section based on detailed mapping Culshaw et al. (1997) and Lithoprobe seismic reflection data White et al. (2000). SoP, Southern Province; BSZ, Boundary shear zone; BD, Britt domain; ABT, Allochthon Boundary Thrust; SSZ, Shawanaga Shear Zone; SD, Shawanaga domain; PSSZ. Parry Sound Shear Zone; PSD, Parry Sound domain; AD, Algonquin domain; MR-S, Moon River–Seguin structures; MD, Muskoka domain; CABBZ, Composite Arc Belt boundary zone.

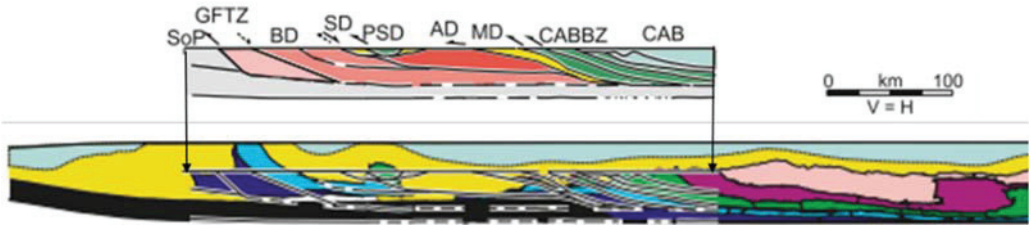

Figure 1.6: Georgian Bay cross-section from Figure 1.5 superimposed on numerical model results of stop-convergence model GO-ST87 from Jamieson et al 2010. Different colours in the numerical model represent variable mechanical properties of blocks within the model. Blocks are described in Jamieson et al 2010.

1.1.2 The Central Gneiss Belt

The Central Gneiss Belt makes up most of the Grenville Province in southeastern Ontario and western Quebec (Wynne-Edwards 1972). Most of the CGB is composed of generally southeast-dipping, upper-amphibolite- to granulite-facies orthogneisses and paragneisses (Rivers et al. 1989, 2012; Davidson 1998; Ketchum and Davidson 2000). The Central Gneiss Belt lithologic domains were part of the Laurentian margin or peri-Laurentian terranes prior to the Grenvillian orogeny (Carr et al. 2000; Condie 2013). Thus, Archean rocks of similar age and tectonic history to those of the Laurentian craton are present in parts of the parautochthonous belt and the GFTZ. Parautochthonous belts are formed near their present locations, whereas allochthonous belts have been transported by tectonic processes. Allochthonous terranes were emplaced on top of parautochthonous belts by northwest-propagating thrusts or shear zones (Figure 1.5). In the CGB, all parautochthonous domains are polycyclic (affected by more than one orogeny) but allochthonous terranes can be either polycyclic or monocyclic (Figure 1.5) (Rivers et al. 1989; Davidson 1998; Ketchum and Davidson 2000). Upright southeast- to south-southeast trending folds are well documented throughout the CGB (Lumbers 1971; Culshaw et al. 1994; Carr et al. 2000).

1.1.3 Huronian Supergroup

The Huronian Supergroup is a 4 to 12 km thick low grade metasedimentary sequence overlying the Laurentian craton, north of the Grenville Front, near Lake Huron and Georgian Bay (Figure 1.7) (Zolnai et al. 1984; Miall 1985; Young et al. 2001). The sediments are interpreted to have been deposited on the rifted, southern margin of the Superior craton during the Paleoproterozoic (ca. 2.5 to 2.2 Ga) (Craddock et al. 2013; Young 2015). The Huronian Supergroup is truncated by the GFTZ, and apparently disappear to the southeast it (Quirke and Collins 1930). However, in this

study, metasedimentary rocks in the Nepewassi domain are tentatively correlated with rocks in the Huronian Supergroup.

The lower Huronian formations are interpreted to have been deposited in transtensional rift basins formed by (oblique-) normal faults, such as the Murray Fault (Figure 1.7) (Fralick and Miall 1989; Long 2004). Rift-facies sedimentary rocks are overlain by passive margin rocks, which make up the upper Huronian formations; foreland basin sedimentary rocks lie unconformably on top of the upper Huronian passive margin sedimentary rocks (Craddock et al. 2013; Young 2015). The variations in thickness of the lower Huronian rocks partially reflect syndepositional, basinward-dipping, normal faulting (Zolnai et al. 1984). During the first phase of the Penokean orogeny (ca. 1900 Ma), the more distal, thicker sedimentary rocks, south of the Murray fault were overridden and depressed to mid-crustal levels, presumably because they were overridden by an allochthonous terrane (Zolnai et al. 1984). The early normal faults were reactivated and became north-verging reverse faults (Murray Fault Zone), that placed deformed and metamorphosed sediments and basement rocks over thinner, non-deformed Huronian sediments (Zolnai et al. 1984). The foreland basin is also interpreted to have formed during the Penokean orogeny (Young 2015).

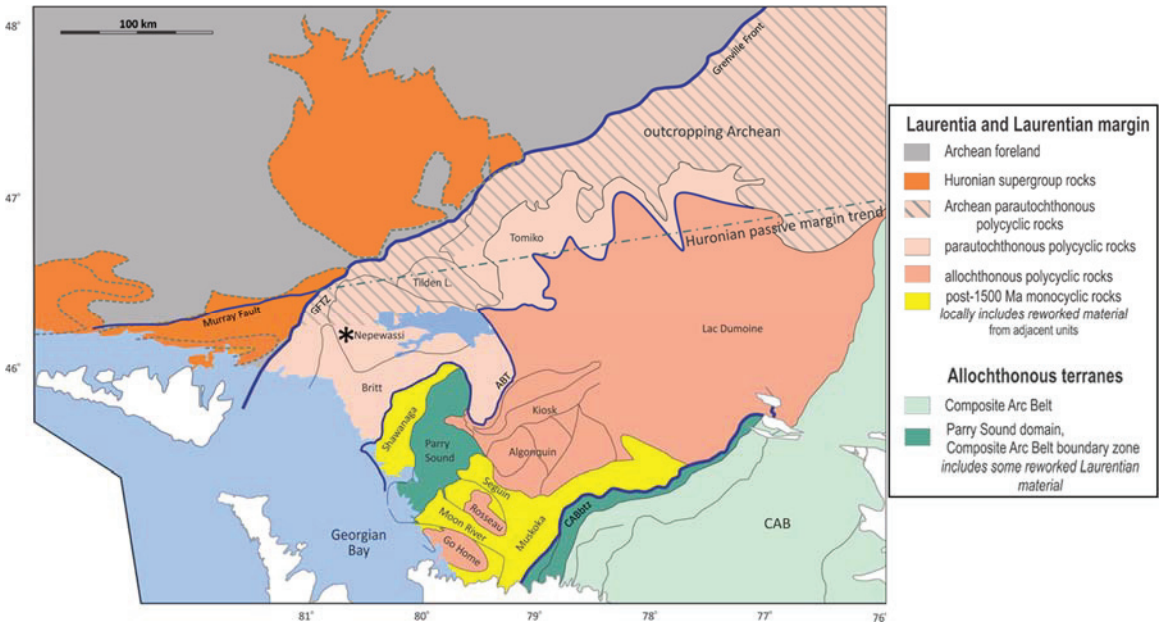

Figure 1.7: Lithotectonic subdivisions of the Central Gneiss Belt in Ontario extended to show corresponding domains in western Quebec, and the Huronian Supergroup north of the GF on the Laurentian craton. GFTZ, Grenville Front Tectonic Zone; ABT, allochthon boundary thrust; CABbtz, Composite Arc Belt boundary thrust zone; CAB, Composite Arc Belt. Modified from N. Culshaw, pers. com. 2016; Davidson 1986; Davidson and van Breemen 1988; Rivers et al. 1989; Culshaw et al. 1997; Ketchum and Davidson 2000.

1.1.4 The Nepewassi domain

This study focuses on the Nepewassi domain, which is located 10 to 20 km south of the Grenville Front within the parautochthonous Central Gneiss Belt, Grenville Province, Ontario (Figure 1.5 and Figure 1.7). The Nepewassi domain was first defined Easton (1992) and was distinguished from its neighbours on based on structural trends as well as rock types. Regional mapping, including what is now the Nepewassi domain, was completed in the late 1960s at 1:126 720 scale by Lumbers (1974, 1975). Prior to this study, the only U-Pb ages from the domain were a few igneous ca. 2.7 Ga ages for tonalitic grey gneisses in the northern portion of the domain, a ca. 1.42 Ga igneous age for a granitoid (Cosby pluton)(Lumbers 1975) and two ca. 1.2 Ga igneous ages for anorthosite bodies (St. Charles anorthosite and Mercer anorthosite)(Prevec 1992, 1993, 2004).

Based on reconnaissance mapping in 2013 (Culshaw et al. 2013a), the Nepewassi domain was divided into distinct subdomains. The Northern and Southern subdomains are separated by a straight high-strain zone of northwest-trending structures, the St. Charles–Lavigne straight zone (SCLSZ) (Culshaw et al. 2013a). Easton (2014) defined the Cosby subdomain, located south of the Southern subdomain, based on structural trends and the presence of the Cosby pluton, which differs in age and composition from the dominant granitoid pluton in the Southern subdomain, the West Bay batholith. An area in the Southern subdomain was chosen for detailed mapping in 2014 based on the presence of metasedimentary rocks and structures oriented oblique to the surrounding (sub)domains. The map area and subdomains of the Nepewassi domain are described fully in Chapter 2.

1.2 Objectives

It is hypothesized that Archean basement rocks and overlying sedimentary rocks, now cropping out in the Nepewassi domain, were part of a rifted passive margin in the early Paleoproterozoic that was inverted, shortened, and re-worked. The inversion of the passive margin and accompanying accretionary orogenies would have reversed previously normal faults, thrusting Archean basement rocks up so that they are imbricated with passive margin sediments (Figure 1.8). The purpose of this project is to test the hypothesis that rocks in the Nepewassi domain were part of a Paleoproterozoic passive margin by geological mapping, petrography, metamorphic studies and geochronology.

This thesis will supplement the overall goal of investigating the role of inheritance in orogens, particularly large, hot, orogens, as they propagate into the foreland (Beaumont et al. 2001, 2004, 2006, Rivers 2009, 2012; Hynes and Rivers 2010; Jamieson and Beaumont 2013), investigating pre-Grenvillian structures in the Nepewassi domain. This study will also supplement research on the tectonic history of the Grenville Province in Ontario by Dalhousie researchers (e.g., Culshaw et al. 1994, 1997, 2006, 2010, 2013b, 2016) and the Ontario Geological Survey (Easton 1992, 2011; Easton et al. 1999; Easton and Heaman 2011). This study may provide insight and support for a similar study by Dufréchou and Harris (2013) and Dufréchou et al. (2014) in southwest Quebec on the role of pre-existing Paleoproterozoic structures in the Archean basement on formation and preservation of linear structures throughout the formation of the Grenville Province, if similar structures can be identified in the Nepewassi domain,

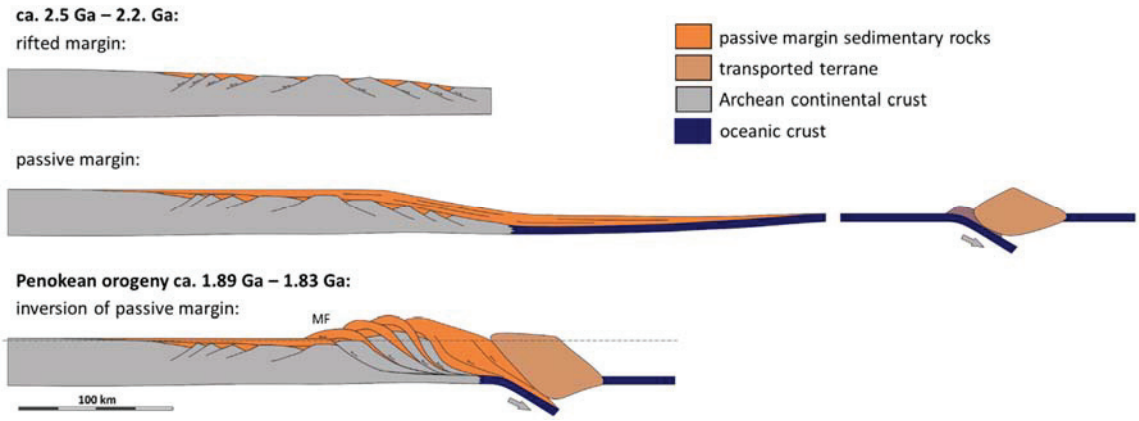

Figure 1.8: Schematic cross sections of a passive margin inversion on the southeast margin of the Laurentian craton during the Paleoproterozoic. The bottom cross section depicts passive margin sediments thrust on top of themselves, like the Huronian Supergroup (Zolnai et al. 1984). Dashed line indicates a modern erosional surface. MF, Murray Fault.

The Nepewassi domain is distinct from surrounding domains in terms of geology, isotopic signature and deformational history (Easton 1992; Dickin 1998b). The Nepewassi domain includes rocks that have yielded igneous Archean U/Pb ages (Chen et al. 1995) and Paleoproterozoic and Mesoproterozoic plutons; therefore rocks in the Nepewassi domain likely have remnant pre-Grenvillian structural features. Similarly-aged Archean rocks are found in the foreland, the GFTZ, and parautochthonous domains to the north and east of the Nepewassi domain (Figure 1.7), but not in domains to the west and south.

The objectives of this study are: a) to document features preserved in the Nepewassi domain by mapping lithological, structural and metamorphic features and comparing their geometry and age with similar features of known age outside the Nepewassi domain; b) to determine which pre-Grenvillian orogenic events affected the Nepewassi domain; and c) to constrain the possible tectonic setting(s) of supracrustal rocks in the Nepewassi domain prior to the Grenvillian orogeny. In order to achieve these objectives, the following tasks were completed: a) a detailed lithological and structural field study of a portion of the Nepewassi domain was done and a bedrock geology map was created; b) the geometry and of structural features of the Nepewassi domain were compared with similar features of known age outside it; c) petrographic and thermobarometric data were acquired to study metamorphism in Nepewassi domain; d) detrital zircon ages of metasedimentary rocks and igneous crystallization ages of orthogneisses were obtained in order to provide insight into the tectonic setting and provenance of Nepewassi domain rocks by comparison with similar rock types outside the Nepewassi domain; and e) ages of high-grade metamorphism within Nepewassi domain were determined in order to determine which pre-Grenvillian orogenic events affected the Nepewassi domain.

CHAPTER 2

LITHOLOGIES

2.1 Introduction

A three-month mapping season in 2014 was supported by Ontario Geological Survey (OGS) as part of a mapping agreement with Dalhousie University. Field equipment, lodging and a field assistant were all supplied; Dr. Michael Easton, from the OGS, provided advice and assistance. Summary of Field Work and Other Activities Reports, and Miscellaneous Release-Data which includes geochemical data, field data, photos, petrography and maps, are publicly available as part of OGS Project Unit 13-029 (Van De Kerckhove and Easton 2016).

Detailed mapping of the Nepewassi domain is crucial in developing a better understanding of the rock types and their protoliths and to provide context for other research in the area. Previous mapping by Lumbers (1974) defined one main unit of layered gneisses which formed the country rock to the West Bay batholith and other intrusive bodies in the Southern subdomain (Figure 2.1). The goal of this mapping project was to provide a more detailed map of a portion of the Southern subdomain, with a focus on dividing the gneissic country rock unit (Layered gneisses, Figure 2.1) into multiple units. The aim was to define lithologies or packages of lithologies that provide information about the tectonic setting during the formation of the rocks. In order to extrapolate tectonic information from a rock unit or units, the protolith of the rock must be accurately determined. Metasedimentary rocks were identified and are focused on because they have the potential to provide information about depositional setting. In this thesis, the hypothesis that the metasedimentary package of rocks in the Nepewassi Domain was initially deposited on a passive margin is tested.

Mapping was done at 1:20 000 on an area within the Southern subdomain where outcrop of desired rock types (metasedimentary rocks – namely quartzite) is relatively abundant, and easily accessed. The area was also chosen because it displays trends that are oblique to the trends of surrounding domains. The structure of this area will be discussed in Chapter 3.

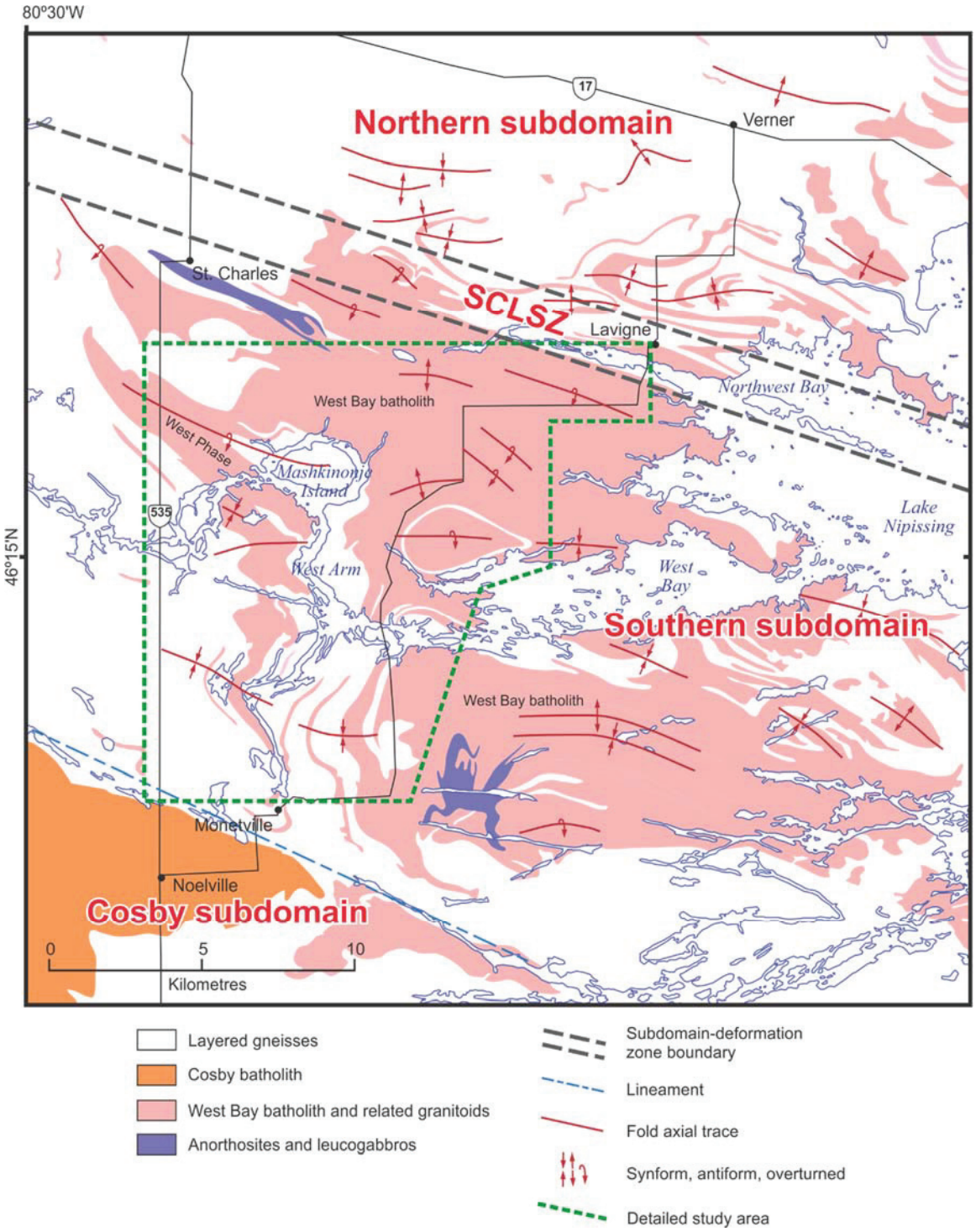

Figure 2.1: Simplified map of the Nepewassi domain, highlighting contrasting metaplutonic units. SCLSZ, St. Charles-Lavigne straight zone.

2.1.1 Previous Work

The Nepewassi domain in the Central Gneiss Belt has not been studied in detail except for regional mapping in the 1970s (Lumbers 1974, 1975) when a 1:126 720 scale map was created. The domain consists of Archean grey gneisses and a variety of biotite gneiss units intruded by large granitoid plutons, such as the West Bay batholith and the Cosby pluton, and the Geon 12 St. Charles anorthosite and Mercer anorthosite (Carr et al. 2000, Culshaw et al. 2013b). Studies by Dickin (1998a, 1998b) and Prevec (1992, 2004) provided some ages for Archean grey gneiss and Geon 12 anorthosites. The Cosby pluton is assigned an age of ca 1420 Ma based on preliminary U-Pb ages reported by L.T. Silver (pers. comm, reported in Lumbers 1975).

During reconnaissance mapping between 2011 and 2013 a type 1 transitional to type 2 fold interference pattern (Ramsay 1967) in the eastern portion of the Nepewassi domain was documented (Culshaw et al. 2013a) and the Nepewassi domain has been divided into 3 subdomains: Northern, Southern and Cosby, which are described as follows.

Northern subdomain:

Located immediately north of the SCLSZ, the Northern subdomain consists of a grey gneiss complex, intruded by a granitoid pluton known as the Sturgeon Falls batholith The grey gneiss complex (unit 6a, Lumbers 1974; unit 1, section 2.2) consists of cm- to m-scale interlayered leucocratic grey biotite-hornblende tonalite, a darker hornblende-biotite tonalite and subordinate pink leucogranite, along with less common centimetre- to decimetre-scale amphibolite bands, and pegmatitic veins and layers (Culshaw et al. 2013a). Granitic leucosomes filling internal boudin necks can be seen in some outcrops. Geochronology by Chen et al. (1995) yielded several ca. 2.7 Ga Archean zircon ages for this tonalite-trondhjemite grey gneiss complex. Lumbers (1975) also described a paragneiss country rock associated with the Archean grey gneiss suite; however, this unit was not observed during this study, despite attempts to locate it in the field. A few relatively small gabbroic and dioritic intrusions are present (Lumbers 1974) along with the Sturgeon Falls batholith, which consists of parallel, folded quartz monzonitic bodies (Figure 2.1), nearly identical to those of the West Bay batholith.

Folds in the Northern subdomain are commonly upright, open, and plunge shallowly east-southeast (Culshaw et al. 2013a). Also present are decimetre- to metre-scale recumbent folds that occur immediately north of the SCLSZ.

St. Charles–Lavigne straight zone:

The SCLSZ is a near-vertical, consistently oriented, strongly foliated zone that affects rock units from the adjacent subdomains, including the West Bay batholith. The foliation of the SCLSZ is stronger and at an angle to the orientation of adjacent subdomains. A steep north-northeast dip is the dominant orientation of the SCLSZ, as exposed in the eastern part of the study area. The northeast dip is approximately parallel to the dip of the axial planes of the second phase folds in the Southern subdomain, suggesting a genetic relationship between the SCLSZ and the second phase folds (Culshaw et al. 2013a). The SCLZ also includes three elongate bodies of St. Charles-like leucogabbro (unit 20a, section 2.2) oriented the same as the SCLSZ. The leucogabbros display foliations that are either transposed or were initiated parallel to the SCLSZ trend (Culshaw et al. 2013a).

Southern subdomain:

The Southern subdomain contains the same rocks types as the Northern subdomain, and an additional suite of supracrustal rocks which are layered and vary in thickness from 1 metre to 100s of metres. A large migmatitic quartz monzonite body in the Southern subdomain, named the West Bay batholith (Lumbers 1974, 1975), is compositionally and texturally akin to the Sturgeon Falls batholith in the Northern subdomain (Lumbers 1974, 1975). A significant number of small mafic intrusions are found in the Southern subdomain, particularly in the western half. The St. Charles anorthosite, akin to unit MA described in section 2.1.2, is a leucogabbroic to anorthositic body located in the northwest corner of the Southern subdomain, just south of the SCLSZ. The St. Charles anorthosite ranges from undeformed to weakly foliated gneiss.

Mapping in the 2014 season was concentrated in the Southern subdomain around the West Arm of Lake Nipissing (Figure 2.1); rock types from this subdomain are divided into units and described in detail in section 2.2. Polyphase fold interference structures, documented in 2013, are present in the Southern subdomain, but are apparently absent in the Northern and Cosby subdomains.

Cosby subdomain:

The Cosby subdomain, defined by Easton in 2014, is separated from the Southern subdomain by a northwest-trending lineament, coinciding with the Wolseley River. This boundary is also marked by a change in the gravity field (Gupta 1991, 1992) from higher in the Southern subdomain to

lower in the Cosby subdomain. The Cosby subdomain is made up of country rocks seemingly similar to those observed in the Southern subdomain including feldspathic paragneiss (unit 8a, Lumbers 1974), and tonalitic and granodioritic grey gneisses. There are no documented U-Pb Archean ages in the Cosby subdomain, but Pb isotope studies by Dickin (1998a) suggest that Archean rocks are present. Intrusive bodies in the Cosby subdomain include minor mafic intrusions and quartz monzonitic intrusions, such as the Cosby pluton and the Pine Cove pluton; the Pine Cove pluton is lithologically similar to the West Bay batholith (Lumbers 1974, 1975). Also present is the thick, laterally extensive, French River quartzite. Whether or not the French River quartzite is correlative with the thin quartzite units observed in the Southern subdomain has yet to be established. Structural data from the Cosby subdomain are limited to structural trend lines on Map 2271 (Lumbers 1974).

During the 2013 field season, important packages of rocks were recognized and chosen as the focus of mapping for the following season. Tonalitic and granodioritic gneisses in the western portion of the Southern subdomain (Figure 2.1) have a similar appearance to rocks of known Archean age in the Northern subdomain, and were thus hypothesized to also be Archean. Metasedimentary rocks were located within a package of layered gneisses along the West Arm of Lake Nippissing (Figure 2.1). The West Bay batholith is the prominent granitoid metaplutonic rock in the Southern subdomain.

2.1.2 Map Area and Access

Although information from the entire Nepewassi domain and its surroundings is considered in this study, a smaller area was studied in detail. The project location was originally defined as an approximately 1400 km^2 area west of Lake Nipissing, bounded to the north by Highway 17, to the south by the French River, and extending about 2 km west of Highway 535 (Culshaw et al. 2013a). In 2014, the map area was narrowed to an approximately 250 km^2 area bounded to the north by Lavigne, to the east by Highway 64, to the south by Monetville on Highway 64, and to the west by Highway 535. This area is referred to as “the map area” and is outlined in Figure 2.1. Based largely on data from the 2014 field season, a 1:20 000 bedrock map of the map area was created. Two versions of the bedrock map are in Appendix A; Structural measurements are depicted in Appendix A.1, and station locations and landmarks referenced in this thesis are shown in Appendix A.2. Geographical coordinates of map stations are listed in Appendix A.3.

Bedrock was accessed from hiking trails, minor roads, highway road cuts, and from the shorelines of the West Arm of Lake Nipissing, Warren Bay, and Shanty Bay.

2.2 Map Units

The following map legend describes the lithologic units from the 1:20 000 scale maps included in this thesis as Appendix A, and follows the same order, interpreted youngest to oldest, as the Appendix A map legend. The unit descriptions are grouped by protolith (or assumed protolith) and estimated age. Age groups are estimates, and the order of units within each group does not necessarily imply chronological order.

Table 2.1. Map Legend. Unit IDs combine capital letters, which indicate composition and/or protolith type, and lower case letters, which are descriptors.

Age	Protolith Group	Unit	Unit name
Neoproterozoic or younger (≤ 1.0 Ga)	Small mafic bodies	Nd	Unmetamorphosed nephelinite dike
Mesoproterozoic or younger (≤ 1.6 Ga)	Small mafic bodies	Md_3	Amphibolite dikes
Mesoproterozoic or younger (≤ 1.6 Ga)	Small mafic bodies	Md_2	Garnet-bearing, amphibolite dikes
Paleoproterozoic to Mesoproterozoic	Small mafic bodies	Md_1	Metadiabase dikes (similar to Sudbury dike swarm)
Paleoproterozoic to Mesoproterozoic (2.5 – 1.0 Ga)	Small mafic bodies	Mmd	Dioritic and gabbroic metatexite and diatexite dikes and sills
Paleoproterozoic to Mesoproterozoic (2.5 – 1.0 Ga)	Mafic and intermediate metaplutonic rocks	QD	Quartz dioritic gneiss
Paleoproterozoic to Mesoproterozoic (2.5 – 1.0 Ga)	Mafic and intermediate metaplutonic rocks	Mm_1	Dioritic metatexite and diatexite
Paleoproterozoic to Mesoproterozoic (2.5 – 1.0 Ga)	Mafic and intermediate metaplutonic rocks	Mm_2	Dioritic stromatic metatexite
Paleoproterozoic to Mesoproterozoic (2.5 – 1.0 Ga)	Mafic and intermediate metaplutonic rocks	Mn	Diorite and gabbro gneiss
Paleoproterozoic to Mesoproterozoic (2.5 – 1.0 Ga)	Mafic and intermediate metaplutonic rocks	GMb	Intrusion breccia; gabbroic xenoliths in syenogranite to monzogranite matrix
Paleoproterozoic to Mesoproterozoic (2.5 – 1.0 Ga)	Mafic and intermediate metaplutonic rocks	MA	Gneissic to massive leucogabbro, gabbroic anorthosite, anorthositic gabbro, and anorthosite

Table 2.1: *Continued.*

Age	Protolith Group	Unit	Unit name
Paleoproterozoic to Mesoproterozoic (2.5 – 1.0 Ga)	Mafic and intermediate metaplutonic rocks	UM	Pyroxene hornblendite
Paleoproterozoic to Mesoproterozoic (2.5 – 1.0 Ga)	Felsic metaplutonic rocks	Gd	Monzogranite dikes and sills
Paleoproterozoic to Mesoproterozoic (2.5 – 1.0 Ga)	Felsic metaplutonic rocks	Gnm	Quartz monzonitic gneiss and migmatite (West Bay batholith)
Paleoproterozoic to Mesoproterozoic	Felsic metaplutonic rocks	Gn_1	Leucocratic quartz monzonitic gneiss (West Phase)
Paleoproterozoic to Mesoproterozoic (2.5 – 1.0 Ga)	Felsic metaplutonic rocks	GMn	Undivided leucocratic quartz monzonitic gneiss (Gn1) with Dioritic stromatic metatexite (Mm2), Amphibolite dikes (Md3), and Monzogranite dikes and sills (Gd)
Paleoproterozoic to Mesoproterozoic (2.5 – 1.0 Ga)	Felsic metaplutonic rocks	Gn_2	Magnetite-bearing leucocratic monzogranitic gneiss
Paleoproterozoic to Mesoproterozoic (2.5 – 1.0 Ga)	Felsic metaplutonic rocks	Gn_3	Monzonitic gneiss with minor syenite and quartz syenite
Paleoproterozoic to Mesoproterozoic (2.5 – 1.0 Ga)	Gneiss of uncertain protolith	lm_2	Heterogeneous, layered metatexite of multiple compositions
Paleoproterozoic to Mesoproterozoic (2.5 – 1.0 Ga)	Gneiss of uncertain protolith	lm_3	Heterogeneous, layered garnet, hornblende, biotite, plagioclase, quartz, K-feldspar metatexite
Paleoproterozoic to Mesoproterozoic (2.5 – 1.0 Ga)	Gneiss of uncertain protolith	Bn	Biotite gneiss
Paleoproterozoic to Mesoproterozoic (2.5 – 1.0 Ga)	Probable supracrustal rocks	Pm	Garnet, biotite, plagioclase migmatite
Paleoproterozoic to Mesoproterozoic (2.5 – 1.0 Ga)	Probable supracrustal rocks	Fm	Feldspathic migmatite
Paleoproterozoic to Mesoproterozoic (2.5 – 1.0 Ga)	Probable supracrustal rocks	Fn	Feldspathic gneiss
Paleoproterozoic to Mesoproterozoic (2.5 – 1.0 Ga)	Probable supracrustal rocks	lm_1	Layered tonalitic to granodioritic gneiss and metatexite

Table 2.1: *Continued.*

Age	Protolith Group	Unit	Unit name
Paleoproterozoic to Mesoproterozoic (2.5 – 1.0 Ga)	Probable supracrustal rocks	lnFm	Undivided layered gneiss and minor migmatite (ln) and Feldspathic migmatite (Fm) with Monzogranite dikes and sills (Gd), Pelite/semipelite (Sn2), Leucocratic gneiss with probable volcanic protolith (VFn), Dioritic stromatic metatexite (Mm2), and Quartz dioritic gneiss (QD)
Paleoproterozoic to Mesoproterozoic (2.5 – 1.0 Ga)	Probable supracrustal rocks	ln	Layered gneiss and minor migmatite
Paleoproterozoic to Mesoproterozoic (2.5 – 1.0 Ga)	Probable supracrustal rocks	VGMn	Undivided felsic gneiss with probable volcanic protolith (VFn), Gn2, and Mn1 with minor Monzogranite dikes and sills (Gd), Dioritic metatexite and diatexite dikes and sills (Mmd) and Amphibolite dikes (Md3)
Paleoproterozoic to Mesoproterozoic (2.5 – 1.0 Ga)	Probable supracrustal rocks	VFn	Leucocratic gneiss; probable volcanic protolith
Paleoproterozoic to Mesoproterozoic (2.5 – 1.0 Ga)	Supracrustal: Metasedimentary rocks	Sn_1	Paragneiss: Quartzite
Paleoproterozoic to Mesoproterozoic (2.5 – 1.0 Ga)	Supracrustal: Metasedimentary rocks	Sn_2	Paragneiss: Pelite/semipelite
Paleoproterozoic to Mesoproterozoic (2.5 – 1.0 Ga)	Supracrustal: Metasedimentary rocks	Sn_3	Paragneiss: Psammite
Archean (≥2.5 Ga)	Tonalitic grey gneisses	Tn	Tonalitic and granodioritic gneiss and migmatites

G, granitoids: granitic, monzogranite, quartz monzonite, minor syenite and quartz syenite; F, felsic; M, mafic; UM, ultramafic; A, anorthosite; N, nephelinite; D, diorite; T, tonalitic; Q, quartz; B, biotite; P, plagioclase; S, sedimentary; V, volcanic; n, gneiss; m, migmatite; d, dike/sill; b, breccia; l, layered

Criteria used for categorizing rock-types and naming rocks are as follows:

Rocks with intrusive protoliths are determined by the presence of a remnant, medium to coarse grained igneous texture. Actual crystal size is highly varied, because original grains were recrystallized during high grade metamorphism. Deformed coarse plutonic textures are recognized by flattened or elongate aggregates of minerals. Units with intrusive protoliths tend to be compositionally homogeneous at outcrop scale, although variation in texture is common.

Furthermore, if contacts are observed cutting the host rock fabric or layering, an intrusive protolith is likely.

Metasedimentary rocks were distinguished based on texture and mineralogy. Rocks with sedimentary protoliths are compositionally layered, have a granular texture, and are fine- to medium-grained. The presence of the aluminosilicate minerals kyanite and/or sillimanite, together with abundant mica, confirms the rock had an aluminous (clay-rich) protolith. Metasandstones with less aluminous protoliths may not contain aluminosilicate minerals or garnets, however high quartz content (> 60%) is an indicator that the rock is sedimentary, because igneous rocks do not commonly contain more than 60% quartz. Metamorphosed quartz arenites (quartzites) in the map area are texturally and compositionally homogeneous because they are composed almost exclusively of quartz. Feldspathic sandstone protoliths are difficult to determine because they have a similar mineral assemblage (quartz + 2 feldspars + biotite) to many felsic igneous rocks. Where possible, field relations were used to distinguish between rocks with feldspathic sandstone and felsic igneous protoliths. Calc-silicate rocks are interpreted to be derived from rocks with calcareous mudstone or siltstone protoliths and contain a large portion of garnet and calcareous minerals. No evidence was observed in the field to suggest that the calc-silicate rocks may have been metasomatic or due to localized alteration.

Supracrustal rocks may be sedimentary or volcanic, but it is impossible to determine the exact protolith of many rock units. Rocks interpreted as supracrustal in origin are compositionally layered, have a granular texture, and are fine- to medium grained. Compositional layering varies from mm scale to dm scale. In the case of fine-grained leucocratic gneiss of probable volcanic protolith (VFn), which is texturally and mineralogically homogeneous, they are less migmatitic relative to the granitic plutonic rock units. This relative difference is a local phenomenon, potentially because the supracrustal rocks are older and were depleted in fluids during previous metamorphic events.

The Archean grey gneiss association consists of tonalitic to granodioritic orthogneiss with outcrop-scale mafic and granitic dikes. It is not grouped with the rest of the intrusive protolith rock types because its strongly resembles rocks with known Archean ages in the Northern subdomain. It is described separately because it is likely basement or host rock to all the other units.

Nearly all units in the Nepewassi domain are gneisses. The term gneiss refers to a high grade metamorphic rock (medium- to coarse-grained) with an L-S tectonic fabric. An L-fabric is a

marked linear fabric and an S-fabric is planar (Chapter 3). The L-S fabrics are defined by the separation of mafic and quartzofeldspathic minerals, or the shape of minerals and mineral aggregates. Many gneisses are migmatitic; for migmatites, the distinction between diatexite and metatexite is the same as Ontario Geological Survey's definition based on Sawyer (2008). Metatexites have <20 % (leucosome), and diatexites have 20 % or more leucosome. When a gneissic rock unit has less than 5 % leucosome (migmatitic gneiss), or is only locally migmatitic, it is still named gneiss.

During the 2014 field season, 42 samples were collected from within the map area for geochemical analysis. In some units, the resulting data were used to help characterize the rock units and supplement mapping. All geochemical data are found in Ontario Geological Survey Miscellaneous Release-Data 338 (Van De Kerckhove and Easton 2016).

Surficial lake, stream and swamp deposits in the map area were not subdivided nor were they assigned unit names. Instead bedrock unit contacts have been extrapolated across these surficial deposits using structural trends from adjacent outcrops.

2.3 Small mafic bodies

2.3.1 Nd

Nd is an unmetamorphosed nephelinite dike, light- to medium-grey, sharp-walled, very fine-grained, containing olivine + clinopyroxene + biotite ± analcime ± nepheline. This unit was documented in two locations along highway 64, only one of which is located within the map area. Both dikes are approximately 40 to 50 cm wide, cut the fabric of surrounding rocks, and are undeformed. These dikes have similar compositions and orientations to dikes of the Neoproterozoic Ottawa-Bonnechere graben alkaline magmatic suite, intruded at ca. 590 Ma (Halls et al. 2015). An approximate age of 590 Ma was assigned to unit Nd based on this association.

2.3.2 Md_3

Unit Md_3 consists of amphibolite dikes and sills composed of hornblende + plagioclase ± biotite but tend to be smaller and more deformed the garnet-bearing, amphibolite dikes (Md_2). They are fine- to medium-grained, commonly folded, and typically cut the country rock foliation. Both units, Md_2 and Md_3, have ≥ 50% mafic minerals, and although they are compositionally similar, it is not known if they formed during the same magmatic episode.

2.3.3 Md_2

Md_2 consists of fine-grained, garnet-bearing, amphibolite dikes, composed of hornblende + plagioclase + garnet. They are typically 3- to 4-m wide, vertical, straight-walled, compositionally and texturally homogeneous and low strain; some local granitic veins and/or leucosomes are present. Dike contacts cut gneissosity in the host rock at a low angle (Figure 2.2). Garnet aggregates in Md_2 dikes in the Southern subdomain are notably elongated along the foliation; however, this elongation texture is not present in dikes of the same unit in the Northern subdomain.

Figure 2.2: Garnet-bearing, amphibolite dikes, Md_2, cutting the West Bay batholith, Gnm. White line highlights the contact of the dike and red line highlight the layering in the West Bay batholith.

Figure 2.3: Heterogeneous dike with dark inclusions (bottom) on highway 535 (station 14SV339, Appendix A.2) cutting light grey tonalitic-granodioritic gneiss (top).

A second, but compositionally and texturally distinctive dike type is also included in unit Md_2. It crops out as an approximately 5-metre-wide, heterogeneous, garnet amphibolite dike on highway 535, north of Noelville (station 14SV339, Appendix A.2) and has different textures than any other dike documented in the Nepewassi domain. It intrudes tonalitic and granodioritic grey gneiss (unit Tn), obviously cutting the gneissic fabric, and has dark internal inclusions (Figure 2.3). It is lineated and foliated, ranging from L>S to L<S. The distribution of garnet porphyroblasts and plagioclase and amphibole phenocrysts is heterogeneous.

2.3.4 Md_1

Md_1 rocks are medium-grained garnet amphibolite or metadiabase intrusions. They are composed of plagioclase + amphibole + garnet ± clinopyroxene ± biotite ± ilmenite. One of the two documented outcrops in the map area displays coronitic texture, which is common in metamorphosed Sudbury dikes (Bethune and Davidson 1997). The Sudbury dike swarm is dated at approximately 1235 Ma (Krogh et al. 1987).

2.3.5 Mmd

Dioritic and gabbroic metatexite and diatexite dikes and sills (Mmd) are similar to dioritic metatexite and diatexite, unit Mm1, but crops out as smaller metre-scale bodies. Mmd dikes and sills are composed of plagioclase + amphibole ± biotite ± titanite ± apatite ± allanite ± quartz ± scapolite ± chlorite ± K-feldspar ± opaque minerals. They characteristically form migmatitic amphibolite lenses and layers, typically highly strained. Both leucosomes and body shape are concordant with the foliation of the rock it intrudes, which is typically leucocratic gneiss with probable volcanic protolith (VFn). Unlike those in dioritic metatexite and diatexite (Mm_1), leucosomes in dioritic and gabbroic metatexite and diatexite dikes and sills (Mmd) are either plagioclase-rich or K-feldspar rich.

2.4 Mafic and intermediate metaplutonic rocks

2.4.1 QD

Unit QD is medium- to coarse-grained quartz diorite, with roughly 25 to 30 volume % mafic minerals, it is made of plagioclase + quartz + amphibole + biotite ± chlorite ± K-feldspar ± titanite ± apatite ± calcite ± clinopyroxene. It is generally gneissic, locally migmatitic, and commonly veined by granitic pegmatite.

2.4.2 Mm_1

Dioritic metatexite and diatexite, Mm_1, is characterized by large volumes of leucosomes in a medium- to coarse-grained diorite host (Figure 2.4). The matrix is made up of hornblende + plagioclase + quartz + biotite and the leucosomes are composed of predominantly plagioclase with small amounts of quartz. This unit is typically diatexite, locally metatexite, stromatic or net-veined, and derived from gabbro and diorite. Unit Mm_1 is commonly garnet-bearing. The leucosomes are medium- to coarse-grained and plagioclase-rich, whereas the mesosome is typically medium- to fine-grained with ≤ 50% mafic minerals. Dioritic metatexite and diatexite (Mm_1) crops out as metre to decametre-scale bodies, the largest of which is approximately 85 m long.

Figure 2.4: Dioritic diatexite, Mm_1, on the northern shoreline of Mashkinonje Island.

2.4.3 Mm_2

Mm_2 is dioritic stromatic metatexite composed of amphibole + quartz + calcite ± chlorite ± epidote ± zoisite. In some locations, melanosomes or amphibole lenses and coarse-grained plagioclase and quartz leucosomes are very distinctive and are centimetres wide and tens of centimetres long. Dioritic stromatic metatexite (Mm_2) is similar to dioritic metatexite and diatexite (Mm_1) and dioritic and gabbroic metatexite and diatexite dikes and sills (Mmd), however rocks in this unit have more plagioclase and quartz overall and are generally medium- to coarse-grained. Furthermore, units Mm_1 and Mmd do not crop out within the West Bay batholith (Gnm), and contacts between these units are not exposed. Because dioritic stromatic metatexite (Mm_2) cuts the West Bay batholith (Gnm), it is interpreted as younger than the West Bay batholith, but this relative age constraint cannot be placed on Mm_1 and Mmd. The age of migmatization in dioritic stromatic metatexite (Mm_2) (or the West Bay batholith (Gnm)) is not constrained.

2.4.4 Mn

Diorite and gabbro gneisses, unit Mn_1, are medium- to coarse-grained, massive to weakly foliated. They are locally migmatitic, but typically stromatic. This unit is composed of plagioclase + amphibole + quartz ± biotite ± garnet ± titanite (metamict) ± epidote ± clinopyroxene ± orthopyroxene ± scapolite ± allanite (metamict) ± chlorite ± apatite ± K-feldspar ± magnetite.

Many samples contain minerals from multiple metamorphic assemblages implying multiple generations of metamorphism. For examples, in some samples metamict orthopyroxene and clinopyroxene (granulite facies) are present amongst hornblende, biotite, quartz and plagioclase (amphibolite facies). Leucosomes are composed of quartz and feldspar; where present, K-feldspar is only found in leucosomes. It is not clear if the leucosomes were injected from an external location, or formed by partial melting of the host rock. In some non-foliated outcrops there are two orientations of leucosomes (Figure 2.5 A). Locally, there are coarse to very coarse amphibole crystals throughout the rock (Figure 2.5 B). It is unclear if the original crystals developed during metamorphism or if they were igneous.

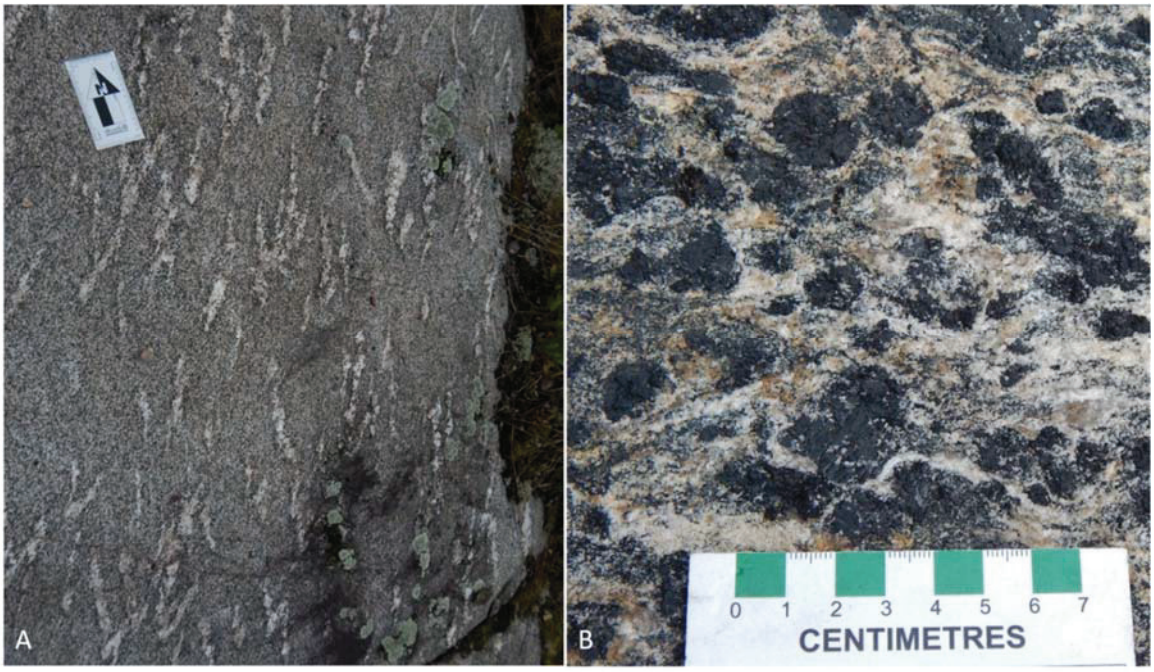

Figure 2.5: A) Unit Mn_1, medium grained diorite with two orientations of leucosomes. Arrow on the scale card points north. B) Unit Mn_1 with coarse amphibole crystals. The ocher mineral is scapolite and the white is plagioclase.

2.4.5 GMb

GMb is an intrusion breccia that crops out in only one location at the southern edge of the map area. It consists of coarse-grained gabbro fragments in a matrix of magnetic syenogranite to monzogranite. The fragments range from 1 cm to > 1 m across. The gabbro is apparently undeformed, but is recrystallized and composed predominantly of amphibole + plagioclase. Some coarse plagioclase phenocrysts are replaced by aggregates of fine-grained plagioclase. Thin (≤ 1 cm), fine-grained chilled margins in the granitic matrix surround the gabbro xenoliths. Most of the

matrix is a medium- to fine-grained leucosyenogranite to monzogranite, but there are some areas with coarse hornblende phenocrysts (Figure 2.6 A).

Figure 2.6: Unit GMb, intrusion breccia. A) Internal contact in the host rock. Coarse-grained syenogranite with biotite and amphibole phenocrysts and fine-grained leucosyenogranite. Short dashes on the hammer handle are 1 cm apart, and black circumferential line is 10 cm from the end of the handle. B) Intrusion breccia; leucosyenogranite (matrix) intrusion with abundant gabbro fragments.

2.4.6 MA

Unit MA is gneissic to massive leucogabbro, gabbroic anorthosite, anorthositic gabbro, and anorthosite containing plagioclase megacrysts. Variants include minor amounts of gneissic gabbro, diorite, tonalite and ultramafic rocks. Unit MA is composed of plagioclase + amphibole + biotite ± quartz ± clinozoisite ± titanite ± sericite. This unit has a similar mineralogy and textures to parts of the St. Charles anorthosite and the Mercer anorthosite, both located adjacent to the map area.

2.4.7 UM

Unit UM is an undeformed, very coarse-grained pyroxene hornblendite. It has a basaltic komatiite composition (Van De Kerckhove and Easton 2016), and is composed of clinopyroxene + hornblende + orthopyroxene, with dusty inclusions of a fine-grained opaque mineral within the hornblende and clinopyroxene. The only outcrop is a 40-metre-long island in Warren Bay; because the entire island is pyroxene hornblendite, the nature of the contact is unknown.

2.5 Felsic metaplutonic rocks

2.5.1 Gd

Monzogranite dikes and sills of unit Gd are pink, medium- to fine-grained, and generally massive, although they can be locally gneissic. Monzogranite dikes and sills are compositionally and texturally homogeneous with a very low mafic mineral content (< 5%); they are made up of K-feldspar + plagioclase + quartz ± biotite. Monzogranite dikes and sills (unit Gd) are characteristically bright orange-pink relative to the pale pink Gn_2. They form metre-scale sills and dikes, or veinlets. Where monzogranite dikes and sills (Gd) intrude the West Phase, Gn_1, the contact is typically concordant with foliation (Figure 2.7), although it locally cuts foliation at a very low angle. The small-scale dikes and veinlets of this unit commonly intrude tonalitic and granodioritic gneiss and migmatites (Tn).

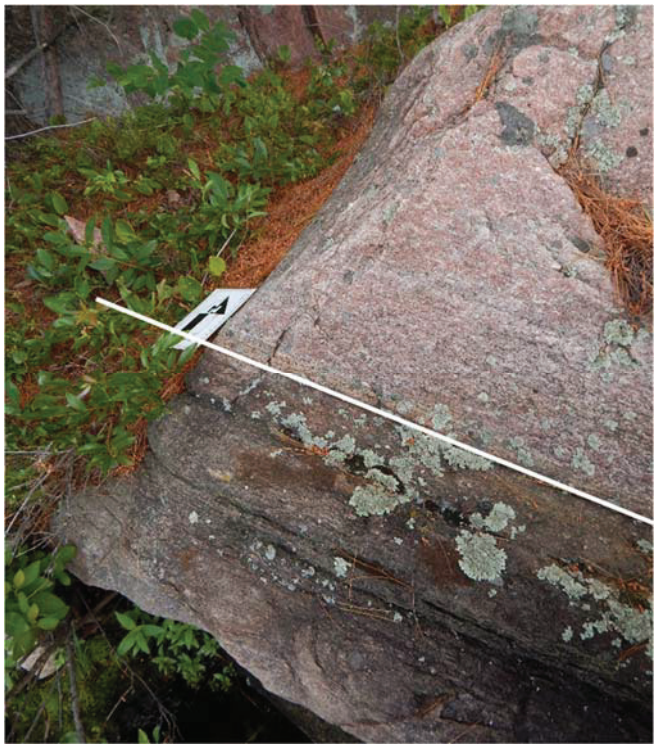

Figure 2.7: Foliated monzogranite sill, Gd (top), showing concordant contact with the West Phase, Gn_1 (bottom).

2.5.2 Gnm

The West Bay batholith (Lumbers 1974, 1975), Gnm, consists of intermediate to felsic orthogneiss and migmatite. It is composed of K-feldspar + plagioclase + quartz + biotite ± amphibole ± calcite ± chlorite. The West Bay batholith is a migmatitic to gneissic, medium- to coarse-grained quartz

monzonite, commonly garnet- and/or hornblende-bearing, with minor granodiorite and quartz syenite. Gnm typically displays about 20 % mafic minerals with a low quartz content, typically 5-10%. Rocks of this unit generally contain deformed aggregates of mafic minerals interpreted to represent a relict coarse-grained igneous texture, although locally they lack a remnant coarse igneous texture and have low mafic content. Rocks of this unit are most commonly stromatic migmatites, but are locally gneissic. Quartzofeldspathic leucosomes are on average 1-2 cm wide, typically with very thin melanosomes (Figure 2.8 A and B). Porphyroblasts within the West Bay batholith are typically 1 mm to 1 cm garnet, amphibole, and in some locations, magnetite crystals, although many outcrops have coarse to megacrystic porphyroblasts. In some locations, amphibole porphyroblasts are localized in the leucosomes (Figure 2.8 B). Many porphyroblasts are disaggregated and composed of a combination of garnet, amphibole and/or plagioclase (Figure 2.8 C and D). The relationships or replacement reactions between the minerals within the porphyroblasts aggregates is unclear. Foliation in this unit is defined by the orientation of leucosomes and gneissosity, which is folded on the map scale. There are very few outcrop-scale enclaves of other rock units within the West Bay batholith (unit Gnm).

Unit Gnm crops out in the eastern half of the map as a very large body along the western shore of Lake Nipissing, extending beyond the map area boundaries. Van de Kerckhove (2014), introduced the term the "West Phase" (unit Gn_1) for quartz monzonite rocks located in the western half of the map area, but which are typically less migmatitic than unit Gnm. Lumbers (1974) included these plutonic rocks as part of the West Bay batholith.

2.5.3 Gn_1

The West Phase, Gn_1, is medium- to coarse-grained quartz monzonite, gneissic to weakly migmatitic, with a low mafic mineral content (≤ 5%) (Figure 2.9). It is composed of K-feldspar + quartz + plagioclase + biotite + opaque minerals ± garnet. The West Phase typically has more quartz than the West Bay batholith (Gnm), and in some locations, preserves coarse K-feldspar phenocrysts. The most notable difference between the two units is that the West Phase is spatially associated with mafic rocks including diorite and gabbro gneiss (Mn_1), massive to gneissic gabbro (Mn_2), dioritic and gabbroic metatexite and diatexite dikes and sills (Mmd), amphibolite dikes (Md_3), and monzogranite dikes and sills (Gd). In the northwestern corner of the map area, some metagabbro bodies of diorite and gabbro gneiss (Mn_1) are enclosed and intruded by the West Phase (Gn_1). In one location on highway 535, (sub)metre-scale bodies of diorite and

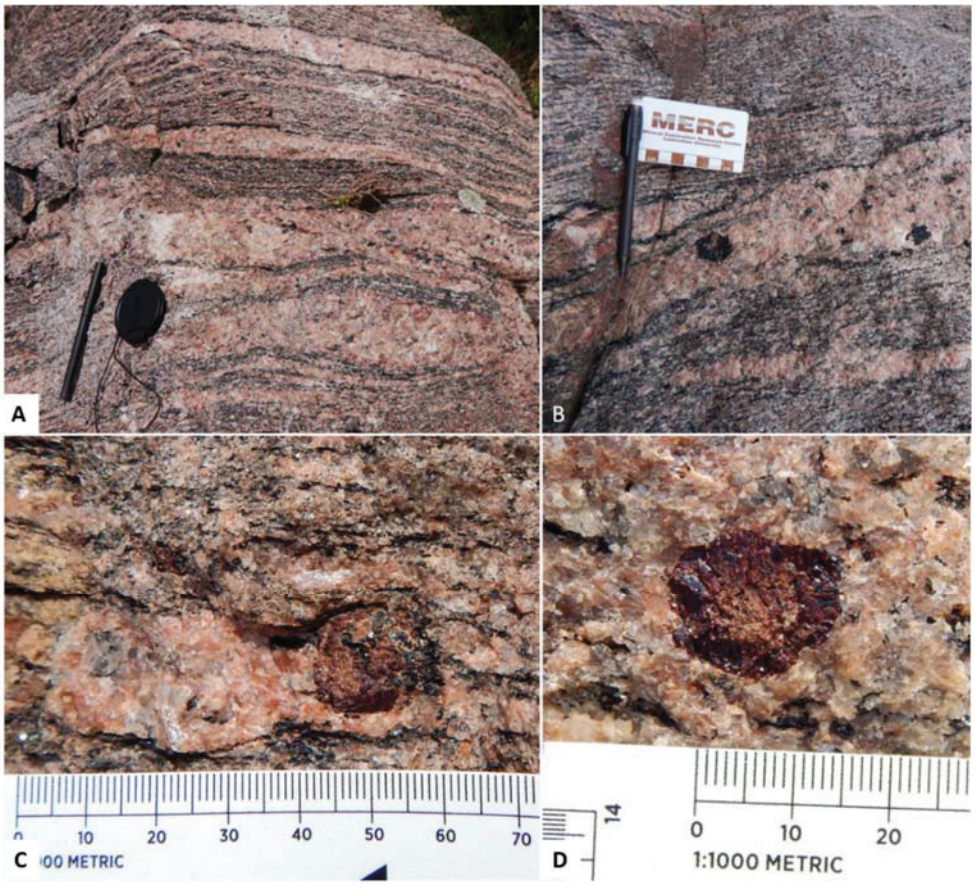

Figure 2.8: The West Bay batholith, unit Gnm. A) Typical stromatic leucosomes with thin melanosomes. B) Typical stromatic leucosomes with thin melanosomes, containing amphibole porphyroblasts. C) Garnet porphyroblast intergrown with plagioclase and amphibole. D) Garnet porphyroblast with plagioclase core.

Figure 2.9: Typical texture and composition of West Phase, Gn_1, (bottom) in contact with fine-grained, high strain rock of the same unit (top right of image).

gabbro gneiss (Mn_1) and the West Phase (Gn_1) intrude one another with layers of intermediate composition between the units. This compositional mixing is potentially a deformed magma mingling texture. In the central portion of the map area, along the shoreline of the West Arm, the West Phase is distinguished by numerous outcrop-scale lenses of highly strained, fine-grained mafic rocks and other enclaves, concordant to foliation, that range from a few cm to a few m long. Figure 2.10 displays the REE patterns of the West Bay batholith (Gnm) and the quartz monzonites only of the West Phase (Gn_1). The sample with a positive Eu anomaly within the West Phase may represent an accumulation of plagioclase within the pluton. As discussed in sections 3.3.2 and 3.5.2, the West Bay batholith and the West Phase are separated by the WAHSZ. Nowhere are the two phases seen in non-tectonic contact, consequently, it is not known for sure if the two phases are different parts of the same intrusion (i.e. both are West Bay batholith), or if they represent two distinct plutonic bodies. Data from two geochemical samples of the West Phase plot as volcanic-arc granites (VAG) using discrimination diagrams of Pearce et al. (1984) from Rollinson (1993). Using the same discrimination diagrams, geochemical data from samples of the West Bay batholith, Gnm, plot as within-plate granites (WPG).

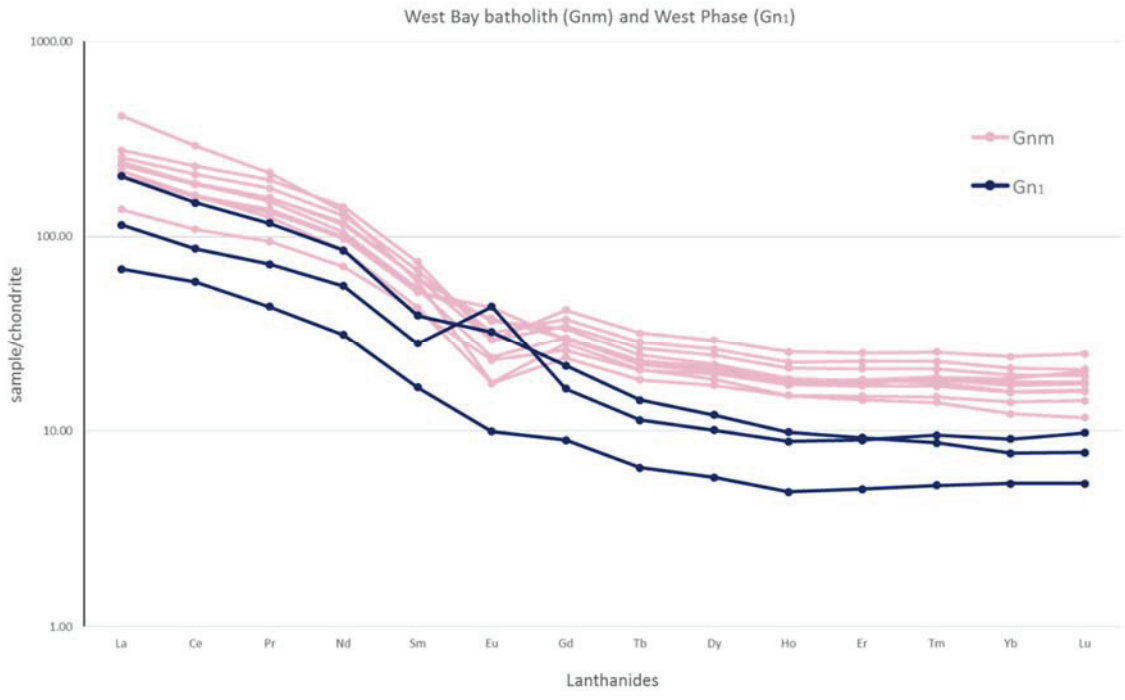

Figure 2.10: Chondrite normalized diagram of quartz monzonite samples from the West Bay batholith, Gnm, and the West Phase Gn_1. Normalizing values of Taylor and McLennan (1985, p.298) are used.

2.5.4 GMn

The proportion of other rock units, including mafic rocks, is so high in some areas that a grouping of rock units, GMn, was used to describe these rocks on the map. Unit GMn includes dioritic and gabbroic metatexite and diatexite dikes and sills (Mmd), amphibolite dikes (Md_3) and monzogranite dikes and sills (Gd) associated with the West Phase (Gn_1). A few outcrops have an abnormally high number of enclaves of varied lithologies and levels of deformation (Figure 2.11 A). In a number of locations in the northern half of the map, small calc-silicate enclaves are found within the West Phase (Gn_1) and the undivided group of units, GMn (Figure 2.11 B).

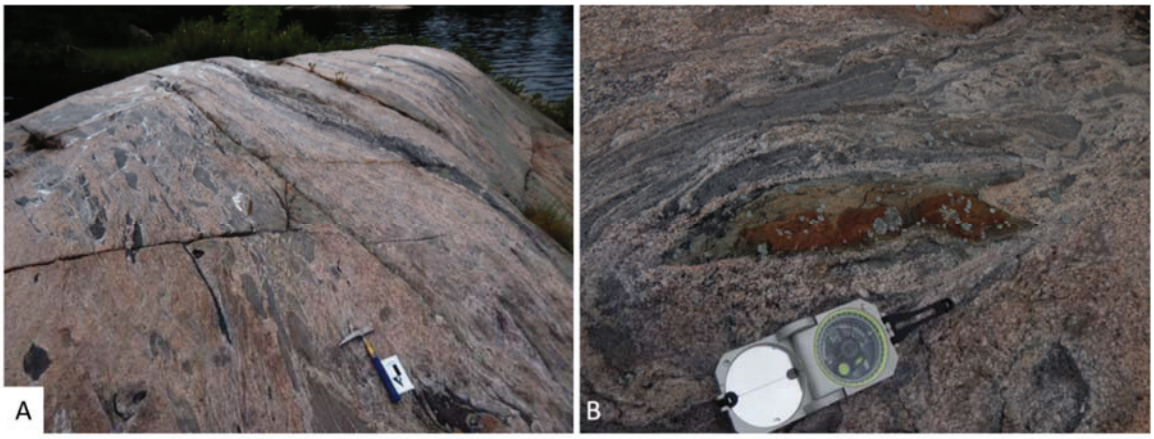

Figure 2.11: A) The West Phase, unit Gn_1, containing many enclaves with varying degrees of strain. B) Deformed enclaves within the West Phase, including red and green calc-silicate enclave.

2.5.5 Gn_2

Gn_2 is a magnetite-bearing leucocratic monzogranitic gneiss that is spatially associated with the West Bay batholith (Gnm). It is light pink, medium- to fine-grained, and generally massive. Magnetite-bearing leucocratic monzogranitic gneiss (Gn_2) is compositionally and texturally homogeneous with a very low mafic mineral content (< 5%). Rocks of this unit have a distinctive rare earth element signature from other granitoid units in the map area, and is similar to that for anorogenic (A-type) granites. The bulk composition and texture of unit Gn_2 are similar to the monzogranite dikes and sills (Gd) but magnetite-bearing leucocratic monzogranitic gneiss (Gn_2) is paler in colour, is magnetite-bearing and forms larger rock bodies than the monzogranite dikes and sills (Gd). No contacts between magnetite-bearing leucocratic monzogranitic gneiss, Gn_2, and adjacent units are exposed.

2.5.6 Gn_3

Gn_3 is monzonitic gneiss with minor syenite and quartz syenite. Rocks of this unit are red-pink or grey, gneissic to massive, with minor gneissic syenite and quartz syenite. This unit is medium-grained, with remnant coarse igneous texture. It is composed of K-feldspar + plagioclase + quartz ± amphibole ± biotite. In outcrop, rocks of this unit are similar to the 1420 Ma Cosby pluton (Lumbers 1975) which is located immediately southwest of the map area, in the Cosby subdomain. Its contacts are not exposed; however, monzonitic gneiss with minor syenite and quartz syenite (Gn_3) and the Cosby pluton are less deformed than the West Bay batholith (Gnm), which is otherwise similar in composition and texture. REE diagrams were made from samples of unit Gn_3 to characterize the unit better (Figure 2.12). Based on the REE plots alone, unit Gn_3, monzonitic gneiss with minor syenite and quartz syenite, does not appear to be related to the Cosby pluton (Figure 2.12). Positive Eu values may represent an accumulation of plagioclase within these rocks.

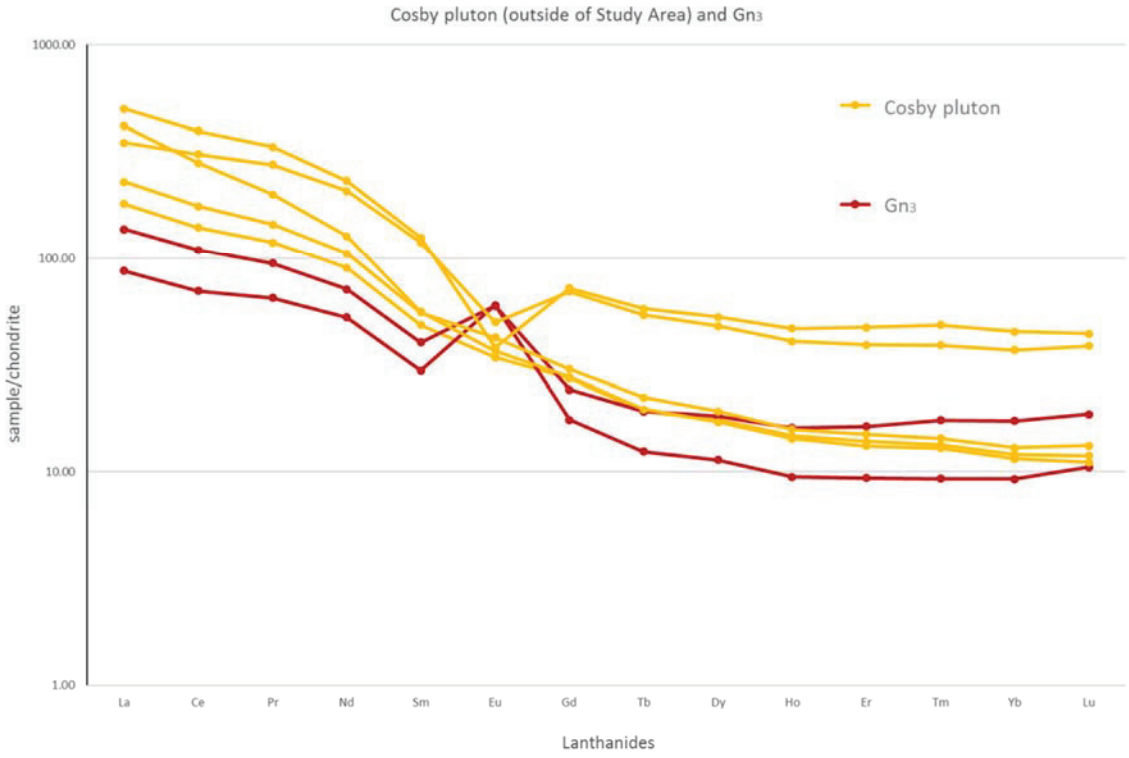

Figure 2.12: Chondrite normalized diagram of samples from unit Gn_3, monzonitic gneiss with minor syenite and quartz syenite, and from the Cosby pluton, south of the map area (normalized after Taylor and McLennan 1985, p.298). This diagram was constructed to help determine if unit Gn_3 is the same as the Cosby pluton in the Cosby subdomain. The Eu anomaly is positive in monzonitic gneiss with minor syenite and quartz syenite, Gn_3, but is negative or non-existent in the Cosby pluton.

2.6 Gneiss of uncertain protolith

2.6.1 lm_2

Unit lm_2 is a heterogeneous layered metatexite with highly varied compositional layering. Exposure is poor, and the large body of this unit in the northwest corner of the map area was projected based on satellite imagery and aeromagnetic data. Layers range from fine- to coarse-grained diorite, granodiorite, quartz monzonite, and monzogranite; biotite concentration in these layers also varies significantly. Centimetre-scale lenses and pods of amphibole are common. Compositional layering and texture varies on a decimetre-scale.

2.6.2 lm_3

Layered migmatite, lm_3, is a medium-grained, garnet + hornblende + biotite metatexite, with composition varying on a decimetre to metre scale. Layering is usually distinct (Figure 2.13). Migmatization varies from 5 to 15 volume % leucosomes. Centimetre-scale lenses and pods of amphibole are common.

Figure 2.13: Tonalitic and granodioritic gneiss and migmatite, Tn, (massive body) overlying heterogeneous, layered garnet, hornblende, biotite, plagioclase, quartz, K-feldspar metatexite, lm_3. The contact is highlighted with a dashed line. There is a boudinaged amphibolite layer within lm_3 just above the waterline.

2.6.3 Bn

Biotite gneiss, Bn, is a grey, medium-grained gneiss. It is composed of predominantly plagioclase + biotite but may contain small amounts of amphibole and/or garnet. It contains > 25 volume % biotite.

2.7 Probable supracrustal rocks

2.7.1 Pm:

Unit Pm is a stromatic migmatite, composed of garnet + plagioclase + biotite. It typically has 10 % plagioclase-rich leucosomes. Garnet porphyroblasts are typically about 1 mm across but can be larger, and are abundant throughout the whole rock, including the leucosomes (Figure 2.14 A). The overall texture does not vary significantly throughout the unit. Leucosomes range from a few mm to about 1 cm wide and from 5 cm to > 1 m long (Figure 2.14 B). The rare earth signature for a sample from this unit (station 14SV506), (Van De Kerckhove and Easton 2016) is similar to post-Archean Australian Shale composite from Taylor and McLennan (1985). Furthermore, Ni/Co and Cu/Zn ratios from this unit are comparable to other paragneiss samples from this area.

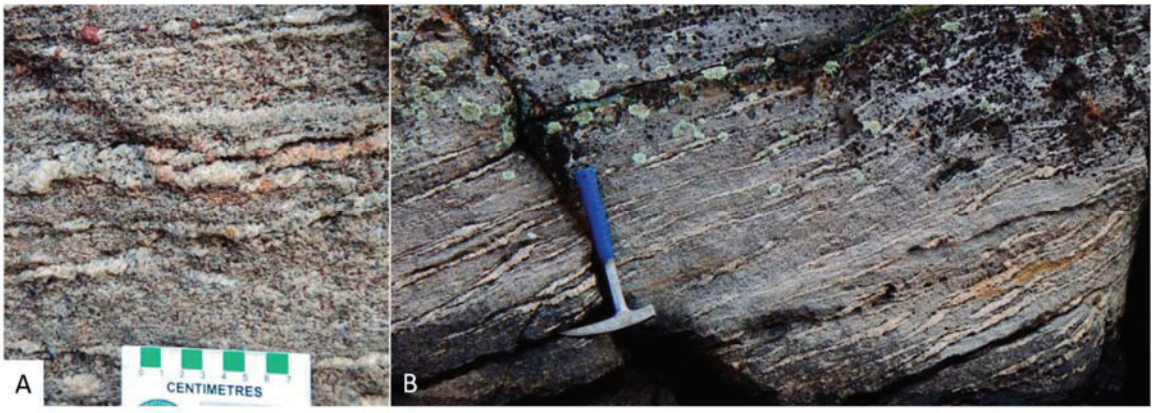

Figure 2.14: A) Garnet, biotite, plagioclase migmatite, unit Pm, showing garnets in the leucosomes and the paleosome. B) Overall texture typical of garnet, biotite, plagioclase migmatite.

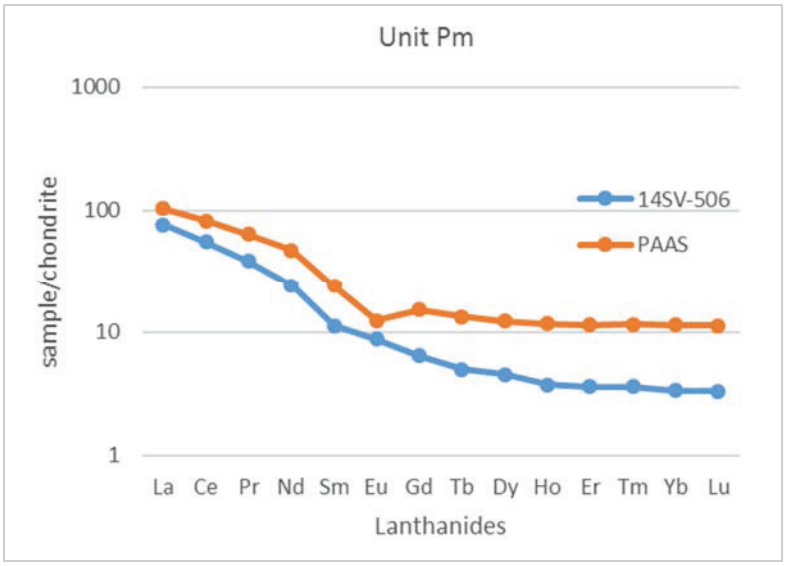

Figure 2.15: Chondrite normalized diagram comparing unit Pm, stromatic migmatite (14SV506) to post-Archean Australian Shale (PAAS). Normalizing values of Taylor and McLennan (1985) are used.

2.7.2 Fm

Feldspathic migmatite, Fm, is the same composition as feldspathic gneiss, Fn, but it is migmatitic, with up to 10% quartzofeldspathic leucosomes. The two units have never been mapped in contact with one another.

2.7.3 Fn

Feldspathic gneiss, Fn, is a pink, plagioclase + K-feldspar + quartz gneiss, with minor grey quartz + plagioclase gneiss, possibly derived from a feldspathic arenite protolith. It is fine- to medium-grained and there are no remnants of primary textures.

2.7.4 lm_1

Layered migmatite (1), lm_1, is a medium-grained tonalitic gneiss to metatexite. It contains K-feldspar + quartz + biotite + plagioclase, and commonly contains hornblende, magnetite and/or garnet. It has approximately 10-25 % mafic mineral content. Composition varies gradationally on a metre scale. The migmatite contains up to 5 volume % plagioclase-rich leucosome. Some areas contain centimetre- to decimetre scale, fine-grained, mafic lenses and layers similar to the amphibolite dikes (Md_3) found within unit VFn (leucocratic gneiss).

2.7.5 lnFm

Unit lnFm is also a grouping of rock units. It consists predominantly of units ln and feldspathic migmatite (Fm), with monzogranite dikes and sills (Gd), pelite/semipelite (Sn_2) and leucocratic gneiss with probable volcanic protolith (VFn), and/or dioritic stromatic metatexite (Mm_2), and quartz dioritic gneiss (QD) (Figure 2.16).

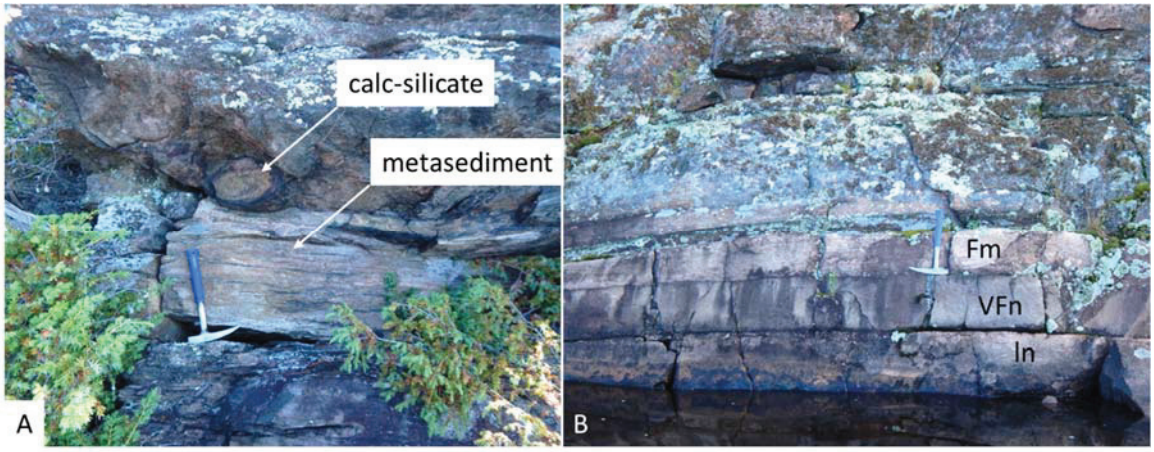

Figure 2.16: A) Metasedimentary, psammitic to semipelitic rock layer and calc-silicate pod within unit lnFm. B) Layering of rocks within lnFm. From bottom up: ln, leucocratic gneiss with probable volcanic protolith (VFn) and feldspathic migmatite (Fm).

2.7.6 ln

Consisting of layered gneiss and minor migmatite, unit ln is characteristically a light pink to purple-grey, fine- to medium-grained, quartz + biotite + plagioclase + K-feldspar gneiss with mm- to dm-scale layering; mm-scale layers can be found within apparent larger scale layers (Figure 2.17 A and C). Layering is consistently planar. The rock is locally magnetite-, hornblende- and garnet-bearing. Some locations have extremely garnet-rich layers with ≥ 30 % garnet (Figure 2.17 B).

Figure 2.17: A) Typical layered gneiss and minor migmatite, ln, with extremely garnet-rich layer at the rock hammer handle. B) Garnet rich layer within unit ln. C) Characteristic layered gneiss and minor migmatite, ln, texture and layering.

2.7.7 VGMn

Undivided felsic gneiss, VGMn, is a grouping of rock units. It consists of m-scale intercalated layers of gneiss of leucocratic gneiss with probable volcanic protolith (VFn), the West Phase (Gn_1), magnetite-bearing leucocratic monzogranitic gneiss (Gn_2), monzogranite dikes and sills (Gd), diorite and gabbro gneiss (Mn_1), dioritic and gabbroic metatexite and diatexite dikes and sills (Mmd) and amphibolite dikes (Md_3). Leucocratic gneiss with probable volcanic protolith (VFn) and the West Phase (Gn_1) are the most prominent units. Along the shoreline of the West Arm, southwest from Mashkinonje Island, units Mn_1, leucocratic gneiss with probable volcanic protolith (VFn) and the West Phase (Gn_1) are subhorizontally interlayered.

2.7.8 VFn

Leucocratic gneiss, VFn, is light grey to light pink, homogeneous, medium- to fine-grained, biotite + quartz + K-feldspar + plagioclase gneiss, locally migmatitic, and has low mafic mineral content (< 5 %). Leucosomes are composed of quartz and plagioclase, never exceed 5 % of the rock volume, and are thin - ≤ 1 cm wide. This unit has a granular texture and does not display any remnant igneous textures. It is probable that the protolith was supracrustal, possibly intermediate to felsic volcanic or volcaniclastic rocks. Unit VFn also contains cm- to dm-scale, fine-grained, mafic dikes and concordant lenses and layers, interpreted as unit Md_3, amphibolite dikes. It is unknown if the mafic rocks found in the leucocratic gneiss (VFn) are the same generation as the amphibolite dikes, Md_3, found within the West Phase, Gn_1.

2.8 Supracrustal: Metasedimentary rocks

2.8.1 Sn_1

Quartzite (Sn_1) is a quartzose gneiss derived from quartz arenite. It is composed of 90 to 95% quartz and the remainder is made up of muscovite ± sillimanite ± K-feldspar ± kyanite ± sillimanite ± opaque minerals. This unit crops out in small, metre-scale pods within a larger package of supracrustal rocks along the West Arm from Mashkinonje Island to Monetville (Figure 2.1). The rock is white to light pink, fine- to medium-grained with equant to elongate interlocking grains. Interstitial sillimanite and/or mica is common, forming veinlets or streaks that define the foliation. In some samples, elongate quartz crystals appear to be oblique to the sillimanite orientation. This is the most easily identified of all the metasedimentary rock units. The discovery of this rock type inspired the focus and rationale for this thesis.

2.8.2 Sn_2

Sn_2 is pelitic to semipelitic paragneiss. This is a grey-brown to dark grey, sillimanite + kyanite ± sulphides + garnet + muscovite + K-feldspar + plagioclase + quartz + biotite gneiss, derived from aluminous sedimentary rocks. This unit is fine- to medium-grained with a sugary or granular texture. Garnet porphyroblasts are pink-mauve and typically small, 1 mm or less, but ranging up to 1 cm. In some locations mats of sillimanite within biotite layers range from 0.1-1 cm long (Figure 2.18). Kyanite is too fine to be seen in hand sample. Banding varies on the mm-scale from Al_2SiO_5-rich layers to quartz- and feldspar-rich layers, however the entire rock is very biotite-rich (65 %). There are a few thin (m-scale) pink, quartz-rich leucosomes which lack biotite. One-metre-wide layers of calc-silicate gneiss are found locally adjacent to unit 11. These calc-silicate layers are extremely garnet-rich (approximately 50 %).

2.8.3 Sn_3

Sn_3 is psammitic paragneiss. The rocks consist of light grey to pink, fine-grained, biotite + muscovite + plagioclase + K-feldspar + quartz gneiss. Fresh surfaces normally have a granular or sugary texture, although more quartz-rich outcrops have an interlocking crystalline texture. Psammitic gneiss, Sn_3, has an overall very low mafic content (≤ 5 %) although there are thin, mm-scale, discontinuous, biotite-rich layers. Layering in the psammite tends to be on the decimetre scale (Figure 2.19), although in some outcrops layering is absent. In two locations, stations

14SV434 and 14SV095 (Appendix A.2), psammitic paragneisses are in contact with dioritic metatexite and diatexite (Mm_1) bodies.

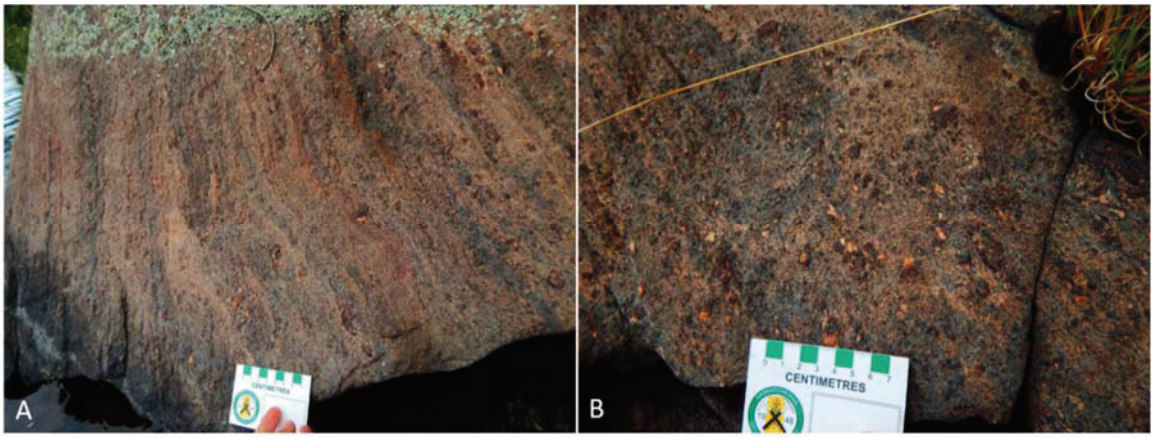

Figure 2.18: A) Compositional layering within pelitic gneiss, Sn2. B) Large garnet porphyroblasts and sillimanite mats within the pelite (Sn2).

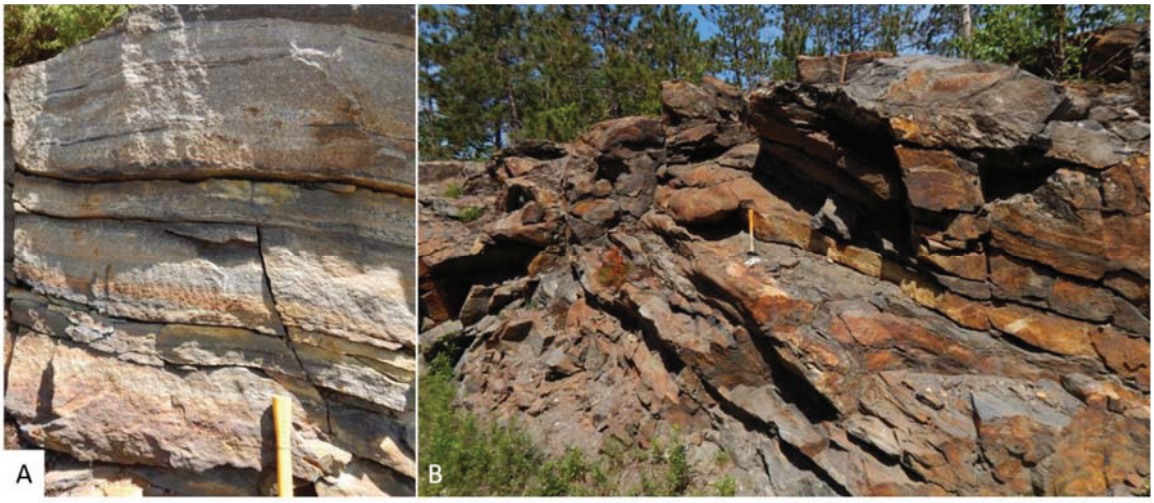

Figure 2.19: A) Layering in psammitic gneiss (Sn_3) with thin, discontinuous biotite-rich layers. B) Isoclinally folded layers of psammite. Hammer is located on the trace of the fold hinge.

2.9 Tonalitic grey gneisses

2.9.1 Tn

Tonalitic and granodioritic gneiss and migmatites (Tn) are believed to be components of a tonalite-trondhjemite-granodiorite grey gneiss complex. Referred to informally as Archean grey gneiss, it is a dark-grey to light-grey, medium-grained biotite-hornblende tonalite to granodiorite with mafic layers. This unit is composed of plagioclase + quartz + biotite ± K-feldspar. This unit commonly contains cross-cutting mafic dikes which may be genetically similar to the garnet-

bearing, amphibolite dikes (Md_2) or amphibolite dikes (Md_3) (Figure 2.20). There are also many dikes and sills of pink leucogranite, potentially related to the West Phase (Gn_1) and/or monzogranite dikes and sills (Gd) (Figure 2.20). The unit is locally veined, brecciated and can have centimetre- to decimetre-scale amphibolite lenses, and pegmatitic veins and layers. This rock resembles the grey gneiss complex in the Northern subdomain, and is interpreted to be the same (described in Chapter 1). In the Northern subdomain, geochronology by Chen et al. (1995) yielded ca. 2.7 Ga Archean ages for this tonalite-trondhjemite grey gneiss complex. The presence of this unit provides significant information about the architecture of the map area; because these rocks are the same type and age as the cratonic foreland (Card 1990), they are basement rocks that are now at the same structural level as younger rocks.

Figure 2.20: Cross-cutting relationships between tonalitic-granodioritic gneiss, granitic gneiss, and fine-grained, relatively undeformed mafic dikes at three different locations within the Archean grey gneiss complex. A) Mafic dike cuts both the tonalitic gneiss and the granitic gneiss. B) Granitic and mafic dike within a larger tonalitic body. Both dikes are oriented slightly oblique to gneissosity. C) Internal breccia within unit 1. Light grey tonalitic veins separate darker grey tonalite fragments.

2.10 Summary

Following the approach of Culshaw et al. (1988), the various map units that have been described in this chapter were grouped into gneiss associations in order to better display the key tectonic packages present in the map area, as shown in Figure 2:20. The predominant map units, or groups of units are the Archean grey gneisses, the supracrustal units - particularly the metasedimentary rocks, and the plutonic bodies. Figure 2.21 depicts the main gneiss associations in the map; the maps in Appendix A show the detailed rock units. The western portion of the map area is dominated by Archean grey gneisses, with the two main plutonic associations separated by a thin package of supracrustal rocks that trends north-south.

If the inferred Archean grey gneisses (unit Tn) correlate with the Archean basement rocks exposed north of the Grenville Front, the question arises about what potential processes could have brought basement rocks to the same elevation as supracrustal packages. The structures of the map area, discussed in Chapter 3, may provide insight into this question.

Supracrustal rocks, particularly metasedimentary rocks, add crucial information about the tectonic history of the Nepewassi domain prior to the Grenvillian orogeny. The Nepewassi domain metasedimentary rocks are potentially correlative with the ca. 2.5 and 2.2 Ga Huronian Supergroup, which was deposited on the passive margin of the Superior craton in the Paleoproterozoic. This possible correlation is based on both proximity to the exposed Southern Province, and the fact that the continental shelf related to the Huronian passive margin likely extended to the south-southeast of Sudbury. Metamorphic and geochronological studies, Chapter 4 and 5 respectively, have been done to test if the Nepewassi sediments can be correlated with the Huronian Supergroup.

The West Bay batholith is predominantly one granitoid unit, that is migmatitic, whereas the West Phase association is made up of multiple units. The West Phase (Gn_1) is the main unit in the West Phase association, but it also includes other felsic intrusive rocks, mafic intrusions, and supracrustal rocks such as leucocratic gneiss of probable volcanic protolith (VFn). The West Phase was previously mapped as part of the West Bay batholith (Gnm), but was mapped as a separate unit here based on slight compositional and textural differences, and because the West Phase (Gn_1) is spatially associated with multiple mafic intrusive rocks, namely diorite and gabbro gneiss (Mn_1). The West Bay batholith and the West Phase may be different pulses or phases of the same pluton, or they may be different plutons entirely. The geochemistry of these units (Van De Kerckhove and Easton 2016) is slightly different. Furthermore, in the West Phase association,

compositional mixing or mingling between the diorite and gabbro gneiss, Mn_1, and the West Phase (Gn_1) implies bimodal magmatism. Bimodal magmatism is typical of crustal thinning, which may indicate extensional processes. A detailed geochronological study of the West Phase association and the West Bay batholith is needed to better understand the compositional differences in these units and their tectonic significance.

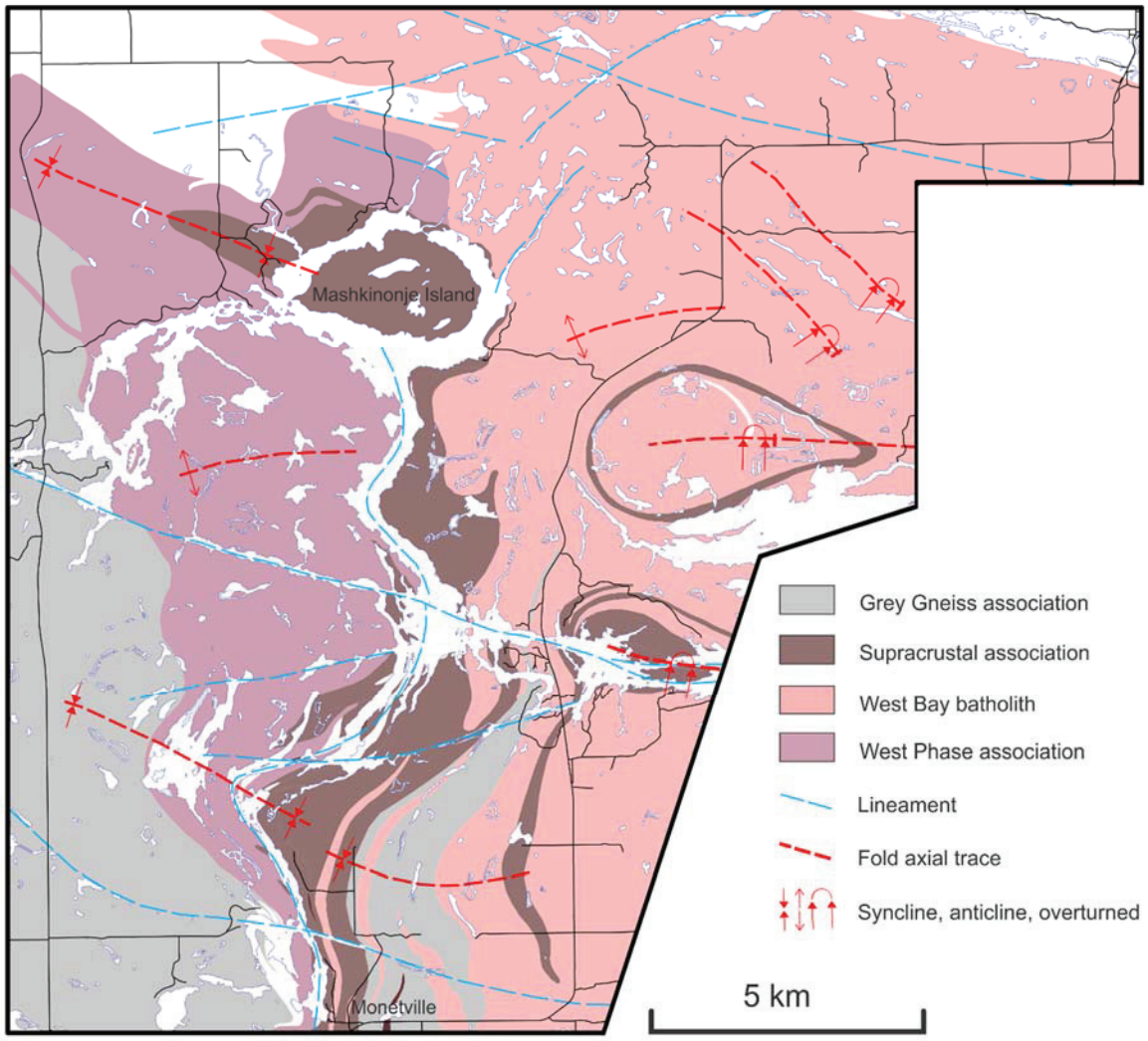

Figure 2.21: Simplified map depicting gneiss associations and the predominant metaplutonic unit, the West Bay batholith.

CHAPTER 3

STRUCTURAL GEOLOGY

3.1 Introduction

This structural study of the Nepewassi domain, in conjunction with lithological studies from Chapter 2, provides context for metamorphic and geochronologic studies. Understanding the structure of the geology in the map area (outlined in Figure 3.1) inherently provides a greater understanding of the tectonic history in the Nepewassi domain. The large-scale goal in the Nepewassi domain is to study structural (and metamorphic, Chapter 4,) inheritance by relating the structures in the map area to known tectonic events prior to, and including the Grenvillian orogeny. It is very important to understand the local structures thoroughly before they can be accurately compared with regional structures.

As discussed in Chapter 1, west-northwest – east-southeast trending structures in the Nepewassi domain are slightly oblique to those in surrounding domains. The shear zones that bound the Southern subdomain, the SCLSZ and the Wolseley River lineament, are oriented west-northwest, similar to faults in the Southern Superior Provinces, west of the GF. Map-scale folds in the Northern subdomain are upright, open, and plunge shallowly east-southeast and there are no map-scale polyphase folds recognized. The Northern subdomain and Southern subdomain are separated by the St. Charles Lavigne Shear Zone, which trends east-southeast and is characterized by near-vertical, high-strain gneisses. The Southern subdomain is the only subdomain in the Nepewassi where map-scale polyphase fold interference structures are documented. Thus, a portion of the Southern subdomain, including the fold interference structures, was chosen as a target for detailed mapping. Structural features in the map area were systematically mapped during the 2014 field season. Structural data from 2014 and previous years (Tyler 2013) are compiled on stereonets (section 3.3.1), in order to gain insight into the structural geometry within the map area. Satellite imagery and trend lines from previous maps were used to interpret map-scale structures.

Two versions of the bedrock map, including the rock unit legend, are in Appendix A. Station locations and landmarks referenced in this thesis are shown in map Appendix A. Structural measurements are depicted in Appendix A.1 and station locations and landmarks referenced in

this thesis are shown in Appendix A.2. Geographical coordinates of map stations are listed in Appendix A.3.

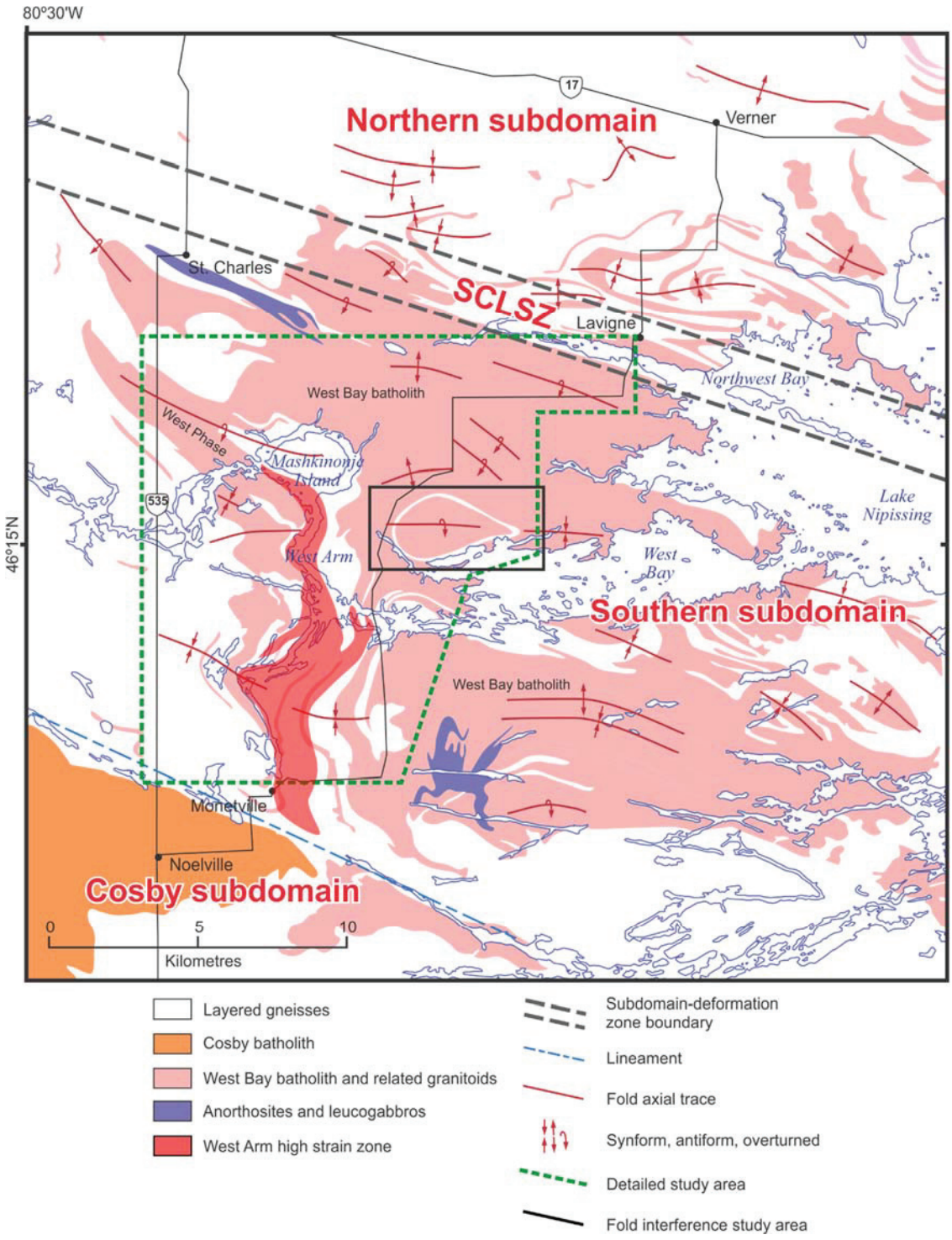

Figure 3.1: Simplified map of the Nepewassi domain with major folds marked. The fold interference study area and the map area (detailed study area) are outlined.

In this chapter, the fabrics (section 3.2) and structures (section 3.3 and 3.4) in the Nepewassi domain are described and discussed. The structural geometry of the map area provides context for the metamorphic (Chapter 4) and geochronological (Chapter 5) work.

3.2 Fabric descriptions

3.2.1 L-S tectonites

In chapter 2, it is mentioned that nearly all the rock units in the Nepewassi domain are gneisses. Gneisses are medium- to coarse-grained L-S tectonites formed by high-grade metamorphism and bulk strain (Myers 1978). L-S tectonites are rocks that have penetrative linear (L) and/or planar (S) fabric. Fabrics are defined by the separation of mafic and quartzofeldspathic minerals, or the shape of minerals and mineral aggregates. Where there is very high strain, the resulting gneiss is uniformly layered (Myers 1978). In addition, it is common for the rocks in this domain to be migmatitic, or have evidence for the former presence of partial melt.

Where the S-fabric is strongly developed, with straight, parallel layers, rocks are termed straight gneisses. Straight gneisses have relatively uniform layer thickness (Figure 3.2 B) and typically have S>>L fabrics (Davidson 1984). They contain intrafolial isoclinal folds (Figure 3.2 D), elongate enclaves, (Figure 3.2 E), internal boudins and boudinaged pegmatites that are parallel to layering (Figure 3.2 F). Relative to typical gneisses in the Nepewassi domain, straight gneisses have finer and more uniform grain size, more pervasive layering and fewer cross-cutting features. These features are caused by high strain so straight gneisses are interpreted to have formed within shear zones.

Most gneisses in the map area are S > L or S ≥ L tectonites, meaning the planar fabric is stronger than the linear fabric. Where visible, linear fabrics are defined by elongate minerals, aggregates of minerals, enclaves and leucosomes that lie along a foliation plane. In many places, linear fabrics are located within, and likely represent, hinge zones of a map-scale fold (Appendix A.1).

Mylonitic foliation is distinguishable from straight gneisses and other planar fabrics in the Nepewassi domain because of its fine grain size. Rocks with mylonitic fabric, or mylonites, typically have L=S fabric, defined by fine-scale banding. They commonly contain micron quartz ribbons, and coarse quartz or rotated porphyroclasts. Mylonitic fabric is formed by grain-size reduction through ductile crystal-plastic deformation and indicates ductile shearing at middle crustal levels.

Figure 3.2: Straight gneisses. A) Typical straight layered gneiss with elongate enclaves on the east shoreline station 14SV319. B) 14SV302 and C) Shoreline of just east of the Hwy before the mouth of the West Arm to West Bay. typical outcrops of straight layered gneiss. D) West of Station 14SV493 Intrafolial isoclinal fold. E) 14SV2492 Elongate enclaves. F) Internally boudinaged layers and boudinaged pegmatite layer on the shoreline near the Little Cut and station14SV504 (Appendix A.2)

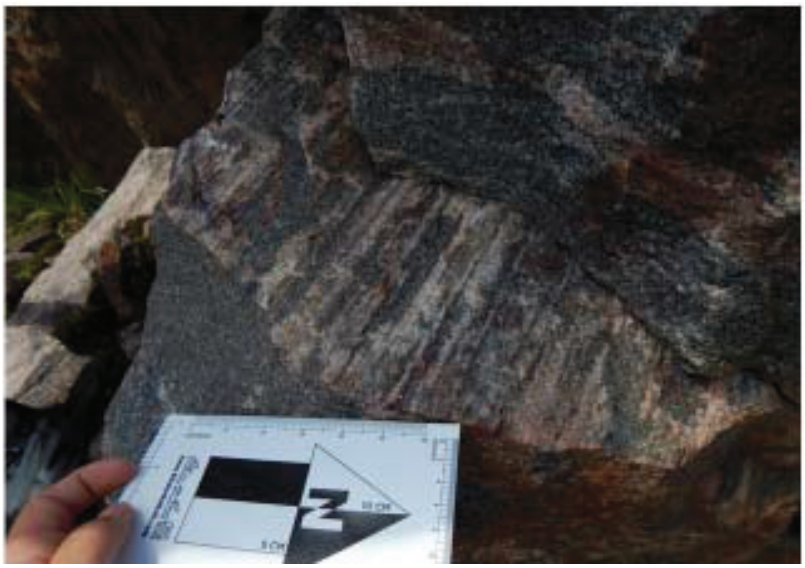

Figure 3.3: L=S fabric in a deformed quartzofeldspathic layer within granodioritic gneiss (unit Tn) on a roadside outcrop off highway 535, north of Noelville (station 14SV336, Appendix A.2). The lineation is defined by elongate aggregates of quartzofeldspathic minerals.

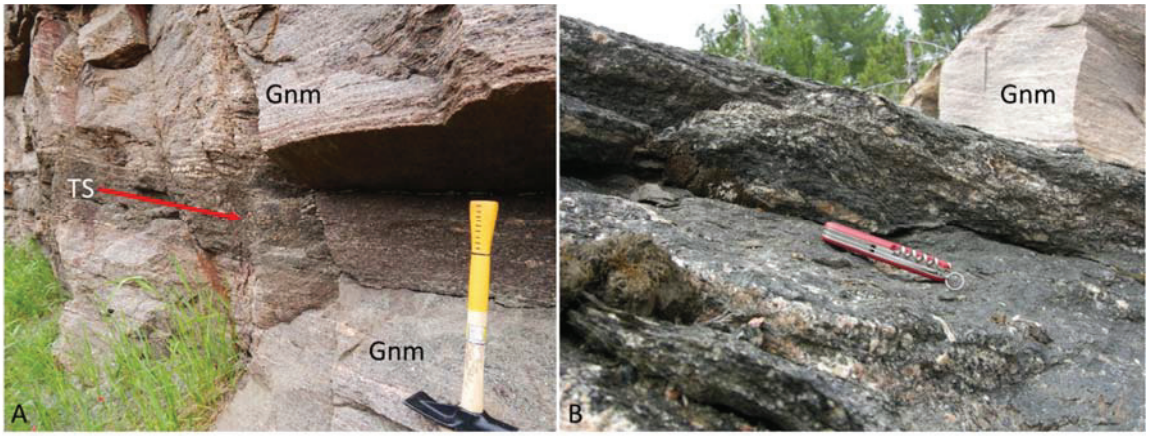

Figure 3.4: A) A layer of tectonic schist (TS), along highway 64 (station 14SV074), within the West Bay batholith (Gnm). Small notches on hammer handle are 1 centimetre apart. B) Tectonic schist (foreground) along highway 64 with coarse feldspar crystals (station 14SV061), within the West Bay batholith (Gnm)(background).

There are a few outcrops of thin pervasive schist layers amongst the gneisses in the Nepewassi domain. They are composed of well foliated medium to coarse biotite crystals, with garnet and aggregates of fine to coarse K-feldspar which may be disaggregated veins or pegmatites; some coarse amphibole crystals are present. Schists are only documented as 10 to 50 cm wide concordant layers within the West Bay batholith (Gnm) (Figure 3.4). The schists in the

map area are termed tectonic schists because they are interpreted as ductile formed isochronously with metamorphism (Hutton 1979).

3.2.2 Orthogneisses

Gneisses with plutonic protoliths tend to be more texturally and compositionally uniform at the outcrop scale relative to layered (typically supracrustal) gneisses; however, orthogneisses with very high strain can also be uniformly layered, making the distinction between compositionally similar orthogneisses and quartzofeldspathic supracrustal gneisses difficult. Coarse plutonic textures are typically preserved as flattened lenses of dark and/or light minerals. This fabric is less obvious in gneisses whose initial igneous texture was relatively finer-grained, but a plutonic protolith is generally assumed where cross-cutting relationships are observed.

3.2.3 Layered gneisses

Gneisses of supracrustal or unknown origin typically have pervasive compositional layering at various scales, defining an S-fabric. Fabrics in mica-rich gneisses, such as paragneisses, are easily recognized because mica-rich layers and the mica crystals themselves define the fabric. These samples tend to have a relatively smaller grain size because biotite and muscovite crystals pin quartz and feldspar grain boundaries during recovery and recrystallization.

When gneisses are very quartzofeldspathic and mica-poor, L-S fabrics are less obvious; compositional layering is very subtle and there are few mica-bearing layers or lenses. Furthermore, except for quartzite (unit Sn_1), recrystallized grains are typically equant rather than elongate. The quartzite unit is too quartz-rich to display typical gneissic fabric. The unit is massive, but foliation can be recognized by elongate grains of quartz and the orientation of interstitial minerals at some outcrops. Linear fabrics are not recognizable in any of the quartzite samples. Because of the competent nature of the quartzite unit, it forms map-scale boudins within a package of layered gneisses.

3.2.4 Migmatites

Many rock units in the map area are migmatitic. Migmatites form when partial melt is trapped and crystallizes within a metamorphic rock, forming leucosomes, which are bands or lenses of light-coloured granitic material. Where a gneiss contains less than 5 % leucosomes, it is still named a gneiss or migmatitic gneiss. Where there are significant leucosomes (≥ 5%) the term migmatite is used. Migmatites are separated into two different types, metatexites and diatexites,

following the Ontario Geological Survey's definition based on Sawyer (2008). Metatexites have <20 % leucosome, and diatexites have 20 % or more leucosome. Nearly all the migmatites in the Nepewassi domain are stromatic (layered), according to nomenclature by Sawyer (2008). Stromatic migmatites in the Nepewassi domain have multiple laterally pervasive leucosomes, parallel to gneissosity. According to Sawyer (2008), stromatic migmatites typically form when partial melting is accompanied by deformation. Alternatively, stromatic migmatites may form from preferential melting of a rock with pre-existing compositional layers.

3.3 Map-scale Structures

3.3.1 Folds

Folds in the Nepewassi domain (and Central Gneiss Belt) are defined by the orientation of planar fabrics and sheets of rock units. Since primary layering in the Nepewassi domain have been obliterated, a foliation-forming deformation (D_1) must have occurred prior to fold-forming deformation event(s).

A fold interference pattern was documented by Culshaw and Tyler (2013) near the shoreline, northwest of the West Bay of Lake Nipissing (fold interference study area, Figure 3.1). Another fold interference pattern with similar geometry crops out immediately south of the fold interference study area, but is cut off by the shoreline (Figure 3.1); based on satellite imagery, there are possibly two more to the north of the fold interference study area. These fold interference patterns imply that two separate phases of folding affected the map area. The interference pattern is a teardrop-shaped, type 1 transitional to type 2 fold interference pattern (Figure 3.5 D and E; Ramsay 1967). For this map pattern to be recognized, lithologic layering must have been present prior to folding.

Outside of the fold interference study area, there are metre-scale, open dome-and-basin structures within the overall east-dipping fabric in many locations across the map area. Based on the map pattern and stereonet projections of foliations and lineations (Fig. 3.5), fold hinges in the map area typically plunge shallowly east-southeast, parallel to the average stretching lineation (Stereonet B, Figure 3.6). Most lineations are defined by stretched mineral aggregates; however, fold hinges and elongate mineral lineations are also included in the stereonet. Mylonitic lineations (L_3) are interpreted to have formed much later than the folds, and are excluded from the stereonet. The poles to generally south-dipping foliation (northern hemisphere of stereonet A, Figure 3.6) are scattered compared to the relatively concentrated poles of north- to east-

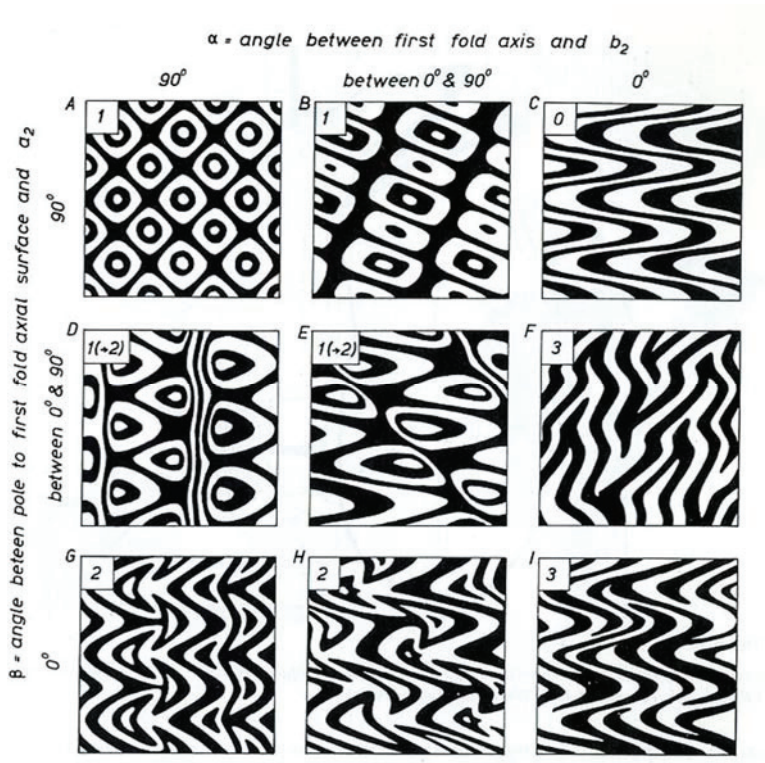

Figure 3.5: Fold interference patterns (Ramsay 1967) produced by two successive phases of folding. a_2 = axial plane of the second fold. b_2 = fold axis of the second fold.

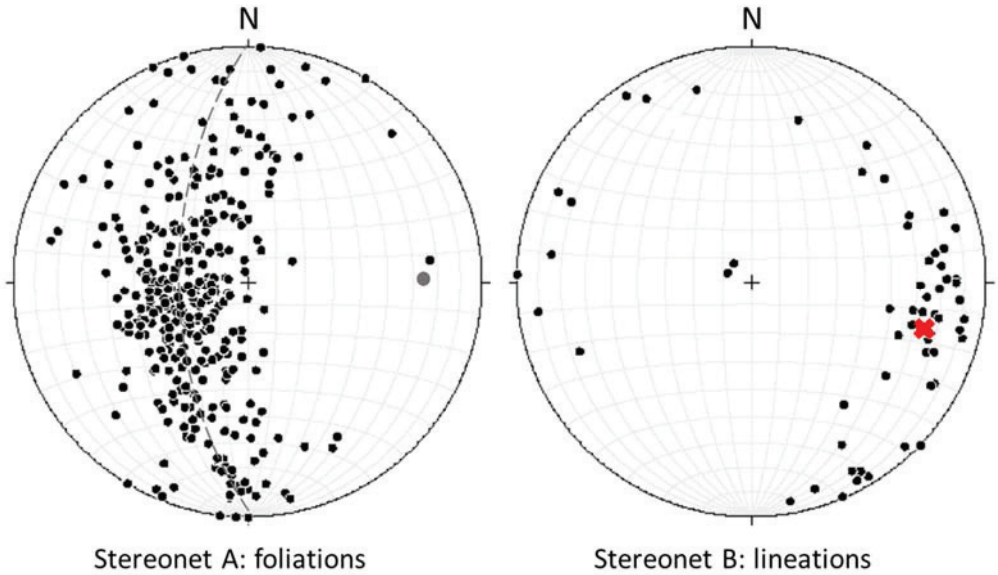

Figure 3.6: A) Poles to foliation measurements in the map area, excluding the interference study area. B) Lineation measurments from the map area, excluding mylonitic lineations (L_3). Average lineation, 105-25, is marked in red. Structural measurements are in Appendix A.1 and Van De Kerckhove and Easton (2016).

dipping foliations (center and southern hemisphere of stereonet A, Figure 3.6). This suggests that north dipping limbs are consistently oriented (relative to one another) compared to the south-dipping limbs. Lineations, which are generally parallel to fold axes, have an average orientation of 105-25. In strongly lineated outcrops, there are ptygmatically and irregularly folded leucosomes with hinges parallel to lineation.

Stereonets of the foliation measurements collected by Tyler (2013) from the fold interference study area (Figure 3.7) differ from those from the rest of the map area (Figure 3.6). The stereonet from the fold interference study area depicts two trends of great circles, or girdles. The second girdle indicates a west-northwest plunging fold, which is not observed in the rest of the map area.

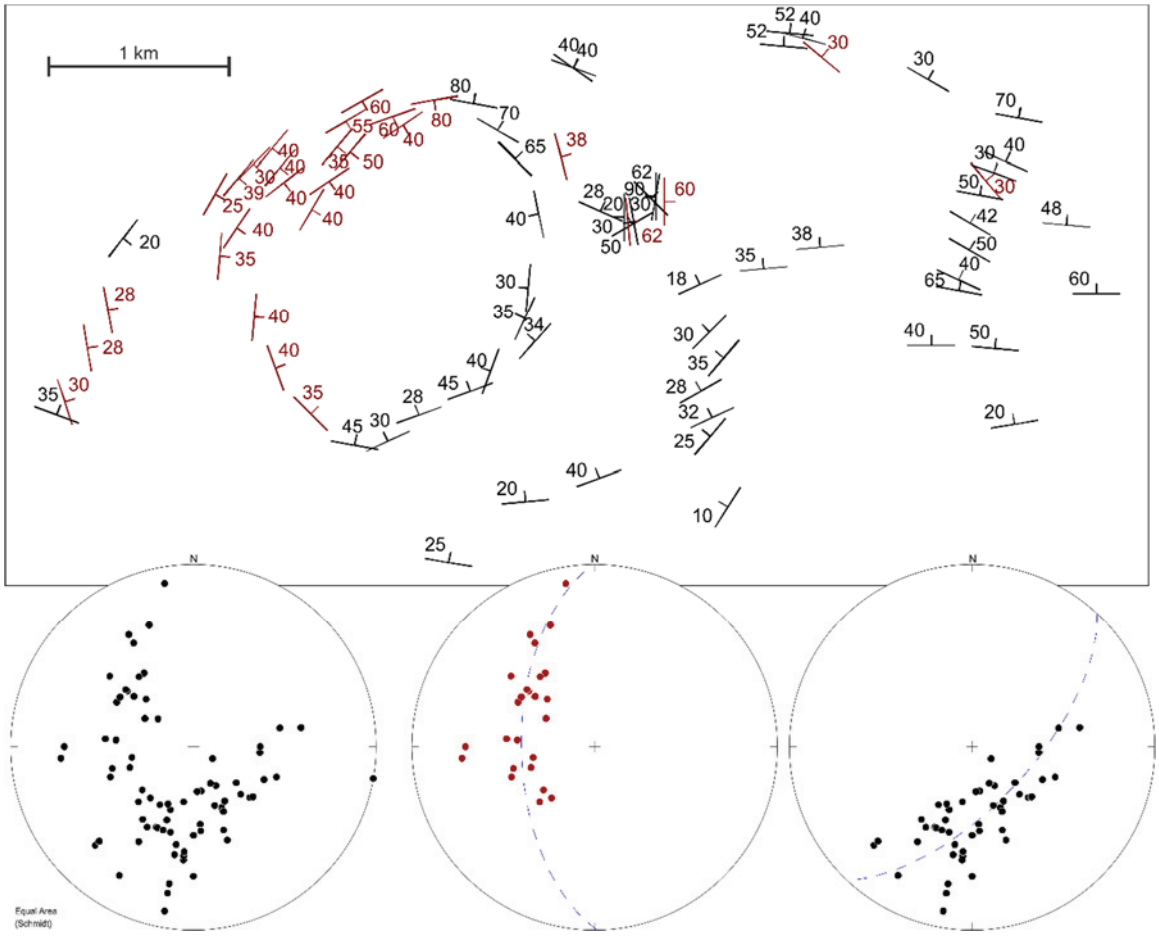

Figure 3.7: A) Foliations measured within the interference pattern from Tyler (2013). The bounding rectangle matches that of Figure 3.1. B) A stereonet containing all foliation data from A. C) A stereonet containing all the generally east and south dipping foliations from A, marked in red, that define a great circle similar to the rest of the map area. D) North to northwest dipping foliations plotted on a stereonet. This stereonet defines a second great circle that is not present in data from the rest of the map area

3.3.2 West Arm high-strain zone

A shallowly east-dipping zone of straight gneisses is located west of the fold interference pattern. This zone, highlighted in red in Figure 3.9 and Figure 3.10, is observed mostly along the shorelines of the West Arm, south of Mashkinonje Island down to Monetville (Figure 3.1) and is termed the West Arm high-strain zone (WAHSZ). The nature, or existence, of the WAHSZ to the south and north of where it is mapped in the Southern subdomain is unknown. It is also not known if the WAHSZ is truncated against the SCLSZ in the north and the Cosby-Southern subdomain boundary to the south, or whether it is offset across either or both of those bounding structures. Isoclinal sheath folds are found within the WAHSZ at the south edge of the map area, which is consistent with a high degree of shear (Figure 3.8). These isoclinal folds are west-verging, implying the WAHSZ is a shear that placed rocks to the east over rocks to the west. Abundant boudins within the WAHSZ, including map scale boudins of quartzite, is consistent with a high degree of simple shear.

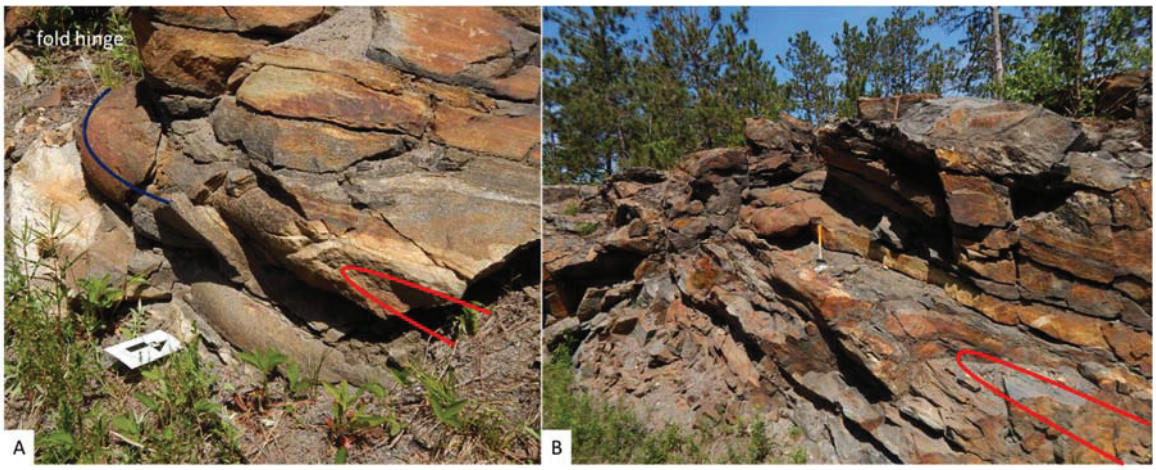

Figure 3.8: Sheath folds at the south end of the West Arm high strain zone, near Monetville. Station SV-14-095. Red lines trace the folded rock layering and the blue line traces the curved fold axis. Images A and B are different locations along the same outcrop.

The east-west cross sections (B-B', Figure 3.10) depicts the WAHSZ as a detachment caused by westward thrusting and ductile folding. In map pattern, the West Bay batholith crops out mostly on the east side of the WAHSZ, and the West Phase crops out mainly west of the WAHSZ. Thus, the cross section shows the West Bay batholith and the West Phase as different plutonic bodies separated by a shear zone. However, the nature of the original contact between the two units is unknown. If the West Phase and the West Bay batholith are the same body, it was

shortened by the WAHSZ, but if the two units are different plutons, they were juxtaposed against one another by the WAHSZ.

Tectonic schists, discussed previously, are oriented similar to the WAHSZ, but are only mapped east of, and structurally above, the high strain zone along Highway 64. In one location (station 14SV061) a pegmatite associated with the tectonic schist cuts the gneissic fabric.

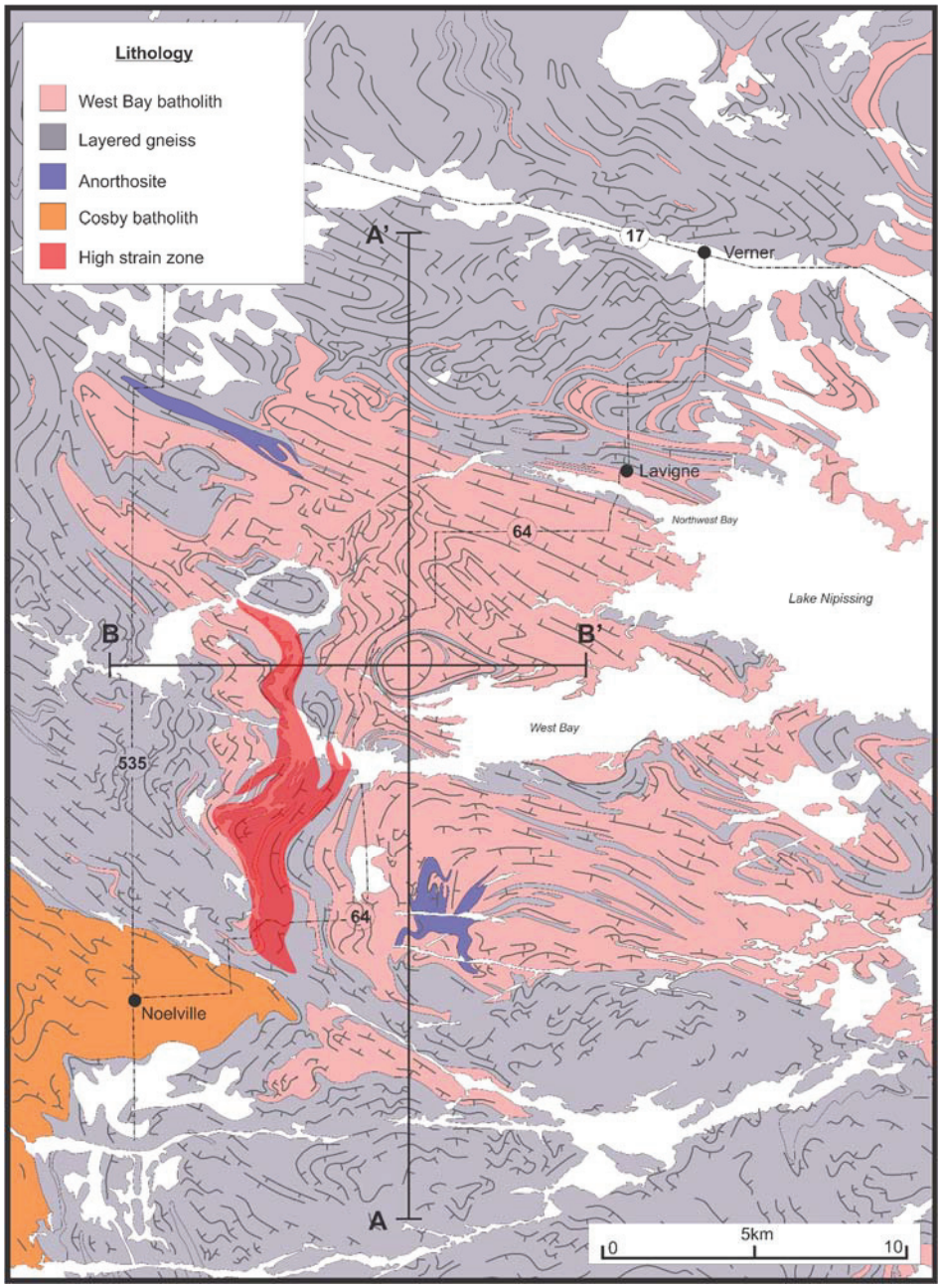

Figure 3.9: Simplified geological map of the Nepewassi domain indicating the locations of cross-sections in Figure 3.10. Cross section lines intersect in the center of the fold interference pattern documented by Tyler (2013). Cross section B-B' intersects the WAHSZ (red) and cross section A-A' runs parallel to it. Lithological contacts and structural trend lines are from Lumbers (1974).

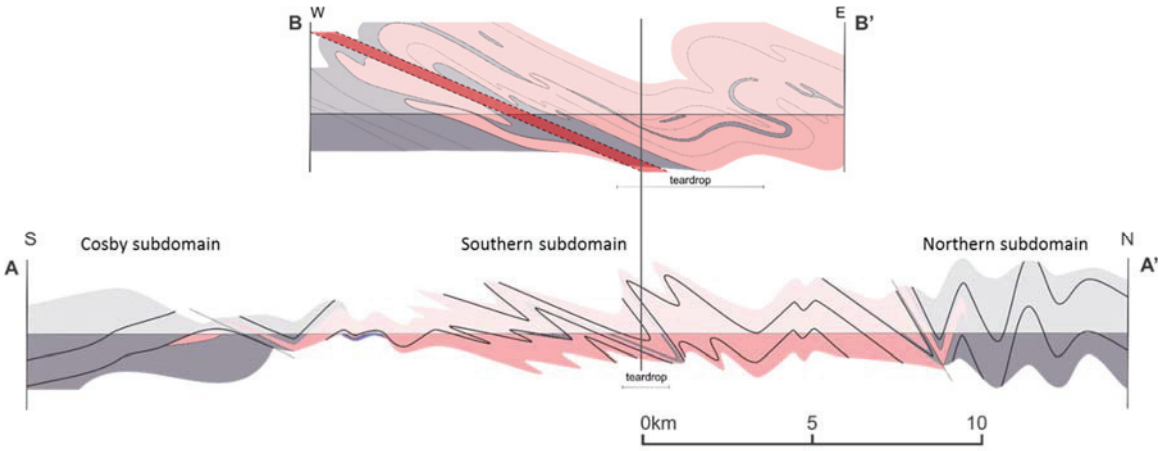

Figure 3.10: Cross sections of the Nepewassi domain, corresponding to Figure 3.9. Section A-A' was constructed by Tyler (2013). Cross-section B-B' was constructed from data compiled from Lumbers (1974), Tyler (2013), and the 2014 field season. The West Arm high-strain zone (WAHSZ) is highlighted in red on the map and cross-section B-B'.

3.3.3 Late shear zones

Mylonites in the map area are interpreted to have formed in shear zones. The mylonitic fabric overprints other fabrics, so these shear zones formed after the previously described structures. Where measured, mylonitic lineations, L_3, are shallow and trend generally northwest-southeast (335° or 155°), which is similar to Grenvillian lineations in other areas of the CGB (Krogh 1994; Jamieson et al. 1995; Culshaw et al. 2016). In the map area, mylonites are found at stations 14SV102, 14SV534, 14SV230 and 14SV145 to 149, mostly along the West Arm from north of Mashkinonje Island to the shoreline across from Shanty Bay (Appendix A.2), suggesting an association with the WAHSZ. Oriented samples from mylonites were taken to find and interpret shear sense indicators. Mylonites dip shallowly between north and east (Figure 3.11) and overprint earlier fabrics. Mylonites are typically a few metres wide or less, apart from the mylonite that runs from station 14SV145 to 14SV149 which is approximately 10 metres wide. Mylonites represent ductile faults or shear zones, with lineation marking the transport direction.

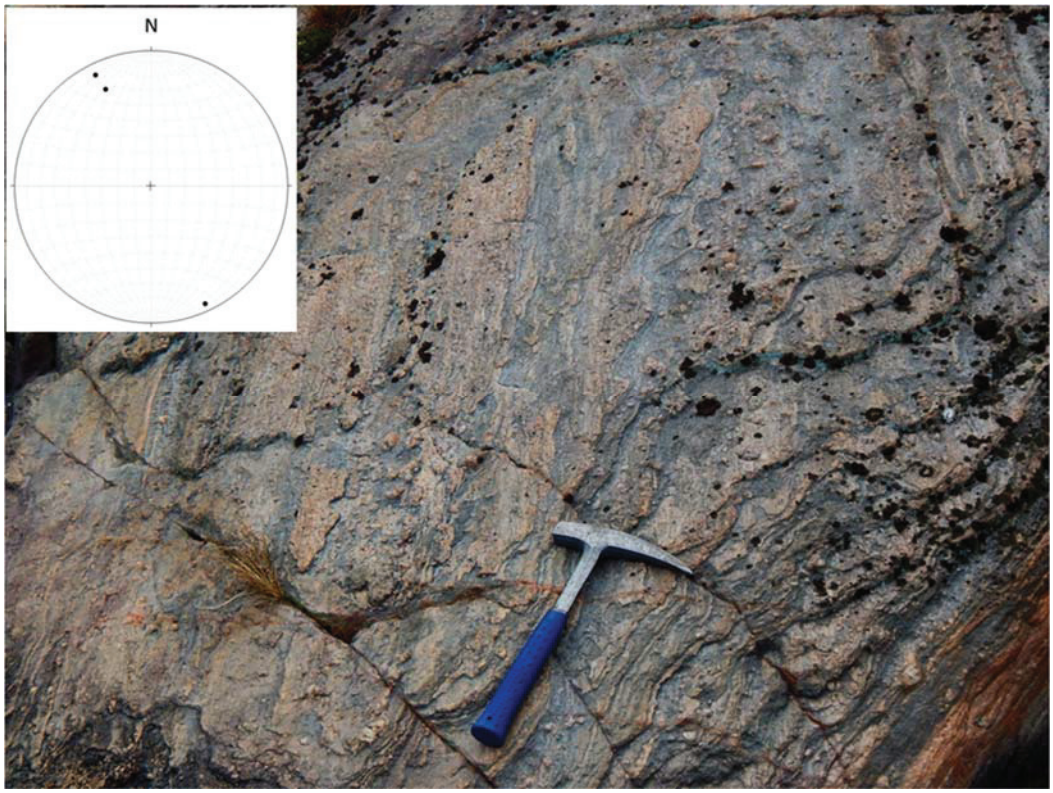

Figure 3.11: Northeast-dipping, fine-grained mylonite on the West Arm across from Shanty Bay (14SV534, Appendix A.2) depicting mm-scale banding and feldspar porphyroclasts. Lineation, defined by aggregates of minerals, is oriented at 335-23. The rock hammer handle points north. Stereonet in the top left corner of the image shows L_3 orientations from the map area.

3.3.4 Lineaments

Map-scale linear landscape features, or lineaments, are recognized in satellite imagery as rivers and valleys. In the center of the map area a west-northwest trending fault offsets the map pattern and the aeromagnetic pattern. This lineament trends parallel to an inlet oriented west-northwest from Warren Bay and out to the West Arm at highway 535. This lineament does not have its own aeromagnetic signature, nor were and mafic dike fragments observed along its exposed length in the map area. This fault or lineament is parallel to the St. Charles-Lavigne Straight Zone (SCLSZ), described in Chapter 1, and the lineament marking the boundary between the Southern subdomain and the Cosby subdomain. Another similarly oriented lineament cuts across Shanty Bay; mylonites have been found along it at stations 14SV534 and 14SV102 (Appendix A.2). A second set of smaller lineaments trends west and west-southwest.

3.4 Microstructure

Microstructures were inspected and described for several samples in the Nepewassi study area to identify and interpret kinematic indicators, overprinting fabrics and mineral assemblages, and recrystallization textures. Oriented mylonite samples cut perpendicular to foliation and parallel to lineation were studied to determine shear-sense in the late shear zones. Other, non-oriented, samples from the Nepewassi study area were studied to determine deformation mechanisms and succession of deformation events.

Analysis of an oriented sample from a shallowly east-dipping mylonite (station 14SV146, northeast of Mashkinonje Island), shows sigmoidal shear-sense indicators (Figure 3.12) formed by non-coaxial deformation and oblique, dextral-normal movement, i.e., top- side down and south; the lineation plunges shallowly 155°. This mylonite sample has lattice preferred orientation (LPO) characterized by quartz c-axes lying in the foliation plane, perpendicular to lineation. LPO forms from simple and/or pure shear at medium to high grade (Passchier and Trouw 2005).

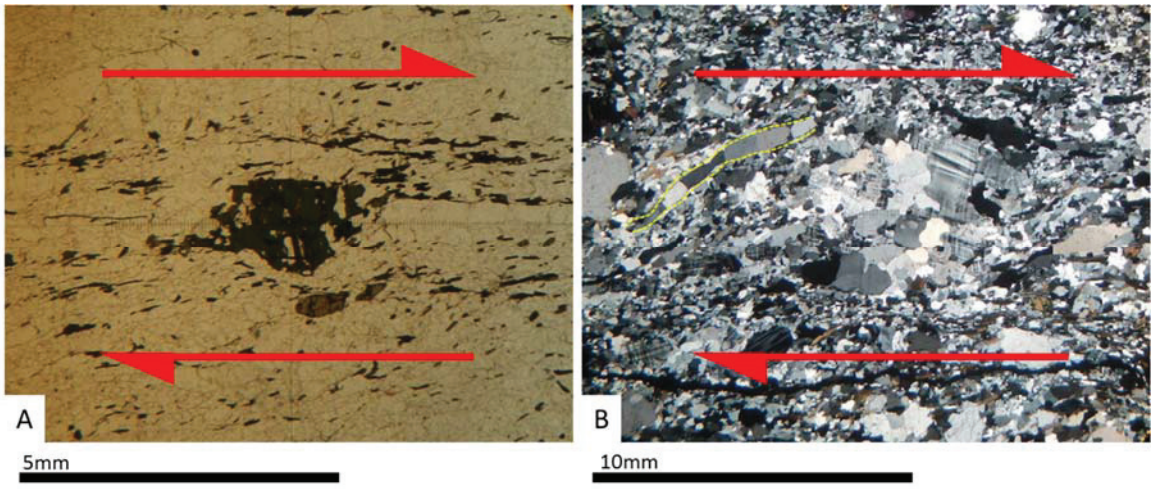

Figure 3.12: A sample of the West Bay batholith with a shallow east-dipping mylonitic fabric from station 14SV146, northeast of Mashkinonje Island. A) PPL. Sigmoidal amphibole porphyroclast indicating dextral movement. B) XPL. Dextral sigmoidal aggregate of quartz and feldspar, potentially originally a K-feldspar megacryst. There is a quartz ribbon along the upper left edge of the aggregate (outlined in dashed yellow), indicating a high degree of strain. The shape of the sigmoidal aggregate and quartz ribbon indicates dextral shear-sense. The orientation of kinematic indicators in this sample show that the mylonite formed during oblique-extensional (top-down, dextral) shearing.

Unlike mylonites, which have undergone grain-size reduction during late-stage ductile shear, most rocks in the study area are medium- to coarse-grained, reflecting high-temperature recrystallization and recovery (>550°C for feldspar and > 400°C for quartz) (Vernon 2004). High-

temperature metamorphism promotes crystal growth, which typically overprints previous microstructures and textures (S_{hg}). Most quartzofeldspathic rocks in the Nepewassi domain have undulose extinction in quartz, deformation twins in feldspar, myrmekite texture, sutured and interlocking grain boundaries between feldspars and quartz, and subgrain formation (Figure 3.13). These textures form during lower grade ductile deformation (S_{lg}) relative to the grain-coarsening high-temperature event Most quartzofeldspathic gneisses and migmatites have some melt film pseudomorphs along quartz and feldspar grain boundaries, which is evidence that melt was present during or after the crystallization of quartz and feldspar.

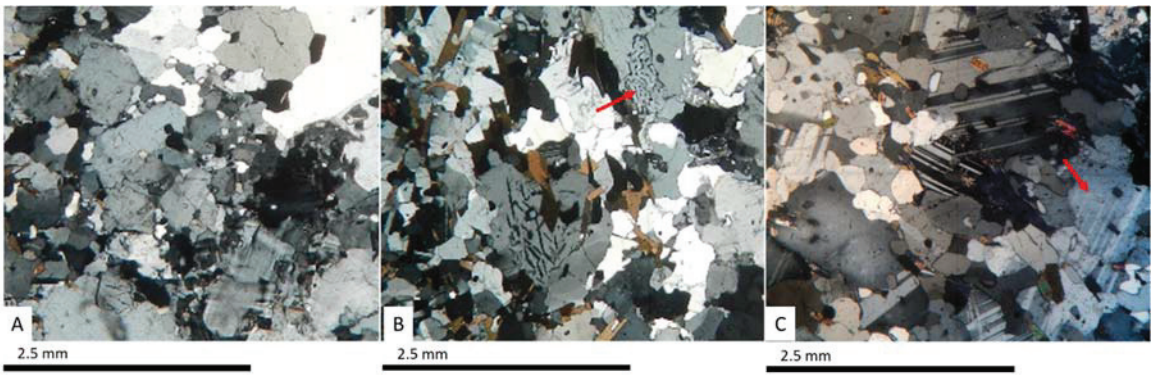

Figure 3.13: Evidence of ductile deformation in quartzofeldspathic gneisses. A) A granodioritic sample (unit Tn, sample 14SV528-NEP-S-1) showing interlocking grain boundaries. B) Myrmekite texture (arrow) in a layered tonalitic to granodioritic gneiss and metatexite (unit lm_1, sample 14SV323A). C) Deformation twins in a psammitic paragneiss (unit Sn_3, sample 14SV095A). Arrow points to tapered deformation twins in plagioclase.

Micro-scale fabrics are visible in some mica-rich gneisses. A biotite-rich metapelite within the high-strain zone (station 14SV543/N13029) near the Big Cut on West Arm displays foliation defined by biotite, sillimanite and kyanite, and crenulations defined by folded biotite and sillimanite (Figure 3.14 B). In this sample, kyanite is typically broken perpendicular to its long axis, apparently boudinaged (Figure 3.14 A), similar to outcrop and map-scale boudins in the map area, and the West Arm high strain zone in particular. The space between the broken pieces of kyanite is filled with matrix minerals, typically biotite or quartz. In some locations, these kyanite fragments are oriented slightly oblique to one another, apparently re-oriented during the formation of crenulations in the rocks (Figure 3.14 A). There is no obvious replacement reaction between kyanite and sillimanite. Sillimanite typically forms acicular, fibrolite masses, but fine prismatic crystals are also present. Sillimanite is folded with biotite (Figure 3.14 B), and does not display any alteration or retrograde reactions. Kyanite is interpreted to have formed earlier because it is commonly embayed, fractured and broken but sillimanite is always intact. Thus,

kyanite likely crystallized during the formation of foliation, and sillimanite crystallized after kyanite crystals were broken, but before or during the formation of crenulations. Garnet crystals are broken, with no replacement textures; they lack inclusion trails (Figure 3.14).

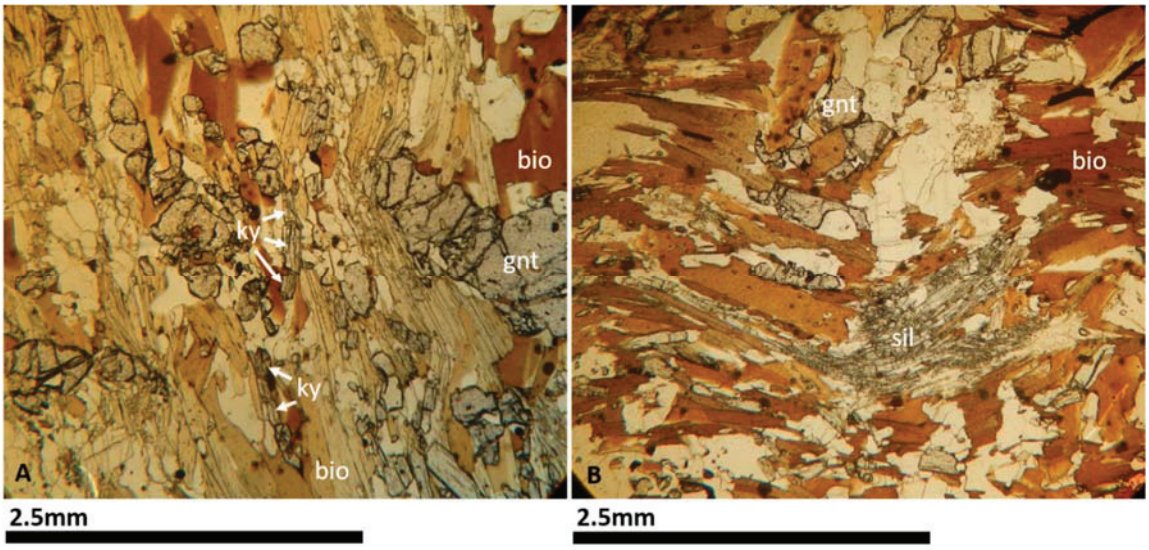

Figure 3.14: Metapelite (station 14SV542). A) Boudinaged/broken kyanite crystals oriented parallel to foliation. Note fractured garnet porphyroblasts. B) Crenulated biotite and sillimanite.

Figure 3.15 displays contrasting textures from four different quartzite samples in the Nepewassi domain. Three samples are located within the WAHSZ; sample 14SV493A is just east of the Big Cut, sample SV14557A is at the mouth of Shanty Bay and sample 14SV003 (NEP-Q) is located just north of Monetville (Appendix A.2). Sample 14SV434A is the only one outside of the WAHSZ; it is located 3 km east in the center of a fold interference pattern (Appendix A.2). Samples 14SV493A and 14SV557A show signs of dynamic recrystallization including sutured grain boundaries, subgrains, and undulose extinction (Figure 3.15 A and B), indicating ductile deformation (Vernon 2004; Passchier and Trouw 2005). Sample 14SV003 (Nep Q) contains elongate quartz crystals with a shape preferred orientation (SPO), pinned by muscovite, that define a foliation (S_{hg}) (Figure 3.15 C). The coarse elongate crystals, formed by exaggerated grain growth, have near simultaneous extinction, indicating grains or groups of grains with similar orientations. A secondary fabric is defined in sample 14SV003 by aggregates of subgrains (S_{lg}) overprinting the large elongate grains at a slight angle, implying simple shear (Figure 3.15 C). Thus, 14SV003 (NEP-Q), had exaggerated grain growth during medium to high grade deformation (S_{hg}) and was overprinted by a relatively lower grade foliation with a faster strain-rate (S_{lg}). It is likely that the grain boundary migration and other deformation in 14SV493A and 14SV557A

corresponds to S_{lg} in 14SV003 (NEP-Q), although not as well developed. The relationship of these fabrics to the map-scale features, boudinaged quartzite bodies, F_2, F_3 and the WAHSZ, is unknown. Quartz grains in sample 14SV434A have more consistent LPO than 14SV003 (Figure 3.15 D). Quartz crystals in this sample are pinned by muscovite crystals and have irregular grain shapes indicating exaggerated grain growth, and have a lower degree of grain boundary migration relative to the other quartzite samples, indicating the last deformation event to affect this sample was relatively lower strain rate and/or higher temperatures (S_{hg}) (Figure 3.15 D). Sample 14SV434A does not have the same, relatively low grade fabric (S_{lg}), seen in other samples from the Nepewassi domain, potentially because S_{lg} is associated with the WAHSZ, and sample 14SV434A is located outside of the WAHSZ.

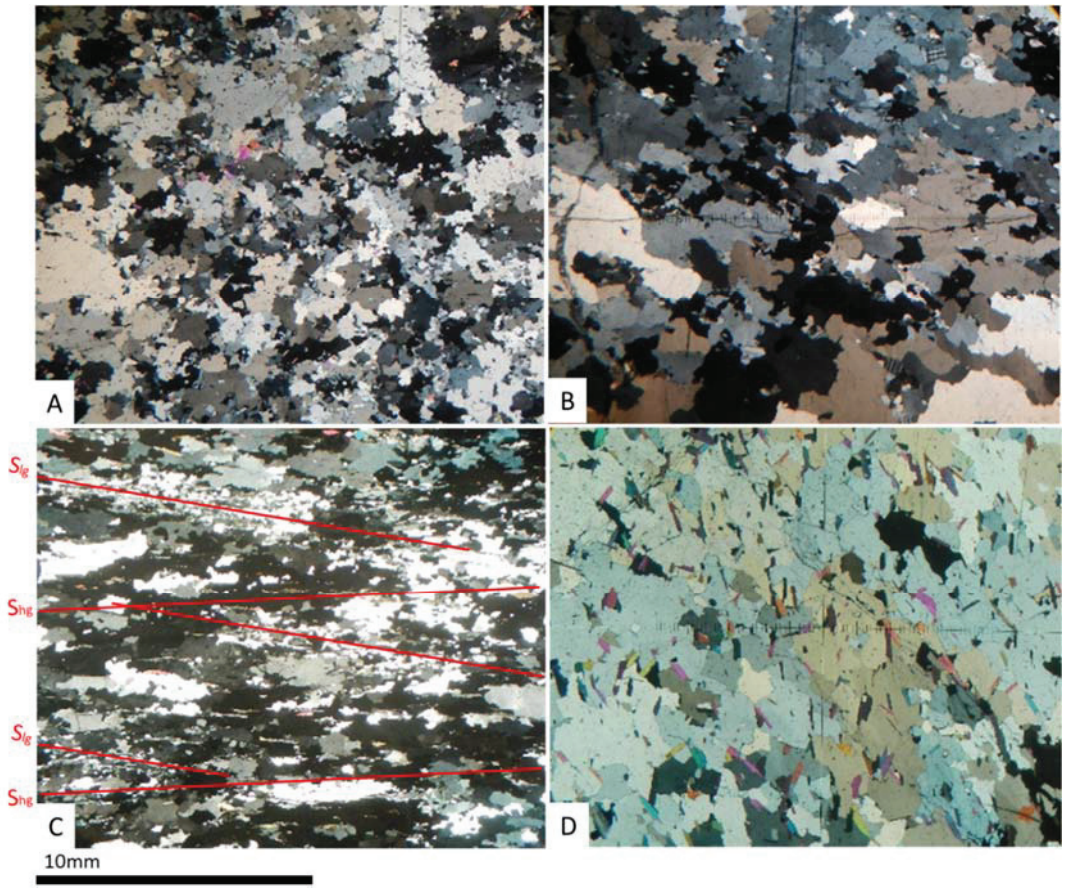

Figure 3.15: Quartzite samples in XPL. A) Sample 14SV493: sutured grain boundaries, inequigranular grainsize, and undulose extinction indicating dynamic recrystallization. B) Sample 14SV557A: sutured grain boundaries, inequigranular grainsize, and undulose extinction indicating dynamic recrystallization. C) Sample 14SV003/Nep-Q: elongate coarse quartz (S_{hg}) and aggregates of quartz subgrains (S_{lg}). D) Sample 14SV434A: LPO indicated by simultaneous extinction of quartz, or groupings of simultaneous extinction. Quartz boundaries are irregular, and locally pinned by muscovite indicating exaggerated grain growth. These samples were used for U-Pb zircon geochronology and are described in more detail in Chapter 5

3.5 Discussion

3.5.1 Folds:

At some point prior to folding in the Nepewassi domain, D_1 created foliation and layering, which was subsequently folded. Based on the fold interference pattern, at least two phases of folding, here termed F_2 and F_3 (corresponding to deformation phases D_2 and D_3) in the Nepewassi domain.

Based on three dimensional conceptual diagrams (Figure 3.16) and stereonet projections, the first phase of folding (F_2) produced upright folds with north-trending fold axes. The second phase of folding (F_3) formed open to tight, overturned, south-verging folds. Where the teardrop-shaped fold interference pattern forms, F_3 folds are tight and have shallowly west-plunging axes (Figure 3.10 and Figure 3.16). Gently plunging, east-west trending F_3 folds are restricted to the Nepewassi domain; in the rest of the Central Gneiss Belt and elsewhere in the Grenville Province in Ontario, folds are typically southeast to south-southeast trending (orthogonal to the Grenville Front), long and cylindrical with axes parallel to stretching lineation (Ontario Geological Survey 1991; Davidson 1998). Based on this model, east-southeast trending fold hinges (and most lineations) are likely associated with D_3/F_3.

Fold interference patterns are apparently absent from the Northern subdomain, and so presumably the Northern subdomain did not contain F_2 folds. F_3 folds are upright in the Northern subdomain but south-verging in the Southern subdomain; south-verging folds are uncommon in the Grenville Province. Furthermore, F_3 folds are truncated at the boundary with the Cosby subdomain.

Within the Central Gneiss Belt, fold interference pattern(s) like those seen in the Southern subdomain are rare, and apparently only form in the parautochthonous belt (Culshaw et al. 1994; Ketchum and Davidson 2000; Rivers et al. 2012). Northwest-trending Type 3 fold interference patterns (Figure 3.5) (Ramsay 1967) appear in the geological map pattern (Lumbers 1974), 3 to 25 km west of the map area. This suggests that the orientation of F_2 folds changes from east (north-trending) to west (northwest-trending) across the Southern subdomain.

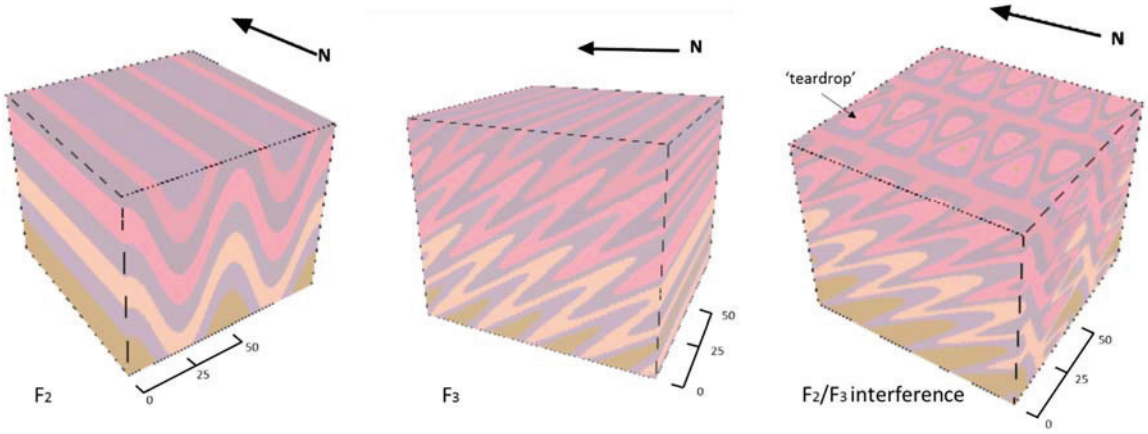

Figure 3.16: Three-dimensional view of the two phases of folding showing the geometry of each phase separately, and the result of both phases combined (fold interference pattern). The first phase of folding (F_2) produced upright folds with north-trending fold axes. The second phase of folding (F_3) formed tight, overturned, south-verging folds with west-trending fold axes. The interference of these two folds creates a teardrop shaped map pattern. Modified from N. Culshaw pers. com., 2016.

3.5.2 West Arm high strain zone:

The WAHSZ has a curved and sinuous map pattern defined by sub-parallel layers of high strain separated by relatively less strained rocks. The sinuous map pattern indicates that the shear zone was folded after it formed. Thus, the WAHSZ was likely formed syn- or post-D_2 and pre-D_3. Assuming F_2 folds plunge slightly north, the nature of the WAHSZ and the West Bay batholith-West Phase contact as they project above the surface and north of Mashkinonje Island on the map, is not well known because of a lack of outcrop.

3.5.3 Tectonic schist:

Tectonic schists in the Nepewassi domain, described in section 3.2.1, are interpreted to have formed in a ductile fault roughly concordant with the WAHSZ. Tectonic schists are concordant to the regional fabric; they are axial plane-parallel and are located within the fold limbs of major folds. On the east-west cross section of the map area (B-B', Figure 3.10), the tectonic schists lie within the upper limb of a kilometre-scale, west-verging, overturned fold. In some locations, tectonic schist is associated with pegmatites. The association with pegmatites, and high concentration of biotite and K-feldspar suggests the schists probably formed by enhanced fluid flow and K-metasomatism. The associated pegmatite cuts gneissic fabric, so the tectonic schists formed post-D_1, and syn- or post-D_2.

3.5.4 Mylonites:

Mylonites overprint earlier gneissic and migmatitic fabrics indicating that they formed later than the other map-scale structures. Mylonites are typically shallowly east-dipping, like the WAHSZ and tectonic schists. Mylonites cut the fabrics in the WAHSZ, and are thus younger than them, but a relative age between the mylonites and the tectonic schists cannot be confirmed.

The mylonite sample at station 14SV146 has LPO characterized by quartz c-axes lying in the foliation plane, perpendicular to lineation; this texture is common in amphibolite facies, Grenvillian shear zones in the Britt domain, and at the base of the Kiosk domain (pers. com. N. Culshaw, 2016). Furthermore, the southeast-trending lineations of the mylonites are oriented the same as lineations in Britt, Kiosk and Shawanaga shear zones that are interpreted to have formed during northwest-directed Ottawan thrusting, followed by oblique-normal ductile extension. (Culshaw et al. 1994, 1997; Jamieson et al. 1995; Rivers et al. 2012). Thus, mylonites in the Nepewassi domain may have formed in response to the overthrusting of and extension in surrounding domains such as the Brit to the south.

3.5.5 Subdomain boundaries:

The boundary between the Southern subdomain and the Cosby subdomain is defined by a lineament or fault. Greenschist facies mylonites are present at this boundary (pers. com. N. Culshaw, 2016). Bouguer gravity maps (Gupta 1991, 1992), especially the first derivative of the gravity field display higher anomalies (denser rocks) in the Southern subdomain and lower in the Cosby subdomain, and south-verging folds are truncated.

The Northern subdomain and Southern subdomain are separated by the SCLSZ, which is oriented parallel to the boundary between the Cosby subdomain and the Southern subdomain; however, rather than a sharp lineament, the SCLSZ is a 3 to 5 km wide vertical ductile shear zone. As described in Chapter 1, the SCLSZ is composed of near-vertical, east-southeast-trending, straight gneisses and affects rock units from the adjacent subdomains. The SCLSZ likely formed from a high degree of simple shear, which implies a significant amount of relative transport between the subdomains. Transpressional forces that drove the formation of the SCLSZ are likely related to, or the same as D_3.

CHAPTER 4

METAMORPHISM

4.1 Introduction

Metamorphic mineral assemblages and textures provide another method of characterizing the orogenic events that affected the Nepewassi domain. Metamorphic grade, paired with deformation style, can be used to estimate crustal depths and temperatures during metamorphism. This, in turn, provides information about the size and history of the orogen.

One goal of this study was to determine if there were multiple episodes of metamorphism and/or retrograde metamorphism, typical of polycyclic orogenic belts. Mineral assemblages and textures were studied during field work to determine metamorphic facies. Following detailed petrographic and microprobe analysis, pressure-temperature (P-T) conditions were determined using thermobarometry in order to quantify the metamorphic grade of these samples. In the context of the present study, a specific goal was to use metamorphic P-T data to test the hypothesis that the rocks on the east side of the WAHSZ were thrust over rocks to the west (Chapter 3).

4.2 Petrography

Major map units and units with mineral assemblages suitable for determining P-T conditions are described in this section. These units are grouped based on protolith (cf. Chapter 2).

4.2.1 Felsic metaplutonic rocks

West Bay batholith (unit Gnm):

The West Bay batholith is typically a pink, stromatic metatexite, although it can range from red to grey; leucosomes are typically light pink. It is medium- to coarse-grained with 20-35% mafic minerals. In hand sample, flattened aggregates of feldspar, quartz, amphibole, and biotite are interpreted as deformed relict phenocrysts. Foliation is defined by stromatic leucosomes and gneissosity. Leucosomes make up ≤ 10% of the rock volume.

The minerals present include K-feldspar + plagioclase + quartz + biotite ± amphibole ± garnet ± calcite ± titanite ± chlorite with accessory apatite and zircon. Leucosomes are composed mainly

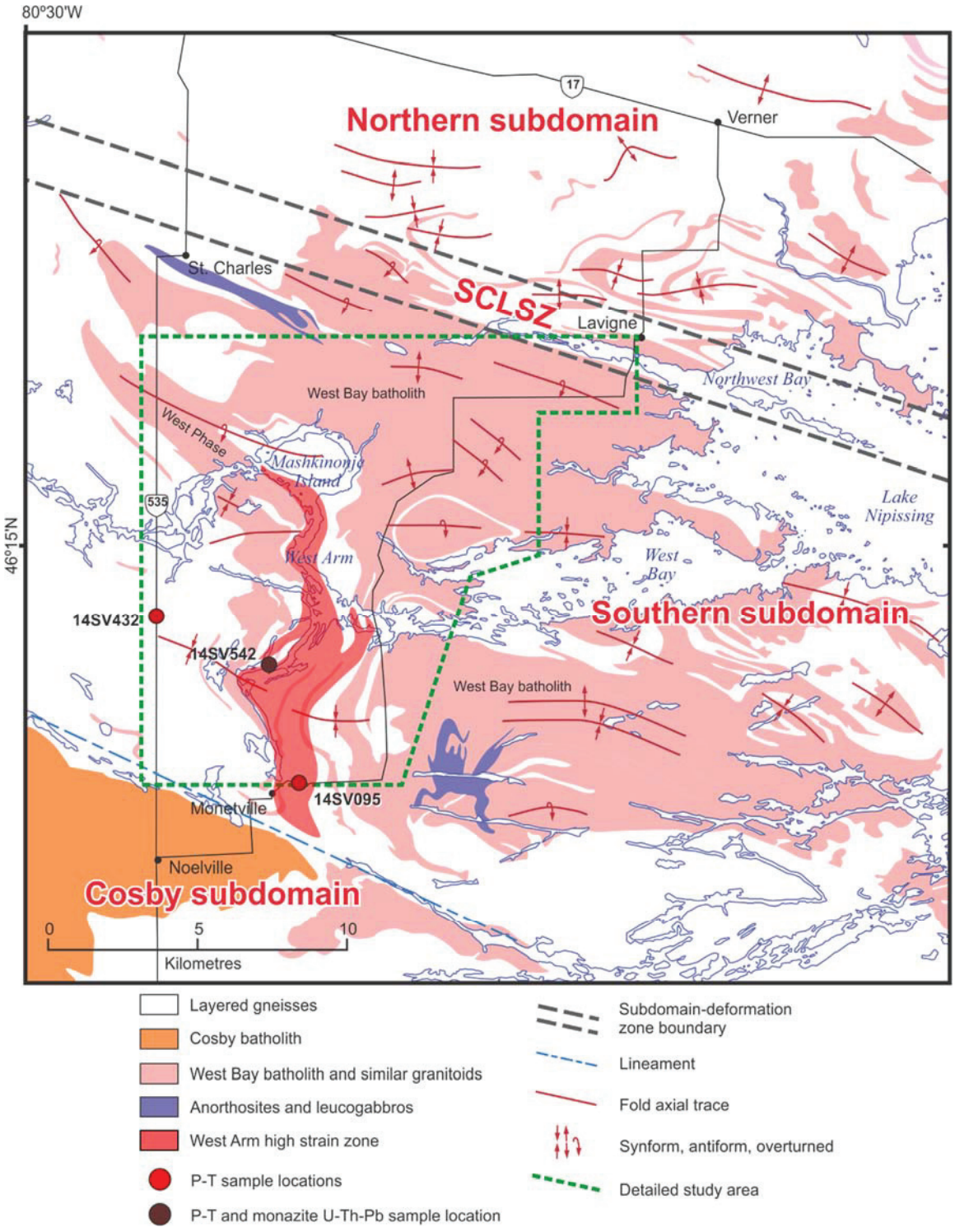

Figure 4.1: Simplified map of the Nepewassi domain displaying locations of the samples analyzed for P-T.

of K-feldspar and quartz. Hornblende grains are commonly fragmented along cleavage planes, and chlorite replaces hornblende along the cracks. In this coarse-grained unit, foliation is difficult

to recognized in thin section. In some samples, foliation is defined by compositional layering of mafic minerals, but biotite does not display a well-defined preferred orientation, potentially because of overprinting fabrics that are no longer recognizable.

Crystals range from 0.05-6 mm in diameter, with some hornblende porphyroblasts reaching up to 7 mm. Felsic minerals are xenoblastic and equant whereas mafic minerals are subidioblastic. Deformation textures include poorly developed subgrains, interlocking and embayed grain boundaries between felsic minerals, undulose extinction in quartz, myrmekitic intergrowths of quartz and feldspar, and antiperthite texture in plagioclase. Feldspar crystals generally have dusty sericite alteration. Thin films of quartz, plagioclase and/or K-feldspar along grains boundaries, melt films, are present locally and represent crystalized melt.

Based on the presence of K-feldspar + plagioclase + quartz + hornblende + garnet, this rock unit is metamorphosed to amphibolite facies. Dynamic recrystallization textures indicate the most recent ductile deformation event happened at a relatively low temperature and/or high strain rate, compared to the grain coarsening event. Leucosomes and melt film pseudomorphs indicate there was partial melting.

West Phase (unit Gn_1):

The West Phase of the West Bay batholith is a leucocratic (≤10% mafic minerals), fine- to coarse-grained, locally porphyroblastic, light pink orthogneiss. West Phase is composed predominantly of K-feldspar + quartz + plagioclase, with small amounts of biotite ± garnet ± opaque minerals, likely magnetite. Unlike the West Bay batholith (Gnm), the West Phase (Gn_1) apparently lacks amphibole and leucosomes are rare to absent. Grainsize is bimodal, with 2-3 to 7 mm to ≥ 1 cm quartz or K-feldspar porphyroblasts, and matrix crystals averaging 1 to 0.25 mm across. Garnet is highly fragmented, and typically rimmed by quartz and opaque minerals. In thin section, foliation is defined by elongate quartz and feldspar crystals and, and in some samples the trend of undulose extinction in quartz is parallel to foliation. Other microscopic textures include subgrains and embayed and sutured grain boundaries. At some quartz and feldspar grain boundaries, small amounts of myrmekitic texture and melt films are present. Feldspar crystals have dusty sericite alteration.

As with almost all units in the Nepewassi domain, dynamic recrystallization textures indicate that the last deformation event occurred under ductile conditions at relatively low temperature and/or high strain rate, compared to the earlier high-temperature grain coarsening event.

Myrmekitic texture, which forms by grain-scale diffusion between quartz and feldspar, is common in medium-grade deformed rocks (Vernon 2004). Melt films indicate the former presence of interstitial melt, but there are very few leucosomes in this unit. Former melt likely migrated out of the pluton, or this part (phase) of the pluton. Some samples display shape preferred orientations (SPO) of quartz, feldspar and biotite.

4.2.2 Mafic and intermediate metaplutonic rocks

Dioritic and gabbroic gneiss (unit Mn):

The dioritic and gabbroic gneisses are medium- to coarse-grained with a black and white speckled texture; they typically have around 50% mafic minerals. This unit is typically equigranular, but in some samples, very coarse amphibole porphyroblasts reach up to 2 cm in length. The gabbro and diorite typically have a weak gneissic foliation, and are locally migmatitic with up to 20% leucosomes. Leucosomes can be K-feldpsar-dominated, but are typically plagioclase-dominated.

The minerals observed in this unit are hornblende + plagioclase (oligoclase to andesine) + quartz ± biotite + titanite ± clinopyroxene (augite) ± orthopyroxene (hypersthene) ± allanite ± chlorite ± scapolite ± apatite ± epidote ± actinolite. K-feldspar is present only in the leucosomes of a few samples. Grain size is bimodal, ranging from 0.1 mm to 1.5 mm. Hornblende, plagioclase and quartz are typically xenoblastic and relatively equant. Titanite is commonly metamict, dark and cloudy. Allanite is typically xenoblastic, yellow and surrounded by radiation halos and radial fractures. The large (>1cm) porphyroblasts of hornblende are typically clusters of fine crystals. Hornblende crystals are randomly oriented. Where hornblende is oriented c-axis perpendicular to the slide, it tends to be very fragmented and broken along well-defined cleavage planes. There is also spongy-looking hornblende replacing pyroxene; pyroxene is xenoblastic, metamict, and small (<0.1 mm) and is interpreted as metamorphic. Less common textures include scapolite intergrown with hornblende, fibrous orange-yellow chlorite replacing scapolite and hornblende, and hornblende intergrown with actinolite along cleavage planes. Biotite pleochroism is dark chestnut, to khaki brown, to pale tan. Feldspar crystals have a small amount of dusty sericite alteration and fracturing. Boundaries between felsic minerals are interlocking, locally with subgrains of quartz and feldspar along grain boundaries. In some samples, melt films can be found locally along grain boundaries of feldspar. Antiperthite texture, (irregular K-feldspar exsolution lamellae in plagioclase) is found locally indicating slow cooling of high-temperature K-rich plagioclase.

The major mineral phases in all samples, plagioclase + hornblende + quartz + titanite, indicate that this rock is amphibolite facies. In some samples, retrograde actinolite after hornblende, epidote, and chlorite indicate a greenschist facies overprint. Clinopyroxene (augite) and orthopyroxene (hypersthene), interpreted as metamorphic (granulite facies), are found in small amounts in some dioritic and gabbroic gneiss samples (unit Mn). Since hornblende replaces pyroxene in many samples, the amphibolite facies assemblage may be retrograde after granulite. Antiperthite texture is formed by slow cooling from a much higher temperature, 800-900°C (Kay 1977). Based on these observations, the rocks were probably recrystallized at granulite facies, retrogressed to amphibolite facies, and then partially retrogressed to greenschist facies.

Sample 14SV095B from unit Mn was chosen for P-T analysis because it contains relatively fresh, unaltered minerals needed for garnet-biotite (GB) thermometry, garnet-hornblende (GH) thermometry, and garnet-plagioclase-hornblende-quartz barometry (GPHQ), and because it is located on the east edge of the WAHSZ (Figure 4.1). The WAHSZ is interpreted as an east-over-west shear, so this sample may provide support for this interpretation.

4.2.3 Metasedimentary rocks

Quartzite (unit Sn_1):

In hand sample, this unit is white to pink and glassy on fresh surfaces; it is almost entirely composed of quartz. The quartzite is foliated locally lineated, with interstitial sillimanite and muscovite defining the foliation. It is fine- to medium-grained with interlocking quartz grains. In one sample, elongate quartz grains appear to be oriented slightly oblique to layering potentially because of overprinting fabrics and/or simple shear.

In thin section, samples are composed of 90 to 95% quartz. Sillimanite, muscovite and accessory zircon are common in this unit, and kyanite, K-feldspar and opaque minerals are locally present as minor phases. In one sample (14SV003/NEP-Q), muscovite and sillimanite are intergrown. Quartz has undulose extinction, and the boundaries are interlocking, embayed, sutured, and in some cases subgrains have formed. In some samples, quartz has lattice preferred orientation (LPO). Four samples of quartzite were selected for structural and geochronological analysis. They are described in Chapter 3, section 3.4 and Chapter 5, section 5.2.3.

The quartzite unit is a metamorphosed quartz arenite; its protolith is interpreted to have contained a small amount of clay, contributing the Al_2O_3 and K_2O needed to form muscovite, K-feldspar, sillimanite, and/or kyanite during metamorphism. The presence of sillimanite and/or

kyanite indicates that the sample has been metamorphosed to amphibolite facies or higher. LPO in quartz is formed during shear strain, and is common in medium- to high-grade facies rocks (Passchier and Trouw 2005). In one quartzite sample (14SV493A), kyanite and sillimanite coexist, but there is no evidence suggesting which Al-silicate formed first.

Quartzite samples were chosen for detrital zircon geochronological studies (Chapter 5) because they contain ample zircon grains, and are the most easily recognized metasedimentary rock in the map area. Three samples are located within the WAHSZ and one is located approximately 3 km west of it (Figure 4.1).

Pelite/semi-pelite (unit Sn_2):

Pelitic to semi-pelitic gneisses are light grey-brown to dark grey, garnet-bearing, quartz- and mica-rich rocks. They are foliated and fine- to medium-grained with a sugary or granular texture. Foliation is defined by mica, weak compositional layering, and thin streaks of unidentified black minerals. Rocks of unit Sn_2 are layered on the mm- to cm-scale and contain sparse mm-scale leucosomes. Pelitic to semi-pelitic rocks contain sillimanite and/or kyanite. In most pelites, kyanite is only visible at microscopic scale, but sillimanite is visible in hand sample. In hand sample, sillimanite commonly forms < 1 mm interstitial crystals and radiating mats, up to 1 cm, that lie parallel to foliation. Garnets are typically mauve, small, ≤ 1 mm, although rare porphyroblasts up to 1 cm across are present.

Pelites and semi-pelites contain 20-80% quartz and 20-65% biotite. Other major mineral phases include muscovite + garnet + K-feldspar + plagioclase ± sillimanite ± kyanite ± rutile. Pleochroic halos within biotite indicate the presence of accessory zircon and monazite. In some samples, chlorite replaces biotite. Felsic minerals are equant and xenoblastic to subidioblastic with irregular and sutured grain boundaries, although quartz crystals have a weak shape preferred orientation (SPO). Plagioclase typically displays a mottled texture because of sericite alteration (Figure 4.6 A). Some quartz displays undulose extinction. Pelites and semi-pelites are inequigranular but the average crystal size is 0.5 mm, apart from garnet and Al_2SiO_5 porphyroblasts, which are notably bigger in some samples. Garnet porphyroblasts make up to 10 modal %, and are xenoblastic and poikiloblastic, but lack inclusion trails (Figure 4.2 B). Biotite commonly replaces garnet. Sillmanite porphyroblasts are lath-shaped or form fibrous masses, and kyanite crystals are euhedral to subhedral, and locally fractured or embayed. Some kyanite crystals have simple twins. Plagioclase is twinned and commonly contains inclusions of biotite and

rutile. Thin layers of rutile and iron oxide minerals likely make up the streaks of unidentified black minerals visible in hand sample. Minor myrmekitic texture is present in most samples along with melt films of plagioclase and quartz along the grain boundaries of plagioclase and quartz.

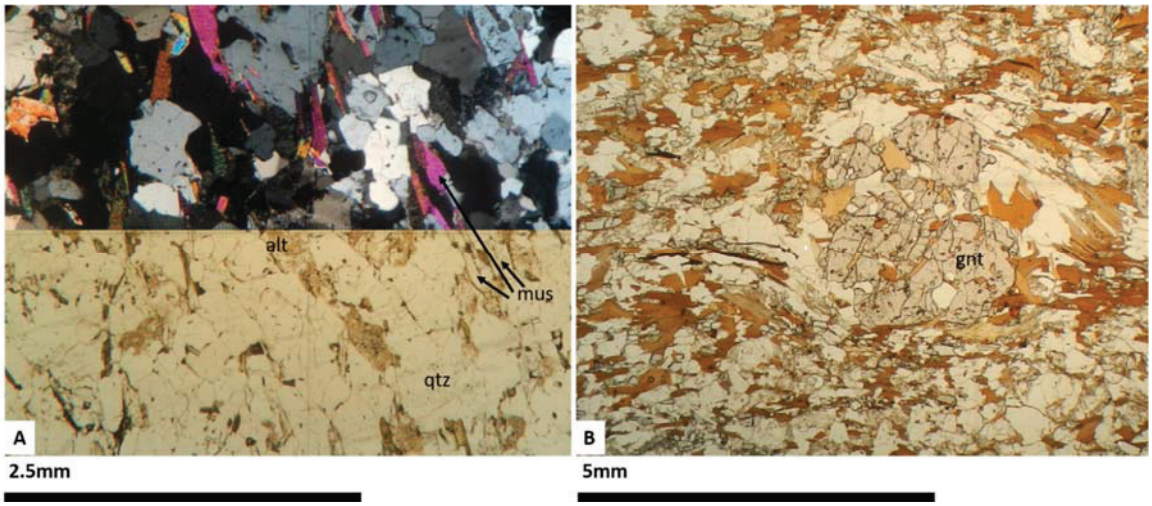

Figure 4.2: A) Sample 14SV432A displaying the typical appearance of semi-pelites in thin section. Single field of view, with the top half displayed in XPL, and the bottom half in PPL. B) Sample 14SV542A in PPL. Garnet porphyroblasts within foliation defined by biotite. gnt = garnet. qtz = quartz. alt = sericite alteration. mus = muscovite.

The presence of garnet + biotite + muscovite + quartz + plagioclase ± kyanite ± sillimanite indicates that this rock unit is amphibolite facies to upper amphibolite. Chlorite replacing some biotite crystals indicates minor retrogression. As with most units in the Nepewassi map area, interlocking grain boundaries between felsic minerals and myrmekite indicate ductile deformation, and melt films provide evidence that there has been partial melting.

Two pelite samples, 14SV432 and 14SV542, were chosen for P-T analysis because they contain the necessary mineral assemblage for garnet-biotite (GB), garnet-biotite-plagioclase-quartz (GBPQ) and garnet-aluminosilicate-quartz-plagioclase (GASP) thermobarometry. Sample 14SV542A is located within the WAHSZ and sample 14SV432 is located west, on highway 535, structurally below the WAHSZ. In addition, monazite from pelite sample 14SV542 was analyzed for metamorphic ages (Chapter 5), to determine a potential P-T-t path for this sample.

4.2.4 Tonalitic grey gneisses

Tonalitic and granodioritic gneiss and migmatites (unit Tn):

Tonalitic gneisses in the Nepewassi map area are typically medium-grained, compositionally homogeneous, foliated to massive gneisses. They are typically light grey with ≤ 10% mafic

minerals, however there are also some layers enriched in mafic minerals. This unit is cut by cm- to mm-scale granitoid dikes and sills.

In thin section, tonalitic gneisses are composed predominantly of plagioclase + quartz, but can also contain biotite ± amphibole ± K-feldspar ± titanite ± apatite ± epidote ± pyrite ± calcite ± chlorite. Quartz range from 7 mm by 1mm in size, but the average crystal size is 0.5 mm. Felsic minerals have interlocking grain boundaries with minor embayments, sutures, and subgrains. Quartz crystals display undulose extinction. Locally biotite crystals have two poorly defined preferred orientations, but in most samples, foliation is defined by aligned biotite and amphibole aggregates and/or elongate quartz crystals. Grains are inequigranular or bimodal but with no porphyroblasts. Felsic minerals are typically xenoblastic. Local antiperthite and myrmekite are present. Feldspar typically has dusty sericite alteration. In many samples, chlorite almost completely replaces amphibole. Biotite is khaki green in PPL and locally replaced by epidote or hematite.

4.3 Thermobarometry

4.3.1 Methods

Pressures (P) and temperatures (T) of metamorphism were calculated from two pelites and one garnet amphibolite using two different thermometers and three different barometers (Table 4.1). Samples were chosen based on mineral assemblages and location relative to the north-south trending WAHSZ.

Table 4.1: A list of all the thermometers and barometers used in this study.

Method	Reference
garnet-biotite thermometer (GB)	(Holdaway 2000)
garnet-hornblende thermometer (GH)	(Graham and Powell 1984)
garnet-biotite-plagioclase-quartz barometer(GBPQ)	(Wu 2004)
garnet-plagioclase-hornblende-quartz barometer (GPHQ)	(Kohn and Spear 1990)
garnet-aluminosilicate-silica (quartz)-plagioclase barometer (GASP)	(Holdaway 2001, 2004)

GB:

Garnet-biotite thermometry is based on Mg-Fe^{2+} exchange between biotite and garnet through the following reaction:

$$Fe_3Al_2Si_3O_{12}(almandine) + KMg_3AlSi_3O_{10}(OH)_2(phlogopite) = Mg_3Al_2Si_3O_{12}(pyrope) + KFe_3AlSi_3O_{10}(OH)_2(annite) \quad (4.1)$$

The reaction was experimentally calibrated by Ferry and Spear (1978); the formulation reported by Holdaway (2000) has been used here:

$$T(°C) = \frac{40198 + 0.295P + G + B}{7.802 + 3RlnK_D} - 273 \quad (4.2)$$

where R = 8.31441 J/(mol*K) and P is in bar. Variables G and B, and K_D, are defined by:

$$G = 3RTln\left(\frac{\gamma_{Mg}^{Grt}}{\gamma_{Fe}^{Grt}}\right) \quad (4.3)$$

$$B = 3RTln\left(\frac{\gamma_{Fe}^{Bt}}{\gamma_{Mg}^{Bt}}\right) \quad (4.4)$$

$$K_D = \frac{X_{Mg}^{Grt}/X_{Fe}^{Grt}}{X_{Mg}^{Bt}/X_{Mg}^{Bt}} \quad (4.5)$$

GB thermometer calculations, including activity coefficients (γ) and mole fraction (X) were completed on a spreadsheet provided by Rebecca Jamieson, adapted from Holdaway (2000).

The GB thermometer was calibrated over the range 550-800°C, and is normally used to calculate equilibrium temperatures < 800°C (Ferry and Spear 1978) in medium-grade pelitic metamorphic rocks (Holdaway et al. 1997). Biotite is particularly susceptible to post-peak metamorphism cation exchange, particularly with garnet. Thus, results could potentially yield lower T than peak metamorphism temperatures. For this reason, compositions used for P-T calculations were measured where biotite is not in contact with garnet.

This method yields a nominal uncertainty of ± 25°C (Holdaway 2000).

GH:

The Mg and Fe^{2+} exchange reaction between garnet and hornblende is represented by the following reaction (Graham and Powell 1984):

$$\frac{1}{4}NaCa_2Fe_4Al_3Si_6O_{22}(ferro-pargasite) + \frac{1}{3}Mg_3Al_2Si_3O_{12}(pyrope) = \frac{1}{4}NaCa_2Mg_4Al_3Si_6O_{22}(OH)_2(pargasite) + \frac{1}{3}Fe_3Al_2Si_3O_{12}(almandine) \quad (4.6)$$

The formulation as derived by Graham and Powell (1984) is:

$$T(°C) = \frac{2880 + 3280X_{Ca}^{Grt}}{lnK_D + 2.426} - 273 \quad (4.7)$$

where

$$K_D = \frac{X_{Fe}^{Grt}/X_{Mg}^{Grt}}{X_{Fe}^{Hb}/X_{Mg}^{Hb}} \quad (4.8)$$

Unlike the GB thermometer, GH was not calibrated as a function of P. The GH thermometer is applied to rocks with T_{max} < 850°C and yields useful results for a wide range of hornblende compositions. According to Graham and Powell (1984) there is no reliable data for activity composition relationships of end-member components in calciferous amphibole solid solutions. In this method, non-ideality is assumed to be assigned to the well-known non-ideality of Ca-substitution in garnet (Graham and Powell 1984).

Nominal uncertainty used for this method is ± 20°C (Graham and Powell 1984).

GBPQ:

The garnet-biotite-plagioclase-quartz barometer is based on two model reactions involving Mg- and Fe- end member components (Wu 2004):

$$Mg_3Al_2Si_3O_{12}(pyrope) + 2Ca_3Al_2Si_3O_{12}(grossular) + 3K(Mg_2Al)(Si_2Al_2)O_{10}(OH)_2(eastonite) + 6SiO_2(quartz) = 6CaAl_2Si_2O_8(anorthite) + 3KMg_3(AlSi_3)O_{10}(OH)_2(phlogopite) \quad (4.9)$$

$$Fe_3Al_2Si_3O_{12}(almandine) + 2Ca_3Al_2Si_3O_{12}(grossular) + 3K(Fe_2Al)(Si_2Al_2)O_{10}(OH)_2(siderophyllite) + 6SiO_2(quartz) = 6CaAl_2Si_2O_8(anorthite) + 3KFe_3(AlSi_3)O_{10}(OH)_2(annite) \quad (4.10)$$

Activity models and equilibrium constants for each mineral were derived as a function of P by Wu (2004), and he obtained the following GBPQ barometry equations:

$$P_{Mg}(bars)[1 - 0.081(-6\mathrm{Fb} + \mathrm{Mgb} + 2\mathrm{Cab})] = -24450.7 + 40.238\mathrm{T(K)} + 59256.2X_{Fe}^{bio} + 5173.9\left(X_{Mg}^{bio} - X_{Al}^{bio}\right) + 6393.4X_{Ti}^{bio} + 0.081[T(K)\left(-R\,lnK_{(Mg)}^{ideal} - 6Fa + Mga + 2Caa - 788.7X_{Fe}^{bio}\right) - 6Fe + Mgc + 2Cac] \quad (4.11)$$

$$P_{Fe}(bars)[1 - 0.081(-6\mathrm{Fb} + \mathrm{Feb} + 2\mathrm{Cab})] = -19871.0 + 30.75\mathrm{T(K)} + 66622.5\left(X_{Fe}^{bio} - X_{Al}^{bio}\right) + 1363.1X_{Mg}^{bio} - 74704.2X_{Ti}^{bio} + 0.081 * \left[T(K)\left(-R\,lnK_{(Fe)}^{ideal} - 6Fa + Fea + 2Caa - 840.9X_{Fe}^{bio} + 52.2X_{Mg}^{bio} + 840.9X_{Al}^{bio} + 1111.2X_{Ti}^{bio}\right) - 6Fc + Fec + 2Cac\right] \quad (4.12)$$

where *Caa, Cab, Cac, Fea, Feb, Fec, Mga, Mgb* and *Mgc* are polynomial expressions for the end-member compositions of garnet, and Fa, Fb and Fc are polynomial expressions for the end-member compositions of plagioclase, X is mole fraction, and K is equilibrium constant (Wu, 2004).

Equations for the above-mentioned variables are listed in Appendix B.1. These variables are used to account for non-ideal end-member concentrations relative to the model reactions.

This method was calibrated over the P-T range 1.0 to 11.4 kbar and 515 to 878°C, and thus is most suitable for amphibolite facies assemblages.

The uncertainty cannot be assessed directly as the reactions were not experimentally calibrated. However, GBPQ barometry reproduced GASP results within error of ± 1 kbar, although most results were actually within ± 0.5 kbar (Wu 2004). Furthermore, experimental results from GBPQ and GASP are in 1:1 linear accordance (Wu 2004). A nominal error of ± 1 kbar is used in this study.

GPHQ:

This barometer is based on a net transfer reaction involving garnet, plagioclase, hornblende and quartz. There are two different reactions for the Mg- and Fe-end member components of garnet and hornblende (equations 4.13, and 4.14)(Kohn and Spear 1990).

$$\begin{aligned} 6CaAl_2Si_2O_8(anorthite) + 3Ca_2Mg_5Si_8O_{22}(OH)_2(tremolite) = \\ 2Ca_3Al_2Si_3O_{12}(grossular) + Mg_3Al_2Si_3O_{12}(pyrope) + \\ 3Ca_2Mg_4Al_2Si_7O_{22}(OH)_2(tschermakite) + 6SiO_2(quartz) \end{aligned} \quad (4.13)$$

and

$$\begin{aligned} 6CaAl_2Si_2O_8(anorthite) + 3Ca_2Fe_5Si_8O_{22}(OH)_2(Fe-actinolite) \\ = 2Ca_3Al_2Si_3O_{12}(grossular) \\ + Fe_3Al_2Si_3O_{12}(almandine) \\ + 3Ca_2Fe_4Al_2Si_7O_{22}(OH)_2(Fe-tschermakite) \\ + 18SiO_2(quartz) \end{aligned} \quad (4.14)$$

The equations derived by Kohn and Spear (1990) are:

$$P_{Mg}(bars) = [79507 + T(°K)(29.14 + 83144 * \ln K_{eq})]/10.988 \quad (4.15)$$

$$P_{Fe}(bars) = [35327 + T(°K)(56.09 + 83144 * \ln K_{eq})]/11.906 \quad (4.16)$$

where

$$K_{eq}(Mg) = \frac{(a_{Grs})^2 * (a_{Prp}) * (a_{Tsch})^3 * (a_{Qtz})^6}{(a_{An})^6 * (a_{Tr})^3} \quad (4.17)$$

$$K_{eq}(Fe) = \frac{(a_{Grs})^2 * (a_{Alm}) * (a_{Fe-Tsch})^3 * (a_{Qtz})^6}{(a_{An})^6 * (a_{Fe-Act})^3} \quad (4.18)$$

The activity models and compositional parameters used for this barometer are listed in Appendix B.2.

Kohn and Spear (1990) calculated a typical error for this method to be ± 0.5 kbar. This barometer was calibrated over the range 2.5-13 kbar and 500-800°C, and is most suitable for amphibolite facies assemblages.

GASP:

The garnet-aluminosilicate-silica-plagioclase barometer was originally suggested by Ghent (1976), experimentally calibrated by Newton and Haselton (1983) and Koziol and Newton (ca 1990), and re-formulated by Holdaway (2001, 2004). The equilibrium reaction, equation (4.19), was used to derive the barometer, equation (4.20).

$$Ca_3Al_2Si_3O_{12}(grossular) + 2Al_2SiO_5(kyanite\ or\ sillimanite) + SiO_2 = 3CaAl_2Si_2O_8(anorthite) \quad (4.19)$$

$$P(bar) = \frac{\Delta H - T\Delta S}{-\Delta V} + \frac{RTlnK_{eq}}{-\Delta V} + \frac{RTlnK_{\gamma}}{-\Delta V} + 1.0 \quad (4.20)$$

where

$$K_{eq} = \frac{(X_{An})^3}{(X_{Grs})^3} \quad (4.21)$$

$$K_{\gamma} = \frac{(a_{An})^3}{(a_{Grs})^3} \quad (4.22)$$

and ΔH, ΔS, ΔV are changes in molar enthalpy, entropy, and volume for the reaction, R = 8.31441 J/(mol*K). (Holdaway 2001). Two different values for thermodynamic parameters are required, depending on which aluminosilicate polymorph (kyanite or sillimanite) is in equilibrium with the garnet and plagioclase (Ghent 1976; Holdaway 2001). The calculations for all these parameters were completed on a spreadsheet provided by Rebecca Jamieson, adapted from Holdaway (2000).

Nominal uncertainty used for this method is ± 0.8 kbar (Holdaway 2001).

Uncertainties:

The largest assumption in thermobarometry is that the mineral compositions used represent an equilibrium assemblage. Where mineral compositions vary in a sample, the mineral assemblage may be at equilibrium but the specific compositions used for thermobarometry might not be. Based on petrographic studies, most rocks in this study display evidence of minor retrograde and/or alteration reactions. Because the samples can be analyzed in situ, visible retrograde

reactions can be avoided, however retrogression can affect the compositions beyond the area of retrograde minerals. Areas that lack visible replacement textures and have sharp grain boundaries were targeted. However, in these polycylic rocks, some minerals, notably garnet, may have inherited their chemical compositions from a previous metamorphic event. As previously mentioned, biotite is commonly affected by post-peak metamorphism cation exchange with garnet, so analysis points in biotite and garnet are measured where the two minerals are not in contact with one another.

For thermobarometers involving Fe^{2+}end-members, uncertainty arises because Fe^{3+} is not known and may be significant. $Fe^{2+} = Fe_{total}$ was assumed in this study because all the thermobarometers used were calibrated on the same assumption.

The results from the GASP barometer can be checked by comparing calculated P-T conditions against the known position of the kyanite-sillimanite phase boundary.

4.3.2 Analytical Procedure

In each polished section, an area was chosen for analysis based on mineral assemblage and textures. The areas chosen contained all the minerals included in each thermometer and barometer, with little or no evidence for retrogression. Grains susceptible to reactions were avoided where possible. For example, resorbed garnets or garnets with plagioclase rims were avoided, as well as biotite in contact with garnet.

The JEOL 8200 Superprobe at Dalhousie University was used to take backscatter (BSE) images of selected areas to reveal textural details, and WDS X-ray chemical maps of the garnet and amphibole crystals were made to reveal any internal structure or zoning (Figure 4.3). Using the chemical maps and BSE images to target chemically homogeneous locations in each mineral, 10-15 points from each mineral were analyzed for major elements in WDS mode, at 15 kV and 20 na. A single point per mineral was chosen for calculations based on the best major element total.

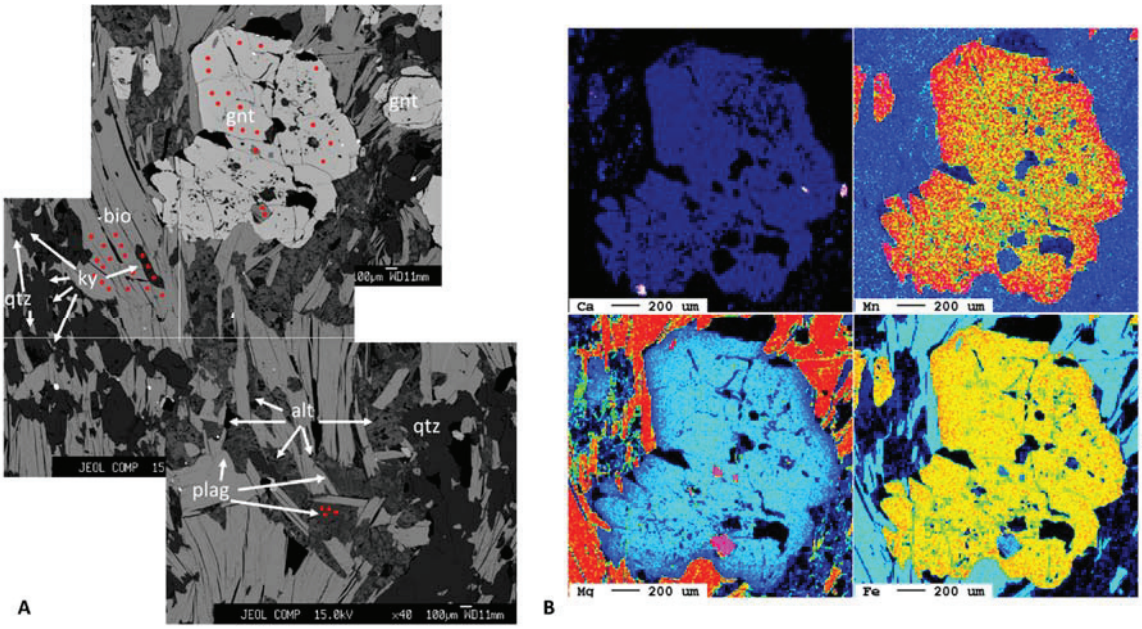

Figure 4.3: An example of the BSE images and chemical maps from sample 14SV542 used for choosing analysis points. A) Composite BSE image of the analyzed area with analysis points marked in red. B) WDS chemical map of the garnet shown in upper part of BSE image. Reds and yellows indicate high concentrations and blue and greens indicate low. Increased Mn and decreased Mg and Fe at grain boundaries is attributed to retrograde exchange with adjacent biotite. BSE images with analysis points and chemical maps for all samples are in Appendix B.3.

4.3.3 Results

14SV095B:

Sample 14SV095B is a medium-coarse-grained migmatitic garnet amphibolite within a metasedimentary package exposed in a roadcut near the southern border of the map area (Figure 4.1). The location is significant because it lies within the WAHSZ (described in section 3.3.2). Obtaining P-T conditions across the WAHSZ offers a potential test of the thrust interpretation for this structure (section 3.5.2). A higher PT result for this sample relative to samples on the west of the WAHSZ would suggest the east-over-west thrust interpretation is correct; however, similar results could simply mean metamorphism occurred after thrusting.

The mafic body is approximately 10 m long and cut by a large plagioclase + quartz pegmatite with tourmaline (Figure 4.5 A). Smaller (50-60 cm) pods and boudinaged layers of garnet amphibolite are oriented parallel to the metasedimentary rock layers (Figure 4.5 E). The mesosome is mostly hornblende + garnet + biotite + plagioclase + quartz. Composition of the mesosome does not vary noticeably across the outcrop. The crystals are typically xenoblastic to

subidioblastic, equant (apart from biotite), and equigranular with and average crystal size of 1-2 mm. Many of the garnet crystals have plagioclase reaction rims (Figure 4.4 B) and contain inclusions of quartz, biotite and ilmenite. Leucosomes, concentrated within the main body, contain mostly plagioclase (oligoclase to andesine) + quartz, and cm-scale euhedral titanite crystals (Figure 4.5 F). Leucosomes, which vary from absent to stromatic to net-structured, make up < 10 % of the rock volume (Figure 4.5 C and D). There are no melt films or other evidence of partial melt in the samples analyzed. It is unclear if the leucosomes were derived from melting of the amphibolite or if they were injected from surround rocks.

To avoid retrogression induced by the tourmaline-bearing vein, the sample analyzed was taken several metres away from the vein.

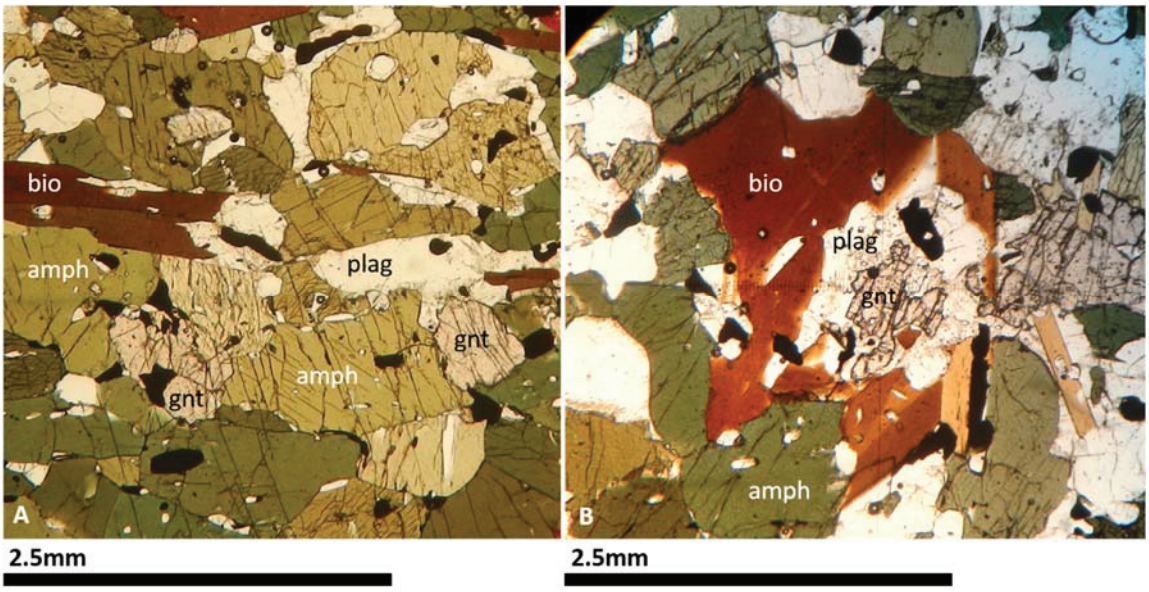

Figure 4.4: Sample 14SV095B in thin section. A) Typical texture used for thermobarometry analysis. Garnets are fresh and not in contact with biotite. B) Partially resorbed garnet indicating a decompression reaction - not suitable for thermobarometry analysis.

Data used for the calculations are listed in Table 4.1. Thermometer and barometer combinations were chosen based on mineral assemblages present and criteria listed in source papers (Graham and Powell 1984; Kohn and Spear 1990; Holdaway 2000). Results are listed in Table 4.3.

Both T and P estimates from 14SV095Bi and 14SV 095Bii are consistent within error (± 25°C; ± 0.5 kbar).

Figure 4.5: Field images of 14SV095B. A) Roadcut showing large, vertical tourmaline-bearing quartz and feldspar vein near the center of the garnet amphibolite body. B) Contact of the garnet amphibolite (bottom) with interlayered metasedimentary unit and orthogneiss. The metasedimentary rocks are rusty and yellow on the weathered surface while the orthogneiss is grey. C) Variation in leucosome density and style within 14SV095B, ranging from net-structured to stromatic or absent. D) Stromatic leucosomes. E) Boudinaged mafic layer within psammite. F) Euhedral titanite crystals within a quartz-feldspar leucosome.

Table 4.2: Major element data of thermobarometry analysis points used for sample 14SV095.

	14SV095Bi				14SV095Bii			
No.	**25**	**69**	**73**	**95**	**118**	**128**	**139**	**178**
	plag 10	**amph 15**	**bio 4**	**gnt 5**	**plag 10**	**amph 2**	**bio 1**	**gnt 12**
oxides(wt%):								
SiO2	60.721	41.025	36.34	37.326	58.774	41.5	36.077	37.451
TiO2	0	1.403	3.286	0.049	0	1.39	3.66	0
Al2O3	24.739	13.938	16.197	20.869	26.021	14.676	15.93	21.08
Cr2O3	0	0.066	0.08	0.05	0	0.024	0.001	0
FeO	0.034	18.123	18.493	26.445	0.002	17.808	17.93	26.716
MnO	0	0.189	0.033	1.586	0	0.206	0.063	1.357
MgO	0	8.919	11.901	4.568	0	9.08	11.922	4.82
CaO	6.241	11.39	0.218	8.459	7.61	11.46	0.027	8.172
Na2O	8.165	1.808	0.312	0.003	7.414	1.888	0.287	0
K2O	0.172	1.189	8.604	0.028	0.07	1.092	8.796	0
Total	100.072	98.05	95.464	99.383	99.891	99.124	94.693	99.596
cations(pfu):								
Si	2.7	6.1985	5.4912	2.9652	2.628	6.1778	5.4912	2.964
Ti	0	0.1587	0.374	0.0024	0	0.1564	0.418	0
Al	1.2968	2.4817	2.8842	1.9548	1.3712	2.576	2.8578	1.9668
Cr	0	0.0069	0.0088	0.0036	0	0.0023	0	0
Fe	0.0016	2.2908	2.3364	1.7568	0	2.2172	2.2814	1.7688
Mn	0	0.0253	0.0044	0.1068	0	0.0253	0.0088	0.0912
Mg	0	2.0102	2.6796	0.5412	0	2.0148	2.7038	0.5688
Ca	0.2976	1.8446	0.0352	0.72	0.3648	1.8285	0.0044	0.6936
Na	0.704	0.529	0.0924	0	0.6424	0.5451	0.0836	0
K	0.0096	0.23	1.6588	0.0024	0.004	0.207	1.7072	0
Total	5.0096	15.7757	15.565	8.0532	5.0104	15.7504	15.5562	8.0532

Cations pfu were calculated using the following values of oxygen pfu: 8 for plagioclase, 23 for amphibole, 11 for biotite, and 12 for garnet. For GPHQ calculations, biotite cations pfu values use 22 oxygen pfu.

Table 4.3: Pressure and temperature results for garnet amphibolite sample 14SV095B using different thermometers and barometers.

Sample	GB T(°C)	GH T(°C)	GB-GPHQ P (kbars)	GH-GPHQ P (kbars)
14SV095Bi	773 ± 25	774 ± 25	10.9 ± 0.5	11.2 ± 0.5
14SV095Bii	774 ± 25	769 ± 25	9.9 ± 0.5	10.2 ± 0.5

14SV432:

Sample 14SV432 is part of a thin (2-3m thick) package of metasedimentary rocks exposed in a large roadside outcrop of dioritic diatexite on Hwy 535 (Appendix A.2). The metasedimentary

rocks range in composition from psammitic to pelitic, with compositional layering on a mm- to cm-scale. The pelite was chosen for analysis because it contains the necessary mineral assemblage for GB, GBPQ and GASP thermobarometry. The sample is quartz-rich with abundant muscovite and biotite, fibrous sillimanite masses, and garnet porphyroblasts. Mica crystals define a foliation and sillimanite crystals appear to grow along that foliation (Figure 4.6 A). Garnets lack inclusion trails, or any other kinematic indicators. Inclusions are mostly quartz, biotite and rutile. Plagioclase crystals usually have a mottled texture where sericite replaces the plagioclase (Figure 4.6 B); fresh plagioclase was targeted for thermobarometry. Biotite is variably replaced by chlorite; analyses were taken from fresh grains lacking visible alteration. Although this sample displays some retrogression, it was chosen for analysis because it is the only known pelite west of the WAHSZ supracrustal package that contains the necessary mineral assemblage.

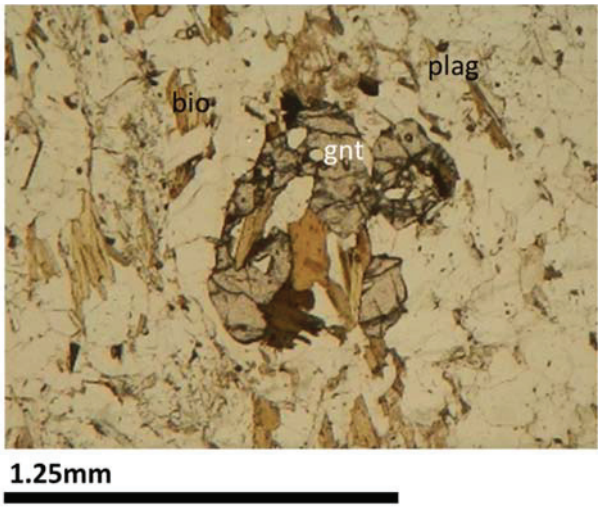

Figure 4.6: Thin section 14SV432A in PPL displaying the area chosen for analysis. bio = biotite. plag = plagioclase. gnt = garnet.

Major element compositions used in the thermobarometers are listed in Table 4.4, and results are listed in Table 4.5.

For sample 14SV432A, both GB-GBPQ and GB-GASP yield similar results. The mineral assemblage contains only sillimanite, so GASP was calculated using sillimanite parameters. When plotted on the Al_2SiO_5 phase diagram, sample 14SV432A lies within the kyanite field, within error of the sillimanite-kyanite boundary (see discussion section 4.3.4).

Table 4.4: Major element data of thermobarometry analysis points used for sample 14SV432A.

	14SV432A		
No.	**195**	**215**	**228**
	plag 8	**bio 8**	**gnt 5**
oxides (wt%):			
SiO2	63.311	35.534	36.183
TiO2	0	3.303	0.026
Al2O3	22.896	17.988	20.855
Cr2O3	0.013	0.145	0.044
FeO	0.02	19.153	27.462
MnO	0	0.253	9.799
MgO	0	9.523	3.388
CaO	4.118	0.029	1.545
Na2O	9.442	0.158	0.028
K2O	0.165	10.049	0.013
Total	99.965	96.135	99.343
cations (pfu):			
Si	2.8016	5.39	2.9472
Ti	0	0.3762	0.0012
Al	1.1944	3.2164	2.0016
Cr	0.0008	0.0176	0.0024
Fe	0.0008	2.4288	1.8708
Mn	0	0.033	0.6756
Mg	0	2.1538	0.4116
Ca	0.1952	0.0044	0.1344
Na	0.8104	0.0462	0.0048
K	0.0096	1.9448	0.0012
Total	5.0128	15.6112	8.0508

Cations pfu were calculated using the following values of oxygen pfu: 8 for plagioclase, 23 for amphibole, 11 for biotite, and 12 for garnet. Analysis points are mapped in Appendix B.3.

Table 4.5: Pressure and temperature results for pelitic sample 14SV432A using GB thermometer and two different barometers.

	GB-GBPQ		GB-GASP (sil)	
Sample	**T°C**	**P(kbars)**	**T°C**	**P(kbars)**
432A	656 ± 25	7.3 ± 1	656 ± 25	7.2 ± 0.8

14SV542 (N13-029):

This sample crops out along the shoreline near the big cut on the West Arm (Figure 4.1) for approximately 10 metres along strike. The sample is part of a small sliver within a package of supracrustal rocks in the WAHSZ.

14SV542 is a grey-brown to dark grey-brown pelitic paragneiss, containing biotite + quartz + plagioclase + K-feldspar + muscovite + garnet + sillimanite + kyanite + rutile. The sample is very biotite-rich (approximately 65 %) and contains a significant amount of sillimanite and kyanite (approximately 1-2 % each). It has a fine-grained (average 0.5 mm) sugary or granular texture, with cm-scale banding defined by biotite-rich layers *vs* feldspar + quartz-rich layers. There are some thin streaks of very fine grained muscovite, sillimanite, rutile, and opaque. Biotite orientation and compositional layering define the main foliation, which is weakly folded into poorly developed crenulations. A few thin (< 10 mm) quartz- and feldspar-dominant stromatic leucosomes with very thin melanosomes along their edges make up less than 3% of the rock volume.

Sillimanite crystals are typically unaltered and form prismatic or fibrous crystals. Fibrous masses of sillimanite are concentrated in biotite-rich layers. These masses vary in size from microscopic to clearly visible in hand sample (up to 1.5 centimetres) across the outcrop. Kyanite is microscopic and more abundant than sillimanite. As discussed in Chapter 3, the kyanite in this sample is interpreted to have formed during the formation of the main foliation, broken parallel to foliation and then folded during formation of weak crenulations. Sillimanite crystallized after the main foliation formed, but before or during the formation of crenulations.

Large garnet porphyroblasts are abundant and typically wrapped by the mica fabric and fine-grained matrix crystals (Figure 4.7). Garnets are typically inclusion-rich, containing quartz, biotite, plagioclase, rutile and accessory phases. Some garnets are broken, while others are intact, and some garnets are wrapped by the mica fabric while others are not; there are no inclusion trails within the garnet. Rutile inclusions within garnet suggest the garnet grew at a higher metamorphic grade than the current metamorphic assemblage. Chemical maps of garnets used for thermobarometry (Figure 4.3, Appendix B.3) do not exhibit any zoning. However, based on relationships with the fabric, garnets may have different ages from one another; most garnets grew before or during the formation of the main foliation, and before the crenulation fabrics.

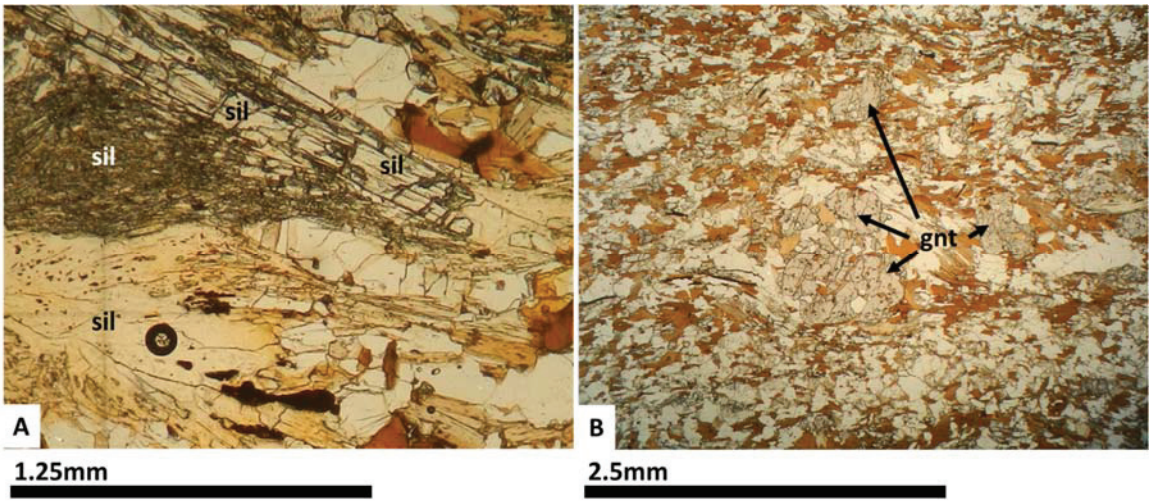

Figure 4.7: Sample 14SV542 in PPL. A) Fibrous and prismatic sillimanite. B) Garnet porphyroblasts with biotite and quartz inclusions.

Similar to sample 14SV432, most of the plagioclase crystals in 14SV542 have a mottled or dusty texture caused by sericite alteration; these grains were avoided during analysis.

Data used to calculate the pressure and temperature regime of sample 14SV542 and the results are listed in Table 4.6 and Table 4.7.

Sample 14SV542 contains both sillimanite and kyanite, so results from both sillimanite and kyanite parameters are listed. Regardless of which parameters or barometer is used, results from both samples 14SV542A and 14SV542B plot within error of the kyanite-sillimanite phase boundary (Figure 4.8). Because there are higher temperature mineral inclusions in this sample, such as rutile, these results likely represent a retrograde metamorphic reaction, or the last of two or more metamorphic events. Because this sample, and 14SV432, have polymetamorphic histories, the results are likely to have been affected by inherited compositions.

Table 4.6: Major element data of thermobarometry analysis points used for sample 14SV542.

	14SV542A			14SV542B		
No.	**256**	**266**	**291**	**306**	**319**	**333**
	plag 12	**bio 7**	**gnt 8**	**plag 5**	**bio 1**	**gnt 3**
oxides (wt%):						
SiO2	61.25	36.05	36.717	61.769	36.111	36.676
TiO2	0	2.62	0	0.005	2.482	0.055
Al2O3	24.269	19.877	21.046	23.864	19.744	21.102
Cr2O3	0	0.046	0.028	0.003	0.149	0.073
FeO	0.053	17.269	33.143	0.019	17.571	34.604
MnO	0.008	0.028	1.354	0.004	0.068	1.739
MgO	0.004	10.35	4.546	0.001	10.177	3.671
CaO	5.711	0.022	2.312	5.294	0.025	1.794
Na2O	8.553	0.134	0.004	8.864	0.146	0.016
K2O	0.148	9.749	0.023	0.22	9.81	0.029
Total	99.996	96.145	99.173	100.043	96.283	99.759
cation (pfu):						
Si	2.7224	5.3768	2.9604	2.7424	5.39	2.9604
Ti	0	0.2948	0	0	0.2794	0.0036
Al	1.2712	3.4936	2.0004	1.2488	3.4738	2.0076
Cr	0	0.0044	0.0012	0	0.0176	0.0048
Fe	0.0016	2.1538	2.2356	0.0008	2.1934	2.3364
Mn	0	0.0044	0.0924	0	0.0088	0.1188
Mg	0	2.3012	0.546	0	2.2638	0.4416
Ca	0.272	0.0044	0.1992	0.252	0.0044	0.1548
Na	0.7368	0.0396	0.0012	0.7632	0.0418	0.0024
K	0.008	1.8546	0.0024	0.0128	1.8678	0.0024
Total	5.012	15.5276	8.0388	5.02	15.5408	8.0328

Cations pfu were calculated using the following values of oxygen pfu: 8 for plagioclase, 23 for amphibole, 11 for biotite, and 12 for garnet. Analysis points are mapped in Appendix B.3.

Table 4.7: Thermobarometry results for pelitic sample 14SV542 using GB thermometer, and GBPQ and GASP barometers.

	GB-GBPQ		GB-GASP (sil)		GB-GASP (ky)	
Sample	**T°C**	**P(kbars)**	**T°C**	**P(kbars)**	**T°C**	**P(kbars)**
542A	632 ± 25	6.9 ± 1	632 ± 25	6.8 ± 0.8	632 ± 25	6.7 ± 0.8
542B	605 ± 25	5.0 ± 1	606 ± 25	5.5 ± 0.8	606 ± 25	5.6 ± 0.8

4.4 Discussion and Conclusions

The field relations and petrography suggest that the rocks in the Nepewassi domain have been subjected to at least two ductile deformation phases. Microstructures in sample 14SV542

indicate there may have been foliation-parallel extension between two events. Recrystallization textures in quartzofeldspathic gneisses suggest the last deformation event happened at relatively low temperature and/or a high strain rates compared to an earlier, coarse-grain forming, high temperature event.

Many of the rocks in the Nepewassi are migmatites, indicating a high temperature regime (> 700°C). Plutonic rocks, particularly the West Bay batholith, are more strongly migmatitic than their country rocks. This is potentially because the country rocks were metamorphosed, dehydrated, and/or partially melted prior to the emplacement of the plutonic bodies. The younger plutonic rocks may have been fluid rich during emplacement and were more easily melted.

Based on observed mineral assemblages, rocks have been metamorphosed to amphibolite facies, with minor retrogression to greenschist facies. Some dioritic and gabbroic gneisses contain evidence of granulite facies metamorphism (metamorphic pyroxene), suggesting at least some of the rocks in the Nepewassi domain are retrograde amphibolite facies after granulite facies. The timing of granulite facies metamorphism is unconstrained. Based on thermobarometry, two pelite samples, one west of the WAHSZ and one within it (Figure 4.1) are both amphibolite facies, and the garnet amphibolite sample, near the east edge of the WAHSZ is upper amphibolite facies. Results are plotted in Figure 4.8. These results are consistent with other rocks in the Central Gneiss Belt (Rivers et al. 2012), apart from sample 14SV542B, which yields lower than expected results. For this sample, the pressure results from GB-GBPQ and GB-GASP are consistent within error, but inconsistent relative to results from the other pelite samples. This analysis was potentially affected by retrograde composition, because GB-GBPQ yielded a lower result than GB-GASP (Table 4.7).

The garnet amphibolite, 14SV095, yields a higher P-T estimate than either of the pelite samples. This result is consistent with the hypothesis that rocks on the east side of the WAHSZ were thrust over those on the west side (Figure 4.7), although the results could simply mean the pelite samples were more susceptible to retrograde metamorphism than the garnet amphibolite. Assuming the WAHSZ is a west-directed thrust, the West Bay batholith, which crops out almost entirely to the east of the WAHSZ, may have been subjected to higher P-T conditions than its less migmatitic counterpart, the West Phase, which crops out west of the WAHSZ. This suggests that the West Bay batholith and West Phase may be unrelated plutons.

The pelite samples all yield middle amphibolite facies results. Sample 14SV432 contains only one Al_2SiO_5 polymorph, sillimanite, and does not have textural evidence for a previous metamorphic event. Sample 14SV542 contains both kyanite and sillimanite, with textures suggesting that kyanite may have formed earlier (discussed in Chapter 3). Results from this sample are the same whether kyanite or sillimanite parameters are used (Table 4.7), so they likely formed one after the other during one (most recent) metamorphic event, or they both represent cooling and/or decompression during retrograde metamorphism.

Geochronological studies of accessory phases within the garnet (Chapter 5) will provide information about the age of metamorphism studied in this chapter.

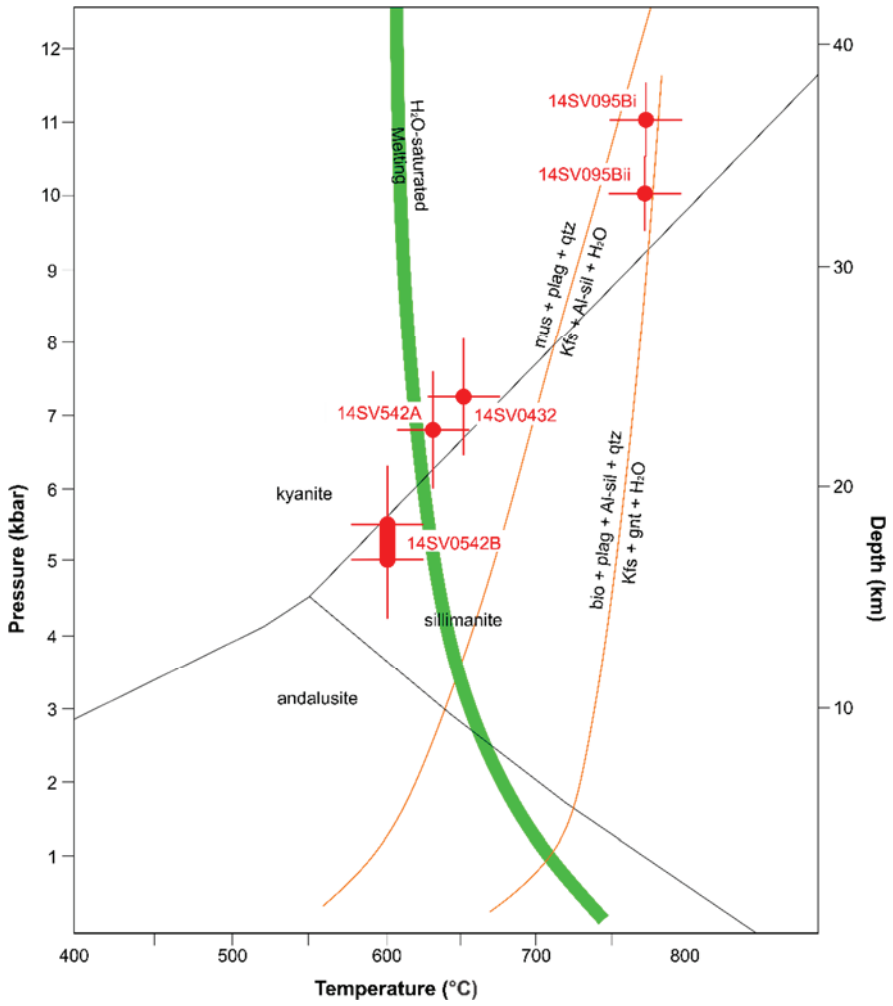

Figure 4.8: Simplified P-T phase diagram with results and uncertainties (red) superimposed. Diagram includes Al_2SiO_5 phase diagram (black) (Pattison 1992), H_2O saturated solidus (green) and muscovite and biotite dehydration reaction boundaries (orange)(Winter 2001).

CHAPTER 5

GEOCHRONOLOGY

5.1 Introduction

Studying the geochronology of an area adds quantitative constraints to its tectonometamorphic history. In the Nepewassi domain, very few geochronological studies have been done, so zircon and monazite chronology was studied to shed light on the tectonic evolution of this area. A detailed list of previous geochronological data from the Nepewassi and neighbouring domains can be found in Easton (2014).

The overall goal is to determine the age of formation and metamorphism of samples from the Nepewassi map area and, if possible, determine the timing of structures. Three specific problems were addressed. 1) Tonalitic grey gneisses, which have plutonic protoliths, were analyzed to determine if they are the same as the Archean rocks in the Northern subdomain, as is assumed based on field relations. 2) Provenance of metasedimentary rocks within the map area was determined to test the hypothesis that Nepewassi sediments were deposited on a Paleoproterozoic (Huronian) passive margin on the southern edge of the Superior craton. 3) Metamorphic ages were determined from several rock units in order to constrain the times of metamorphism and deformation, and therefore which orogenic events affected the Nepewassi domain.

Methods used for this study were zircon geochronology, using laser ablation inductively coupled plasma mass spectroscopy (LA-ICP-MS), and monazite geochronology, using electron probe microanalysis (EPMA). Dates from igneous zircons in the tonalitic grey gneisses yield crystallization ages for their igneous protoliths; dates from detrital zircon populations in the metasedimentary rocks yield minimum depositional ages and constrain possible source areas, and in situ dating of metamorphic monazite can yield information on when monazite and the associated mineral assemblage formed.

5.1.1 Previous Geochronology:

Before this M.Sc. thesis study, no ages had been determined from rocks within the map area; however, outside the map area, ages are known for a number of rock units. In the Cosby subdomain, the Cosby pluton has an age of 1420 Ma (Figure 5.1, Lumbers 1975), and the French

River granite have igneous ages of ca. 1700 Ma and 1689 ± 16 Ma (Krogh and Davis 1969, 1972). There are two metasedimentary units located west of the Cosby pluton, the French River paragneiss and quartzite. The French River paragneiss has a single detrital population of 1744 ± 11 Ma, and the French River quartzite has only Archean zircons and metamorphic monazites that yield 1062 ± 15 Ma (Krogh 1989). Leucogabbro and anorthositic bodies in the Southern subdomain, the Mercer and St. Charles anorthosites, have igneous U/Pb TIMS and SHRIMP zircon ages, respectively, of 1245 ± 48 Ma and 1233 ± 100 Ma (Prevec 1992, 2004). In the Northern subdomain, tonalitic and granodioritic gneisses have Archean igneous ages ranging from 2678 to 2683 Ma (Figure 5.1), with lower intercepts that represent metamorphic ages of 975 to 996 Ma (Chen et al. 1995). The Archean ages from the Northern subdomain are similar to igneous ages in the Laurentian craton, near the Grenville Front Tectonic Zone (GFTZ) (Card 1990).

The West Bay batholith and mafic plutonic rocks in the Southern subdomain are compositionally similar to, show similar relative age relationships, and have similar potential magma mingling textures to metaplutonic rocks in the Killarney Magmatic Belt and the Wanapitei complex (Easton 2014). The Wanapitei magmatic complex, located northwest of the Nepewassi domain in the Grenville Front Tectonic Zone just south of the Grenville Front Boundary Fault, has ages ranging from 1694 to 1746 Ma (Prevec 1992, 1995; Easton et al. 1999; Rousell et al. 2012). The Killarney Magmatic Belt, located due west of the Nepewassi domain, has igneous ages ranging from 1704 to 1749 Ma, with a younger set of ages from 1429 to 1467 Ma (Davidson and van Breemen 1988; Davidson et al. 1992; Davidson and van Breeman 1994; Krogh 1994; Raharimahefa et al. 2014). All of the geochronology data are summarized in Table 16.1 of Easton (2014).

5.2 Zircon Geochronology

5.2.1 Method: Laser Ablation Inductively Coupled Plasma Mass Spectrometry

Dating of zircon grains has been the main source of geochronological data for the past half century (Corfu 2012). Many different methods for collecting isotopic data have been developed since the 1950s, but the method used for this study, laser ablation inductively coupled plasma mas spectroscopy (LA-ICP-MS), was developed in the early 1990s (Corfu 2012). LA-ICP-MS provides less precise results than other U-Pb methods (such as isotope dilution-thermal ionization mass spectrometry (ID TIMS) but it can analyze large populations of data, making it ideal for the study of detrital zircons.

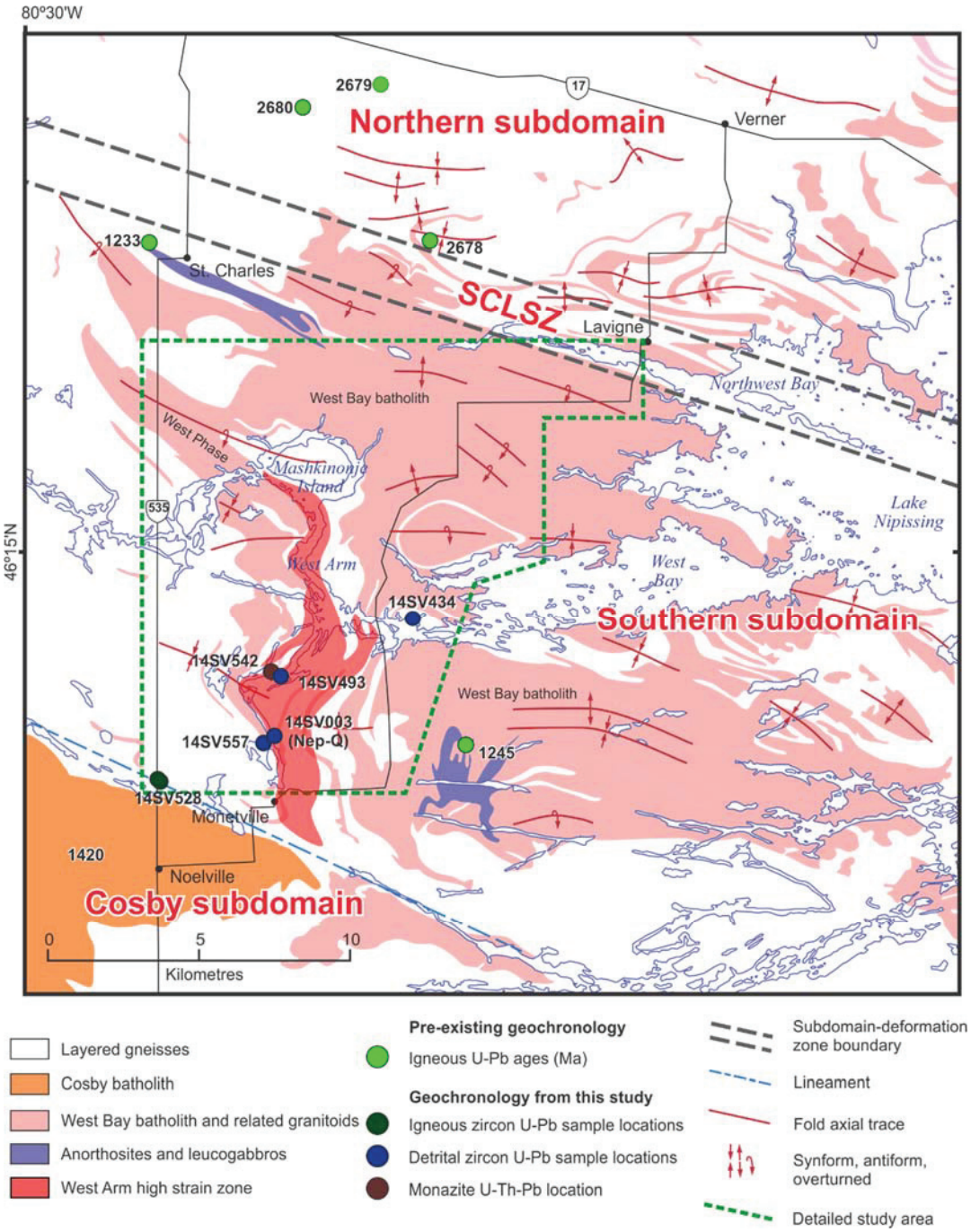

Figure 5.1: Simplified geological map of the study area with zircon and monazite geochronology locations from this study and ages from previous geochronological studies. Pre-existing U/Pb TIMS and SHRIMP zircon geochronology (igneous ages), displayed in Ma, are from Chen et al. (1995) in the Northern subdomain and Prevec (1992, 1993, 2004) in the Southern subdomain. The igneous age of the Cosby batholith is from Lumbers (1975), but the sample location is unknown.

LA-ICP-MS analysis can be done in situ or on grain mounts of zircon separates. For the present study, which was done using separates, analysis begins with the extraction of zircon grains from the sample. At Dalhousie University, samples were crushed and separated using a Wilfley table. Water flowing over the crushed sample on a pulsating, ridged Wilfley table separates the crystals based on density. After that, crystals are separated based on their variable magnetic properties using a Franz magnetic separator. The last stage of separation involves heavy liquid separation, which extracts targeted grains based on density. The separates were sent to the Geological Survey of Norway (NGU) where zircons were separated from other minerals by Trond Slagstad using a microscope. He mounted the grains in epoxy, polished them, and took cathodoluminescence (CL) images of them using a scanning electron microscope (SEM).

At the NGU, isotopic analyses were carried out on an ELEMENT XR single-collector, high-resolution ICP–MS, coupled to a UP193–FX 193 nm short-pulse excimer laser ablation system manufactured by New Wave Research. Using a spot size of 15 mm, a repetition rate of 10 Hz and an energy corresponding to a fluence of 4–5 J/cm^2, the laser was set to ablate single lines. Each analysis included 30 s of background measurement followed by 30 s of ablation. The masses 202, 204, 206–208, 232 and 238 were measured. The reference material GJ–1 (Jackson et al. 2004) was used for correction of isotopic ratios, whereas 91500 (Wiedenbeck et al. 1995) and an in-house standard (OS–99–14; 1797 ± 3 Ma; Skår 2002) were used to check precision and accuracy. The data were not corrected for common lead, but monitoring of the signal for 204 allowed exclusion of data affected by 204 isotope from further calculations. The data were reduced using the GLITTER® software (Van Achterbergh et al. 2001).

Isotopic ratios are used to calculate the age of sample. Uranium (parent) is radioactive and will decay to lead (daughter) over time; half of the initial parent isotope will become daughter isotopes in a half-life ($t_{1/2}$). Ages can be calculated using two different decay systems, $^{207}Pb/^{235}U$ and $^{206}Pb/^{238}U$, assuming the system is closed (no loss of lead). The following equations are used to calculate the age based on the U/Pb ratios.

$$D^*/P = e^{\lambda t} - 1 \text{ (decay equation)}$$

$$t = ln(D^*/P + 1) / \lambda \text{ (age equation)}$$

where D*/P is the ratio of daughter isotopes to parent isotopes, t is time, and λ is the decay constant ($\lambda = ln2/ t_{1/2}$). Decay constants used are 1.55125E-10 with 2 σ uncertainty 0.107% for ^{238}U and 9.8485E-10 with 2 σ uncertainty 0.136% for ^{235}U (Jaffey et al. 1971).

Ratios of $^{207}Pb/^{235}U$ and $^{206}Pb/^{238}U$ are plotted on concordia diagrams. A concordant age, which plots on the concordia curve, means that the two age calculations (from $^{207}Pb/^{235}U$ and $^{206}Pb/^{238}U$) agree within error. Concordant ages generally mean that the crystals have remained geochemically undisturbed since their formation. If an age plots off the concordia curve, it is discordant; a discordant age may result from Pb loss since original crystallization, interference of age domains in the zircon, intermediate daughter product disequilibrium, or uncertainties from correction for initial Pb (Schoene 2014). An array of discordant data may define a line referred to as discordia. In many cases, the upper intercept between a concordia curve and a discordia line can be interpreted as the age of igneous crystallization and the lower intercept as the time of Pb loss or metamorphic overgrowth (Schoene 2014). A concordia age is the most-probable age for a weighted mean (or data point) where the true location of the mean is assumed to fall precisely on the concordia curve. This calculation makes optimal use of all the radiogenic Pb/U ratios, meaning it will be slightly to significantly more precise than any single U/Pb age (Ludwig 2008).

For detrital populations, data are also plotted using a probability density graph. For this plot, calculated ages are plotted by proportion relative to the data set. The peaks on the diagram represent the main age populations in the detrital zircon sample, which can be readily compared with data from possible source areas or correlative units.

When using this method, the analyzed zircon population is assumed to represent all the zircons in the rock, and the youngest detrital zircon is used as maximum limit for deposition age. However, randomly sampling host sediments is unlikely to yield an exact representation of the age distribution of the zircons, and using the youngest zircon as a limit is statistically unreliable (Andersen 2005), as it is possible for the rocks to have been deposited significantly later than the youngest zircon.

For metasedimentary rocks, the morphology of zircons must be studied to separate detrital ages from metamorphic ages; zircons that are concentrically zoned are interpreted as igneous in origin, and are now detrital. In this study, homogeneous, typically dark, zircons, with relatively low Th/U ratios are interpreted as metamorphic.

Four samples were chosen for detrital zircon studies and two samples were chosen to determine igneous crystallization ages. The igneous samples are from tonalitic and granodioritic grey gneisses that resemble gneisses from the Northern subdomain, which are known to be Archean. The detrital samples are quartzites that contain sufficient accessory zircon for analysis, roughly 100 grains (Andersen 2005). Sample locations are shown in Figure 5.1.

5.2.2 Tonalitic grey gneisses

Two samples of tonalitic grey gneiss (unit Tn), NEP-S-1 and NEP-S-3, were chosen for zircon geochronology. The samples were taken from station 14SV528 along highway 535, north of Noelville (Figure 5.1), and were chosen based on their resemblance to Archean gneisses in the Northern subdomain.

14SV528 - NEP-S-1:

This sample is a medium-grained, purple-grey tonalitic gneiss with coarse-grained granitic veins. The rock consists mostly of plagioclase + quartz with 5 to 10 volume % biotite. The biotite is not well aligned. This sample is typically medium-grained with fine subgrains. Quartz boundaries are interlocking and sutured and quartz crystals have undulose extinction (Figure 5.2). There is some myrmekite texture present. The coarse granitic veins are composed of microcline, plagioclase and quartz. Feldspar crystals have fine grained, dusty alteration.

Dynamic recrystallization of the quartz and feldspar grains indicates there has been at least one episode of ductile deformation. Myrmekite, which is forms from grain-scale diffusion between quartz and feldspar, is common in medium-grade, ductile, deformed rocks. Alteration indicates that lower greenschist facies retrograde reactions partially overprint amphibolite facies rocks.

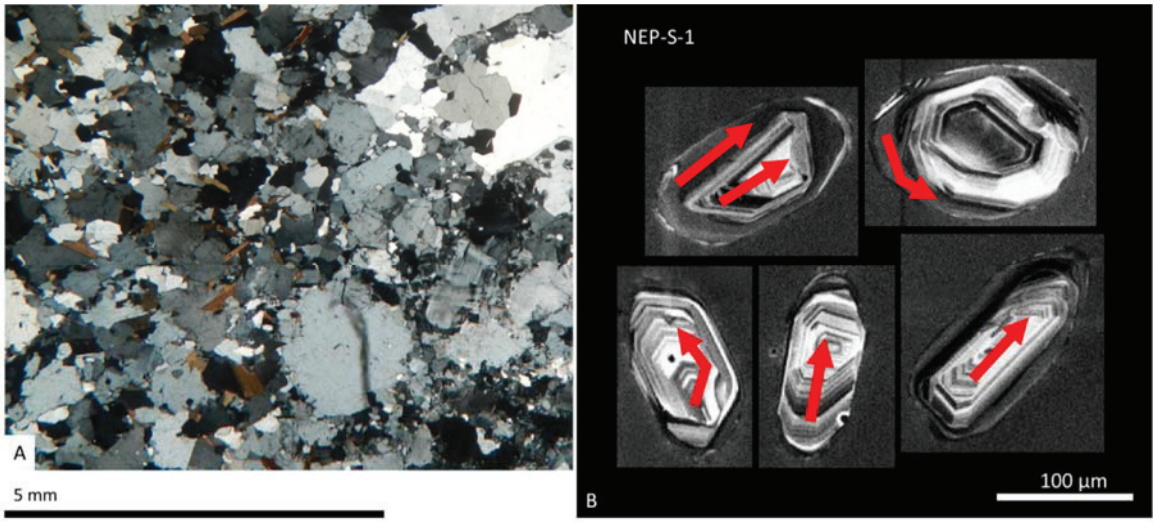

Figure 5.2: Grey gneiss geochronology sample NEP-S-1. A) Typical texture of sample NEP-S-1 in XPL on the left half of the image, and a relatively coarse granitic vein on the right half. B) Cathodoluminescence (CL) images of zircons; arrows represent laser ablation lines followed during LA-ICP-MS analysis. Most lines targeted zoned cores, but some lines targeted rims/overgrowths, probably of metamorphic origin (e.g., upper right).

Accessory zircon is found as inclusions in quartz, feldspar and biotite. They are concentrically zoned. Some zircons have homogeneous overgrowths/rims which are interpreted as metamorphic in origin (Figure 5.2).

14SV528 - NEP-S-3:

The hand sample is fine- to medium-grained and light grey with low mafic content. The sample is composed mostly of plagioclase + quartz, but also contains K-feldspar + epidote + pyrite. Biotite is a khaki dark green in PPL, and is locally replaced by epidote (Figure 5.3). A lineation is defined by streaks of red-stained plagioclase and biotite. In thin section, textures are nearly identical to NEP-S-1; the biotite is weakly aligned, quartz boundaries are slightly embayed and sutured, quartz crystals have undulose extinction and there is some myrmekite. Grain size varies slightly, but the sample does not have a strong bimodal texture.

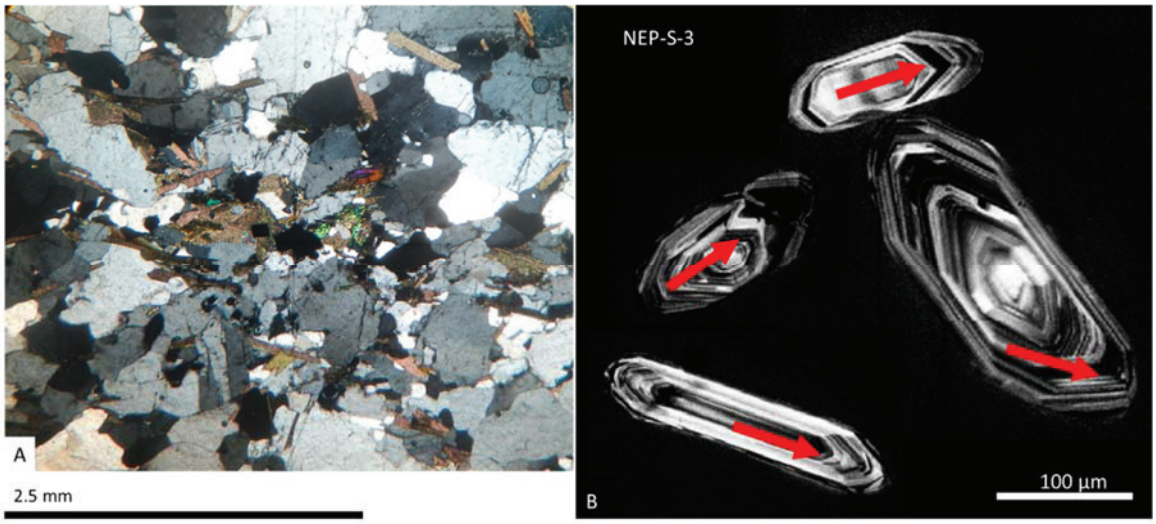

Figure 5.3: Grey gneiss geochronology sample NEP-S-3. A) Sample NEP-S-3 in XPL showing a cluster of biotite, epidote and pyrite. B) Cathodoluminescence (CL) images of zircons in sample NEP-S-3; arrows represent laser ablation lines followed during LA-ICP-MS analysis.

Zircons in this sample are inclusions in quartz, feldspar and biotite. They are concentrically zoned and some appear to have very thin overgrowths, none of which are large enough to analyze.

Results:

Ages were calculated for sixteen analysis lines from each sample, and plotted on concordia diagrams using Isoplot 4.15. Table 5.1 summarizes the results, and all the LA-ICP-MS data are included in Appendix C. Figure 5.4 displays all data on concordia diagrams.

Table 5.1. Summary of age results for 14SV528 tonalitic and granodioritic gneisses.

		NEP-S-1	NEP-S-3
concordia (all data)	upper intercept	2701 ± 36	2697 ± 21
	lower intercept	1704 ± 560	1136 ± 410
concordia age (data <2% discordant)		2684.4 ± 13	2685.6 ± 3.8
weighted average age (all data)		2675 ± 12	2681 ± 13
weighted average age (data <2% discordant)		2680 ± 11	2692 ± 13

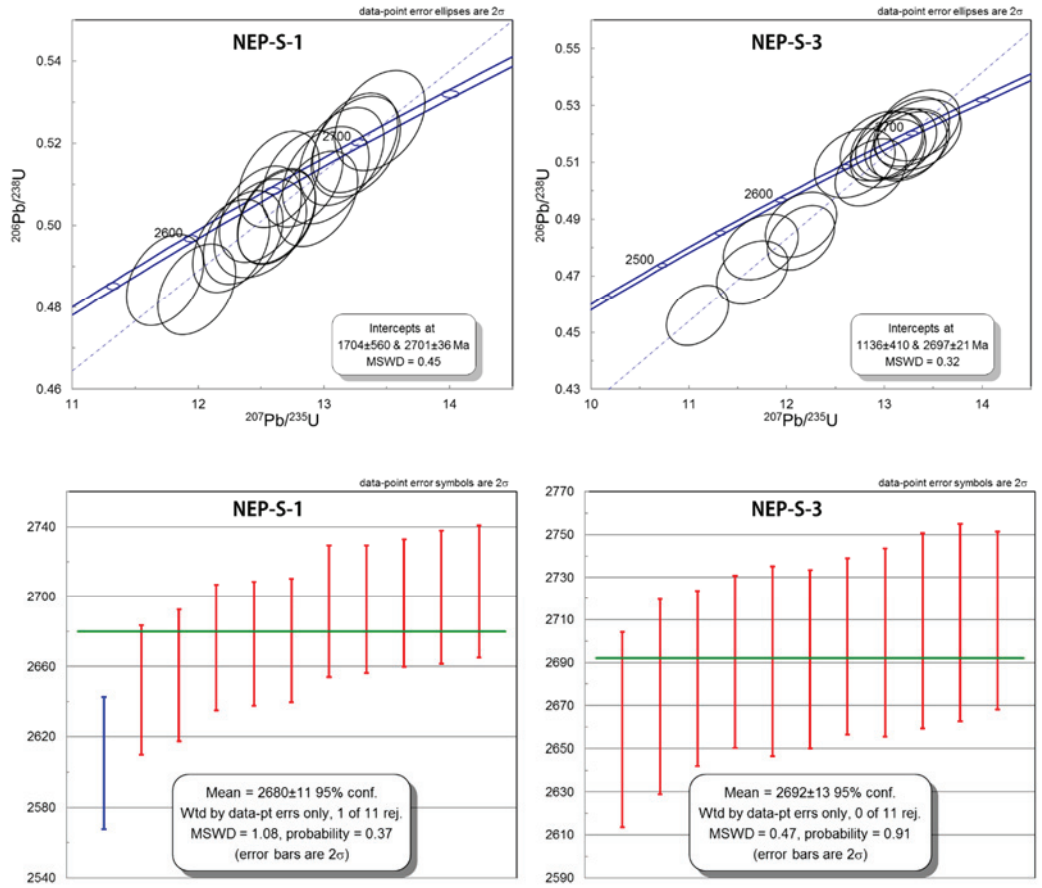

Figure 5.4: Concordia diagrams (top) and weighted average charts (bottom) of the results from 14SV528 – NEP-S-1 and NEP-S-3. All data are plotted using Isoplot 4.15. The blue bar was recognized as statistical outlier and excluded by Isoplot. MSWD = mean square of weighted deviates.

The upper intercept ages, concordia ages and weighted averages from both samples, ca. 2.7 Ga, are similar to ages from tonalitic and granodioritic gneisses from the Northern subdomain and the craton foreland (Chen et al 1995; Card 1990; respectively). Metamorphic rims on NEP-S-1 zircons are typically about 55 Ma younger than the core (Figure 5.5), probably representing Archean metamorphism. The resulting ages of rims and cores lie within the range of ages obtained from similar rocks in the cratonic foreland (Card 1990; Easton 2001) The lower intercepts on the concordia diagrams do not coincide with any calculated ages in the samples, but they do correspond with the Yavapai (NEP-S-1) and early Grenville (NEP-S-3) orogenies. However, because the uncertainty is so large, no geological significance is attached to the lower intercept ages.

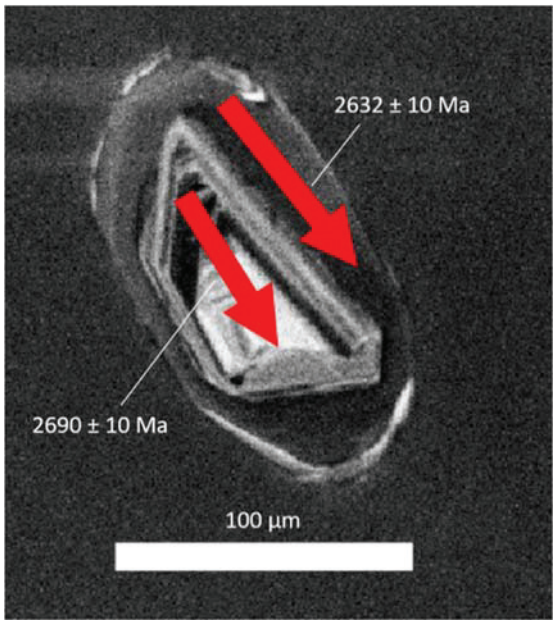

Figure 5.5: CL image of a zircon from NEP-S-1 displaying age calculations $^{207}Pb/^{238}U$ for both the core and the rim.

5.2.3 Quartzites

Four samples of quartzite, unit Sn_1, were chosen for detrital zircon geochronology. These samples were chosen because they are known metasedimentary rocks, with quartz arenite protoliths, which are likely to contain abundant detrital zircon. Three of the samples are located within the WAHSZ and the fourth is located 3 km east on the shoreline of the West Arm, near its opening into the West Bay (Figure 5.1).

14SV003 (NEP Q):

This sample is from an approximately 3 m-thick outcrop beside a small access road near Monetville (Appendix A.2). It is white, homogeneous, foliated, and lineated with interlocking quartz grains and interstitial sillimanite. The sillimanite forms mm-scale seams. Quartz makes up 95% or more of the rock volume, with the remainder composed of sillimanite and muscovite. In thin section, large elongate quartz crystals, muscovite, and sillimanite crystals define the foliation. Sillimanite and muscovite typically pin the boundaries of the quartz crystals, and some are completely encompassed by the larger quartz crystals (Figure 5.6). Muscovite forms mica fish oriented in two directions, however the kinematic significance of this is not known because the L fabric was too weak in hand sample to cut properly oriented thin sections.

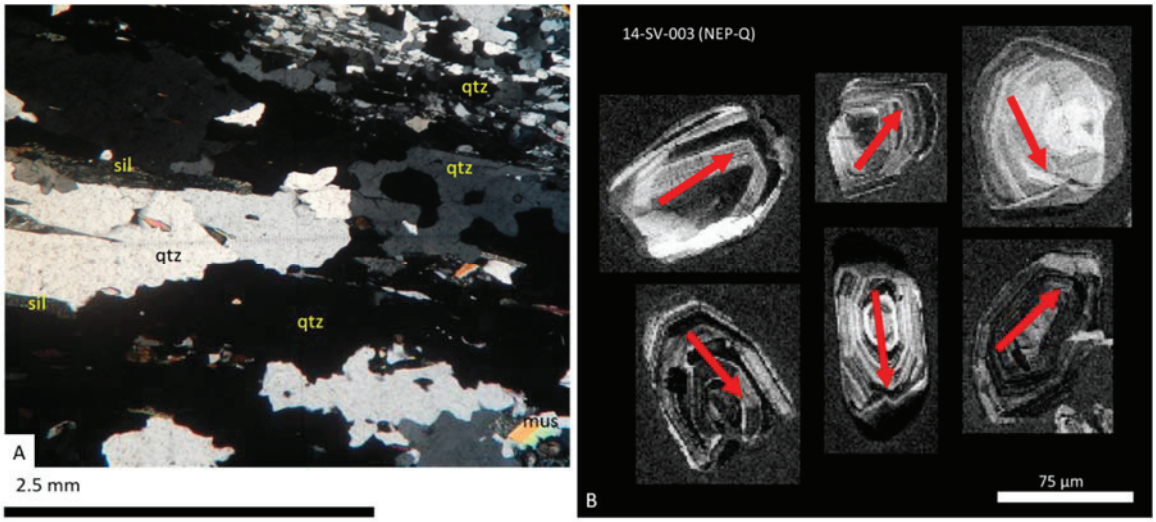

Figure 5.6: Quartzite geochronology sample 14SV003/NEP-Q. A) Texture of 14SV003/NEP-Q in XPL. Many large elongate quartz crystals that define S_{hg} are extinct. Sillimanite crystals pin the edges of the elongate quartz. Where quartz is bounded by quartz, the boundaries are embayed and sutured. Some small muscovite and sillimanite crystals (not labelled) are completely encompassed by the quartz. An aggregate of quartz subgrains (S_{lg}) is shown in the top right corner. B) CL images of zircons; arrows represent laser ablation lines followed during LA-ICP-MS analysis. There were no metamorphic rims large enough to analyze in this sample.

Accessory zircon is found as inclusions in quartz. The grains display concentric zoning (Figure 5.6) and some thin metamorphic overgrowths. Zircons in this samples are all interpreted as detrital; they have concentric zoning, are typically subrounded and some are broken or chipped. Based on the mineral assemblage, this quartzite has been subjected to (at least) one high grade metamorphic event, but none of the rims were large enough to analyze.

14SV493A:

This sample is from one of two metre-scale pods of quartzite on the shoreline of the West Arm. It is white on fresh faces, fine-grained, and foliated. Foliation is defined by streaks of black minerals and white-pink minerals interstitial to quartz. On broken faces, elongate quartz crystals appear to be oblique to the foliation defined by the opaque minerals. In thin section, more than 90 % of the rock volume is quartz, with minor muscovite + microcline + sillimanite + kyanite. Sillimanite forms fibrous, radiating masses and kyanite forms short prismatic crystals (Figure 5.7).

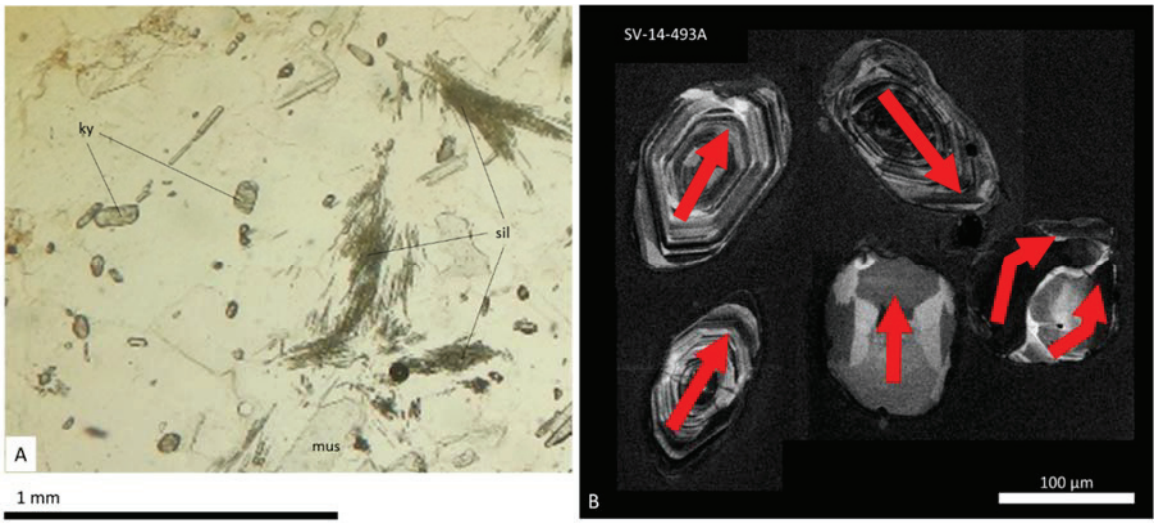

Figure 5.7: Geochronology sample 14SV493A. A) PPL image displaying fine kyanite (ky), sillimanite (sil) and muscovite (mus) within the quartzite sample. B) CL images of zircons; arrows represent laser ablation lines followed during LA-ICP-MS analysis.

Zircon grains are inclusions in quartz. They are mostly subrounded, concentrically zoned, and interpreted as detrital (Figure 5.7). Almost all the zircons have extremely thin outer rims. Only four grains had outer rims large enough to analyze, and because these rims are significantly wider than the rest (Figure 5.7), the rims are interpreted to have formed while the zircon was in the source rock, before it was eroded and deposited in the quartzite. The presence of both kyanite and sillimanite suggests this rock has been subjected to at least one high-grade metamorphic event; however, the narrow overgrowths were too small to analyzed by LA-ICP-MS.

14SV557A:

This sample was taken along the shoreline of Shanty Bay (Figure 5.1, Appendix A.2). This sample is white and glassy on the fresh face, has a bimodal grain size, and is weakly foliated. The rock consists of > 95 % quartz. The remaining minerals are microcline and opaque metallic minerals.

Apart from the lack of aluminosilicate minerals, this sample appears very similar to 14SV493A in thin section.

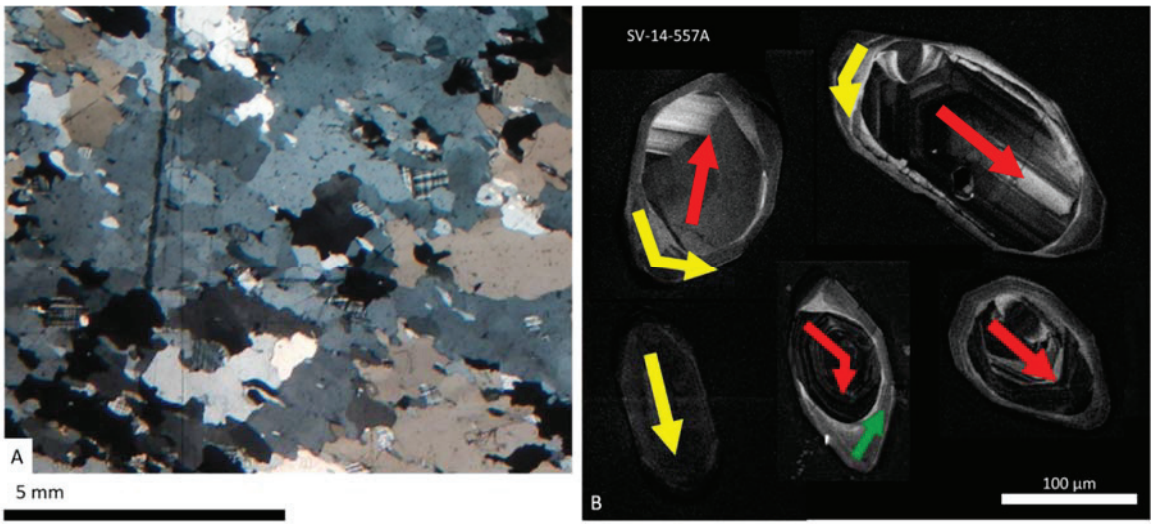

Figure 5.8: Geochronology sample 14V557A. A) Overall texture, in XPL, composed mostly of quartz and microcline with sutured and embayed grain boundaries. B) CL images of zircons; arrows represent laser ablation lines followed during LA-ICP-MS analysis. Lines shown in red targeted zoned cores, and lines shown in yellow and green targeted dark and homogeneous zircons and rims interpreted as metamorphic.

Zircon is found as inclusions in quartz and feldspar. They are typically subrounded, have concentrically zoned igneous cores and distinct overgrowths (Figure 5.8). Two of the grains analyzed are dark in CL, and lack concentric zoning (Figure 5.8). These grains are interpreted as metamorphic in origin. Eleven overgrowths, interpreted as metamorphic, were analyzed to determine the age of metamorphism.

14SV434A:

Sample 14SV434A comes from one of the only two, small, quartzite outcrops found well to the east of the WAHSZ. They are located approximately 200 m apart, in the center of a fold interference pattern, approximately 3 km east of the WAHSZ (Figure 5.1). The hand sample is glassy, pink and white, with interstitial muscovite. More than 95% of the rock is quartz; most of the rest is muscovite, with some very fine kyanite crystals. Quartz overgrows fine-grained muscovite and grain boundaries are locally pinned by muscovite. Muscovite does not define a foliation but quartz displays crystallographic preferred orientation (Figure 5.9), potentially because the muscovite crystallized before the high strain event that affected the quartz.

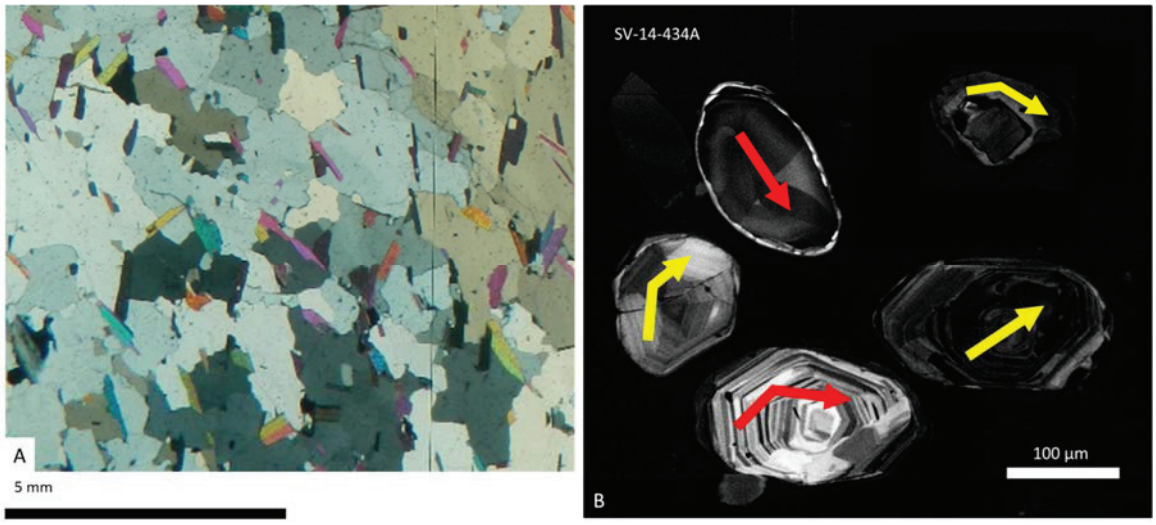

Figure 5.9: Geochronology sample 14SV434A. A) Typical texture in XPL. B) CL images of zircons; arrows represent laser ablation lines followed during LA-ICP-MS analysis. All analyses targeted zoned cores, except one zircon, displayed in the top right corner.

Detrital zircons from this sample are subrounded, are located within quartz and muscovite, and have concentrically zoned igneous cores with thin metamorphic overgrowths (Figure 5.9), mostly too narrow for analysis. A single thicker rim was analyzed to determine the metamorphic age (top right, Figure 5.9); however, this may be a thin metamorphic overgrowth, like many others in this sample, that just appears thicker in the CL image (Figure 5.11 A) because of the angle of the polished grain mount. If that is the case, it is likely that the ablation line sampled both the rim and the underlying core, in which case the result is a meaningless mixed age.

Results:

The data are interpreted based on zircon chemistry and morphology. Magmatic zircons (now detrital) typically show oscillatory zoning whereas metamorphic zircon tends to lack oscillatory zoning and to be relatively U-rich, which makes the CL images darker (Figure 5.8 B and Figure 5.9 B) (Corfu 2003; Kirkland et al. 2009). During metamorphism, growth of Th-rich metamorphic minerals such as monazite can lead to low Th/U in coexisting metamorphic zircon (Trond Slagstad, pers. comm. 2015, Kirkland et al. 2009). On this basis, samples 14SV434A, 14SV493A and 14SV003/NEP-Q yield detrital populations and sample 14SV557A yields a detrital population, and a metamorphic age. Furthermore, the analyses interpreted as metamorphic in sample 14SV557A have relatively lower Th/U ratios than the detrital data (Table 5.2, Appendix C).

Table 5.2. Th and U ratios and concentrations in zircons for Nepewassi quartzite samples

	average Th/U	U ppm	Th ppm	No. of analyses
14SV434 all data	0.80	115.71	92.11	122
14SV434 ca. 1750 Ma data	0.78	139.77	108.16	61
14SV434 ca. 2700 Ma data	0.82	91.65	76.05	61
14SV557A all data	0.81	134.36	101.40	100
14SV557A ca. 1750 Ma data	0.25	178.79	42.69	14
14SV557A ca. 2700 Ma data	0.90	127.13	110.96	86
14SV493A all data	1	170	127	106
NEP-Q/14SV003 all data	0.90	103.39	93.43	100

The age results, summarized in Table 5.3, show that all the quartzite samples have a similar peak of detrital ages at ca. 2.7 Ga (Figure 5.10), similar to the igneous crystallization ages determined from the two tonalitic grey gneiss samples. Samples 14SV557A and 14SV493A have population peaks at circa 2690 Ma, and zircons younger than 2700 Ma dominate the population in both samples. In contrast, sample NEP-Q has nearly equal proportions of <2700 Ma and >2700 Ma zircons. None of the samples have concordant grains younger than circa 2580 Ma.

Sample 14SV434A, has a second detrital population of ca. 1750 Ma (Figure 5.10) and sample 14SV557A yields a metamorphic age at the same time, ca. 1750 Ma (Figure 5.11). Thus, sample 14SV434A is interpreted to have formed after ca. 1750 and after the other three quartzite samples.

Outliers in the data include, a single, discordant, metamorphic overgrowth in sample 14SV557A that yielded an age of ca. 2300 Ma (green arrow, Figure 5.8); however, because this age is so discordant, the result is disregarded. Only one overgrowth was analyzed for in sample 14SV434A and yielded a concordant age of 1304 Ma. It is interpreted as metamorphic because it is an overgrowth; however, it has a high Th/U, likely because of signal interference from the adjacent detrital core (top right, Figure 5.9 B; Table 5.3).

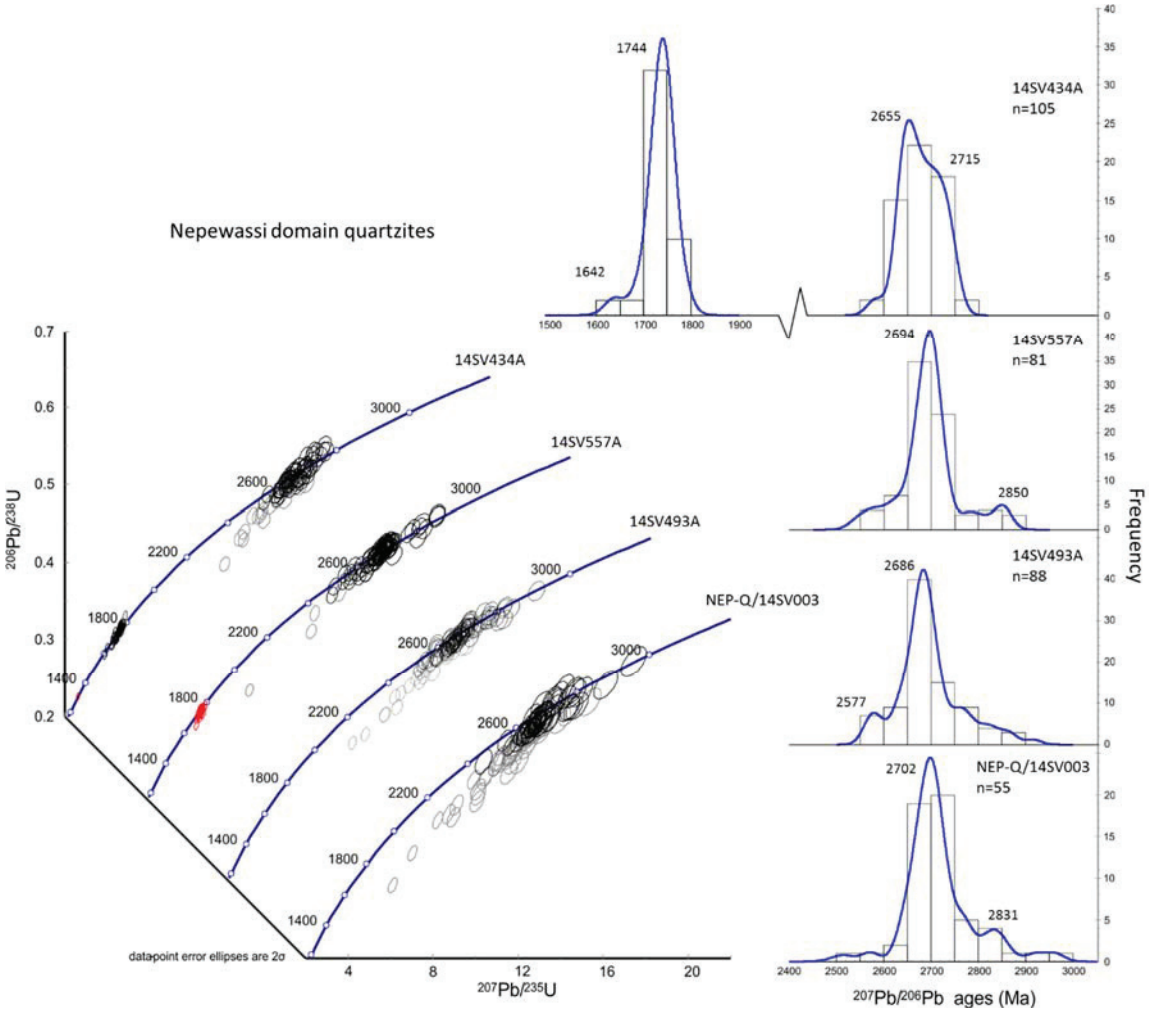

Figure 5.10: Detrital zircon results from four Nepewassi domain quartzites. Nested concordia plots (bottom left) display all data; black ellipses indicate ages from zoned cores interpreted to represent the igneous age of the source rock, red ellipses indicate metamorphic ages, and grey ellipses are > 5% discordant. Probability density plots (right) show $^{207}Pb/^{206}Pb$ ages for detrital ages that are between 95% and 105% concordant. Original plots were made using Isoplot 4.15.

Table 5.3: Summary of U-Pb zircon ages from four quartzite samples. Detrital age peaks are taken from the probability density plots in Figure 5.10. Metamorphic age for sample 14SV434A (red) comes from a single analysis of an outer rim that may have interference from the igneous core. Metamorphic age for sample 14SV557A is the weighted average of 95-105% concordant data from metamorphic zircons or overgrowths. All the U/Pb data can be found in Appendix C.

sample	major detrital peaks (Ma)		minor detrital peaks (Ma)		metamorphic ages (Ma) ($^{207}Pb/^{206}Pb$)
14SV434A	2655	1744	2715	1642	1304 ± 42
14SV557A	2694		2850		1755 ± 11
14SV493A	2686		2577		
NEP-Q/14SV003	2702		2831		

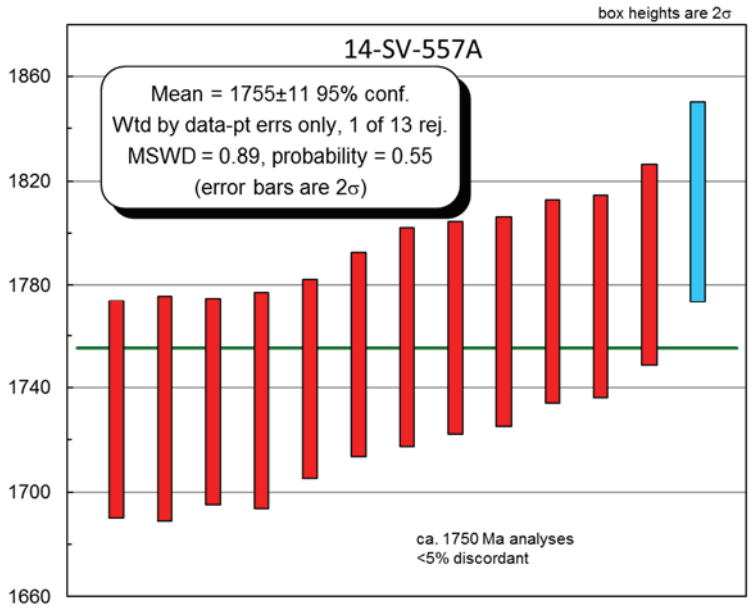

Figure 5.11: Weighted average $^{207}Pb/^{206}Pb$ ages of <5% discordant, ca. 1.75 Ga analyses for sample 14SV557A, interpreted as metamorphic ages. The blue bar was recognized as statistical outlier and excluded by Isoplot. MSWD = mean square of weighted deviates.

5.3 Monazite Geochronology

5.3.1 Background

Metamorphic ages were determined using monazite geochronology by electron probe microanalysis (EPMA). Monazite is a light-rare-earth-element (LREE)-bearing phosphate that can contain U and Th in its crystal structure, but does not readily incorporate Pb (Parrish 1990; Cottle et al. 2012). Monazite can also contain minor heavy rare-earth-elements (HREE) and Y. It is a common accessory mineral in peraluminous granitoid rocks and pelitic metasedimentary rocks. This method is most useful for determining the age of crystallization for peraluminous granitoid rocks and the timing of metamorphism (Williams and Jercinovic 2002).

Monazite is commonly analyzed for U-Pb isotopes using TIMS, LA-ICP-MS, and other methods. However, because monazite rarely contains initial Pb, a chemical geochronometer was developed in the early 1990s using EPMA compositional data (Suzuki et al. 1994; Montel et al. 1996; Williams and Jercinovic 2002; Williams et al. 2006, 2007). This method can provide reliable age data without isotopic analysis. EPMA is a particularly useful approach for determining metamorphic ages in polycyclic terranes because the EPMA beam produces a much smaller spot (≤ 5 µm) than laser ablation systems or ion probes (Williams and Jercinovic 2002; Williams et al. 2007). The high spatial resolution makes it possible to analyze multiple crystallization zones or

growth domains within a single grain. Another advantage of the EPMA method is that it can analyze crystals in situ, preserving the textural context throughout the analytical process. Caution must be taken when choosing analysis spots to avoid chemical interference from neighboring domains. The EPMA method is limited to rocks with a probable age of ≥ 100 Ma because young samples may have very low concentrations of Pb making count times longer and detection difficult (Montel et al. 1996).

Monazite can form during crystallization of melt or fluid, or by reaction with pre-existing minerals, such as xenotime, apatite, or allanite during prograde metamorphism. During its history, a rock may be affected by several events that could cause monazite growth or dissolution. Each event could be marked by characteristic textural and/or chemical domains within single grains or by populations of distinctive grains in a single sample (Williams et al. 2007). Different chemical domains can have similar ages because local chemistry may vary spatially within any sample; likewise, similar chemical domains may have contrasting ages. The chemistry of each domain can be compared with other mineral phases that contain the same major and trace elements in order to link chemical changes in those phases with monazite growth. For example, garnet in medium to high grade metamorphic rocks readily incorporates HREE and Y into its crystal structure. Thus, monazite grains growing in the presence of garnet will have relatively depleted concentrations of HREE and Y. Conversely, monazite grains growing during the breakdown of garnet will be relatively enriched in HREE and Y (Williams et al. 2007).

A microprobe measures only the total concentration of an element in a mineral, not the individual isotopes. For the chemical dating approach, the Montel equation (Montel et al. 1996), which uses total concentrations of elements rather than isotopic concentration measurements, is applied:

$$Pb = \frac{Th}{232}\{e^{\lambda^{232}t} - 1\}208 + \frac{U}{238.04}0.9928 \times \{e^{\lambda^{238}t} - 1\}206 + \frac{U}{238.04}0.0072 \times \{e^{\lambda^{235}t} - 1\}207 \quad (5.1)$$

where Pb, Th and U represent the corresponding element concentrations, λ is the decay constant for the given isotope, and 206, 207 and 208 correspond to the daughter isotopes of Pb. The Montel equation is solved iteratively for time (t). The method assumes that the ratio of U-Th-Pb changes over time only because of radioactive decay, that the decay rate for each isotope has remained constant over geological time, and that non-radiogenic Pb is negligible.

5.3.2 Analytical Procedure

Thin and polished sections were made at Dalhousie University. Before analysis, the polished sections were re-polished with a Pb-free polish to ensure that no Pb from the polishing lap would contaminate the sample. Possible monazites were located and marked using a petrographic microscope. A double-thickness carbon coat was applied to the section to limit thermal damage from the electron beam. Analysis was done using the JEOL JXA-8200 Superprobe at the Robert MacKay Electron Microprobe Laboratory. The analytical procedure used was described by (Pyle et al. 2002, 2005) Pyle et al. (2002, 2005) and adapted for the instrument configuration by Gagné (2004), and Steenkamp (2012).

Following preliminary petrographic inspection, monazite was located using BSE imaging to detect high atomic number (bright) grains, with possible targets confirmed by EDS analysis. High-contrast BSE images were used to pick crystals for analysis based on internal zoning patterns, petrographic setting, and grain morphology. The chosen crystals were then mapped for Y, Th, U and Pb using wavelength dispersive spectroscopy (WDS) (Figure 5.12 C). The WDS maps were used to identify chemical zones within each crystal (Figure 5.12), which were then grouped into domains. Domains are chemically similar zones in crystals that have the same textural setting. Monazite grains were grouped based on textural context, and chemical domains were chosen within each group.

Each chemical domain was quantitatively analyzed for major element concentrations at standard EMP operating conditions (15kV, 20nA). The major element concentrations are used to determine the ZAF (atomic number, absorption, fluorescence) corrections needed for subsequent trace element analysis (Pyle et al. 2002). The analytical precision was periodically checked against the in-house ‘Monazite53’ major-element standard and the Geological Society of Canada’s standard monazite.

Each chemical domain was then analyzed for the trace elements Y, Th, U and Pb at 15kV and 200nA. Peak scans (Fig. 5.13) were performed for each element in order to identify background levels and possible peak overlaps. Multiple points were then analyzed in each zone for Th, U and Pb, to use in the age calculation, and Y, which is analyzed to correct for its interference on Pb and because it provides petrogenetic information. Concentration corrections, age calculations, and error calculations were completed in an Excel spreadsheet (Steenkamp, 2012).

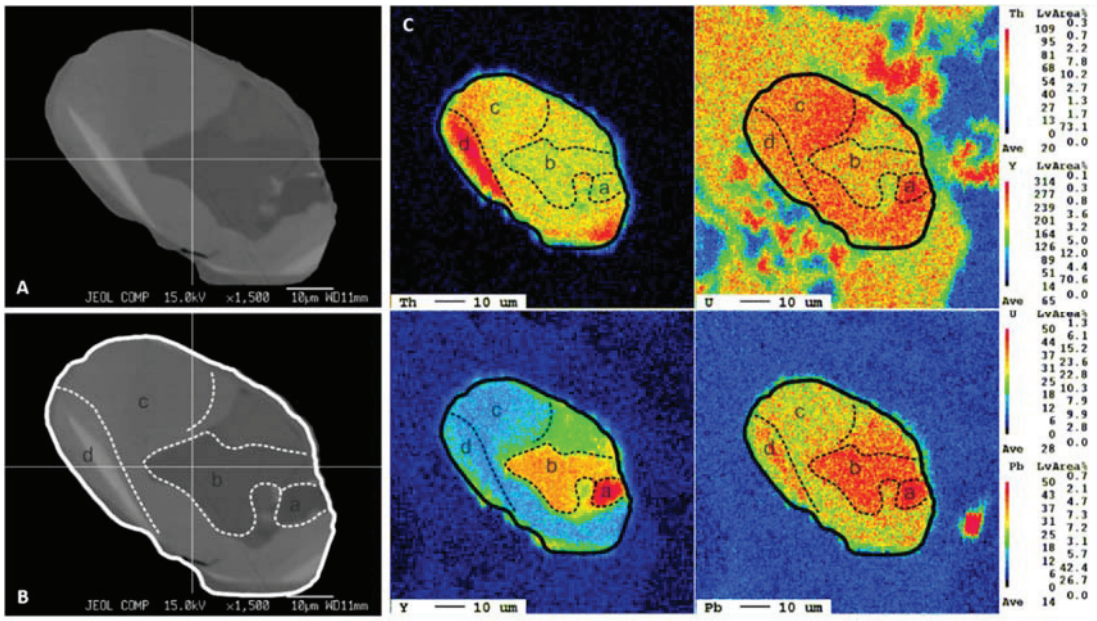

Figure 5.12: Representative zoned monazite (monazite grain 23). A) BSE image used to assist in choosing suitable monazite grains, based on internal zoning and texture of the crystal. B) The same BSE image as A, with chemical domains outlined. C) WDS chemical maps of Y, Th, U and Pb. While all element maps were used to identify chemical domains, in most cases the Y map tends to show the largest contrast between domains, making it the most useful. These images are of monazite grain 23.

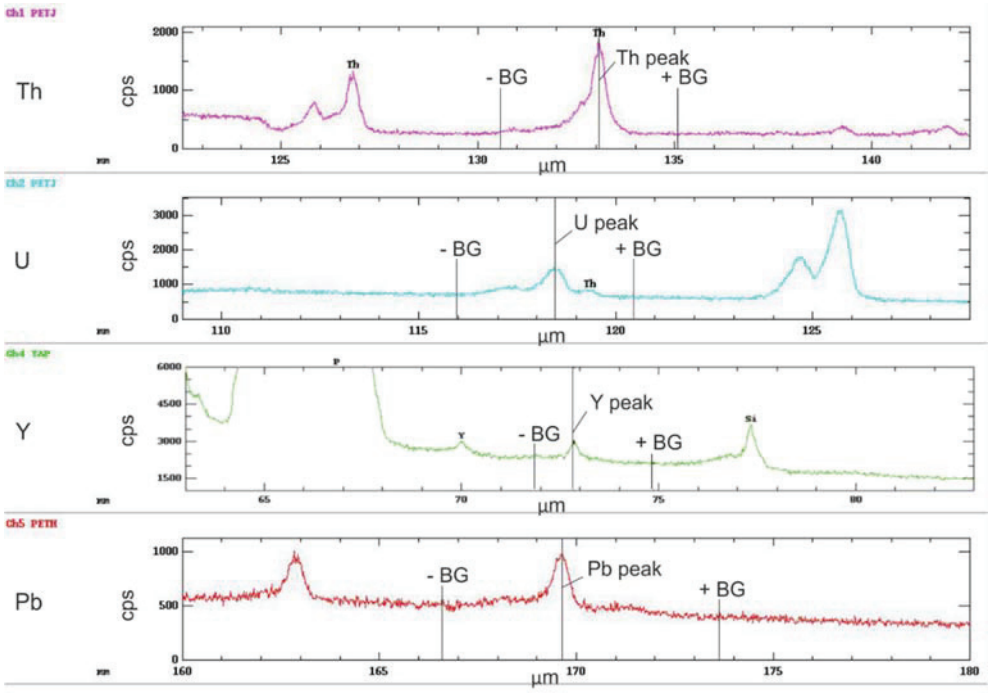

Figure 5.13: Example of background selection procedure for high and low background positions on the element peaks from WDS scan of monazite. Background positions (horizontal axes) are in µm and are measured in cps, counts per second (vertical axes). BG, background.

5.3.3 Sample Description

Pelitic samples from station 14SV542/N13-029 were chosen because of their location within the map area (Figure 5.1) and presence of monazite in thin section. This station/sample is within the WAHSZ, near one of the quartzite samples used for detrital zircon geochronology. The same sample was also used for thermobarometry, and is described in detail in Chapter 4.

Monazite grains are found in a variety of textural settings (Figure 5.14), most commonly in the matrix or within biotite and feldspar crystals. Numerous monazites are also found in the leucosome, although these crystals display textural evidence of extreme dissolution (Figure 5.15). This textural relationship implies that the leucosomes formed after the monazites within them. Only two crystals within and on the edge of the leucosome were suitable for analysis (Figure 5.14 B). Three monazite grains were located within larger garnet crystals (Figure 5.14 C and D), and one small monazite was situated immediately adjacent to an embayed kyanite crystal (Figure 5.14 A).

Monazite grains are typically xenoblastic and vary from small (approximately 20 µm across), weakly zoned crystals to large (up to 70 µm across) complexly zoned crystals (Figure 5.12). BSE images and chemical maps for each analyzed grain can be found in Appendix D.1. As described in section 5.3.1, data from texturally and compositionally similar zones from multiple grains were grouped for purposes of calculating domain ages.

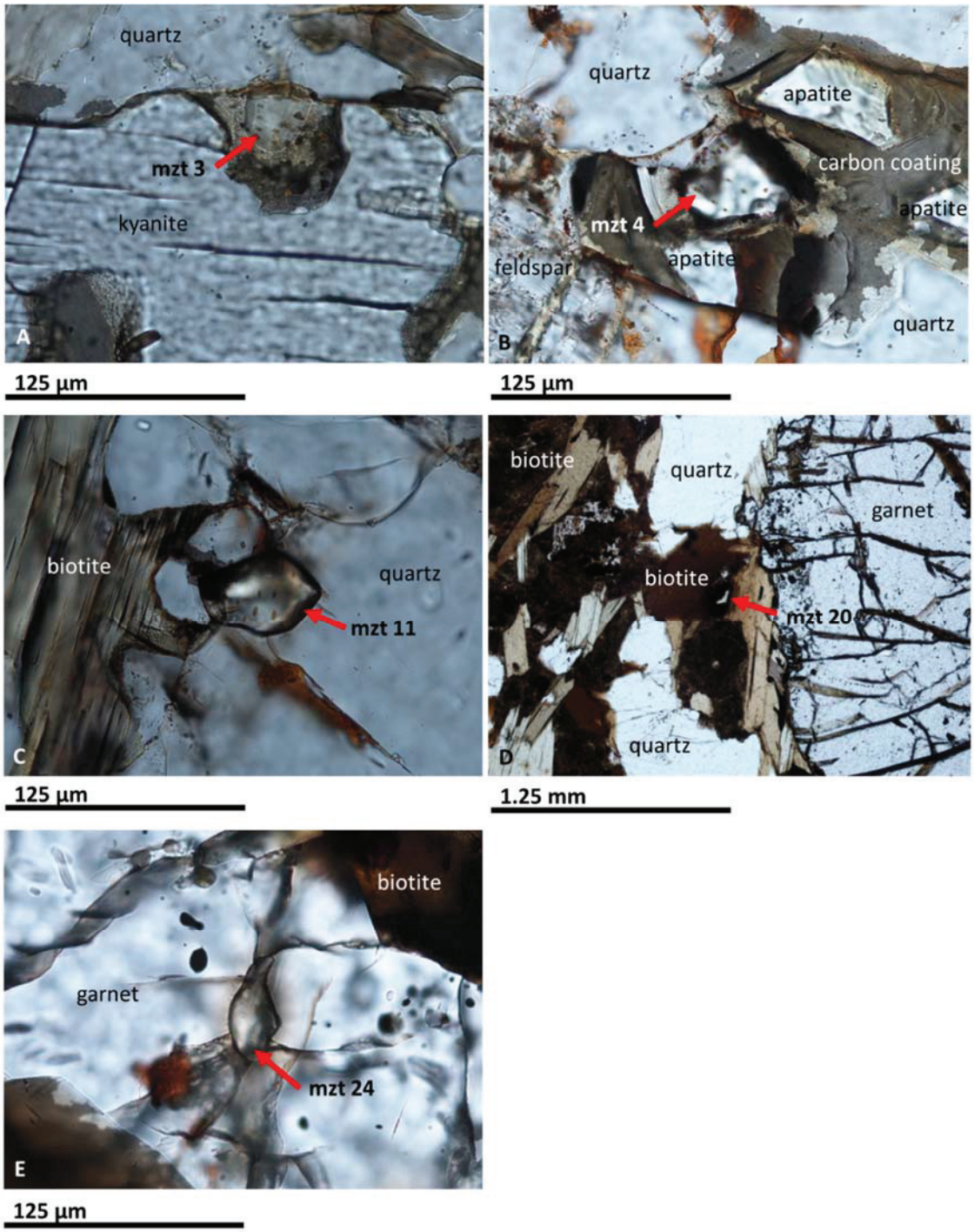

Figure 5.14: Textural settings of monazite grains in sample N13-029. A) Monazite 3 within an embayment of a kyanite crystal. B) Monazite grain 4 with fragments of apatite, between quartz and feldspar crystals. C) Monazite 11 on the edge of a leucosome (right of image). D) Monazite grain 20 is an inclusion in biotite adjacent to a garnet porphyroblast. D) Monazite grain 24 is an inclusion in garnet with a narrow overgrowth (top of grain) that follows along a fracture in the garnet.

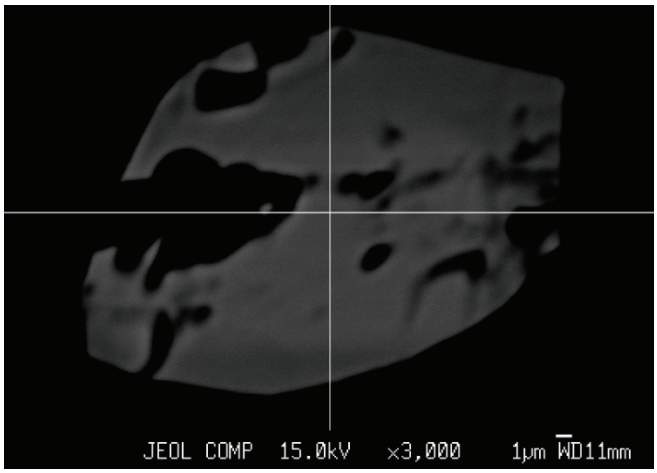

Figure 5.15: BSE image of a monazite from sample N13-029ii Ⱶ with highly resorbed texture found within the leucosome. This monazite was not analyzed.

5.3.4 Results

Many different domains were determined based on textural setting and chemical composition, as discussed in section 5.3.2 (Table 5.4). Most domains can be grouped based on relative Y concentrations into high Y cores, low Y cores, low Y rims and high Y rims. Domains that have high Y likely grew at a time when garnet was not present or was breaking down. Domains with low Y likely grew when garnet was present or crystallizing. High Y cores (domains 1-3, 5, Table 5.4) yield Paleoproterozoic ages from 1608 Ma – 1828 Ma that correspond to the Yavapai-Penokean orogenies. Low Y rims (domains 6-9, Table 5.4) have ages from 988 Ma to 1293 Ma, but are mostly Ottawan. Low Y cores (domains 10-14, Table 5.4) yield ages from 971 Ma – 1033 Ma, mostly Rigolet ages. High Y rims (domains 15-21, Table 5.4) yield 963 Ma – 1025 Ma. Based on these domain groups, garnet was not present or was breaking down during the Penokean-Yavapai (high Y cores), then garnet (and/or apatite) likely grew during the Ottawan (low Y rims), and may have been breaking down and/or growing simultaneously (low Y cores and high Y rims) during the Rigolet phase. Domain 5, inclusion in garnet, high Y inner core, is the only domain with two age populations; monazite 24a yields an average age of 1684 ± 37 Ma, and monazite 21a yields a single point analysis of 1028 ± 19 Ma (Table 5.4). Monazite grains 24 and 21 are both inclusions within different garnets, indicating there are at least two ages of garnet. Thus, according to these results, garnets formed in this sample after ca. 1680 Ma, likely were breaking down before ca. 1030 Ma, and then crystallized again after ca. 1020 Ma. Furthermore, monazite 24 has an overgrowth that follows a crack in the garnet crystal (24b) which yields individual spot

ages of 1293 and 1054 Ma. This implies that this garnet grew before 1293 Ma, cracked, and then the younger monazite tail grew within the fracture.

Table 5.4: Age results for individual spot analyses in monazites from 14SV542/N13-029, organized by zone and chemical domain.

	compositional domain	zone	analysis point ages	zone median	domain average
1	matrix, high Y and Pb inner core	12a (core1)	1813, 1818, 1824, 1839, 1828, 1818	1821	1813
		15a (core1)	1748	1748	
2	matrix, intermediate Y and Pb, low U and Th core	12b (core2)	1809, 1780, 1815, 1814	1811	1763
		23b (core1)	1743, 1733, 1734, 1735	1735	
		15b (core2)	1721, 1743	1732	
3	edge of leucosome, high Y, Pb and Th, low U	11a (core1)	1750, 1778	1764	1764
4	high Th and Pb core	4a (core)	1764, 1758, 1772, 1769, 1738, 1473	1761	1712
5	inclusion in garnet, high Y inner core	24a (core)	1772, 1751, 1729, 1690, 1608, 1554	1709	
		21a (core1)	1028	1028	
6	inclusion in garnet, low Y rim	24b (rim/tail)	1293, 1054	1173	1046
		22b (main body)	1008, 1006, 1002, 1007	1007	
		21c (rim)	1007, 988	998	
7	edge of leucosome, intermediate Y and U, low Pb and Th	11c (rim1)	1022, 1228	1125	1125
8	edge of leucosome, intermediate U, low Th Y and Pb	11d (rim2)	1096, 1154	1125	1096
9	matrix, low Y and Pb rim	15c (rim)	1018, 1055, 1026, 1027, 1031, 1029, 1032, 1024, 1028, 1056	1028	1041
		12c (rim1)	1057, 1039, 1050, 1058, 1051, 1056, 1057, 1073, 1217, 1039, 1048	1056	
		23c (core2)	1096,1033, 1037, 1035, 1029, 1031, 1035	1035	
10	edge of leucosome, high Th, intermediate Pb and U, low Y	11b (core2)	1033	1033	1033
11	in leucosome, core	7b (core)	1021, 1026	1023	1023
12	matrix average to low Y core	19a (core)	992, 1007, 1011, 993, 999, 1006, 1014, 1014, 1000, 992	1003	991
		17a (core)	994, 984, 998, 986	990	
		20a (core)	991, 989, 978, 980, 985, 965	983	
		18a (core)	986, 979, 979, 975, 979, 987, 990, 971, 985, 987	982	

Table 5.4: *Continued.*

	compositional domain	zone	analysis point ages	zone median	domain average
13	grain within embayment in kyanite, low Y core	3a (core)	1011, 1002	1007	1007
14	matrix average to low Y core, lower Th	20d (zone)	979, 991, 1002, 988, 987	988	989
15	inclusion in garnet, outer core	21b (core2)	1017, 1025, 1023	1023	1022
		22a (corner)	1024	1024	
16	high Y and U edge	4b (rim)	999, 989, 1018	999	1002
17	grain within embayment in kyanite, relatively high Y rim	3b (rim)	1010, 1002, 1011, 1008, 996, 0	1005	838
18	matrix, intermediate to high Y rim	19b (rim1)	1001, 984, 995	995	988
		18c (rim2)	60, 993	526	
		20c (zone)	965, 988	977	
19	matrix, high Y rim	19c (rim2)	1017, 997, 1000	1000	984
		17b (rim)	968,992, 983, 967, 968, 986	975	
		20b (rim)	999	999	
		18b (rim1)	963, 995, 995	995	
20	in leucosome, high Y rim	7a (rim)	992	992	992
21	matrix, high Th rim	23d (rim)	988	988	988

Ages in green font are Grenvillian ages, blue fonts are generally Paleoproterozoic ages, and red font indicates that the analysis was eliminated from the results due to textural or analytical interference. Zones are annotated with a number that represents the monazite grain, followed by a letter that represents the chemical zone within that grain. BSE images and chemical maps of each grain are found in Appendix D.1.

Associations between textures and ages can provide insight into the metamorphic setting. Monazite grains in or adjacent to leucosomes are typically highly embayed and have complicated zoning (Figure 5.16). Complicated zoning suggests the grain has been exposed to a series of different growth and/or dissolution stages. Where the dissolution is on the outside, or affects all the zones, as it typically does for monazite grains in the leucosome (Figure 5.15 and Figure 5.17), we can assume the dissolution, and probably partial melting, was the last thing to affect the grain. However, in most monazites, such as monazite 23 (Figure 5.12) and monazite 12 (Figure 5.16), the inner zones are embayed and then subsequent monazite growth filled in the embayments. Zones in monazite 12 have significantly different ages, ranging from 1039 ± 15 to 1839 ± 39 Ma. All points within each chemical domain have similar ages to one another. Monazite 12 is the only grain that yields ca. 1820 Ma ages (Penokean). As previously mentioned, all Paleoproterozoic ages come from high Y cores or inclusions, all of which are embayed. The core

of monazite 4 (4a) is the only excluded analysis (Table 5.4, Appendix D.1). These data suggest that there were likely at least two episodes of dissolution or partial melting; the first after ca. 1720 but before ca. 1080 Ma (Figure 5.16; Figure 5.17 A; Table 5.4) and another after ca. 1020 Ma (Figure 5.17 B; Table 5.4). Dissolution of monazite, and probably partial melting, may have occurred at the same time as garnet growth.

The core of monazite 4 is the only relatively low Y core that yields a Paleoproterozoic age. Low Y in monazite suggests that garnet was present, or growing at the same time, however this contradicts the interpretation that all the high Y cores are of similar age. Figure 5.14 B shows how monazite 4 is located within a pit, along with fragments of apatite. The pit formed during polishing, when carbon coating from the microprobe analysis remains caught in crevices on the surface of the thin section. This relationship suggests that monazite 4 may have previously been an inclusion within an apatite crystal. Apatite also incorporates Y into its crystal structure, so if the two minerals grew together, that could account for the relatively low Y values in monazite 4.

A lower age limit on the timing of kyanite crystallization may be determined based on the textural setting of monazite 3. This monazite grain is located within an embayment in a kyanite crystal (Figure 5.14 A), thus, kyanite must have formed, and been dissolved, prior to the age of the monazite core at ca. 1010 Ma. Alternatively, the kyanite may have grown around the monazite and is relatively younger, however

All the viable data from sample N13-029 (Table 5.4) are plotted in a probability density diagram (Figure 5.18). Some analysis points were eliminated using post-analysis BSE images (Figure 5.17; Appendix D.1), based on textural or analytical interference. Monazite data were reported using methods described by (Williams et al. 2007). Each individual point analysis yields an age; individual analyses are compiled in an age histogram, or probability density plot. These data yield a large 993 Ma (Grenvillian Rigolet phase) age peak and two Paleoproterozoic peaks with a slightly larger one at 1761 Ma and the other at 1818 Ma (Yavapai – Penokean). All these data are interpreted as metamorphic ages, based on correlation with detrital zircon results from metasedimentary rocks in the same package (sample 14SV557A, section 5.2.3), which has metamorphic ages, ca. 1750 Ma, similar to the monazite Yavapai peak at 1761 Ma (Figure 5.18 A). It is, however, possible that Yavapai-Penokean monazite core ages are detrital.

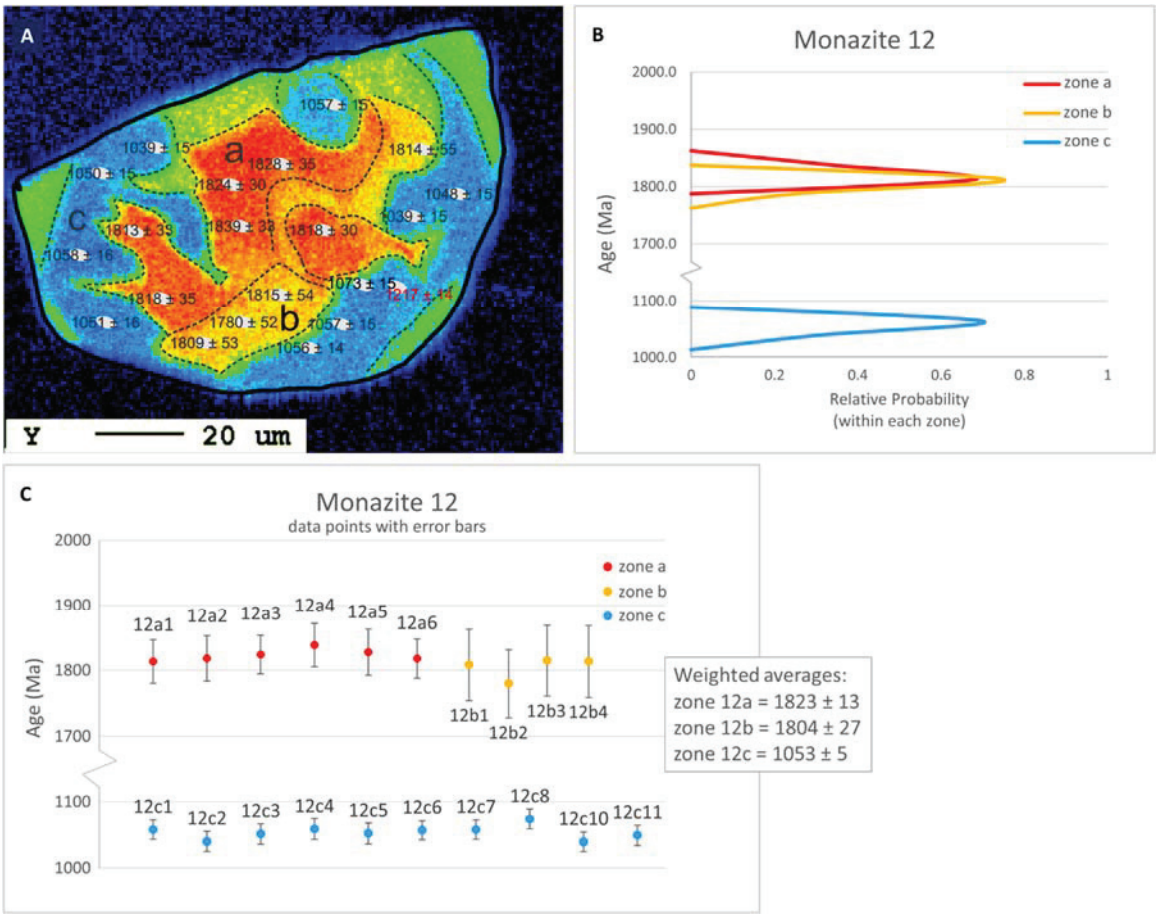

Figure 5.16: Monazite data from grain 12, sample N13-029ii. A) Y map; reds and yellows indicate high concentrations, blue and greens indicate low. Distinct chemical zones depicted by dotted lines. Spot analyses are shown to scale as grey dots, annotated with the calculated age and errors in Ma. Ages annotated in red represent spots that were removed from the domain age calculations set because they were deemed unreliable (see section 5.3.1). B) Probability density plot for data from age domains a (red; high Y), b (yellow; moderate Y), and c (blue; low Y). C) Ages and uncertainties for individual spot analyses from domains a, b, and c; horizontal scale represents analysis number. Weighted averages for each zone are: 12a = 1823 ± 13 Ma, 12b = 1804 ± 27 and 12c = 1053 ± 5 Ma

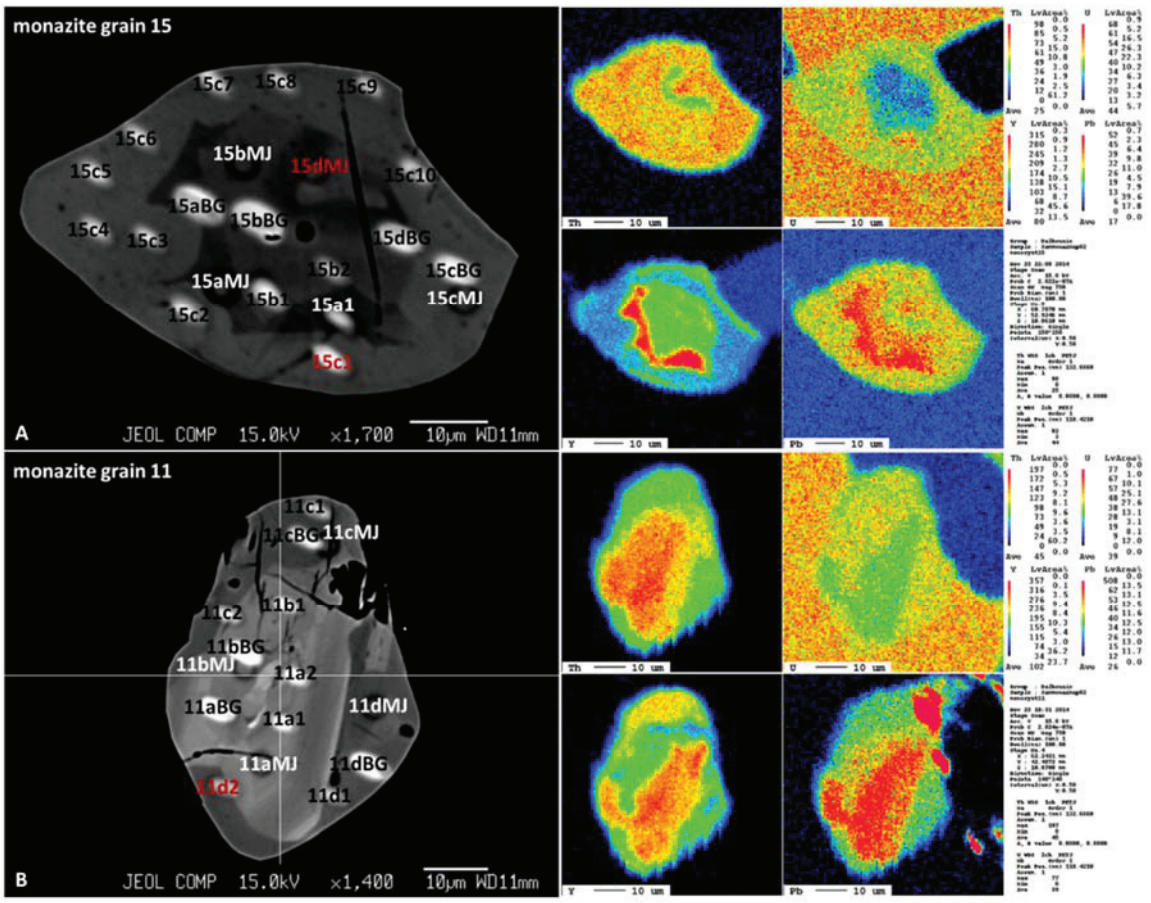

Figure 5.17: Representative monazites used for constraining the age of dissolution, displaying BSE images with annotated analysis points (corresponding to Table 5.4 and Appendix D.1) and minor element maps. Analyses in red were eliminated due to textural or analytical interference. A) Monazite grain 15. The age of embayed cores provides an upper age limit, and the age of the rim provides a lower age limit. B) Monazite grain 11. The outer rim is embayed and thus provides an upper age limit for another episode of dissolution.

A sample from the same outcrop, N13-029, was analyzed using the same method (P. Regan 2014, unpublished ERTH 6400 report). This sample had smaller monazite grains and, thus, fewer points were analyzed, making the results less statistically robust. The probability density chart from this analysis yields age peaks at 1007 (Grenvillian) Ma, 1412 Ma, and 1783 Ma (Yavapai – Penokean) (Figure 5.18 B). The Grenvillian and Yavapai – Penokean age peaks generally line up with results from this study, but the ca. 1410 Ma age population does not correspond to any domains recognized in the present study.

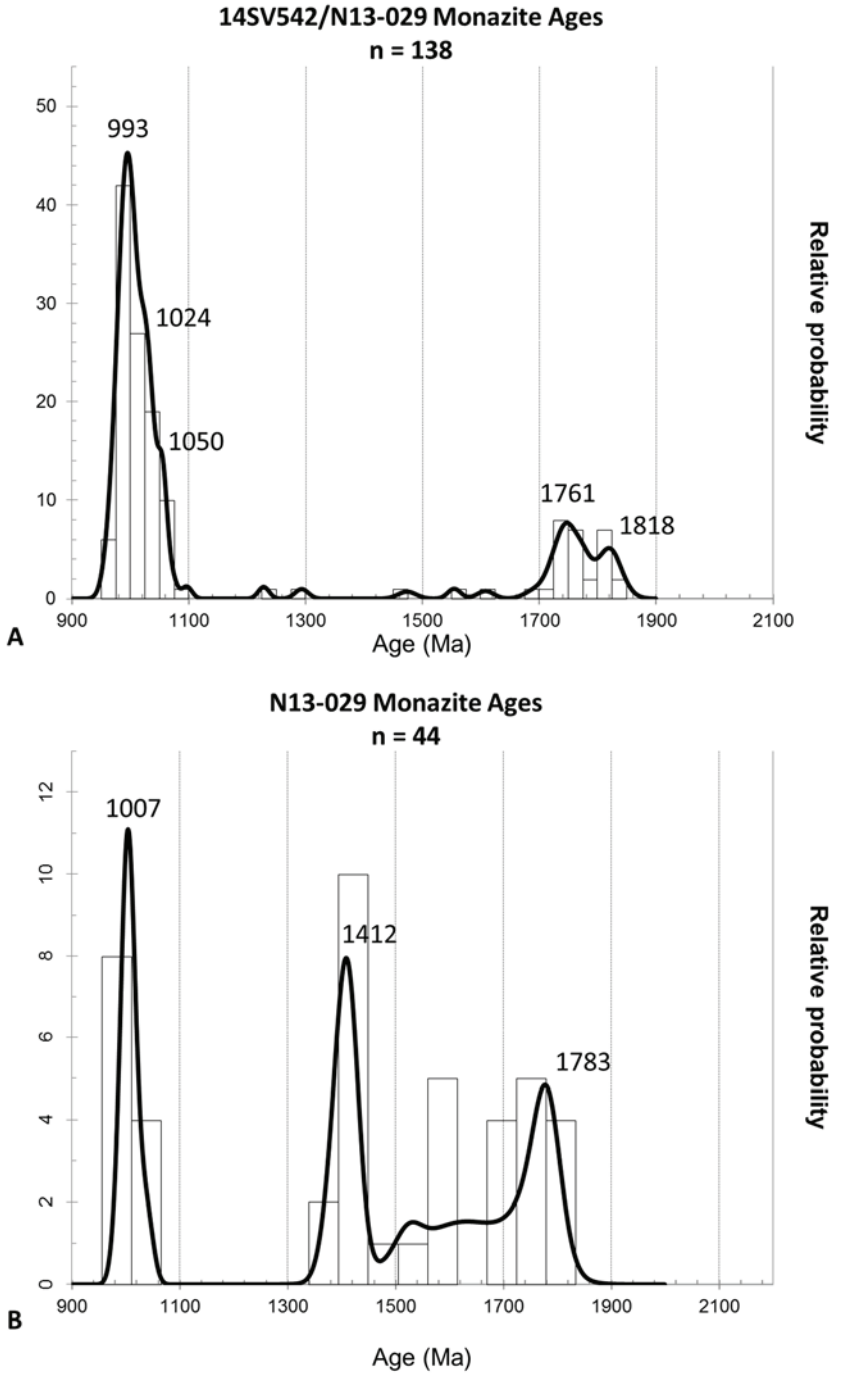

Figure 5.18: A) Probability density graph containing all viable data points from this study. The dominant age peaks correspond to the Grenville, with a strong Rigolet peak and a side Ottawan peak. There are also Yavapai, 1761 Ma, and Penokean, 1818 Ma, peaks. B) Probability density chart of monazite ages from N13-029 from a previous study (Regan, 2014, unpublished ERTH 6400 report).

5.4 Discussion

5.4.1 Igneous Zircon Ages:

The two tonalitic grey gneisses analyzed were chosen to test the hypothesis that Archean basement rocks are present in the study area, and if so, whether these rocks could have been the source of the detrital zircon in nearby sedimentary rocks. The tonalitic grey gneisses in the Southern subdomain are Neoarchean, and potentially basement rocks, because they yield similar ages, ca. 2.68 Ga, to similar rocks in the Northern subdomain gneissic rocks in the cratonic foreland north of the Grenville Front (e.g. Levack gneiss complex, Wodicka and Card 1995). The similarity of these ages to the detrital zircon age peak in metasedimentary rocks in the Southern subdomain suggests that these metasedimentary rocks were derived from, and possibly deposited on, Archean basement.

Tonalitic gneisses (unit Tn) are mapped to the east and west of the metasedimentary rocks (Appendix A.1). Assuming the tonalitic gneisses to the east are the same age as the ones analyzed to the west, Archean rocks are both structurally above and below the (relatively younger) metasedimentary rocks. This repeat of tectonic stratigraphy may indicate significant thrusting along the WAHSZ, or significant pre-Grenvillian folding and thrusting

5.4.2 Detrital Zircons:

The main age peak in the Nepewassi domain detrital zircon samples, ca. 2.7 Ga, is very similar to the detrital peak age for samples from sandstone units throughout the complete the Huronian Supergroup succession (Figure 5.19; Rainbird and Davis 2006; Craddock et al. 2013). The Huronian Supergroup is a 4- to 12-kilometre-thick package of magmatic and sedimentary rocks deposited between 2.5 and 2.2 Ga on the southern margin of the Laurentian Archean craton (Zolnai et al. 1984; Fralick and Miall 1989; Card 1990; Corfu and Easton 2000; Craddock et al. 2013). The upper Huronian formations (or Cobalt Group), as defined by Young (2015), are interpreted to have been deposited on a passive margin, with the lowermost group interpreted to have been deposited in a rift basin, which was the early stages of the passive margin (Young 2015).

The upper Huronian succession consists of repeated successions of conglomerate, siltstone and/or carbonate, and sandstone, with sandstone commonly being the thickest and most abundant of the 3 rock types in each group Because of the proximity to Huronian Supergroup strata to the map area, and the southward-facing orientation of the Huronian passive margin, it is

logical to examine the possibility that the Nepewassi sediments may be equivalents of the Huronian Supergroup. Unfortunately, the high metamorphic grade and tectonic disruption of the Nepewassi sediments, as described in Chapters 2, 3 and 4, means that conventional stratigraphic correlation tools cannot be utilized in such a comparison. As a substitute, the detrital zircon populations of the Huronian Supergroup (Easton and Heaman 2011; Craddock et al. 2013) can be compared with those obtained from the Nepewassi sediments in this study to determine if this suggestion can be validated.

As noted previously, samples 14SV557A and 14SV493A both have population peaks at circa 2690 Ma, but with zircons younger than 2700 Ma dominating the population in both samples. In fact, sample 14SV493A is dominated almost completely by circa 2680-2690 Ma zircons. Of all the Huronian Supergroup sandstone units, only the Matinenda Formation, near the base of the Huronian Supergroup is dominated by 2680-2690 Ma zircons (Easton and Heaman 2011; Craddock et al 2013). In contrast, sample NEP-Q has roughly equal proportions of zircons <2700 Ma and >2700 Ma, and thus it is harder to assign to a single Huronian Supergroup unit, however, either the Mississagi, Serpent or Lorrain formations show the closest match (Craddock et al. 2013). The Mississagi Formation contains interbedded siltstones and sandstones, which may be equivalent to metasedimentary rocks in the Nepewassi domain. The Lorrain Formation contains aluminous quartzites (Chandler et al. 1969) which are similar in composition to the Nepewassi quartzites, and could represent lower grade equivalents.-Despite having somewhat different zircon populations, samples NEP-Q, 14SV493A and 14SV434A all have similar rare earth element patterns characterized by low total rare earth element contents, no europium anomaly, and a concave upward sloping heavy rare earth element pattern. Insufficient geochemical data are available from the Archean gneiss complex in Nepewassi domain to determine if this unusual pattern might be the result of a local, distinctive, source rock.

Some, but not all, Huronian Supergroup sandstones contain 2450-2480 Ma old grains (Easton and Heaman 2008), which are likely sourced from Huronian Supergroup metavolcanic rocks or circa 2460 to 2480 Ma mafic and felsic intrusive rocks associated with the early rifting phase of the Huronian continental margin. The presence of such zircons in the Nepewassi sediments would strengthen the comparison to the Huronian Supergroup. Unfortunately, the grains in this age range in samples 14SV493A, 14SV557A and NEP-Q are all highly discordant, and thus it can not reliably be determined if circa 2460 to 2480 Ma zircons are present in the Nepewassi samples.

It should be noted that it cannot be entirely ruled out that 3 of the 4 Nepewassi quartzite units are Archean, given that all of the concordant grains are Archean. If this were the case, then they would likely be equivalent to either the Pontiac Group or Temiskaming assemblage metasedimentary rocks that are common in the craton north of the Grenville Front near Temagami. However, the presence of associated aluminosilicate-bearing metapelite rocks with the Nepewassi quartzites would appear to favour the comparison with The Huronian Supergroup.

Quirke and Collins (1930) described how the Huronian Supergroup extends to the Grenville Front and then disappears. However, the apparent correlation of the Huronian Supergroup with the metasedimentary rocks in the Nepewassi domain suggests that the Huronian rocks do not disappear south of the Grenville Front, but are simply deformed and/or reworked beyond recognition.

Sample 14SV434A is interpreted to have a second detrital peak at ca. 1750 Ma, because all analyses were from concentrically zoned zircons, implying they were magmatic in origin and are now detrital. Thus, sample 14SV434 was deposited much later than the other three quartzites. Two detrital peaks also imply that, unlike the other quartzites, sample 14SV434 had two distinct source rocks. This sample lies to the west and structurally above the other three samples, which are located roughly along strike within the WAHSZ. Sample 14SV434A likely has the same source rocks as the older quartzites, plus and additional Proterozoic, ca. 1750 Ma, source. Alternatively, this package of metasedimentary rocks might have been derived from reworking of the older sedimentary rocks plus an additional Proterozoic source. As mentioned in section 5.1.1, the French River paragneiss in the Cosby subdomain has a single detrital population of 1744 ± 11 Ma, and thus could be coeval with deposition of the sediments associated with sample 14SV434. The French River quartzite in Cosby subdomain has only Archean zircons, and metamorphic monazites that yield 1062 ± 15 Ma (Krogh 1989). However, this was a U-Pb TIMS study, so only a limited number of grains were studied, which does not allow for a direct comparison between sample 14SV434 and the French River quartzite.

Of the three older quartzites, only sample 14SV557A yielded a ca. 1750 Ma metamorphic age. This result could mean that 14SV557A was affected by a metamorphic event at 1750 Ma, and the others were not. However, it is more likely is that samples 14SV557A, 14SV493 and NEP-Q were all affected by the same metamorphic event, but only 14SV557A had sufficient fluid flow and free Zr to crystallize large metamorphic zircon overgrowths. It is assumed that the metamorphic rims grew in situ, rather than before transport, as it is probable that transport

would have removed or damaged the rims. The rock(s) provided detritus for sample 14SV434A formed at the same time as metamorphism in the other three quartzite samples at ca. 1750 Ma.

Finally, quartzites do occur in Tomiko terrane, located northeast of North Bay and also part of the parautochthonous belt (Krogh 1989; Easton 2006). The Tomiko quartzites also have Archean ages as well as a population at circa 1685 Ma, which is distinct from that found in sample 14SV434A. Again, this was a U-PB TIMS study, so only a limited number of grains were studied, which does not allow for a direct comparison between sample 14SV434.

The presence of quartzites with similar age populations to the Huronian passive margin sediments supports the hypothesis that metasedimentary rocks in the Nepewassi domain were deposited originally on the distal edge of the Laurentian craton.

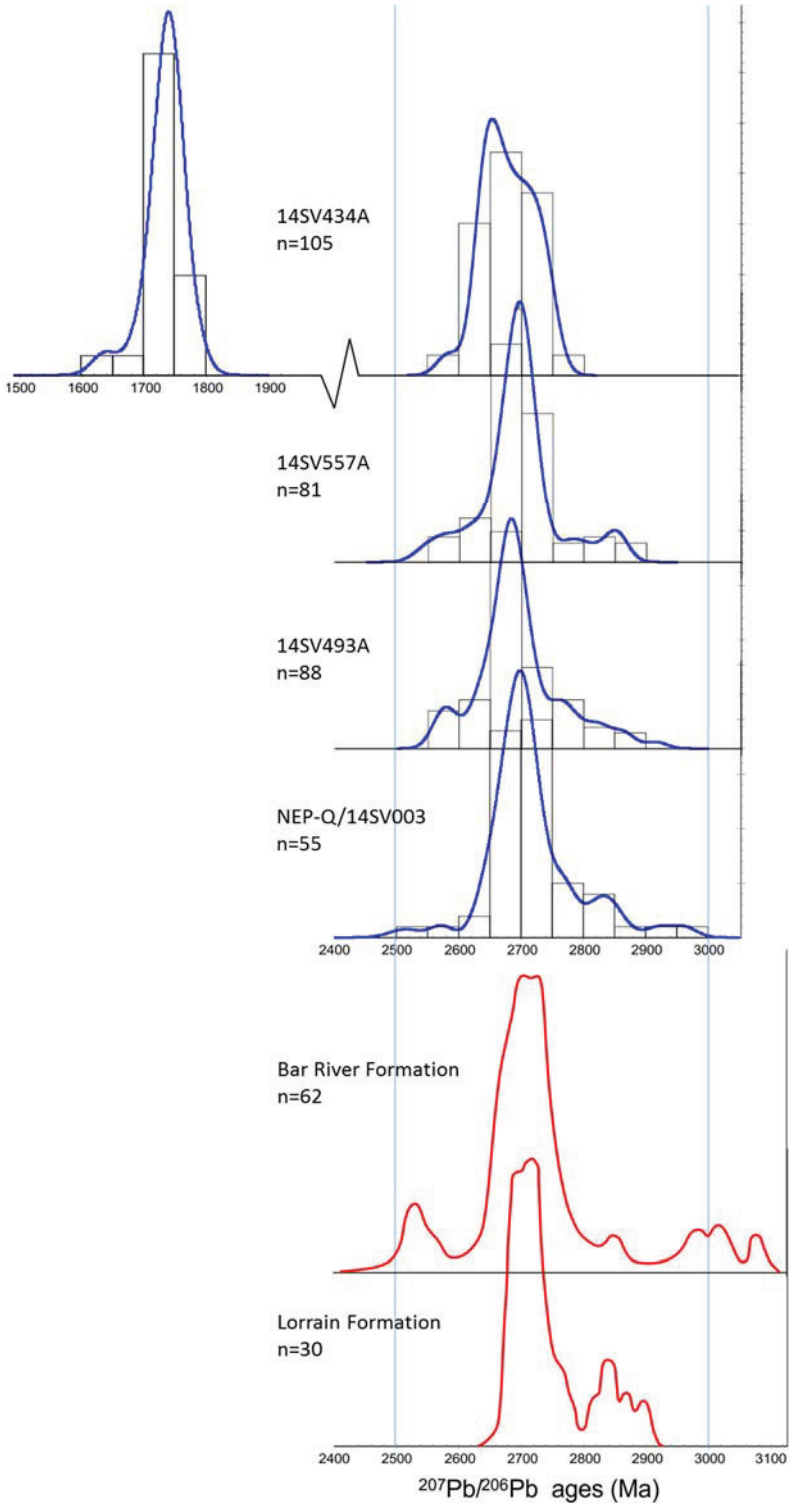

Figure 5.19: Detrital zircon data from the Lorrain Formation and Bar River Formation in the Huronian Supergroup (red) from Craddock et al. (2013) aligned with the data from the Nepewassi domain (blue). The alignment of the ca. 2.7 Ga peaks suggests that the Southern domain metasedimentary rocks are correlative with the Huronian or shared a similar source.

5.4.3 Metamorphic ages:

Prior to ca 1 Ga Grenvillian orogeny, southeast Laurentia was an active continental margin that was affected by several regionally significant tectonic events. These include the Penokean orogeny (1.89 – 1.83 Ga), the Yavapai orogeny (1.75 – 1.70 Ga), the Mazatzal/Labradorian orogeny (1.65 – 1.60 Ga), the Pinwarian orogeny (1.52 – 1.45 Ga) and the Elzevirian orogeny (1245 – 1220 Ma) (Hynes and Rivers 2010; Craddock et al. 2013). Some or all of these events may have affected rocks now in the Nepewassi domain.

The monazite analysis yielded three main metamorphic ages. The largest peak is a late Grenvillian, Rigolet phase peak at ca. 990 Ma, with a subsidiary Ottawan peak. The second prominent peak is a Yavapai peak at ca. 1750 Ma, and the smallest peak is late-Penokean at ca. 1820 Ma. The ca. 1410 Ma age determined by Regan (unpublished, 2014) corresponds within error to the Pinwarian orogeny, and also to ca. 1470 – 1340 Ma high-grade metamorphism and plutonism in the Kiosk domain (Ketchum et al. 1994; Corrigan et al. 1994; Culshaw et al. 2016) to the southeast. Although the ca. 1410 Ma age from the same sample is not statistically robust, it is included for comparison because monazite growth can be heterogeneous.

Based on the ages and petrographic context of monazite in sample 14SV542/N13-029, the relative chronology includes, but is not limited to, the events listed in Table 5.5.

Table 5.5: Summary of age constraints on multiple stages of monazite crystallization, garnet crystallization, kyanite crystallization and potentially partial melt.

Event	Age constraint
monazite growth possibly with no garnet growth or garnet break-down	Penokean-Yavapai ca. 1820 and ca. 1760 Ma
garnet crystallization (encasing monazite)	post-ca. 1600 Ma; pre-ca. 1290 Ma,
dissolution of monazites that were not encompassed by garnet (probably partial melting)	post-ca. 1720 Ma; pre-ca. 1080 Ma
monazite growth	ca. 1410 Ma
fracturing of garnet porphyroblasts,	pre-ca. 1290 Ma
formation and dissolution of kyanite	pre-ca. 1010 Ma
monazite growth (low Y rims) with garnet present or growing	Ottawan phase ca. 1050 Ma
garnet crystallized again	post-ca. 1020 Ma.
dissolutions of monazites (probably partial melting)	post-ca. 1020 Ma
monazite growth (low Y cores and high Y rims) while garnet is both breaking down and growing	Rigolet phase ca. 990 Ma

CHAPTER 6

DISCUSSION

This chapter is intended to synthesize data discussed in previous chapters into a timeline of tectonic development of the Nepewassi domain study area and hypothesize how the study area fits into the regional tectonic architecture. Suggestions are made for future research in the area.

6.1 Tectonic History

Based on conclusions from the previous chapters, the following tectonic history for rocks in the Southern subdomain of the Nepewassi domain is suggested.

6.1.1 Deposition of sediments along a Paleoproterozoic passive margin

Quartzites in the Nepewassi domain are similar in composition to aluminous quartzites in the Lorrain Formation (Chandler et al. 1969; Long 2004; Young 2015). Three quartzite samples, located roughly along strike of one another, also have a very similar detrital population to the Lorrain Formation, and other Huronian sediments. The Lorrain Formation is within the upper Huronian succession, which is interpreted to have been deposited on Archean basement as part of the Paleoproterozoic passive margin on the southern Laurentian margin (Zolnai et al. 1984; Young et al. 2001; Rainbird and Davis 2006b; Craddock et al. 2013; Young 2015). Although Lorrain Formation chemistry and Nepewassi quartzite chemistry do not precisely match (pers. com. M. Easton, 2016; Van De Kerckhove and Easton 2016), it is possible that there were chemical differences laterally along the passive margin, or that metasedimentary rocks found in the Nepewassi domain correlate with lesser known units of the Huronian Supergroup.

The thick Huronian Supergroup was faulted and reworked during the Penokean, Yavapai and/or other pre-Grenvillian orogenies (Zolnai et al. 1984; Fueten and Redmond 1994; Young 2015). During the Grenvillian orogeny, the already folded, faulted and probably disaggregated Huronian rocks would have been highly attenuated and deformed. Thus, if any Huronian rocks remain in the Grenville Province, they would occur as thin slivers and layers of metasedimentary and volcanic rocks. Their primary features and thicknesses would have been destroyed. This deformation could account for the present state of the supracrustal rocks in the Nepewassi domain. Thus, the Nepewassi quartzites are interpreted to have been deposited on the distal part of the Huronian passive margin (Figure 6.1 and Figure 6.3).

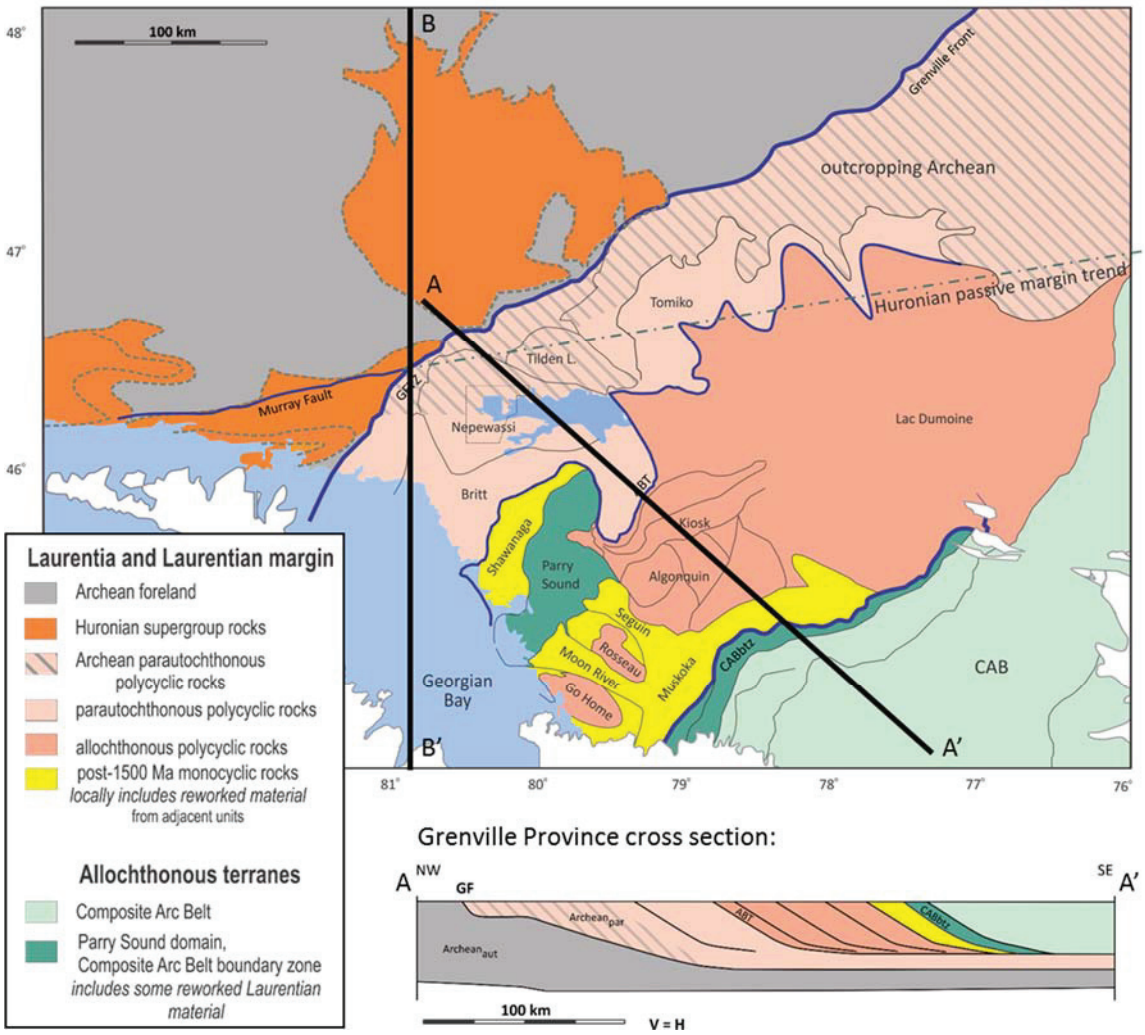

Figure 6.1: Map of the Grenville Province and adjacent Laurentian craton in Ontario and Quebec, with corresponding cross-section across the Nepewassi domain. Detailed map area in the Nepewassi domain is outlined and corresponds to Figure 6.2. The Murray Fault and trend of outcropping Archean rocks in the Grenville Province correspond to the Huronian passive margin trend. The deformation front of the Penokean orogeny is traced through the craton and Grenville Province. GFTZ, Grenville Front Tectonic Zone; ABT, allochthon boundary thrust; CABbtz, Composite Arc Belt boundary thrust zone; CAB, Composite Arc Belt; GF = Grenville Front; aut, autochthon; par, parautochthon. (pers. com. N. Culshaw, 2016, modified from Davidson 1986; Davidson and van Breemen 1988; Rivers et al. 1989; Culshaw et al. 1997; Carr et al. 2000; Ketchum and Davidson 2000; White et al. 2000)

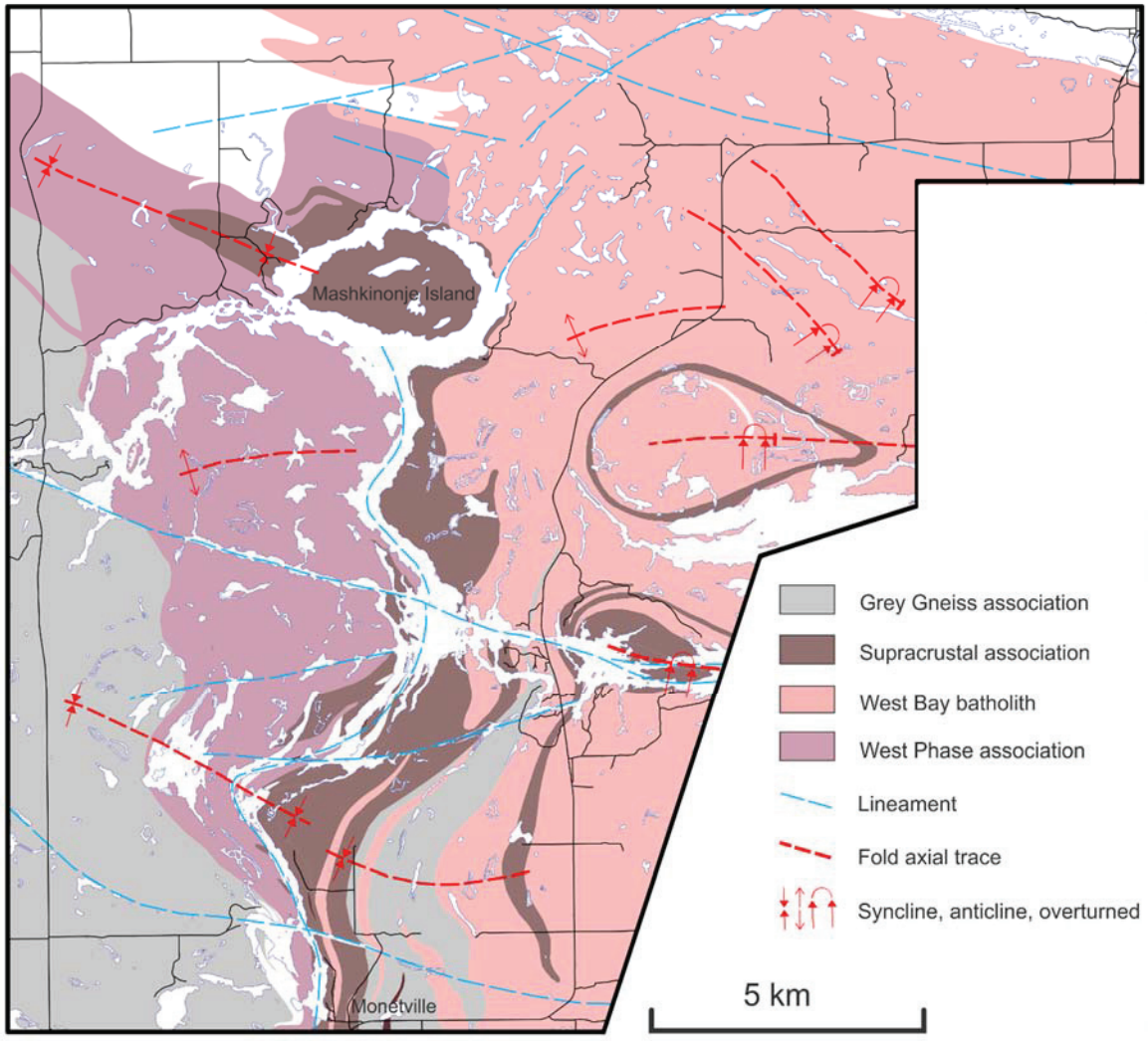

Figure 6.2: Simplified map of the detailed study area in the Southern subdomain of the Nepewassi domain. Map boundaries are outlined in Figure 6.1. The Grey Gneiss association represents predominantly tonalitic and granodioritic grey gneiss, and has an Archean igneous age from a sample taken from the southwest corner of the map area. West Phase association is predominantly leucocratic quartz monzonitic gneiss (West Phase) and monzogranite and diorite and gabbro gneiss.

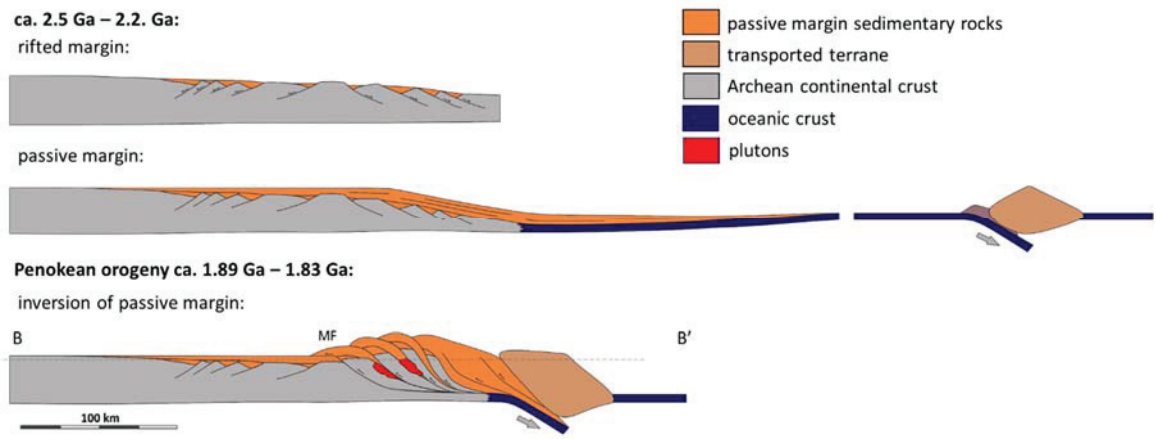

Figure 6.3: Schematic north – south cross section of the rifted margin and passive margin on the southwest edge of the Laurentian craton (upper panels), and the inversion of that passive margin during an accretionary orogeny (lower panel). The latter depicts thrust faults, a thickened sedimentary sequence, and plutonism. The cross section, B – B', corresponds to the map in Figure 6.1. Dashed line represents current erosional surface.

6.1.2 Inversion of the passive margin

The Great Proterozoic Accretionary Orogen (GPAO) was a protracted series of accretionary tectonic episodes including the Penokean orogeny (1.89 – 1.83 Ga), the Yavapai orogeny (1.75 – 1.70 Ga), the Mazatzal/Labradorian orogeny (1.65 – 1.60 Ga), all of which involved subduction and collision. The passive margin where the Nepewassi quartzites were deposited must have been inverted after deposition but before or during the Penokean orogeny. Monazite from a metasedimentary rock in the Nepewassi domain yielded late Penokean ages, interpreted as metamorphic, at ca. 1820 Ma, so the passive margin likely inverted before 1820 Ma (Figure 6.3), when normal faults were reactivated as thrusts. If the Archean tonalitic gneisses in the Southern subdomain are basement rocks, they may have been thrust up and imbricated with passive margin sediments during inversion (Figure 6.3).

6.1.3 Yavapai orogeny

Metamorphic monazites in the Nepewassi domain yield Yavapai (1608 Ma to 1780 Ma with a ca. 1760 Ma peak) ages, indicating the Nepewassi domain was affected by the Yavapai orogeny. Detrital igneous zircons in one quartzite sample with Yavapai (ca. 1750 Ma) ages, indicate that there was plutonism in or near the Nepewassi domain at this time (Figure 6.3). Similar igneous ages are documented for the nearby Killarney Magmatic Belt (1704 to 1749 Ma) and the Wanapitei complex (1694 to 1746 Ma) (Davidson and van Breemen 1988; Davidson et al. 1992;

Prevec 1992, 1995; Davidson and van Breeman 1994; Krogh 1994; Easton et al. 1999; Rousell et al. 2012; Raharimahefa et al. 2014).

6.1.4 Great Proterozoic Accretionary Orogen and Pre-Grenvillian

Metamorphic ages indicate that the Penokean and Yavapai orogenies affected the Nepewassi domain, but evidence for other GPAO and pre-Grenvillian orogenies (e.g., the Pinwarian orogeny from 1.52 – 1.45 Ga and the Elzevirian orogeny from 1.245 – 1.22 Ga) is sparse. Multiple metamorphic events occurred between the Yavapai and the Grenvillian orogenies, but the timing of these events is not well constrained. These events included: post-Yavapai sedimentation, indicated by a quartzite with a ca. 1750 Ma detrital population, dissolution of monazites and probably partial melting at some time between ca. 1720 Ma and ca. 1080 Ma, garnet crystallization sometime between ca. 1600 Ma and ca. 1290 Ma, metamorphism ca. 1410 Ma, kyanite formation and dissolution pre-1010 Ma. Furthermore, zircon yielded a ca. 1250 Ma age for the West Bay batholith (Aldis 2016). If the West Phase, which has a strong association with mafic plutons, is the same age as the West Bay batholith, there may have been bimodal magmatism at ca. 1250 Ma, suggesting possible rifting, potentially in a back arc to the Central Metasedimentary Belt. A deformation event, D_1, created a foliation which affects the West Bay batholith and defines folds in the Nepewassi domain, thus, D_1 occurred after or potentially syn-emplacement of the ca. 1250 Ma West Bay batholith, but before D_2/F_2. D_1 created the earliest fabric that is mapped; however, there would have been multiple deformation events and fabrics in the Nepewassi prior to D_1.

6.1.5 Grenvillian – Ottawan phase

Folding (F_2):

The fold interference pattern (D_2/F_2 and D_3/F_3) that affects the West Bay batholith, so D_2 must have occurred after ca. 1250 Ma. Monazite associated with garnets in the Nepewassi domain metapelites yielded Ottawan metamorphic ages. Based on relict granulite facies metamorphic minerals in some samples, this metamorphic event may have been granulite facies; however, there is no constraint on the age of granulite facies metamorphism. It is possible that granulite facies metamorphism is relict from the earliest, Archean, events. If Ottawan aged metamorphism occurred congruently with deformation, structures associated with these rocks, including F_2 and fold hinge-parallel lineations, likely formed during the Ottawan phase of the Grenvillian orogeny.

Westward thrusting:

The WAHSZ is interpreted to have formed during or after F_2, but before F_3. Thermobarometry from a garnet amphibolite on the east edge of the WAHSZ suggests that rocks to the east of the WAHSZ were thrust over those on the west. The ages of tectonic schists in the Nepewassi domain are not well constrained; a pegmatite associated with one of them cuts gneissic layering suggesting it formed after D_1. Because the tectonic schists, which are also interpreted to have formed during shearing, have a similar orientation as the WAHSZ, they are interpreted to have formed around the same time.

Folding (F_3):

The second phase of folding (F_3) likely formed late in the Ottawan age phase and because the hinges trend parallel to the SCLSZ, F_3 may corresponds to transpression that formed the SCLSZ. This deformation (D_3) was likely a response to thrusting in the Britt domain (Culshaw et al. 1994). Monazite metamorphic ages from the late Ottawan likely correspond to D_3.

6.1.6 Grenvillian – Rigolet phase

Metamorphic monazite from a pelite in the WAHSZ yielded a strong Rigolet peak at ca. 990 Ma, possibly recording the time of amphibolite facies metamorphism in the same sample and another to the west. Dissolution textures of monazites suggests partial melting and/or dissolution of monazite after 1020 Ma. Kinematic indicators in the mylonites (corresponding to L_3) show oblique-normal shear. Ductile extension has been documented in the Central Gneiss Belt between ca. 1040 Ma and ca. 990 Ma, and continues as lower grade extension late in the Grenvillian orogeny, and afterward (Culshaw et al. 1994, 1997, 2016; Ketchum 1994; Ketchum et al. 1998). Relatively low-grade ductile deformation seen in thin section (S_{lg}) may have formed during this time as well. Tectonic schists have similar orientations to the mylonites; however, it is not known whether they formed at the same time.

6.1.7 Late to post-Grenvillian

Petrographic studies show that many rocks have evidence of partial greenschist facies retrogression, and several relatively low grade lineaments overprint previous structures in the Nepewassi domain.

6.1.8 Summary

The following table summarizes tectonic and metamorphic events documented in the Nepewassi domain. They are listed, based on present data, in chronological order.

Table 6.1: Summary table of the tectonic and metamorphic events in the Nepewassi domain.

Event	Age constraint
formation of tonalitic and granodioritic grey gneisses	ca. 2.7 Ga
deposition of sediments on the Huronian passive margin	inferred between ca. 2.4 and 2.2 Ga
inversion of passive margin	inferred early Penokean
monazite growth possibly with no garnet growth or garnet break-down	Penokean ca. 1820 Ma
monazite growth possibly with no garnet growth or garnet break-down	Yavapai ca. 1760 Ma
nearby plutonism, based on detrital igneous zircons	ca. 1750 Ma
deposition of sediments	post-ca. 1630 Ma
dissolution of monazites that were not encompassed by garnet (probably partial melting)	post-ca. 1720 Ma; pre-ca. 1080 Ma.
garnet crystallization (encasing monazite)	post-ca. 1600 Ma; pre-ca. 1290 Ma,
metamorphic monazite	ca. 1410 Ma
fracturing of garnet porphyroblasts,	pre-ca. 1290 Ma
West Bay batholith and probably bimodal magmatism	ca. 1250 Ma
foliation forming deformation (D_1)	syn- to post-ca. 1250 Ma
D_2/ F_2/stretching lineations	post-ca. 1250 Ma
monazite growth (low Y rims) with garnet present or growing	Ottawan phase ca. 1050 Ma
? granulite facies metamorphism	inferred Ottawan phase ca. 1050 Ma
WAHSZ and tectonics schists(?)	inferred Ottawan phase ca. 1050 Ma
D_3/F_3/SCLSZ	inferred late Ottawan phase
garnet crystallized again	post-ca. 1020 Ma.
dissolutions of monazites (probably partial melting)	post-ca. 1020 Ma
formation and dissolution of kyanite	pre-ca. 1010 Ma
monazite growth (low Y cores and high Y rims) while garnet is both breaking down and growing	Rigolet phase ca. 990 Ma
amphibolite facies metamorphism	inferred Rigolet phase ca. 990 Ma
oblique extensional shear (mylonites) L_3	inferred ca. 1040 Ma to ca. 990 Ma
relatively low grade ductile deformation	inferred late to post-Grenvillian
greenschist facies retrogression, and lineaments	inferred late to post-Grenvillian

6.2 Regional Implications

Metasedimentary rocks in the Nepewassi domain, interpreted as passive margin sediments, fall along the projected trend of the Paleoproterozoic (Huronian) passive margin, relative to the Grenville Front (Figure 6.1). At ca. 2.5 Ga, the margin of the Laurentian/Superior craton trended generally northeast, relative to modern landforms (Whitmeyer and Karlstrom 2007); however, north and west of Georgian Bay, it likely trended approximately east–northeast, like the trend of outcropping of Archean rocks within the Grenville Province (Figure 6.1). Seismic reflection profiles show that inferred Archean rocks underlie much of the northern flank of the Grenville Province (Hynes et al. 2000; Ludden and Hynes 2000; Hynes and Rivers 2010). The inferred Archean indentor is thin and deep along Georgian Bay, but thickens along strike to the northeast (Figure 6.4), suggesting that an Archean ramp may have been oriented parallel to the interpreted trend of the Superior passive margin. Northwest of the study ares, the Murray Fault originated as a normal fault, dipping towards the basin, that was reactivated during the Penokean as a north-verging reverse fault(s) (Zolnai et al. 1984; Fueten and Redmond 1994). Similar reversal of pre-existing normal faults may have brought Archean basement rocks to the same level as passive margin sediments in the Southern subdomain (Figure 6.3). The Murray Fault runs through Huronian sedimentary rocks with Penokean-aged folds, suggesting the inversion of faults and folding are related, and thus, inversion occurred during the Penokean orogeny (Young 2015). The Murray Fault and related faults were overprinted by the Grenvillian structures.

Apart from the emplacement of a few plutonic bodies (West Bay batholith, Cosby pluton, Mercer anorthosite, and St. Charles anorthosite), the tectonic evolution of the Nepewassi domain is poorly constrained after ca 1750 Ma (Yavapai) and before ca 1080 Ma (Ottawan). It is therefore not known how the crustal architecture evolved from the (hypothesized) post-Penokean/Yavapai, cross-section (B-B', Figure 6.3) to the current, post-Grenvillian cross-section (A-A', Figure 6.1).

Fold interference patterns, interpreted to have resulted from two generations of Grenvillian deformation, are apparently found only in parautochthonous belts of the Grenville Province. Interference patterns similar to the ones in the Nepewassi domain are located in the Tomiko domain (pers. com. M. Easton, 2016), and Type 3 interference patterns (Ramsay 1967), with northwest-trending hinges, are present to the west of the Southern subdomain (Lumbers 1974). As depicted in Figure 6.4, much of the parautochthonous belt is underlain by a thick Archean indentor, or basement. F_2 folds likely formed on top of relatively shallow detachment faults in relatively weaker material than the underlying Archean ramp or indentor, making them slightly

different from folds in the rest of the Central Gneiss Belt. Fold geometry changes from east of the WAHSZ to the west of it, suggesting the WAHSZ may be a shallow detachment fault. The subsequent, F_3 folds in the late Ottawan are likely similar to folds in the rest of the Central Gneiss Belt.

On a regional scale, southeast to northwest emplacement of allochthonous terranes began ca. 1190 Ma in the Central Metasedimentary Belt boundary thrust zone and Parry Sound domain (van Breemen et al. 1986; Culshaw et al. 1997). Northwest-directed Ottawan thrusting is interpreted to have occurred in the Central Gneiss Belt after ca. 1080 Ma (Culshaw et al. 1994, 1997). Extension on the SSZ is bracketed between 1040 and 990 Ma (Ketchum 1994; Ketchum et al. 1998), and thrusting in the GFTZ was active at ca 1000 Ma. If the WAHSZ, which is interpreted as a thrust, is related to thrusting in the surrounding (sub)domains, it is still unknown why it has a different orientation. Similarly, south-verging folds in the Nepewassi domain are a different orientation than folds in surrounding domains. The south-verging folds and WAHSZ are apparently truncate at the boundary with the Cosby subdomain. The Britt domain (and probably the Cosby subdomain) is interpreted to have been emplaced upon the Nepewassi domain by northwest-directed thrusting (Culshaw et al. 1994; Jamieson et al. 1995). If emplacement of the Britt domain was the driving force for folding in the Nepewassi domain, northwest verging folds are expected; however, that is not the case. South verging F_3 folds are potentially a product of the orientation of the transpressional stresses that formed the SCLSZ and possibly, in part, an effect of the shape of underlying Archean ramp. However, the oblique nature of structures in the Southern subdomain, relative to surrounding domains, is poorly understood and requires further investigation.

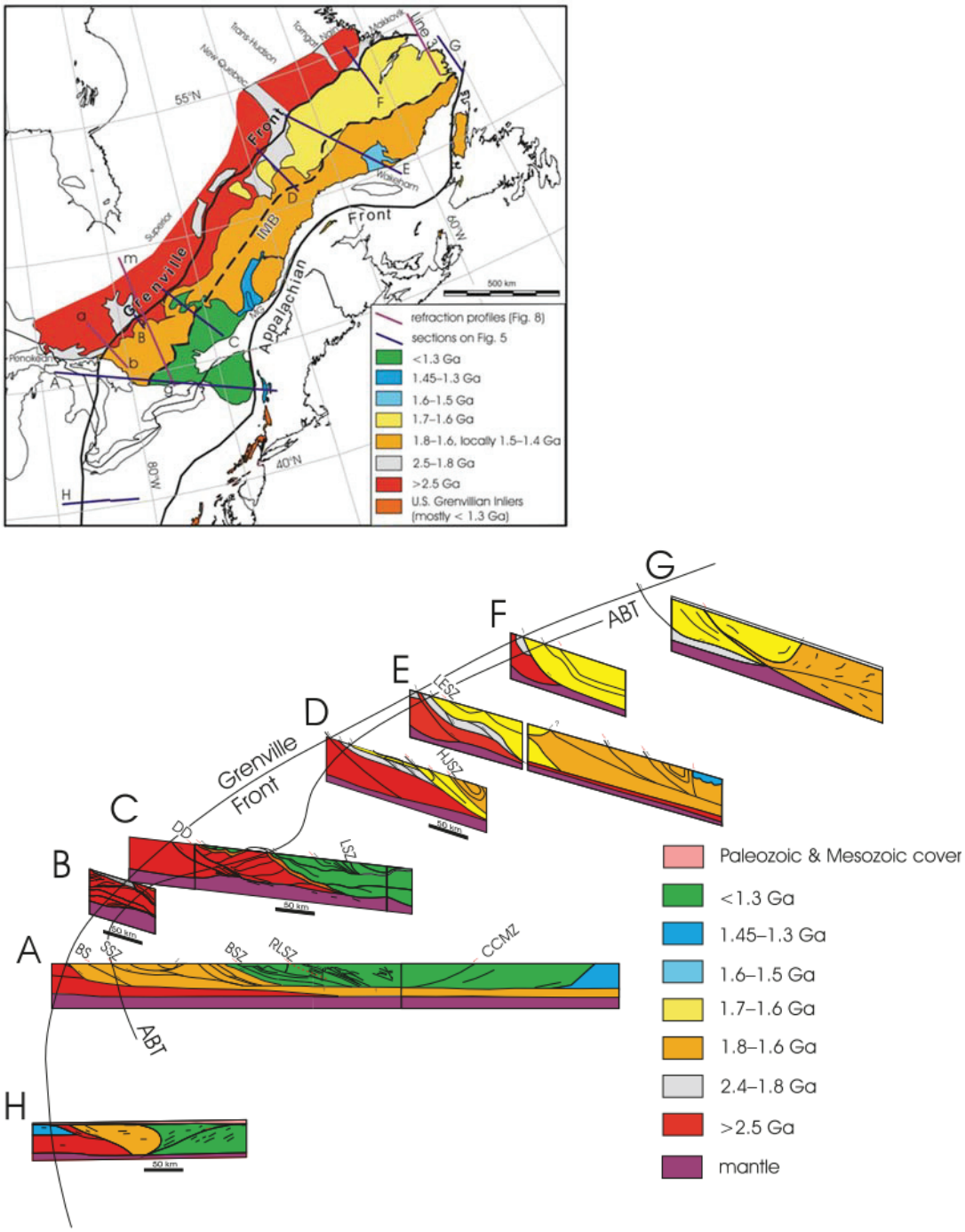

Figure 6.4: Map and interpreted crustal-scale cross-sections of the Grenville Orogen compiled by Hynes and Rivers (2010). The red depicts an inferred Archean indentor that thickens to northeast along-strike, eventually tapering out and disappearing in Labrador. ABT, Allochthon Boundary Thrust; BS, Boundary shear; SSZ, Shawanaga shear zone; BSZ, Bancroft shear zone; RLSZ, Robertson Lake shear zone; CCMZ, Cartage–Colton shear zone; DD, Dorval detachment; LSZ, Labelle shear zone; HJSZ, Hart-Jaune shear zone; LESZ, Lac Émerillon shear zone.

6.3 Future Work

Continued geochronological, geochemical and field studies are needed in order to constrain the tectonic history of the Nepewassi domain better. Below is a list of recommended targets for study.

The first recommendation is to determine the protolith ages of tonalitic gneisses mapped to the east of the WAHSZ (Figure 6.2). If these gneisses prove to be Archean, like the tonalitic and granodioritic gneiss to the west of the WAHSZ (Figure 6.2), then Archean (possible basement) rocks sit structurally both below and above a Paleoproterozoic supracrustal package and the WAHSZ. This would provide substantial evidence for significant westward-verging imbrication.

One way to test whether the Archean rocks in the Southern subdomain are cratonic basement, or part of a separate but similarly aged terrane, would be to study the geochemistry and geochronology of metadiabase dikes within them. Well documented dikes that cut the Laurentian craton include the ca. 1240 Ma Sudbury diabase dike swarm (Krogh et al. 1987; Bethune and Davidson 1997), and ca. 2220 Ma Nippissing diabase suite (Corfu and Andrews 1986). If tonalitic and granodioritic grey gneisses in the Nepewassi domain are cratonic basement, both types of dikes would be expected also to cut rocks in the Nepewassi domain. If the Archean rocks in the Nepewassi domain were originally a separate, similarly aged terrane, emplaced during the GPAO, Sudbury dikes, but no Nippissing dikes are expected. However, the original spatial distribution of both types of dikes may result in a lack of dispersion in the Nepewassi domain, regardless of its origin. In addition, the Nippissing diabase suite forms sills, typically along unconformities, so a similar contact would need to be present in the Nepewassi domain for Nippissing diabase rocks to have been emplaced. Numerous dikes of unknown affinity cut the tonalitic gneiss north of Noelville on highway 535 (Appendix A) in the Southern subdomain. Two metadiabase dikes with similar chemistry to the Sudbury dike swarm intruded the West Phase, one on highway 535 and one on the shoreline near the Little Cut (stations 14SV299 and 14SV503 Appendix A.2; Van De Kerckhove and Easton 2016). Because the West Phase intruded the tonalitic gneisses, these dikes are recommended targets for geochemical and metamorphic study. Studying the metamorphism of Sudbury dikes would yield Grenvillian results, without inheritance from pre-Grenvillian metamorphism. In addition, a foliated and lineated heterogeneous dike on highway 535, north of Noelville (station 14SV339, Appendix A.2) is dissimilar to any other dike documented in the Nepewassi domain and warrants further investigation (Chapter 2, section 2.3.2).

The West Bay batholith was initially interpreted to have formed at 1700 ± 150 Ma (Lumbers 1975) but recent U-Pb igneous zircon studies yielded an age of ca. 1250 Ma (Aldis 2016). No ages have been obtained from the West Phase. The Cosby pluton yielded ca. 1420 Ma (Lumbers 1975), 1434 ± 30 Ma and 1488 ± 16 Ma (Aldis 2016) ages. The Sturgeon Falls batholith (in the Northern subdomain) and Pine Cove pluton (in the Cosby subdomain) are similar in composition and texture to the West Bay batholith (Lumbers 1975) and have 1245 ± 12 Ma and 1451 ± 7 ages respectively (Aldis 2016). The Cosby pluton cuts the migmatitic Pine Cove pluton (Lumbers 1975), indicating the Cosby pluton is younger than the Pine Cove pluton; however, their ages are the same within error. The West Bay batholith is similar in composition and texture to the Wanapitei magmatic complex (Easton 2014) and the older plutons of the Killarney Magmatic Belt (ca. 1740 Ma and ca 1450 Ma) (Davidson and van Breeman 1994; Krogh 1994; Easton 2014; Raharimahefa et al. 2014; Aldis 2016). Geochronological studies on the French River granite (Nepewassi domain, southwest of the Cosby pluton), yield similar igneous ca. 1700 Ma ages (Krogh and Davis 1969, 1972; Easton 2014). In addition, the composition and textures of the West Phase and associated diorite units are similar to those described in the Wanapitei complex, particularly the probable magma mingling textures in the on highway 535 (Easton 2014). A detailed geochronological study of the granitoid plutons in the Nepewassi domain is recommended, particularly the West Phase. The lower, migmatitic the West Bay batholith is interpreted to have thrust over the non-migmatitic West Phase, but it is still unclear if the two were originally part of the same pluton or not. The West Phase is closely associated with mafic intrusions, suggesting bimodal magmatism at the time of emplacement, but the West Bay batholith is not. Furthermore, detailed geochronological, and geochemical, studies are needed in order to investigate the apparent correlation between the West Phase and the Wanapitei magmatic complex and/or the Killarney Magmatic Belt. It would also be useful to target anatectic melts in the West Bay batholith in order to constrain the timing of migmatization.

In addition to igneous geochronology, a detailed study of metamorphic ages, using monazite and/or zircon from supracrustal rocks along the West Arm, is recommended. Analyzing a large number of metamorphic grains or overgrowths would improve the statistical significance of the results from this study, and potentially provide better age constraints on metamorphism and deformation in the Nepewassi domain between the Yavapai and Grenvillian orogenies.

The last recommendation is for field work targeted on the WAHSZ north and south of where it is currently mapped. The relationship of this structure to bounding subdomains is unknown.

Field work could answer the following questions: Does the WAHSZ terminate near Mashkinonje Island, or does it continue north or northwest? Does the WAHSZ connect with the SCLSZ or is it cut off by it? Similarly, is the WAHSZ cut off by the boundary between the Southern subdomain and the Cosby subdomain? The answer to these questions may provide insight into the relationships between subdomains. Limited accessible outcrop in these areas poses a problem, but geophysical maps may be able to supplement field work.

CHAPTER 7

CONCLUSIONS

The Nepewassi domain is composed of tonalitic and granodioritic grey gneiss intruded by large granitoid plutons, and smaller mafic plutons. The Southern subdomain is composed of tonalitic and granodioritic grey gneiss and a north-south trending package of supracrustal rocks; both are intruded by a large migmatitic quartz monzonite pluton (West Bay batholith) on the eastern portion, and bimodal magmatism in the west.

Multiple deformation events have affected the Southern subdomain, forming fold interference patterns and a shallow, westward thrusting shear zone, the West Arm high strain zone. Folds verge south in the Southern subdomain, but are generally upright in the surrounding subdomains. Fold interference patterns are found within the parautochthonous belt of the Grenville Province, but are apparently absent in allochthonous belts. Southeast-trending, oblique-extensional shears the Southern subdomain overprint earlier structures.

A garnet amphibolite sample on the east edge of the WAHSZ yielded upper amphibolite facies P-T results, average 10.6 ± 0.5 kbar - 773 ± 25°C. Two pelite samples, one within the WAHSZ and one to the west of it, both yield amphibolite facies P-T results, averaging 6.8 ± 1 kbar - 632 ± 25°C and 7.3± 1 kbar - 656 ± 25°C respectively. Mineral assemblages in most rocks indicate amphibolite facies, but in some samples, relict granulite facies minerals are present, and in many samples, there is partial retrogression to greenschist facies.

Archean tonalitic and granodioritic grey gneisses, similar in age, ca. 2.7 Ga, and composition to rock in Laurentian craton near the Grenville Front, outcrop in the Northern and Southern subdomains of the Nepewassi domain. Quartzites in the Nepewassi domain have a very similar detrital population to rocks in the Huronian Supergroup. This detrital age, ca. 2.7 Ga, is similar to Archean rocks in the Nepewassi domain and Laurentian craton. One quartzite from the Nepewassi domain has an additional, younger detrital population with an age of ca. 1750 Ma.

Multiple metamorphic ages are documented in metasedimentary rocks in the Nepewassi domain corresponding to known orogenic events. They are: late Penokean, ca. 1820 Ma; Yavapai, ca. 1720 to ca. 1750 Ma; late- to post-Pinwarian, ca. 1410 Ma; and two Grenvillian phases - Ottawan, ca. 1050 Ma; and Rigolet, ca. 990 Ma.

Metasedimentary rocks in the Nepewassi domain were likely deposited on the southern edge of the Superior craton in Paleoproterozoic (Huronian) passive margin. The passive margin was inverted, probably just before or during the Penokean orogeny. There was plutonism in or near the Nepewassi during the Yavapai and subsequent sedimentation. The rocks of the Nepewassi domain were affected by one or more post-Yavapai, pre-Grenvillian event before being folded and sheared in the Grenvillian orogeny.

APPENDIX A

GEOLOGICAL MAPS AND GEOGRAPHICAL INFORMATION

A.1 FIGURE 1 Precambrian Geology of the West Arm of Lake Nipissing, Grenville Province

Figure 1, attached as a fold out in the back of the thesis, is a lithological and structural map of the chosen study area in the Southern subdomain.

A.2 FIGURE 2 Precambrian Geology of the West Arm of Lake Nipissing, Grenville Province

Figure 2, attached as a fold out in the back of the thesis, is a lithological map of the chosen study area in the Southern subdomain with station locations.

A.3 Geographical coordinates of map stations

Table A.1: Geographical location of map stations in latitude longitude, and Universal Transverse Mercator projection.

STATION NUMBER	LATITUDE	LONGITUDE	Nad 83, Zone 17 EASTING (in metres)	Nad 83, Zone 17 NORTHING (in metres)
14SV003	46.18268870	-80.36946644	548663	5114538
14SV005	46.25022534	-80.43314352	543695	5122005
14SV006	46.24580697	-80.43326686	543689	5121514
14SV007	46.24085672	-80.43321407	543697	5120964
14SV008	46.23832219	-80.43391462	543645	5120682
14SV009	46.19024362	-80.43201100	543830	5115341
14SV028	46.31478259	-80.17583948	563454	5129352
14SV029	46.31514771	-80.17530147	563495	5129393
14SV030	46.31765625	-80.17371808	563614	5129673
14SV031	46.30772875	-80.19380214	562079	5128554
14SV032	46.30761506	-80.19682972	561846	5128539
14SV033	46.30771284	-80.20697093	561065	5128542
14SV034	46.30816079	-80.22904210	559365	5128575
14SV035	46.30825542	-80.22972907	559312	5128585
14SV036	46.30813101	-80.23130222	559191	5128570
14SV037	46.30779626	-80.23372245	559005	5128531
14SV038	46.30774479	-80.24220351	558352	5128519
14SV039	46.30771715	-80.24619082	558045	5128513

Table A.1: *Continued.* Geographical location of map stations in latitude longitude, and Universal Transverse Mercator projection.

STATION NUMBER	LATITUDE	LONGITUDE	Nad 83, Zone 17 EASTING (in metres)	Nad 83, Zone 17 NORTHING (in metres)
14SV040	46.23571479	-80.25262465	557625	5128508
14SV041	46.30762885	-80.26023067	556964	5128493
14SV042	46.30698802	-80.26273272	556772	5128420
14SV043	46.30561054	-80.26545235	556567	5128310
14SV044	46.30561054	-80.26545235	556564	5128265
14SV045	46.29655811	-80.26989711	556231	5127256
14SV046	46.29552271	-80.26983297	556237	5127141
14SV047	46.29266848	-80.26963721	556255	5126824
14SV048	46.29039278	-80.26983623	556242	5126571
14SV049	46.28663996	-80.26986014	556244	5126154
14SV050	46.27861174	-80.27405544	555929	5125259
14SV051	46.27771077	-80.27674114	555723	5125157
14SV052	46.27243719	-80.28972402	554728	5124562
14SV053	46.26993618	-80.29570016	554270	5124280
14SV054	46.26713894	-80.30038181	553912	5123966
14SV055	46.26419980	-80.30396177	553639	5123637
14SV056	46.26255839	-80.30487789	553570	5123454
14SV057	46.25911655	-80.30572585	553508	5123071
14SV058	46.25601708	-80.30663426	553441	5122726
14SV059	46.25357839	-80.30816998	553325	5122454
14SV060	46.25290815	-80.30895683	553265	5122379
14SV061	46.25162650	-80.30984215	553198	5122236
14SV062	46.24948123	-80.31079014	553127	5121997
14SV063	46.24726082	-80.30972827	553211	5121751
14SV064	46.24273086	-80.30774857	553368	5121249
14SV065	46.23881540	-80.31065132	553148	5120812
14SV066	46.23780380	-80.31154596	553080	5120699
14SV067	46.23814225	-80.31095807	553125	5120737
14SV068	46.24072129	-80.30881152	553288	5121025
14SV069	46.22847582	-80.31388013	552909	5119661
14SV070	46.22263162	-80.31185234	553071	5119013
14SV071	46.22103476	-80.31121101	553122	5118836
14SV072	46.21864329	-80.31013883	553207	5118571
14SV073	46.21724424	-80.30946919	553260	5118416
14SV074	46.21523488	-80.30907950	553292	5118193
14SV075	46.21348720	-80.30880323	553315	5117999
14SV076	46.21225280	-80.30857240	553334	5117862
14SV077	46.21083028	-80.30848654	553342	5117704
14SV078	46.20845170	-80.30806267	553377	5117440

Table A.1: *Continued.* Geographical location of map stations in latitude longitude, and Universal Transverse Mercator projection.

STATION NUMBER	LATITUDE	LONGITUDE	Nad 83, Zone 17 EASTING (in metres)	Nad 83, Zone 17 NORTHING (in metres)
14SV079	46.19943171	-80.30625765	553525	5116439
14SV080	46.19773217	-80.30649938	553508	5116250
14SV081	46.19184779	-80.30233567	553835	5115599
14SV082	46.19180791	-80.29875938	554111	5115597
14SV083	46.19166080	-80.29532702	554376	5115583
14SV084	46.19073081	-80.30661336	553506	5115472
14SV085	46.17215432	-80.30656185	553528	5113408
14SV086	46.17178401	-80.30634628	553545	5113367
14SV087	46.16734957	-80.30677768	553516	5112874
14SV088	46.16310581	-80.32098823	552423	5112393
14SV089	46.16313323	-80.32409653	552183	5112394
14SV090	46.16313563	-80.32755486	551916	5112392
14SV091	46.16317260	-80.32925121	551785	5112395
14SV092	46.16315631	-80.33261911	551525	5112391
14SV093	46.16314252	-80.33488599	551350	5112388
14SV094	46.16313507	-80.33825377	551090	5112385
14SV095	46.16305617	-80.35118145	550092	5112368
14SV098	46.16699115	-80.35950319	549446	5112800
14SV099	46.16783289	-80.35874210	549504	5112894
14SV100	46.16903866	-80.35709588	549630	5113029
14SV101	46.17294323	-80.35364323	549893	5113465
14SV102	46.17475504	-80.35254670	549976	5113667
14SV103	46.16307889	-80.35360333	549905	5112369
14SV104	46.27892677	-80.33008561	551612	5125256
14SV105	46.28161955	-80.32885858	551704	5125556
14SV106	46.28610546	-80.32953077	551648	5126054
14SV107	46.28978904	-80.33305600	551373	5126461
14SV108	46.29131770	-80.33591964	551151	5126629
14SV109	46.29190517	-80.33789894	550998	5126693
14SV110	46.29401747	-80.34524810	550430	5126923
14SV111	46.29418096	-80.34866082	550167	5126939
14SV112	46.29401500	-80.34954566	550099	5126920
14SV113	46.29386290	-80.34970326	550087	5126903
14SV114	46.29338926	-80.35029312	550042	5126850
14SV115	46.29285254	-80.35087073	549998	5126790
14SV116	46.29196038	-80.35384139	549770	5126689
14SV117	46.29179657	-80.35511565	549672	5126670
14SV118	46.29145102	-80.35608044	549598	5126631
14SV119	46.29929773	-80.34950908	550097	5127507

Table A.1: *Continued.* Geographical location of map stations in latitude longitude, and Universal Transverse Mercator projection.

STATION NUMBER	LATITUDE	LONGITUDE	Nad 83, Zone 17 EASTING (in metres)	Nad 83, Zone 17 NORTHING (in metres)
14SV120	46.30181132	-80.34838854	550181	5127787
14SV121	46.30198179	-80.34829562	550188	5127806
14SV122	46.30455529	-80.34821314	550192	5128092
14SV123	46.30535771	-80.34846334	550172	5128181
14SV124	46.30664086	-80.34937015	550101	5128323
14SV125	46.29093756	-80.35920232	549358	5126572
14SV126	46.28882018	-80.36522481	548896	5126333
14SV127	46.28628040	-80.36814906	548673	5126049
14SV128	46.28482559	-80.36872398	548630	5125887
14SV129	46.28074908	-80.35910044	549375	5125440
14SV130	46.27894441	-80.35826481	549441	5125240
14SV131	46.27860012	-80.35625696	549596	5125203
14SV132	46.27768092	-80.35285408	549859	5125103
14SV133	46.27139710	-80.34149430	550740	5124412
14SV134	46.27691084	-80.35037109	550051	5125019
14SV135	46.27680829	-80.34816580	550221	5125009
14SV136	46.27635054	-80.34209691	550689	5124962
14SV137	46.27672193	-80.34095028	550777	5125004
14SV138	46.27569909	-80.33993719	550856	5124891
14SV139	46.27620864	-80.33623198	551141	5124950
14SV140	46.27704242	-80.33413221	551302	5125044
14SV141	46.27590287	-80.32703341	551850	5124922
14SV142	46.27668160	-80.32631001	551905	5125009
14SV143	46.27821945	-80.32459082	552036	5125181
14SV144	46.27913139	-80.32356717	552114	5125283
14SV145	46.28375286	-80.32129053	552285	5125798
14SV146	46.28665900	-80.32115078	552293	5126121
14SV147	46.28774522	-80.32068300	552328	5126242
14SV148	46.28934767	-80.31924810	552437	5126421
14SV149	46.29160285	-80.31559793	552716	5126674
14SV150	46.29648241	-80.31136925	553037	5127219
14SV151	46.29731543	-80.31070960	553087	5127312
14SV152	46.29962453	-80.30857708	553249	5127570
14SV153	46.29962021	-80.30786297	553304	5127570
14SV154	46.30118090	-80.30550597	553484	5127745
14SV155	46.30155546	-80.30346254	553641	5127788
14SV156	46.30273270	-80.29875983	554002	5127922
14SV157	46.30105147	-80.29319768	554432	5127739
14SV158	46.30263360	-80.29581338	554229	5127913

Table A.1: *Continued.* Geographical location of map stations in latitude longitude, and Universal Transverse Mercator projection.

STATION NUMBER	LATITUDE	LONGITUDE	Nad 83, Zone 17 EASTING (in metres)	Nad 83, Zone 17 NORTHING (in metres)
14SV159	46.29395697	-80.31345230	552879	5126937
14SV160	46.28806358	-80.32125027	552284	5126277
14SV161	46.28599336	-80.32424863	552055	5126045
14SV162	46.28646447	-80.32477508	552014	5126097
14SV163	46.28761952	-80.32529315	551973	5126225
14SV164	46.28798971	-80.32549632	551957	5126266
14SV165	46.29200410	-80.32862787	551712	5126710
14SV166	46.29138338	-80.32867441	551709	5126641
14SV167	46.29133411	-80.32947995	551647	5126635
14SV168	46.29159844	-80.33004797	551603	5126664
14SV169	46.29223879	-80.33181884	551466	5126734
14SV170	46.29598167	-80.34249806	550640	5127143
14SV171	46.29650901	-80.34499767	550447	5127200
14SV172	46.29776623	-80.34451525	550483	5127340
14SV173	46.29731664	-80.34458553	550478	5127290
14SV174	46.29736379	-80.34496151	550449	5127295
14SV175	46.29683809	-80.34746074	550257	5127235
14SV176	46.30749114	-80.35012629	550042	5128417
14SV177	46.30819338	-80.35016993	550038	5128495
14SV178	46.31149686	-80.35026071	550028	5128862
14SV179	46.31192322	-80.35085310	549982	5128909
14SV180	46.31300748	-80.35002203	550045	5129030
14SV181	46.29416846	-80.35919060	549356	5126931
14SV182	46.31355481	-80.34972982	550067	5129091
14SV183	46.31430587	-80.34886369	550133	5129175
14SV184	46.31543115	-80.34891529	550121	5129239
14SV185	46.29616943	-80.35492149	550128	5129300
14SV186	46.29618472	-80.35444091	549683	5127156
14SV187	46.29618472	-80.35444091	549720	5127158
14SV188	46.29456171	-80.35549867	549640	5126977
14SV189	46.29300988	-80.35961958	549324	5126802
14SV190	46.29246216	-80.36145658	549183	5126740
14SV191	46.29240329	-80.36219730	549126	5126733
14SV192	46.29240145	-80.36348265	549027	5126732
14SV193	46.29187793	-80.36482596	548924	5126673
14SV194	46.29107185	-80.36878205	548620	5126581
14SV195	46.29067709	-80.36900729	548603	5126537
14SV196	46.29033335	-80.37032248	548502	5126498
14SV197	46.29067461	-80.37018874	548512	5126536

Table A.1: *Continued.* Geographical location of map stations in latitude longitude, and Universal Transverse Mercator projection.

STATION NUMBER	LATITUDE	LONGITUDE	Nad 83, Zone 17 EASTING (in metres)	Nad 83, Zone 17 NORTHING (in metres)
14SV198	46.29054919	-80.37029404	548504	5126522
14SV199	46.29178096	-80.37007220	548520	5126659
14SV200	46.29650703	-80.37684763	547994	5127180
14SV201	46.31643566	-80.34830589	550174	5129412
14SV202	46.31679571	-80.34831461	550173	5129452
14SV203	46.31803694	-80.34818297	550182	5129590
14SV204	46.31971117	-80.34822803	550177	5129776
14SV205	46.32015480	-80.34869039	550141	5129825
14SV206	46.32104802	-80.34908248	550110	5129924
14SV207	46.32169059	-80.34971137	550061	5129995
14SV208	46.32246298	-80.35101423	549960	5130080
14SV209	46.32269385	-80.36165053	549141	5130099
14SV210	46.32225875	-80.36270779	549060	5130050
14SV211	46.32219135	-80.36515072	548872	5130041
14SV212	46.32206637	-80.36533403	548858	5130027
14SV213	46.32200550	-80.36897196	548578	5130018
14SV214	46.32213350	-80.36933422	548550	5130032
14SV215	46.32216373	-80.37155518	548379	5130034
14SV216	46.32208573	-80.37210166	548337	5130025
14SV217	46.32215635	-80.37349080	548230	5130032
14SV218	46.32206908	-80.37728491	547938	5130020
14SV219	46.32238523	-80.38247740	547538	5130052
14SV220	46.32216843	-80.41133093	545317	5130011
14SV221	46.32223932	-80.41638334	544928	5130016
14SV222	46.32199886	-80.41864617	544754	5129988
14SV223	46.32229828	-80.41912364	544717	5130021
14SV224	46.32212047	-80.41955420	544684	5130001
14SV225	46.32225291	-80.42082583	544586	5130015
14SV226	46.32218429	-80.42506134	544260	5130005
14SV227	46.31677535	-80.43226186	543710	5129400
14SV228	46.28673818	-80.37119451	548438	5126098
14SV229	46.28498631	-80.37669268	548016	5125900
14SV230	46.28506932	-80.37871684	547860	5125908
14SV231	46.28134277	-80.37530615	548126	5125496
14SV232	46.28084007	-80.37389700	548235	5125441
14SV233	46.28059850	-80.37415936	548215	5125414
14SV234	46.27838728	-80.37138090	548431	5125170
14SV235	46.27842712	-80.36881045	548629	5125176
14SV236	46.27744450	-80.36526533	548903	5125069

Table A.1: *Continued.* Geographical location of map stations in latitude longitude, and Universal Transverse Mercator projection.

STATION NUMBER	LATITUDE	LONGITUDE	Nad 83, Zone 17 EASTING (in metres)	Nad 83, Zone 17 NORTHING (in metres)
14SV237	46.27645982	-80.36460177	548955	5124960
14SV238	46.27584972	-80.36332389	549054	5124893
14SV239	46.27626181	-80.36298165	549080	5124939
14SV240	46.27721382	-80.36424261	548982	5125044
14SV241	46.27465833	-80.36271470	549102	5124761
14SV242	46.27505671	-80.36152899	549193	5124806
14SV243	46.27554391	-80.36013456	549300	5124861
14SV244	46.27453502	-80.35836820	549437	5124750
14SV245	46.27438858	-80.35953800	549347	5124733
14SV246	46.27304804	-80.35961851	549342	5124584
14SV247	46.27162054	-80.35863582	549419	5124426
14SV248	46.27050801	-80.35764950	549496	5124303
14SV249	46.27284794	-80.35603878	549618	5124564
14SV250	46.27215053	-80.35525527	549679	5124487
14SV251	46.26943726	-80.35449545	549740	5124186
14SV252	46.26706874	-80.35104539	550008	5123925
14SV253	46.26693752	-80.35012556	550079	5123911
14SV254	46.26630741	-80.35010705	550081	5123841
14SV255	46.26660786	-80.34913023	550156	5123875
14SV256	46.26578778	-80.34736211	550293	5123785
14SV257	46.26509172	-80.34682535	550335	5123708
14SV258	46.26442762	-80.34715765	550310	5123634
14SV259	46.26163948	-80.35064232	550044	5123322
14SV260	46.26142528	-80.34622010	550385	5123301
14SV261	46.25925021	-80.34830903	550226	5123058
14SV262	46.25534560	-80.35171564	549967	5122622
14SV263	46.25391533	-80.35662370	549590	5122460
14SV264	46.25069374	-80.35829600	549464	5122101
14SV265	46.25077080	-80.35759454	549518	5122110
14SV266	46.24722220	-80.35713005	549557	5121716
14SV267	46.24702538	-80.35733990	549541	5121694
14SV268	46.24463719	-80.35517555	549710	5121430
14SV269	46.24441257	-80.35364752	549828	5121406
14SV270	46.24287187	-80.35175881	549975	5121236
14SV271	46.24158262	-80.34977645	550129	5121094
14SV272	46.23916411	-80.34705526	550341	5120827
14SV273	46.23866522	-80.34637375	550394	5120772
14SV274	46.23722719	-80.34357631	550611	5120614
14SV275	46.23544761	-80.34243026	550701	5120417

Table A.1: *Continued.* Geographical location of map stations in latitude longitude, and Universal Transverse Mercator projection.

STATION NUMBER	LATITUDE	LONGITUDE	Nad 83, Zone 17 EASTING (in metres)	Nad 83, Zone 17 NORTHING (in metres)
14SV276	46.23459744	-80.34483977	550516	5120321
14SV277	46.23556936	-80.34639754	550395	5120428
14SV278	46.23542440	-80.34623065	550408	5120412
14SV279	46.23484466	-80.34557609	550459	5120348
14SV280	46.27077531	-80.33668691	551111	5124346
14SV281	46.27114544	-80.33843449	550976	5124386
14SV282	46.27040410	-80.34410178	550540	5124300
14SV283	46.26975191	-80.34494013	550476	5124227
14SV284	46.26908759	-80.34523355	550454	5124153
14SV285	46.26870895	-80.34512126	550463	5124111
14SV286	46.27008656	-80.32055079	552355	5124280
14SV287	46.27002098	-80.32619696	551920	5124269
14SV288	46.27026062	-80.32868577	551728	5124294
14SV289	46.27006239	-80.33018064	551613	5124271
14SV290	46.26939331	-80.33273242	551417	5124195
14SV291	46.26979836	-80.33274048	551416	5124240
14SV292	46.26780812	-80.34497626	550475	5124011
14SV293	46.31488609	-80.30228033	553719	5129270
14SV294	46.31472420	-80.43242595	543699	5129172
14SV295	46.31284867	-80.43352333	543616	5128963
14SV296	46.31164860	-80.43471759	543525	5128829
14SV297	46.30991915	-80.43624192	543409	5128636
14SV298	46.30838453	-80.43712779	543342	5128465
14SV299	46.30432916	-80.43602660	543430	5128015
14SV300	46.29730538	-80.43342396	543636	5127236
14SV301	46.29454775	-80.43268636	543695	5126930
14SV302	46.26628114	-80.34393034	550557	5123842
14SV303	46.26502591	-80.34319267	550615	5123703
14SV304	46.26277813	-80.34201274	550708	5123454
14SV305	46.26106217	-80.34253932	550669	5123263
14SV306	46.25941501	-80.34407712	550552	5123079
14SV307	46.25765226	-80.34429276	550537	5122883
14SV308	46.25614184	-80.34614018	550396	5122714
14SV309	46.25318250	-80.34800466	550255	5122384
14SV310	46.25184625	-80.34883783	550192	5122235
14SV311	46.25131943	-80.34957057	550136	5122176
14SV312	46.25075467	-80.35154919	549984	5122112
14SV313	46.25034430	-80.35218971	549935	5122066
14SV314	46.24849950	-80.35222440	549934	5121861

Table A.1: *Continued.* Geographical location of map stations in latitude longitude, and Universal Transverse Mercator projection.

STATION NUMBER	LATITUDE	LONGITUDE	Nad 83, Zone 17 EASTING (in metres)	Nad 83, Zone 17 NORTHING (in metres)
14SV315	46.24716583	-80.35192876	549958	5121713
14SV316	46.24695730	-80.35165880	549979	5121690
14SV317	46.24636187	-80.35140637	549999	5121624
14SV318	46.24307758	-80.34678832	550358	5121262
14SV319	46.24184789	-80.34422165	550557	5121127
14SV320	46.23845465	-80.33948898	550925	5120753
14SV321	46.23245536	-80.34013159	550881	5120086
14SV322	46.23389666	-80.34662490	550379	5120242
14SV323	46.23569097	-80.34878252	550211	5120440
14SV324	46.23838902	-80.35002170	550113	5120739
14SV325	46.24097036	-80.35131425	550011	5121025
14SV326	46.24052913	-80.35286299	549892	5120975
14SV327	46.23479465	-80.34942863	550162	5120340
14SV328	46.23480016	-80.35198356	549965	5120339
14SV329	46.23612139	-80.35805085	549496	5120482
14SV330	46.23575315	-80.36140134	549238	5120439
14SV331	46.23675920	-80.36428197	549015	5120549
14SV332	46.23685381	-80.36511096	548951	5120559
14SV333	46.23697000	-80.36658820	548837	5120571
14SV334	46.23832973	-80.37325228	548322	5120718
14SV335	46.29017634	-80.43319887	543659	5126444
14SV336	46.28690503	-80.43232389	543729	5126081
14SV337	46.28246759	-80.43222693	543740	5125588
14SV338	46.28143317	-80.43234146	543732	5125473
14SV339	46.27819472	-80.43264748	543711	5125113
14SV340	46.27565796	-80.43289431	543694	5124831
14SV341	46.23832004	-80.37476992	548205	5120716
14SV342	46.24039060	-80.38149123	547685	5120942
14SV343	46.24049284	-80.38710646	547252	5120950
14SV344	46.24134691	-80.38861456	547135	5121044
14SV345	46.24124592	-80.38992575	547034	5121032
14SV346	46.24224671	-80.39195115	546877	5121142
14SV347	46.24201790	-80.39462575	546671	5121115
14SV348	46.23716009	-80.37331748	548318	5120588
14SV349	46.23692985	-80.36909187	548644	5120565
14SV350	46.23644861	-80.36669796	548829	5120513
14SV351	46.23488594	-80.35442082	549777	5120347
14SV352	46.23394742	-80.35238267	549935	5120244
14SV353	46.23235717	-80.35286826	549899	5120067

Table A.1: *Continued.* Geographical location of map stations in latitude longitude, and Universal Transverse Mercator projection.

STATION NUMBER	LATITUDE	LONGITUDE	Nad 83, Zone 17 EASTING (in metres)	Nad 83, Zone 17 NORTHING (in metres)
14SV354	46.22788067	-80.34908238	550195	5119572
14SV355	46.22522894	-80.34807634	550275	5119278
14SV356	46.23670540	-80.33892632	550970	5120559
14SV357	46.23558077	-80.33743534	551086	5120435
14SV358	46.23408097	-80.33334211	551403	5120271
14SV359	46.23175059	-80.33344814	551397	5120012
14SV360	46.23135575	-80.33364745	551382	5119968
14SV361	46.23068337	-80.33409652	551348	5119893
14SV362	46.22737154	-80.27779163	555693	5119563
14SV363	46.23047990	-80.28261404	555318	5119905
14SV364	46.23264622	-80.28794202	554905	5120142
14SV365	46.23248523	-80.28955225	554781	5120123
14SV366	46.23329294	-80.29208379	554585	5120211
14SV367	46.23511911	-80.29486173	554369	5120412
14SV368	46.23521057	-80.29655958	554238	5120421
14SV369	46.23554155	-80.29916226	554037	5120456
14SV370	46.23472687	-80.30133854	553870	5120364
14SV371	46.23525155	-80.30325138	553722	5120421
14SV372	46.23812445	-80.30504383	553581	5120739
14SV373	46.23976050	-80.30620351	553490	5120920
14SV374	46.23041006	-80.33352921	551392	5119863
14SV375	46.23028958	-80.33139087	551557	5119851
14SV376	46.23044482	-80.32564395	552000	5119872
14SV377	46.21617090	-80.28565273	555098	5118313
14SV378	46.20966399	-80.28567228	555103	5117590
14SV379	46.20771592	-80.28935314	554821	5117371
14SV380	46.20556011	-80.29293270	554547	5117129
14SV381	46.20763276	-80.30362661	553720	5117352
14SV382	46.21085918	-80.30287282	553775	5117711
14SV383	46.21236830	-80.30239997	553810	5117879
14SV384	46.21464212	-80.30631247	553506	5118129
14SV385	46.21801547	-80.30308046	553752	5118506
14SV386	46.21880063	-80.30343357	553724	5118593
14SV387	46.22198829	-80.30370445	553700	5118947
14SV388	46.21958332	-80.30190666	553841	5118681
14SV389	46.21816178	-80.29465097	554402	5118528
14SV390	46.22230510	-80.29372915	554469	5118989
14SV391	46.22253836	-80.29360946	554478	5119015
14SV392	46.22382786	-80.29547313	554333	5119157

Table A.1: *Continued.* Geographical location of map stations in latitude longitude, and Universal Transverse Mercator projection.

STATION NUMBER	LATITUDE	LONGITUDE	Nad 83, Zone 17 EASTING (in metres)	Nad 83, Zone 17 NORTHING (in metres)
14SV393	46.28026697	-80.37938119	547813	5125374
14SV394	46.28101013	-80.38033335	547739	5125456
14SV395	46.28055989	-80.39712195	546446	5125396
14SV396	46.27824684	-80.40397467	545920	5125135
14SV397	46.27704011	-80.41428048	545127	5124995
14SV398	46.27310103	-80.41660666	544951	5124556
14SV399	46.27427076	-80.41832043	544818	5124685
14SV400	46.27208530	-80.42039413	544660	5124441
14SV401	46.27160110	-80.41720660	544906	5124389
14SV402	46.26773331	-80.42117970	544603	5123957
14SV403	46.26492686	-80.42148175	544582	5123645
14SV404	46.26576085	-80.42266684	544490	5123737
14SV405	46.26435745	-80.42278539	544482	5123581
14SV406	46.26501516	-80.42650278	544195	5123652
14SV407	46.26061747	-80.42357722	544424	5123165
14SV408	46.25928515	-80.42709451	544154	5123015
14SV409	46.25929470	-80.42900177	544007	5123015
14SV410	46.25857338	-80.42873678	544028	5122935
14SV411	46.25649089	-80.42445084	544360	5122706
14SV412	46.25841991	-80.42148531	544587	5122922
14SV413	46.25667183	-80.41929800	544757	5122729
14SV414	46.25109641	-80.42554514	544280	5122106
14SV415	46.25196541	-80.42833835	544064	5122201
14SV416	46.25099623	-80.42710298	544160	5122094
14SV417	46.24876240	-80.42315656	544466	5121848
14SV418	46.24805992	-80.41950565	544748	5121772
14SV419	46.24446381	-80.42027000	544692	5121372
14SV420	46.24893548	-80.41647374	544981	5121871
14SV421	46.27345078	-80.43244985	543730	5124586
14SV422	46.27246006	-80.43230433	543742	5124476
14SV423	46.26903858	-80.43200224	543768	5124096
14SV424	46.26690571	-80.43202427	543768	5123859
14SV425	46.26477251	-80.43198142	543773	5123622
14SV426	46.26298135	-80.43194801	543777	5123423
14SV427	46.26130680	-80.43183555	543787	5123237
14SV428	46.25938342	-80.43236145	543748	5123023
14SV429	46.25651252	-80.43237810	543749	5122704
14SV430	46.25209389	-80.43244964	543747	5122213
14SV431	46.22778920	-80.43330968	543700	5119512

Table A.1: *Continued.* Geographical location of map stations in latitude longitude, and Universal Transverse Mercator projection.

STATION NUMBER	LATITUDE	LONGITUDE	Nad 83, Zone 17 EASTING (in metres)	Nad 83, Zone 17 NORTHING (in metres)
14SV432	46.22290585	-80.43223182	543787	5118970
14SV433	46.22543770	-80.29528396	554346	5119336
14SV434	46.22629671	-80.29593431	554295	5119431
14SV435	46.22723990	-80.29710231	554204	5119535
14SV436	46.22750740	-80.29669690	554235	5119565
14SV437	46.22559983	-80.30116906	553892	5119350
14SV438	46.22611819	-80.30500085	553596	5119405
14SV439	46.22847643	-80.30949693	553247	5119664
14SV440	46.22629687	-80.31073024	553154	5119421
14SV441	46.23369678	-80.34787232	550283	5120219
14SV442	46.22989850	-80.34467522	550533	5119799
14SV443	46.22838734	-80.34325376	550644	5119632
14SV444	46.23198490	-80.34754244	550310	5120029
14SV445	46.23282598	-80.34825874	550254	5120122
14SV446	46.24939459	-80.41649482	544979	5121922
14SV447	46.25259569	-80.41592895	545020	5122278
14SV448	46.25347741	-80.41411621	545159	5122377
14SV449	46.25223489	-80.41226124	545303	5122240
14SV450	46.25181491	-80.41109811	545393	5122194
14SV451	46.25409973	-80.40912755	545543	5122449
14SV452	46.25454716	-80.40862972	545581	5122499
14SV453	46.25638519	-80.40728656	545683	5122704
14SV454	46.25959975	-80.40758928	545657	5123061
14SV455	46.26284195	-80.40110523	546154	5123425
14SV456	46.26943766	-80.39915163	546299	5124159
14SV457	46.27203535	-80.40023937	546213	5124447
14SV458	46.27498097	-80.39391243	546698	5124778
14SV459	46.27830120	-80.39547234	546575	5125146
14SV460	47.17837178	-80.38275818	546770	5125170
14SV461	47.17995274	-80.38057540	546934	5125347
14SV462	46.28069247	-80.38651557	547263	5125417
14SV463	46.27838558	-80.37765016	547948	5125166
14SV464	46.27565016	-80.43132391	545815	5124831
14SV465	46.27647608	-80.40095671	546154	5124940
14SV466	46.27320922	-80.40097933	546155	5124577
14SV467	46.26873945	-80.40503807	545846	5124078
14SV468	46.26466079	-80.40644473	545741	5123624
14SV469	46.26426731	-80.40866795	545570	5123579
14SV470	46.26192411	-80.41153487	545351	5123317

Table A.1: *Continued.* Geographical location of map stations in latitude longitude, and Universal Transverse Mercator projection.

STATION NUMBER	LATITUDE	LONGITUDE	Nad 83, Zone 17 EASTING (in metres)	Nad 83, Zone 17 NORTHING (in metres)
14SV471	46.25952064	-80.41494714	545090	5123048
14SV472	46.25744236	-80.41508602	545081	5122817
14SV473	46.25986018	-80.41799275	544855	5123084
14SV474	46.26182517	-80.41858183	544808	5123302
14SV475	46.26262160	-80.41945578	544740	5123390
14SV476	46.25879837	-80.41274905	545260	5122969
14SV477	46.25445083	-80.41263977	545272	5122486
14SV478	46.25983721	-80.41000015	545471	5123086
14SV479	46.25874218	-80.40883115	545562	5122965
14SV480	46.25572750	-80.40888950	545560	5122630
14SV481	46.26439121	-80.40134789	546134	5123597
14SV482	46.26471802	-80.40880585	545859	5123629
14SV483	46.22925482	-80.34700419	550354	5119726
14SV484	46.22527407	-80.34495070	550516	5119285
14SV485	46.22650949	-80.34694597	550361	5119421
14SV486	46.21658079	-80.34351121	550635	5118320
14SV487	46.22108242	-80.34222576	550730	5118821
14SV488	46.22075888	-80.34230742	550724	5118785
14SV489	46.21591340	-80.34641038	550412	5118244
14SV490	46.21838201	-80.34844262	550253	5118517
14SV491	46.21291368	-80.35544323	549718	5117905
14SV492	46.21079059	-80.35720522	549584	5117668
14SV493	46.20517159	-80.36634454	548884	5117038
14SV494	46.20407135	-80.37082917	548539	5116913
14SV495	46.20509287	-80.37001383	548601	5117027
14SV496	46.20648734	-80.36828680	548733	5117183
14SV497	46.20631315	-80.37589796	548146	5117159
14SV498	46.20837799	-80.37330784	548344	5117390
14SV499	46.21435796	-80.36911705	548662	5118057
14SV500	46.20485954	-80.37670513	548085	5116997
14SV501	46.20434331	-80.37942010	547876	5116938
14SV502	46.20297431	-80.38590356	547377	5116782
14SV503	46.20230408	-80.38679243	547309	5116707
14SV504	46.20076885	-80.38749647	547256	5116536
14SV505	46.20013878	-80.38413352	547516	5116468
14SV506	46.19912522	-80.37977695	547853	5116358
14SV507	46.19554316	-80.38309620	547600	5115958
14SV508	46.19195112	-80.37792670	548002	5115562
14SV509	46.18792547	-80.37414937	548297	5115117

Table A.1: *Continued.* Geographical location of map stations in latitude longitude, and Universal Transverse Mercator projection.

STATION NUMBER	LATITUDE	LONGITUDE	Nad 83, Zone 17 EASTING (in metres)	Nad 83, Zone 17 NORTHING (in metres)
14SV510	46.18642404	-80.37443853	548276	5114950
14SV511	46.18344327	-80.37247690	548430	5114620
14SV512	46.26987087	-80.30119060	553847	5124269
14SV513	46.27256253	-80.30721732	553380	5124564
14SV514	46.27258001	-80.30861876	553272	5124565
14SV515	46.27294767	-80.30988604	553174	5124605
14SV516	46.27302564	-80.31386947	552867	5124611
14SV517	46.27321822	-80.32505459	552005	5124625
14SV518	46.21872819	-80.43189888	543816	5118506
14SV519	46.21797197	-80.43185482	543820	5118422
14SV520	46.21469600	-80.43186267	543822	5118058
14SV521	46.21324713	-80.43189058	543821	5117897
14SV522	46.20881086	-80.43204002	543813	5117404
14SV523	46.19754281	-80.43203948	543822	5116152
14SV524	46.19596781	-80.43204275	543823	5115977
14SV525	46.19367182	-80.43184608	543840	5115722
14SV526	46.18621160	-80.43201366	543833	5114893
14SV527	46.18277220	-80.43173810	543857	5114511
14SV528	46.16750948	-80.43202483	543847	5112815
14SV529	46.16447577	-80.43188766	543860	5112478
14SV530	46.18261783	-80.37130718	548521	5114529
14SV531	46.18032711	-80.37045223	548589	5114275
14SV532	46.17837607	-80.36917888	548689	5114059
14SV533	46.17737904	-80.36790764	548788	5113949
14SV534	46.17738119	-80.36829629	548758	5113949
14SV535	46.17172031	-80.36670291	548886	5113321
14SV536	46.16529084	-80.36609018	548939	5112607
14SV537	46.16333586	-80.36573700	548968	5112390
14SV538	46.16366025	-80.36743009	548837	5112425
14SV539	46.16499434	-80.36943548	548681	5112572
14SV540	46.16537527	-80.37323936	548387	5112612
14SV541	46.16890549	-80.36873013	548732	5113007
14SV542	46.20634642	-80.37211244	548438	5117165
14SV543	46.17081182	-80.36842332	548754	5113219
14SV544	46.17787562	-80.37309735	548387	5114001
14SV545	46.17693500	-80.37389835	548326	5113896
14SV546	46.17200921	-80.37339719	548369	5113349
14SV547	46.17116595	-80.37389904	548331	5113255
14SV548	46.17357243	-80.37617774	548153	5113521

Table A.1: *Continued.* Geographical location of map stations in latitude longitude, and Universal Transverse Mercator projection.

STATION NUMBER	LATITUDE	LONGITUDE	Nad 83, Zone 17 EASTING (in metres)	Nad 83, Zone 17 NORTHING (in metres)
14SV549	46.17523999	-80.37829654	547988	5113705
14SV550	46.17794281	-80.38046862	547818	5114004
14SV551	46.17513528	-80.38222323	547685	5113691
14SV552	46.17684563	-80.38395312	547550	5113880
14SV553	46.17929222	-80.37704592	548081	5114156
14SV554	46.17973131	-80.37504565	548235	5114206
14SV555	46.17696956	-80.37692964	548092	5113898
14SV556	46.17790561	-80.37528659	548218	5114003
14SV557	46.18019297	-80.37388728	548324	5114258
14SV558	46.17890922	-80.37283943	548406	5114116
14SV559	46.18486734	-80.37449506	548273	5114777
14SV560	46.19140041	-80.37926772	547899	5115500
14SV561	46.19513232	-80.38368401	547555	5115912
14SV562	46.20244768	-80.38839811	547185	5116722
14SV563	46.20617784	-80.38247161	547639	5117140
14SV564	46.20657095	-80.38193573	547680	5117184
14SV565	46.20561005	-80.37077272	548542	5117084
14SV566	46.20604651	-80.36831778	548731	5117134
14SV567	46.20991041	-80.36074160	549312	5117568
14SV568	46.21624654	-80.35435406	549799	5118276
14SV569	46.22225324	-80.34865616	550233	5118947
14SV570	46.27215993	-80.32874045	551722	5124505

APPENDIX B

THERMOBAROMETRY FORMULAS AND ANALYTICAL DATA

B.1 GBPQ Formulas

Compositional parameters used for garnet biotite plagioclase quartz thermobarometry from Wu 2004. Element concentrations in cations per formula unit (pfu). R (gas constant) = 8.31441 J/(mol*K) (J = Joules). X = mole fraction.

Ideal activity of the mineral phases:

Garnet:

$X_{Fe}^{grt} = Fe^{2+}/(Fe^{2+} + Mg + Ca + Mn)$,

$X_{Mg}^{grt} = Mg/(Fe^{2+} + Mg + Ca + Mn)$,

$X_{Ca}^{grt} = Ca/(Fe^{2+} + Mg + Ca + Mn)$,

$X_{Mn}^{grt} = Mn/(Fe^{2+} + Mg + Ca + Mn)$,

$X_{alm}^{gnt} = (X_{Fe}^{gnt})^3,\ X_{pyr}^{gnt} = (X_{Mg}^{gnt})^3, X_{gros}^{gnt} = (X_{Ca}^{gnt})^3, X_{sps}^{gnt} = (X_{Mn}^{gnt})^3$

Biotite:

$X_{ann}^{bio} = (X_{Fe}^{bio})^3,\ X_{phl}^{bio} = (X_{Mg}^{bio})^3,\ X_{eas}^{bio} = \frac{27}{4}(X_{Mg}^{bio})^3 X_{Al}^{bio},\ X_{sid}^{bio} = \frac{27}{4}(X_{Fe}^{bio})^2 X_{Al}^{bio}$

$X_{Fe}^{bio} = Fe^{2+}/(Fe^{2+} + Mg + Al^{VI} + Ti)$,

$X_{Mg}^{bio} = Mg/(Fe^{2+} + Mg + Al^{VI} + Ti)$,

$X_{Al}^{bio} = Al^{VI}/(Fe^{2+} + Mg + Al^{VI} + Ti)$,

$X_{Ti}^{bio} = Ti/(Fe^{2+} + Mg + Al^{VI} + Ti)$

Plagioclase:

$X_{an}^{pl} = 0.25X_{Ca}^{pl}(1 + X_{Ca})^2,\ X_{ab}^{pl} = X_{Na}^{pl},\ X_{or}^{pl} = X_K^{pl}$,

$X_{Ca}^{pl} = Ca/(Ca + Na + K), X_{Na}^{pl} = Na/(Ca + Na + K)$,

$X_K^{pl} = K/(Ca + Na + K)$

Equilibrium constants:

$$K_{(Mg)}^{ideal} = \frac{(X_{an}^{pl})^6 (X_{phl}^{bio})^3}{(X_{pyr}^{grt})(X_{gros}^{grt})^2 (X_{eas}^{bio})^3 (X_{qtz}^{qtz})^6} = \frac{(X_{Ca}^{pl})^6 (1 + X_{Ca}^{pl})^{12} (X_{Mg}^{bio})^3}{1259712.0 (X_{Mg}^{grt})^3 (X_{Ca}^{grt})^6 (X_{Al}^{bio})^3}$$

$$K_{(Fe)}^{ideal} = \frac{(X_{an}^{pl})^6 (X_{ann}^{bio})^3}{(X_{alm}^{grt})(X_{gros}^{grt})^2 (X_{sid}^{bio})^3 (X_{qtz}^{qtz})^6} = \frac{(X_{Ca}^{pl})^6 (1 + X_{Ca}^{pl})^{12} (X_{Mg}^{bio})^3}{1259712.0 (X_{Fe}^{grt})^3 (X_{Ca}^{grt})^6 (X_{Al}^{bio})^3}$$

Polynomial expressions for garnet end-members:

$$\begin{aligned}
\mathrm{Caa} = {} & 0{\cdot}337(X_{\mathrm{Fe}}^{\mathrm{grt}})^2 - 18{\cdot}983(X_{\mathrm{Mg}}^{\mathrm{grt}})^2 \\
& - 9{\cdot}5725(X_{\mathrm{Fe}}^{\mathrm{grt}})(X_{\mathrm{Mg}}^{\mathrm{grt}}) - 19{\cdot}34(X_{\mathrm{Fe}}^{\mathrm{grt}})(X_{\mathrm{Ca}}^{\mathrm{grt}}) \\
& - 4{\cdot}6665(X_{\mathrm{Fe}}^{\mathrm{grt}})(X_{\mathrm{Mn}}^{\mathrm{grt}}) - 25{\cdot}746(X_{\mathrm{Mg}}^{\mathrm{grt}})(X_{\mathrm{Ca}}^{\mathrm{grt}}) \\
& - 38{\cdot}938(X_{\mathrm{Mg}}^{\mathrm{grt}})(X_{\mathrm{Mn}}^{\mathrm{grt}}) + 11{\cdot}006(X_{\mathrm{Fe}}^{\mathrm{grt}})^2 (X_{\mathrm{Mg}}^{\mathrm{grt}}) \\
& - 0{\cdot}674(X_{\mathrm{Fe}}^{\mathrm{grt}})^2 (X_{\mathrm{Ca}}^{\mathrm{grt}}) - 11{\cdot}986(X_{\mathrm{Mg}}^{\mathrm{grt}})^2 (X_{\mathrm{Fe}}^{\mathrm{grt}}) \\
& + 37{\cdot}966(X_{\mathrm{Mg}}^{\mathrm{grt}})^2 (X_{\mathrm{Ca}}^{\mathrm{grt}}) + 46{\cdot}02(X_{\mathrm{Mg}}^{\mathrm{grt}})^2 (X_{\mathrm{Mn}}^{\mathrm{grt}}) \\
& + 19{\cdot}34(X_{\mathrm{Ca}}^{\mathrm{grt}})^2 (X_{\mathrm{Fe}}^{\mathrm{grt}}) + 25{\cdot}746(X_{\mathrm{Ca}}^{\mathrm{grt}})^2 (X_{\mathrm{Mg}}^{\mathrm{grt}}) \\
& + 46{\cdot}02(X_{\mathrm{Mn}}^{\mathrm{grt}})^2 (X_{\mathrm{Mg}}^{\mathrm{grt}}) + 19{\cdot}145(X_{\mathrm{Fe}}^{\mathrm{grt}})(X_{\mathrm{Mg}}^{\mathrm{grt}})(X_{\mathrm{Ca}}^{\mathrm{grt}}) \\
& + 45{\cdot}53(X_{\mathrm{Fe}}^{\mathrm{grt}})(X_{\mathrm{Mg}}^{\mathrm{grt}})(X_{\mathrm{Mn}}^{\mathrm{grt}}) \\
& + 9{\cdot}333(X_{\mathrm{Fe}}^{\mathrm{grt}})(X_{\mathrm{Ca}}^{\mathrm{grt}})(X_{\mathrm{Mn}}^{\mathrm{grt}}) \\
& + 77{\cdot}876(X_{\mathrm{Mg}}^{\mathrm{grt}})(X_{\mathrm{Ca}}^{\mathrm{grt}})(X_{\mathrm{Mn}}^{\mathrm{grt}})
\end{aligned}$$

$$\begin{aligned}
\mathrm{Cab} = {} & 0{\cdot}04(X_{\mathrm{Fe}}^{\mathrm{grt}})^2 + 0{\cdot}068(X_{\mathrm{Mg}}^{\mathrm{grt}})^2 + 0{\cdot}065(X_{\mathrm{Mn}}^{\mathrm{grt}})^2 \\
& - 0{\cdot}0515(X_{\mathrm{Fe}}^{\mathrm{grt}})(X_{\mathrm{Mg}}^{\mathrm{grt}}) + 0{\cdot}27(X_{\mathrm{Fe}}^{\mathrm{grt}})(X_{\mathrm{Ca}}^{\mathrm{grt}}) \\
& + 0{\cdot}1765(X_{\mathrm{Fe}}^{\mathrm{grt}})(X_{\mathrm{Mn}}^{\mathrm{grt}}) + 0{\cdot}28(X_{\mathrm{Mg}}^{\mathrm{grt}})(X_{\mathrm{Ca}}^{\mathrm{grt}}) \\
& + 0{\cdot}207(X_{\mathrm{Mg}}^{\mathrm{grt}})(X_{\mathrm{Mn}}^{\mathrm{grt}}) + 0{\cdot}13(X_{\mathrm{Ca}}^{\mathrm{grt}})(X_{\mathrm{Mn}}^{\mathrm{grt}}) \\
& - 0{\cdot}1(X_{\mathrm{Fe}}^{\mathrm{grt}})^2 (X_{\mathrm{Mg}}^{\mathrm{grt}}) - 0{\cdot}08(X_{\mathrm{Fe}}^{\mathrm{grt}})^2 (X_{\mathrm{Ca}}^{\mathrm{grt}}) \\
& - 0{\cdot}048(X_{\mathrm{Fe}}^{\mathrm{grt}})^2 (X_{\mathrm{Mn}}^{\mathrm{grt}}) + 0{\cdot}068(X_{\mathrm{Mg}}^{\mathrm{grt}})^2 (X_{\mathrm{Fe}}^{\mathrm{grt}}) \\
& - 0{\cdot}136(X_{\mathrm{Mg}}^{\mathrm{grt}})^2 (X_{\mathrm{Ca}}^{\mathrm{grt}}) - 0{\cdot}076(X_{\mathrm{Mg}}^{\mathrm{grt}})^2 (X_{\mathrm{Mn}}^{\mathrm{grt}}) \\
& - 0{\cdot}27(X_{\mathrm{Ca}}^{\mathrm{grt}})^2 (X_{\mathrm{Fe}}^{\mathrm{grt}}) - 0{\cdot}28(X_{\mathrm{Ca}}^{\mathrm{grt}})^2 (X_{\mathrm{Mg}}^{\mathrm{grt}}) \\
& - 0{\cdot}13(X_{\mathrm{Ca}}^{\mathrm{grt}})^2 (X_{\mathrm{Mn}}^{\mathrm{grt}}) - 0{\cdot}048(X_{\mathrm{Mn}}^{\mathrm{grt}})^2 (X_{\mathrm{Fe}}^{\mathrm{grt}}) \\
& - 0{\cdot}076(X_{\mathrm{Mn}}^{\mathrm{grt}})^2 (X_{\mathrm{Mg}}^{\mathrm{grt}}) - 0{\cdot}13(X_{\mathrm{Mn}}^{\mathrm{grt}})^2 (X_{\mathrm{Ca}}^{\mathrm{grt}}) \\
& + 0{\cdot}103(X_{\mathrm{Fe}}^{\mathrm{grt}})(X_{\mathrm{Mg}}^{\mathrm{grt}})(X_{\mathrm{Ca}}^{\mathrm{grt}}) - 0{\cdot}14(X_{\mathrm{Fe}}^{\mathrm{grt}})(X_{\mathrm{Mg}}^{\mathrm{grt}})(X_{\mathrm{Mn}}^{\mathrm{grt}}) \\
& - 0{\cdot}353(X_{\mathrm{Fe}}^{\mathrm{grt}})(X_{\mathrm{Ca}}^{\mathrm{grt}})(X_{\mathrm{Mn}}^{\mathrm{grt}}) - 0{\cdot}414(X_{\mathrm{Mg}}^{\mathrm{grt}})(X_{\mathrm{Ca}}^{\mathrm{grt}})(X_{\mathrm{Mn}}^{\mathrm{grt}})
\end{aligned}$$

$$
\begin{aligned}
\mathrm{Cac} = & -1304{\cdot}0(X_{\mathrm{Fe}}^{\mathrm{grt}})^2 + 66114{\cdot}0(X_{\mathrm{Mg}}^{\mathrm{grt}})^2 + 1425{\cdot}0(X_{\mathrm{Mn}}^{\mathrm{grt}})^2 \\
& + 31326{\cdot}5(X_{\mathrm{Fe}}^{\mathrm{grt}})(X_{\mathrm{Mg}}^{\mathrm{grt}}) + 39864{\cdot}0(X_{\mathrm{Fe}}^{\mathrm{grt}})(X_{\mathrm{Ca}}^{\mathrm{grt}}) \\
& + 12356{\cdot}0(X_{\mathrm{Fe}}^{\mathrm{grt}})(X_{\mathrm{Mn}}^{\mathrm{grt}}) + 51518{\cdot}0(X_{\mathrm{Mg}}^{\mathrm{grt}})(X_{\mathrm{Ca}}^{\mathrm{grt}}) \\
& + 88610{\cdot}5(X_{\mathrm{Mg}}^{\mathrm{grt}})(X_{\mathrm{Mn}}^{\mathrm{grt}}) + 2850{\cdot}0(X_{\mathrm{Ca}}^{\mathrm{grt}})(X_{\mathrm{Mn}}^{\mathrm{grt}}) \\
& - 23244{\cdot}0(X_{\mathrm{Fe}}^{\mathrm{grt}})^2(X_{\mathrm{Mg}}^{\mathrm{grt}}) + 2608{\cdot}0(X_{\mathrm{Fe}}^{\mathrm{grt}})^2(X_{\mathrm{Ca}}^{\mathrm{grt}}) \\
& - 3234{\cdot}0(X_{\mathrm{Fe}}^{\mathrm{grt}})^2(X_{\mathrm{Mn}}^{\mathrm{grt}}) + 11344{\cdot}0(X_{\mathrm{Mg}}^{\mathrm{grt}})^2(X_{\mathrm{Fe}}^{\mathrm{grt}}) \\
& - 132228{\cdot}0(X_{\mathrm{Mg}}^{\mathrm{grt}})^2(X_{\mathrm{Ca}}^{\mathrm{grt}}) - 82498{\cdot}0(X_{\mathrm{Mg}}^{\mathrm{grt}})^2(X_{\mathrm{Mn}}^{\mathrm{grt}}) \\
& - 39864{\cdot}0(X_{\mathrm{Ca}}^{\mathrm{grt}})^2(X_{\mathrm{Fe}}^{\mathrm{grt}}) - 51518{\cdot}0(X_{\mathrm{Ca}}^{\mathrm{grt}})^2(X_{\mathrm{Mg}}^{\mathrm{grt}}) \\
& - 2850{\cdot}0(X_{\mathrm{Ca}}^{\mathrm{grt}})^2(X_{\mathrm{Mn}}^{\mathrm{grt}}) - 3234{\cdot}0(X_{\mathrm{Mn}}^{\mathrm{grt}})^2(X_{\mathrm{Fe}}^{\mathrm{grt}}) \\
& - 82498{\cdot}0(X_{\mathrm{Mn}}^{\mathrm{grt}})^2(X_{\mathrm{Mg}}^{\mathrm{grt}}) - 2850{\cdot}0(X_{\mathrm{Mn}}^{\mathrm{grt}})^2(X_{\mathrm{Ca}}^{\mathrm{grt}}) \\
& - 62653{\cdot}0(X_{\mathrm{Fe}}^{\mathrm{grt}})(X_{\mathrm{Mg}}^{\mathrm{grt}})(X_{\mathrm{Ca}}^{\mathrm{grt}}) \\
& - 91682{\cdot}0(X_{\mathrm{Fe}}^{\mathrm{grt}})(X_{\mathrm{Mg}}^{\mathrm{grt}})(X_{\mathrm{Mn}}^{\mathrm{grt}}) \\
& - 24712{\cdot}0(X_{\mathrm{Fe}}^{\mathrm{grt}})(X_{\mathrm{Ca}}^{\mathrm{grt}})(X_{\mathrm{Mn}}^{\mathrm{grt}}) \\
& - 177221{\cdot}0(X_{\mathrm{Mg}}^{\mathrm{grt}})(X_{\mathrm{Ca}}^{\mathrm{grt}})(X_{\mathrm{Mn}}^{\mathrm{grt}})
\end{aligned}
$$

$$
\begin{aligned}
\mathrm{Fea} = & 5{\cdot}993(X_{\mathrm{Mg}}^{\mathrm{grt}})^2 - 9{\cdot}67(X_{\mathrm{Ca}}^{\mathrm{grt}})^2 - 11{\cdot}006(X_{\mathrm{Fe}}^{\mathrm{grt}})(X_{\mathrm{Mg}}^{\mathrm{grt}}) \\
& + 0{\cdot}674(X_{\mathrm{Fe}}^{\mathrm{grt}})(X_{\mathrm{Ca}}^{\mathrm{grt}}) - 9{\cdot}5725(X_{\mathrm{Mg}}^{\mathrm{grt}})(X_{\mathrm{Ca}}^{\mathrm{grt}}) \\
& - 22{\cdot}765(X_{\mathrm{Mg}}^{\mathrm{grt}})(X_{\mathrm{Mn}}^{\mathrm{grt}}) - 4{\cdot}6665(X_{\mathrm{Ca}}^{\mathrm{grt}})(X_{\mathrm{Mn}}^{\mathrm{grt}}) \\
& + 11{\cdot}006(X_{\mathrm{Fe}}^{\mathrm{grt}})^2(X_{\mathrm{Mg}}^{\mathrm{grt}}) - 0{\cdot}674(X_{\mathrm{Fe}}^{\mathrm{grt}})^2(X_{\mathrm{Ca}}^{\mathrm{grt}}) \\
& - 11{\cdot}986(X_{\mathrm{Mg}}^{\mathrm{grt}})^2(X_{\mathrm{Fe}}^{\mathrm{grt}}) + 37{\cdot}966(X_{\mathrm{Mg}}^{\mathrm{grt}})^2(X_{\mathrm{Ca}}^{\mathrm{grt}}) \\
& + 46{\cdot}02(X_{\mathrm{Mg}}^{\mathrm{grt}})^2(X_{\mathrm{Mn}}^{\mathrm{grt}}) + 19{\cdot}34(X_{\mathrm{Ca}}^{\mathrm{grt}})^2(X_{\mathrm{Fe}}^{\mathrm{grt}}) \\
& + 25{\cdot}746(X_{\mathrm{Ca}}^{\mathrm{grt}})^2(X_{\mathrm{Mg}}^{\mathrm{grt}}) + 46{\cdot}02(X_{\mathrm{Mn}}^{\mathrm{grt}})^2(X_{\mathrm{Mg}}^{\mathrm{grt}}) \\
& + 19{\cdot}145(X_{\mathrm{Fe}}^{\mathrm{grt}})(X_{\mathrm{Mg}}^{\mathrm{grt}})(X_{\mathrm{Ca}}^{\mathrm{grt}}) \\
& + 45{\cdot}53(X_{\mathrm{Fe}}^{\mathrm{grt}})(X_{\mathrm{Mg}}^{\mathrm{grt}})(X_{\mathrm{Mn}}^{\mathrm{grt}}) \\
& + 9{\cdot}333(X_{\mathrm{Fe}}^{\mathrm{grt}})(X_{\mathrm{Ca}}^{\mathrm{grt}})(X_{\mathrm{Mn}}^{\mathrm{grt}}) \\
& + 77{\cdot}876(X_{\mathrm{Mg}}^{\mathrm{grt}})(X_{\mathrm{Ca}}^{\mathrm{grt}})(X_{\mathrm{Mn}}^{\mathrm{grt}})
\end{aligned}
$$

$$
\begin{aligned}
\mathrm{Feb} = {} & -0{\cdot}034(X_{\mathrm{Mg}}^{\mathrm{grt}})^2 + 0{\cdot}135(X_{\mathrm{Ca}}^{\mathrm{grt}})^2 + 0{\cdot}024(X_{\mathrm{Mn}}^{\mathrm{grt}})^2 \\
& + 0{\cdot}1(X_{\mathrm{Fe}}^{\mathrm{grt}})(X_{\mathrm{Mg}}^{\mathrm{grt}}) + 0{\cdot}08(X_{\mathrm{Fe}}^{\mathrm{grt}})(X_{\mathrm{Ca}}^{\mathrm{grt}}) \\
& + 0{\cdot}048(X_{\mathrm{Fe}}^{\mathrm{grt}})(X_{\mathrm{Mn}}^{\mathrm{grt}}) - 0{\cdot}0515(X_{\mathrm{Mg}}^{\mathrm{grt}})(X_{\mathrm{Ca}}^{\mathrm{grt}}) \\
& + 0{\cdot}07(X_{\mathrm{Mg}}^{\mathrm{grt}})(X_{\mathrm{Mn}}^{\mathrm{grt}}) + 0{\cdot}1765(X_{\mathrm{Ca}}^{\mathrm{grt}})(X_{\mathrm{Mn}}^{\mathrm{grt}}) \\
& - 0{\cdot}1(X_{\mathrm{Fe}}^{\mathrm{grt}})^2(X_{\mathrm{Mg}}^{\mathrm{grt}}) - 0{\cdot}08(X_{\mathrm{Fe}}^{\mathrm{grt}})^2(X_{\mathrm{Ca}}^{\mathrm{grt}}) \\
& - 0{\cdot}048(X_{\mathrm{Fe}}^{\mathrm{grt}})^2(X_{\mathrm{Mn}}^{\mathrm{grt}}) + 0{\cdot}068(X_{\mathrm{Mg}}^{\mathrm{grt}})^2(X_{\mathrm{Fe}}^{\mathrm{grt}}) \\
& - 0{\cdot}136(X_{\mathrm{Mg}}^{\mathrm{grt}})^2(X_{\mathrm{Ca}}^{\mathrm{grt}}) - 0{\cdot}076(X_{\mathrm{Mg}}^{\mathrm{grt}})^2(X_{\mathrm{Mn}}^{\mathrm{grt}}) \\
& - 0{\cdot}27(X_{\mathrm{Ca}}^{\mathrm{grt}})^2(X_{\mathrm{Fe}}^{\mathrm{grt}}) - 0{\cdot}28(X_{\mathrm{Ca}}^{\mathrm{grt}})^2(X_{\mathrm{Mg}}^{\mathrm{grt}}) \\
& - 0{\cdot}13(X_{\mathrm{Ca}}^{\mathrm{grt}})^2(X_{\mathrm{Mn}}^{\mathrm{grt}}) - 0{\cdot}048(X_{\mathrm{Mn}}^{\mathrm{grt}})^2(X_{\mathrm{Fe}}^{\mathrm{grt}}) \\
& - 0{\cdot}076(X_{\mathrm{Mn}}^{\mathrm{grt}})^2(X_{\mathrm{Mg}}^{\mathrm{grt}}) - 0{\cdot}13(X_{\mathrm{Mn}}^{\mathrm{grt}})^2(X_{\mathrm{Ca}}^{\mathrm{grt}}) \\
& + 0{\cdot}103(X_{\mathrm{Fe}}^{\mathrm{grt}})(X_{\mathrm{Mg}}^{\mathrm{grt}})(X_{\mathrm{Ca}}^{\mathrm{grt}}) - 0{\cdot}14(X_{\mathrm{Fe}}^{\mathrm{grt}})(X_{\mathrm{Mg}}^{\mathrm{grt}})(X_{\mathrm{Mn}}^{\mathrm{grt}}) \\
& - 0{\cdot}353(X_{\mathrm{Fe}}^{\mathrm{grt}})(X_{\mathrm{Ca}}^{\mathrm{grt}})(X_{\mathrm{Mn}}^{\mathrm{grt}}) - 0{\cdot}414(X_{\mathrm{Mg}}^{\mathrm{grt}})(X_{\mathrm{Ca}}^{\mathrm{grt}})(X_{\mathrm{Mn}}^{\mathrm{grt}})
\end{aligned}
$$

$$
\begin{aligned}
\mathrm{Fec} = {} & -5672{\cdot}0(X_{\mathrm{Mg}}^{\mathrm{grt}})^2 + 19932{\cdot}0(X_{\mathrm{Ca}}^{\mathrm{grt}})^2 + 1617{\cdot}0(X_{\mathrm{Mn}}^{\mathrm{grt}})^2 \\
& + 23244{\cdot}0(X_{\mathrm{Fe}}^{\mathrm{grt}})(X_{\mathrm{Mg}}^{\mathrm{grt}}) - 2608{\cdot}0(X_{\mathrm{Fe}}^{\mathrm{grt}})(X_{\mathrm{Ca}}^{\mathrm{grt}}) \\
& + 3234{\cdot}0(X_{\mathrm{Fe}}^{\mathrm{grt}})(X_{\mathrm{Mn}}^{\mathrm{grt}}) + 31326{\cdot}5(X_{\mathrm{Mg}}^{\mathrm{grt}})(X_{\mathrm{Ca}}^{\mathrm{grt}}) \\
& + 45841{\cdot}0(X_{\mathrm{Mg}}^{\mathrm{grt}})(X_{\mathrm{Mn}}^{\mathrm{grt}}) + 12356{\cdot}0(X_{\mathrm{Ca}}^{\mathrm{grt}})(X_{\mathrm{Mn}}^{\mathrm{grt}}) \\
& - 23244{\cdot}0(X_{\mathrm{Fe}}^{\mathrm{grt}})^2(X_{\mathrm{Mg}}^{\mathrm{grt}}) + 2608{\cdot}0(X_{\mathrm{Fe}}^{\mathrm{grt}})^2(X_{\mathrm{Ca}}^{\mathrm{grt}}) \\
& - 3234{\cdot}0(X_{\mathrm{Fe}}^{\mathrm{grt}})^2(X_{\mathrm{Mn}}^{\mathrm{grt}}) + 11344{\cdot}0(X_{\mathrm{Mg}}^{\mathrm{grt}})^2(X_{\mathrm{Fe}}^{\mathrm{grt}}) \\
& - 132228{\cdot}0(X_{\mathrm{Mg}}^{\mathrm{grt}})^2(X_{\mathrm{Ca}}^{\mathrm{grt}}) - 82498{\cdot}0(X_{\mathrm{Mg}}^{\mathrm{grt}})^2(X_{\mathrm{Mn}}^{\mathrm{grt}}) \\
& - 39864{\cdot}0(X_{\mathrm{Ca}}^{\mathrm{grt}})^2(X_{\mathrm{Fe}}^{\mathrm{grt}}) - 51518{\cdot}0(X_{\mathrm{Ca}}^{\mathrm{grt}})^2(X_{\mathrm{Mg}}^{\mathrm{grt}}) \\
& - 2850{\cdot}0(X_{\mathrm{Ca}}^{\mathrm{grt}})^2(X_{\mathrm{Mn}}^{\mathrm{grt}}) - 3234{\cdot}0(X_{\mathrm{Mn}}^{\mathrm{grt}})^2(X_{\mathrm{Fe}}^{\mathrm{grt}}) \\
& - 82498{\cdot}0(X_{\mathrm{Mn}}^{\mathrm{grt}})^2(X_{\mathrm{Mg}}^{\mathrm{grt}}) - 2850{\cdot}0(X_{\mathrm{Mn}}^{\mathrm{grt}})^2(X_{\mathrm{Ca}}^{\mathrm{grt}}) \\
& - 62653{\cdot}0(X_{\mathrm{Fe}}^{\mathrm{grt}})(X_{\mathrm{Mg}}^{\mathrm{grt}})(X_{\mathrm{Ca}}^{\mathrm{grt}}) \\
& - 91682{\cdot}0(X_{\mathrm{Fe}}^{\mathrm{grt}})(X_{\mathrm{Mg}}^{\mathrm{grt}})(X_{\mathrm{Mn}}^{\mathrm{grt}}) \\
& - 24712{\cdot}0(X_{\mathrm{Fe}}^{\mathrm{grt}})(X_{\mathrm{Ca}}^{\mathrm{grt}})(X_{\mathrm{Mn}}^{\mathrm{grt}}) \\
& - 177221{\cdot}0(X_{\mathrm{Mg}}^{\mathrm{grt}})(X_{\mathrm{Ca}}^{\mathrm{grt}})(X_{\mathrm{Mn}}^{\mathrm{grt}})
\end{aligned}
$$

$$
\begin{aligned}
\mathrm{Mga} = {} & -5{\cdot}503(X_{\mathrm{Fe}}^{\mathrm{grt}})^2 - 12{\cdot}873(X_{\mathrm{Ca}}^{\mathrm{grt}})^2 - 23{\cdot}01(X_{\mathrm{Mn}}^{\mathrm{grt}})^2 \\
& + 11{\cdot}986(X_{\mathrm{Fe}}^{\mathrm{grt}})(X_{\mathrm{Mg}}^{\mathrm{grt}}) - 9{\cdot}5725(X_{\mathrm{Fe}}^{\mathrm{grt}})(X_{\mathrm{Ca}}^{\mathrm{grt}}) \\
& - 22{\cdot}765(X_{\mathrm{Fe}}^{\mathrm{grt}})(X_{\mathrm{Mn}}^{\mathrm{grt}}) - 37{\cdot}966(X_{\mathrm{Mg}}^{\mathrm{grt}})(X_{\mathrm{Ca}}^{\mathrm{grt}}) \\
& - 46{\cdot}02(X_{\mathrm{Mg}}^{\mathrm{grt}})(X_{\mathrm{Mn}}^{\mathrm{grt}}) - 38{\cdot}938(X_{\mathrm{Ca}}^{\mathrm{grt}})(X_{\mathrm{Mn}}^{\mathrm{grt}}) \\
& + 11{\cdot}006(X_{\mathrm{Fe}}^{\mathrm{grt}})^2(X_{\mathrm{Mg}}^{\mathrm{grt}}) - 0{\cdot}674(X_{\mathrm{Fe}}^{\mathrm{grt}})^2(X_{\mathrm{Ca}}^{\mathrm{grt}}) \\
& - 11{\cdot}986(X_{\mathrm{Mg}}^{\mathrm{grt}})^2(X_{\mathrm{Fe}}^{\mathrm{grt}}) + 37{\cdot}966(X_{\mathrm{Mg}}^{\mathrm{grt}})^2(X_{\mathrm{Ca}}^{\mathrm{grt}}) \\
& + 46{\cdot}02(X_{\mathrm{Mg}}^{\mathrm{grt}})^2(X_{\mathrm{Mn}}^{\mathrm{grt}}) + 19{\cdot}34(X_{\mathrm{Ca}}^{\mathrm{grt}})^2(X_{\mathrm{Fe}}^{\mathrm{grt}}) \\
& + 25{\cdot}746(X_{\mathrm{Ca}}^{\mathrm{grt}})^2(X_{\mathrm{Mg}}^{\mathrm{grt}}) + 46{\cdot}02(X_{\mathrm{Mn}}^{\mathrm{grt}})^2(X_{\mathrm{Mg}}^{\mathrm{grt}}) \\
& + 19{\cdot}145(X_{\mathrm{Fe}}^{\mathrm{grt}})(X_{\mathrm{Mg}}^{\mathrm{grt}})(X_{\mathrm{Ca}}^{\mathrm{grt}}) \\
& + 45{\cdot}53(X_{\mathrm{Fe}}^{\mathrm{grt}})(X_{\mathrm{Mg}}^{\mathrm{grt}})(X_{\mathrm{Mn}}^{\mathrm{grt}}) \\
& + 9{\cdot}333(X_{\mathrm{Fe}}^{\mathrm{grt}})(X_{\mathrm{Ca}}^{\mathrm{grt}})(X_{\mathrm{Mn}}^{\mathrm{grt}}) \\
& + 77{\cdot}876(X_{\mathrm{Mg}}^{\mathrm{grt}})(X_{\mathrm{Ca}}^{\mathrm{grt}})(X_{\mathrm{Mn}}^{\mathrm{grt}})
\end{aligned}
$$

$$
\begin{aligned}
\mathrm{Mgb} = {} & 0{\cdot}05(X_{\mathrm{Fe}}^{\mathrm{grt}})^2 + 0{\cdot}14(X_{\mathrm{Ca}}^{\mathrm{grt}})^2 + 0{\cdot}038(X_{\mathrm{Mn}}^{\mathrm{grt}})^2 \\
& - 0{\cdot}068(X_{\mathrm{Fe}}^{\mathrm{grt}})(X_{\mathrm{Mg}}^{\mathrm{grt}}) - 0{\cdot}0515(X_{\mathrm{Fe}}^{\mathrm{grt}})(X_{\mathrm{Ca}}^{\mathrm{grt}}) \\
& + 0{\cdot}07(X_{\mathrm{Fe}}^{\mathrm{grt}})(X_{\mathrm{Mn}}^{\mathrm{grt}}) + 0{\cdot}136(X_{\mathrm{Mg}}^{\mathrm{grt}})(X_{\mathrm{Ca}}^{\mathrm{grt}}) \\
& + 0{\cdot}076(X_{\mathrm{Mg}}^{\mathrm{grt}})(X_{\mathrm{Mn}}^{\mathrm{grt}}) + 0{\cdot}207(X_{\mathrm{Ca}}^{\mathrm{grt}})(X_{\mathrm{Mn}}^{\mathrm{grt}}) \\
& - 0{\cdot}1(X_{\mathrm{Fe}}^{\mathrm{grt}})^2(X_{\mathrm{Mg}}^{\mathrm{grt}}) - 0{\cdot}08(X_{\mathrm{Fe}}^{\mathrm{grt}})^2(X_{\mathrm{Ca}}^{\mathrm{grt}}) \\
& - 0{\cdot}048(X_{\mathrm{Fe}}^{\mathrm{grt}})^2(X_{\mathrm{Mn}}^{\mathrm{grt}}) + 0{\cdot}068(X_{\mathrm{Mg}}^{\mathrm{grt}})^2(X_{\mathrm{Fe}}^{\mathrm{grt}}) \\
& - 0{\cdot}136(X_{\mathrm{Mg}}^{\mathrm{grt}})^2(X_{\mathrm{Ca}}^{\mathrm{grt}}) - 0{\cdot}076(X_{\mathrm{Mg}}^{\mathrm{grt}})^2(X_{\mathrm{Mn}}^{\mathrm{grt}}) \\
& - 0{\cdot}27(X_{\mathrm{Ca}}^{\mathrm{grt}})^2(X_{\mathrm{Fe}}^{\mathrm{grt}}) - 0{\cdot}28(X_{\mathrm{Ca}}^{\mathrm{grt}})^2(X_{\mathrm{Mg}}^{\mathrm{grt}}) \\
& - 0{\cdot}13(X_{\mathrm{Ca}}^{\mathrm{grt}})^2(X_{\mathrm{Mn}}^{\mathrm{grt}}) - 0{\cdot}048(X_{\mathrm{Mn}}^{\mathrm{grt}})^2(X_{\mathrm{Fe}}^{\mathrm{grt}}) \\
& - 0{\cdot}076(X_{\mathrm{Mn}}^{\mathrm{grt}})^2(X_{\mathrm{Mg}}^{\mathrm{grt}}) - 0{\cdot}13(X_{\mathrm{Mn}}^{\mathrm{grt}})^2(X_{\mathrm{Ca}}^{\mathrm{grt}}) \\
& + 0{\cdot}103(X_{\mathrm{Fe}}^{\mathrm{grt}})(X_{\mathrm{Mg}}^{\mathrm{grt}})(X_{\mathrm{Ca}}^{\mathrm{grt}}) - 0{\cdot}14(X_{\mathrm{Fe}}^{\mathrm{grt}})(X_{\mathrm{Mg}}^{\mathrm{grt}})(X_{\mathrm{Mn}}^{\mathrm{grt}}) \\
& - 0{\cdot}353(X_{\mathrm{Fe}}^{\mathrm{grt}})(X_{\mathrm{Ca}}^{\mathrm{grt}})(X_{\mathrm{Mn}}^{\mathrm{grt}}) - 0{\cdot}414(X_{\mathrm{Mg}}^{\mathrm{grt}})(X_{\mathrm{Ca}}^{\mathrm{grt}})(X_{\mathrm{Mn}}^{\mathrm{grt}})
\end{aligned}
$$

$$
\begin{aligned}
\mathrm{Mgc} = {} & 11622{\cdot}0(X_{\mathrm{Fe}}^{\mathrm{grt}})^2 + 25759{\cdot}0(X_{\mathrm{Ca}}^{\mathrm{grt}})^2 \\
& + 41249{\cdot}0(X_{\mathrm{Mn}}^{\mathrm{grt}})^2 - 11344{\cdot}0(X_{\mathrm{Fe}}^{\mathrm{grt}})(X_{\mathrm{Mg}}^{\mathrm{grt}}) \\
& + 31326{\cdot}5(X_{\mathrm{Fe}}^{\mathrm{grt}})(X_{\mathrm{Ca}}^{\mathrm{grt}}) + 45841{\cdot}0(X_{\mathrm{Fe}}^{\mathrm{grt}})(X_{\mathrm{Mn}}^{\mathrm{grt}}) \\
& + 132228{\cdot}0(X_{\mathrm{Mg}}^{\mathrm{grt}})(X_{\mathrm{Ca}}^{\mathrm{grt}}) + 82498{\cdot}0(X_{\mathrm{Mg}}^{\mathrm{grt}})(X_{\mathrm{Mn}}^{\mathrm{grt}}) \\
& + 88610{\cdot}5(X_{\mathrm{Ca}}^{\mathrm{grt}})(X_{\mathrm{Mn}}^{\mathrm{grt}}) - 23244{\cdot}0(X_{\mathrm{Fe}}^{\mathrm{grt}})^2(X_{\mathrm{Mg}}^{\mathrm{grt}}) \\
& + 2608{\cdot}0(X_{\mathrm{Fe}}^{\mathrm{grt}})^2(X_{\mathrm{Ca}}^{\mathrm{grt}}) - 3234{\cdot}0(X_{\mathrm{Fe}}^{\mathrm{grt}})^2(X_{\mathrm{Mn}}^{\mathrm{grt}}) \\
& + 11344{\cdot}0(X_{\mathrm{Mg}}^{\mathrm{grt}})^2(X_{\mathrm{Fe}}^{\mathrm{grt}}) - 132228{\cdot}0(X_{\mathrm{Mg}}^{\mathrm{grt}})^2(X_{\mathrm{Ca}}^{\mathrm{grt}}) \\
& - 82498{\cdot}0(X_{\mathrm{Mg}}^{\mathrm{grt}})^2(X_{\mathrm{Mn}}^{\mathrm{grt}}) - 39864{\cdot}0(X_{\mathrm{Ca}}^{\mathrm{grt}})^2(X_{\mathrm{Fe}}^{\mathrm{grt}}) \\
& - 51518{\cdot}0(X_{\mathrm{Ca}}^{\mathrm{grt}})^2(X_{\mathrm{Mg}}^{\mathrm{grt}}) - 2850{\cdot}0(X_{\mathrm{Ca}}^{\mathrm{grt}})^2(X_{\mathrm{Mn}}^{\mathrm{grt}}) \\
& - 3234{\cdot}0(X_{\mathrm{Mn}}^{\mathrm{grt}})^2(X_{\mathrm{Fe}}^{\mathrm{grt}}) - 82498{\cdot}0(X_{\mathrm{Mn}}^{\mathrm{grt}})^2(X_{\mathrm{Mg}}^{\mathrm{grt}}) \\
& - 2850{\cdot}0(X_{\mathrm{Mn}}^{\mathrm{grt}})^2(X_{\mathrm{Ca}}^{\mathrm{grt}}) - 62653{\cdot}0(X_{\mathrm{Fe}}^{\mathrm{grt}})(X_{\mathrm{Mg}}^{\mathrm{grt}})(X_{\mathrm{Ca}}^{\mathrm{grt}}) \\
& - 91682{\cdot}0(X_{\mathrm{Fe}}^{\mathrm{grt}})(X_{\mathrm{Mg}}^{\mathrm{grt}})(X_{\mathrm{Mn}}^{\mathrm{grt}}) \\
& - 24712{\cdot}0(X_{\mathrm{Fe}}^{\mathrm{grt}})(X_{\mathrm{Ca}}^{\mathrm{grt}})(X_{\mathrm{Mn}}^{\mathrm{grt}}) \\
& - 177221{\cdot}0(X_{\mathrm{Mg}}^{\mathrm{grt}})(X_{\mathrm{Ca}}^{\mathrm{grt}})(X_{\mathrm{Mn}}^{\mathrm{grt}})
\end{aligned}
$$

Polynomial expressions for plagioclase end-members:

$$
\begin{aligned}
\mathrm{Fa} = {} & 20{\cdot}6(X_{\mathrm{Ab}}^{\mathrm{pl}})^2(X_{\mathrm{Or}}^{\mathrm{pl}}) + 20{\cdot}6(X_{\mathrm{Or}}^{\mathrm{pl}})^2(X_{\mathrm{Ab}}^{\mathrm{pl}}) \\
& - 10{\cdot}3(X_{\mathrm{Ab}}^{\mathrm{pl}})(X_{\mathrm{Or}}^{\mathrm{pl}}) + 20{\cdot}6(X_{\mathrm{Ab}}^{\mathrm{pl}})(X_{\mathrm{An}}^{\mathrm{pl}})(X_{\mathrm{Or}}^{\mathrm{pl}})
\end{aligned}
$$

$$
\begin{aligned}
\mathrm{Fb} = {} & -0{\cdot}788(X_{\mathrm{Ab}}^{\mathrm{pl}})^2(X_{\mathrm{Or}}^{\mathrm{pl}}) - 0{\cdot}788(X_{\mathrm{Or}}^{\mathrm{pl}})^2(X_{\mathrm{Ab}}^{\mathrm{pl}}) \\
& + 0{\cdot}24(X_{\mathrm{Or}}^{\mathrm{pl}})^2(X_{\mathrm{An}}^{\mathrm{pl}}) - 0{\cdot}12(X_{\mathrm{Or}}^{\mathrm{pl}})^2 \\
& - 0{\cdot}76(X_{\mathrm{Ab}}^{\mathrm{pl}})(X_{\mathrm{Or}}^{\mathrm{pl}}) + 1{\cdot}52(X_{\mathrm{Ab}}^{\mathrm{pl}})(X_{\mathrm{An}}^{\mathrm{pl}})(X_{\mathrm{Or}}^{\mathrm{pl}})
\end{aligned}
$$

$$
\begin{aligned}
\mathrm{Fc} = {} & -16942{\cdot}0(X_{\mathrm{Ab}}^{\mathrm{pl}})^2(X_{\mathrm{An}}^{\mathrm{pl}}) - 54640{\cdot}0(X_{\mathrm{Ab}}^{\mathrm{pl}})^2(X_{\mathrm{Or}}^{\mathrm{pl}}) \\
& - 56452{\cdot}0(X_{\mathrm{An}}^{\mathrm{pl}})^2(X_{\mathrm{Ab}}^{\mathrm{pl}}) - 94792{\cdot}0(X_{\mathrm{An}}^{\mathrm{pl}})^2(X_{\mathrm{Or}}^{\mathrm{pl}}) \\
& - 37620{\cdot}0(X_{\mathrm{Or}}^{\mathrm{pl}})^2(X_{\mathrm{Ab}}^{\mathrm{pl}}) - 104936{\cdot}0(X_{\mathrm{Or}}^{\mathrm{pl}})^2(X_{\mathrm{An}}^{\mathrm{pl}}) \\
& + 8471{\cdot}0(X_{\mathrm{Ab}}^{\mathrm{pl}})^2 + 52468{\cdot}0(X_{\mathrm{Or}}^{\mathrm{pl}})^2 \\
& + 56452{\cdot}0(X_{\mathrm{Ab}}^{\mathrm{pl}})(X_{\mathrm{An}}^{\mathrm{pl}}) + 100045{\cdot}5(X_{\mathrm{Ab}}^{\mathrm{pl}})(X_{\mathrm{Or}}^{\mathrm{pl}}) \\
& + 94792{\cdot}0(X_{\mathrm{An}}^{\mathrm{pl}})(X_{\mathrm{Or}}^{\mathrm{pl}}) - 200091{\cdot}0(X_{\mathrm{Ab}}^{\mathrm{pl}})(X_{\mathrm{An}}^{\mathrm{pl}})(X_{\mathrm{Or}}^{\mathrm{pl}}).
\end{aligned}
$$

B.2 GPHQ Formulas

Compositional parameters used for garnet plagioclase hornblende quartz barometery from Kohn and Spear 1990. Element concentrations in cations per formula unit (pfu). R (gas constant) = 8.31441 J/(mol*K) (J = Joules). X = mole fraction.

Garnet:

((Ca + Mn + Fe^{2+} + Mg) ≈ 3.0; T = °K)

$X_{Fe}^{grt} = Fe^{2+}/(Fe^{2+} + Mg + Ca + Mn)$,

$X_{Mg}^{grt} = Mg/(Fe^{2+} + Mg + Ca + Mn)$,

$X_{Ca}^{grt} = Ca/(Fe^{2+} + Mg + Ca + Mn)$,

$X_{Mn}^{grt} = Mn/(Fe^{2+} + Mg + Ca + Mn)$,

$a_{prp} = \{X_{Mg} * \exp[(13800 - 6.28T) * ({X^2}_{Ca} + X_{Fe} + X_{Ca} + X_{Ca} + X_{Mn})/RT]\}^3$,

$a_{grs} = \{X_{Ca} * \exp[(13800 - 6.28T) * ({X^2}_{Mg} + X_{Fe} + X_{Mg} + X_{Mg} + X_{Mn})/RT]\}^3$,

$a_{alm} = \{X_{Fe} * \exp[(13800 - 6.28T) * (-{X^2}_{Mg} * X_{Ca})/RT]\}^3$

Plagioclase:

(T = °K)

$X_{An} = Ca/(Ca + Na + K)$,

$a_{An} = X_{An} * \exp[(610.34/T) - 0.3837]$

Hornblende:

$T1Si = Si - 4.0,\ X_{T1Si} = T1Si/4.0$,

$T1Al = 8.0 - Si, X_{T1Al} = T1Al/4.0$,

$a_{tsch} = (256/27) * (X_{T1Al}) * (X_{T1Si})^3 * [Mg/(Fe + Mg)]_{hbl}$

$a_{tr} = (X_{T1Si})^4 * {[Mg/(Fe + Mg)]^2}_{hbl}$,

$a_{Fe-tsch} = (256/27) * (X_{T1Al}) * (X_{T1Si})^3 * [Fe/(Fe + Mg)]_{hbl}$

$a_{Fe-act} = (X_{T1Si})^4 * {[Fe/(Fe + Mg)]^2}_{hbl}$

B.3 Analytical Data

For each thermobarometry sample there are BSE images with annotated analysis points, Ca, Mn, Mg and Fe chemical maps of garnet in the selected area, and compositional data. Compositional data in bold font was used for thermobarometry.

14SV095B:

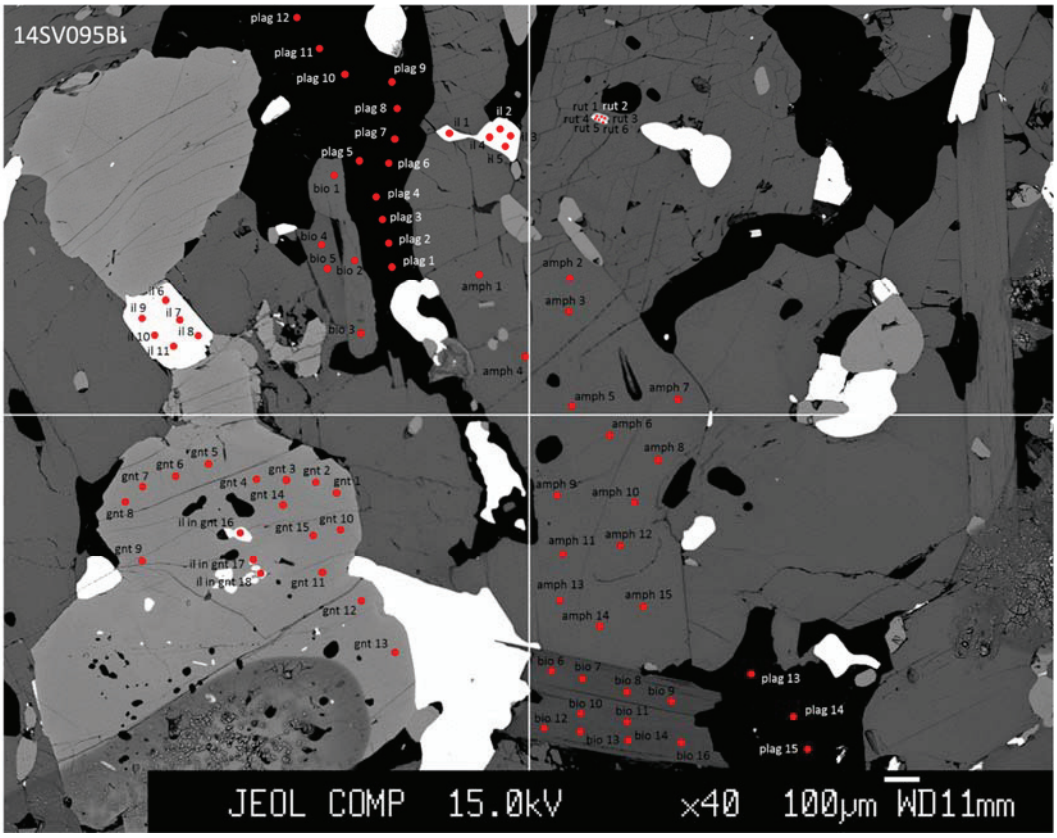

Figure B.1: BSE image of sample 14SV095Bi with annotated analysis points.

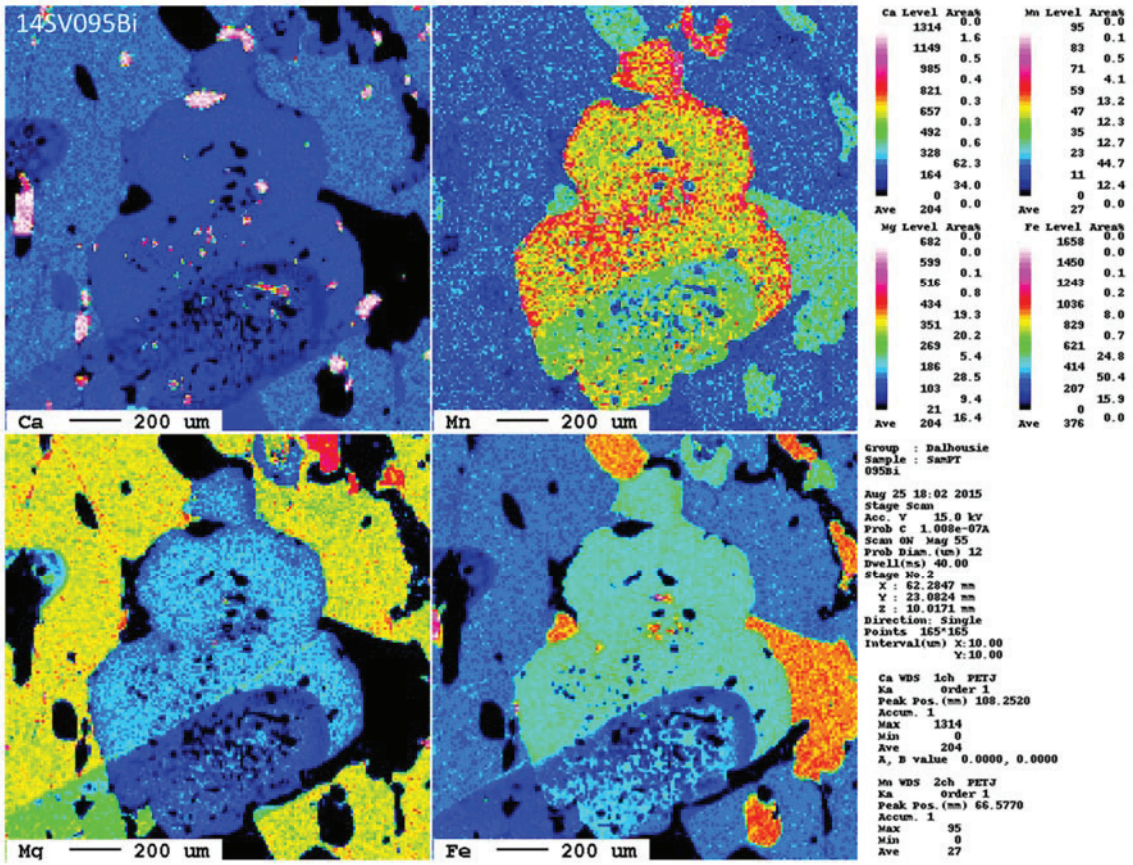

Figure B.2: Ca, Mn, Mg and Fe maps of the garnet analyzed in sample 14SV095Bi.

Table B.1: Analytical data from sample 14SB095i.

No.	16	17	18	19	20	21	22
	095Bi_plag01	095Bi_plag02	095Bi_plag03	095Bi_plag04	095Bi_plag05	095Bi_plag06	095Bi_plag07
oxides(wt%):							
CaO	6.959	7.013	6.135	6.89	7.003	7.158	6.182
TiO2	0	0	0	0	0	0	0
Na2O	7.63	7.671	7.711	7.844	7.713	7.554	7.851
SiO2	59.1	59.227	59.63	59.742	58.949	58.939	60.057
MnO	0	0	0	0	0	0	0
K2O	0.175	0.124	0.44	0.142	0.131	0.129	0.613
Cr2O3	0	0	0	0	0	0	0
MgO	0	0	0	0	0	0	0
Al2O3	24.824	25.008	25.095	25.176	24.829	25.533	24.405
FeO	0.088	0.039	0.056	0.05	0.026	0.07	0.054
Total	98.776	99.082	99.067	99.844	98.651	99.383	99.162
cations:							
Ca	0.0421	0.0423	0.0369	0.0412	0.0424	0.0431	0.0372
Ti	0	0	0	0	0	0	0
Na	0.0835	0.0837	0.084	0.0849	0.0845	0.0822	0.0856
Si	0.3337	0.3332	0.335	0.3335	0.3333	0.3308	0.3375
Mn	0	0	0	0	0	0	0
K	0.0013	0.0009	0.0032	0.001	0.0009	0.0009	0.0044
Cr	0	0	0	0	0	0	0
Mg	0	0	0	0	0	0	0
Al	0.1652	0.1659	0.1662	0.1657	0.1655	0.1689	0.1617
Fe	0.0004	0.0002	0.0003	0.0002	0.0001	0.0003	0.0003
Total	0.6263	0.6263	0.6256	0.6265	0.6268	0.6262	0.6268

Table B.1: *Continued.* Analytical data from sample 14SB095i.

No.	23	24	**25**	26	27	28	29
	095Bi_plag08	095Bi_plag09	**095Bi_plag10**	095Bi_plag11	095Bi_plag12	095Bi_plag13	095Bi_plag14
oxides(wt%):							
CaO	6.209	6.551	**6.241**	6.145	6.246	7.301	6.415
TiO2	0	0	**0**	0	0	0	0
Na2O	8.039	8.085	**8.165**	8.165	8.111	7.558	7.987
SiO2	60.008	60.195	**60.721**	60.554	59.925	59.216	60.048
MnO	0	0	**0**	0	0	0	0
K2O	0.135	0.109	**0.172**	0.176	0.183	0.09	0.242
Cr2O3	0	0	**0**	0	0	0	0
MgO	0	0	**0**	0	0	0	0
Al2O3	24.587	25.111	**24.739**	24.637	24.642	25.676	25.006
FeO	0.02	0.052	**0.034**	0.025	0.02	0.034	0.028
Total	98.998	100.103	**100.072**	99.702	99.127	99.875	99.726
cations:							
Ca	0.0374	0.039	**0.0372**	0.0367	0.0376	0.0437	0.0384
Ti	0	0	**0**	0	0	0	0
Na	0.0876	0.0872	**0.088**	0.0883	0.0883	0.0818	0.0865
Si	0.3371	0.3349	**0.3375**	0.3377	0.3365	0.3307	0.3353
Mn	0	0	**0**	0	0	0	0
K	0.001	0.0008	**0.0012**	0.0013	0.0013	0.0006	0.0017
Cr	0	0	**0**	0	0	0	0
Mg	0	0	**0**	0	0	0	0
Al	0.1628	0.1647	**0.1621**	0.162	0.1631	0.169	0.1646
Fe	0.0001	0.0002	**0.0002**	0.0001	0.0001	0.0002	0.0001
Total	0.626	0.6269	**0.6262**	0.6262	0.627	0.626	0.6267

Table B.1: *Continued.* Analytical data from sample 14SB095i.

No.	30	31	32	33	34	35	36	37
	095Bi_plag15	095Bi_rut01	095Bi_rut02	095Bi_rut03	095Bi_rut04	095Bi_rut05	095Bi_rut06	095Bi_il01
oxides(wt%):								
CaO	6.292	0.203	0.19	0.227	0.331	0.355	0.349	0.104
TiO2	0	100.76	100.559	100.982	100.618	100.348	100.31	48.567
Na2O	8.142	0	0	0.002	0	0	0.002	0
SiO2	60.599	0.093	0.079	0.091	0.105	0.146	0.108	0.096
MnO	0	0.065	0.055	0.058	0.069	0.073	0.065	0.548
K2O	0.149	0.063	0.074	0.07	0.076	0.085	0.08	0.079
Cr2O3	0	0.219	0.191	0.152	0.184	0.21	0.187	0.301
MgO	0.001	0.033	0.013	0.014	0.016	0.02	0.019	0.104
Al2O3	24.662	0.026	0.034	0.034	0.044	0.025	0.033	0.041
FeO	0.039	0.723	0.673	0.683	0.885	0.875	0.902	50.533
Total	99.884	102.185	101.868	102.313	102.328	102.137	102.055	100.373
cations:								
Ca	0.0375	0.0014	0.0013	0.0016	0.0023	0.0025	0.0025	0.001
Ti	0	0.4952	0.4957	0.4956	0.4943	0.494	0.4942	0.3129
Na	0.0879	0	0	0	0	0	0	0
Si	0.3375	0.0006	0.0005	0.0006	0.0007	0.001	0.0007	0.0008
Mn	0	0.0004	0.0003	0.0003	0.0004	0.0004	0.0004	0.004
K	0.0011	0.0005	0.0006	0.0006	0.0006	0.0007	0.0007	0.0009
Cr	0	0.0011	0.001	0.0008	0.001	0.0011	0.001	0.002
Mg	0	0.0003	0.0001	0.0001	0.0002	0.0002	0.0002	0.0013
Al	0.1619	0.0002	0.0003	0.0003	0.0003	0.0002	0.0003	0.0004
Fe	0.0002	0.004	0.0037	0.0037	0.0048	0.0048	0.0049	0.3621
Total	0.6262	0.5038	0.5035	0.5037	0.5046	0.5049	0.5049	0.6855

Table B.1: *Continued.* Analytical data from sample 14SB095i.

No.	38	39	40	41	42	43	44	45	46
	095Bi_il02	095Bi_il03	095Bi_il04	095Bi_il05	095Bi_il06	095Bi_il07	095Bi_il08	095Bi_il09	095Bi_il10
oxides(wt%):									
CaO	0.079	0.061	0.072	0.088	0.069	0.073	0.069	0.059	0.057
TiO2	48.573	48.408	48.444	48.563	50.098	49.146	49.656	49.294	49.649
Na2O	0.002	0	0.018	0	0	0.015	0	0.003	0
SiO2	0.111	0.085	0.076	0.095	0.099	0.076	0.117	0.103	0.08
MnO	0.606	0.53	0.564	0.588	0.53	0.525	0.543	0.514	0.54
K2O	0.075	0.073	0.068	0.08	0.077	0.066	0.065	0.086	0.079
Cr2O3	0.302	0.28	0.298	0.301	0.292	0.314	0.342	0.284	0.306
MgO	0.38	0.453	0.432	0.465	0.677	0.638	0.556	0.634	0.618
Al2O3	0.05	0.02	0.042	0.068	0.025	0.035	0.018	0.039	0.037
FeO	50.508	50.177	50.593	50.411	49.005	49.686	49.872	49.806	49.454
Total	100.686	100.087	100.607	100.659	100.872	100.574	101.238	100.822	100.82
cations:									
Ca	0.0007	0.0006	0.0007	0.0008	0.0006	0.0007	0.0006	0.0005	0.0005
Ti	0.3117	0.3124	0.3114	0.3116	0.3179	0.3143	0.3152	0.3144	0.3161
Na	0	0	0.0003	0	0	0.0002	0	0	0
Si	0.001	0.0007	0.0006	0.0008	0.0008	0.0006	0.001	0.0009	0.0007
Mn	0.0044	0.0039	0.0041	0.0042	0.0038	0.0038	0.0039	0.0037	0.0039
K	0.0008	0.0008	0.0007	0.0009	0.0008	0.0007	0.0007	0.0009	0.0009
Cr	0.002	0.0019	0.002	0.002	0.002	0.0021	0.0023	0.0019	0.002
Mg	0.0048	0.0058	0.0055	0.0059	0.0085	0.0081	0.007	0.008	0.0078
Al	0.0005	0.0002	0.0004	0.0007	0.0002	0.0004	0.0002	0.0004	0.0004
Fe	0.3605	0.3601	0.3616	0.3597	0.3458	0.3534	0.352	0.3533	0.3502
Total	0.6865	0.6865	0.6873	0.6867	0.6805	0.6844	0.6829	0.684	0.6826

Table B.1: *Continued.* Analytical data from sample 14SB095i.

No.	47	55	56	57	58	59	60
	095Bi_il11	095Bi_amph01	095Bi_amph02	095Bi_amph03	095Bi_amph04	095Bi_amph05	095Bi_amph06
oxides(wt%):							
CaO	0.07	11.328	11.379	11.469	11.397	11.375	11.236
TiO2	49.344	1.63	1.506	1.493	1.586	1.589	1.47
Na2O	0	1.861	1.855	1.834	1.852	1.811	1.838
SiO2	0.104	41.071	40.899	40.91	40.899	40.79	40.554
MnO	0.569	0.2	0.18	0.209	0.204	0.188	0.194
K2O	0.069	1.115	1.14	1.088	1.15	1.178	1.183
Cr2O3	0.296	0.08	0.058	0.069	0.092	0.065	0.083
MgO	0.43	8.927	8.862	8.949	9.004	8.918	8.887
Al2O3	0.027	13.776	13.918	14.028	13.941	13.871	14
FeO	49.865	17.735	17.795	17.752	17.679	17.765	17.989
Total	100.774	97.723	97.592	97.801	97.804	97.55	97.434
cations:							
Ca	0.0006	0.0799	0.0804	0.0808	0.0803	0.0804	0.0796
Ti	0.3151	0.0081	0.0075	0.0074	0.0078	0.0079	0.0073
Na	0	0.0237	0.0237	0.0234	0.0236	0.0232	0.0236
Si	0.0009	0.2702	0.2696	0.269	0.269	0.2691	0.2682
Mn	0.0041	0.0011	0.001	0.0012	0.0011	0.001	0.0011
K	0.0007	0.0094	0.0096	0.0091	0.0097	0.0099	0.01
Cr	0.002	0.0004	0.0003	0.0004	0.0005	0.0003	0.0004
Mg	0.0054	0.0875	0.0871	0.0877	0.0883	0.0877	0.0876
Al	0.0003	0.1068	0.1081	0.1087	0.1081	0.1079	0.1091
Fe	0.3541	0.0976	0.0981	0.0976	0.0972	0.098	0.0995
Total	0.6833	0.6848	0.6855	0.6853	0.6856	0.6855	0.6865

Table B.1: *Continued.* Analytical data from sample 14SB095i.

No.	61	62	63	64	65	66	67
	095Bi_amph07	095Bi_amph08	095Bi_amph09	095Bi_amph10	095Bi_amph11	095Bi_amph12	095Bi_amph13
oxides(wt%):							
CaO	11.33	11.161	11.414	11.317	11.223	11.261	11.237
TiO2	1.48	1.488	1.589	1.57	1.523	1.497	1.382
Na2O	1.863	1.852	1.767	1.776	1.799	1.778	1.83
SiO2	40.685	40.767	40.648	41.046	40.601	41.035	40.794
MnO	0.19	0.183	0.174	0.21	0.188	0.206	0.196
K2O	1.082	1.09	1.234	1.254	1.238	1.246	1.231
Cr2O3	0.063	0.076	0.085	0.069	0.047	0.087	0.08
MgO	8.83	8.898	8.828	8.846	8.892	8.925	8.771
Al2O3	13.781	13.734	14.182	13.931	13.986	13.983	14.183
FeO	17.885	17.809	17.814	17.906	17.787	17.744	17.977
Total	97.189	97.058	97.735	97.925	97.284	97.762	97.681
cations:							
Ca	0.0804	0.0792	0.0806	0.0797	0.0796	0.0794	0.0794
Ti	0.0074	0.0074	0.0079	0.0078	0.0076	0.0074	0.0069
Na	0.0239	0.0238	0.0226	0.0226	0.0231	0.0227	0.0234
Si	0.2695	0.2701	0.2678	0.2698	0.2687	0.2699	0.2689
Mn	0.0011	0.001	0.001	0.0012	0.0011	0.0011	0.0011
K	0.0091	0.0092	0.0104	0.0105	0.0105	0.0105	0.0104
Cr	0.0003	0.0004	0.0004	0.0004	0.0002	0.0005	0.0004
Mg	0.0872	0.0879	0.0867	0.0867	0.0877	0.0875	0.0862
Al	0.1076	0.1073	0.1101	0.1079	0.1091	0.1084	0.1102
Fe	0.0991	0.0987	0.0981	0.0984	0.0984	0.0976	0.0991
Total	0.6856	0.685	0.6856	0.6851	0.6861	0.6851	0.686

Table B.1: *Continued.* Analytical data from sample 14SB095i.

No.	68	**69**	70	71	72	**73**	74	75
	095Bi_amph14	**095Bi_amph15**	095Bi_bio01	095Bi_bio02	095Bi_bio03	**095Bi_bio04**	095Bi_bio05	095Bi_bio06
oxides(wt%):								
CaO	11.376	**11.39**	0.03	0.052	0.022	**0.218**	0.322	0.329
TiO2	1.353	**1.403**	3.426	3.292	3.447	**3.286**	3.293	3.227
Na2O	1.724	**1.808**	0.186	0.171	0.152	**0.312**	0.28	0.422
SiO2	40.817	**41.025**	35.649	35.421	35.775	**36.34**	35.698	36.068
MnO	0.177	**0.189**	0.059	0.019	0.035	**0.033**	0.046	0.008
K2O	1.151	**1.189**	9.293	9.234	9.157	**8.604**	8.286	8.091
Cr2O3	0.083	**0.066**	0.09	0.061	0	**0.08**	0.068	0
MgO	8.794	**8.919**	11.678	11.749	11.751	**11.901**	11.889	12.941
Al2O3	14.12	**13.938**	15.809	15.996	15.962	**16.197**	15.974	16.489
FeO	18.072	**18.123**	18.467	18.557	18.266	**18.493**	18.538	16.908
Total	97.667	**98.05**	94.687	94.552	94.567	**95.464**	94.394	94.483
cations:								
Ca	0.0803	**0.0802**	0.0002	0.0004	0.0002	**0.0016**	0.0024	0.0024
Ti	0.0067	**0.0069**	0.0179	0.0173	0.018	**0.017**	0.0172	0.0167
Na	0.022	**0.023**	0.0025	0.0023	0.0021	**0.0042**	0.0038	0.0056
Si	0.2691	**0.2695**	0.2483	0.2472	0.2488	**0.2496**	0.2482	0.2479
Mn	0.001	**0.0011**	0.0003	0.0001	0.0002	**0.0002**	0.0003	0
K	0.0097	**0.01**	0.0826	0.0822	0.0812	**0.0754**	0.0735	0.0709
Cr	0.0004	**0.0003**	0.0005	0.0003	0	**0.0004**	0.0004	0
Mg	0.0864	**0.0874**	0.1213	0.1222	0.1218	**0.1218**	0.1232	0.1326
Al	0.1097	**0.1079**	0.1298	0.1316	0.1308	**0.1311**	0.1309	0.1336
Fe	0.0996	**0.0996**	0.1076	0.1083	0.1062	**0.1062**	0.1078	0.0972
Total	0.685	**0.6859**	0.711	0.712	0.7093	**0.7075**	0.7078	0.7069

Table B.1: *Continued.* Analytical data from sample 14SB095i.

No.	76	77	78	79	80	81	82	83
	095Bi_bio07	095Bi_bio08	095Bi_bio09	095Bi_bio10	095Bi_bio11	095Bi_bio12	095Bi_bio13	095Bi_bio14
oxides(wt%):								
CaO	0.402	0.491	0.487	0.441	0.402	0.521	0.411	0.566
TiO2	3.244	3.399	3.406	3.561	3.476	3.334	3.465	3.55
Na2O	0.418	0.491	0.514	0.503	0.522	0.534	0.365	0.578
SiO2	36.198	36.125	36.213	36.141	36.406	36.253	36.475	36.213
MnO	0.04	0.025	0.01	0.041	0.017	0.032	0.031	0.028
K2O	7.605	7.354	7.251	7.583	7.33	7.682	7.375	7.084
Cr2O3	0	0	0.012	0.019	0.048	0.021	0.029	0.013
MgO	12.781	12.796	12.72	12.673	12.703	12.893	12.6	12.636
Al2O3	16.228	16.247	16.163	16.245	16.235	16.442	16.514	16.035
FeO	17.419	17.59	17.575	17.732	17.552	17.143	17.691	17.642
Total	94.335	94.518	94.351	94.939	94.691	94.855	94.956	94.345
cations:								
Ca	0.003	0.0036	0.0036	0.0032	0.003	0.0038	0.003	0.0042
Ti	0.0168	0.0176	0.0176	0.0184	0.0179	0.0172	0.0178	0.0184
Na	0.0056	0.0065	0.0068	0.0067	0.0069	0.0071	0.0048	0.0077
Si	0.2491	0.2481	0.249	0.2476	0.2493	0.248	0.249	0.249
Mn	0.0002	0.0001	0.0001	0.0002	0.0001	0.0002	0.0002	0.0002
K	0.0668	0.0644	0.0636	0.0663	0.064	0.067	0.0642	0.0621
Cr	0	0	0.0001	0.0001	0.0003	0.0001	0.0002	0.0001
Mg	0.1311	0.131	0.1304	0.1295	0.1297	0.1315	0.1282	0.1295
Al	0.1316	0.1315	0.131	0.1312	0.131	0.1326	0.1329	0.13
Fe	0.1003	0.101	0.1011	0.1016	0.1005	0.0981	0.101	0.1015
Total	0.7046	0.7038	0.7034	0.7049	0.7027	0.7057	0.7013	0.7027

Table B.1: *Continued.* Analytical data from sample 14SB095i.

No.	84	91	92	93	94	**95**	96	97	98
	095Bi_bio15	095Bi_gnt 1	095Bi_gnt 2	095Bi_gnt 3	095Bi_gnt 4	**095Bi_gnt 5**	095Bi_gnt 6	095Bi_gnt 7	095Bi_gnt 8
oxides(wt%):									
CaO	0.489	8.181	8.531	8.453	8.564	**8.459**	8.445	8.526	8.662
TiO2	3.501	0.084	0.058	0.049	0.082	**0.049**	0.076	0.047	0.067
Na2O	0.535	0.018	0.001	0.016	0.002	**0.003**	0.006	0.019	0.012
SiO2	36.493	36.803	37.207	37.227	37.127	**37.326**	37.214	37.12	37.149
MnO	0.045	1.97	1.816	1.656	1.496	**1.586**	1.604	1.515	1.54
K2O	7.194	0.028	0.037	0.044	0.039	**0.028**	0.032	0.036	0.021
Cr2O3	0.003	0.029	0.043	0.018	0.011	**0.05**	0.037	0.038	0.017
MgO	12.859	4.164	4.026	4.472	4.565	**4.568**	4.61	4.571	4.559
Al2O3	16.39	20.807	20.786	20.906	20.851	**20.869**	20.889	20.919	20.897
FeO	17.606	26.949	26.595	26.19	26.4	**26.445**	26.202	26.321	26.111
Total	95.115	99.033	99.1	99.031	99.137	**99.383**	99.115	99.112	99.035
cations:									
Ca	0.0036	0.0585	0.0608	0.0601	0.0609	**0.06**	0.06	0.0606	0.0616
Ti	0.0179	0.0004	0.0003	0.0002	0.0004	**0.0002**	0.0004	0.0002	0.0003
Na	0.0071	0.0002	0	0.0002	0	**0**	0.0001	0.0002	0.0002
Si	0.2486	0.2457	0.2476	0.2472	0.2465	**0.2471**	0.2469	0.2464	0.2467
Mn	0.0003	0.0111	0.0102	0.0093	0.0084	**0.0089**	0.009	0.0085	0.0087
K	0.0625	0.0002	0.0003	0.0004	0.0003	**0.0002**	0.0003	0.0003	0.0002
Cr	0	0.0002	0.0002	0.0001	0.0001	**0.0003**	0.0002	0.0002	0.0001
Mg	0.1306	0.0414	0.0399	0.0443	0.0452	**0.0451**	0.0456	0.0452	0.0451
Al	0.1316	0.1638	0.1631	0.1636	0.1632	**0.1629**	0.1633	0.1637	0.1635
Fe	0.1003	0.1505	0.148	0.1455	0.1466	**0.1464**	0.1454	0.1461	0.145
Total	0.7026	0.672	0.6705	0.6709	0.6716	**0.6712**	0.6712	0.6714	0.6715

Table B.1: *Continued.* Analytical data from sample 14SB095i.

No.	99	100	101	102	103	104	105
	095Bi_gnt 9	095Bi_gnt 10	095Bi_gnt 11	095Bi_gnt 12	095Bi_gnt 13	095Bi_gnt 14	095Bi_gnt 15
oxides(wt%):							
CaO	8.528	8.934	8.507	8.825	8.44	8.355	8.431
TiO2	0.073	0.068	0.07	0.1	0.081	0.052	0.014
Na2O	0	0.019	0.008	0	0.007	0	0
SiO2	37	37.102	36.935	37.202	37.135	37.263	37.01
MnO	1.529	1.629	1.765	1.709	1.699	1.518	1.527
K2O	0.035	0.038	0.028	0.032	0.031	0.022	0.03
Cr2O3	0.003	0.03	0.036	0.016	0.027	0.038	0
MgO	4.495	4.422	4.399	4.409	4.463	4.648	4.578
Al2O3	20.819	20.875	20.711	20.634	20.851	20.746	20.907
FeO	26.328	26.077	26.374	26.297	26.497	26.199	26.525
Total	98.81	99.194	98.833	99.224	99.231	98.841	99.022
cations:							
Ca	0.0609	0.0635	0.0608	0.0628	0.06	0.0595	0.0601
Ti	0.0004	0.0003	0.0004	0.0005	0.0004	0.0003	0.0001
Na	0	0.0002	0.0001	0	0.0001	0	0
Si	0.2465	0.2463	0.2464	0.2471	0.2466	0.2477	0.2461
Mn	0.0086	0.0092	0.01	0.0096	0.0096	0.0086	0.0086
K	0.0003	0.0003	0.0002	0.0003	0.0003	0.0002	0.0003
Cr	0	0.0002	0.0002	0.0001	0.0001	0.0002	0
Mg	0.0446	0.0438	0.0437	0.0437	0.0442	0.0461	0.0454
Al	0.1635	0.1633	0.1629	0.1616	0.1632	0.1626	0.1639
Fe	0.1467	0.1448	0.1472	0.1461	0.1471	0.1457	0.1475
Total	0.6715	0.6719	0.672	0.6718	0.6716	0.6709	0.672

Table B.1: *Continued.* Analytical data from sample 14SB095i.

No.	106	107	108
	095Bi_il in gnt 16	095Bi_il in gnt 17	095Bi_il in gnt 18
oxides(wt%):			
CaO	0.093	0.234	0.196
TiO2	49.485	48.258	48.062
Na2O	0.026	0.011	0.025
SiO2	0.066	0.083	0.084
MnO	0.626	0.385	0.388
K2O	0.053	0.035	0.047
Cr2O3	0.154	0.108	0.166
MgO	0.046	1.096	0.992
Al2O3	0.027	0.028	0.043
FeO	49.77	49.116	49.81
Total	100.346	99.354	99.813
cations:			
Ca	0.0008	0.0022	0.0018
Ti	0.3176	0.3122	0.3104
Na	0.0004	0.0002	0.0004
Si	0.0006	0.0007	0.0007
Mn	0.0045	0.0028	0.0028
K	0.0006	0.0004	0.0005
Cr	0.001	0.0007	0.0011
Mg	0.0006	0.0141	0.0127
Al	0.0003	0.0003	0.0004
Fe	0.3552	0.3533	0.3577
Total	0.6817	0.687	0.6885

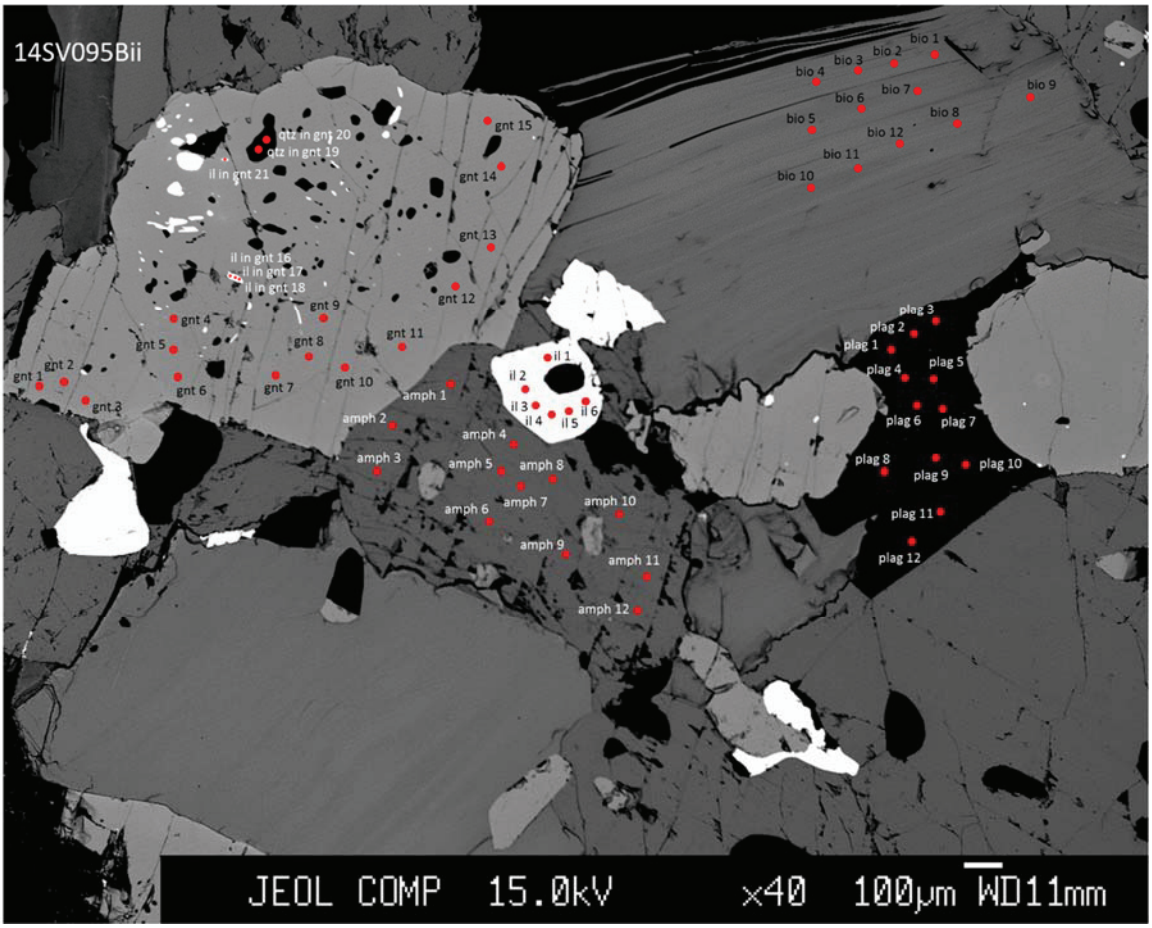

Figure B.3: BSE image of sample 14SV095Bii with annotated analysis points.

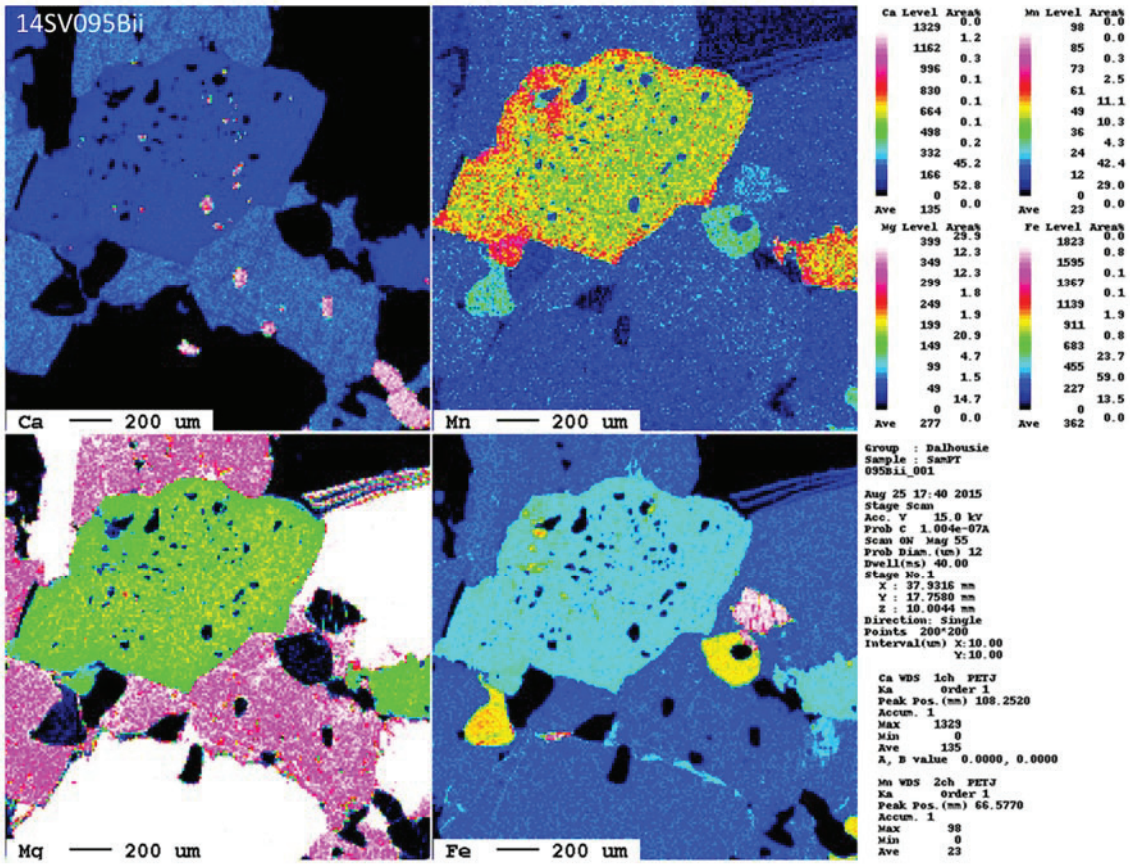

Figure B.4: Ca, Mn, Mg and Fe maps of the garnet analyzed in sample 14SV095Bii.

Table B.2: Analytical data from sample 14SB095ii.

No.	109	110	111	112	113	114	115
	095Bii_plag 1	095Bii_plag 2	095Bii_plag 3	095Bii_plag 4	095Bii_plag 5	095Bii_plag 6	095Bii_plag 7
oxides(wt%):							
CaO	8.196	8.078	7.946	7.969	7.674	8.075	7.876
TiO2	0	0	0	0	0	0	0
Na2O	7.232	7.243	7.422	7.306	7.444	7.243	7.271
SiO2	57.617	58.499	58.744	58.409	59.182	58.581	58.387
MnO	0	0	0	0	0	0	0
K2O	0.086	0.092	0.081	0.091	0.102	0.074	0.067
Cr2O3	0	0	0	0	0	0	0
MgO	0	0	0	0	0	0	0
Al2O3	26.371	26.299	26.234	26.333	25.965	26.389	26.034
FeO	0.043	0.065	0.099	0.045	0.166	0.041	0.024
Total	99.545	100.276	100.526	100.153	100.533	100.403	99.659
cations:							
Ca	0.0494	0.0483	0.0474	0.0477	0.0457	0.0482	0.0473
Ti	0	0	0	0	0	0	0
Na	0.0789	0.0783	0.0801	0.0791	0.0802	0.0782	0.079
Si	0.3242	0.3263	0.3269	0.3261	0.3289	0.3262	0.3274
Mn	0	0	0	0	0	0	0
K	0.0006	0.0007	0.0006	0.0006	0.0007	0.0005	0.0005
Cr	0	0	0	0	0	0	0
Mg	0	0	0	0	0	0	0
Al	0.1749	0.1729	0.1721	0.1733	0.1701	0.1732	0.1721
Fe	0.0002	0.0003	0.0005	0.0002	0.0008	0.0002	0.0001
Total	0.6283	0.6269	0.6277	0.627	0.6265	0.6265	0.6265

Table B.2: *Continued.* Analytical data from sample 14SB095ii.

No.	116	117	**118**	119	120	127	**128**
	095Bii_plag 8	095Bii_plag 9	**095Bii_plag 10**	095Bii_plag 11	095Bii_plag 12	095Bii_amph 1	**095Bii_amph 2**
oxides(wt%):							
CaO	7.991	7.632	**7.61**	7.993	8.11	11.671	**11.46**
TiO2	0	0	**0**	0	0	1.342	**1.39**
Na2O	7.228	7.39	**7.414**	7.315	7.267	1.795	**1.888**
SiO2	58.355	58.561	**58.774**	58.397	58.515	41.004	**41.5**
MnO	0	0	**0**	0	0	0.193	**0.206**
K2O	0.065	0.083	**0.07**	0.068	0.07	1.127	**1.092**
Cr2O3	0	0	**0**	0	0	0.004	**0.024**
MgO	0	0	**0**	0	0	9.024	**9.08**
Al2O3	26.316	26.052	**26.021**	26.272	26.454	14.21	**14.676**
FeO	0.145	0.03	**0.002**	0.141	0.212	17.696	**17.808**
Total	100.1	99.748	**99.891**	100.186	100.628	98.066	**99.124**
cations:							
Ca	0.0478	0.0458	**0.0456**	0.0478	0.0483	0.082	**0.0795**
Ti	0	0	**0**	0	0	0.0066	**0.0068**
Na	0.0783	0.0802	**0.0803**	0.0792	0.0784	0.0228	**0.0237**
Si	0.3261	0.3279	**0.3285**	0.3261	0.3255	0.2688	**0.2686**
Mn	0	0	**0**	0	0	0.0011	**0.0011**
K	0.0005	0.0006	**0.0005**	0.0005	0.0005	0.0094	**0.009**
Cr	0	0	**0**	0	0	0	**0.0001**
Mg	0	0	**0**	0	0	0.0882	**0.0876**
Al	0.1733	0.1719	**0.1714**	0.1729	0.1735	0.1098	**0.112**
Fe	0.0007	0.0001	**0**	0.0007	0.001	0.097	**0.0964**
Total	0.6267	0.6266	**0.6263**	0.6273	0.6272	0.6858	**0.6849**

Table B.2: *Continued.* Analytical data from sample 14SB095ii.

No.	129	130	131	132	133	134	135
	095Bii_amph 3	095Bii_amph 4	095Bii_amph 5	095Bii_amph 6	095Bii_amph 7	095Bii_amph 8	095Bii_amph 9
oxides(wt%):							
CaO	11.512	11.478	11.381	11.464	11.4	11.519	11.275
TiO2	1.284	1.41	1.369	1.348	1.446	1.253	1.37
Na2O	1.877	1.846	1.854	1.867	1.874	1.784	1.856
SiO2	41.096	41.057	40.858	41.055	40.859	41.104	40.381
MnO	0.174	0.202	0.202	0.228	0.182	0.208	0.207
K2O	1.024	1.104	1.136	1.116	1.137	0.987	1.108
Cr2O3	0.029	0.034	0.018	0.022	0.016	0	0.024
MgO	8.971	8.919	8.811	8.794	8.81	8.918	8.9
Al2O3	14.089	14.281	14.072	14.474	14.106	14.255	14.064
FeO	18.031	17.977	18.043	18.11	17.98	17.871	17.886
Total	98.087	98.308	97.744	98.478	97.81	97.899	97.071
cations:							
Ca	0.0809	0.0805	0.0803	0.0803	0.0804	0.081	0.0802
Ti	0.0063	0.0069	0.0068	0.0066	0.0072	0.0062	0.0068
Na	0.0239	0.0234	0.0237	0.0237	0.0239	0.0227	0.0239
Si	0.2695	0.2687	0.2692	0.2683	0.2689	0.2697	0.2679
Mn	0.001	0.0011	0.0011	0.0013	0.001	0.0012	0.0012
K	0.0086	0.0092	0.0095	0.0093	0.0095	0.0083	0.0094
Cr	0.0002	0.0002	0.0001	0.0001	0.0001	0	0.0001
Mg	0.0877	0.087	0.0865	0.0857	0.0864	0.0872	0.088
Al	0.1089	0.1101	0.1093	0.1115	0.1094	0.1102	0.11
Fe	0.0989	0.0984	0.0994	0.099	0.099	0.0981	0.0993
Total	0.6859	0.6856	0.6859	0.6858	0.6858	0.6847	0.6869

Table B.2: *Continued.* Analytical data from sample 14SB095ii.

No.	136	137	138	**139**	140	141	142
	095Bii_amph 10	095Bii_amph 11	095Bii_amph 12	**095Bii_bio 1**	095Bii_bio 2	095Bii_bio 3	095Bii_bio 4
oxides(wt%):							
CaO	11.611	11.609	11.405	**0.027**	0.009	0	0.003
TiO2	1.134	1.168	1.332	**3.66**	3.742	3.681	3.749
Na2O	1.802	1.866	1.89	**0.287**	0.232	0.241	0.244
SiO2	41.474	41.019	41.151	**36.077**	35.165	35.405	35.759
MnO	0.209	0.19	0.183	**0.063**	0.076	0.076	0.065
K2O	0.944	0.977	1.014	**8.796**	9.138	9.095	9.045
Cr2O3	0.042	0.043	0.055	**0.001**	0.012	0.015	0.026
MgO	9.034	8.921	8.934	**11.922**	11.692	11.788	11.63
Al2O3	14.121	14.205	14.188	**15.93**	15.784	15.722	15.757
FeO	17.85	17.855	18.161	**17.93**	18.083	17.994	17.973
Total	98.221	97.853	98.313	**94.693**	93.933	94.017	94.251
cations:							
Ca	0.0813	0.0817	0.08	**0.0002**	0.0001	0	0
Ti	0.0056	0.0058	0.0066	**0.019**	0.0197	0.0194	0.0197
Na	0.0228	0.0238	0.024	**0.0038**	0.0032	0.0033	0.0033
Si	0.271	0.2695	0.2693	**0.2496**	0.2467	0.2478	0.2492
Mn	0.0012	0.0011	0.001	**0.0004**	0.0005	0.0005	0.0004
K	0.0079	0.0082	0.0085	**0.0776**	0.0818	0.0812	0.0804
Cr	0.0002	0.0002	0.0003	**0**	0.0001	0.0001	0.0001
Mg	0.088	0.0874	0.0872	**0.1229**	0.1223	0.123	0.1208
Al	0.1088	0.11	0.1094	**0.1299**	0.1305	0.1297	0.1294
Fe	0.0976	0.0981	0.0994	**0.1037**	0.1061	0.1053	0.1048
Total	0.6844	0.6858	0.6857	**0.7071**	0.7111	0.7104	0.7081

Table B.2: *Continued.* Analytical data from sample 14SB095ii.

No.	143	144	145	146	147	148	149	150
	095Bii_bio 5	095Bii_bio 6	095Bii_bio 7	095Bii_bio 8	095Bii_bio 9	095Bii_bio 10	095Bii_bio 11	095Bii_bio 12
oxides(wt%):								
CaO	0.001	0	0	0.015	0.04	0.003	0	0.004
TiO2	3.721	3.62	3.613	3.695	3.667	3.607	3.561	3.57
Na2O	0.263	0.259	0.22	0.251	0.209	0.223	0.255	0.262
SiO2	35.327	35.747	35.704	35.63	35.743	35.789	35.655	35.197
MnO	0.083	0.07	0.047	0.046	0.052	0.027	0.036	0.057
K2O	9.006	9.027	8.871	8.793	8.856	9.007	9.221	9.042
Cr2O3	0.043	0.038	0.04	0	0	0.014	0	0.019
MgO	11.521	11.708	11.853	11.635	11.804	11.914	11.801	11.493
Al2O3	15.901	15.94	16.042	15.827	15.866	16.002	15.766	15.845
FeO	18.125	18.028	18.181	18.014	18.211	17.865	17.806	17.94
Total	93.991	94.437	94.571	93.906	94.448	94.451	94.101	93.429
cations:								
Ca	0	0	0	0.0001	0.0003	0	0	0
Ti	0.0196	0.0189	0.0189	0.0194	0.0192	0.0188	0.0187	0.0189
Na	0.0036	0.0035	0.003	0.0034	0.0028	0.003	0.0035	0.0036
Si	0.2474	0.2486	0.2479	0.249	0.2485	0.2485	0.249	0.2478
Mn	0.0005	0.0004	0.0003	0.0003	0.0003	0.0002	0.0002	0.0003
K	0.0805	0.0801	0.0786	0.0784	0.0786	0.0798	0.0822	0.0812
Cr	0.0002	0.0002	0.0002	0	0	0.0001	0	0.0001
Mg	0.1203	0.1214	0.1227	0.1212	0.1224	0.1233	0.1229	0.1206
Al	0.1312	0.1307	0.1313	0.1303	0.13	0.131	0.1298	0.1315
Fe	0.1061	0.1049	0.1056	0.1053	0.1059	0.1038	0.104	0.1056
Total	0.7095	0.7088	0.7086	0.7075	0.708	0.7085	0.7103	0.7096

Table B.2: *Continued.* Analytical data from sample 14SB095ii.

No.	151	152	153	154	155	156	163	164	165
	095Bii_il 1	095Bii_il 2	095Bii_il 3	095Bii_il 4	095Bii_il 5	095Bii_il 6	095Bii_il 7	095Bii_il 8	095Bii_il 9
oxides(wt%):									
CaO	0.045	0.047	0.066	0.047	0.033	0.049	0.056	0.05	0.015
TiO2	49.824	49.07	49.002	49.127	49.338	49.909	49.527	49.434	49.395
Na2O	0	0	0.007	0	0	0.006	0.013	0	0
SiO2	0.105	0.08	0.107	0.098	0.095	0.093	0.103	0.12	0.024
MnO	0.633	0.614	0.632	0.585	0.61	0.605	0.584	0.587	0.487
K2O	0.055	0.053	0.061	0.057	0.056	0.038	0.056	0.06	0.028
Cr2O3	0.199	0.217	0.176	0.228	0.227	0.181	0.198	0.181	0
MgO	0.075	0.098	0.122	0.146	0.141	0.081	0.472	0.5	0.502
Al2O3	0.021	0.043	0.056	0.069	0.042	0.038	0.05	0.062	0.029
FeO	50.029	50.432	50.62	50.356	50.142	49.553	49.836	49.661	49.349
Total	100.986	100.654	100.849	100.713	100.684	100.553	100.895	100.655	99.829
cations:									
Ca	0.0004	0.0004	0.0006	0.0004	0.0003	0.0004	0.0005	0.0005	0.0001
Ti	0.3176	0.3148	0.3139	0.3147	0.3159	0.3189	0.3156	0.3156	0.3179
Na	0	0	0.0001	0	0	0.0001	0.0002	0	0
Si	0.0009	0.0007	0.0009	0.0008	0.0008	0.0008	0.0009	0.001	0.0002
Mn	0.0045	0.0044	0.0046	0.0042	0.0044	0.0044	0.0042	0.0042	0.0035
K	0.0006	0.0006	0.0007	0.0006	0.0006	0.0004	0.0006	0.0006	0.0003
Cr	0.0013	0.0015	0.0012	0.0015	0.0015	0.0012	0.0013	0.0012	0
Mg	0.0009	0.0012	0.0015	0.0019	0.0018	0.001	0.006	0.0063	0.0064
Al	0.0002	0.0004	0.0006	0.0007	0.0004	0.0004	0.0005	0.0006	0.0003
Fe	0.3546	0.3598	0.3606	0.3587	0.357	0.3521	0.3532	0.3526	0.3532
Total	0.6811	0.6838	0.6848	0.6836	0.6828	0.6798	0.6831	0.6827	0.6819

Table B.2: *Continued.* Analytical data from sample 14SB095ii.

No.	166	167	168	169	170	171	172	173
	095Bii_il 10	095Bii_gnt 1	095Bii_gnt 2	095Bii_gnt 3	095Bii_gnt 4	095Bii_gnt 5	095Bii_gnt 6	095Bii_gnt 7
oxides(wt%):								
CaO	0.03	8.328	8.223	8.186	8.395	8.486	8.438	8.451
TiO2	49.406	0	0	0	0	0	0	0
Na2O	0	0	0.002	0	0	0	0.002	0
SiO2	0.012	37.17	37.191	37.09	37.302	37.431	37.378	37.036
MnO	0.47	1.665	1.627	1.747	1.607	1.464	1.522	1.42
K2O	0.027	0	0	0.026	0.003	0.005	0	0
Cr2O3	0	0	0	0	0	0	0	0
MgO	0.506	4.448	4.521	4.319	4.528	4.524	4.486	4.547
Al2O3	0.026	20.854	20.984	20.979	21.043	20.921	20.91	21.06
FeO	49.739	26.582	26.606	26.66	26.673	26.437	26.421	26.335
Total	100.216	99.047	99.154	99.007	99.551	99.268	99.157	98.849
cations:								
Ca	0.0003	0.0593	0.0585	0.0584	0.0595	0.0602	0.0599	0.0602
Ti	0.3171	0	0	0	0	0	0	0
Na	0	0	0	0	0	0	0	0
Si	0.0001	0.2471	0.2468	0.2468	0.2467	0.2478	0.2478	0.2463
Mn	0.0034	0.0094	0.0091	0.0098	0.009	0.0082	0.0085	0.008
K	0.0003	0	0	0.0002	0	0	0	0
Cr	0	0	0	0	0	0	0	0
Mg	0.0064	0.0441	0.0447	0.0428	0.0446	0.0446	0.0443	0.0451
Al	0.0003	0.1634	0.1642	0.1646	0.164	0.1633	0.1634	0.1651
Fe	0.355	0.1478	0.1477	0.1484	0.1475	0.1464	0.1465	0.1465
Total	0.6829	0.6712	0.6711	0.6711	0.6714	0.6706	0.6704	0.6712

Table B.2: *Continued.* Analytical data from sample 14SB095ii.

No.	174	175	176	177	**178**	179	180	181
	095Bii_gnt 8	095Bii_gnt 9	095Bii_gnt 10	095Bii_gnt 11	**095Bii_gnt 12**	095Bii_gnt 13	095Bii_gnt 14	095Bii_gnt 15
oxides(wt%):								
CaO	8.332	8.213	8.211	8.037	**8.172**	8.397	7.918	7.797
TiO2	0	0	0	0	**0**	0	0	0
Na2O	0	0	0	0	**0**	0	0.003	0
SiO2	37.223	37.262	37.202	37.313	**37.451**	37.436	37.162	37.256
MnO	1.434	1.429	1.489	1.405	**1.357**	1.42	1.381	1.531
K2O	0	0.002	0	0.017	**0**	0.008	0.015	0.007
Cr2O3	0	0	0	0	**0**	0	0	0
MgO	4.674	4.668	4.725	4.694	**4.82**	4.712	4.792	4.685
Al2O3	20.881	20.957	21.02	20.905	**21.08**	21.19	20.925	21.027
FeO	26.469	26.534	26.486	26.6	**26.716**	26.43	26.657	26.792
Total	99.013	99.065	99.133	98.971	**99.596**	99.593	98.853	99.095
cations:								
Ca	0.0593	0.0584	0.0583	0.0572	**0.0578**	0.0593	0.0564	0.0554
Ti	0	0	0	0	**0**	0	0	0
Na	0	0	0	0	**0**	0	0	0
Si	0.2471	0.2472	0.2467	0.2477	**0.247**	0.2468	0.247	0.2472
Mn	0.0081	0.008	0.0084	0.0079	**0.0076**	0.0079	0.0078	0.0086
K	0	0	0	0.0001	**0**	0.0001	0.0001	0.0001
Cr	0	0	0	0	**0**	0	0	0
Mg	0.0463	0.0462	0.0467	0.0465	**0.0474**	0.0463	0.0475	0.0463
Al	0.1634	0.1639	0.1643	0.1636	**0.1639**	0.1647	0.164	0.1644
Fe	0.147	0.1472	0.1469	0.1477	**0.1474**	0.1457	0.1482	0.1487
Total	0.6712	0.6709	0.6714	0.6708	**0.6712**	0.6708	0.6711	0.6707

Table B.2: *Continued.* Analytical data from sample 14SB095ii.

No.	182	183	184	185	186	187
	095Bii_il in gnt 16	095Bii_il in gnt 17	095Bii_il in gnt 18	095Bii_qtz in gnt 19	095Bii_qtz in gnt 20	095Bii_il in gnt 21
oxides(wt%):						
CaO	0.121	0.121	0.122	0.004	0.008	0.284
TiO2	48.154	48.239	48.65	0	0	48.425
Na2O	0	0	0.014	0	0.007	0.003
SiO2	0.04	0.01	0.014	100.117	99.83	0.11
MnO	0.538	0.549	0.553	0.014	0.007	0.574
K2O	0.038	0.035	0.043	0.02	0.015	0.048
Cr2O3	0	0.017	0	0	0	0.276
MgO	0.013	0.014	0.014	0	0.002	0.405
Al2O3	0.027	0.024	0.024	0	0	0
FeO	50.216	50.438	50.697	0.381	0.346	49.959
Total	99.147	99.447	100.131	100.536	100.215	100.084
cations:						
Ca	0.0011	0.0011	0.0011	0	0	0.0026
Ti	0.3144	0.3142	0.3146	0	0	0.3124
Na	0	0	0.0002	0	0.0001	0.0001
Si	0.0003	0.0001	0.0001	0.4991	0.4992	0.0009
Mn	0.004	0.004	0.004	0.0001	0	0.0042
K	0.0004	0.0004	0.0005	0.0001	0.0001	0.0005
Cr	0	0.0001	0	0	0	0.0019
Mg	0.0002	0.0002	0.0002	0	0	0.0052
Al	0.0003	0.0002	0.0002	0	0	0
Fe	0.3646	0.3653	0.3645	0.0016	0.0014	0.3583
Total	0.6854	0.6857	0.6855	0.5009	0.5008	0.6862

14SV432A:

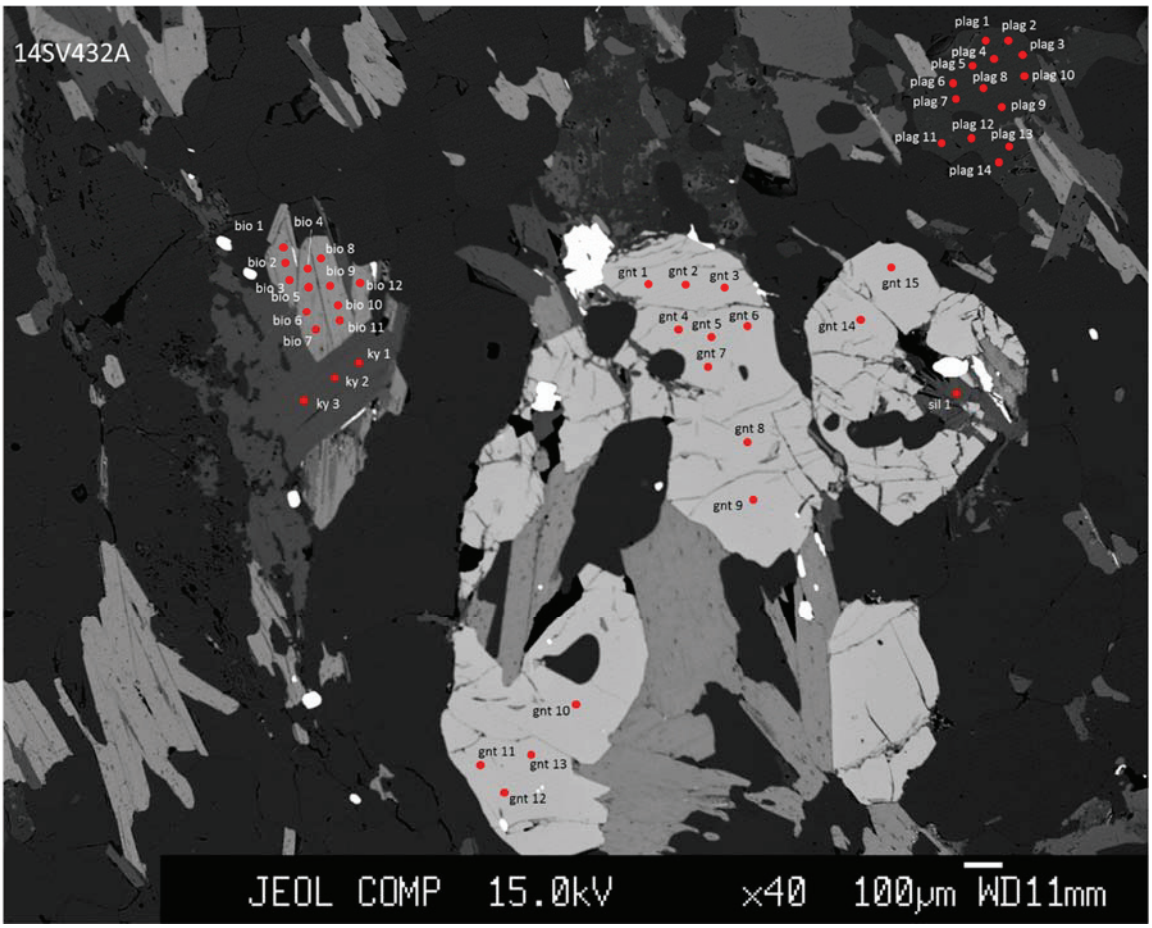

Figure B.5: BSE image of sample 14SV432A with annotated analysis points.

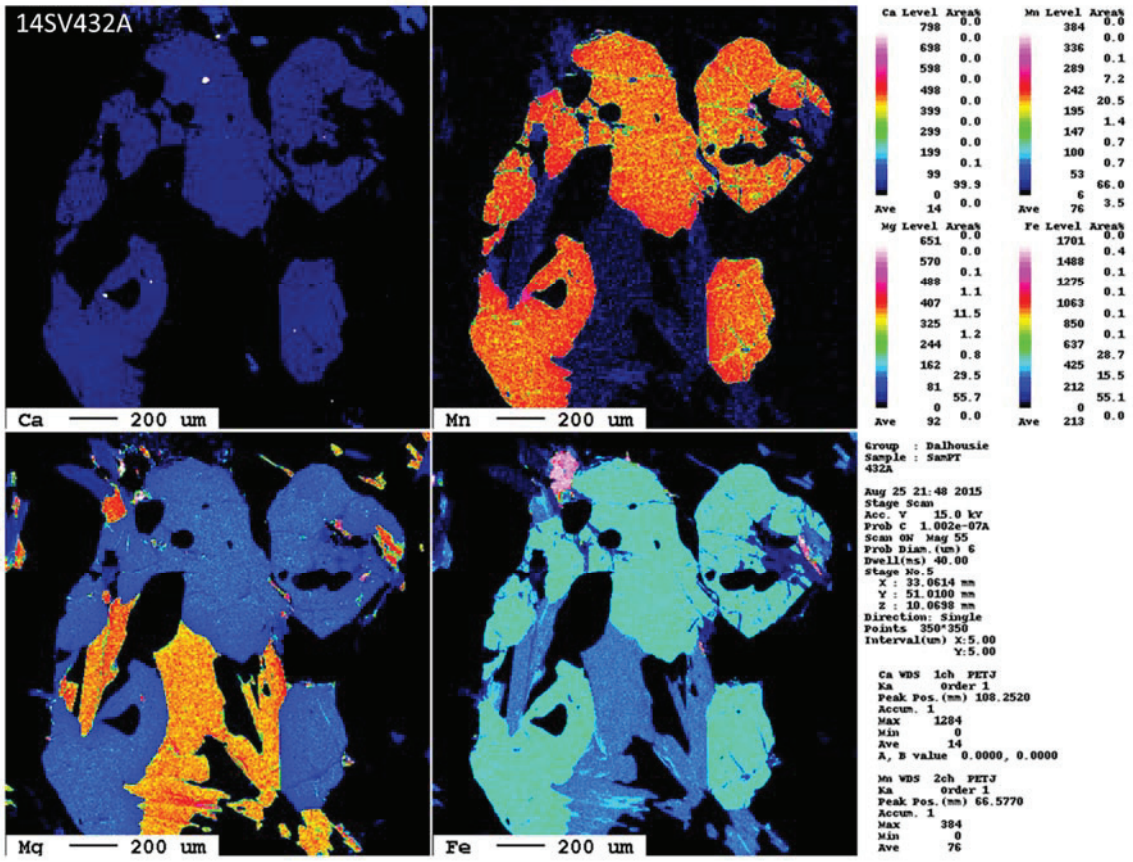

Figure B.6: Ca, Mn, Mg and Fe maps of the garnet analyzed in sample 14SV432A.

Table B.3: Analytical data from sample 14SV432A.

No.	188	189	190	191	192	193	194	**195**
	432A_plag 1	432A_plag 2	432A_plag 3	432A_plag 4	432A_plag 5	432A_plag 6	432A_plag 7	**432A_plag 8**
oxides(wt%):								
CaO	4.182	4.125	4.105	4.034	4.209	4.08	4.199	**4.118**
TiO2	0.009	0.015	0	0.035	0.016	0.004	0.009	**0**
Na2O	9.474	9.515	9.559	9.433	9.569	9.655	9.541	**9.442**
SiO2	63.156	62.874	63.381	63.045	63.257	63.432	63.412	**63.311**
MnO	0	0.015	0	0	0.016	0.01	0	**0**
K2O	0.197	0.188	0.201	0.196	0.123	0.151	0.169	**0.165**
Cr2O3	0.017	0.05	0.025	0.011	0	0.019	0.009	**0.013**
MgO	0	0	0	0	0	0	0	**0**
Al2O3	22.999	22.942	22.908	22.785	22.966	23.046	23.03	**22.896**
FeO	0.03	0.018	0.037	0	0.023	0.049	0.016	**0.02**
Total	100.064	99.742	100.216	99.539	100.179	100.446	100.385	**99.965**
cations:								
Ca	0.0248	0.0245	0.0243	0.024	0.0249	0.0241	0.0248	**0.0244**
Ti	0	0.0001	0	0.0001	0.0001	0	0	**0**
Na	0.1016	0.1024	0.1023	0.1016	0.1025	0.1031	0.102	**0.1013**
Si	0.3493	0.3489	0.3499	0.3502	0.3494	0.3495	0.3495	**0.3502**
Mn	0	0.0001	0	0	0.0001	0	0	**0**
K	0.0014	0.0013	0.0014	0.0014	0.0009	0.0011	0.0012	**0.0012**
Cr	0.0001	0.0002	0.0001	0	0	0.0001	0	**0.0001**
Mg	0	0	0	0	0	0	0	**0**
Al	0.1499	0.1501	0.1491	0.1492	0.1495	0.1497	0.1496	**0.1493**
Fe	0.0001	0.0001	0.0002	0	0.0001	0.0002	0.0001	**0.0001**
Total	0.6273	0.6277	0.6273	0.6266	0.6276	0.6278	0.6273	**0.6266**

Table B.3: *Continued.* Analytical data from sample 14SV432A.

No.	196	197	198	199	200	201	208	209
	432A_plag 9	432A_plag 10	432A_plag 11	432A_plag 12	432A_plag 13	432A_plag 14	432A_bio 1	432A_bio 2
oxides(wt%):								
CaO	3.676	3.613	4.181	3.972	3.795	3.971	0.066	0.074
TiO2	0	0	0	0	0	0	3.273	3.234
Na2O	9.658	9.723	9.479	9.706	9.724	9.677	0.181	0.203
SiO2	64.154	63.985	63.375	63.727	64.296	63.648	35.643	35.66
MnO	0	0	0.005	0.008	0.002	0.001	0.252	0.231
K2O	0.201	0.224	0.173	0.169	0.167	0.167	9.921	9.763
Cr2O3	0.047	0.035	0.017	0.007	0.025	0.027	0.119	0.148
MgO	0	0	0	0	0	0	9.469	9.332
Al2O3	22.725	22.646	23.127	22.87	22.8	22.962	18.201	18.134
FeO	0.021	0.025	0.03	0.017	0.029	0.025	18.989	18.797
Total	100.482	100.251	100.387	100.476	100.838	100.478	96.114	95.576
cations:								
Ca	0.0216	0.0213	0.0247	0.0234	0.0223	0.0234	0.0005	0.0005
Ti	0	0	0	0	0	0	0.0169	0.0168
Na	0.1029	0.1039	0.1013	0.1036	0.1033	0.1033	0.0024	0.0027
Si	0.3525	0.3525	0.3492	0.3507	0.3522	0.3503	0.2453	0.2464
Mn	0	0	0	0	0	0	0.0015	0.0014
K	0.0014	0.0016	0.0012	0.0012	0.0012	0.0012	0.0871	0.086
Cr	0.0002	0.0002	0.0001	0	0.0001	0.0001	0.0006	0.0008
Mg	0	0	0	0	0	0	0.0971	0.0961
Al	0.1472	0.1471	0.1502	0.1484	0.1472	0.149	0.1476	0.1477
Fe	0.0001	0.0001	0.0001	0.0001	0.0001	0.0001	0.1093	0.1086
Total	0.626	0.6268	0.6269	0.6274	0.6265	0.6274	0.7084	0.7071

Table B.3: *Continued.* Analytical data from sample 14SV432A.

No.	210	211	212	213	214	**215**	216	217	218
	432A_bio 3	432A_bio 4	432A_bio 5	432A_bio 6	432A_bio 7	**432A_bio 8**	432A_bio 9	432A_bio 10	432A_bio 11
oxides(wt%):									
CaO	0.166	0.048	0.054	0.058	0.085	**0.029**	0.018	0.033	0.009
TiO2	3.285	3.376	3.313	3.32	3.374	**3.303**	3.299	3.299	3.38
Na2O	0.178	0.144	0.146	0.161	0.169	**0.158**	0.158	0.165	0.136
SiO2	35.651	35.107	35.546	35.38	35.453	**35.534**	35.249	35.504	35.564
MnO	0.242	0.221	0.215	0.219	0.194	**0.253**	0.224	0.25	0.221
K2O	9.213	10.058	9.992	9.982	9.746	**10.049**	9.988	9.874	10.094
Cr2O3	0.156	0.144	0.134	0.155	0.15	**0.145**	0.177	0.158	0.153
MgO	9.477	9.339	9.546	9.498	9.571	**9.523**	9.42	9.563	9.573
Al2O3	18.161	17.927	18.072	17.939	17.99	**17.988**	18.051	18.06	17.912
FeO	18.793	18.726	18.93	18.795	18.833	**19.153**	18.835	19.013	18.979
Total	95.322	95.09	95.948	95.507	95.565	**96.135**	95.419	95.919	96.021
cations:									
Ca	0.0012	0.0004	0.0004	0.0004	0.0006	**0.0002**	0.0001	0.0002	0.0001
Ti	0.0171	0.0177	0.0172	0.0173	0.0175	**0.0171**	0.0172	0.0171	0.0175
Na	0.0024	0.0019	0.002	0.0022	0.0023	**0.0021**	0.0021	0.0022	0.0018
Si	0.2462	0.2446	0.2451	0.2452	0.2451	**0.245**	0.2446	0.2449	0.2453
Mn	0.0014	0.0013	0.0013	0.0013	0.0011	**0.0015**	0.0013	0.0015	0.0013
K	0.0812	0.0894	0.0879	0.0883	0.086	**0.0884**	0.0884	0.0869	0.0888
Cr	0.0009	0.0008	0.0007	0.0008	0.0008	**0.0008**	0.001	0.0009	0.0008
Mg	0.0976	0.097	0.0981	0.0981	0.0987	**0.0979**	0.0974	0.0984	0.0984
Al	0.1478	0.1472	0.1469	0.1465	0.1466	**0.1462**	0.1476	0.1469	0.1456
Fe	0.1085	0.1091	0.1092	0.1089	0.1089	**0.1104**	0.1093	0.1097	0.1095
Total	0.7044	0.7095	0.7089	0.7091	0.7077	**0.7097**	0.709	0.7088	0.7092

Table B.3: *Continued.* Analytical data from sample 14SV432A.

No.	219	220	221	222	223	224	225	226	227
	432A_bio 12	432A_ky 1	432A_ky 2	432A_ky 3	432A_sil 1	432A_gnt 1	432A_gnt 2	432A_gnt 3	432A_gnt 4
oxides(wt%):									
CaO	0.006	0.017	0.02	0.007	0.023	1.614	1.523	1.407	1.588
TiO2	3.309	0.934	0.883	0.905	0	0.09	0.011	0.003	0.012
Na2O	0.133	0.453	0.508	0.473	0.196	0.019	0.045	0.024	0.034
SiO2	35.475	45.706	45.783	45.709	48.497	36.306	36.036	35.922	36.002
MnO	0.244	0	0.005	0.002	0.012	9.921	9.843	9.936	9.725
K2O	10.047	9.609	9.655	9.491	7.396	0.04	0.02	0.018	0.016
Cr2O3	0.156	0.049	0.064	0	0	0.104	0.015	0.106	0.047
MgO	9.499	0.805	0.838	0.905	1.277	3.245	3.335	3.322	3.334
Al2O3	17.932	34.231	34.172	34.254	33.882	20.777	20.941	20.85	20.964
FeO	18.813	2.843	2.862	3.006	3.825	27.236	27.351	27.393	27.142
Total	95.614	94.647	94.79	94.752	95.108	99.352	99.12	98.981	98.864
cations:									
Ca	0	0.0001	0.0001	0	0.0001	0.0117	0.0111	0.0103	0.0116
Ti	0.0172	0.0043	0.0041	0.0042	0	0.0005	0.0001	0	0.0001
Na	0.0018	0.0054	0.006	0.0056	0.0023	0.0003	0.0006	0.0003	0.0004
Si	0.2456	0.2794	0.2797	0.2792	0.2905	0.2463	0.2451	0.2449	0.2453
Mn	0.0014	0	0	0	0.0001	0.057	0.0567	0.0574	0.0561
K	0.0887	0.0749	0.0752	0.074	0.0565	0.0003	0.0002	0.0002	0.0001
Cr	0.0009	0.0002	0.0003	0	0	0.0006	0.0001	0.0006	0.0003
Mg	0.098	0.0073	0.0076	0.0082	0.0114	0.0328	0.0338	0.0338	0.0339
Al	0.1463	0.2467	0.246	0.2466	0.2392	0.1661	0.1679	0.1676	0.1683
Fe	0.1089	0.0145	0.0146	0.0154	0.0192	0.1545	0.1556	0.1562	0.1546
Total	0.7089	0.6328	0.6337	0.6332	0.6194	0.6701	0.6712	0.6714	0.6707

Table B.3: *Continued.* Analytical data from sample 14SV432A.

No.	**228**	229	230	231	232	233	234	235
	432A_gnt 5	432A_gnt 6	432A_gnt 7	432A_gnt 8	432A_gnt 9	432A_gnt 10	432A_gnt 11	432A_gnt 12
oxides(wt%):								
CaO	**1.545**	1.409	1.578	1.705	1.605	1.463	1.768	1.64
TiO2	**0.026**	0.001	0.011	0.003	0.011	0	0	0.004
Na2O	**0.028**	0.029	0.025	0.04	0.036	0.038	0.03	0.038
SiO2	**36.183**	36.122	36.237	36.308	36.191	36.001	36.336	35.83
MnO	**9.799**	9.839	9.628	9.839	9.834	9.848	9.776	9.676
K2O	**0.013**	0.021	0.032	0.029	0.013	0.013	0.026	0.029
Cr2O3	**0.044**	0.045	0.035	0.042	0.023	0.048	0	0.011
MgO	**3.388**	3.366	3.42	3.347	3.229	3.228	3.307	3.351
Al2O3	**20.855**	20.79	20.846	20.687	20.772	20.685	20.79	20.893
FeO	**27.462**	27.533	27.136	26.959	27.161	27.446	26.721	27.04
Total	**99.343**	99.155	98.948	98.959	98.875	98.77	98.754	98.512
cations:								
Ca	**0.0112**	0.0103	0.0115	0.0124	0.0117	0.0107	0.0129	0.012
Ti	**0.0001**	0	0.0001	0	0.0001	0	0	0
Na	**0.0004**	0.0004	0.0003	0.0005	0.0005	0.0005	0.0004	0.0005
Si	**0.2456**	0.2458	0.2464	0.247	0.2466	0.246	0.2473	0.245
Mn	**0.0563**	0.0567	0.0555	0.0567	0.0568	0.057	0.0564	0.056
K	**0.0001**	0.0002	0.0003	0.0003	0.0001	0.0001	0.0002	0.0003
Cr	**0.0002**	0.0002	0.0002	0.0002	0.0001	0.0003	0	0.0001
Mg	**0.0343**	0.0341	0.0347	0.0339	0.0328	0.0329	0.0336	0.0342
Al	**0.1668**	0.1667	0.1671	0.1659	0.1668	0.1666	0.1668	0.1684
Fe	**0.1559**	0.1567	0.1543	0.1534	0.1548	0.1568	0.1521	0.1546
Total	**0.6709**	0.6712	0.6705	0.6704	0.6703	0.6709	0.6698	0.6712

Table B.3: *Continued.* Analytical data from sample 14SV432A.

No.	236	237	238
	432A_gnt 13	432A_gnt 14	432A_gnt 15
oxides(wt%):			
CaO	1.758	1.336	1.305
TiO2	0.009	0.006	0.009
Na2O	0.015	0.02	0.063
SiO2	36.085	36.061	35.653
MnO	9.863	9.712	9.883
K2O	0.01	0.021	0.025
Cr2O3	0.054	0	0
MgO	3.342	3.37	3.191
Al2O3	20.894	20.874	20.788
FeO	27.125	27.308	27.231
Total	99.155	98.708	98.148
cations:			
Ca	0.0128	0.0098	0.0096
Ti	0	0	0
Na	0.0002	0.0003	0.0008
Si	0.2453	0.246	0.2451
Mn	0.0568	0.0561	0.0576
K	0.0001	0.0002	0.0002
Cr	0.0003	0	0
Mg	0.0339	0.0343	0.0327
Al	0.1674	0.1678	0.1685
Fe	0.1542	0.1558	0.1566
Total	0.6711	0.6704	0.6712

14SV542:

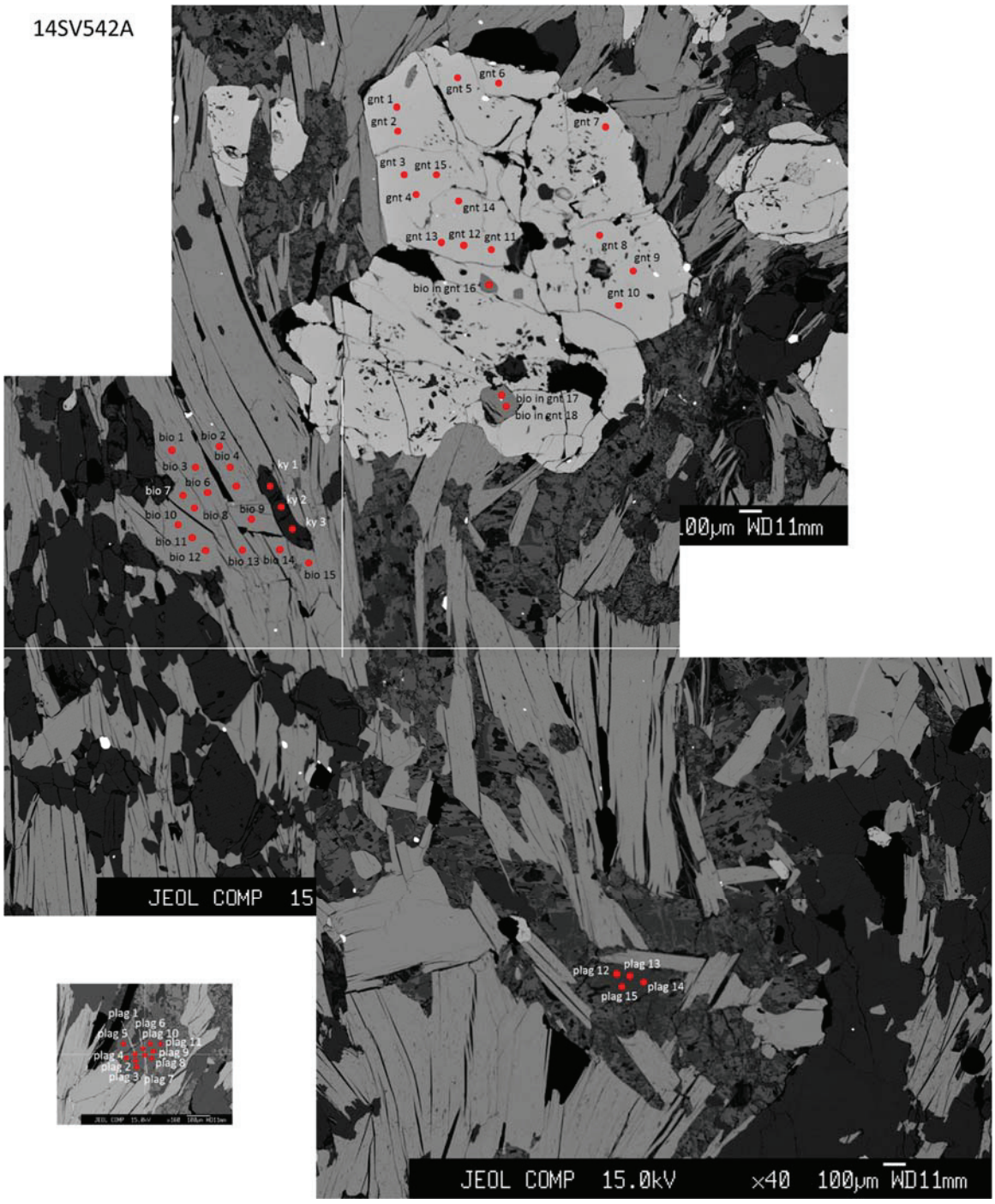

Figure B.7: BSE images of sample 14SV542A with annotated analysis points.

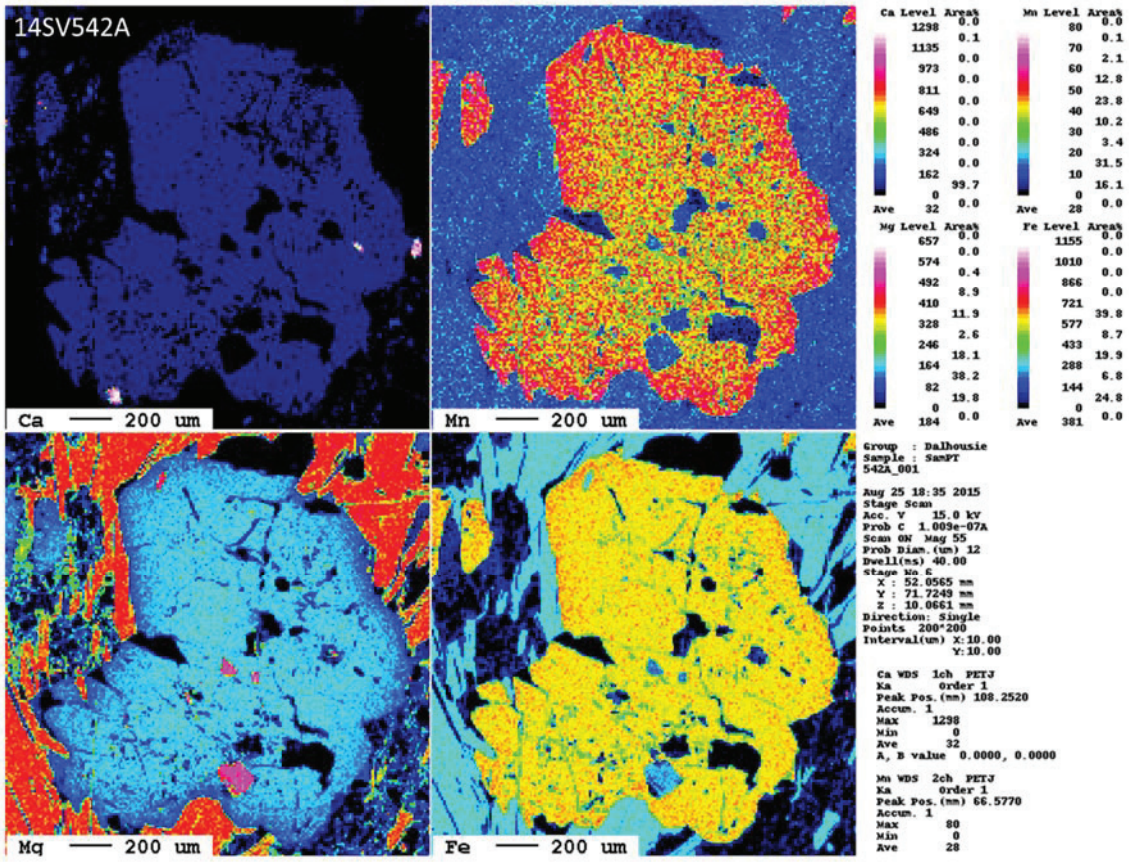

Figure B.8: Ca, Mn, Mg and Fe maps of the garnet analyzed in sample 14SV542A.

Table B.4: Analytical data from sample 14SV542A.

No.	245	246	247	248	249	250	251	252
	542A_plag 1	542A_plag 2	542A_plag 3	542A_plag 4	542A_plag 5	542A_plag 6	542A_plag 7	542A_plag 8
oxides(wt%):								
CaO	5.869	5.925	5.878	6.393	6.401	5.846	5.876	5.877
TiO2	0	0	0	0	0	0	0	0
Na2O	8.466	8.413	8.404	8.212	8.148	8.608	8.446	8.406
SiO2	60.915	60.193	60.709	60.289	60.214	61.005	60.808	61.074
MnO	0	0	0	0	0	0	0	0
K2O	0.21	0.21	0.179	0.195	0.164	0.217	0.212	0.207
Cr2O3	0	0	0	0	0	0	0	0
MgO	0.006	0.008	0.009	0	0.005	0	0.001	0.006
Al2O3	24.195	24.189	24.319	24.601	24.997	24.155	24.302	24.266
FeO	0.026	0.04	0.075	0.095	0.071	0.028	0.028	0.028
Total	99.687	98.978	99.573	99.785	100	99.859	99.673	99.864
cations:								
Ca	0.0351	0.0357	0.0352	0.0382	0.0382	0.0349	0.0351	0.0351
Ti	0	0	0	0	0	0	0	0
Na	0.0916	0.0917	0.091	0.0889	0.088	0.093	0.0914	0.0907
Si	0.3398	0.3385	0.3391	0.3366	0.3354	0.3399	0.3393	0.3399
Mn	0	0	0	0	0	0	0	0
K	0.0015	0.0015	0.0013	0.0014	0.0012	0.0015	0.0015	0.0015
Cr	0	0	0	0	0	0	0	0
Mg	0	0.0001	0.0001	0	0	0	0	0
Al	0.1591	0.1603	0.1601	0.1619	0.1641	0.1586	0.1598	0.1592
Fe	0.0001	0.0002	0.0003	0.0004	0.0003	0.0001	0.0001	0.0001
Total	0.6273	0.628	0.6271	0.6274	0.6272	0.6281	0.6273	0.6266

Table B.4: *Continued.* Analytical data from sample 14SV542A.

No.	253	254	255	**256**	257	258	259	260
	542A_plag 9	542A_plag 10	542A_plag 11	**542A_plag 12**	542A_plag 13	542A_plag 14	542A_plag 15	542A_bio 1
oxides(wt%):								
CaO	5.794	5.751	5.785	**5.711**	5.777	5.548	5.451	0.058
TiO2	0	0	0	**0**	0	0	0	2.44
Na2O	8.454	8.488	8.429	**8.553**	8.574	8.587	8.654	0.154
SiO2	60.98	60.787	60.692	**61.25**	60.949	61.4	62.324	35.959
MnO	0.001	0	0	**0.008**	0	0	0.005	0.033
K2O	0.214	0.228	0.234	**0.148**	0.187	0.145	0.174	9.646
Cr2O3	0.003	0	0	**0**	0	0	0	0.135
MgO	0.012	0.005	0	**0.004**	0.011	0	0.015	10.347
Al2O3	24.085	24.064	24.124	**24.269**	24.073	24.066	24.015	19.712
FeO	0.024	0.017	0.04	**0.053**	0.074	0.053	0.025	17.225
Total	99.567	99.34	99.304	**99.996**	99.645	99.799	100.663	95.709
cations:								
Ca	0.0347	0.0345	0.0347	**0.034**	0.0346	0.0331	0.0322	0.0004
Ti	0	0	0	**0**	0	0	0	0.0125
Na	0.0915	0.0921	0.0915	**0.0921**	0.0928	0.0926	0.0924	0.002
Si	0.3404	0.3402	0.3398	**0.3403**	0.3402	0.3416	0.3434	0.2449
Mn	0	0	0	**0**	0	0	0	0.0002
K	0.0015	0.0016	0.0017	**0.001**	0.0013	0.001	0.0012	0.0838
Cr	0	0	0	**0**	0	0	0	0.0007
Mg	0.0001	0	0	**0**	0.0001	0	0.0001	0.1051
Al	0.1585	0.1587	0.1592	**0.1589**	0.1584	0.1578	0.156	0.1583
Fe	0.0001	0.0001	0.0002	**0.0002**	0.0003	0.0002	0.0001	0.0981
Total	0.6269	0.6273	0.6271	**0.6265**	0.6277	0.6263	0.6255	0.7061

Table B.4: *Continued.* Analytical data from sample 14SV542A.

No.	261	262	263	264	265	**266**	267	268
	542A_bio 2	542A_bio 3	542A_bio 4	542A_bio 5	542A_bio 6	**542A_bio 7**	542A_bio 8	542A_bio 9
oxides(wt%):								
CaO	0.053	0.05	0.029	0.043	0.043	**0.022**	0.015	0.026
TiO2	2.402	2.46	2.449	2.452	2.339	**2.62**	2.501	2.436
Na2O	0.177	0.162	0.154	0.175	0.148	**0.134**	0.161	0.137
SiO2	35.811	36.074	35.803	35.573	35.937	**36.05**	35.747	35.813
MnO	0.034	0.034	0.047	0.057	0.033	**0.028**	0.044	0.035
K2O	9.561	9.715	9.858	9.867	9.385	**9.749**	9.736	9.852
Cr2O3	0.171	0.098	0.147	0.129	0.035	**0.046**	0.096	0.081
MgO	10.212	10.417	10.351	10.182	10.352	**10.35**	10.216	10.292
Al2O3	19.553	19.846	19.649	19.327	19.791	**19.877**	19.481	19.48
FeO	17.376	17.163	17.542	17.383	17.272	**17.269**	17.515	16.963
Total	95.35	96.019	96.029	95.188	95.335	**96.145**	95.512	95.115
cations:								
Ca	0.0004	0.0004	0.0002	0.0003	0.0003	**0.0002**	0.0001	0.0002
Ti	0.0124	0.0126	0.0125	0.0127	0.012	**0.0134**	0.0129	0.0126
Na	0.0023	0.0021	0.002	0.0023	0.002	**0.0018**	0.0021	0.0018
Si	0.2451	0.2448	0.2439	0.2446	0.2453	**0.2444**	0.2447	0.2456
Mn	0.0002	0.0002	0.0003	0.0003	0.0002	**0.0002**	0.0003	0.0002
K	0.0835	0.0841	0.0857	0.0866	0.0817	**0.0843**	0.085	0.0862
Cr	0.0009	0.0005	0.0008	0.0007	0.0002	**0.0002**	0.0005	0.0004
Mg	0.1042	0.1054	0.1051	0.1044	0.1053	**0.1046**	0.1042	0.1052
Al	0.1577	0.1587	0.1578	0.1566	0.1592	**0.1588**	0.1572	0.1574
Fe	0.0995	0.0974	0.0999	0.1	0.0986	**0.0979**	0.1003	0.0973
Total	0.7063	0.7063	0.7083	0.7086	0.7049	**0.7058**	0.7074	0.707

Table B.4: *Continued.* Analytical data from sample 14SV542A.

No.	269	270	271	272	273	274	281	282
	542A_bio 10	542A_bio 11	542A_bio 12	542A_bio 13	542A_bio 14	542A_bio 15	542A_ky 1	542A_ky 2
oxides(wt%):								
CaO	0.062	0.016	0.013	0.008	0.008	0.01	0	0
TiO2	1.963	2.327	2.433	2.424	2.442	2.462	0	0
Na2O	0.161	0.144	0.135	0.144	0.131	0.136	0	0
SiO2	37.016	35.557	35.742	35.755	35.617	35.618	37.019	36.737
MnO	0.027	0.043	0.033	0.03	0.026	0.059	0	0
K2O	8.43	9.86	9.61	9.84	9.794	9.885	0.008	0.005
Cr2O3	0.031	0.047	0.067	0.062	0.059	0.062	0	0
MgO	10.324	10.35	10.158	10.279	9.995	10.229	0.008	0.003
Al2O3	20.786	19.757	19.661	19.503	19.49	19.786	63.517	63.701
FeO	15.415	16.966	17.01	17.363	16.994	17.477	0.275	0.249
Total	94.215	95.067	94.862	95.408	94.556	95.724	100.827	100.695
cations:								
Ca	0.0005	0.0001	0.0001	0.0001	0.0001	0.0001	0	0
Ti	0.01	0.012	0.0126	0.0125	0.0127	0.0127	0	0
Na	0.0021	0.0019	0.0018	0.0019	0.0018	0.0018	0	0
Si	0.2507	0.244	0.2454	0.2449	0.2457	0.2434	0.1984	0.1972
Mn	0.0002	0.0002	0.0002	0.0002	0.0002	0.0003	0	0
K	0.0728	0.0863	0.0842	0.086	0.0862	0.0862	0.0001	0
Cr	0.0002	0.0003	0.0004	0.0003	0.0003	0.0003	0	0
Mg	0.1042	0.1059	0.104	0.105	0.1028	0.1042	0.0001	0
Al	0.1659	0.1598	0.1591	0.1574	0.1585	0.1593	0.4013	0.403
Fe	0.0873	0.0974	0.0977	0.0995	0.098	0.0999	0.0012	0.0011
Total	0.694	0.7079	0.7056	0.7078	0.7064	0.7082	0.6012	0.6014

Table B.4: *Continued.* Analytical data from sample 14SV542A.

No.	283	284	285	286	287	288	289	290	**291**
	542A_ky 3	542A_gnt 1	542A_gnt 2	542A_gnt 3	542A_gnt 4	542A_gnt 5	542A_gnt 6	542A_gnt 7	**542A_gnt 8**
oxides(wt%):									
CaO	0	2.346	2.292	2.304	2.268	2.433	2.359	2.177	**2.312**
TiO2	0	0	0	0	0	0	0	0	**0**
Na2O	0	0.011	0.007	0.013	0.006	0.011	0.006	0.011	**0.004**
SiO2	37.049	36.637	36.822	36.401	36.627	36.789	36.649	36.501	**36.717**
MnO	0	1.59	1.506	1.487	1.533	1.456	1.419	1.518	**1.354**
K2O	0.007	0.026	0.022	0.023	0.014	0.02	0.016	0.029	**0.023**
Cr2O3	0	0.063	0.007	0	0.003	0	0.022	0	**0.028**
MgO	0.009	4.14	4.26	4.177	4.006	4.184	4.386	4.017	**4.546**
Al2O3	63.701	20.964	21.038	20.973	20.967	21.044	20.933	21.106	**21.046**
FeO	0.221	33.157	33.197	33.388	33.582	33.198	33.083	33.221	**33.143**
Total	100.987	98.934	99.151	98.766	99.006	99.135	98.873	98.58	**99.173**
cations:									
Ca	0	0.017	0.0165	0.0167	0.0164	0.0175	0.017	0.0158	**0.0166**
Ti	0	0	0	0	0	0	0	0	**0**
Na	0	0.0001	0.0001	0.0002	0.0001	0.0001	0.0001	0.0001	**0.0001**
Si	0.1982	0.2472	0.2476	0.2463	0.2473	0.2475	0.2472	0.2471	**0.2467**
Mn	0	0.0091	0.0086	0.0085	0.0088	0.0083	0.0081	0.0087	**0.0077**
K	0	0.0002	0.0002	0.0002	0.0001	0.0002	0.0001	0.0003	**0.0002**
Cr	0	0.0003	0	0	0	0	0.0001	0	**0.0001**
Mg	0.0001	0.0416	0.0427	0.0421	0.0403	0.042	0.0441	0.0405	**0.0455**
Al	0.4017	0.1667	0.1667	0.1673	0.1668	0.1669	0.1664	0.1684	**0.1667**
Fe	0.001	0.1871	0.1867	0.1889	0.1896	0.1868	0.1866	0.1881	**0.1863**
Total	0.6011	0.6693	0.6691	0.6702	0.6694	0.6694	0.6698	0.669	**0.67**

Table B.4: *Continued.* Analytical data from sample 14SV542A.

No.	292	293	294	295	296	297	298
	542A_gnt 9	542A_gnt 10	542A_gnt 11	542A_gnt 12	542A_gnt 13	542A_gnt 14	542A_gnt 15
oxides(wt%):							
CaO	2.2	2.328	2.415	2.373	2.491	2.201	2.438
TiO2	0	0	0	0	0	0	0
Na2O	0.002	0	0	0.001	0.008	0	0.003
SiO2	36.329	36.411	36.3	36.573	36.223	36.525	36.307
MnO	1.382	1.332	1.294	1.329	1.35	1.33	1.402
K2O	0.029	0.019	0.024	0.03	0.017	0.027	0.022
Cr2O3	0.005	0.032	0	0.023	0	0.001	0.011
MgO	4.488	4.597	4.592	4.648	4.661	4.693	4.573
Al2O3	21.154	20.928	21.21	20.883	20.999	21.071	21.101
FeO	33.174	32.718	32.496	32.619	32.585	33.057	32.68
Total	98.763	98.365	98.331	98.479	98.334	98.905	98.537
cations:							
Ca	0.0159	0.0169	0.0175	0.0172	0.0181	0.0159	0.0177
Ti	0	0	0	0	0	0	0
Na	0	0	0	0	0.0001	0	0
Si	0.2454	0.2465	0.2456	0.2471	0.2454	0.246	0.2455
Mn	0.0079	0.0076	0.0074	0.0076	0.0077	0.0076	0.008
K	0.0003	0.0002	0.0002	0.0003	0.0001	0.0002	0.0002
Cr	0	0.0002	0	0.0001	0	0	0.0001
Mg	0.0452	0.0464	0.0463	0.0468	0.0471	0.0471	0.0461
Al	0.1684	0.167	0.1691	0.1663	0.1677	0.1673	0.1682
Fe	0.1874	0.1852	0.1839	0.1843	0.1846	0.1862	0.1848
Total	0.6705	0.6701	0.6701	0.6697	0.6708	0.6704	0.6706

Table B.4: *Continued.* Analytical data from sample 14SV542A.

No.	299	300	301
	542A_bio in gnt 16	542A_bio in gnt 17	542A_bio in gnt 18
oxides(wt%):			
CaO	0	0	0
TiO2	2.253	2.146	2.11
Na2O	0.271	0.215	0.209
SiO2	35.792	36.388	36.044
MnO	0	0	0
K2O	9.364	9.312	9.473
Cr2O3	0	0	0
MgO	12.94	13.064	13.186
Al2O3	20.357	19.235	19.216
FeO	12.704	14.397	14.231
Total	93.681	94.757	94.469
cations:			
Ca	0	0	0
Ti	0.0115	0.0109	0.0108
Na	0.0036	0.0028	0.0028
Si	0.2433	0.2464	0.2451
Mn	0	0	0
K	0.0812	0.0805	0.0822
Cr	0	0	0
Mg	0.1311	0.1319	0.1337
Al	0.1631	0.1535	0.154
Fe	0.0722	0.0815	0.0809
Total	0.7061	0.7076	0.7096

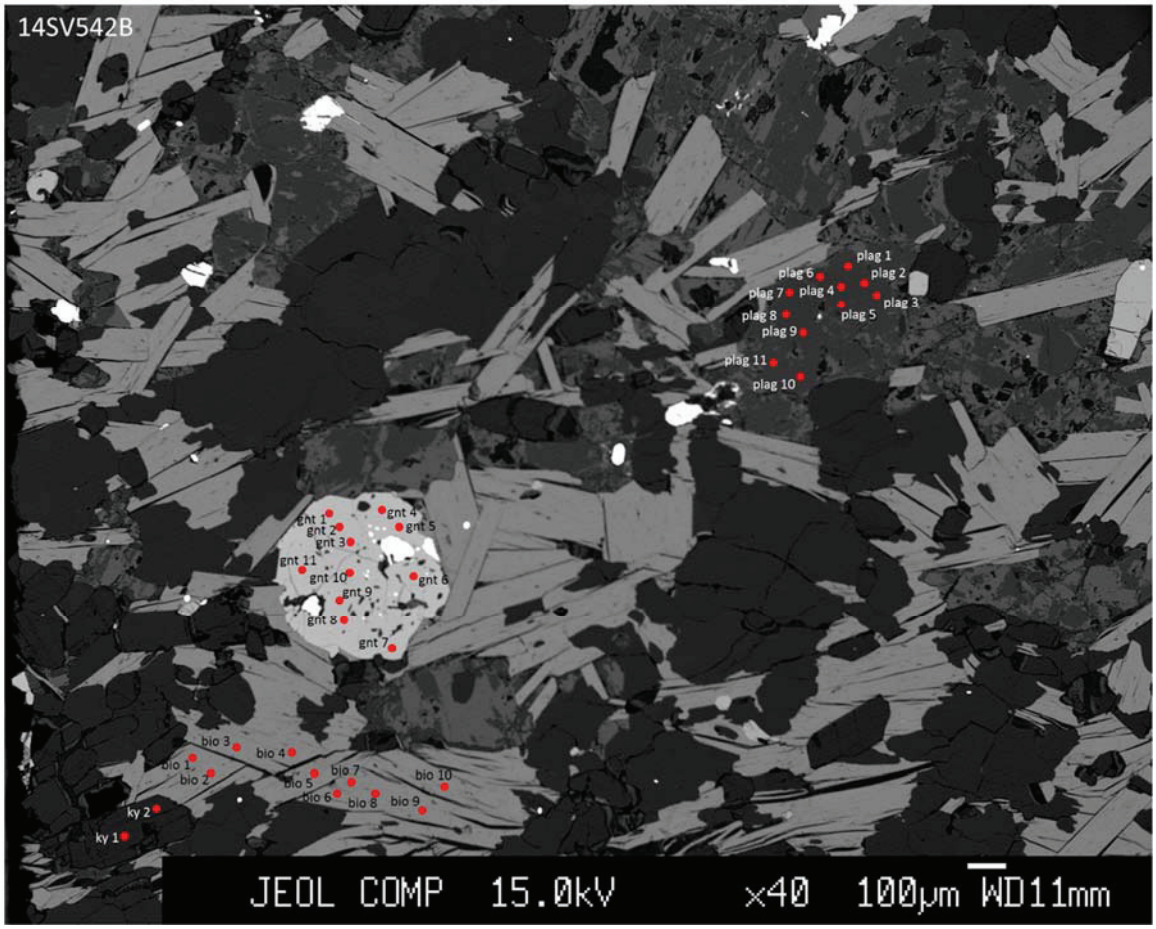

Figure B.9: BSE image of sample 14SV542B with annotated analysis points.

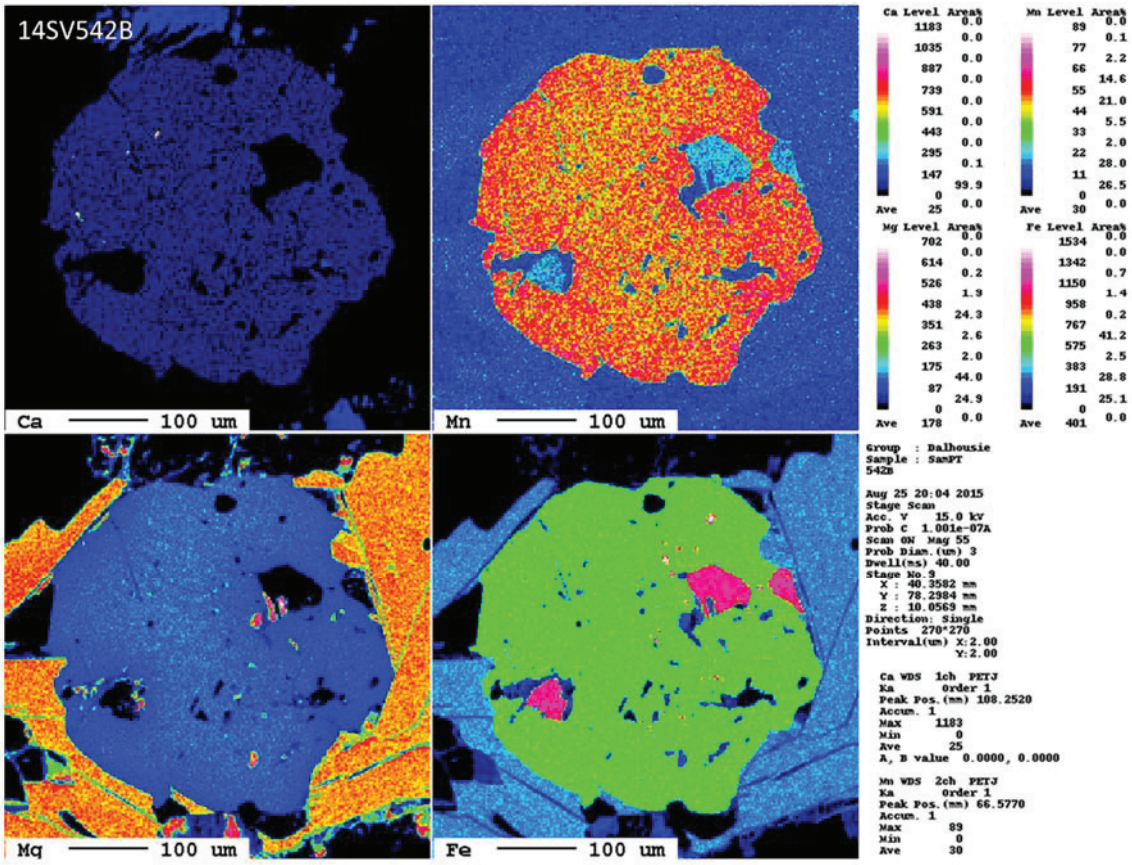

Figure B.10: Ca, Mn, Mg and Fe maps of the garnet analyzed in sample 14SV432B.

Table B.5: Analytical data from sample 14SV542B.

No.	302	303	304	305	**306**	307	308	309
	542B_plag 1	542B_plag 2	542B_plag 3	542B_plag 4	**542B_plag 5**	542B_plag 6	542B_plag 7	542B_plag 8
oxides(wt%):								
CaO	5.577	5.492	5.647	5.184	**5.294**	5.319	5.065	5.12
TiO2	0	0	0	0.009	**0.005**	0.023	0.011	0.026
Na2O	8.701	8.784	8.62	8.966	**8.864**	8.883	8.966	9.011
SiO2	61.813	62.149	61.61	62.581	**61.769**	61.984	62.715	62.483
MnO	0	0	0	0	**0.004**	0.007	0.001	0.003
K2O	0.186	0.192	0.17	0.184	**0.22**	0.203	0.208	0.194
Cr2O3	0	0	0	0.019	**0.003**	0	0.014	0
MgO	0	0	0	0	**0.001**	0.006	0	0
Al2O3	24.165	24.149	24.515	23.806	**23.864**	24.031	23.786	24.04
FeO	0	0	0	0.02	**0.019**	0.043	0.056	0.06
Total	100.442	100.766	100.562	100.769	**100.043**	100.499	100.822	100.937
cations:								
Ca	0.033	0.0324	0.0334	0.0306	**0.0315**	0.0315	0.0298	0.0302
Ti	0	0	0	0	**0**	0.0001	0	0.0001
Na	0.0933	0.0938	0.0923	0.0957	**0.0954**	0.0952	0.0956	0.0961
Si	0.3417	0.3424	0.3402	0.3445	**0.3428**	0.3425	0.3449	0.3435
Mn	0	0	0	0	**0**	0	0	0
K	0.0013	0.0013	0.0012	0.0013	**0.0016**	0.0014	0.0015	0.0014
Cr	0	0	0	0.0001	**0**	0	0.0001	0
Mg	0	0	0	0	**0**	0	0	0
Al	0.1575	0.1568	0.1596	0.1545	**0.1561**	0.1565	0.1542	0.1558
Fe	0	0	0	0.0001	**0.0001**	0.0002	0.0003	0.0003
Total	0.6269	0.6268	0.6267	0.6269	**0.6276**	0.6274	0.6265	0.6274

Table B.5: *Continued.* Analytical data from sample 14SV542B.

No.	310	311	312	**319**	320	321	322	323
	542B_plag 9	542B_plag 10	542B_plag 11	**542B_bio 1**	542B_bio 2	542B_bio 3	542B_bio 4	542B_bio 5
oxides(wt%):								
CaO	5.292	6.498	6.299	**0.025**	0.034	0.026	0.009	0.025
TiO2	0.009	0.004	0.008	**2.482**	2.458	2.43	2.542	2.512
Na2O	8.796	8.265	8.2	**0.146**	0.138	0.143	0.15	0.102
SiO2	61.879	60.508	60.555	**36.111**	36.143	35.851	35.881	35.818
MnO	0.007	0.012	0.013	**0.068**	0.05	0.078	0.052	0.062
K2O	0.225	0.197	0.187	**9.81**	9.929	9.887	10.003	9.92
Cr2O3	0	0.003	0.012	**0.149**	0.109	0.174	0.148	0.139
MgO	0	0.005	0.003	**10.177**	10.139	10.109	10.064	10.239
Al2O3	23.91	24.732	24.765	**19.744**	19.825	19.821	19.779	19.696
FeO	0.032	0.023	0.043	**17.571**	17.402	17.401	17.346	17.465
Total	100.15	100.247	100.085	**96.283**	96.227	95.92	95.974	95.978
cations:								
Ca	0.0314	0.0387	0.0375	**0.0002**	0.0002	0.0002	0.0001	0.0002
Ti	0	0	0	**0.0127**	0.0125	0.0125	0.013	0.0129
Na	0.0945	0.0891	0.0884	**0.0019**	0.0018	0.0019	0.002	0.0013
Si	0.343	0.3364	0.3368	**0.245**	0.2452	0.2443	0.2444	0.244
Mn	0	0.0001	0.0001	**0.0004**	0.0003	0.0005	0.0003	0.0004
K	0.0016	0.0014	0.0013	**0.0849**	0.0859	0.0859	0.0869	0.0862
Cr	0	0	0.0001	**0.0008**	0.0006	0.0009	0.0008	0.0008
Mg	0	0	0	**0.1029**	0.1026	0.1027	0.1022	0.104
Al	0.1562	0.162	0.1624	**0.1579**	0.1586	0.1592	0.1588	0.1582
Fe	0.0001	0.0001	0.0002	**0.0997**	0.0988	0.0992	0.0988	0.0995
Total	0.6269	0.6278	0.6269	**0.7065**	0.7066	0.7074	0.7074	0.7076

Table B.5: *Continued.* Analytical data from sample 14SV542B.

No.	324	325	326	327	328	329	330	331	332
	542B_bio 6	542B_bio 7	542B_bio 8	542B_bio 9	542B_bio 10	542B_ky 1	542B_ky 2	542B_gnt 1	542B_gnt 2
oxides(wt%):									
CaO	0.015	0	0.008	0	0	0	0	1.793	1.702
TiO2	2.418	2.412	2.428	2.432	2.451	0	0	0.064	0.039
Na2O	0.127	0.113	0.112	0.102	0.13	0	0	0.012	0.023
SiO2	35.876	35.68	35.471	35.58	35.621	37.228	37.356	36.527	36.53
MnO	0.077	0.031	0.048	0.031	0.025	0	0	1.727	1.737
K2O	10.013	9.928	9.957	9.86	9.947	0.003	0.012	0.044	0.025
Cr2O3	0.151	0.056	0.042	0.044	0.059	0	0	0.063	0.082
MgO	10.095	10.182	10.088	10.006	10.003	0	0	3.595	3.738
Al2O3	19.878	19.827	19.827	19.591	19.951	64.209	63.964	20.939	20.846
FeO	17.302	17.779	17.437	17.77	17.405	0.197	0.252	34.785	34.44
Total	95.952	96.008	95.418	95.416	95.592	101.637	101.584	99.549	99.162
cations:									
Ca	0.0001	0	0.0001	0	0	0	0	0.013	0.0123
Ti	0.0124	0.0124	0.0125	0.0126	0.0126	0	0	0.0003	0.0002
Na	0.0017	0.0015	0.0015	0.0014	0.0017	0	0	0.0002	0.0003
Si	0.2443	0.2433	0.2432	0.2442	0.2436	0.1979	0.1987	0.2466	0.2472
Mn	0.0004	0.0002	0.0003	0.0002	0.0001	0	0	0.0099	0.01
K	0.087	0.0864	0.0871	0.0863	0.0868	0	0.0001	0.0004	0.0002
Cr	0.0008	0.0003	0.0002	0.0002	0.0003	0	0	0.0003	0.0004
Mg	0.1025	0.1035	0.1031	0.1024	0.102	0	0	0.0362	0.0377
Al	0.1596	0.1594	0.1603	0.1585	0.1608	0.4023	0.401	0.1666	0.1663
Fe	0.0986	0.1014	0.1	0.102	0.0995	0.0009	0.0011	0.1964	0.1949
Total	0.7074	0.7085	0.7084	0.7079	0.7074	0.6011	0.601	0.67	0.6696

Table B.5: *Continued.* Analytical data from sample 14SV542B.

No.	**333**	334	335	336	337	338	339	340	341
	542B_gnt 3	542B_gnt 4	542B_gnt 5	542B_gnt 6	542B_gnt 7	542B_gnt 8	542B_gnt 9	542B_gnt 10	542B_gnt 11
oxides(wt%):									
CaO	**1.794**	1.772	1.731	1.742	1.743	1.77	1.772	1.749	1.689
TiO2	**0.055**	0.039	0.05	0.07	0.092	0.049	0.053	0.062	0.053
Na2O	**0.016**	0.019	0	0.004	0.007	0.012	0.019	0.006	0.01
SiO2	**36.676**	36.308	36.312	36.518	36.484	36.529	36.463	36.287	36.454
MnO	**1.739**	1.809	1.83	1.921	1.811	1.825	1.763	1.757	1.747
K2O	**0.029**	0.037	0.037	0.032	0.045	0.027	0.029	0.036	0.039
Cr2O3	**0.073**	0.077	0.105	0.095	0.081	0.084	0.061	0.07	0.041
MgO	**3.671**	3.558	3.441	3.141	3.443	3.566	3.642	3.697	3.611
Al2O3	**21.102**	21.122	20.974	20.835	20.927	20.922	20.891	20.789	20.907
FeO	**34.604**	34.525	34.758	35.185	34.873	34.88	34.452	34.429	34.711
Total	**99.759**	99.266	99.238	99.543	99.506	99.664	99.145	98.882	99.262
cations:									
Ca	**0.0129**	0.0129	0.0126	0.0126	0.0126	0.0128	0.0129	0.0127	0.0122
Ti	**0.0003**	0.0002	0.0003	0.0004	0.0005	0.0002	0.0003	0.0003	0.0003
Na	**0.0002**	0.0003	0	0.0001	0.0001	0.0002	0.0003	0.0001	0.0001
Si	**0.2467**	0.2457	0.2461	0.2472	0.2466	0.2465	0.2469	0.2465	0.2467
Mn	**0.0099**	0.0104	0.0105	0.011	0.0104	0.0104	0.0101	0.0101	0.01
K	**0.0002**	0.0003	0.0003	0.0003	0.0004	0.0002	0.0002	0.0003	0.0003
Cr	**0.0004**	0.0004	0.0006	0.0005	0.0004	0.0004	0.0003	0.0004	0.0002
Mg	**0.0368**	0.0359	0.0348	0.0317	0.0347	0.0359	0.0368	0.0374	0.0364
Al	**0.1673**	0.1685	0.1676	0.1663	0.1667	0.1664	0.1667	0.1665	0.1668
Fe	**0.1947**	0.1954	0.197	0.1992	0.1971	0.1969	0.1951	0.1956	0.1965
Total	**0.6695**	0.67	0.6699	0.6693	0.6696	0.67	0.6697	0.67	0.6696

Table B.6: Analytical data for in-house feldspar and garnet controls.

No.	1	2	3	4	5	6	7	8	9	10	11
	KK ctrl 1	KK ctrl 2	San ctrl 1	San ctrl 2	Gnt ctrl 1	Gnt ctrl 2	KK ctrl 1	San ctrl 1	Gnt ctrl 1	KK ctrl 1	KK ctrl 2
oxides(wt%):											
CaO	10.433	10.274	0.016	0.005	4.355	4.464	10.209	0	4.281	10.419	10.361
TiO2	4.731	4.807	0.03	0.083	0.064	0.055	4.798	0.043	0.059	4.742	4.825
Na2O	2.671	2.598	2.971	3.008	0.003	0.02	2.66	3.027	0.004	2.59	2.708
SiO2	40.403	40.722	64.387	64.191	38.75	38.871	40.525	64.066	38.766	40.069	40.059
MnO	0.067	0.08	0	0	0.485	0.481	0.119	0.023	0.522	0.073	0.055
K2O	2.079	2.106	11.975	11.938	0.034	0.039	2.092	12.258	0.028	2.085	2.139
Cr2O3	0.014	0	0	0	0.022	0.017	0	0	0.003	0	0
MgO	12.692	11.69	0	0	11.423	11.369	12.578	0	11.382	12.749	12.541
Al2O3	14.382	14.781	18.411	18.31	21.865	21.914	14.345	18.692	22.091	14.235	14.4
FeO	10.028	9.844	0.141	0.139	22.045	21.986	10.152	0.13	21.918	10.022	10.024
Total	97.5	96.902	97.931	97.674	99.046	99.216	97.478	98.239	99.054	96.984	97.112
cations:											
Ca	0.0717	0.0708	0.0001	0	0.0298	0.0304	0.0702	0	0.0283	0.0721	0.0716
Ti	0.0228	0.0233	0.0001	0.0004	0.0003	0.0003	0.0232	0.0002	0.0003	0.023	0.0234
Na	0.0332	0.0324	0.0335	0.034	0	0.0002	0.0331	0.0341	0.0001	0.0324	0.0339
Si	0.2593	0.262	0.3743	0.3742	0.2471	0.2473	0.2601	0.3722	0.2487	0.2587	0.2584
Mn	0.0004	0.0004	0	0	0.0026	0.0026	0.0006	0.0001	0.0027	0.0004	0.0003
K	0.017	0.0173	0.0888	0.0888	0.0003	0.0003	0.0171	0.0909	0.0002	0.0172	0.0176
Cr	0.0001	0	0	0	0.0001	0.0001	0	0	0	0	0
Mg	0.1214	0.1121	0	0	0.1086	0.1078	0.1203	0	0.104	0.1227	0.1206
Al	0.1088	0.1121	0.1262	0.1258	0.1643	0.1644	0.1085	0.128	0.1694	0.1083	0.1095
Fe	0.0538	0.053	0.0007	0.0007	0.1175	0.117	0.0545	0.0006	0.1127	0.0541	0.0541
Total	0.6885	0.6834	0.6238	0.624	0.6707	0.6704	0.6877	0.6262	0.6664	0.6889	0.6894

Table B.6: *Continued.* Analytical data for in-house feldspar and garnet controls.

No.	12	13	14	15	48	49	50	51	52	53	85
	San ctrl 1	San ctrl 2	KGnt ctrl 1	KGnt ctrl 2	KK ctrl 1	KK ctrl 2	San ctrl 1	San ctrl 2	KGnt ctrl 1	KGnt ctrl 2	KK ctrl 1
oxides(wt%):											
CaO	0	0.01	5.303	5.244	10.689	10.105	0.015	0.026	5.268	5.339	10.31
TiO2	0.083	0.061	0.403	0.369	4.848	4.846	0.134	0.093	0.39	0.411	4.816
Na2O	3.055	3.087	0.01	0.028	2.538	2.626	2.957	3.009	0.013	0.028	2.655
SiO2	64.041	64.293	40.45	40.45	39.948	40.589	64.016	63.51	40.262	40.413	40.206
MnO	0	0	0.292	0.276	0.098	0.124	0	0	0.311	0.324	0.062
K2O	12.15	12.368	0.021	0.02	2.07	2.145	12.194	12.203	0.013	0.021	2.096
Cr2O3	0	0	0.064	0.065	0.079	0.081	0.007	0.009	0.104	0.096	0
MgO	0	0	19.173	19.166	12.92	12.555	0	0	19.339	19.166	12.629
Al2O3	18.582	18.699	22.687	22.717	14.241	14.261	18.69	18.768	22.753	22.686	14.331
FeO	0.152	0.142	10.415	10.363	9.688	10.154	0.182	0.174	10.409	10.427	10.238
Total	98.063	98.66	98.818	98.698	97.119	97.486	98.195	97.792	98.862	98.911	97.343
cations:											
Ca	0	0.0001	0.0345	0.0341	0.0738	0.0695	0.0001	0.0002	0.0342	0.0347	0.0711
Ti	0.0004	0.0003	0.0018	0.0017	0.0235	0.0234	0.0006	0.0004	0.0018	0.0019	0.0233
Na	0.0345	0.0347	0.0001	0.0003	0.0317	0.0327	0.0333	0.0341	0.0002	0.0003	0.0331
Si	0.3725	0.3722	0.2452	0.2454	0.2575	0.2605	0.372	0.3709	0.2441	0.2449	0.2587
Mn	0	0	0.0015	0.0014	0.0005	0.0007	0	0	0.0016	0.0017	0.0003
K	0.0902	0.0913	0.0002	0.0002	0.017	0.0176	0.0904	0.0909	0.0001	0.0002	0.0172
Cr	0	0	0.0003	0.0003	0.0004	0.0004	0	0	0.0005	0.0005	0
Mg	0	0	0.1733	0.1733	0.1241	0.1201	0	0	0.1748	0.1732	0.1212
Al	0.1274	0.1276	0.1621	0.1625	0.1082	0.1079	0.128	0.1292	0.1626	0.1621	0.1087
Fe	0.0007	0.0007	0.0528	0.0526	0.0522	0.0545	0.0009	0.0008	0.0528	0.0529	0.0551
Total	0.6258	0.627	0.6719	0.6719	0.689	0.6874	0.6253	0.6266	0.6727	0.6725	0.6888

Table B.6: *Continued.* Analytical data for in-house feldspar and garnet controls.

No.	86	87	88	89	90	121	122	123	124	125	126
	KK ctrl 2	San ctrl 1	San ctrl 2	KGnt ctrl 1	KGnt ctrl 2	KK ctrl 1	KK ctrl 2	San ctrl 1	San ctrl 2	KGnt ctrl 1	KGnt ctrl 2
oxides(wt%):											
CaO	10.285	0	0.002	5.283	5.235	10.387	10.149	0	0	5.243	5.281
TiO2	4.887	0.075	0.043	0.373	0.374	4.766	4.662	0.018	0.002	0.434	0.362
Na2O	2.616	3.016	2.978	0.032	0.036	2.731	2.749	3.018	2.989	0.027	0.034
SiO2	40.025	63.953	63.745	40.303	40.189	39.934	40.396	63.752	63.554	40.135	40.251
MnO	0.075	0	0	0.289	0.283	0.074	0.063	0	0	0.334	0.321
K2O	2.106	12.292	12.192	0.021	0.014	2.136	2.131	12.209	12.282	0.027	0.016
Cr2O3	0	0	0	0.023	0	0	0	0	0	0.017	0.035
MgO	12.677	0	0	19.103	19.246	12.442	12.276	0	0	19.146	19.254
Al2O3	14.269	18.642	18.428	22.738	22.821	14.383	14.457	18.649	18.678	22.686	22.755
FeO	10.233	0.173	0.127	10.374	10.428	10.295	10.355	0.141	0.124	10.37	10.263
Total	97.173	98.151	97.515	98.539	98.626	97.148	97.238	97.787	97.629	98.419	98.572
cations:											
Ca	0.0711	0	0	0.0344	0.0341	0.0719	0.07	0	0	0.0331	0.0333
Ti	0.0237	0.0003	0.0002	0.0017	0.0017	0.0231	0.0226	0.0001	0	0.0019	0.0016
Na	0.0327	0.034	0.0338	0.0004	0.0004	0.0342	0.0343	0.0342	0.0339	0.0003	0.0004
Si	0.2581	0.3721	0.373	0.245	0.2442	0.2579	0.2602	0.3721	0.3717	0.2463	0.2464
Mn	0.0004	0	0	0.0015	0.0015	0.0004	0.0003	0	0	0.0017	0.0016
K	0.0173	0.0912	0.091	0.0002	0.0001	0.0176	0.0175	0.0909	0.0916	0.0002	0.0001
Cr	0	0	0	0.0001	0	0	0	0	0	0.0001	0.0002
Mg	0.1219	0	0	0.1731	0.1743	0.1198	0.1179	0	0	0.1678	0.1683
Al	0.1085	0.1278	0.1271	0.1629	0.1634	0.1095	0.1097	0.1283	0.1288	0.1664	0.1665
Fe	0.0552	0.0008	0.0006	0.0527	0.053	0.0556	0.0558	0.0007	0.0006	0.0511	0.0505
Total	0.689	0.6263	0.6258	0.672	0.6727	0.69	0.6884	0.6263	0.6266	0.669	0.6689

Table B.6: *Continued.* Analytical data for in-house feldspar and garnet controls.

No.	157	158	159	160	161	162	202	203	204	205	206
	KK ctrl 1	KK ctrl 2	San ctrl 1	San ctrl 2	KGnt ctrl 1	KGnt ctrl 2	KK ctrl 1	KK ctrl 2	San ctrl 1	San ctrl 2	KGnt ctrl 1
oxides(wt%):											
CaO	10.402	10.365	0	0	5.345	5.286	10.372	10.366	0.037	0.025	5.259
TiO2	4.808	4.826	0.053	0.017	0.367	0.302	4.877	4.729	0.113	0.087	0.421
Na2O	2.662	2.67	3.118	3.018	0.009	0.003	2.689	2.756	3.067	3.137	0.029
SiO2	40.448	39.741	64.151	64.449	40.482	40.375	40.308	40.188	64.133	64.023	39.901
MnO	0.086	0.066	0	0	0.3	0.29	0.098	0.118	0.011	0.012	0.323
K2O	2.127	2.107	12.236	12.254	0.009	0.005	2.155	2.109	12.242	12.13	0.026
Cr2O3	0	0	0	0	0	0.021	0.094	0.035	0.047	0	0.065
MgO	12.685	12.28	0	0	19.102	19.299	12.687	12.621	0.004	0	19.155
Al2O3	14.449	14.304	18.805	18.831	22.832	22.904	14.509	14.456	18.783	18.81	22.712
FeO	10.009	10.253	0.086	0.119	10.189	10.343	10.351	10.327	0.187	0.192	10.382
Total	97.676	96.612	98.449	98.688	98.635	98.828	98.14	97.705	98.624	98.416	98.273
cations:											
Ca	0.0714	0.0721	0	0	0.0347	0.0343	0.071	0.0713	0.0002	0.0002	0.0344
Ti	0.0232	0.0236	0.0002	0.0001	0.0017	0.0014	0.0234	0.0228	0.0005	0.0004	0.0019
Na	0.0331	0.0336	0.035	0.0338	0.0001	0	0.0333	0.0343	0.0344	0.0353	0.0003
Si	0.2591	0.258	0.3718	0.3724	0.2455	0.2446	0.2576	0.258	0.3714	0.3713	0.2435
Mn	0.0005	0.0004	0	0	0.0015	0.0015	0.0005	0.0006	0.0001	0.0001	0.0017
K	0.0174	0.0175	0.0905	0.0903	0.0001	0	0.0176	0.0173	0.0904	0.0898	0.0002
Cr	0	0	0	0	0	0.0001	0.0005	0.0002	0.0002	0	0.0003
Mg	0.1211	0.1189	0	0	0.1727	0.1743	0.1209	0.1208	0	0	0.1743
Al	0.1091	0.1095	0.1285	0.1283	0.1632	0.1636	0.1093	0.1094	0.1282	0.1286	0.1634
Fe	0.0536	0.0557	0.0004	0.0006	0.0517	0.0524	0.0553	0.0554	0.0009	0.0009	0.053
Total	0.6885	0.6894	0.6265	0.6255	0.6713	0.6722	0.6895	0.6902	0.6263	0.6266	0.673

Table B.6: *Continued.* Analytical data for in-house feldspar and garnet controls.

No.	207	239	240	241	242	243	244	275	276	277	278
	KGnt ctrl 2	KK ctrl 1	KK ctrl 2	San ctrl 1	San ctrl 2	KGnt ctrl 1	KGnt ctrl 2	KK ctrl 1	KK ctrl 2	San ctrl 1	San ctrl 2
oxides(wt%):											
CaO	5.295	10.308	10.394	0	0	5.241	5.241	10.373	10.444	0.012	0.003
TiO2	0.399	4.77	4.732	0.028	0	0.374	0.328	4.841	4.864	0.064	0.042
Na2O	0.026	2.742	2.691	3.048	3.115	0.043	0.029	2.639	2.668	3.108	3.016
SiO2	39.939	40.044	39.803	63.718	64.149	40.128	40.353	40.062	39.968	63.746	63.796
MnO	0.325	0.032	0.025	0	0	0.234	0.258	0.085	0.09	0.006	0
K2O	0	2.145	2.15	12.282	12.303	0.006	0.007	2.172	2.117	12.336	12.239
Cr2O3	0.03	0	0	0	0	0	0	0	0.001	0	0
MgO	19.26	12.736	12.556	0	0	19.235	19.307	12.635	12.32	0.004	0
Al2O3	22.855	14.206	14.118	18.445	18.621	22.749	22.74	14.271	14.236	18.577	18.67
FeO	10.3	10.045	10.103	0.084	0.122	10.267	10.274	10.127	10.318	0.098	0.126
Total	98.429	97.028	96.572	97.605	98.31	98.277	98.537	97.205	97.026	97.951	97.892
cations:											
Ca	0.0345	0.0713	0.0723	0	0	0.0342	0.0341	0.0717	0.0724	0.0001	0
Ti	0.0018	0.0232	0.0231	0.0001	0	0.0017	0.0015	0.0235	0.0237	0.0003	0.0002
Na	0.0003	0.0343	0.0339	0.0346	0.0351	0.0005	0.0003	0.033	0.0335	0.0352	0.0341
Si	0.2432	0.2586	0.2585	0.3727	0.3725	0.2444	0.2451	0.2583	0.2585	0.3719	0.372
Mn	0.0017	0.0002	0.0001	0	0	0.0012	0.0013	0.0005	0.0005	0	0
K	0	0.0177	0.0178	0.0917	0.0912	0.0001	0.0001	0.0179	0.0175	0.0918	0.091
Cr	0.0001	0	0	0	0	0	0	0	0	0	0
Mg	0.1748	0.1226	0.1216	0	0	0.1747	0.1748	0.1215	0.1188	0	0
Al	0.164	0.1081	0.1081	0.1272	0.1275	0.1633	0.1628	0.1085	0.1085	0.1277	0.1283
Fe	0.0525	0.0542	0.0549	0.0004	0.0006	0.0523	0.0522	0.0546	0.0558	0.0005	0.0006
Total	0.6729	0.6902	0.6903	0.6268	0.6269	0.6724	0.6723	0.6895	0.6893	0.6276	0.6262

Table B.6: *Continued.* Analytical data for in-house feldspar and garnet controls.

No.	279	280	313	314	315	316	317	318	342	343	344
	KGnt ctrl 1	KGnt ctrl 2	KK ctrl 1	KK ctrl 2	San ctrl 1	San ctrl 2	KGnt ctrl 1	KGnt ctrl 2	KK ctrl 1	KK ctrl 2	San ctrl 1
oxides(wt%):											
CaO	5.265	5.18	10.157	10.303	0.021	0.016	5.446	5.305	10.43	10.401	0
TiO2	0.355	0.357	4.899	4.962	0.111	0.106	0.424	0.45	4.832	4.627	0.065
Na2O	0.021	0.018	2.746	2.661	3.038	3.03	0.016	0.027	2.706	2.661	3.018
SiO2	40.071	40.003	40.326	40.362	63.689	64.071	40.356	40.531	40.119	40.45	64.392
MnO	0.304	0.318	0.107	0.117	0.01	0.014	0.307	0.34	0.093	0.07	0
K2O	0.011	0.011	2.147	2.113	12.376	12.399	0.015	0.012	2.176	2.116	12.459
Cr2O3	0	0.007	0.095	0.054	0.016	0.033	0.079	0.121	0	0	0
MgO	19.333	19.277	12.538	12.882	0.003	0.005	19.236	19.442	12.57	12.635	0
Al2O3	22.734	22.735	14.223	14.497	18.675	18.666	22.851	22.862	14.336	14.298	18.669
FeO	10.391	10.298	10.359	10.256	0.184	0.21	10.303	10.458	10.168	10.193	0.154
Total	98.485	98.204	97.597	98.207	98.123	98.55	99.033	99.548	97.43	97.451	98.757
cations:											
Ca	0.0343	0.0339	0.0699	0.0704	0.0001	0.0001	0.0353	0.0342	0.0719	0.0716	0
Ti	0.0016	0.0016	0.0237	0.0238	0.0005	0.0005	0.0019	0.002	0.0234	0.0224	0.0003
Na	0.0002	0.0002	0.0342	0.0329	0.0343	0.0341	0.0002	0.0003	0.0338	0.0332	0.0338
Si	0.2439	0.244	0.2591	0.2575	0.3711	0.3716	0.2442	0.2441	0.2582	0.2599	0.3724
Mn	0.0016	0.0016	0.0006	0.0006	0.0001	0.0001	0.0016	0.0017	0.0005	0.0004	0
K	0.0001	0.0001	0.0176	0.0172	0.092	0.0918	0.0001	0.0001	0.0179	0.0173	0.0919
Cr	0	0	0.0005	0.0003	0.0001	0.0002	0.0004	0.0006	0	0	0
Mg	0.1754	0.1753	0.1201	0.1225	0	0	0.1735	0.1746	0.1206	0.121	0
Al	0.1631	0.1635	0.1077	0.109	0.1283	0.1276	0.163	0.1623	0.1088	0.1083	0.1273
Fe	0.0529	0.0525	0.0557	0.0547	0.0009	0.001	0.0521	0.0527	0.0547	0.0548	0.0007
Total	0.6732	0.6727	0.6892	0.689	0.6274	0.627	0.6723	0.6727	0.6898	0.6889	0.6265

Table B.6: *Continued.* Analytical data for in-house feldspar and garnet controls.

No.	345	346	347	348
	San ctrl 2	KGnt ctrl 1	KGnt ctrl 2	Gnt std no PS
oxides(wt%):				
CaO	0.016	5.276	5.316	4.419
TiO2	0.066	0.427	0.4	0.049
Na2O	3.045	0.019	0.017	0.004
SiO2	64.058	40.146	40.505	38.567
MnO	0.032	0.318	0.371	0.469
K2O	12.281	0.003	0.011	0.025
Cr2O3	0	0.108	0.047	0.011
MgO	0.004	19.198	19.145	11.517
Al2O3	18.714	22.727	22.807	22.141
FeO	0.144	10.477	10.495	22.251
Total	98.36	98.699	99.114	99.453
cations:				
Ca	0.0001	0.0344	0.0345	0.0301
Ti	0.0003	0.0019	0.0018	0.0002
Na	0.0343	0.0002	0.0002	0.0001
Si	0.3719	0.2439	0.245	0.2452
Mn	0.0002	0.0016	0.0019	0.0025
K	0.091	0	0.0001	0.0002
Cr	0	0.0005	0.0002	0.0001
Mg	0	0.1739	0.1726	0.1091
Al	0.1281	0.1628	0.1626	0.1659
Fe	0.0007	0.0532	0.0531	0.1183
Total	0.6266	0.6725	0.672	0.6718

APPENDIX C

ZIRCON ANALYTICAL DATA

Appendix C presents LA-ICP-MS analytical data of zircons analysed in this study. This appendix is subdivided by sample. For each sample, there are annotated CL images and trace-element data collected during U-Pb isotopic analyses from Trond Slagstad at the Norweigeon Geological Survey.

14SV528/NEP-S-1 and NEP-S-3

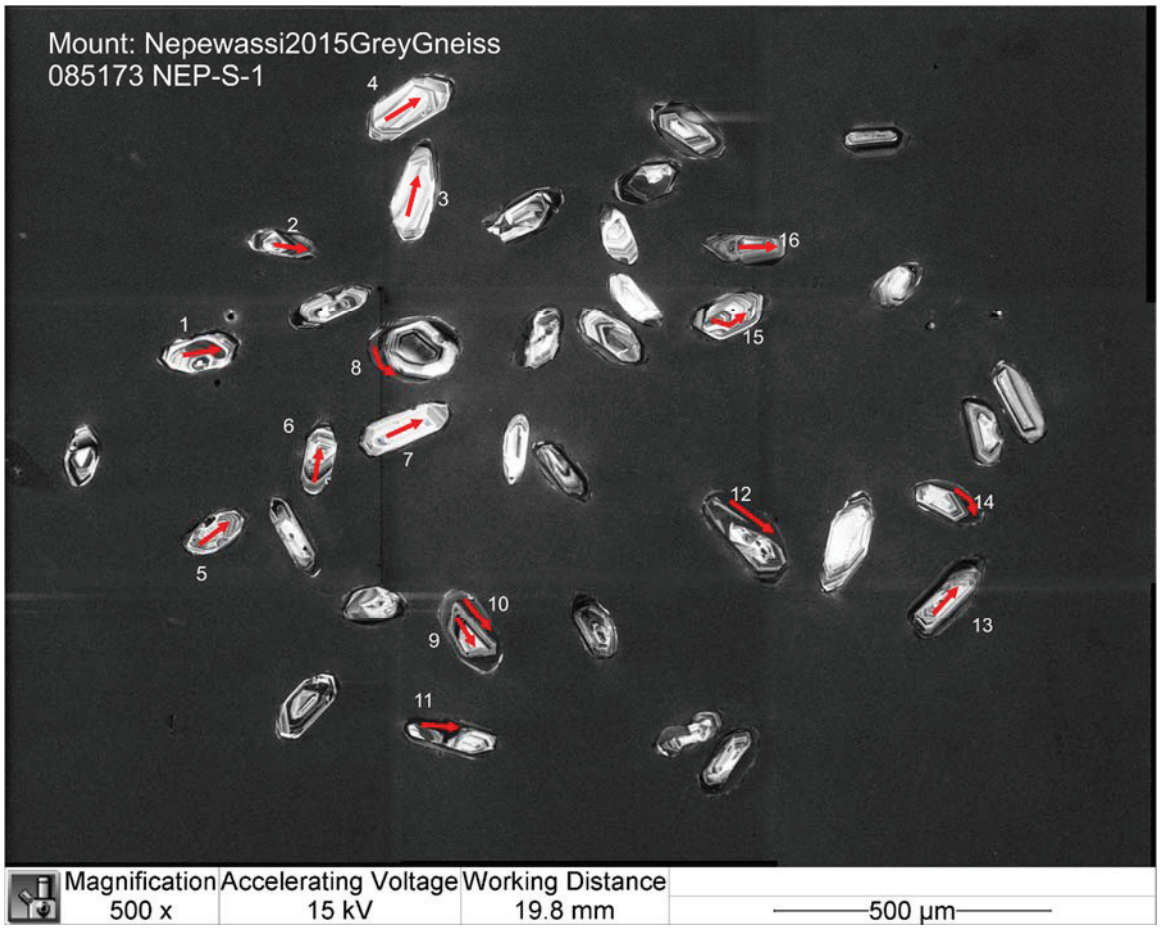

Figure C.1: Annotated CL images of zircon grains from sample 14SV528 NEP-S-1.

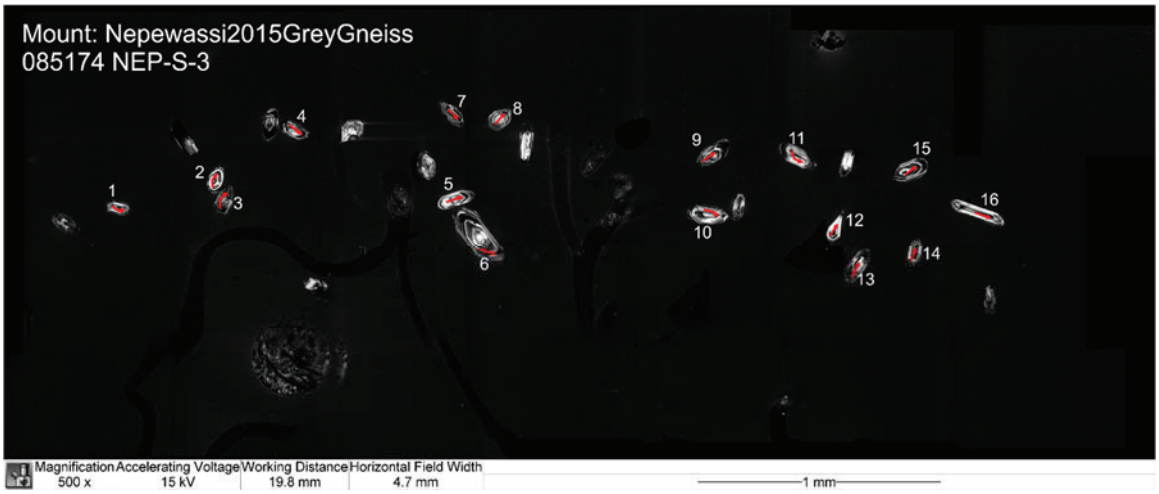

Figure C.2: Annotated CL images of zircon grains from sample 14SV528 NEP-S-3.

Table C.1: Zircon U-Pb Analytical data for sample 14SV528 NEP-S-1 and NEP-S-3.

	Isotope ratios									Age estimates (ma)							Concentrations (ppm)				
	Concordia output					Terra-Wasserburg output															Pb com.
Analysis_#	Pb207/ U235	1s%	Pb206/ U238	1s%	roh	238/206	1s%	207/206	1s%	Pb207/ Pb206	1s	Pb207/ U235	1s	Pb206/ U238	1s	conc	Th/U	U	Th	Pbtot	>LLD (%)
NEP-S-1_01	12.6208	1.003581	0.50235	0.935603	0.386233	1.990644	0.935603	0.1822	1.075741	2673	17.72	2651.8	9.44	2623.9	20.15	98.16311	0.22394	129.4217	28.98271	81.15834	-
NEP-S-1_02	12.6271	1.00229	0.50204	0.934189	0.385875	1.991873	0.934189	0.1824	1.074561	2674.9	17.69	2652.2	9.43	2622.6	20.12	98.04479	0.534859	246.4396	131.8106	165.3508	0.079368
NEP-S-1_03	13.2514	1.043512	0.52012	0.947858	0.376276	1.922633	0.947858	0.18477	1.1149	2696.2	18.27	2697.7	9.85	2699.7	20.91	100.1298	0.378136	65.25746	24.6762	43.77728	-
NEP-S-1_04	13.2545	1.095481	0.51916	0.966947	0.371308	1.926188	0.966947	0.18515	1.161221	2699.6	19.05	2697.9	10.34	2695.6	21.29	99.85183	0.454568	86.39844	39.274	58.97188	0.482145
NEP-S-1_05	12.2612	1.018988	0.49503	0.937317	0.380232	2.02008	0.937317	0.17963	1.091132	2649.4	17.99	2624.6	9.57	2592.4	20.02	97.84857	0.483732	107.0084	51.76343	70.0237	-
NEP-S-1_06	12.947	1.018384	0.50652	0.937771	0.381696	1.974256	0.937771	0.18537	1.089712	2701.5	17.89	2675.8	9.6	2641.7	20.32	97.78641	0.673341	149.7292	100.8189	104.0036	-
NEP-S-1_07	12.4949	1.069719	0.50277	0.954711	0.37307	1.988981	0.954711	0.18023	1.137435	2655	18.74	2642.3	10.06	2625.7	20.58	98.89642	0.337464	82.97329	28.00054	53.22611	1.074071
NEP-S-1_08	12.83	1.022446	0.51135	0.936736	0.37943	1.955608	0.936736	0.18196	1.093647	2670.8	18	2667.3	9.63	2662.4	20.44	99.68549	0.209741	192.4878	40.37258	122.0977	0.258279
NEP-S-1_09	13.1396	1.045691	0.51679	0.940421	0.371028	1.935022	0.940421	0.18439	1.117197	2692.8	18.32	2689.7	9.87	2685.5	20.65	99.72891	0.437228	140.2901	61.33881	94.59371	0.626648
NEP-S-1_10	12.3594	1.041072	0.49704	0.93755	0.369059	2.011911	0.93755	0.18033	1.114623	2655.9	18.32	2632.1	9.78	2601.1	20.06	97.93667	0.237422	296.2938	70.34678	183.6207	-
NEP-S-1_11	12.6426	1.041876	0.51125	0.936919	0.368616	1.95599	0.936919	0.17934	1.1152	2646.7	18.35	2653.4	9.8	2662	20.42	100.5781	0.131653	423.669	55.7774	263.4123	0.189763
NEP-S-1_12	11.9901	1.057127	0.4844	0.939306	0.369371	2.06441	0.939306	0.17951	1.125285	2648.3	18.58	2603.6	9.91	2546.4	19.78	96.15225	0.243751	259.2733	63.19803	156.7352	0.271567
NEP-S-1_13	13.0162	1.079044	0.51224	0.946822	0.366946	1.95221	0.946822	0.18428	1.144997	2691.7	18.83	2680.8	10.17	2666.2	20.67	99.05264	0.502263	84.75839	42.57101	57.67156	0.803143
NEP-S-1_14	11.7379	1.063049	0.48671	0.938957	0.365734	2.054612	0.938957	0.1749	1.132075	2605.1	18.75	2583.7	9.95	2556.4	19.82	98.13059	0.228116	327.1719	74.63309	196.9405	-
NEP-S-1_15	12.4959	1.199514	0.49935	0.987283	0.346759	2.002603	0.987283	0.18148	1.261847	2666.4	20.73	2642.4	11.28	2611	21.21	97.92229	0.721247	63.86254	46.06066	44.46863	0.33485
NEP-S-1_16	13.4451	1.086348	0.5256	0.945586	0.361916	1.902588	0.945586	0.18551	1.153577	2702.8	18.93	2711.4	10.27	2722.9	20.98	100.7437	0.470459	127.2824	59.88119	88.15291	0.193613
NEP-S-3_01	12.1481	1.161083	0.48348	0.953504	0.343063	2.068338	0.953504	0.18222	1.223795	2673.2	20.16	2615.9	10.89	2542.4	20.04	95.10699	0.689419	138.6422	95.58248	92.78654	0.493271
NEP-S-3_02	12.8596	1.161779	0.50646	0.951704	0.338772	1.97449	0.951704	0.18414	1.227327	2690.5	20.14	2669.4	10.95	2641.5	20.63	98.17878	0.864871	150.3013	129.9912	108.6647	0.108556
NEP-S-3_03	11.0885	1.167063	0.45608	0.951587	0.338968	2.192598	0.951587	0.17632	1.230717	2618.5	20.36	2530.6	10.87	2422.2	19.21	92.50334	0.582938	177.1427	103.2633	108.7229	0.33742
NEP-S-3_04	13.0302	1.17834	0.51557	0.954284	0.334207	1.939601	0.954284	0.18328	1.243998	2682.8	20.41	2681.8	11.11	2680.4	20.91	99.91054	0.302574	159.7463	48.33502	105.0306	0.415444
NEP-S-3_05	13.2491	1.205518	0.51573	0.961744	0.333655	1.938999	0.961744	0.18631	1.266706	2709.8	20.78	2697.6	11.38	2681	21.1	98.93719	0.504418	117.8755	59.45847	80.72278	0.425709
NEP-S-3_06	13.2776	1.194489	0.52068	0.954521	0.329108	1.920565	0.954521	0.18493	1.259936	2697.6	20.64	2699.6	11.28	2702.1	21.07	100.1668	0.786771	161.8037	127.3024	118.2694	-
NEP-S-3_07	13.0378	1.206488	0.51312	0.956891	0.328577	1.948862	0.956891	0.18427	1.269876	2691.7	20.84	2682.4	11.38	2669.9	20.91	99.1901	0.692855	146.6954	101.6387	104.0888	0.470313
NEP-S-3_08	12.1491	1.225198	0.48809	0.960888	0.32205	2.048802	0.960888	0.18051	1.290787	2657.6	21.2	2616	11.49	2562.4	20.32	96.41782	0.546095	102.1107	55.76219	66.53307	0.314311
NEP-S-3_09	13.1213	1.287298	0.51663	0.971682	0.315152	1.935621	0.971682	0.18419	1.346436	2690.9	22.1	2688.4	12.15	2684.9	21.34	99.77703	0.516721	125.1783	64.68226	86.0819	-
NEP-S-3_10	13.3522	1.28084	0.52301	0.965565	0.314754	1.912009	0.965565	0.18514	1.339527	2699.5	21.99	2704.9	12.1	2711.9	21.38	100.4593	0.426598	100.3739	42.81932	68.54198	0.71321
NEP-S-3_11	11.6501	1.28583	0.4712	0.963497	0.306731	2.122241	0.963497	0.1793	1.349693	2646.4	22.19	2576.7	12.02	2488.8	19.91	94.04474	0.288581	272.7014	78.69657	161.9264	-
NEP-S-3_12	11.7361	1.32446	0.48022	0.976636	0.308085	2.082379	0.976636	0.17723	1.382384	2627.1	22.83	2583.6	12.39	2528.2	20.43	96.23539	0.48876	84.97089	41.53038	53.58295	1.262979
NEP-S-3_13	12.6991	1.319545	0.50976	0.971045	0.306115	1.961707	0.971045	0.18066	1.37828	2658.9	22.68	2657.6	12.42	2655.6	21.15	99.87589	0.696189	118.8267	82.72583	84.18858	0.876957
NEP-S-3_14	12.967	1.31773	0.51576	0.967504	0.304877	1.938886	0.967504	0.18233	1.376625	2674.2	22.63	2677.3	12.42	2681.2	21.23	100.2618	0.794297	229.9785	182.6712	165.7174	-
NEP-S-3_15	13.2307	1.334018	0.51652	0.971889	0.300874	1.936033	0.971889	0.18576	1.394272	2705	22.82	2696.3	12.59	2684.4	21.33	99.23845	0.559634	256.5343	143.5654	178.1335	0.257433
NEP-S-3_16	13.3454	1.351398	0.5198	0.975375	0.296777	1.923817	0.975375	0.18619	1.412536	2708.8	23.08	2704.4	12.77	2698.3	21.5	99.61237	0.798337	97.86401	78.12845	71.41735	-

14SV003/NEP-Q:

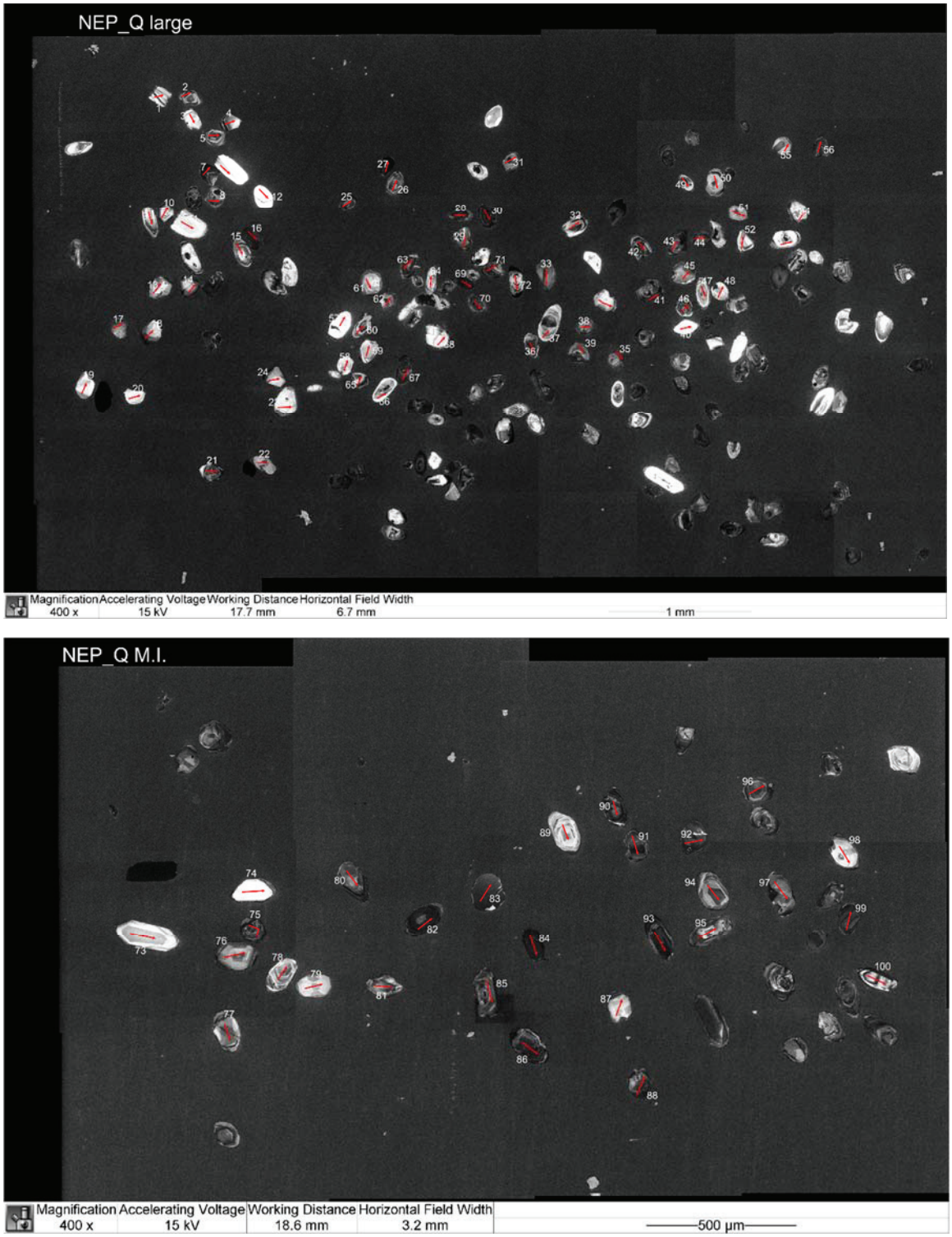

Figure C.3: Annotated CL images of zircon grains from sample 14SV003/NEP-Q.

Table C.2: U-Pb analytical data for sample 14SV003/NEP-Q.

	Isotope ratios									Age estimates (ma)							Concentrations (ppm)				
	Concordia output					Terra-Wasserburg output															Pb com.
Analysis_#	Pb207/U235	1s%	Pb206/U238	1s%	roh	238/206	1s%	207/206	1s%	Pb207/Pb206	1s	Pb207/U235	1s	Pb206/U238	1s	conc	Th/U	U	Th	Pbtot	>LLD (%)
NEPQ_042	6.0602	1.387752	0.2944	1.344972	0.579958	3.396393	1.344972	0.14925	1.252931	2337.3	21.36	1984.5	12.09	1663.6	19.72	71.17614	0.820761	325.4625	267.1269	130.6894	0.635081
NEPQ_029	6.9895	1.223975	0.3354	1.136059	0.548039	2.981781	1.136059	0.15117	1.124562	2359.2	19.08	2110.1	10.87	1864.4	18.37	79.02679	0.834251	139.9252	116.7327	62.51379	-
NEPQ_088	8.9362	1.373513	0.3814	1.329174	0.56593	2.621644	1.329174	0.16988	1.259713	2556.5	20.92	2331.5	12.54	2083	23.68	81.47858	1.144983	213.809	244.8075	117.5649	-
NEPQ_090	10.051	1.37165	0.4022	1.327797	0.566013	2.486511	1.327797	0.18123	1.25807	2664.2	20.71	2439.5	12.67	2179	24.56	81.78815	0.81695	214.5813	175.3022	118.4815	-
NEPQ_045	10.108	1.417531	0.4112	1.354737	0.567634	2.432202	1.354737	0.17827	1.290178	2636.9	21.28	2444.7	13.1	2220.2	25.44	84.19735	0.740037	77.05509	57.02362	43.22831	-
NEPQ_093	8.6923	1.365802	0.3859	1.326872	0.565885	2.591546	1.326872	0.16335	1.254974	2490.6	20.97	2306.3	12.44	2103.7	23.8	84.46559	1.101548	402.8313	443.738	221.6319	0.322496
NEPQ_007	8.1828	1.173198	0.3776	1.144189	0.594862	2.648586	1.144189	0.15719	1.043323	2425.6	17.58	2251.4	10.62	2064.9	20.2	85.12945	1.845014	243.8202	449.8518	131.2333	-
NEPQ_058	11.538	1.412186	0.4394	1.351936	0.56391	2.275986	1.351936	0.19043	1.291813	2745.8	21.05	2567.7	13.2	2347.8	26.59	85.50514	0.755419	63.193	47.73719	38.00023	-
NEPQ_075	9.0681	1.38188	0.3973	1.336522	0.568871	2.51699	1.336522	0.16551	1.262764	2512.7	21.09	2344.9	12.64	2156.6	24.48	85.82799	0.777982	234.5795	182.4986	130.2518	0.56195
NEPQ_085	10.084	1.375176	0.417	1.330871	0.566528	2.397967	1.330871	0.17534	1.260408	2609.3	20.83	2442.5	12.7	2246.9	25.26	86.11122	0.567735	164.0557	93.14012	90.53463	-
NEPQ_077	12.04	1.392722	0.4525	1.339375	0.565111	2.210189	1.339375	0.19296	1.274876	2767.6	20.79	2607.5	13.06	2406.1	26.91	86.93814	0.482155	138.3789	66.72003	83.66799	-
NEPQ_066	11.717	1.430792	0.4525	1.354726	0.555134	2.209994	1.354726	0.18777	1.315439	2722.8	21.5	2582.1	13.39	2406.3	27.2	88.37594	1.03439	94.10303	97.33923	61.82161	1.126394
NEPQ_095	10.432	1.409278	0.4318	1.338614	0.552352	2.315941	1.338614	0.17518	1.301518	2607.8	21.54	2473.9	13.06	2313.8	26.01	88.72613	1.439117	78.62296	113.1476	52.7219	-
NEPQ_005	10.488	1.211431	0.4346	1.155085	0.580079	2.300966	1.155085	0.17503	1.085528	2606.4	17.97	2478.9	11.23	2326.4	22.57	89.25721	0.859771	113.7364	97.78732	69.63768	-
NEPQ_006	12.392	1.213844	0.4705	1.158441	0.579578	2.125579	1.158441	0.19104	1.088777	2751.1	17.78	2634.6	11.4	2485.6	23.87	90.34931	0.901722	54.52823	49.16929	35.7998	-
NEPQ_041	11.565	1.375788	0.4579	1.343205	0.58465	2.184074	1.343205	0.18315	1.239421	2681.6	20.38	2569.8	12.86	2430.1	27.2	90.62127	0.724598	159.2612	115.4004	98.47715	-
NEPQ_097	10.957	1.38035	0.449	1.32971	0.560307	2.22732	1.32971	0.17696	1.271474	2624.6	20.99	2519.5	12.84	2390.7	26.54	91.08817	0.848528	115.4054	97.92473	70.63815	-
NEPQ_081	11.262	1.374702	0.4544	1.331485	0.568592	2.200801	1.331485	0.17973	1.257442	2650.4	20.72	2545.1	12.82	2414.7	26.83	91.107	0.794636	123.8409	98.40844	79.4215	-
NEPQ_032	11.982	1.221787	0.4668	1.13539	0.54853	2.142245	1.13539	0.18619	1.122509	2708.8	18.4	2603	11.45	2469.5	23.31	91.16583	0.625047	71.47066	44.67256	43.99065	-
NEPQ_069	10.967	1.380825	0.4495	1.33719	0.570438	2.224942	1.33719	0.17695	1.260243	2624.5	20.79	2520.4	12.85	2392.8	26.74	91.17165	1.115892	179.3461	200.1309	117.0319	-
NEPQ_030	9.8839	1.200839	0.4296	1.128878	0.558318	2.327584	1.128878	0.16687	1.096662	2526.5	18.32	2424	11.07	2304	21.89	91.19335	0.961109	125.326	120.452	74.63478	-
NEPQ_062	11.666	1.426428	0.4624	1.353718	0.559422	2.162489	1.353718	0.18294	1.306439	2679.7	21.45	2578	13.34	2450.3	27.61	91.43934	1.110154	93.71707	104.0404	63.30331	-
NEPQ_099	11.622	1.373831	0.463	1.326277	0.562522	2.16006	1.326277	0.18203	1.263528	2671.5	20.78	2574.4	12.84	2452.6	27.06	91.8061	0.737391	153.1679	112.9446	96.46422	-
NEPQ_100	12.54	1.405854	0.4793	1.337339	0.55043	2.086332	1.337339	0.18971	1.301987	2739.6	21.23	2645.7	13.22	2524.2	27.92	92.13754	0.428277	105.2522	45.07714	64.8455	-
NEPQ_092	11.664	1.384025	0.4655	1.332044	0.56243	2.148458	1.332044	0.18171	1.271256	2668.6	20.93	2577.8	12.94	2463.6	27.27	92.31807	1.067852	143.1985	152.9147	96.81201	-
NEPQ_080	11.134	1.382365	0.4565	1.336342	0.566446	2.190724	1.336342	0.17687	1.266467	2623.8	20.89	2534.4	12.88	2423.9	26.98	92.38128	0.822064	119.1425	97.94272	75.21081	-
NEPQ_084	11.009	1.370327	0.4549	1.330109	0.569421	2.198527	1.330109	0.17551	1.25349	2610.9	20.73	2523.9	12.76	2416.8	26.81	92.56578	0.744221	313.9392	233.6401	191.4197	-
NEPQ_003	11.816	1.220268	0.4707	1.160024	0.579362	2.124586	1.160024	0.18208	1.092926	2671.9	17.99	2590	11.42	2486.6	23.94	93.06486	1.307732	46.58382	60.91916	33.3081	-
NEPQ_046	13.132	1.385315	0.4925	1.346302	0.580479	2.030622	1.346302	0.19336	1.251552	2770.9	20.41	2689.2	13.07	2581.3	28.64	93.15746	0.80205	129.5558	103.9102	87.74018	-
NEPQ_064	13.965	1.405967	0.5059	1.349962	0.566488	1.976519	1.349962	0.20015	1.284037	2827.4	20.79	2747.3	13.32	2639.3	29.23	93.34724	0.578654	78.89353	45.65204	53.03773	-
NEPQ_023	12.413	1.346747	0.4819	1.186919	0.517255	2.075033	1.186919	0.18682	1.252543	2714.3	20.5	2636.2	12.66	2535.6	24.86	93.41635	1.022677	37.92928	38.78939	26.33387	-
NEPQ_025	12.13	1.198289	0.4783	1.133227	0.561932	2.090825	1.133227	0.18395	1.092688	2688.8	17.92	2614.5	11.24	2519.8	23.64	93.71467	0.930559	91.47689	85.12467	60.84394	-
NEPQ_028	11.842	1.185447	0.4735	1.127748	0.564615	2.111888	1.127748	0.1814	1.080485	2665.7	17.76	2592	11.1	2498.9	23.36	93.74273	0.645624	128.0379	82.66427	81.26572	-
NEPQ_002	11.154	1.180691	0.4615	1.148404	0.594025	2.1668	1.148404	0.17528	1.049749	2608.7	17.34	2536	11	2446.2	23.38	93.77084	0.438282	122.5314	53.70334	72.33441	-
NEPQ_087	11.961	1.408142	0.4757	1.341322	0.557775	2.102386	1.341322	0.18235	1.294214	2674.4	21.31	2601.4	13.19	2508.3	27.88	93.78926	0.859448	59.08699	50.7822	38.88921	-
NEPQ_021	14.317	1.177584	0.5134	1.133619	0.577502	1.947799	1.133619	0.20226	1.062988	2844.5	17.2	2770.9	11.18	2671.1	24.77	93.90403	0.711232	117.0818	83.27237	81.697	-
NEPQ_068	12.685	1.412294	0.4892	1.349279	0.562906	2.044363	1.349279	0.18805	1.29221	2725.2	21.16	2656.6	13.29	2567	28.55	94.19492	0.93346	56.35639	52.60644	38.5996	-
NEPQ_047	15.367	1.414895	0.5301	1.358286	0.571618	1.886508	1.358286	0.21021	1.28443	2907.2	20.69	2838.3	13.49	2741.8	30.31	94.31068	0.590598	62.46023	36.88886	44.89627	-
NEPQ_013	12.638	1.247067	0.4893	1.160913	0.56029	2.043861	1.160913	0.18734	1.131632	2719	18.55	2653	11.73	2567.5	24.6	94.4281	0.771719	60.62667	46.78675	40.36815	-
NEPQ_083	12.419	1.367949	0.4861	1.331057	0.569778	2.057275	1.331057	0.18527	1.252226	2700.7	20.51	2636.6	12.85	2553.7	28.05	94.55697	0.917376	171.7891	157.5953	118.1958	-
NEPQ_026	12.742	1.207676	0.4917	1.136918	0.560198	2.033843	1.136918	0.18797	1.10124	2724.5	18.04	2660.8	11.37	2577.9	24.14	94.6192	0.896918	76.55464	68.66326	51.73766	-
NEPQ_059	13.338	1.434237	0.5013	1.358414	0.560151	1.994734	1.358414	0.19293	1.311356	2767.3	21.39	2703.9	13.55	2619.5	29.26	94.65905	0.580957	73.06321	42.4466	48.7104	1.684482

Table C.2: Continued. U-Pb analytical data for sample 14SV003/NEP-Q.

	Isotope ratios									Age estimates (ma)							Concentrations (ppm)				Pb com.
	Concordia output					Terra-Wasserburg output															
Analysis_#	Pb207/U235	1s%	Pb206/U238	1s%	roh	238/206	1s%	207/206	1s%	Pb207/Pb206	1s	Pb207/U235	1s	Pb206/U238	1s	conc	Th/U	U	Th	Pbtot	>LLD (%)
NEPQ_072	13.002	1.412415	0.4962	1.348138	0.560853	2.015154	1.348138	0.18999	1.294805	2742.1	21.14	2679.8	13.32	2597.6	28.82	94.73032	0.874011	73.57046	64.3014	49.67003	-
NEPQ_053	13.165	1.465297	0.4994	1.369726	0.551995	2.002523	1.369726	0.19116	1.344424	2752.2	21.94	2691.5	13.83	2611.1	29.43	94.87319	0.767501	45.76541	35.12501	30.81003	-
NEPQ_094	12.505	1.386131	0.4888	1.331969	0.558831	2.046036	1.331969	0.18552	1.27749	2702.9	20.91	2643.1	13.03	2565.3	28.19	94.90917	1.154448	115.6076	133.4629	82.11581	-
NEPQ_014	11.625	1.200467	0.4739	1.145763	0.577664	2.110061	1.145763	0.1779	1.079258	2633.4	17.85	2574.7	11.22	2500.7	23.75	94.96089	0.865375	62.70915	54.26691	40.48893	-
NEPQ_054	14.762	1.472393	0.5241	1.375718	0.551539	1.908069	1.375718	0.20424	1.351351	2860.4	21.84	2800	14	2716.5	30.49	94.96924	1.200975	49.35764	59.27729	38.44198	-
NEPQ_009	14.591	1.262602	0.5218	1.172841	0.557067	1.916406	1.172841	0.20281	1.148859	2848.9	18.56	2789	12	2706.8	25.9	95.01211	0.483001	46.1214	22.27667	31.57135	-
NEPQ_091	12.049	1.381293	0.4815	1.331312	0.563863	2.076929	1.331312	0.18146	1.267497	2666.3	20.88	2608.2	12.95	2533.7	27.89	95.02682	0.943392	166.0161	156.6183	112.6301	-
NEPQ_024	12.544	1.224028	0.4899	1.145062	0.558956	2.041108	1.145062	0.1857	1.114701	2704.5	18.31	2646	11.51	2570.4	24.27	95.0416	0.878651	51.61008	45.34723	35.74819	-
NEPQ_086	12.565	1.372346	0.4911	1.331623	0.568833	2.036121	1.331623	0.18551	1.255997	2702.8	20.6	2647.6	12.91	2575.6	28.26	95.29377	1.1962	201.8765	241.4846	147.5795	0.467991
NEPQ_043	12.608	1.392195	0.492	1.349539	0.57842	2.032438	1.349539	0.18581	1.259351	2705.4	20.65	2650.8	13.1	2579.4	28.67	95.34265	0.875414	99.39368	87.01064	67.19545	-
NEPQ_010	13.516	1.203282	0.5072	1.14938	0.578238	1.971492	1.14938	0.19326	1.081445	2770.1	17.63	2716.4	11.38	2644.8	24.95	95.4767	0.722503	55.23084	39.90446	37.88673	-
NEPQ_011	14.44	1.255203	0.5218	1.167047	0.558283	1.916333	1.167047	0.2007	1.141006	2831.9	18.47	2779.1	11.92	2706.9	25.82	95.586	0.864559	42.60378	36.83349	31.18604	1.806026
NEPQ_055	13.11	1.43627	0.5015	1.359866	0.559778	1.993938	1.359866	0.18956	1.313568	2738.3	21.45	2687.6	13.55	2620.3	29.3	95.69076	0.719651	55.27767	39.78064	37.48806	-
NEPQ_074	10.344	1.60537	0.4526	1.398586	0.502784	2.209456	1.398586	0.16573	1.508478	2515	25.16	2466.1	14.86	2406.8	28.09	95.69781	1.437582	21.76526	31.28935	15.57422	5.613696
NEPQ_034	13.465	1.458161	0.5075	1.371429	0.559138	1.970443	1.371429	0.19238	1.3307	2762.6	21.67	2712.8	13.78	2645.9	29.77	95.77572	0.589237	42.09801	24.80568	28.55795	-
NEPQ_063	12.35	1.372097	0.4893	1.338538	0.577806	2.043569	1.338538	0.18302	1.245765	2680.4	20.45	2631.4	12.89	2567.8	28.34	95.79913	1.180561	164.3282	193.9995	116.2953	-
NEPQ_036	14.37	1.3869	0.5221	1.348297	0.580763	1.915195	1.348297	0.19956	1.252756	2822.6	20.28	2774.5	13.17	2708.3	29.83	95.95054	1.104684	105.0846	116.0853	78.97262	-
NEPQ_098	12.306	1.403115	0.4894	1.336385	0.554498	2.043402	1.336385	0.18234	1.294285	2674.3	21.3	2628	13.18	2568	28.3	96.02513	1.200088	57.15127	68.58657	40.25907	-
NEPQ_019	12.87	1.304808	0.499	1.174372	0.533516	2.004048	1.174372	0.18707	1.202758	2716.6	19.7	2670.2	12.29	2609.5	25.21	96.05757	1.023048	32.16035	32.90158	22.67058	-
NEPQ_048	13.034	1.535946	0.5022	1.393978	0.534731	1.991397	1.393978	0.18821	1.418628	2726.5	23.21	2682.1	14.48	2623.1	30.05	96.20759	1.73907	38.57926	67.09204	30.04067	-
NEPQ_016	12.696	1.196113	0.4977	1.143167	0.577918	2.009081	1.143167	0.185	1.075676	2698.3	17.68	2657.4	11.26	2604.1	24.5	96.50891	1.142047	115.1181	131.4703	82.64436	-
NEPQ_033	12.851	1.401865	0.5011	1.353077	0.576126	1.995689	1.353077	0.18597	1.269022	2706.8	20.76	2668.8	13.21	2618.4	29.12	96.73415	1.040996	87.14556	90.71816	62.30227	-
NEPQ_027	12.087	1.186695	0.4882	1.128705	0.565605	2.048467	1.128705	0.17958	1.080298	2649	17.8	2611.1	11.13	2562.7	23.87	96.74217	0.610091	194.9667	118.9475	125.8698	-
NEPQ_012	12.688	1.33719	0.4986	1.19136	0.531926	2.005656	1.19136	0.18457	1.229886	2694.3	20.21	2656.8	12.59	2607.7	25.54	96.78581	0.862362	28.29097	24.39705	19.22196	4.954548
NEPQ_050	12.915	1.397481	0.5023	1.34971	0.572206	1.990723	1.34971	0.18643	1.271255	2710.9	20.78	2673.4	13.17	2623.8	29.07	96.78704	0.676353	63.20668	42.75003	43.41728	-
NEPQ_067	12.419	1.372989	0.4941	1.335897	0.573873	2.024087	1.335897	0.18228	1.250823	2673.7	20.54	2636.6	12.9	2588.2	28.49	96.80218	0.666803	236.2015	157.4999	156.0705	-
NEPQ_082	12.186	1.363171	0.4901	1.328409	0.570436	2.040566	1.328409	0.18032	1.247782	2655.8	20.5	2618.9	12.79	2570.9	28.17	96.80322	1.118255	268.1883	299.903	192.6968	-
NEPQ_017	12.609	1.184943	0.4974	1.137871	0.5794	2.010374	1.137871	0.18386	1.066028	2688	17.54	2650.9	11.15	2602.7	24.35	96.82664	0.618209	96.32927	59.55159	63.53358	-
NEPQ_089	12.927	1.381947	0.5031	1.331717	0.561052	1.987637	1.331717	0.18631	1.272073	2709.9	20.79	2674.3	13.02	2627.1	28.74	96.94454	1.133902	94.13167	106.7361	67.81933	-
NEPQ_037	16.133	1.396533	0.5518	1.351964	0.580473	1.812284	1.351964	0.212	1.259434	2920.9	20.27	2884.7	13.35	2832.6	31.01	96.97696	0.385415	66.90188	25.78498	48.29975	-
NEPQ_052	13.244	1.421647	0.5089	1.355972	0.563976	1.965177	1.355972	0.18872	1.29822	2731	21.18	2697.2	13.42	2651.8	29.49	97.09996	0.78111	50.99436	39.83221	35.2587	-
NEPQ_020	12.866	1.251538	0.5034	1.156207	0.551247	1.98661	1.156207	0.18538	1.143597	2701.6	18.77	2669.9	11.79	2628.3	24.96	97.28679	0.973929	38.22502	37.22844	26.87818	-
NEPQ_056	12.575	1.384048	0.4995	1.343451	0.577376	2.002162	1.343451	0.18257	1.254313	2676.4	20.63	2648.4	13.02	2611.5	28.85	97.5751	0.951491	99.29239	94.47582	69.08223	-
NEPQ_096	12.509	1.371764	0.4993	1.327806	0.56426	2.002724	1.327806	0.18165	1.260666	2668	20.73	2643.4	12.9	2610.9	28.49	97.85982	1.005927	156.3817	157.3087	110.6318	-
NEPQ_044	13.234	1.415394	0.5125	1.355992	0.569282	1.951067	1.355992	0.18723	1.287187	2718	21.04	2696.5	13.36	2667.4	29.62	98.13834	1.011962	91.66364	92.76008	67.62468	-
NEPQ_018	11.348	1.195888	0.4797	1.138283	0.574257	2.084767	1.138283	0.17159	1.078151	2573.2	17.95	2552.2	11.16	2525.8	23.81	98.15794	0.815776	74.13251	60.47553	48.14116	-
NEPQ_008	12.712	1.180438	0.5045	1.145598	0.592289	1.982003	1.145598	0.18274	1.050673	2677.9	17.29	2658.6	11.11	2633.3	24.77	98.33452	0.848427	98.82077	83.84224	68.16214	-
NEPQ_038	12.851	1.404352	0.5071	1.35279	0.573884	1.971998	1.35279	0.18375	1.273469	2687	20.86	2668.8	13.23	2644.2	29.36	98.40715	0.936007	80.43002	75.28303	58.14904	-
NEPQ_070	13.165	1.394668	0.5135	1.343693	0.567092	1.947382	1.343693	0.18591	1.27481	2706.3	20.88	2691.6	13.16	2671.6	29.37	98.71781	0.816407	117.6953	96.0873	83.6233	-
NEPQ_015	13.162	1.208128	0.5135	1.148955	0.571738	1.947382	1.148955	0.1859	1.091985	2706.2	17.87	2691.3	11.4	2671.6	25.11	98.72145	0.595546	57.67092	34.34567	38.90739	-
NEPQ_061	12.943	1.523817	0.5099	1.386574	0.532262	1.961207	1.386574	0.18406	1.412583	2689.8	23.15	2675.5	14.36	2656.2	30.19	98.75084	1.667455	41.66551	69.47536	33.04105	-
NEPQ_078	12.86	1.446683	0.5086	1.356745	0.547309	1.966298	1.356745	0.18337	1.336096	2683.6	21.91	2669.5	13.63	2650.5	29.48	98.76658	1.180603	51.5174	60.8216	39.56986	-

Table C.2: Continued. U-Pb analytical data for sample 14SV003/NEP-Q.

	Isotope ratios									Age estimates (ma)							Concentrations (ppm)				
	Concordia output					Terra-Wasserburg output															Pb com.
Analysis_#	Pb207/U235	1s%	Pb206/U238	1s%	roh	238/206	1s%	207/206	1s%	Pb207/Pb206	1s	Pb207/U235	1s	Pb206/U238	1s	conc	Th/U	U	Th	Pbtot	>LLD (%)
NEPQ_065	13.113	1.387276	0.5138	1.340963	0.570845	1.946245	1.340963	0.18506	1.264455	2698.7	20.74	2687.8	13.09	2672.9	29.35	99.04398	0.756486	76.3257	57.7393	53.6587	-
NEPQ_031	12.838	1.207932	0.5093	1.133039	0.556192	1.963672	1.133039	0.18285	1.104731	2678.9	18.18	2667.8	11.38	2653.4	24.64	99.04812	0.956734	66.0802	63.22116	47.43707	-
NEPQ_057	14.931	1.580581	0.543	1.412445	0.522608	1.841519	1.412445	0.19937	1.469629	2821.1	23.82	2810.8	15.04	2796.1	32.04	99.11382	0.540491	25.72219	13.90263	18.46356	-
NEPQ_001	13.661	1.207446	0.5241	1.158198	0.584548	1.908069	1.158198	0.18905	1.07908	2733.9	17.62	2726.5	11.42	2716.5	25.68	99.36355	0.980911	64.10285	62.8792	47.47865	1.881547
NEPQ_022	13.223	1.22026	0.5171	1.144891	0.560618	1.933937	1.144891	0.18549	1.110572	2702.5	18.22	2695.7	11.52	2686.8	25.17	99.41906	1.490938	67.96947	101.3382	52.94698	-
NEPQ_049	17.459	1.378954	0.5822	1.344991	0.581633	1.717741	1.344991	0.21746	1.246206	2962	19.97	2960.4	13.24	2957.5	31.89	99.84808	0.942415	90.86286	85.63051	76.21874	-
NEPQ_073	14.62	1.5774	0.5414	1.405615	0.515472	1.847063	1.405615	0.19582	1.475845	2791.7	23.94	2790.9	14.99	2789.3	31.83	99.91403	0.791827	27.73182	21.95881	21.12886	6.997951
NEPQ_004	14.268	1.20865	0.5361	1.15828	0.582123	1.865184	1.15828	0.19301	1.082845	2768	17.61	2767.7	11.47	2767.3	26.05	99.97471	0.576203	61.91293	35.67444	43.86859	-
NEPQ_071	12.636	1.405719	0.5098	1.345626	0.564357	1.961554	1.345626	0.17974	1.28519	2650.4	21.19	2652.9	13.23	2655.8	29.29	100.2037	0.835749	96.31312	80.49359	67.01644	-
NEPQ_076	13.769	1.450131	0.529	1.359245	0.54634	1.890466	1.359245	0.18875	1.340397	2731.3	21.86	2734	13.73	2737.1	30.32	100.2124	1.480298	43.07903	63.76981	35.07712	-
NEPQ_051	14.546	1.416975	0.5441	1.356418	0.568323	1.837965	1.356418	0.19386	1.28959	2775.2	21	2786	13.46	2800.5	30.8	100.9116	0.851274	50.84149	43.28006	37.99993	-
NEPQ_040	13.602	1.522471	0.5291	1.390963	0.541126	1.889895	1.390963	0.18639	1.40029	2710.6	22.94	2722.4	14.4	2737.8	31.04	101.0035	0.448296	26.21576	11.75243	17.86114	-
NEPQ_060	13.542	1.376648	0.5325	1.34082	0.578932	1.877899	1.34082	0.1844	1.247289	2692.8	20.49	2718.2	13.02	2752	30.02	102.1985	0.524807	150.6733	79.07447	105.1409	-
NEPQ_035	13.834	1.388033	0.5382	1.348866	0.583001	1.857942	1.348866	0.18637	1.250201	2710.4	20.5	2738.4	13.14	2776	30.43	102.4203	0.936869	100.1627	93.83925	74.9124	-
NEPQ_079	13.066	1.517387	0.5259	1.378668	0.529574	1.901611	1.378668	0.18017	1.40978	2654.4	23.22	2684.4	14.31	2724	30.64	102.6221	0.716857	29.92864	21.45455	21.52971	-
NEPQ_039	14.114	1.42335	0.5472	1.359649	0.568449	1.827485	1.359649	0.18702	1.293979	2716.2	21.14	2757.4	13.5	2813.5	31.01	103.5822	1.168803	52.30386	61.13293	40.79759	-

14SV493A:

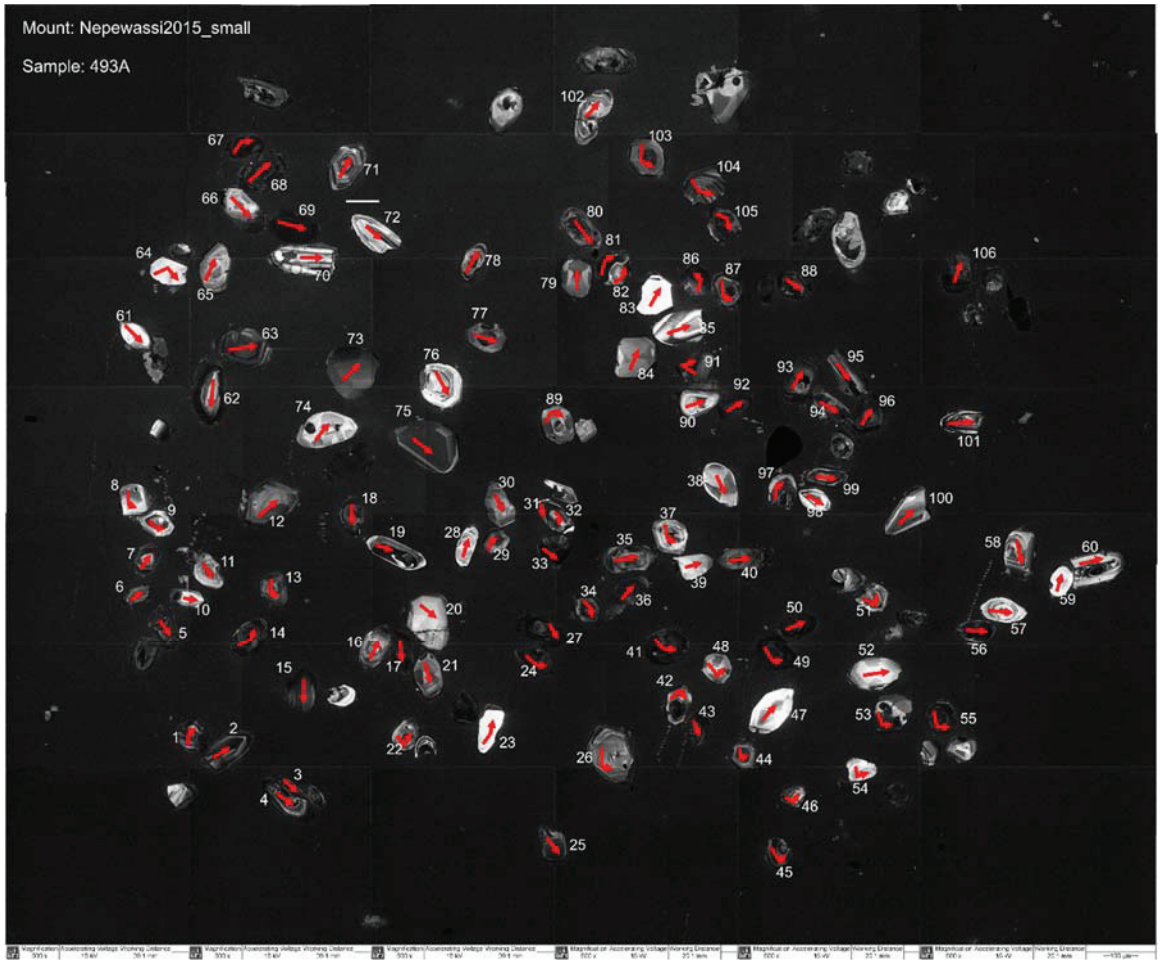

Figure C.4: Annotated CL images of zircon grains from sample 14SV493A.

Table C.3: Zircon U-Pb Analytical data for sample 14SV943A.

	Isotope ratios									Age estimates (ma)							Concentrations (ppm)				
	Concordia output					Terra-Wasserburg output															Pb com.
Analysis_#	Pb207/U235	1s%	Pb206/U238	1s%	roh	238/206	1s%	207/206	1s%	Pb207/Pb206	1s	Pb207/U235	1s	Pb206/U238	1s	conc	Th/U	U	Th	Pbtot	>LLD (%)
493A_80	8.5562	0.946686	0.38531	0.897978	0.353651	2.595313	0.897978	0.16104	1.049429	2466.6	17.67	2291.9	8.61	2101	16.1	85.17798	0.863543	402.5645	347.6319	220.6727	0.299519
493A_43	7.9537	0.931638	0.37432	0.892285	0.344385	2.671511	0.892285	0.1541	1.044776	2391.9	17.67	2225.8	8.4	2049.7	15.65	85.69338	0.970045	362.2457	351.3947	196.7306	-
493A_28	10.048	1.03087	0.41944	0.922659	0.330216	2.384131	0.922659	0.17373	1.133943	2593.9	18.83	2439.2	9.52	2257.9	17.57	87.04653	0.478313	75.39116	36.0606	41.45647	-
493A_54	9.4817	1.112665	0.40976	0.949336	0.320015	2.440453	0.949336	0.16782	1.209629	2536	20.14	2385.8	10.22	2213.8	17.78	87.29495	0.863545	58.92324	50.88288	34.66897	-
493A_94	9.4705	0.973654	0.41076	0.905638	0.345524	2.434512	0.905638	0.16721	1.076491	2529.9	17.93	2384.7	8.94	2218.4	16.99	87.68726	0.866228	232.6062	201.4899	136.2793	-
493A_81	11.142	0.943986	0.45257	0.897099	0.353667	2.209603	0.897099	0.17855	1.047326	2639.4	17.32	2535.1	8.8	2406.7	18.02	91.1836	0.01926	470.1763	9.055579	251.7882	-
493A_72	11.766	1.001709	0.46371	0.916521	0.341205	2.15652	0.916521	0.18402	1.103141	2689.4	18.11	2586	9.37	2455.9	18.73	91.31777	0.811999	153.8775	124.9484	100.6531	0.88219
493A_88	10.226	0.958187	0.43775	0.902342	0.34895	2.284409	0.902342	0.16941	1.062511	2551.8	17.67	2455.4	8.86	2340.5	17.69	91.71957	0.906358	286.8153	259.9574	179.8238	-
493A_50	9.939	0.925748	0.43293	0.891599	0.346716	2.309842	0.891599	0.1665	1.039039	2522.7	17.33	2429.1	8.54	2318.9	17.36	91.92135	0.959549	333.3012	319.8188	209.4625	-
493A_79	11.331	0.996957	0.45994	0.915337	0.344292	2.174197	0.915337	0.17867	1.096994	2640.6	18.11	2550.8	9.3	2439.3	18.58	92.37673	0.857488	112.8537	96.77074	75.44473	-
493A_55	10.624	0.923813	0.4474	0.891819	0.352312	2.235136	0.891819	0.17222	1.033562	2579.3	17.2	2490.8	8.57	2383.7	17.75	92.41655	0.955226	268.6435	256.6152	176.7323	-
493A_33	10.963	0.934609	0.45706	0.892662	0.34499	2.187897	0.892662	0.17395	1.046278	2596	17.37	2520	8.7	2426.6	18.06	93.47458	0.84799	262.7973	222.8494	169.7584	0.521522
493A_91	13.342	0.959853	0.49839	0.902907	0.3523	2.006461	0.902907	0.19414	1.06109	2777.5	17.3	2704.1	9.07	2606.9	19.35	93.85779	0.462701	265.6062	122.8963	176.9992	-
493A_69	13.155	0.930122	0.49749	0.89449	0.353621	2.010091	0.89449	0.19177	1.037701	2757.4	16.96	2690.9	8.78	2603	19.14	94.40052	0.390417	418.2698	163.2995	270.5109	-
493A_007	12.424	0.95	0.48619	0.9	0.34	2.056809	0.9	0.18541	1.06	2701.9	17.44	2637	8.95	2554.2	19	94.53348	1.170765	127.4211	149.1802	94.10477	0.723529
493A_106	11.42	0.970181	0.46891	0.904225	0.349749	2.132605	0.904225	0.17661	1.070155	2621.3	17.69	2558	9.06	2478.8	18.61	94.56377	0.989573	210.9988	208.7987	143.5421	-
493A_68	11.171	0.95437	0.46451	0.902026	0.348107	2.152806	0.902026	0.17441	1.060719	2600.4	17.57	2537.5	8.89	2459.4	18.42	94.57776	0.826818	304.2551	251.5636	201.3638	-
493A_90	12.73	0.969152	0.49178	0.904876	0.348683	2.03343	0.904876	0.18772	1.070744	2722.3	17.53	2659.9	9.12	2578.4	19.24	94.71403	0.914579	129.9019	118.8055	94.38435	-
493A_97	11.676	0.966997	0.47652	0.904474	0.348681	2.098548	0.904474	0.1777	1.069218	2631.5	17.64	2578.8	9.04	2512.1	18.81	95.46266	0.7956	184.355	146.6728	124.6891	-
493A_005	11.983	0.92	0.48311	0.89	0.35	2.069922	0.89	0.17997	1.03	2652.6	17.05	2603	8.62	2540.8	18.67	95.78527	0.594753	307.4373	182.8494	201.6439	0.286118
493A_016	12.423	1.02	0.49073	0.92	0.33	2.03778	0.92	0.18368	1.12	2686.4	18.44	2636.9	9.58	2573.8	19.46	95.80852	1.011822	69.17031	69.98804	49.61095	-
493A_31	13.546	0.93627	0.50898	0.893945	0.340307	1.964714	0.893945	0.19302	1.051704	2768.1	17.12	2718.5	8.85	2652.3	19.45	95.81663	0.337808	307.3958	103.8407	201.9851	0.498548
493A_102	15.086	1.000612	0.53264	0.918068	0.350588	1.877441	0.918068	0.2054	1.095424	2869.6	17.72	2820.7	9.53	2752.6	20.55	95.92278	0.329491	115.0741	37.91594	79.66761	-
493A_105	11.929	0.977219	0.48365	0.907681	0.346453	2.067611	0.907681	0.17887	1.078996	2642.4	17.76	2598.8	9.16	2543.1	19.05	96.24205	0.945391	304.1898	287.5784	214.7007	-
493A_83	14.857	1.023765	0.53092	0.928577	0.346701	1.883523	0.928577	0.20294	1.118557	2850	18.11	2806.1	9.74	2745.3	20.75	96.32632	0.450762	35.64821	16.06886	25.30316	-
493A_56	11.082	0.928681	0.4687	0.891828	0.350338	2.133561	0.891828	0.17148	1.038022	2572.1	17.28	2530.1	8.65	2477.9	18.36	96.33762	0.628718	256.6965	161.3898	164.0251	-
493A_104	12.341	0.970798	0.49126	0.903798	0.349744	2.035582	0.903798	0.18219	1.070311	2672.9	17.61	2630.7	9.12	2576.1	19.21	96.37847	0.750695	159.856	120.003	110.3229	-
493A_53	12.846	0.926661	0.50012	0.891786	0.351249	1.99952	0.891786	0.18628	1.036075	2709.6	17.03	2668.4	8.73	2614.3	19.18	96.48288	0.738224	186.8511	137.938	132.9396	-
493A_024	11.887	1.03	0.48393	0.91	0.32	2.066415	0.91	0.17823	1.13	2636.5	18.69	2595.5	9.62	2544.4	19.1	96.50673	0.773993	203.8393	157.7702	137.8773	0.532093
493A_103	12.594	0.968156	0.49679	0.903802	0.352931	2.012923	0.903802	0.18385	1.066086	2687.9	17.55	2649.8	9.11	2600	19.34	96.72979	0.971962	173.7091	168.8386	128.2536	-
493A_74	12.893	0.98141	0.50222	0.90996	0.343714	1.991159	0.90996	0.18617	1.08503	2708.6	17.76	2671.8	9.25	2623.3	19.63	96.85077	0.658972	79.08824	52.11695	54.39625	-
493A_001	12.473	0.96	0.49559	0.9	0.34	2.017797	0.9	0.18263	1.07	2676.9	17.54	2640.7	8.99	2594.8	19.24	96.93302	1.065515	162.9021	173.5746	120.5803	1.15763
493A_93	12.378	0.973919	0.49391	0.907048	0.350996	2.02466	0.907048	0.18175	1.072902	2668.9	17.68	2633.5	9.15	2587.6	19.33	96.9538	0.681249	189.0272	128.7745	128.4271	-
493A_014	11.898	0.96	0.48589	0.9	0.33	2.058079	0.9	0.17768	1.07	2631.3	17.71	2596.4	9.02	2552.9	18.94	97.02048	0.654289	206.9107	135.3793	138.0591	-
493A_92	12.663	0.954586	0.49936	0.901153	0.354821	2.002563	0.901153	0.1839	1.054921	2688.4	17.37	2654.9	8.98	2611.1	19.33	97.12468	0.722772	252.7157	182.6557	178.0806	-
493A_89	12.737	0.968233	0.50098	0.904228	0.350386	1.996088	0.904228	0.18438	1.068446	2692.6	17.56	2660.4	9.12	2618	19.48	97.22944	0.731663	106.6814	78.05483	76.80633	-
493A_017	12.641	0.98	0.49966	0.9	0.33	2.001361	0.9	0.18358	1.08	2685.4	17.83	2653.3	9.19	2612.3	19.28	97.27787	0.732042	259.0734	189.6527	179.0274	-
493A_96	12.452	0.963858	0.49638	0.902534	0.348598	2.014586	0.902534	0.18193	1.066344	2670.5	17.53	2639.1	9.06	2598.2	19.31	97.29264	0.626986	188.4443	118.1519	127.2941	-
493A_47	13.05	0.941815	0.50659	0.898162	0.343939	1.973983	0.898162	0.18683	1.054435	2714.4	17.25	2683.3	8.88	2642.1	19.45	97.33643	0.83853	91.19003	76.46555	66.00416	-
493A_36	12.653	0.916458	0.50004	0.887929	0.348747	1.99984	0.887929	0.18351	1.029917	2684.9	16.96	2654.2	8.62	2614	19.08	97.35931	0.530182	290.273	153.8975	195.0037	-
493A_65	11.265	0.99361	0.47609	0.913693	0.342467	2.100443	0.913693	0.1716	1.095571	2573.3	18.19	2545.3	9.27	2510.2	18.99	97.5479	0.908223	82.92339	75.31291	56.88995	-
493A_013	12.703	0.99	0.50179	0.91	0.33	1.992866	0.91	0.18369	1.09	2686.4	17.94	2657.9	9.28	2621.5	19.54	97.58413	0.849082	142.3252	120.8457	100.9892	0.837868

Table C.3: *Continued*. Zircon U-Pb Analytical data for sample 14SV943A.

	Isotope ratios									Age estimates (ma)							Concentrations (ppm)				
	Concordia output					Terra-Wasserburg output															Pb com.
Analysis_#	Pb207/ U235	1s%	Pb206/ U238	1s%	roh	238/206	1s%	207/206	1s%	Pb207/ Pb206	1s	Pb207/ U235	1s	Pb206/U 238	1s	conc	Th/U	U	Th	Pbtot	>LLD (%)
493A_87	12.779	0.949444	0.50319	0.898269	0.351087	1.987321	0.898269	0.18418	1.053317	2690.9	17.3	2663.5	8.94	2627.5	19.4	97.64391	0.982923	233.606	229.6167	173.9771	-
493A_67	11.51	0.960184	0.48095	0.902381	0.346282	2.079218	0.902381	0.17356	1.065914	2592.3	17.66	2565.4	8.97	2531.4	18.9	97.65073	0.934515	338.1168	315.9753	236.196	-
493A_020	12.672	1.03	0.50189	0.91	0.32	1.992468	0.91	0.18321	1.14	2682.2	18.64	2655.6	9.71	2621.9	19.7	97.75185	0.960267	53.61142	51.48128	39.09521	-
493A_82	12.71	0.966703	0.50267	0.905166	0.349328	1.989377	0.905166	0.18337	1.068877	2683.6	17.57	2658.4	9.1	2625.3	19.52	97.82755	0.434025	174.493	75.73432	115.7133	-
493A_70	14.767	0.974895	0.53565	0.911043	0.351275	1.866891	0.911043	0.19993	1.075376	2825.6	17.48	2800.3	9.27	2765.2	20.47	97.8624	0.49991	76.75278	38.36947	55.0971	-
493A_84	13.177	0.965094	0.51094	0.904216	0.346936	1.957177	0.904216	0.18703	1.069347	2716.2	17.49	2692.4	9.11	2660.6	19.72	97.95302	0.75603	96.60932	73.03958	69.90297	-
493A_58	13.758	0.965375	0.52083	0.906246	0.34761	1.920012	0.906246	0.19158	1.070049	2755.8	17.48	2733.2	9.14	2702.7	20.01	98.07315	0.787782	88.6526	69.83892	65.26677	-
493A_019	12.788	0.99	0.505	0.9	0.33	1.980198	0.9	0.18374	1.1	2686.9	18.03	2664.1	9.32	2635.3	19.48	98.07957	0.525347	163.8392	86.07249	109.8767	0.520276
493A_66	12.801	0.957497	0.50514	0.90272	0.350479	1.979649	0.90272	0.18378	1.061051	2687.3	17.46	2665.1	9.02	2635.9	19.53	98.0873	0.689773	97.78954	67.45256	68.41892	-
493A_60	12.416	1.020578	0.49884	0.924144	0.341058	2.004651	0.924144	0.18051	1.119052	2657.6	18.44	2636.4	9.59	2608.8	19.83	98.16376	0.637946	66.87604	42.66333	46.19093	1.73164
493A_85	15.431	0.972492	0.54671	0.909074	0.349002	1.829123	0.909074	0.2047	1.074744	2864	17.35	2842.3	9.27	2811.5	20.71	98.1669	0.415856	75.941	31.58051	55.15498	-
493A_006	13.715	0.93	0.52092	0.89	0.35	1.919681	0.89	0.19104	1.04	2751.1	17.06	2730.2	8.82	2703.1	19.74	98.25524	0.709145	186.7359	132.4228	136.3653	-
493A_008	14.48	0.93	0.53296	0.9	0.35	1.876313	0.9	0.19713	1.04	2802.6	16.99	2781.7	8.86	2753.9	20.06	98.26233	0.699067	134.0896	93.73765	100.3324	-
493A_64	11.337	0.985439	0.47999	0.910436	0.346003	2.083377	0.910436	0.17129	1.085878	2570.3	18.08	2551.3	9.2	2527.2	19.04	98.32315	0.592445	53.38889	31.62995	34.71374	1.852739
493A_86	12.291	0.945571	0.49724	0.896951	0.352975	2.011101	0.896951	0.17926	1.048756	2646.1	17.32	2626.9	8.88	2601.9	19.22	98.32962	0.502936	396.6943	199.5119	265.7119	-
493A_59	13.369	0.997674	0.51548	0.917591	0.341985	1.939939	0.917591	0.18809	1.100537	2725.5	17.99	2706.1	9.43	2680	20.12	98.33058	0.676035	61.24254	41.40211	43.6748	1.345486
493A_37	12.822	0.973108	0.50663	0.90796	0.343818	1.973827	0.90796	0.18354	1.078784	2685.1	17.76	2666.6	9.17	2642.2	19.66	98.40229	0.863779	97.61719	84.31969	71.04433	-
493A_009	13.159	0.94	0.5128	0.9	0.34	1.950078	0.9	0.18619	1.05	2708.8	17.28	2691.1	8.89	2668.6	19.55	98.51595	0.697255	159.4133	111.1518	113.6861	-
493A_63	13.118	0.939109	0.51243	0.895732	0.352051	1.951486	0.895732	0.18565	1.044977	2704	17.18	2688.2	8.86	2667	19.58	98.63166	0.961022	147.6085	141.855	111.8294	-
493A_52	14.322	0.994498	0.53193	0.917414	0.34499	1.879947	0.917414	0.19526	1.095975	2787	17.86	2771.3	9.44	2749.6	20.54	98.65806	0.545982	37.80129	20.63884	27.24382	-
493A_003	12.089	0.94	0.49597	0.9	0.35	2.016251	0.9	0.17686	1.05	2623.6	17.41	2611.3	8.83	2596.5	19.15	98.96707	0.343713	277.3735	95.33696	175.7027	-
493A_41	12.535	0.933499	0.50376	0.893283	0.343195	1.985072	0.893283	0.18045	1.047382	2657	17.23	2645.3	8.78	2630	19.3	98.98382	0.644469	223.7939	144.2282	155.2733	-
493A_29	13.708	0.928065	0.52377	0.891613	0.343285	1.909235	0.891613	0.18981	1.043148	2740.5	17.05	2729.8	8.78	2715.2	19.75	99.07681	0.515645	136.8735	70.57805	96.83081	0.711956
493A_101	13.966	0.975914	0.52797	0.907249	0.351501	1.894047	0.907249	0.19184	1.073812	2758	17.55	2747.4	9.25	2732.9	20.21	99.08992	0.809376	210.1741	170.1099	157.2676	-
493A_004	12.495	0.94	0.50363	0.9	0.34	1.985585	0.9	0.18003	1.05	2653.1	17.28	2642.4	8.8	2629.4	19.32	99.10671	1.499712	188.7981	283.1428	151.1605	-
493A_012	13.141	0.97	0.51483	0.9	0.34	1.942389	0.9	0.18521	1.07	2700.1	17.64	2689.8	9.12	2677.2	19.74	99.15188	0.78043	82.11323	64.08364	59.19783	-
493A_27	12.764	0.919552	0.50835	0.887184	0.340429	1.967149	0.887184	0.1821	1.037891	2672.1	17.04	2662.4	8.66	2649.6	19.29	99.15797	0.79528	310.0225	246.5547	224.6661	0.536133
493A_25	12.819	0.925651	0.50944	0.889212	0.34232	1.96294	0.889212	0.18249	1.041153	2675.6	17.12	2666.4	8.72	2654.2	19.36	99.20018	0.534381	164.8789	88.10815	112.4633	0.589895
493A_011	12.641	0.98	0.50659	0.9	0.34	1.973983	0.9	0.18105	1.08	2662.5	17.83	2653.2	9.17	2642.1	19.61	99.2338	0.867587	127.0899	110.2615	91.06788	0.672989
493A_51	12.638	0.962909	0.50677	0.903763	0.340938	1.973282	0.903763	0.18086	1.072653	2660.7	17.63	2653	9.06	2642.8	19.61	99.32724	0.786103	133.9811	105.3229	96.04383	-
493A_76	14.499	0.969745	0.5373	0.908245	0.348399	1.861158	0.908245	0.19569	1.073126	2790.6	17.45	2782.9	9.21	2772.2	20.45	99.34064	0.475963	72.54137	34.52701	51.8237	-
493A_018	12.795	0.99	0.50968	0.9	0.33	1.962015	0.9	0.18215	1.1	2672.5	18.03	2664.6	9.31	2655.3	19.61	99.35641	0.707269	168.9311	119.4796	119.2945	-
493A_100	14.202	0.991259	0.53297	0.913747	0.351454	1.876278	0.913747	0.19325	1.086675	2770	17.75	2763.3	9.4	2753.9	20.47	99.41877	1.061401	99.18543	105.2755	79.03939	-
493A_62	12.832	0.964393	0.5106	0.904818	0.346128	1.95848	0.904818	0.18226	1.0699	2673.5	17.59	2667.4	9.08	2659.2	19.72	99.46512	0.607232	87.03125	52.84817	60.11419	-
493A_78	15.075	0.945975	0.54691	0.8996	0.352847	1.828454	0.8996	0.1999	1.050525	2825.4	17.05	2820	9.01	2812.3	20.49	99.53635	0.592573	165.0157	97.78391	122.9725	-
493A_44	13.308	0.941657	0.51913	0.897656	0.343748	1.9263	0.897656	0.18592	1.054217	2706.4	17.26	2701.8	8.89	2695.5	19.76	99.59725	1.331081	153.6459	204.5152	125.5996	-
493A_38	16.598	0.937341	0.56943	0.897389	0.345364	1.756142	0.897389	0.21139	1.050192	2916.2	16.88	2911.9	8.98	2905.5	20.97	99.63308	0.676742	77.64779	52.54753	62.0096	-
493A_95	12.967	0.9584	0.51355	0.901568	0.352402	1.94723	0.901568	0.18312	1.059415	2681.4	17.43	2677.3	9.03	2671.8	19.72	99.64198	1.283828	252.1404	323.7048	202.5067	-
493A_002	13.535	0.92	0.52324	0.89	0.34	1.911169	0.89	0.18769	1.04	2722	17	2717.7	8.74	2712.9	19.71	99.66569	0.747654	246.2995	184.1467	180.2294	0.450661
493A_71	13.097	0.98198	0.51606	0.910747	0.342663	1.937759	0.910747	0.18405	1.086661	2689.8	17.8	2686.7	9.26	2682.4	20	99.72489	0.886915	138.4344	122.7795	102.4328	-
493A_010	11.967	1.04	0.49692	0.93	0.33	2.012396	0.93	0.17474	1.14	2603.6	18.94	2601.8	9.78	2600.5	19.86	99.88093	0.667586	78.16839	52.18409	53.42624	-
493A_34	12.975	0.919542	0.51461	0.888051	0.346432	1.943219	0.888051	0.18285	1.033634	2678.9	17.01	2677.8	8.67	2676.3	19.47	99.90295	0.589898	210.0272	123.8947	147.4483	-

Table C.3: *Continued*. Zircon U-Pb Analytical data for sample 14SV943A.

	Isotope ratios									Age estimates (ma)							Concentrations (ppm)				
	Concordia output					Terra-Wasserburg output															Pb com.
Analysis_#	Pb207/U235	1s%	Pb206/U238	1s%	roh	238/206	1s%	207/206	1s%	Pb207/Pb206	1s	Pb207/U235	1s	Pb206/U238	1s	conc	Th/U	U	Th	Pbtot	>LLD (%)
493A_40	13.415	0.949095	0.52209	0.900228	0.347392	1.915379	0.900228	0.18635	1.057151	2710.2	17.37	2709.3	8.97	2708	19.89	99.91883	0.748889	113.2851	84.83795	82.99202	-
493A_61	14.357	0.977	0.53756	0.911526	0.348698	1.860257	0.911526	0.19369	1.079044	2773.8	17.6	2773.6	9.27	2773.2	20.53	99.97837	0.490152	50.52342	24.76413	36.34939	-
493A_32	15.109	0.962354	0.54936	0.904689	0.340833	1.8203	0.904689	0.19946	1.072897	2821.8	17.39	2822.1	9.16	2822.5	20.68	100.0248	0.453844	131.1065	59.50198	96.01472	-
493A_42	12.776	0.961239	0.51212	0.904085	0.340407	1.952667	0.904085	0.18093	1.072238	2661.4	17.62	2663.3	9.05	2665.7	19.72	100.1616	0.610603	156.2196	95.3882	110.8476	-
493A_75	13.376	0.950937	0.52266	0.901159	0.350758	1.91329	0.901159	0.1856	1.056034	2703.6	17.32	2706.6	8.98	2710.5	19.92	100.2552	1.674271	128.7368	215.5403	111.5336	-
493A_39	13.298	0.944082	0.52157	0.897291	0.344811	1.917288	0.897291	0.1849	1.054624	2697.3	17.32	2701	8.92	2705.8	19.83	100.3151	0.884725	76.85119	67.99217	57.9881	-
493A_021	13.359	1	0.52282	0.9	0.32	1.912704	0.9	0.1854	1.11	2701.8	18.19	2705.3	9.47	2711.1	19.99	100.3442	0.852374	128.7098	109.7089	95.42149	-
493A_48	13.065	0.967346	0.51785	0.905668	0.340504	1.931061	0.905668	0.18296	1.076738	2679.9	17.67	2684.3	9.12	2690.1	19.92	100.3806	1.050334	81.93583	86.06002	63.38	-
493A_99	11.77	0.977897	0.49512	0.906851	0.346561	2.019712	0.906851	0.1724	1.078886	2581.1	17.88	2586.3	9.15	2592.8	19.36	100.4533	0.916826	128.1184	117.4623	92.21859	-
493A_73	12.993	0.951262	0.51699	0.901371	0.347643	1.934273	0.901371	0.18227	1.058869	2673.6	17.38	2679.2	8.97	2686.4	19.78	100.4788	0.981719	122.5359	120.2958	92.39382	-
493A_45	12.472	0.936823	0.50803	0.895616	0.343599	1.968388	0.895616	0.17804	1.050326	2634.7	17.31	2640.6	8.81	2648.2	19.44	100.5124	0.780325	221.5348	172.8691	158.4933	0.401454
493A_77	13.208	0.946123	0.52159	0.899174	0.352125	1.917215	0.899174	0.18364	1.050969	2686	17.28	2694.6	8.93	2705.9	19.86	100.7409	0.980405	172.3078	168.9315	131.5683	-
493A_46	12.507	0.943857	0.51007	0.897916	0.348864	1.960515	0.897916	0.17783	1.051566	2632.7	17.41	2643.3	8.87	2656.9	19.54	100.9192	0.717236	152.7994	109.5933	108.6824	-
493A_49	11.833	0.934743	0.49837	0.894917	0.347857	2.006541	0.894917	0.1722	1.045296	2579.1	17.36	2591.3	8.75	2606.8	19.18	101.074	0.731413	236.7212	173.141	164.443	-
493A_98	14.421	0.983146	0.5429	0.909928	0.3514	1.84196	0.909928	0.19264	1.079734	2764.8	17.64	2777.8	9.34	2795.6	20.65	101.114	0.594744	102.107	60.72751	75.6577	-
493A_35	13.203	0.927999	0.5229	0.891184	0.343013	1.912412	0.891184	0.18311	1.043089	2681.3	17.13	2694.2	8.76	2711.5	19.74	101.1263	0.641623	125.062	80.24268	89.44356	-
493A_015	13.407	0.96	0.52769	0.89	0.34	1.895052	0.89	0.18435	1.06	2692.4	17.5	2708.7	9.03	2731.7	19.94	101.4597	0.766872	204.4263	156.7688	151.2799	-
493A_023	11.876	1.11	0.50164	0.94	0.31	1.993461	0.94	0.17178	1.21	2575	19.98	2594.6	10.37	2620.8	20.18	101.7786	1.703597	35.25106	60.05359	29.09209	-
493A_30	13.363	0.928865	0.52914	0.892013	0.344525	1.889859	0.892013	0.18315	1.042861	2681.6	17.15	2705.6	8.77	2737.8	19.89	102.0958	0.860026	115.503	99.33564	87.40213	-
493A_022	13.472	1.02	0.53161	0.91	0.32	1.881078	0.91	0.18388	1.13	2688.2	18.49	2713.3	9.65	2748.2	20.34	102.232	0.709407	133.7676	94.89568	98.99808	-
493A_57	14.074	0.990117	0.54192	0.915264	0.343097	1.845291	0.915264	0.18835	1.093709	2727.8	17.87	2754.7	9.39	2791.5	20.74	102.3352	0.660016	81.30986	53.66583	60.60374	-
493A_26	13.395	0.930926	0.53114	0.89242	0.344559	1.882743	0.89242	0.1829	1.044286	2679.4	17.19	2707.9	8.8	2746.3	19.95	102.4968	0.957336	103.5415	99.12405	80.38079	0.710303

14SV557A:

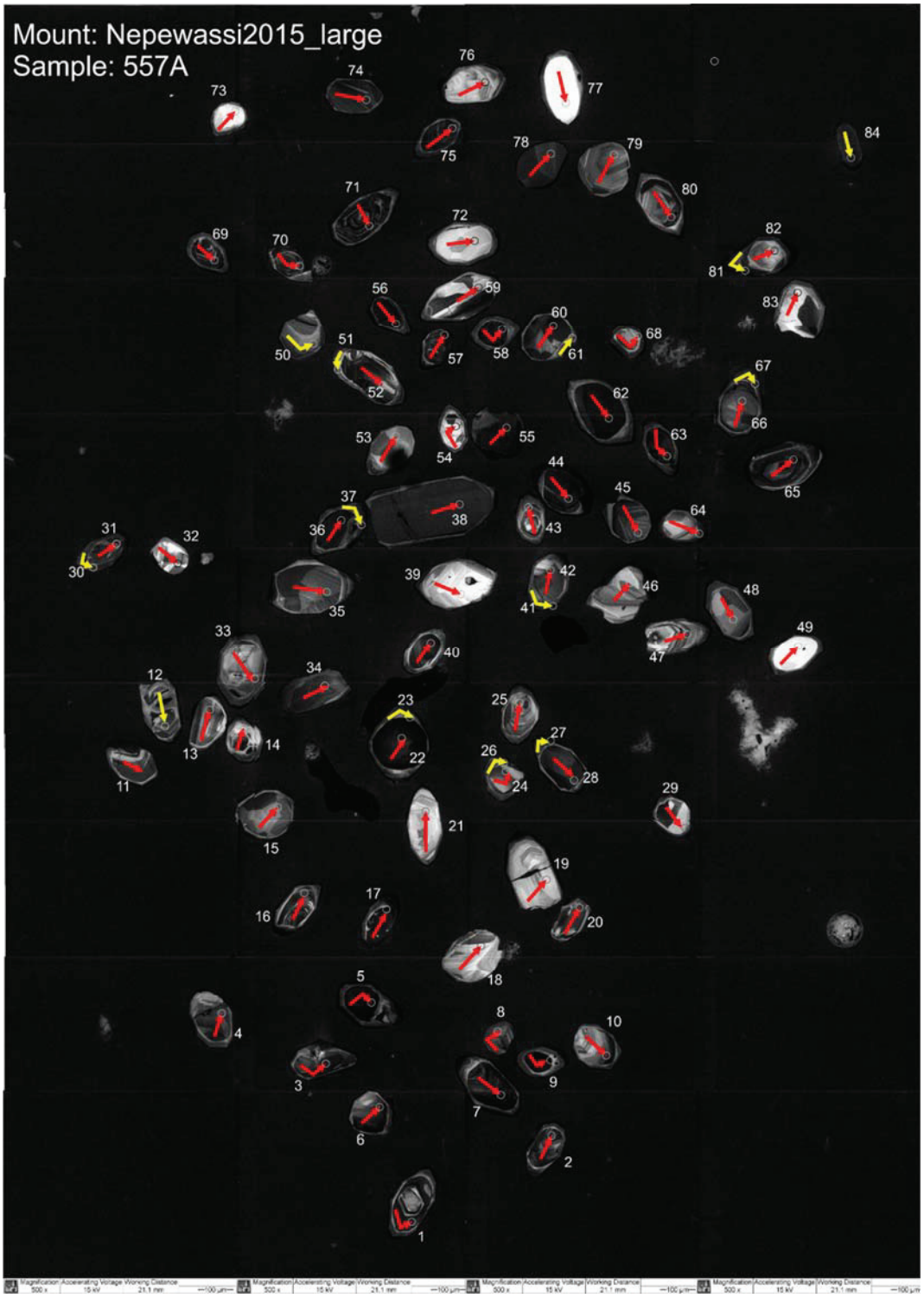

Figure C.5: Annotated CL images of zircon grains 1-84 from sample 14SV557A. Archean analyses are annotated in red and Paleoproterozoic analyses are in yellow.

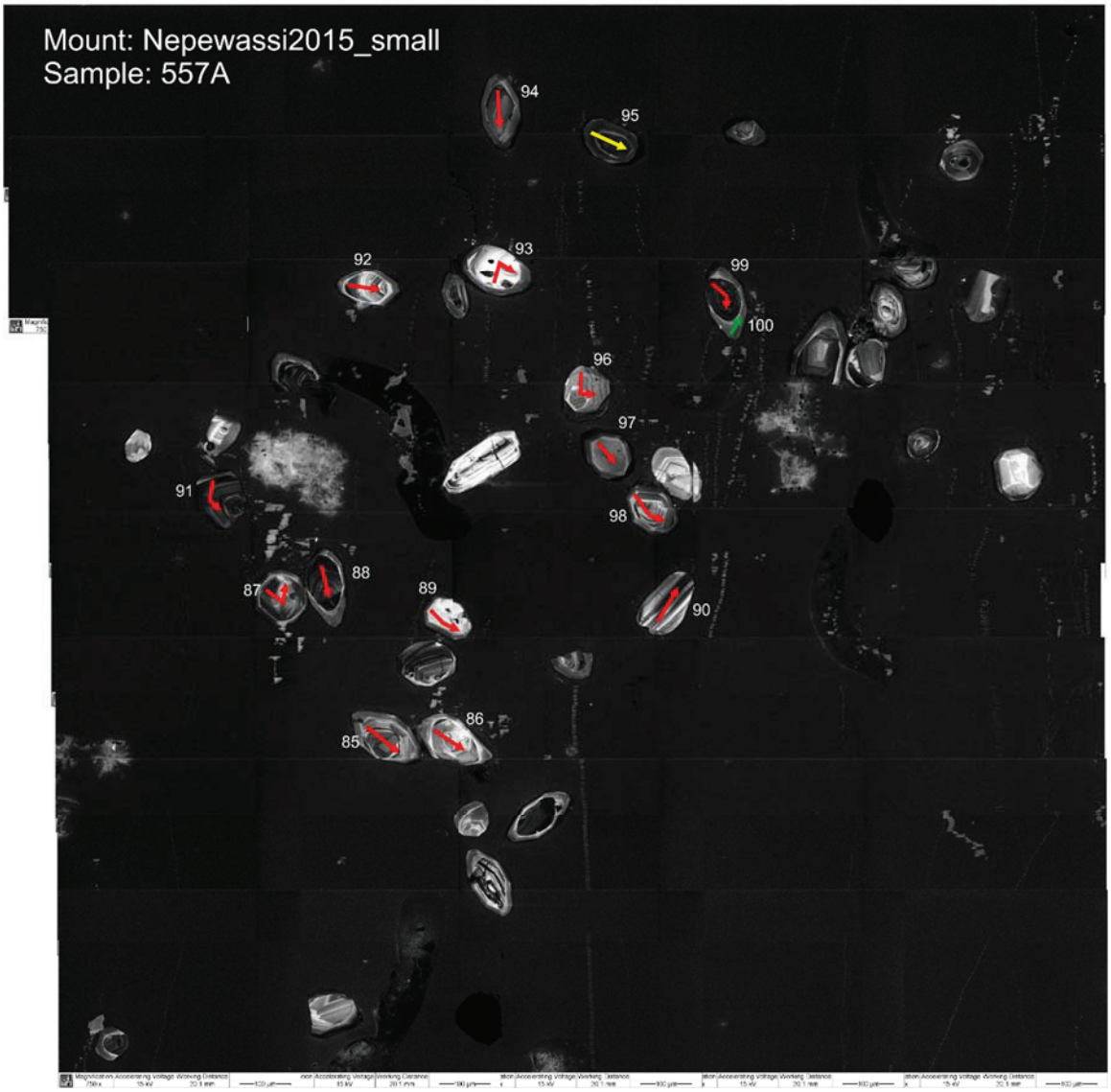

Figure C.6: Annotated CL images of zircon grains 1-84 from sample 14SV557A. Archean analyses are annotated in red and Paleoproterozoic analyses are in yellow. Green analysis is a ca. 2.3 Ga outlier.

Table C.4: Zircon U-Pb Analytical data for sample 14SV557A.

	Isotope ratios									Age estimates (ma)							Concentrations (ppm)				
	Concordia output					Terra-Wasserburg output															Pb com.
Analysis_#	Pb207/U235	1s%	Pb206/U238	1s%	roh	238/206	1s%	207/206	1s%	Pb207/Pb206	1s	Pb207/U235	1s	Pb206/U238	1s	conc	Th/U	U	Th	Pbtot	>LLD (%)
557A_01	9.97479	0.94027	0.4375	0.900571	0.362009	2.285714	0.900571	0.16535	1.040218	2511.1	17.42	2432.5	8.68	2339.5	17.69	93.16634	0.712596	272.0613	193.8698	163.2633	0.40823
557A_02	13.4646	0.957918	0.52881	0.907698	0.360206	1.891038	0.907698	0.18466	1.055995	2695.2	17.36	2712.8	9.05	2736.4	20.25	101.5286	0.807045	132.2054	106.6957	98.00245	-
557A_03	13.4379	0.968978	0.52598	0.912582	0.356129	1.901213	0.912582	0.18529	1.068595	2700.8	17.51	2710.9	9.16	2724.5	20.27	100.8775	1.064305	119.934	127.6464	94.43137	-
557A_04	14.5761	0.956357	0.54361	0.90874	0.361927	1.839554	0.90874	0.19446	1.054201	2780.3	17.2	2788	9.09	2798.6	20.62	100.6582	0.664349	118.7448	78.88799	88.97559	-
557A_05	13.3135	0.941302	0.5196	0.902617	0.359441	1.924557	0.902617	0.18582	1.044021	2705.5	17.1	2702.1	8.89	2697.5	19.9	99.70431	0.584673	339.7453	198.6398	240.8206	0.251595
557A_06	13.1432	0.977464	0.51068	0.914467	0.35353	1.958173	0.914467	0.18665	1.076882	2712.9	17.61	2690	9.22	2659.5	19.94	98.03163	0.611254	114.075	69.72878	79.16943	0.893697
557A_07	13.1558	0.940648	0.51551	0.902019	0.360079	1.939827	0.902019	0.18508	1.042792	2698.9	17.1	2690.9	8.88	2680.1	19.79	99.30342	0.666239	270.8396	180.444	192.6567	-
557A_08	13.3635	0.955811	0.52252	0.907142	0.357433	1.913802	0.907142	0.18548	1.056718	2702.5	17.32	2705.7	9.03	2709.9	20.09	100.2738	1.107202	89.48687	99.08001	69.59333	-
557A_09	11.6447	0.936303	0.48845	0.900809	0.365362	2.047292	0.900809	0.1729	1.035281	2585.9	17.22	2576.3	8.75	2564	19.07	99.1531	0.759473	404.8569	307.4777	278.1573	-
557A_10	13.3332	0.960837	0.5185	0.910318	0.357072	1.92864	0.910318	0.18649	1.061719	2711.5	17.37	2703.5	9.08	2692.8	20.03	99.31034	0.866796	75.24214	65.21959	55.45257	-
557A_100	6.88797	1.033541	0.33854	0.921605	0.342168	2.953861	0.921605	0.14755	1.125042	2317.8	19.14	2097.1	9.16	1879.6	15.04	81.09414	0.40468	173.8427	70.3507	75.79675	-
557A_11	12.7552	0.952086	0.50843	0.906713	0.362878	1.966839	0.906713	0.18194	1.049797	2670.7	17.31	2661.7	8.96	2649.9	19.7	99.22118	1.417007	104.2742	147.7572	83.69476	-
557A_12	4.55604	0.980896	0.3044	0.909987	0.352052	3.285151	0.909987	0.10855	1.077844	1775.1	19.61	1741.3	8.17	1713.1	13.67	96.50724	0.117937	366.376	43.20923	127.871	-
557A_13	12.8718	0.957051	0.5041	0.90855	0.357169	1.983733	0.90855	0.18518	1.05843	2699.9	17.33	2670.3	9.02	2631.4	19.63	97.46287	1.264674	87.69539	110.9061	67.91648	0.627726
557A_14	13.0987	0.970478	0.51259	0.91301	0.357772	1.950877	0.91301	0.18533	1.068365	2701.1	17.52	2686.8	9.16	2667.7	19.95	98.76347	0.653571	134.1909	87.7033	94.47319	0.368603
557A_15	13.1191	0.971254	0.5106	0.91461	0.359865	1.95848	0.91461	0.18634	1.06794	2710.1	17.52	2688.3	9.16	2659.2	19.91	98.12184	1.113253	59.62521	66.37793	45.724	-
557A_16	13.0069	0.947345	0.50862	0.906374	0.363873	1.966104	0.906374	0.18547	1.045991	2702.4	17.18	2680.2	8.93	2650.7	19.68	98.08689	1.196973	127.619	152.7565	99.6761	0.52645
557A_17	11.6783	0.938662	0.48395	0.902986	0.362786	2.066329	0.902986	0.17501	1.039941	2606.1	17.21	2579	8.78	2544.5	18.98	97.63631	0.236224	254.5943	60.14136	152.884	-
557A_18	13.5413	0.976788	0.51924	0.916724	0.358731	1.925892	0.916724	0.18913	1.073336	2734.6	17.55	2718.2	9.24	2696	20.19	98.58846	0.587282	53.41556	31.37001	37.43944	-
557A_19	13.1122	0.999301	0.51562	0.92316	0.352958	1.939413	0.92316	0.18443	1.095266	2693.1	17.95	2687.8	9.43	2680.6	20.26	99.53585	1.033822	49.53883	51.21433	37.5935	-
557A_20	13.0419	0.950703	0.52069	0.906489	0.359691	1.920529	0.906489	0.18165	1.051473	2668	17.28	2682.7	8.97	2702.1	20.02	101.2781	1.090851	111.4214	121.5442	85.80267	-
557A_21	12.91	0.977613	0.50346	0.915664	0.356131	1.986255	0.915664	0.18597	1.075442	2706.8	17.61	2673.1	9.21	2628.7	19.78	97.11467	1.101375	53.70447	59.14878	40.13161	-
557A_22	12.7507	0.940344	0.50204	0.90431	0.361859	1.991873	0.90431	0.18419	1.042402	2691	17.09	2661.4	8.85	2622.6	19.47	97.45819	0.829792	203.9334	169.2222	144.8418	-
557A_23	4.79574	0.973364	0.31828	0.908006	0.353937	3.141888	0.908006	0.10928	1.070644	1787.3	19.43	1784.2	8.18	1781.3	14.13	99.6643	0.246004	137.6056	33.85152	51.76466	-
557A_24	13	0.984079	0.5145	0.919339	0.357028	1.943635	0.919339	0.18324	1.08055	2682.5	17.74	2679.7	9.28	2675.8	20.12	99.75023	1.440818	83.28505	119.9986	68.06316	-
557A_25	12.4231	0.970689	0.48835	0.913279	0.358767	2.047712	0.913279	0.18449	1.067809	2693.6	17.53	2636.9	9.12	2563.6	19.33	95.17375	1.003597	89.54991	89.87199	63.88918	-
557A_26	4.57539	0.95511	0.31104	0.903421	0.362849	3.215021	0.903421	0.10668	1.049869	1743.5	19.2	1744.8	7.96	1745.8	13.84	100.1319	0.190008	260.9761	49.58759	94.72424	-
557A_27	4.39151	0.990548	0.2949	0.912174	0.353956	3.39098	0.912174	0.108	1.083333	1765.8	19.77	1710.7	8.19	1666	13.37	94.34817	0.221863	200.7149	44.53123	69.72286	0.929929
557A_28	15.7262	0.946953	0.56025	0.906738	0.363425	1.784917	0.906738	0.20357	1.046323	2855.1	16.92	2860.3	9.04	2867.6	20.99	100.4378	0.502505	118.3251	59.45896	88.872	0.479169
557A_29	13.0672	0.992795	0.51264	0.922675	0.357374	1.950687	0.922675	0.18486	1.087309	2697	17.84	2684.5	9.36	2667.9	20.14	98.92102	0.786759	76.46027	60.15581	54.68795	-
557A_30	4.64592	0.987533	0.31076	0.910671	0.344714	3.217917	0.910671	0.10842	1.08836	1773	19.7	1757.6	8.25	1744.5	13.92	98.39255	0.299512	154.594	46.30274	57.62675	-
557A_31	11.6543	0.947458	0.47816	0.905555	0.362656	2.09135	0.905555	0.17676	1.046617	2622.7	17.3	2577	8.86	2519.2	18.89	96.05369	1.067356	148.627	158.6379	105.177	-
557A_32	15.1519	0.962787	0.54414	0.913368	0.362928	1.837762	0.913368	0.20195	1.059668	2842	17.16	2824.8	9.17	2800.7	20.73	98.5468	0.850517	69.15465	58.81721	53.91531	-
557A_33	13.7153	0.999834	0.5267	0.924625	0.359517	1.898614	0.924625	0.18885	1.090813	2732.2	17.86	2730.2	9.46	2727.5	20.57	99.82798	1.11277	60.69637	67.54107	47.37549	-
557A_34	13.2499	0.969515	0.52314	0.913713	0.359079	1.911534	0.913713	0.18368	1.067073	2686.4	17.5	2697.6	9.15	2712.5	20.23	100.9716	0.780723	98.04998	76.5499	71.6282	-
557A_35	13.3385	0.962178	0.52441	0.911501	0.364342	1.906905	0.911501	0.18446	1.05714	2693.4	17.38	2703.9	9.09	2717.9	20.21	100.9096	1.334917	85.23171	113.7772	69.40878	-
557A_36	13.3918	0.944754	0.51848	0.904567	0.366913	1.928715	0.904567	0.18732	1.040999	2718.8	17.09	2707.7	8.93	2692.7	19.92	99.04002	0.868891	219.4347	190.6648	163.0274	-
557A_37	4.72608	0.97565	0.30954	0.907799	0.350596	3.2306	0.907799	0.11073	1.074686	1811.4	19.36	1771.9	8.18	1738.5	13.86	95.97549	0.224488	343.4534	77.10128	126.7006	3.020321
557A_38	13.511	0.957589	0.52819	0.908764	0.359987	1.893258	0.908764	0.18551	1.056547	2702.8	17.3	2716.1	9.05	2733.8	20.27	101.147	1.463968	104.9958	153.7105	87.90275	-
557A_39	13.6214	1.017006	0.52775	0.930365	0.357696	1.894837	0.930365	0.18718	1.105887	2717.5	18.13	2723.7	9.62	2732	20.72	100.5336	0.466053	34.91435	16.27193	24.17414	1.605575
557A_40	13.2085	0.945832	0.51771	0.905913	0.366037	1.931583	0.905913	0.18503	1.043074	2698.5	17.13	2694.7	8.93	2689.5	19.91	99.66648	0.613444	225.0768	138.0721	157.8167	-
557A_41	4.44691	0.998896	0.30375	0.911934	0.348914	3.292181	0.911934	0.10617	1.092587	1734.7	19.93	1721.1	8.28	1709.9	13.72	98.57036	0.254403	129.1656	32.86009	46.53308	0.876103

Table C.4: Continued. Zircon U-Pb Analytical data for sample 14SV557A.

	Isotope ratios									Age estimates (ma)							Concentrations (ppm)				
	Concordia output					Terra-Wasserburg output															Pb com.
Analysis_#	Pb207/U235	1s%	Pb206/U238	1s%	roh	238/206	1s%	207/206	1s%	Pb207/Pb206	1s	Pb207/U235	1s	Pb206/U238	1s	conc	Th/U	U	Th	Pbtot	>LLD (%)
557A_42	13.0656	0.958626	0.51262	0.909055	0.362841	1.950763	0.909055	0.18484	1.054966	2696.8	17.32	2684.4	9.04	2667.8	19.87	98.92465	0.871941	121.1715	105.6544	88.48452	-
557A_43	12.103	1.006861	0.4841	0.925429	0.35713	2.065689	0.925429	0.18131	1.097568	2664.9	18.09	2612.4	9.44	2545.1	19.46	95.50452	0.713613	119.0967	84.98893	79.24592	-
557A_44	13.3563	0.955282	0.52601	0.908728	0.362007	1.901105	0.908728	0.18415	1.053489	2690.6	17.28	2705.2	9.02	2724.6	20.19	101.2637	1.396239	229.2795	320.129	187.5305	0.194027
557A_45	13.3447	0.974995	0.5223	0.915183	0.362143	1.914608	0.915183	0.18529	1.068595	2700.8	17.55	2704.4	9.21	2708.9	20.24	100.2999	1.040009	85.16736	88.5748	65.07764	-
557A_46	13.0912	0.975008	0.50942	0.914766	0.36288	1.963017	0.914766	0.18637	1.067768	2710.4	17.53	2686.2	9.2	2654.2	19.91	97.92651	0.336714	67.32643	22.66977	43.82469	-
557A_47	13.0898	0.966706	0.51325	0.911836	0.364743	1.948368	0.911836	0.18496	1.059689	2697.9	17.43	2686.1	9.12	2670.5	19.94	98.9844	1.129623	85.68271	96.78918	65.52909	-
557A_48	13.255	1.011617	0.52603	0.927704	0.359182	1.901032	0.927704	0.18274	1.099923	2677.9	18.12	2698	9.55	2724.7	20.62	101.7476	1.259952	65.20575	82.1561	52.09012	-
557A_49	13.7036	1.143423	0.51113	0.978225	0.342389	1.956449	0.978225	0.19443	1.224091	2780	19.88	2729.4	10.82	2661.5	21.34	95.73741	0.466392	30.95109	14.43533	20.94364	-
557A_50	4.59075	1.056472	0.31407	0.923361	0.330243	3.184004	0.923361	0.10601	1.150835	1731.8	20.91	1747.6	8.81	1760.7	14.24	101.6688	0.195467	83.48183	16.31795	30.45994	1.661526
557A_51	4.60351	1.082435	0.31022	0.928373	0.329784	3.223519	0.928373	0.10762	1.170786	1759.5	21.23	1749.9	9.03	1741.8	14.19	98.99403	0.211393	104.8223	22.15868	38.03463	1.486606
557A_52	11.173	0.968761	0.46363	0.912365	0.361067	2.156892	0.912365	0.17477	1.064256	2603.9	17.62	2537.7	9.03	2455.6	18.62	94.3047	1.029989	100.9654	103.9932	68.76318	0.912897
557A_53	13.3808	0.98245	0.51886	0.917396	0.361621	1.927302	0.917396	0.18703	1.074694	2716.2	17.63	2706.9	9.28	2694.3	20.2	99.19373	1.172575	64.61058	75.76077	50.22579	-
557A_54	13.6139	1.071845	0.5262	0.950209	0.350614	1.900418	0.950209	0.18763	1.156531	2721.5	18.92	2723.2	10.14	2725.4	21.11	100.1433	0.527755	39.39968	20.79339	27.73099	1.397066
557A_55	13.2478	0.962724	0.52534	0.909887	0.359273	1.903529	0.909887	0.18288	1.060805	2679.2	17.4	2697.5	9.09	2721.8	20.21	101.59	1.173185	232.9397	273.2814	185.6668	-
557A_56	12.1038	0.952183	0.49787	0.905859	0.363012	2.008556	0.905859	0.17631	1.049288	2618.5	17.35	2612.5	8.93	2604.6	19.42	99.46916	0.774548	340.7014	263.8897	236.4761	-
557A_57	13.2198	0.964465	0.51779	0.909635	0.363105	1.931285	0.909635	0.18516	1.058544	2699.6	17.39	2695.5	9.1	2689.8	20.02	99.63698	1.394458	161.6588	225.4264	129.9566	-
557A_58	11.3364	0.968917	0.47761	0.910785	0.361581	2.093759	0.910785	0.17214	1.063088	2578.5	17.66	2551.2	9.04	2516.8	18.99	97.60714	0.643725	253.0787	162.9131	162.9401	-
557A_59	14.9208	0.978969	0.54583	0.916036	0.3586	1.832072	0.916036	0.19825	1.074401	2811.8	17.41	2810.2	9.32	2807.8	20.85	99.85774	0.205423	104.9033	21.54957	71.74871	-
557A_60	13.001	0.977001	0.50902	0.91352	0.362133	1.964559	0.91352	0.18523	1.068941	2700.3	17.57	2679.7	9.21	2652.4	19.88	98.22612	1.524847	136.5702	208.2487	110.8699	-
557A_61	4.57166	1.057384	0.31219	0.925718	0.334748	3.203178	0.925718	0.1062	1.148776	1735.2	20.91	1744.1	8.81	1751.5	14.18	100.9394	0.210305	107.4781	22.60317	39.10027	-
557A_62	10.8073	0.959075	0.4597	0.907113	0.361003	2.175332	0.907113	0.1705	1.055718	2562.5	17.54	2506.7	8.91	2438.2	18.43	95.14927	1.006487	261.979	263.6786	174.4991	0.18331
557A_63	12.825	0.971778	0.50892	0.911735	0.359581	1.964945	0.911735	0.18276	1.066973	2678.1	17.53	2666.9	9.15	2652	19.83	99.02543	0.655728	185.2216	121.4549	128.4306	0.242616
557A_64	12.8011	0.995068	0.50828	0.920752	0.355214	1.96742	0.920752	0.18265	1.089515	2677.1	17.87	2665.1	9.37	2649.3	19.99	98.96156	0.571782	56.03721	32.04109	38.11469	-
557A_65	12.5229	0.976452	0.50812	0.91317	0.361863	1.968039	0.91317	0.17873	1.068651	2641.2	17.66	2644.4	9.18	2648.6	19.83	100.2802	0.712721	134.7808	96.06118	94.19879	-
557A_66	12.9212	0.984891	0.51588	0.91688	0.357931	1.938435	0.91688	0.18165	1.078998	2668	17.73	2673.9	9.28	2681.7	20.1	100.5135	0.884094	77.71999	68.7118	56.90824	-
557A_67	4.67151	1.048697	0.3142	0.922979	0.336025	3.182686	0.922979	0.10783	1.140684	1763	20.63	1762.2	8.77	1761.3	14.23	99.90357	0.256967	123.8561	31.82695	46.11132	0.760831
557A_68	13.2515	1.005697	0.5236	0.92246	0.357357	1.909855	0.92246	0.18354	1.095129	2685.1	18.01	2697.7	9.49	2714.4	20.45	101.0912	1.100851	80.79936	88.94806	62.63591	-
557A_69	12.263	0.972194	0.49449	0.912051	0.359382	2.022286	0.912051	0.17985	1.067556	2651.5	17.58	2624.7	9.13	2590.1	19.44	97.68433	0.962078	141.9189	136.5371	101.1645	-
557A_70	12.5207	0.975023	0.50642	0.912286	0.357649	1.974646	0.912286	0.1793	1.070831	2646.4	17.63	2644.3	9.17	2641.3	19.77	99.80729	1.11632	184.512	205.9743	138.5846	0.552013
557A_71	9.82297	0.994709	0.41432	0.917165	0.355026	2.413593	0.917165	0.17194	1.087589	2576.6	18.05	2418.3	9.17	2234.6	17.33	86.72669	0.369172	179.1638	66.14218	94.07889	1.252202
557A_72	15.7298	1.001923	0.5614	0.922693	0.357835	1.781261	0.922693	0.2032	1.09252	2852	17.67	2860.5	9.57	2872.4	21.4	100.7153	0.637589	49.56345	31.60109	38.12232	-
557A_73	11.8266	1.071057	0.4971	0.943472	0.349859	2.011668	0.943472	0.17254	1.153356	2582.4	19.17	2590.8	10.03	2601.3	20.2	100.7319	1.89059	30.28672	57.25979	25.28796	-
557A_74	12.8419	0.997591	0.51466	0.919053	0.357049	1.94303	0.919053	0.18096	1.088638	2661.7	17.93	2668.1	9.4	2676.5	20.13	100.556	1.146117	124.2371	142.3903	95.14397	-
557A_75	12.803	0.97282	0.51037	0.911104	0.360696	1.959363	0.911104	0.18193	1.066344	2670.5	17.55	2665.3	9.16	2658.2	19.83	99.53941	0.895599	202.6804	181.5203	147.3889	-
557A_76	11.3564	1.019688	0.48713	0.925831	0.349798	2.05284	0.925831	0.16907	1.111965	2548.4	18.46	2552.9	9.52	2558.3	19.54	100.3885	0.948117	48.54788	46.02909	33.75557	-
557A_77	14.9959	1.114637	0.55099	0.965535	0.351764	1.814915	0.965535	0.19738	1.190597	2804.6	19.38	2815	10.61	2829.3	22.12	100.8807	0.804843	22.12034	17.8034	17.1504	-
557A_78	11.9097	0.993563	0.49054	0.917356	0.357632	2.03857	0.917356	0.17607	1.084796	2616.2	17.95	2597.3	9.31	2573	19.45	98.34875	0.812938	109.5179	89.03122	74.83105	-
557A_79	13.5773	0.995118	0.52536	0.917466	0.354468	1.903457	0.917466	0.18742	1.088464	2719.7	17.79	2720.7	9.41	2721.9	20.38	100.0809	0.814161	79.81139	64.9793	58.76502	-
557A_80	13.1921	1.010224	0.52273	0.923995	0.357915	1.913033	0.923995	0.18302	1.098241	2680.5	18.08	2693.5	9.53	2710.7	20.43	101.1267	0.911529	79.47324	72.4422	59.21638	-
557A_81	4.50587	1.101896	0.3082	0.931213	0.326076	3.244646	0.931213	0.10603	1.188343	1732.2	21.66	1732.1	9.16	1731.8	14.16	99.97691	0.246649	120.6105	29.74851	43.8608	1.603921
557A_82	14.8554	1.055509	0.53266	0.94244	0.350797	1.87737	0.94244	0.20226	1.142094	2844.5	18.46	2806	10.04	2752.6	21.1	96.7692	1.227491	46.91363	57.58608	38.12854	-
557A_83	14.3986	1.025931	0.53914	0.929258	0.352592	1.854806	0.929258	0.19368	1.115242	2773.7	18.15	2776.3	9.74	2779.8	20.97	100.2199	0.448492	43.56009	19.53633	30.8355	-

Table C.4: Continued. Zircon U-Pb Analytical data for sample 14SV557A.

	Isotope ratios									Age estimates (ma)							Concentrations (ppm)				
	Concordia output					Terra-Wasserburg output															Pb com.
Analysis_#	Pb207/U235	1s%	Pb206/U238	1s%	roh	238/206	1s%	207/206	1s%	Pb207/Pb206	1s	Pb207/U235	1s	Pb206/U238	1s	conc	Th/U	U	Th	Pbtot	>LLD (%)
557A_84	4.63652	0.999241	0.3136	0.91199	0.350851	3.188776	0.91199	0.10722	1.091214	1752.7	19.77	1755.9	8.35	1758.4	14.06	100.3252	0.376799	187.9789	70.83019	71.98411	1.238426
557A_85	13.5558	0.993079	0.52029	0.916796	0.356757	1.922005	0.916796	0.18895	1.084943	2733.1	17.74	2719.2	9.39	2700.4	20.21	98.80356	1.072038	104.5416	112.0726	81.78072	-
557A_86	12.515	1.023971	0.50015	0.925722	0.351518	1.9994	0.925722	0.18147	1.113132	2666.3	18.31	2643.9	9.63	2614.5	19.9	98.05723	0.997358	72.865	72.67252	53.84558	1.252242
557A_87	13.0269	0.995943	0.51657	0.915655	0.354407	1.935846	0.915655	0.18289	1.088086	2679.2	17.87	2681.6	9.39	2684.6	20.12	100.2016	0.564406	103.6717	58.513	72.47152	-
557A_88	12.6265	0.989827	0.49845	0.914836	0.355205	2.006219	0.914836	0.18371	1.083229	2686.6	17.77	2652.2	9.31	2607.1	19.6	97.04087	0.570576	206.0174	117.5486	139.3812	0.414002
557A_89	12.0285	1.066299	0.48955	0.939638	0.347508	2.042692	0.939638	0.17819	1.150457	2636.1	19	2606.6	10	2568.7	19.92	97.44319	0.438952	54.96158	24.12552	34.99709	1.996742
557A_90	12.498	0.990396	0.49903	0.913773	0.353293	2.003888	0.913773	0.18163	1.084623	2667.8	17.81	2642.6	9.31	2609.6	19.61	97.81843	1.571275	222.6795	349.8909	180.666	0.240486
557A_91	13.4219	0.987269	0.52294	0.912151	0.355721	1.912265	0.912151	0.18614	1.079832	2708.3	17.69	2709.8	9.33	2711.6	20.21	100.1218	0.970761	197.3101	191.5409	153.758	-
557A_92	13.4438	1.047918	0.51734	0.933622	0.347714	1.932965	0.933622	0.18846	1.135519	2728.7	18.55	2711.3	9.9	2687.9	20.53	98.50478	0.381247	89.72766	34.20837	60.4275	-
557A_93	10.9264	1.103661	0.47113	0.948783	0.342997	2.122556	0.948783	0.16819	1.183186	2539.7	19.75	2516.9	10.27	2488.5	19.61	97.98401	1.997378	40.30633	80.50695	33.20822	2.203125
557A_94	13.2679	1.010262	0.51807	0.920725	0.355821	1.930241	0.920725	0.18573	1.098369	2704.7	18.03	2698.9	9.54	2691	20.24	99.49347	0.904552	112.0286	101.3356	83.28698	0.372384
557A_95	4.68558	1.029115	0.31474	0.918218	0.341839	3.177226	0.918218	0.10796	1.120785	1765.3	20.26	1764.7	8.61	1764	14.17	99.92636	0.422023	181.9321	76.77945	71.14441	-
557A_96	13.0466	1.023179	0.5111	0.923498	0.350003	1.956564	0.923498	0.18512	1.112792	2699.3	18.24	2683	9.65	2661.3	20.15	98.59223	0.946525	93.2528	88.26609	69.35771	-
557A_97	15.7274	1.024833	0.55927	0.926207	0.352511	1.788045	0.926207	0.20394	1.113072	2858	17.99	2860.4	9.78	2863.6	21.42	100.1959	0.962286	93.29253	89.77412	77.39417	-
557A_98	13.2017	1.013434	0.51937	0.920346	0.354551	1.92541	0.920346	0.18434	1.101226	2692.3	18.1	2694.2	9.57	2696.5	20.28	100.156	0.921045	86.53508	79.7027	64.84245	0.541111
557A_99	12.4217	0.997529	0.49296	0.914882	0.354034	2.028562	0.914882	0.18274	1.088979	2677.9	17.89	2636.8	9.37	2583.5	19.47	96.47485	0.800908	313.8624	251.3748	219.7892	0.232451

14SV434A:

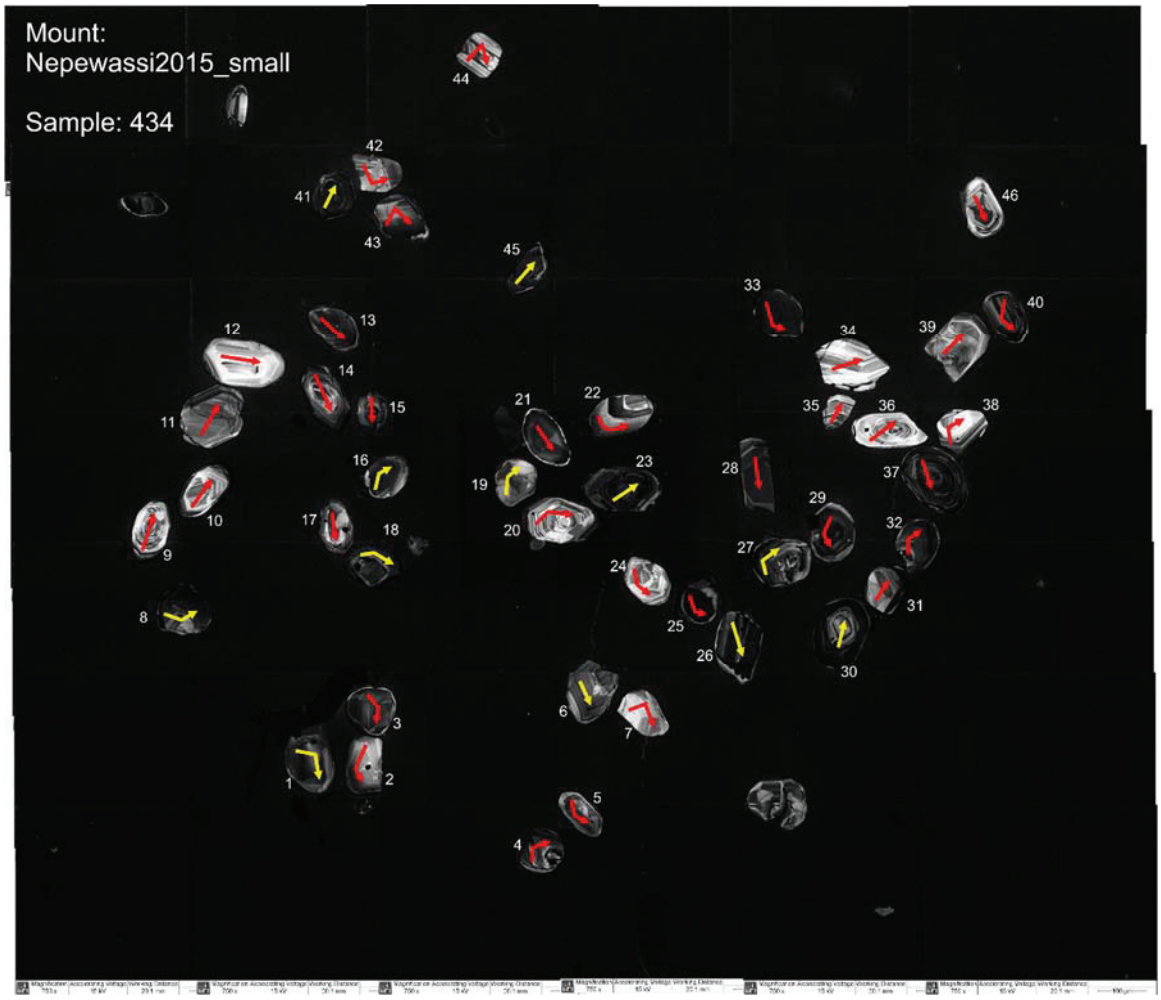

Figure C.7: Annotated CL images of zircon grains 1-46 from sample 14SV434A. Archean analyses are annotated in red and Paleoproterozoic analyses are in yellow.

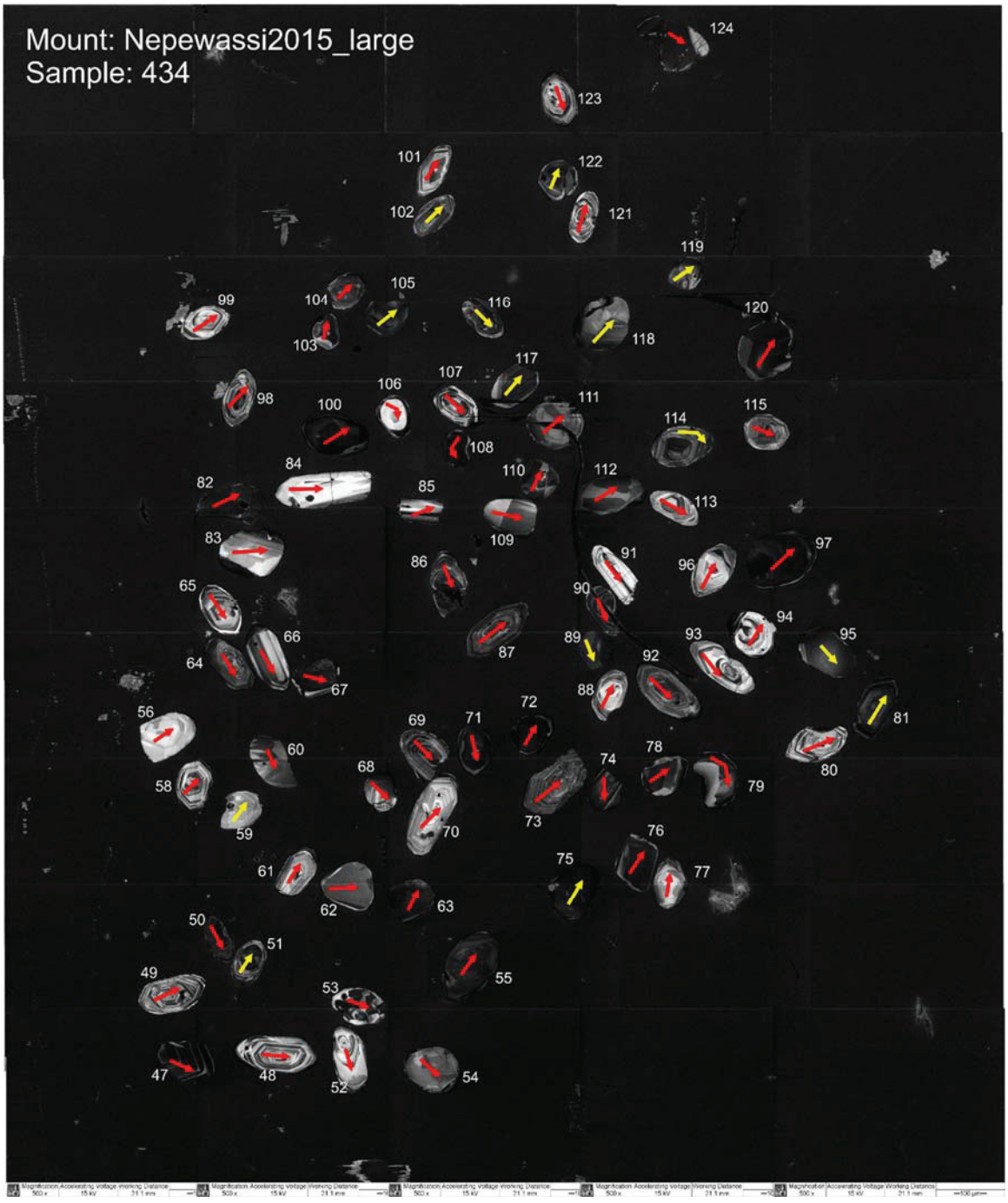

Figure C.8: Annotated CL images of zircon grains 47-124 from sample 14SV434A. Archean analyses are annotated in red and Paleoproterozoic analyses are in yellow.

Table C.5: Zircon U-Pb Analytical data for sample 14SV434A.

	Isotope ratios									Age estimates (ma)							Concentrations (ppm)				
	Concordia output					Terra-Wasserburg output															Pb com.
Analysis_#	Pb207/ U235	1s%	Pb206/ U238	1s%	roh	238/206	1s%	207/206	1s%	Pb207/ Pb206	1s	Pb207/ U235	1s	Pb206/ U238	1s	conc	Th/U	U	Th	Pbtot	>LLD (%)
434_15	9.5384	0.977627	0.3977	0.907697	0.337665	2.514395	0.907697	0.17396	1.086457	2596.2	18.02	2391.3	8.99	2158.5	16.64	83.14074	0.620237	141.5351	87.7853	98.72606	0.322456
434_11	10.42	0.924864	0.4292	0.892379	0.346415	2.32997	0.892379	0.1761	1.039182	2616.5	17.2	2472.8	8.57	2302.1	17.26	87.98395	0.583438	118.6214	69.20827	49.48612	0.662067
434_88	10.264	1.128092	0.4316	0.959155	0.327939	2.316799	0.959155	0.17245	1.217744	2581.6	20.21	2458.9	10.44	2313	18.63	89.5956	1.003858	59.30281	59.53162	44.21604	3.539914
434_91	11.405	0.960249	0.4543	0.904768	0.348377	2.201382	0.904768	0.18207	1.065524	2671.9	17.51	2556.9	8.96	2414.2	18.23	90.35518	0.958621	119.0258	114.1006	78.01211	0.419718
434_73	10.453	1.009117	0.4393	0.919666	0.337319	2.276401	0.919666	0.17256	1.112656	2582.6	18.41	2475.7	9.35	2347.5	18.1	90.89677	0.803092	98.02055	78.71948	43.27281	0.262306
434_07	12.383	0.992818	0.4791	0.916378	0.339838	2.087421	0.916378	0.1875	1.098667	2720.3	18.01	2633.9	9.33	2523.1	19.12	92.7508	0.787545	52.98372	41.72704	24.6894	0.355864
434_46	11.237	0.974665	0.4607	0.909584	0.345057	2.170846	0.909584	0.17692	1.079584	2624.2	17.86	2543	9.09	2442.4	18.48	93.07217	0.618914	144.2148	89.25649	25.07039	1.794019
434_17	11.105	0.935163	0.4597	0.896198	0.34295	2.175237	0.896198	0.17521	1.050168	2608.1	17.35	2532	8.71	2438.3	18.18	93.48951	1.007306	94.43376	95.12365	45.89619	2.401043
434_50	13.381	1.020375	0.5007	0.928774	0.343227	1.997363	0.928774	0.19384	1.11948	2775	18.24	2706.9	9.64	2616.6	19.97	94.29189	0.609453	71.05236	43.3031	13.90429	7.145135
434_42	11.311	0.953072	0.4664	0.902717	0.344657	2.14422	0.902717	0.1759	1.063104	2614.6	17.56	2549.1	8.89	2467.6	18.5	94.37773	0.993158	65.69557	65.24611	14.90667	4.820495
434_83	11.706	1.146898	0.4736	0.969213	0.330536	2.111576	0.969213	0.17926	1.232846	2646	20.33	2581.2	10.73	2499.2	20.09	94.452	0.603697	38.77481	23.40825	27.05418	-
434_44	13.09	0.954959	0.4969	0.903693	0.347532	2.01268	0.903693	0.19107	1.062438	2751.4	17.35	2686.1	9.01	2600.2	19.35	94.50462	0.748402	123.6934	92.57245	25.61167	0.899475
434_34	12.037	0.948258	0.4798	0.90045	0.34943	2.084376	0.90045	0.18197	1.055119	2670.9	17.4	2607.3	8.89	2526.2	18.83	94.58235	0.547102	61.01874	33.38349	16.04199	0.820243
434_54	10.852	0.987728	0.4595	0.914037	0.342863	2.176279	0.914037	0.17128	1.09178	2570.2	18.13	2510.5	9.18	2437.4	18.53	94.83309	1.281987	80.28784	102.928	20.53774	1.818078
434_18	2.6324	0.976288	0.2259	0.894161	0.325234	4.426542	0.894161	0.08452	1.0885	1304.4	21	1309.7	7.18	1313	10.62	100.6593	1.059413	111.436	118.0568	65.43887	0.802038
434_119	4.0015	1.006882	0.289	0.90302	0.322425	3.459848	0.90302	0.10046	1.114872	1632.6	20.52	1634.5	8.18	1636.7	13.06	100.2511	0.677484	114.8833	77.83165	43.07518	-
434_26	3.918	0.946914	0.2817	0.890956	0.334977	3.549624	0.890956	0.10087	1.060771	1640.2	19.54	1617.4	7.66	1600	12.64	97.54908	0.818153	248.2574	203.1127	161.5356	0.324427
434_19	4.3893	1.049607	0.3088	0.910063	0.312982	3.238657	0.910063	0.10311	1.154107	1680.8	21.18	1710.3	8.68	1734.6	13.85	103.2009	0.720087	72.96855	52.54371	46.88751	1.607815
434_116	4.2966	0.999157	0.3007	0.904676	0.324668	3.326016	0.904676	0.1037	1.108968	1691.3	20.24	1692.7	8.23	1694.6	13.46	100.1951	0.598352	119.5407	71.52739	45.64303	-
434_114	4.366	1.027934	0.3037	0.908762	0.322639	3.292615	0.908762	0.10431	1.131243	1702.3	20.69	1705.9	8.49	1709.7	13.65	100.4347	0.35377	108.1776	38.27002	39.63846	-
434_81	4.2469	0.963055	0.2949	0.898701	0.338156	3.391325	0.898701	0.10445	1.072283	1704.6	19.55	1683.1	7.92	1665.8	13.2	97.72381	0.690457	126.7456	87.51235	51.51264	0.733555
434_89	4.2565	1.017505	0.2933	0.910269	0.327397	3.409246	0.910269	0.10523	1.121353	1718.4	20.43	1685	8.37	1658.1	13.29	96.49092	0.708425	151.2028	107.1158	102.0192	0.476603
434_118	4.352	1.01517	0.2996	0.904449	0.324003	3.33745	0.904449	0.10539	1.119651	1721.2	20.44	1703.3	8.38	1689.5	13.46	98.15826	0.864737	86.57412	74.86386	35.09932	1.605331
434_75	4.5298	0.944417	0.3113	0.896184	0.347664	3.212129	0.896184	0.10552	1.051933	1723.4	19.2	1736.5	7.86	1747.2	13.71	101.381	0.543756	184.9684	100.5776	74.16465	0.518692
434_102	4.5683	0.993146	0.3137	0.902078	0.332078	3.187556	0.902078	0.10567	1.097757	1725.9	20.05	1743.5	8.27	1759	13.91	101.9178	1.00243	200.8002	201.2882	89.25945	-
434_105	4.4333	0.97985	0.3044	0.900043	0.332121	3.284827	0.900043	0.10567	1.088294	1726	19.83	1718.6	8.12	1713.3	13.56	99.26419	0.916684	209.2939	191.8564	87.09443	-
434_117	4.4428	1.015573	0.305	0.904799	0.328279	3.278259	0.904799	0.10568	1.116578	1726.2	20.43	1720.4	8.42	1716.3	13.65	99.42649	0.471083	172.3284	81.18101	65.50256	-
434_30	4.6153	1.018354	0.3164	0.907051	0.321909	3.160456	0.907051	0.1058	1.124764	1728.2	20.51	1752	8.5	1772.2	14.04	102.546	1.006966	124.257	125.1226	50.72291	0.507213
434_95	4.658	0.988416	0.3191	0.905757	0.344717	3.134109	0.905757	0.10586	1.08634	1729.4	19.89	1759.7	8.26	1785.2	14.11	103.2266	1.065303	93.31539	99.40919	28.24066	1.118072
434_08	4.5777	0.950914	0.3136	0.892857	0.331212	3.188776	0.892857	0.10588	1.067246	1729.7	19.41	1745.2	7.92	1758.4	13.73	101.6592	0.678677	168.0778	114.0705	117.496	0.386181
434_16	4.4884	0.931523	0.3074	0.888065	0.337114	3.252985	0.888065	0.1059	1.048159	1730.1	19.08	1728.8	7.74	1728	13.48	99.87862	0.407563	179.3941	73.11434	122.3762	-
434_45	4.4601	1.011419	0.305	0.905037	0.330174	3.279119	0.905037	0.10607	1.112473	1733	20.35	1723.6	8.39	1715.8	13.65	99.0075	0.561492	240.0356	134.7781	36.18321	-
434_122	4.6751	1.026923	0.3197	0.907157	0.321393	3.128128	0.907157	0.10612	1.130795	1733.8	20.6	1762.8	8.59	1788.1	14.17	103.1318	0.828897	218.161	180.8329	93.48545	-
434_06	4.4694	0.987613	0.3055	0.897008	0.3187	3.273751	0.897008	0.10613	1.102422	1734	20.02	1725.3	8.19	1718.3	13.55	99.09458	0.898603	75.08906	67.47523	33.27892	1.557322
434_27	4.6075	0.964948	0.3149	0.895636	0.33538	3.176015	0.895636	0.10614	1.074053	1734.2	19.6	1750.6	8.05	1764.6	13.83	101.753	0.728933	94.64374	68.98899	39.52026	0.579105
434_23	4.5495	0.976806	0.3103	0.899101	0.32599	3.222584	0.899101	0.10634	1.090841	1737.7	19.8	1740.1	8.13	1742.2	13.71	100.259	1.037951	209.5782	217.5319	90.36426	0.070058
434_01	4.641	0.961211	0.3163	0.894607	0.335339	3.161156	0.894607	0.10642	1.071227	1739	19.56	1756.7	8.03	1771.8	13.85	101.8861	0.844705	141.3212	119.3747	88.04905	0.572594
434_41	4.5609	0.933366	0.3108	0.891392	0.347622	3.218021	0.891392	0.10645	1.042743	1739.5	19.03	1742.2	7.77	1744.4	13.63	100.2817	0.467389	199.3644	93.18064	28.54848	0.311969
434_59	4.6566	1.065808	0.3172	0.917489	0.317827	3.152883	0.917489	0.10648	1.164538	1739.9	21.3	1759.5	8.91	1775.9	14.24	102.0691	0.625926	50.04434	31.32406	7.963824	5.006932
434_04	4.6512	1.031779	0.3168	0.906049	0.318181	3.156964	0.906049	0.10651	1.136044	1740.5	20.76	1758.5	8.62	1773.9	14.07	101.919	0.725514	111.7038	81.04269	32.43083	1.489893
434_90	4.7137	0.989024	0.3209	0.903849	0.34099	3.116721	0.903849	0.10654	1.088793	1741	19.85	1769.7	8.28	1793.9	14.17	103.0385	0.851215	86.4465	73.58455	60.58311	0.096609
434_67	4.5452	0.98544	0.3093	0.902008	0.337453	3.233002	0.902008	0.10657	1.088486	1741.6	19.78	1739.3	8.2	1737.3	13.75	99.7531	0.498262	133.9568	66.74555	71.83564	0.223435

Table C.5: *Continued*. Zircon U-Pb Analytical data for sample 14SV434A.

	Isotope ratios									Age estimates (ma)							Concentrations (ppm)				
	Concordia output					Terra-Wasserburg output															Pb com.
Analysis_#	Pb207/ U235	1s%	Pb206/ U238	1s%	roh	238/206	1s%	207/206	1s%	Pb207/ Pb206	1s	Pb207/ U235	1s	Pb206/ U238	1s	conc	Th/U	U	Th	Pbtot	>LLD (%)
434_86	4.6497	1.052541	0.3162	0.917141	0.320424	3.162555	0.917141	0.10664	1.153413	1742.7	20.95	1758.2	8.8	1771.1	14.19	101.6297	0.700404	95.31982	66.76235	64.78619	0.198376
434_108	4.698	0.93083	0.3196	0.891684	0.348496	3.128715	0.891684	0.10666	1.04069	1743.1	18.96	1766.9	7.79	1787.9	13.94	102.5701	0.582233	420.4457	244.7974	171.2124	-
434_60	4.6279	0.969774	0.3146	0.899526	0.336766	3.178539	0.899526	0.10668	1.07799	1743.5	19.6	1754.3	8.1	1763.3	13.88	101.1356	0.860264	90.14791	77.55097	16.30079	1.509563
434_120	4.6717	0.991072	0.3174	0.901156	0.332769	3.150896	0.901156	0.10681	1.095403	1745.7	19.88	1762.2	8.29	1776.9	13.99	101.7872	0.795799	246.7987	196.4022	104.8875	-
434_78	4.548	0.958223	0.3086	0.897515	0.340597	3.240126	0.897515	0.10687	1.066717	1746.7	19.29	1739.8	7.98	1734	13.66	99.27291	0.507623	130.4485	66.21867	50.7891	0.290912
434_13	4.4597	0.925849	0.3026	0.888962	0.345833	3.304693	0.888962	0.1069	1.038354	1747.3	18.86	1723.5	7.68	1704.2	13.3	97.53334	1.111696	172.1288	191.3548	123.4036	0.586644
434_47	4.5052	0.981987	0.3056	0.899869	0.337802	3.272251	0.899869	0.10692	1.084923	1747.5	19.74	1731.9	8.16	1719	13.59	98.3691	0.830828	163.6103	135.9321	28.10101	2.916077
434_37	4.6057	0.974455	0.3122	0.900093	0.333161	3.203178	0.900093	0.107	1.084112	1748.9	19.62	1750.3	8.13	1751.5	13.79	100.1487	0.785492	128.1047	100.6253	32.57785	-
434_69	4.6104	0.971291	0.3123	0.899747	0.34278	3.201947	0.899747	0.10706	1.074164	1749.9	19.52	1751.1	8.11	1752.1	13.81	100.1257	0.93354	136.6692	127.5861	82.10955	0.357268
434_71	4.6973	1.045062	0.3181	0.914922	0.319261	3.144061	0.914922	0.10711	1.148352	1750.7	20.76	1766.8	8.75	1780.2	14.22	101.685	0.495081	138.7657	68.70025	81.46839	-
434_72	4.6784	0.935798	0.3167	0.89359	0.347538	3.157562	0.89359	0.10713	1.045459	1751.2	18.92	1763.4	7.83	1773.6	13.86	101.2791	0.659113	227.3478	149.8479	138.536	0.226812
434_82	4.5871	0.94744	0.3101	0.896514	0.348425	3.22487	0.896514	0.10728	1.053318	1753.7	19.1	1746.9	7.9	1741.1	13.68	99.28152	0.75771	173.706	131.6187	71.41508	0.271239
434_28	4.4537	0.943032	0.3011	0.893391	0.343014	3.321156	0.893391	0.10728	1.053318	1753.8	19.12	1722.4	7.82	1696.8	13.31	96.74991	0.727525	138.0655	100.4461	91.66453	0.203339
434_40	4.6165	0.950497	0.3116	0.895494	0.340792	3.209655	0.895494	0.10747	1.060761	1756.9	19.22	1752.3	7.93	1748.4	13.7	99.51619	0.88381	148.8858	131.5868	39.89354	0.957311
434_104	4.6084	0.971051	0.3111	0.900061	0.336635	3.214504	0.900061	0.10749	1.07917	1757.4	19.54	1750.8	8.1	1746.1	13.76	99.357	0.727405	119.0136	86.5711	50.33052	2.800288
434_52	4.714	0.982172	0.3165	0.900502	0.32916	3.159657	0.900502	0.10802	1.09239	1766.3	19.79	1769.7	8.23	1772.6	13.97	100.3567	0.927543	125.4215	116.3338	23.17456	1.516754
434_76	4.7473	0.980555	0.3173	0.901412	0.334585	3.15179	0.901412	0.10851	1.087457	1774.5	19.71	1775.6	8.22	1776.4	14.02	100.1071	1.0271	153.8404	158.0095	61.1833	0.214285
434_100	4.794	0.95495	0.3197	0.897773	0.349737	3.128128	0.897773	0.10875	1.057471	1778.5	19.24	1783.8	8.02	1788.1	14.04	100.5398	0.741359	167.0228	123.8239	45.23135	2.20866
434_29	4.695	0.973581	0.3114	0.899252	0.32705	3.211613	0.899252	0.10937	1.08805	1788.8	19.64	1766.4	8.15	1747.5	13.75	97.69119	1.504596	249.2095	374.9597	160.2132	0.031143
434_02	11.563	0.950557	0.4871	0.899162	0.340714	2.052882	0.899162	0.17218	1.062841	2578.9	17.64	2569.7	8.88	2558.2	19	99.19733	1.373072	58.85469	80.81172	30.40691	1.758239
434_31	11.401	0.941243	0.4775	0.898429	0.348056	2.094241	0.898429	0.17318	1.05093	2588.6	17.45	2556.5	8.79	2516.4	18.7	97.21085	0.819725	91.9715	75.3913	42.15615	0.102497
434_43	12.363	0.926071	0.5053	0.894518	0.351638	1.979022	0.894518	0.17745	1.036912	2629.2	17.13	2632.4	8.7	2636.5	19.34	100.2777	0.56731	112.4681	63.80433	20.78619	0.530627
434_97	12.388	0.935983	0.5046	0.897776	0.358414	1.981846	0.897776	0.17804	1.039092	2634.7	17.2	2634.3	8.79	2633.5	19.4	99.95445	0.763934	183.7198	140.3499	57.78567	0.333102
434_74	12.1	0.954302	0.4927	0.90315	0.348134	2.02955	0.90315	0.17809	1.061261	2635.2	17.49	2612.2	8.95	2582.4	19.22	97.99636	1.147204	88.4281	101.4451	43.65194	0.399868
434_109	12.559	0.951042	0.5112	0.901888	0.346339	1.956373	0.901888	0.17829	1.060071	2637	17.47	2647.1	8.94	2661.5	19.65	100.9291	1.444667	76.4865	110.4975	61.60449	-
434_124	12.235	0.9814	0.4975	0.900539	0.33506	2.010131	0.900539	0.17845	1.087139	2638.6	17.95	2622.6	9.21	2602.9	19.28	98.64701	1.735228	176.4749	306.2241	144.7117	-
434_63	12.699	0.946584	0.5161	0.901041	0.350636	1.937722	0.901041	0.17846	1.053457	2638.6	17.39	2657.6	8.91	2682.5	19.77	101.6638	1.33616	98.43161	131.5204	78.49338	0.234765
434_103	11.952	0.981974	0.4858	0.911823	0.343287	2.058291	0.911823	0.17852	1.086713	2639.1	17.93	2600.7	9.2	2552.6	19.23	96.72237	1.896161	112.6502	213.6029	94.36999	-
434_110	12.398	0.935522	0.5038	0.895161	0.346215	1.984836	0.895161	0.17857	1.047208	2639.6	17.25	2635.1	8.79	2630.2	19.35	99.64389	1.083951	142.2393	154.1805	105.4006	-
434_32	12.766	0.934919	0.5181	0.89558	0.347076	1.930129	0.89558	0.17871	1.046388	2641	17.26	2662.5	8.8	2691.1	19.72	101.897	0.648285	149.0789	96.64567	93.16783	0.522896
434_92	12.168	0.974675	0.4937	0.909514	0.351577	2.025645	0.909514	0.17874	1.074186	2641.3	17.76	2617.5	9.14	2586.5	19.39	97.92526	0.482105	96.81962	46.67722	25.8934	-
434_112	12.497	0.964624	0.5064	0.904477	0.34332	1.974841	0.904477	0.17908	1.072147	2644.4	17.66	2642.5	9.07	2641.1	19.61	99.87521	0.815645	63.04696	51.42394	44.69383	-
434_111	12.522	0.953554	0.5069	0.901594	0.348135	1.972854	0.901594	0.17925	1.059972	2646	17.5	2644.3	8.97	2643.3	19.55	99.89796	0.668788	72.7601	48.66105	50.09822	-
434_39	12.019	0.939666	0.4856	0.897877	0.3511	2.05935	0.897877	0.17952	1.047237	2648.4	17.31	2605.9	8.81	2551.6	18.92	96.34496	0.887708	73.41053	65.16709	22.19316	0.899413
434_56	12.527	0.929466	0.506	0.895222	0.348753	1.976206	0.895222	0.17953	1.041609	2648.6	17.13	2644.7	8.74	2639.6	19.39	99.6602	1.30968	114.2622	149.6469	31.3398	1.31581
434_85	12.21	1.126746	0.493	0.963508	0.333787	2.028439	0.963508	0.17961	1.213741	2649.3	20	2620.7	10.57	2583.6	20.51	97.5201	2.092407	42.31077	88.53136	37.00466	0.437124
434_66	12.965	1.010429	0.5221	0.923159	0.342907	1.915269	0.923159	0.18008	1.110618	2653.6	18.28	2677.1	9.53	2708.2	20.41	102.0576	0.866952	44.39015	38.48415	9.694252	0.403025
434_87	12.609	0.978734	0.5076	0.912064	0.346076	1.9699	0.912064	0.18013	1.082551	2654	17.8	2650.9	9.21	2646.6	19.79	99.72118	0.661672	84.5486	55.94343	59.26419	0.024837
434_09	12.787	0.988205	0.5146	0.913419	0.341439	1.943446	0.913419	0.18025	1.092926	2655.2	18.03	2664.1	9.31	2676	20.02	100.7834	0.851415	114.2727	97.29356	83.07402	0.479837
434_79	12.845	0.945424	0.5163	0.900691	0.350061	1.936971	0.900691	0.18043	1.05304	2656.9	17.32	2668.4	8.91	2683.3	19.77	100.9936	1.283229	82.73602	106.1692	43.68564	0.67794
434_38	12.976	0.984778	0.5215	0.914757	0.341419	1.917729	0.914757	0.18048	1.091534	2657.3	17.94	2677.9	9.28	2705.3	20.19	101.8063	0.636967	42.08412	26.80619	11.96625	1.526891
434_55	13.339	0.965665	0.5357	0.907224	0.350087	1.866716	0.907224	0.18059	1.068719	2658.3	17.63	2703.9	9.12	2765.4	20.41	104.0289	1.085801	63.83086	69.30761	16.20133	0.897026

Table C.5: *Continued*. Zircon U-Pb Analytical data for sample 14SV434A.

	Isotope ratios									Age estimates (ma)							Concentrations (ppm)				
	Concordia output					Terra-Wasserburg output															Pb com.
Analysis_#	Pb207/ U235	1s%	Pb206/ U238	1s%	roh	238/206	1s%	207/206	1s%	Pb207/ Pb206	1s	Pb207/ U235	1s	Pb206/ U238	1s	conc	Th/U	U	Th	Pbtot	>LLD (%)
434_77	12.588	1.017398	0.5053	0.926127	0.347482	1.978905	0.926127	0.18065	1.112649	2658.9	18.37	2649.3	9.57	2636.6	20.02	99.16131	1.106952	43.16331	47.77969	21.96178	-
434_48	12.041	0.955086	0.4819	0.902621	0.343677	2.07499	0.902621	0.18121	1.065063	2663.9	17.5	2607.6	8.95	2535.6	18.94	95.18375	0.676864	77.64182	52.55299	14.35446	4.729131
434_101	12.393	0.943606	0.4949	0.899172	0.350066	2.02061	0.899172	0.18171	1.051125	2668.5	17.32	2634.6	8.87	2591.8	19.19	97.12573	0.631568	105.1197	66.39027	70.02329	-
434_03	12.551	0.927931	0.5008	0.892625	0.34827	1.996925	0.892625	0.18179	1.039661	2669.3	17.15	2646.5	8.73	2617.1	19.21	98.04443	1.2502	146.0478	182.5889	110.0807	0.167936
434_80	12.166	0.964772	0.4851	0.907067	0.351863	2.061516	0.907067	0.18188	1.066637	2670	17.59	2617.3	9.05	2549.4	19.1	95.48315	0.452703	58.24434	26.3674	24.1618	1.319931
434_113	12.687	0.974134	0.505	0.906877	0.341547	1.98008	0.906877	0.18229	1.080696	2673.8	17.75	2656.7	9.17	2635.4	19.64	98.56384	0.516839	97.25458	50.26498	65.0601	1.102973
434_98	12.556	0.949037	0.4995	0.900973	0.35271	2.002162	0.900973	0.1823	1.053209	2673.9	17.33	2646.9	8.93	2611.5	19.36	97.66633	1.118033	96.63263	108.0384	34.72548	0.491905
434_107	12.46	1.004254	0.4948	0.921566	0.34341	2.020978	0.921566	0.18272	1.105517	2677.7	18.18	2639.7	9.44	2591.5	19.66	96.78082	0.48251	89.96069	43.40692	58.707	0.880239
434_36	12.836	0.982189	0.5087	0.912093	0.342748	1.965718	0.912093	0.183	1.087432	2680.2	17.87	2667.7	9.25	2651.2	19.85	98.91799	0.704538	72.27289	50.91899	20.84901	2.146798
434_35	13.701	0.960628	0.5417	0.906473	0.346309	1.846177	0.906473	0.18346	1.068353	2684.4	17.54	2729.3	9.09	2790.4	20.52	103.9487	0.724778	82.5534	59.83287	24.80975	-
434_115	12.681	0.956554	0.5015	0.901224	0.346586	1.993859	0.901224	0.18347	1.062844	2684.5	17.49	2656.2	9	2620.4	19.4	97.61222	1.00127	108.3134	108.451	79.16768	-
434_64	13.273	0.942163	0.5228	0.898937	0.352357	1.912631	0.898937	0.18411	1.048286	2690.2	17.24	2699.2	8.9	2711.2	19.92	100.7806	1.042483	84.0069	87.57574	20.59912	2.791767
434_05	13.647	0.926566	0.5371	0.893688	0.345395	1.861851	0.893688	0.18431	1.041723	2692	17.09	2725.5	8.77	2771.3	20.12	102.9458	0.934304	123.0127	114.9312	89.73173	0.287209
434_62	13.25	0.944977	0.5208	0.90052	0.351602	1.920086	0.90052	0.18451	1.051434	2693.8	17.27	2697.6	8.92	2702.6	19.89	100.3267	0.642098	71.02873	45.60741	13.96354	1.111817
434_123	13.339	1.017555	0.5242	0.915646	0.331086	1.907596	0.915646	0.18464	1.121101	2695	18.37	2703.9	9.61	2717	20.28	100.8163	0.788229	51.79788	40.82857	38.08888	1.348851
434_96	13.223	1.069401	0.5193	0.945485	0.343386	1.925632	0.945485	0.18465	1.158949	2695.1	19.04	2695.7	10.1	2696.2	20.82	100.0408	0.450284	44.30888	19.95157	12.13428	1.289558
434_22	13.812	0.982419	0.5407	0.913681	0.340602	1.849557	0.913681	0.18529	1.090183	2700.8	17.85	2736.9	9.3	2786.3	20.67	103.1657	0.443315	62.21936	27.58274	41.037	0.715627
434_10	12.97	0.93867	0.5071	0.897312	0.345312	1.972114	0.897312	0.18554	1.050986	2703	17.24	2677.5	8.85	2644.1	19.46	97.82094	0.48963	63.98337	31.32817	26.95678	1.017383
434_93	12.645	0.990369	0.4941	0.916763	0.35045	2.023759	0.916763	0.18557	1.088538	2703.3	17.88	2653.6	9.32	2588.5	19.53	95.75334	0.424828	48.74303	20.70739	12.8579	3.148804
434_70	12.918	0.981362	0.5031	0.912416	0.345605	1.987834	0.912416	0.18622	1.084738	2709.1	17.77	2673.7	9.25	2626.9	19.7	96.96578	0.466235	44.7562	20.86689	25.51809	1.065752
434_121	13.594	1.00789	0.5291	0.912854	0.334924	1.889966	0.912854	0.18643	1.110336	2710.9	18.2	2721.8	9.53	2737.7	20.37	100.9886	0.575626	92.61823	53.31345	65.51909	-
434_12	13.062	0.951652	0.5073	0.902765	0.347167	1.971104	0.902765	0.18675	1.060241	2713.7	17.41	2684.1	8.98	2645.2	19.57	97.47577	1.160153	61.78855	71.68419	46.20023	1.027041
434_33	13.423	0.911834	0.5214	0.88998	0.355731	1.91806	0.88998	0.18674	1.022812	2713.7	16.81	2709.9	8.62	2704.9	19.64	99.67572	0.266831	210.2038	56.08882	47.95099	-
434_84	13.086	1.017889	0.5074	0.926291	0.342244	1.970832	0.926291	0.18703	1.117468	2716.2	18.27	2685.9	9.6	2645.5	20.1	97.3971	0.621734	35.78056	22.246	23.96466	1.270224
434_106	13.37	0.971747	0.5181	0.911109	0.345005	1.930316	0.911109	0.18727	1.078656	2718.3	17.63	2706.1	9.18	2690.9	20.04	98.99202	0.692602	40.88752	28.31878	29.10343	1.692869
434_99	14.203	0.994819	0.5492	0.919503	0.349911	1.820797	0.919503	0.18753	1.093158	2720.6	17.9	2763.3	9.44	2821.9	20.99	103.7234	0.578702	46.0996	26.67792	13.32092	2.001967
434_61	12.93	0.947897	0.4983	0.901027	0.353099	2.006743	0.901027	0.18817	1.05224	2726.3	17.27	2674.5	8.93	2606.6	19.34	95.60943	0.83739	120.8376	101.1882	#VALUE!	#VALUE!
434_58	13.533	0.989256	0.5197	0.915931	0.346439	1.924224	0.915931	0.18886	1.090755	2732.3	17.85	2717.6	9.35	2697.9	20.21	98.74099	0.469169	62.49749	29.32188	10.79995	1.206328
434_21	13.295	0.914506	0.5105	0.889394	0.352077	1.959017	0.889394	0.18891	1.026944	2732.7	16.84	2700.8	8.64	2658.6	19.38	97.2884	0.619771	125.444	77.74655	55.06889	0.073647
434_53	13.974	1.067445	0.5357	0.946443	0.338081	1.866751	0.946443	0.1892	1.162791	2735.2	18.97	2748	10.12	2765.4	21.28	101.1041	0.494695	45.48003	22.49874	7.780238	9.880373
434_68	14.153	0.966226	0.5424	0.908923	0.353105	1.843658	0.908923	0.18923	1.067484	2735.5	17.5	2760	9.16	2793.5	20.6	102.1203	0.444813	63.5592	28.27196	35.46315	-
434_24	13.569	0.939821	0.52	0.898025	0.345991	1.922966	0.898025	0.18925	1.051519	2735.7	17.19	2720.1	8.89	2699.3	19.82	98.66944	0.382553	60.17559	23.02033	39.90757	0.373141
434_20	13.161	0.997281	0.5041	0.918541	0.338604	1.983891	0.918541	0.18938	1.103601	2736.8	18.02	2691.2	9.41	2631.2	19.84	96.14148	0.623096	83.81991	52.22789	35.89195	0.369977
434_94	13.788	1.02017	0.5265	0.92874	0.346715	1.899263	0.92874	0.1899	1.116377	2741.3	18.24	2735.2	9.66	2726.8	20.63	99.47105	0.798591	72.93488	58.24516	23.66333	0.455182
434_14	13.46	0.916405	0.5113	0.889941	0.347946	1.955914	0.889941	0.19096	1.03163	2750.5	16.85	2712.5	8.66	2662	19.41	96.7824	0.568778	106.5699	60.61462	73.37068	0.89266
434_65	14.282	1.011675	0.5422	0.925892	0.346585	1.844406	0.925892	0.19104	1.109715	2751.2	18.12	2768.6	9.6	2792.5	20.98	101.5012	0.461466	49.60593	22.89144	8.327827	-
434_51	4.8626	0.945794	0.3306	0.895261	0.338715	3.024529	0.895261	0.10666	1.059441	1743.1	19.21	1795.8	7.97	1841.4	14.34	105.6394	0.738503	218.5799	161.422	37.4022	-
434_25	4.8329	0.912503	0.3296	0.885922	0.350729	3.033981	0.885922	0.10635	1.024918	1737.8	18.72	1790.6	7.68	1836.4	14.17	105.6738	0.649152	337.3586	218.997	223.9946	0.218287

APPENDIX D

MONAZITE ANALYTICAL DATA

D.1 Textural context, analysis locations, and trace element maps

This section includes:

- A table summarizing the textural setting of each monazite.
- Figures depicting the location of each monazite grain within the respective thin section.
- BSE images (left of each image) and qualitative minor element chemical maps (right of each image) for each monazite grain analyzed. Chemical maps depict concentrations from relatively high to low using red, yellow, green and blue respectively. The BSE images were taken after analysis so the disturbance caused by each analysis point can been seen in the image. Each point is annotated using the monazite grain number first, followed by a letter which represents a zone within the monazite, and then an order number for each point within the zone last. Background and major element analyses are notated with BG and MJ respectively instead of an order number. One background and one major element analyses were completed for each compositional domain within each thin section. Analyses annotated in red were eliminated from statistical results due to textural or analytical interference.

Table D.1: A summary of the textural setting of each monazite grain analyzed.

monazite grain	textural setting
3	in an embayment on the edge of a kyanite crystal (Figure 5.14)
4	with fragments of apatite, between quartz and feldspar crystals (Figure 5.14)
7	between quartz crystals in the leucosome
11	at the edge of leucosome between quartz and biotite (Figure 5.14)
12	between quartz and biotite in the matrix, near the leucosome
15	between quartz and biotite in the matrix
17	between biotite crystals in the matrix
18	between feldspar and biotite in the matrix
19	between feldspar crystals adjacent to garnet
20	within a biotite crystal, adjacent to garnet (Figure 5.14)
21	an inclusion within the same garnet as monazite 22
22	an inclusion within the same garnet as monazite 21
23	between quartz and biotite in the matrix
24	an inclusion within a different garnet than monazite 21 and 22 (Figure 5.14)

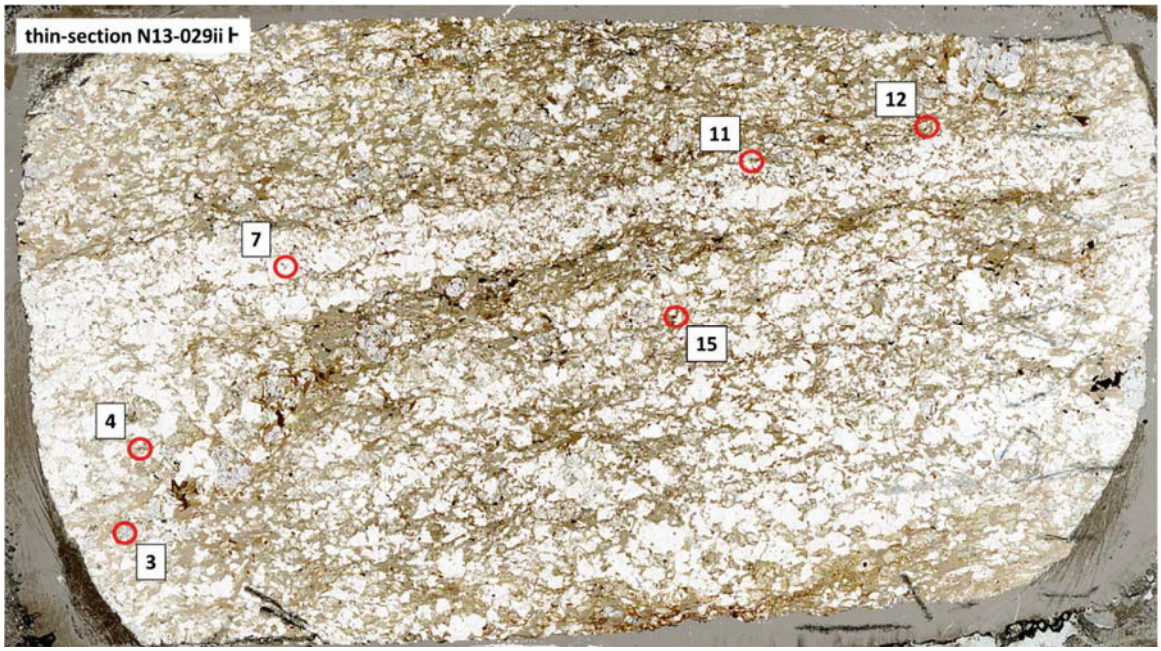

Figure D.1: Scanned polished thin section N13-029ii, perpendicular to foliation, with locations of analyzed monazite grains.

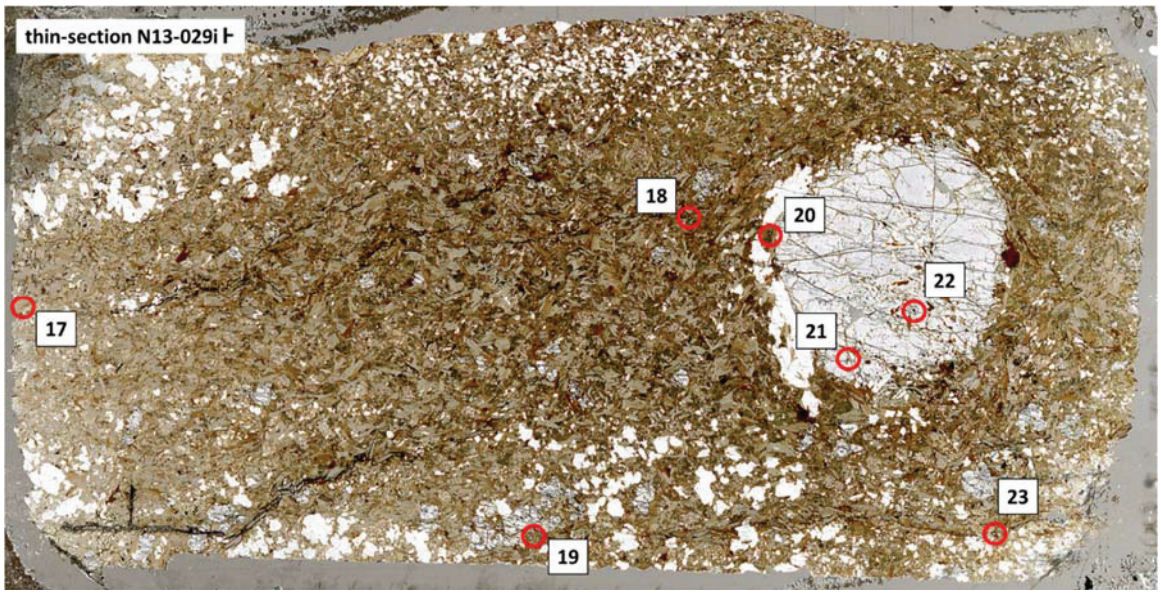

Figure D.2: Scanned polished thin section N13-029i, perpendicular to foliation, with locations of analyzed monazite grains.

Figure D.3: Scanned polished thin section N13-029ii, parallel to foliation, with locations of an analyzed monazite grain.

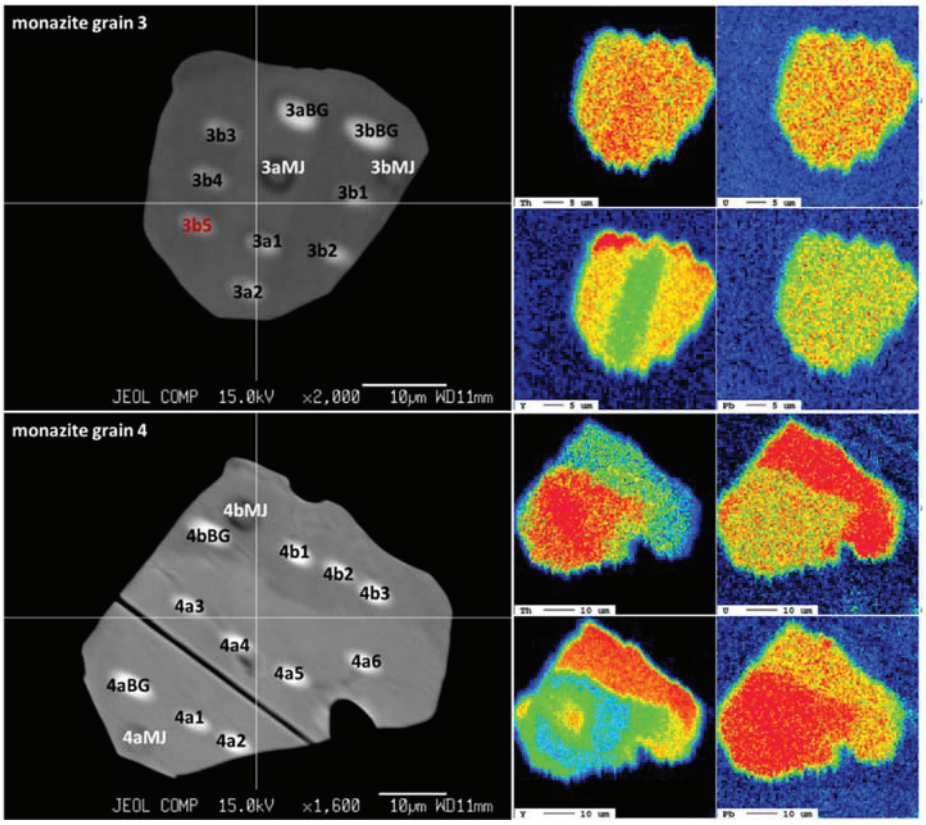

Figure D.4: Analysis locations and chemical maps for monazite grain 3 and 4.

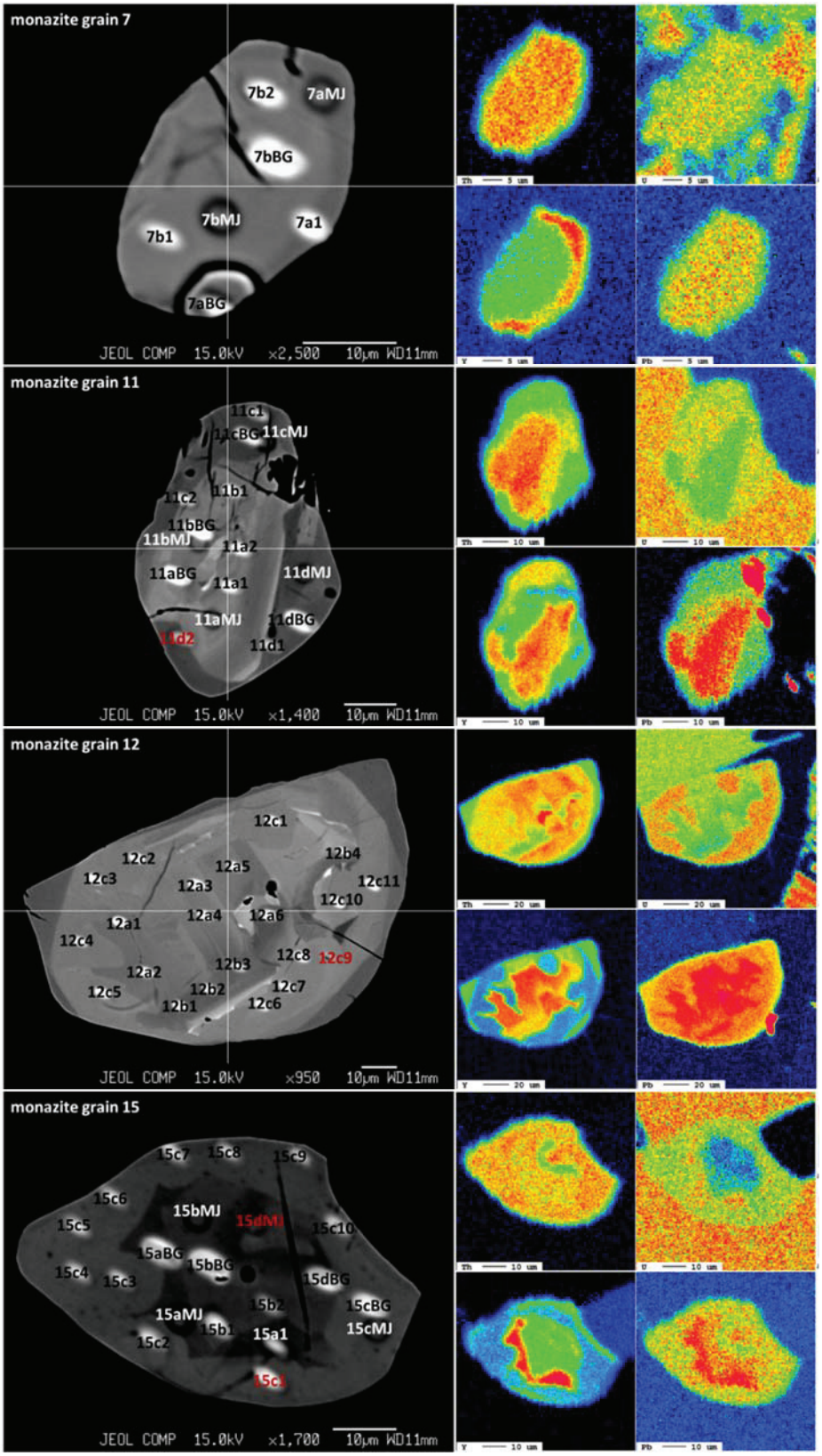

Figure D.5: Analysis locations and chemical maps for monazite grains 7, 11, 12 and 15.

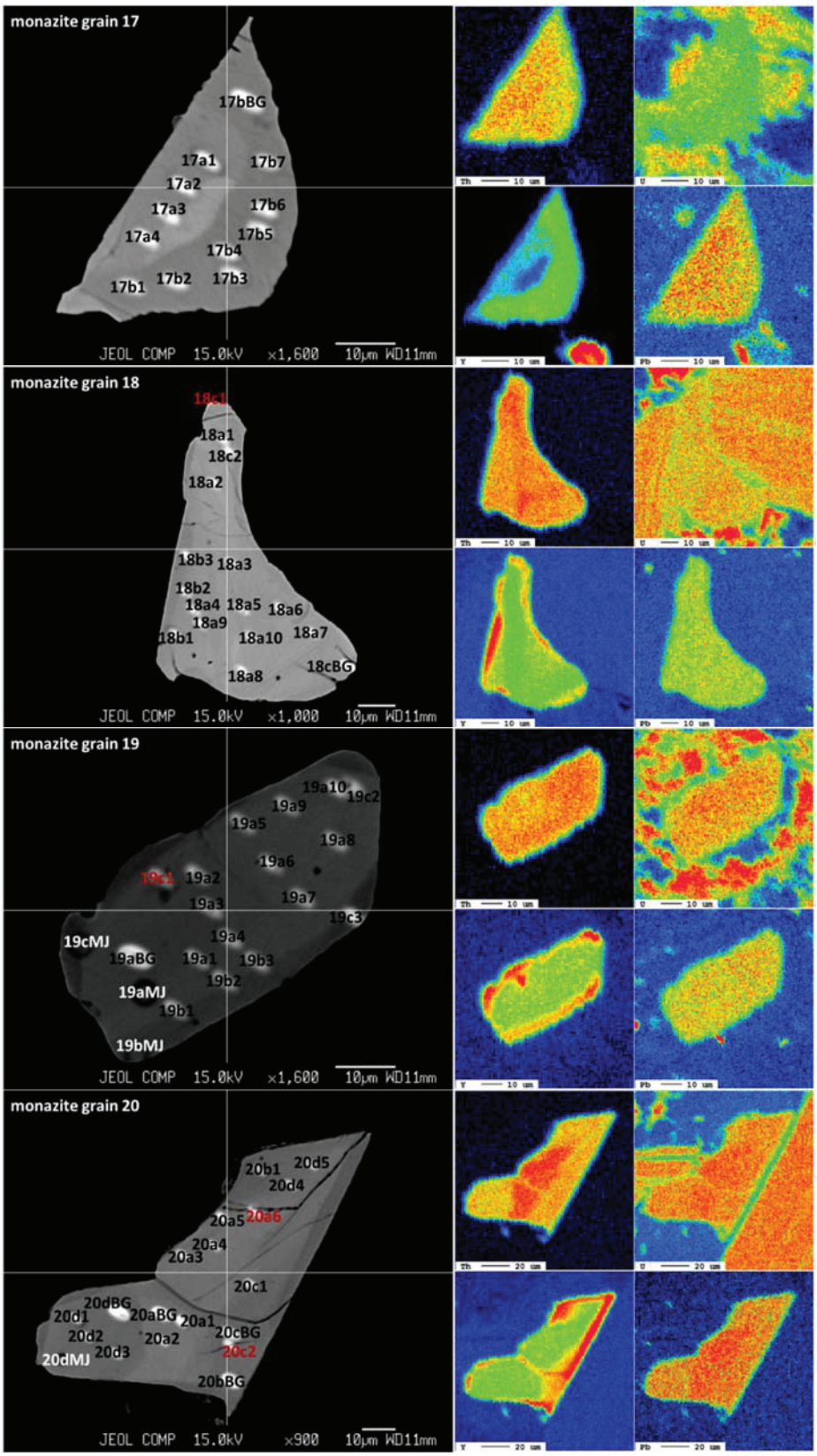

Figure D.6: Analysis locations and chemical maps for monazite grains 17, 18, 19, and 20.

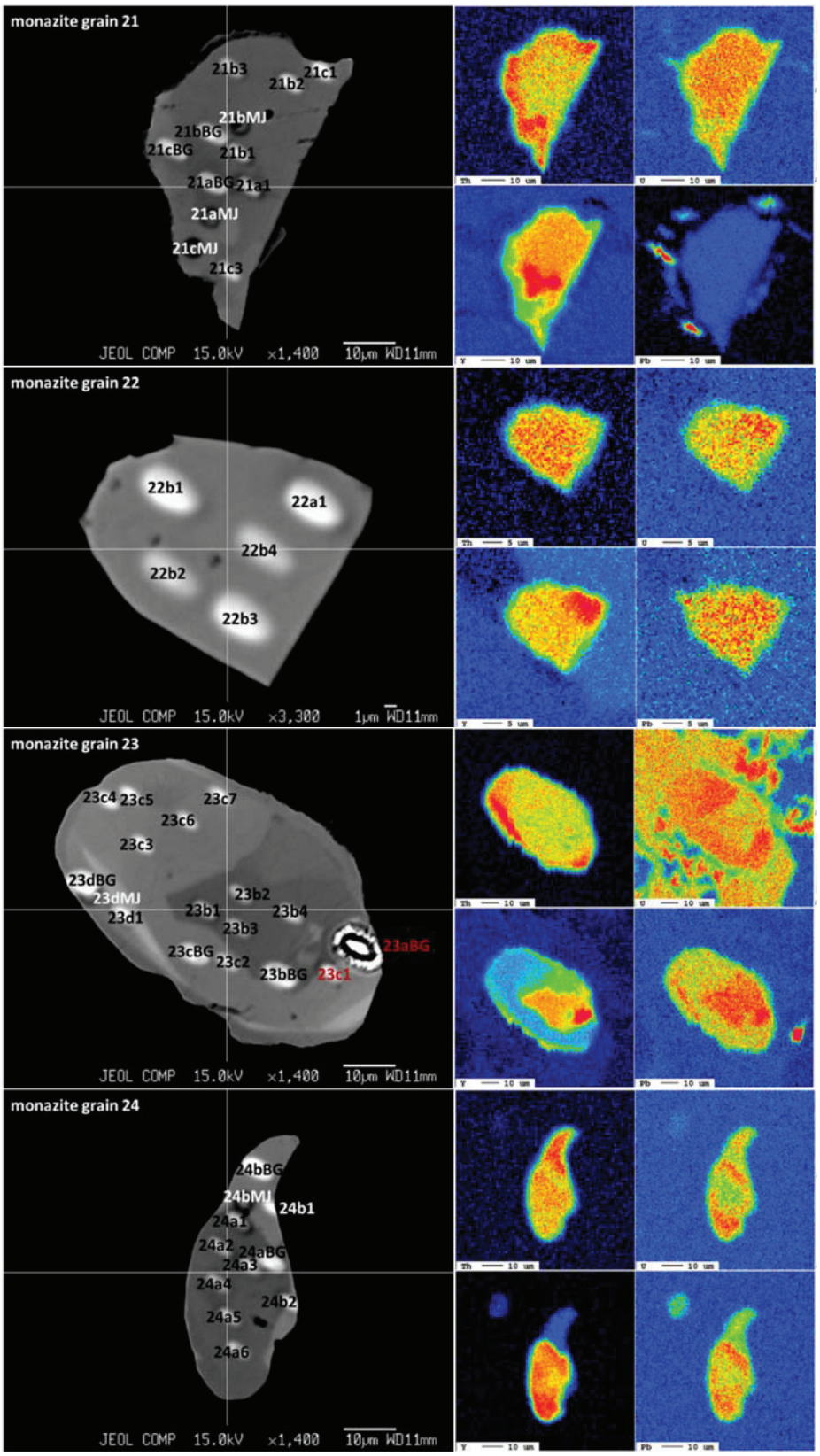

Figure D.7: Analysis locations and chemical maps for monazite grains 21, 22, 23 and 24.

D.2 Quantitative major element analyses

Table D.2: Major element analyses for N13-029 monazite monazite grains.

comp. domain:	grain within embayment in kyanite, low Y core	grain within embayment in kyanite, rim	leucosome, high Y rim	in leucosome, core	edge of leucosome, high Y, Pb and Th, low U	edge of leucosome, high Th, intermediate Pb and U, low Y
zone:	3a	3b	7a	7b	11a	11b
oxides(wt%):						
P2O5	29.02	29.038	28.82	28.342	27.093	27.462
Ce2O3	28.799	27.541	27.444	29.13	24.234	25.463
SiO2	0.402	0.382	0.415	0.523	1.606	1.06
La2O3	14.628	14.063	14.449	15.422	12.193	12.872
SO3	0.026	0.021	0.042	0.012	0	0.012
Dy2O3	0.154	0.411	0.35	0.172	0.573	0.302
Y2O3	0.508	1.323	1.352	0.274	2.456	0.989
Pr2O3	3.221	2.911	2.781	2.884	2.398	2.55
ThO2	4.549	4.275	6.285	6.337	12.172	11.263
Nd2O3	11.9	12.188	11.308	10.31	9.995	10.093
UO2	1.171	1.151	1.149	1.383	0.916	1.453
Sm2O3	1.812	1.862	1.64	1.537	1.536	1.521
CaO	1.089	1.129	1.485	1.418	1.758	2.042
Gd2O3	1.28	1.718	1.446	0.879	1.355	1.065
Eu2O3	0.979	0.931	0.836	0.77	0.537	0.62
TOTAL	99.538	98.944	99.802	99.393	98.822	98.767
cations:						
P	0.2441	0.2446	0.2421	0.2408	0.2315	0.2355
Ce	0.1048	0.1003	0.0997	0.107	0.0895	0.0944
Si	0.004	0.0038	0.0041	0.0052	0.0162	0.0107
La	0.0536	0.0516	0.0529	0.0571	0.0454	0.0481
S	0.0002	0.0002	0.0003	0.0001	0	0.0001
Dy	0.0005	0.0013	0.0011	0.0006	0.0019	0.001
Y	0.0027	0.007	0.0071	0.0015	0.0132	0.0053
Pr	0.0117	0.0106	0.0101	0.0105	0.0088	0.0094
Th	0.0103	0.0097	0.0142	0.0145	0.028	0.026
Nd	0.0422	0.0433	0.0401	0.037	0.036	0.0365
U	0.0026	0.0025	0.0025	0.0031	0.0021	0.0033
Sm	0.0062	0.0064	0.0056	0.0053	0.0053	0.0053
Ca	0.0116	0.012	0.0158	0.0152	0.019	0.0222
Gd	0.0042	0.0057	0.0048	0.0029	0.0045	0.0036
Eu	0.0033	0.0032	0.0028	0.0026	0.0019	0.0021
TOTAL	0.5021	0.5023	0.5033	0.5034	0.5033	0.5035

Table D.2: *Continued.* Major element analyses for N13-029 monazite monazite grains.

comp. domain:	edge of leucosome, intermediate Y and U, low Pb and Th	edge of leucosome, intermediate U, low Th Y and Pb	inclusion in garnet, inner core	inclusion in garnet, outer core	inclusion in garnet, rim	inclusion in garnet, rim
zone:	11c	11d	21a	21b	21c	21c (repeat)
oxides:						
P2O5	28.707	29.129	28.971	29.213	29.346	29.677
Ce2O3	26.308	26.994	24.877	26.306	26.188	27.981
SiO2	0.357	0.334	0.118	0.159	0.144	0.28
La2O3	13.476	13.613	11.983	12.781	12.883	14.184
SO3	0.005	0	0.013	0	0	0
Dy2O3	0.563	0.623	1.165	0.855	0.783	0.3
Y2O3	1.881	1.607	2.676	1.872	1.891	0.705
Pr2O3	2.846	2.707	2.709	2.82	2.68	2.671
ThO2	6.122	6.432	2.774	3.16	2.953	3.885
Nd2O3	11.312	11.138	12.455	12.566	12.725	12.322
UO2	1.349	1.236	1.768	1.773	1.864	1.304
Sm2O3	1.858	1.799	3.793	3.266	3.123	2.679
CaO	1.581	1.658	1.061	1.16	1.112	1.052
Gd2O3	1.58	1.391	4.75	3.76	3.817	2.176
Eu2O3	0.809	0.747	0.835	0.851	0.879	0.83
TOTAL	98.754	99.408	99.948	100.542	100.388	100.046
cations:						
P	0.243	0.2443	0.2437	0.2441	0.245	0.247
Ce	0.0963	0.0979	0.0905	0.0951	0.0945	0.1007
Si	0.0036	0.0033	0.0012	0.0016	0.0014	0.0028
La	0.0497	0.0497	0.0439	0.0465	0.0469	0.0514
S	0	0	0.0001	0	0	0
Dy	0.0018	0.002	0.0037	0.0027	0.0025	0.0009
Y	0.01	0.0085	0.0141	0.0098	0.0099	0.0037
Pr	0.0104	0.0098	0.0098	0.0101	0.0096	0.0096
Th	0.0139	0.0145	0.0063	0.0071	0.0066	0.0087
Nd	0.0404	0.0394	0.0442	0.0443	0.0448	0.0433
U	0.003	0.0027	0.0039	0.0039	0.0041	0.0029
Sm	0.0064	0.0061	0.013	0.0111	0.0106	0.0091
Ca	0.0169	0.0176	0.0113	0.0123	0.0118	0.0111
Gd	0.0052	0.0046	0.0156	0.0123	0.0125	0.0071
Eu	0.0028	0.0025	0.0028	0.0029	0.003	0.0028
TOTAL	0.5034	0.503	0.5041	0.5038	0.5033	0.5012

Table D.2: *Continued.* Major element analyses for N13-029 monazite monazite grains.

comp. domain:	inclusion in garnet, rim	matrix high Y and U edge	matrix high Th and Pb core	matrix, high Th rim	matrix, high Y and Pb inner core	matrix, intermediate Y and Pb, low U and Th core
zone:	24b	4b	4a	32d	15a	15b
oxides:						
P2O5	29.226	28.886	29.188	28.709	29.18	29.131
Ce2O3	30.007	27.637	29.192	29.278	27.435	29.745
SiO2	0.515	0.189	0.309	0.492	0.212	0.235
La2O3	15.668	13.673	14.543	14.922	13.691	15.135
SO3	0.016	0.014	0.006	0.019	0.012	0.014
Dy2O3	0.122	0.72	0.344	0.22	0.785	0.32
Y2O3	0.001	2.217	0.904	0.424	2.72	0.776
Pr2O3	2.737	2.997	2.871	2.87	2.968	2.854
ThO2	5.279	4.088	5.288	5.327	4.2	5.007
Nd2O3	11.103	11.924	11.671	11.761	11.459	11.483
UO2	0.868	1.408	0.492	1.02	1.666	0.571
Sm2O3	1.583	2.233	1.744	1.648	1.872	1.707
CaO	1.064	1.123	1.216	1.09	1.358	1.216
Gd2O3	0.487	1.722	1.099	1.113	1.623	1.104
Eu2O3	1.051	0.875	0.776	0.822	0.685	0.693
TOTAL	99.727	99.706	99.643	99.715	99.866	99.991
cations:						
P	0.2447	0.2431	0.2447	0.2423	0.2436	0.2442
Ce	0.1087	0.1006	0.1058	0.1069	0.0991	0.1078
Si	0.0051	0.0019	0.0031	0.0049	0.0021	0.0023
La	0.0572	0.0501	0.0531	0.0549	0.0498	0.0553
S	0.0001	0.0001	0	0.0001	0.0001	0.0001
Dy	0.0004	0.0023	0.0011	0.0007	0.0025	0.001
Y	0	0.0117	0.0048	0.0022	0.0143	0.0041
Pr	0.0099	0.0109	0.0104	0.0104	0.0107	0.0103
Th	0.0119	0.0092	0.0119	0.0121	0.0094	0.0113
Nd	0.0392	0.0423	0.0413	0.0419	0.0404	0.0406
U	0.0019	0.0031	0.0011	0.0023	0.0037	0.0013
Sm	0.0054	0.0077	0.006	0.0057	0.0064	0.0058
Ca	0.0113	0.012	0.0129	0.0116	0.0143	0.0129
Gd	0.0016	0.0057	0.0036	0.0037	0.0053	0.0036
Eu	0.0036	0.003	0.0026	0.0028	0.0023	0.0023
TOTAL	0.501	0.5038	0.5024	0.5026	0.504	0.503

Table D.2: *Continued.* Major element analyses for N13-029 monazite monazite grains.

comp. domain:	matrix, low Y and Pb rim		matrix, high Y rim	matrix average to low Y core	matrix, intermediate to high Y rim	matrix average to low Y core, lower Th
zone:	15c	15d	19c	19a	19b	20d
oxides:						
P2O5	28.703	29.241	29.115	28.431	28.803	29.855
Ce2O3	29.432	30.566	28.036	29.154	27.842	30.471
SiO2	0.357	0.269	0.376	0.505	0.831	0.383
La2O3	15.447	15.454	14.775	15.244	14.709	15.749
SO3	0	0	0.008	0.009	0.085	0.01
Dy2O3	0.133	0.235	0.513	0.356	0.482	0.21
Y2O3	0.171	0.879	1.704	0.636	1.323	0.438
Pr2O3	2.963	2.944	2.766	3.038	2.92	2.84
ThO2	4.944	4.632	4.8	5.169	4.667	3.884
Nd2O3	11.395	11.307	11.825	11.684	11.38	11.379
UO2	1.402	0.365	0.903	1.208	1.15	0.851
Sm2O3	1.577	1.637	1.656	1.81	1.74	1.575
CaO	1.226	1.077	1.058	1.061	1.15	0.846
Gd2O3	1.014	0.92	1.32	1.11	1.286	1.097
Eu2O3	0.816	0.665	0.756	0.786	0.729	0.904
TOTAL	99.58	100.19	99.611	100.201	99.097	100.492
cations:						
P	0.2429	0.2444	0.244	0.2403	0.2414	0.2468
Ce	0.1077	0.1105	0.1016	0.1066	0.1009	0.1089
Si	0.0036	0.0027	0.0037	0.005	0.0082	0.0037
La	0.057	0.0563	0.0539	0.0561	0.0537	0.0567
S	0	0	0.0001	0.0001	0.0006	0.0001
Dy	0.0004	0.0007	0.0016	0.0011	0.0015	0.0007
Y	0.0009	0.0046	0.009	0.0034	0.007	0.0023
Pr	0.0108	0.0106	0.01	0.0111	0.0105	0.0101
Th	0.0112	0.0104	0.0108	0.0117	0.0105	0.0086
Nd	0.0407	0.0399	0.0418	0.0417	0.0402	0.0397
U	0.0031	0.0008	0.002	0.0027	0.0025	0.0018
Sm	0.0054	0.0056	0.0056	0.0062	0.0059	0.0053
Ca	0.0131	0.0114	0.0112	0.0113	0.0122	0.0089
Gd	0.0034	0.003	0.0043	0.0037	0.0042	0.0036
Eu	0.0028	0.0022	0.0026	0.0027	0.0025	0.003
TOTAL	0.5031	0.5032	0.5023	0.5037	0.5019	0.5002

Table D.3: Major element analyses for in-house Monazite53 standard and the Geological Society of Canada's monazite standard.

Standard	Monazite 53 in-house control							
Analysis No.	1	2	28	29	31	32	41	49
oxides:								
P2O5	27.918	27.648	28.368	28.059	27.808	27.498	27.934	27.468
Ce2O3	32.999	32.529	32.538	33.663	32.967	32.997	33.19	33.14
SiO2	0.889	0.838	0.934	0.873	0.932	0.971	0.755	0.888
La2O3	16.88	16.575	17.078	16.466	16.733	16.812	16.836	16.809
SO3	0.374	0.478	0.457	0.46	0.472	0.47	0.485	0.454
Dy2O3	0.193	0.17	0.133	0.291	0.076	0.066	0.186	0.058
Y2O3	0.507	0.523	0.551	0.586	0.578	0.519	0.593	0.572
Pr2O3	3.119	3.005	2.996	3.134	3.128	3.058	2.925	2.947
ThO2	3.387	3.158	2.851	2.957	3.231	3.534	2.842	3.12
Nd2O3	10.943	11.015	11.307	11.198	10.724	10.873	11.123	11.087
UO2	0.052	0.058	0.049	0	0	0	0.015	0
Sm2O3	0.988	0.94	1.049	1.014	1.006	0.956	0.969	0.969
CaO	0.402	0.552	0.399	0.445	0.477	0.528	0.541	0.43
Gd2O3	0.407	0.481	0.478	0.338	0.546	0.558	0.449	0.543
Eu2O3	0.925	0.926	0.887	0.914	0.872	0.894	0.888	0.868
TOTAL	99.983	98.896	100.075	100.398	99.55	99.734	99.731	99.353
cations:								
P	0.2354	0.235	0.2368	0.235	0.2347	0.2329	0.2354	0.2336
Ce	0.1203	0.1196	0.1174	0.1219	0.1203	0.1208	0.121	0.1219
Si	0.0088	0.0084	0.0092	0.0086	0.0093	0.0097	0.0075	0.0089
La	0.062	0.0614	0.0621	0.0601	0.0615	0.062	0.0618	0.0623
S	0.0028	0.0036	0.0034	0.0034	0.0035	0.0035	0.0036	0.0034
Dy	0.0006	0.0006	0.0004	0.0009	0.0002	0.0002	0.0006	0.0002
Y	0.0027	0.0028	0.0029	0.0031	0.0031	0.0028	0.0031	0.0031
Pr	0.0113	0.011	0.0108	0.0113	0.0114	0.0111	0.0106	0.0108
Th	0.0077	0.0072	0.0064	0.0067	0.0073	0.008	0.0064	0.0071
Nd	0.0389	0.0395	0.0398	0.0396	0.0382	0.0388	0.0395	0.0398
U	0.0001	0.0001	0.0001	0	0	0	0	0
Sm	0.0034	0.0033	0.0036	0.0035	0.0035	0.0033	0.0033	0.0034
Ca	0.0043	0.0059	0.0042	0.0047	0.0051	0.0057	0.0058	0.0046
Gd	0.0013	0.0016	0.0016	0.0011	0.0018	0.0019	0.0015	0.0018
Eu	0.0031	0.0032	0.003	0.0031	0.003	0.0031	0.003	0.003
TOTAL	0.5027	0.5033	0.5017	0.5031	0.503	0.5038	0.5032	0.5039

Table D.3: *Continued.* Major element analyses for in-house Monazite53 standard and the Geological Society of Canada's monazite standard.

Standard	Monazite 53 in-house control			GSC 8153				
Analysis No.	58	60	61	30	50	42	59	62
oxides:								
P2O5	28.01	28.535	28.185	28.435	27.503	27.3	27.478	28.111
Ce2O3	33.249	32.506	32.86	31.46	29.964	30.596	29.816	29.356
SiO2	0.811	0.724	0.957	0.719	1.143	1.035	1.128	1.388
La2O3	16.588	16.315	16.586	14.663	14.213	14.763	14.147	13.844
SO3	0.375	0.417	0.565	0.032	0.017	0.079	0.028	0.087
Dy2O3	0.25	0.25	0.124	0.324	0.26	0.172	0.4	0.366
Y2O3	0.51	0.597	0.557	0.344	0.339	0.231	0.325	0.442
Pr2O3	2.983	2.884	2.806	3.384	3.316	3.165	3.23	3.096
ThO2	2.882	3.344	3.053	4.889	7.077	6.094	6.575	7.66
Nd2O3	11.154	10.749	10.73	11.882	11.716	11.416	11.588	10.879
UO2	0.084	0	0.08	0.148	0.156	0.233	0.137	0.42
Sm2O3	0.949	0.982	1.094	2.406	2.569	2.323	2.38	2.522
CaO	0.441	0.67	0.587	0.528	0.557	0.619	0.518	0.599
Gd2O3	0.447	0.476	0.416	1.007	0.946	0.977	0.97	0.998
Eu2O3	0.833	0.964	1	0.845	0.796	0.79	0.793	0.873
TOTAL	99.566	99.413	99.6	101.066	100.572	99.793	99.513	100.641
cations:								
P	0.2365	0.239	0.2358	0.2389	0.2342	0.2341	0.2354	0.236
Ce	0.1214	0.1177	0.1189	0.1143	0.1103	0.1134	0.1104	0.1066
Si	0.0081	0.0072	0.0095	0.0071	0.0115	0.0105	0.0114	0.0138
La	0.061	0.0595	0.0605	0.0537	0.0527	0.0551	0.0528	0.0506
S	0.0028	0.0031	0.0042	0.0002	0.0001	0.0006	0.0002	0.0006
Dy	0.0008	0.0008	0.0004	0.001	0.0008	0.0006	0.0013	0.0012
Y	0.0027	0.0031	0.0029	0.0018	0.0018	0.0012	0.0017	0.0023
Pr	0.0108	0.0104	0.0101	0.0122	0.0122	0.0117	0.0119	0.0112
Th	0.0065	0.0075	0.0069	0.011	0.0162	0.014	0.0151	0.0173
Nd	0.0397	0.038	0.0379	0.0421	0.0421	0.0413	0.0419	0.0385
U	0.0002	0	0.0002	0.0003	0.0003	0.0005	0.0003	0.0009
Sm	0.0033	0.0033	0.0037	0.0082	0.0089	0.0081	0.0083	0.0086
Ca	0.0047	0.0071	0.0062	0.0056	0.006	0.0067	0.0056	0.0064
Gd	0.0015	0.0016	0.0014	0.0033	0.0032	0.0033	0.0033	0.0033
Eu	0.0028	0.0033	0.0034	0.0029	0.0027	0.0027	0.0027	0.003
TOTAL	0.5028	0.5017	0.5021	0.5027	0.5031	0.5038	0.5024	0.5003

D.3 Background positions for U, Th, Pb and Y trace elements

Table D.4: Background positions for each minor element analysis.

No.	analysis point	Background Position (nm)							
		Th BG+	Th BG-	U BG+	U BG-	Y BG +	Y BG-	Pb BG+	Pb BG-
2	3a1	424.3	443.9	1044.2	1182.5	3973.4	4987.9	638.5	835.1
3	3a2	426.9	449	1048.8	1179.0	3963.3	5018.6	651.1	826.5
4	3b1	424.3	447.5	1044.2	1173.4	3972.4	5294.1	637.5	812.5
5	3b2	424	447.2	1056.3	1171	3985.4	5335.5	640.3	829
6	3b3	419.1	447.2	1049.8	1178.9	3974.9	5253.3	636.2	823.1
7	3b4	422.1	448.7	1052.8	1172.9	3960.3	5250.8	645.2	814.6
8	3b4	423.8	440.9	1039.8	1178.2	3957.2	5246.1	643.7	818.8
9	3b5	845.5	40.8	325.1	64.4	2255.2	822.8	335.7	81.5
10	4a1	432.8	457.8	1060	1183.4	4046	5131.4	645.2	827.6
11	4a2	426.1	454	1040.5	1183.8	4058.4	5111.9	654.3	822.7
12	4a3	421.1	456	1053.9	1179.8	4068.4	5291.2	642.9	814.2
13	4a4	435.9	459.5	1047.1	1179.2	4045.6	5212.7	650.7	825.3
14	4a5	425.1	455.7	1045.1	1184.8	4031.6	5033	645.5	825.7
15	4a6	427.4	450.5	1046.6	1177.2	4012	5221.2	641.1	824.3
16	4b1	429.6	445	1038.5	1179.8	4078.4	5735.3	641.4	810.2
17	4b2	422.1	449.5	1048.9	1173.3	4074.4	5728.8	642.9	816.7
18	4b3	416.7	446.6	1050.9	1169.7	4090.8	5745.5	645.7	811.4
19	7a1	430.1	452.6	1063.4	1185.6	4093.8	5482.5	648.2	843.3
20	7b1	432.2	452.2	1072	1201.6	4021.5	4959	656.3	844.9
21	7b2	434.4	458	1057.1	1194.7	4063.1	5001	652.7	834.3
22	11a1	451	478	1087	1210	4280	6082	659.5	877.5
23	11a2	454.2	478.2	1083	1233.6	4258.6	5956.5	669.8	875.9
24	11b1	440	471	1083	1210.5	4157	5340	657.5	860.5
25	11c1	421.3	453.8	1050	1186.9	4091.9	5657.2	654.2	829.6
26	11c2	427.1	451.2	1057.6	1198.3	4143.7	5645	645.5	835.2
27	11d1	435.1	458.1	1072.2	1191	4045.1	5188.5	648.1	833.6
28	11d2	428.9	446.9	1061.6	1194.9	4067.1	5406.8	654.8	840.7
29	12a1	449.5	471.5	1061.9	1204.3	4225.3	6285.2	656.8	856.1
30	12a2	438.5	474	1065	1193	4208	6239.5	653.5	851.5
31	12a3	452.5	476	1072.5	1208	4260.5	6418.5	667	872.5
32	12a4	452.8	476.8	1072	1217.4	4253.4	6327.3	655.7	853.1
33	12a5	444.5	469.5	1077.5	1218	4208.5	6250	664	856.5
34	12b1	438.9	461	1053.1	1203.2	4131.1	5874.4	650.2	828.3
35	12b2	433.4	460.5	1056.1	1193.2	4135.1	5825.8	651.7	826.8
36	12b3	437.5	463.5	1071	1193.5	4106	5846.5	651.5	841
37	12a6	448	461.5	1063.1	1196.2	4257.3	6295.8	647.2	856.4
38	12b4	440.1	468.2	1072.2	1206.5	4128.8	5862.2	662.2	851.6
39	12c1	452.2	474.2	1094.6	1225.6	4156.1	5243.6	671.3	871.4

Table D.4: *Continued.* Background positions for each minor element analysis

No.	analysis point	Background Position (nm)							
		Th BG+	Th BG-	U BG+	U BG-	Y BG +	Y BG-	Pb BG+	Pb BG-
40	12c2	453.8	471.8	1078.5	1215.9	4135.9	5138.4	662.2	867.6
41	12c3	449.3	476.3	1070.5	1221.4	4132.9	5099.5	659.7	865.1
42	12c4	448.5	470.5	1075	1207.5	4109	5053	665.5	853.5
43	12c5	449.7	471.2	1073.1	1210.8	4149.2	5106.2	656.5	861.8
46	12c6	454.5	481.5	1081.6	1227.2	4172.2	5142.6	672.7	882.9
47	12c7	457.6	474.2	1095.2	1225.1	4162.4	5138.9	673.2	877.7
48	12c8	445.6	478.2	1081.7	1224.1	4172.4	5157.9	669.2	860.2
49	12c9	1	1	0.5	0.5	0.5	1	0.5	0.5
50	12c10	457.8	476.4	1098	1218.1	4112.6	5087.4	674.4	861.8
51	12c11	458.6	472.1	1080.4	1211.4	4080.9	5057.8	662	854.3
52	15a1	427.8	452.9	1038.2	1175.1	4099.1	6219.9	635.6	817.3
53	15b1	420.8	446.5	1037.7	1166.4	3772.2	5026.1	650.1	819.5
54	15b2	428.9	446.6	1053.9	1195.1	3782.8	5014.1	647.7	824.1
55	15c1	429.6	455.3	1045.7	1190.9	3942.2	5005	645.2	819.1
56	15c2	438.1	459.3	1063.9	1197.7	3955.2	5002.5	643.4	821.9
57	15c3	440.2	449.2	1062.3	1180.9	3934.7	4920.6	643.2	832.2
58	15c4	429.6	455.7	1066.9	1194.7	3953.7	4948.7	648.9	821.9
59	15c5	436.5	451	1071.8	1200.4	3966.9	4968.4	645.4	826.7
60	15c6	442.4	451.9	1073	1194.8	3996.5	4986.9	656.3	832.9
61	15c7	432.2	448.7	1051.3	1177.9	4003	5206	639.7	810.5
62	15c8	433.4	451.5	1063.3	1189	3985.4	5113.1	643.5	829.6
63	15c9	435.9	461.5	1058.3	1191.6	4014.6	5239.3	654.6	822.5
64	15c10	431.2	451.3	1056.8	1185.4	4055.8	5120.6	649.2	831.2
65	17a1	430.4	455.6	1044.9	1189	4013.1	5454.6	643.7	808.5
66	17a2	428.6	458.9	1053.4	1188.1	4076.1	5502.3	635.9	822
67	17a3	433.3	454	1049.5	1185.9	4005.6	5293.4	643.4	811.6
68	17a4	434	455.7	1048.1	1187.2	4050.1	5416.3	642.9	819.4
69	17b2	426.2	444.2	1046.5	1174.1	4000.5	5704.9	639.8	820.9
70	17b3	421.3	441.8	1040.5	1170.4	4003	5701.1	639.2	808.6
71	17b4	420.7	434.7	1051	1184.1	4014.5	5734.9	645.3	814.4
72	17b5	422.3	441.8	1038.5	1179.4	3992.5	5666.2	638.2	812.1
73	17b6	417.2	447.7	1045.5	1170.1	3997.5	5697.9	646.3	813.4
74	17b7	420.4	439.9	1055.6	1182.2	4027.5	5670.2	641.6	801.3
75	18a1	440.2	461	1055.2	1182.9	4002	5002.5	645.9	827.8
76	18a2	438.3	467.6	1058.7	1197.9	4009.6	5031.9	645.2	827.9
77	18a3	434.6	462.4	1042.9	1185.9	4001	4998.5	647.3	826.7
78	18a4	428.9	458.2	1059.5	1181.4	4014.1	5068.5	638.1	821.6
79	18a5	433.5	456.6	1057.5	1185.5	4000	5049.9	655.2	821.1
80	18a6	433.2	465.5	1050.4	1184.6	4045.4	5107.4	642.5	831.6
81	18a7	433	457.7	1053.9	1191.5	4044.4	5087.7	647.2	831.2

Table D.4: *Continued.* Background positions for each minor element analysis

No.	analysis point	Background Position (nm)							
		Th BG+	Th BG-	U BG+	U BG-	Y BG +	Y BG-	Pb BG+	Pb BG-
82	18a8	440	460.6	1056	1186.2	4021.2	5053	649.8	822.4
83	18a9	434.9	464.6	1064.1	1182.8	4028.8	5060.1	648	827.3
84	18a10	439.2	467	1049.4	1181	4032.8	5089.8	647.5	821.5
85	18b1	429.7	450.3	1050.7	1177.7	3781.1	4886	646.1	819.8
86	18b2	429.7	447.3	1055.7	1188.2	3787.6	4986.5	635.5	814.8
87	18b3	429	450.1	1043.2	1188.2	3828.4	5254.4	644.2	805.3
88	18c1	240.3	244.9	614.7	664.8	3113.4	2671.9	387.4	462.6
89	18c2	428.5	460.6	1050.2	1190.2	3976.9	4993	631.7	818.9
92	19a1	434.6	466.4	1048	1187.5	4068.2	5214.2	644.3	828.7
93	19a2	437.9	468.2	1058.6	1186.4	4074.8	5257.1	648.5	831.3
94	19a3	436.8	466.6	1057.6	1185.5	4054.1	5225.5	638	819.5
95	19a4	447.6	461.3	1068.3	1190.7	4058.7	5247.3	646.9	828.5
96	19a5	437.3	470.2	1058.7	1188.1	4087	5246.7	642.6	829.1
97	19a6	443.6	471.9	1061.2	1188.7	4115.8	5284.3	644.4	836.1
98	19a7	439.8	465.6	1063.2	1181	4093.5	5275.5	641.6	818.5
99	19a8	446.9	470.6	1063.3	1198.9	4106.3	5271.2	653.8	832
100	19a9	447.1	470.9	1070.8	1194.7	4105.2	5295.4	648.5	832.1
101	19a10	446.4	466.1	1059.7	1192.6	4149.1	5355.4	656.7	830.1
102	19b1	430.3	464	1044.8	1176.2	3931.6	5217.4	635.6	822.8
103	19b2	428.6	452	1057.9	1194	4008.1	5116.3	650.6	827.3
104	19b3	432.6	459.9	1050	1185.8	3974.8	5114.1	650.7	827.9
105	19c1	428.6	452.2	1053.8	1183.1	3893.9	5460.8	637.8	809.4
106	19c2	420	451.6	1052.7	1184.7	3876.1	5024.6	648.8	826.4
107	19c3	410.1	435.2	1016.6	1137.6	3867	5446.8	631.5	809.2
108	20a1	452	479.8	1056.1	1193.1	4133	5279.1	651.7	825.1
109	20a2	450.2	480	1072.8	1202.1	4150.1	5251.1	649.3	835.3
110	20a3	442.6	484.1	1064.7	1195.6	4167.3	5272.4	644.8	833.2
111	20a4	448.5	475.8	1062.1	1189.9	4143.4	5234.9	644.4	827.3
114	20a5	443	476.8	1060	1200.6	4123.5	5275.7	638.6	821.6
115	20a6	447.5	479.8	1051	1194.8	4261.4	5253.3	640.8	817.4
116	20b1	433.2	454.8	1049.7	1192.3	3872	5324.8	640.1	799.7
117	20c1	429.2	457.9	1049.4	1185.9	3984.4	5104.3	646.8	821.7
118	20c2	434.3	455	1051.8	1166.1	3978.4	5230	638.2	814.8
119	20d1	428.9	451.1	1065.5	1200.1	3854.8	4916.3	648.7	821.6
120	20d2	425.8	455.8	1052	1180.4	3816.6	4838.1	634.7	811.6
121	20d3	430.9	448	1051.1	1188.2	3775.3	4807.3	636.1	814.8
122	20d4	430.9	452.9	1052.6	1185.4	3798.1	4887.3	641.3	818.1
123	20d5	427.8	447.3	1056.7	1182.6	3779.3	4864.1	646.4	821.5
124	21a1	423.5	451.2	1036.2	1169.2	4070	6185.3	628.4	805.6
125	21b1	429.4	455.5	1052.8	1176.5	4049.8	5684.8	631.5	814

Table D.4: *Continued.* Background positions for each minor element analysis

No.	analysis point	Background Position (nm)							
		Th BG+	Th BG-	U BG+	U BG-	Y BG +	Y BG-	Pb BG+	Pb BG-
126	21b2	430.4	463	1056.8	1185	4110.1	5655.6	641	815.5
127	21b3	432.2	456.8	1057.8	1186.4	4079.9	5634.2	635.7	812.6
128	21c1	433.1	461.8	1053.8	1189.6	4102.6	5310.4	638.8	823.4
130	21c3	436.3	456.5	1059.9	1189.2	4001	5215.4	644.7	812.3
131	22a1	435.2	458.3	1056.8	1167.8	4126.1	5551.8	632.7	811.6
132	22b1	439.9	462.5	1044.2	1190.6	4068.4	5209.6	648.6	813
133	22b2	433.4	460.5	1048.3	1186	4052.8	5222.7	642	814.5
134	22b3	439.1	467.8	1049.3	1185.3	4060.4	5247.7	642.5	821.8
135	22b4	433.8	456.5	1055.9	1200.3	4069.9	5256.7	647.7	818.8
138	23b1	420.7	444.4	1050.3	1178.7	3787.6	5380	645.2	813.8
139	23b2	418.8	443.4	1041.2	1184.5	3792.4	5380.1	648.1	822.5
140	23b3	424.8	443.9	1051.8	1183	3793.4	5396.2	649.1	819
141	23b4	425.3	446.4	1049.8	1174.6	3798.7	5398.1	637.6	825.9
142	23c1	435	449.5	1045.2	1183.8	4025.1	5287.8	655.5	826.7
143	23c2	435.2	460.8	1065.8	1193	4004	4965.8	648.2	830.7
144	23c3	442.7	467.8	1039.2	1190.9	3979.9	4976.9	656.3	826.1
145	23c4	439.4	468.1	1073.9	1192.1	4034.7	4990.5	646	823.5
146	23c5	446.2	466.8	1054.3	1190.4	4002.5	4994.5	652.3	835.2
147	23c6	441.6	456.2	1046.8	1188.6	4017.1	5037.7	644.4	827.5
148	23c7	441.6	463.2	1054.9	1186.8	4028.7	5055.9	644	832.8
149	23d1	452.8	479.9	1078.9	1223.6	4073.9	5064.8	661.8	854.8
151	24a1	426.7	456.4	1043.3	1178.8	4069.5	5969.3	638.3	810.6
152	24a2	432.2	454.9	1049.4	1176.8	4029.2	5726.5	630.7	806.5
153	24a3	428.5	462.2	1044.8	1174.2	4077.5	5825.3	633.4	818.7
154	24a4	431.5	451.2	1034.7	1172.7	4043.8	5874.6	639	819.2
155	24a5	428.8	455.5	1041.8	1167.1	4048.8	5759.4	640.2	815.8
156	24a6	431.2	455.4	1050.4	1175.3	4088.7	5956.2	642.8	813.6
157	24b2	428.1	452.8	1045.2	1172.9	4077.4	5462.8	650.8	813.6
158	24b1	396.4	414.5	961.8	1088	3840.5	4578	609.7	785.2
standards:									
1	mzt 53	501	519.8	1097.4	1230.5	4505	5670.6	656.3	864.5
181	GSC 1	455.9	475.4	1070.7	1224.7	3764.3	4829	645.9	833.5
182	GSC 2	457.7	489.2	1067.1	1211.3	3788.2	4865.3	638.5	822.2
183	GSC 3	454.7	481.4	1074.4	1210.3	3887.3	4925.5	647.9	828.5
184	GSC 4	456.1	478.3	1068.1	1213.9	3867.8	4898.1	659.4	838
185	GSC 5	472.5	495.7	1080.3	1205.2	3940.9	4997	656.9	840.8
90	GSC 6	461.1	483.9	1070.1	1198.8	3917.8	4965.2	658.4	845.1

D.4 Quantitative minor element (Th, U, Y and Pb) analyses and calculated ages

This sections shows analytical data for minor element (U, Th, Y, and Pb). Concentrations, listed in ppm, were directly converted from raw microprobe output (wt%) by the equation:

$$MicroprobeElementwt\%\times 10,000 = ElementConcentration(ppm)$$

Calculated dates of individual analyses and associated uncertainties following the procedure of Gagne (2004).

Table D.5: Minor element concentrations for monazite analyses in sample N13-029.

No.	Analysis	Th (ppm)	Th error (%)	U (ppm)	U error (%)	Y (ppm)	Y error (%)	Pb (ppm)	Pb error (%)	AGE (Ma)	2σ error (Ma)
2	3a1	42960	0.25	11760	0.56	4320	0.62	3820	0.67	1011	19
3	3a2	42150	0.25	11990	0.55	4510	0.59	3780	0.68	1002	19
4	3b1	39290	0.26	11340	0.58	9940	0.30	3580	0.70	1010	19
5	3b2	39410	0.26	11520	0.57	10210	0.29	3630	0.70	1002	19
6	3b3	39090	0.26	10610	0.61	9390	0.31	3460	0.72	1011	20
7	3b4	39350	0.26	10800	0.60	9320	0.32	3490	0.72	1008	20
8	3b4	38350	0.27	10670	0.61	9150	0.32	3380	0.74	996	20
9	3b5	0	-0.39	0	-0.99	0	-1.55	0	-2.09	0	0
10	4a1	49190	0.23	4720	1.18	4430	0.61	5440	0.51	1764	46
11	4a2	51730	0.22	4870	1.15	4350	0.62	5670	0.49	1758	45
12	4a3	49320	0.23	4900	1.15	8120	0.36	5530	0.50	1772	45
13	4a4	49430	0.23	4970	1.13	6810	0.41	5550	0.50	1769	45
14	4a5	45430	0.24	4460	1.25	3880	0.68	4970	0.55	1738	48
15	4a6	38080	0.27	7410	0.82	7000	0.40	4370	0.60	1473	31
16	4b1	36480	0.28	11280	0.58	16410	0.20	3400	0.72	999	20
17	4b2	36660	0.28	11380	0.57	16470	0.20	3390	0.73	989	19
18	4b3	35490	0.28	11260	0.58	16340	0.20	3420	0.72	1018	20
19	7a1	52190	0.22	11450	0.57	9880	0.30	4110	0.63	992	18
20	7b1	55810	0.21	12050	0.55	2060	1.22	4500	0.59	1021	17
21	7b2	56390	0.21	12480	0.53	2070	1.22	4620	0.58	1026	17
22	11a1	112320	0.14	6940	0.83	20890	0.17	11170	0.30	1750	32
23	11a2	107650	0.15	6460	0.88	18890	0.18	10830	0.31	1778	34
24	11b1	89570	0.16	12450	0.53	7320	0.38	6210	0.45	1033	15
25	11c1	58740	0.21	10640	0.60	15100	0.21	4420	0.59	1022	18
26	11c2	64610	0.20	12050	0.55	14370	0.22	5980	0.47	1228	19

Table D.5: *Continued.* Minor element concentrations for monazite analyses in sample N13-029.

No.	Analysis	Th (ppm)	Th error (%)	U (ppm)	U error (%)	Y (ppm)	Y error (%)	Pb (ppm)	Pb error (%)	AGE (Ma)	2σ error (Ma)
27	11d1	61230	0.20	11490	0.57	7260	0.39	5030	0.54	1096	18
28	11d2	65900	0.19	11160	0.58	10600	0.29	5500	0.50	1154	19
29	12a1	91660	0.16	7040	0.83	25730	0.15	9900	0.33	1813	33
30	12a2	86450	0.17	6690	0.87	24820	0.15	9380	0.34	1818	35
31	12a3	104150	0.15	8410	0.72	27540	0.14	11450	0.30	1824	30
32	12a4	94810	0.16	7200	0.82	26420	0.15	10370	0.32	1839	33
33	12a5	91920	0.16	6570	0.88	25070	0.15	9860	0.33	1828	35
34	12b1	61050	0.20	3800	1.41	18810	0.19	6300	0.45	1809	54
35	12b2	63830	0.20	3930	1.36	17960	0.19	6460	0.44	1780	52
36	12b3	66490	0.19	3790	1.39	18020	0.19	6780	0.43	1815	54
37	12a6	89510	0.16	8340	0.73	25280	0.15	10150	0.32	1818	30
38	12b4	68080	0.19	3700	1.42	17800	0.19	6880	0.43	1814	55
39	12c1	94790	0.16	13470	0.50	5640	0.50	6780	0.44	1057	15
40	12c2	88570	0.16	13060	0.51	3160	0.84	6300	0.46	1039	15
41	12c3	87630	0.16	13140	0.51	3320	0.80	6340	0.46	1050	15
42	12c4	82640	0.17	12370	0.53	2580	1.01	6020	0.48	1058	16
43	12c5	85700	0.17	12510	0.53	2830	0.93	6150	0.47	1051	16
46	12c6	103360	0.15	13680	0.49	3840	0.71	7220	0.42	1056	14
47	12c7	97810	0.15	13440	0.50	3670	0.74	6920	0.43	1057	15
48	12c8	94490	0.16	13380	0.50	3380	0.79	6860	0.43	1073	15
49	12c9	47080	0.21	10760	0.35	6630	0.21	4700	0.37	1217	14
50	12c10	102300	0.15	13030	0.51	3710	0.74	6940	0.43	1039	15
51	12c11	90480	0.16	13060	0.51	3410	0.79	6450	0.45	1048	15
52	15a1	38190	0.27	15660	0.45	25040	0.15	7740	0.39	1748	23
53	15b1	40300	0.26	5590	1.03	7410	0.39	4840	0.56	1721	42

Table D.5: *Continued.* Minor element concentrations for monazite analyses in sample N13-029.

No.	Analysis	Th (ppm)	Th error (%)	U (ppm)	U error (%)	Y (ppm)	Y error (%)	Pb (ppm)	Pb error (%)	AGE (Ma)	2σ error (Ma)
54	15b2	41530	0.26	5090	1.13	7460	0.38	4860	0.55	1743	45
55	15c1	40730	0.26	11240	0.58	3240	0.82	3660	0.69	1018	19
56	15c2	44320	0.25	13450	0.50	3290	0.81	4340	0.61	1055	18
57	15c3	40920	0.26	10740	0.60	2130	1.20	3620	0.70	1026	20
58	15c4	40650	0.26	10350	0.62	1980	1.29	3550	0.71	1027	20
59	15c5	40760	0.26	10340	0.62	2120	1.21	3570	0.71	1031	20
60	15c6	42360	0.26	10860	0.60	2020	1.28	3720	0.69	1029	20
61	15c7	38450	0.27	10760	0.60	5900	0.48	3530	0.71	1032	20
62	15c8	38380	0.27	10650	0.61	4620	0.59	3480	0.72	1024	20
63	15c9	38760	0.27	10890	0.60	7240	0.40	3550	0.71	1028	20
64	15c10	41450	0.26	11100	0.58	3390	0.79	3820	0.67	1056	20
65	17a1	38720	0.27	9300	0.68	11540	0.27	3180	0.77	994	21
66	17a2	39330	0.27	9880	0.65	11530	0.27	3260	0.75	984	20
67	17a3	40280	0.26	9280	0.68	7630	0.38	3260	0.76	998	21
68	17a4	41250	0.26	9790	0.65	10150	0.30	3340	0.74	986	20
69	17b2	38460	0.27	7830	0.78	17130	0.20	2860	0.83	968	23
70	17b3	38130	0.27	8080	0.76	17180	0.20	2960	0.80	992	23
71	17b4	38940	0.26	7780	0.79	17270	0.19	2920	0.81	983	23
72	17b5	35150	0.28	7270	0.83	16170	0.20	2630	0.88	967	24
73	17b6	36310	0.28	7060	0.85	16450	0.20	2650	0.88	968	25
74	17b7	31590	0.30	6980	0.87	15840	0.21	2480	0.93	986	26
75	18a1	41190	0.26	6990	0.86	2810	0.94	2910	0.84	986	24
76	18a2	44160	0.25	7570	0.81	2520	1.04	3110	0.80	979	23
77	18a3	39980	0.27	6820	0.88	2380	1.10	2810	0.87	979	25
78	18a4	38420	0.27	6960	0.86	3620	0.74	2750	0.88	975	25

Table D.5: *Continued.* Minor element concentrations for monazite analyses in sample N13-029.

No.	Analysis	Th (ppm)	Th error (%)	U (ppm)	U error (%)	Y (ppm)	Y error (%)	Pb (ppm)	Pb error (%)	AGE (Ma)	2σ error (Ma)
79	18a5	39450	0.27	7110	0.85	3120	0.85	2830	0.86	979	24
80	18a6	38750	0.27	7340	0.82	3660	0.74	2860	0.85	987	24
81	18a7	40460	0.26	6920	0.87	2760	0.96	2880	0.85	990	25
82	18a8	42650	0.25	7670	0.79	2700	0.98	3030	0.81	971	23
83	18a9	38890	0.27	6820	0.88	3300	0.81	2780	0.87	985	25
84	18a10	41850	0.26	7300	0.83	2970	0.89	2990	0.82	987	24
85	18b1	36790	0.28	7070	0.85	5560	0.49	2660	0.90	963	25
86	18b2	36630	0.28	6770	0.88	6970	0.40	2700	0.88	995	26
87	18b3	36110	0.28	5830	1.00	12460	0.25	2530	0.92	995	28
88	18c1	4970	1.02	4410	1.06	60	34.74	50	28.70	60	34
89	18c2	40530	0.26	6960	0.86	3190	0.82	2900	0.83	993	25
92	19a1	46290	0.24	10130	0.63	5390	0.52	3640	0.70	992	20
93	19a2	44570	0.25	11530	0.57	6140	0.47	3840	0.67	1007	19
94	19a3	42560	0.26	10810	0.60	5890	0.48	3650	0.69	1011	20
95	19a4	46680	0.24	9910	0.64	5400	0.52	3630	0.70	993	20
96	19a5	46950	0.24	10580	0.61	5370	0.53	3770	0.68	999	19
97	19a6	49590	0.23	10990	0.59	5540	0.51	3980	0.65	1006	19
98	19a7	48060	0.24	9940	0.64	5350	0.53	3780	0.68	1014	20
99	19a8	47620	0.24	9950	0.64	5300	0.53	3760	0.68	1014	20
100	19a9	48560	0.24	10210	0.63	5530	0.51	3790	0.68	1000	19
101	19a10	48050	0.24	9140	0.69	6120	0.47	3570	0.71	992	20
102	19b1	46500	0.24	9560	0.66	7480	0.39	3600	0.70	1001	20
103	19b2	46560	0.24	9660	0.66	6440	0.44	3550	0.71	984	20
104	19b3	46290	0.24	9450	0.67	6110	0.46	3550	0.71	995	20
105	19c1	40270	0.26	10510	0.61	15500	0.21	3520	0.70	1017	20

Table D.5: *Continued.* Minor element concentrations for monazite analyses in sample N13-029.

No.	Analysis	Th (ppm)	Th error (%)	U (ppm)	U error (%)	Y (ppm)	Y error (%)	Pb (ppm)	Pb error (%)	AGE (Ma)	2σ error (Ma)
106	19c2	46780	0.24	9200	0.68	6140	0.45	3540	0.71	997	20
107	19c3	42160	0.26	8730	0.70	15310	0.22	3270	0.74	1000	21
108	20a1	44670	0.25	8410	0.74	4060	0.68	3300	0.76	991	22
109	20a2	46100	0.24	8670	0.72	3930	0.70	3400	0.74	989	21
110	20a3	45880	0.24	8940	0.70	3990	0.69	3390	0.74	978	21
111	20a4	47090	0.24	8990	0.70	3860	0.71	3460	0.73	980	21
114	20a5	38360	0.27	7240	0.84	3830	0.71	2820	0.86	985	24
115	20a6	41350	0.26	8520	0.73	3480	0.79	3080	0.80	965	22
116	20b1	34210	0.29	7020	0.86	11250	0.27	2640	0.89	999	26
117	20c1	37840	0.27	7660	0.80	4940	0.56	2800	0.86	965	23
118	20c2	37840	0.27	7590	0.80	7270	0.40	2860	0.84	988	24
119	20d1	35460	0.29	7420	0.82	3950	0.68	2700	0.90	979	25
120	20d2	34600	0.29	7450	0.81	3760	0.70	2700	0.89	991	25
121	20d3	33910	0.29	7440	0.82	3670	0.72	2700	0.89	1002	25
122	20d4	36130	0.28	7190	0.84	4850	0.56	2720	0.88	988	25
123	20d5	34980	0.29	6950	0.87	4190	0.64	2630	0.91	987	26
124	21a1	22190	0.39	15730	0.45	25250	0.15	3550	0.69	1028	19
125	21b1	24540	0.37	17070	0.42	15620	0.22	3830	0.66	1017	18
126	21b2	28500	0.33	16400	0.43	14590	0.23	3940	0.65	1025	18
127	21b3	28710	0.33	16470	0.43	14070	0.24	3950	0.65	1023	18
128	21c1	41250	0.26	10910	0.60	7110	0.41	3590	0.70	1007	20
130	21c3	32150	0.31	9720	0.66	6500	0.44	2930	0.83	988	22
131	22a1	32400	0.30	16120	0.44	12510	0.26	4070	0.63	1024	17
132	22b1	38010	0.27	11310	0.58	6720	0.43	3510	0.72	1008	20
133	22b2	36890	0.28	11300	0.58	6930	0.42	3450	0.73	1006	20

Table D.5: *Continued.* Minor element concentrations for monazite analyses in sample N13-029.

No.	Analysis	Th (ppm)	Th error (%)	U (ppm)	U error (%)	Y (ppm)	Y error (%)	Pb (ppm)	Pb error (%)	AGE (Ma)	2σ error (Ma)
134	22b3	38140	0.27	11610	0.57	6970	0.42	3540	0.71	1002	19
135	22b4	38170	0.27	11870	0.56	7420	0.40	3600	0.70	1007	19
138	23b1	41480	0.26	6940	0.86	14840	0.22	5400	0.51	1743	36
139	23b2	41460	0.26	7090	0.85	14910	0.22	5410	0.51	1733	36
140	23b3	41440	0.26	6910	0.87	14940	0.22	5360	0.51	1734	36
141	23b4	42360	0.26	6890	0.87	14900	0.22	5430	0.51	1735	36
142	23c1	42950	0.25	11280	0.58	6530	0.44	4080	0.64	1096	20
143	23c2	40870	0.26	9140	0.69	1450	1.75	3390	0.74	1033	22
144	23c3	44020	0.25	8580	0.72	1270	1.98	3460	0.73	1037	22
145	23c4	51110	0.23	8480	0.73	1380	1.84	3770	0.68	1035	21
146	23c5	46730	0.24	8400	0.73	1250	2.03	3530	0.72	1029	22
147	23c6	41890	0.26	10200	0.63	2090	1.24	3600	0.70	1031	20
148	23c7	41880	0.26	10000	0.64	2070	1.25	3580	0.71	1035	21
149	23d1	72150	0.19	7800	0.78	3040	0.88	4430	0.60	988	20
151	24a1	37750	0.28	15670	0.45	22170	0.17	7830	0.39	1772	24
152	24a2	42950	0.26	6880	0.87	17420	0.20	5530	0.50	1751	37
153	24a3	39960	0.27	8680	0.72	18060	0.20	5740	0.48	1729	32
154	24a4	41410	0.26	7390	0.82	20510	0.18	5340	0.51	1690	34
155	24a5	40750	0.26	9350	0.67	17500	0.20	5530	0.50	1608	29
156	24a6	39770	0.27	14660	0.47	21260	0.17	6620	0.44	1554	22
157	24b2	39390	0.27	10800	0.60	11160	0.28	4570	0.58	1293	23
158	24b1	39930	0.26	9280	0.66	400	6.06	3440	0.72	1054	22

Table D.6: Minor element concentrations for in-house Monazite53 standard and the Geological Society of Canada's monazite standard.

No.	Analysis	Th (ppm)	Th error (%)	U (ppm)	U error (%)	Y (ppm)	Y error (%)	Pb (ppm)	Pb error (%)	AGE (Ma)	2σ error (Ma)
1	Mzt 53	98010	0.15	3310	1.47	5650	0.51	6700	0.43	1333	41
181	GSC 1	65590	0.20	2910	1.73	3800	0.69	1730	1.29	513	22
182	GSC 2	68480	0.19	3040	1.66	3950	0.67	1750	1.27	497	21
183	GSC 3	68660	0.19	3040	1.66	4040	0.66	1760	1.27	499	21
184	GSC 4	67660	0.19	3100	1.64	4050	0.66	1740	1.29	498	21
185	GSC 5	69030	0.19	2910	1.72	3870	0.70	1760	1.28	499	22
90	GSC 6	69240	0.19	2930	1.71	3990	0.67	1720	1.31	486	21

References

Aldis, C.H. 2016. Geochronology and Geochemistry of Mesoproterozoic Granitoids in the Nepewassi Domain, Grenville Orogen. B.Sc. thesis, University of Waterloo, Waterloo, Ontario.

Andersen, T. 2005. Detrital zircons as tracers of sedimentary provenance: limiting conditions from statistics and numerical simulation. Chemical Geology **216**: 249–270. doi: 10.1016/j.chemgeo.2004.11.013.

Beaumont, C., Jamieson, R.A., Nguyen, M.H., and Lee, B. 2001. Himalayan tectonics explained by extrusion of a low-viscosity crustal channel coupled to focused surface denudation. Nature **414**: 738–42. doi: 10.1038/414738a.

Beaumont, C., Jamieson, R.A., Nguyen, M.H., and Medvedev, S. 2004. Crustal channel flows: 1. Numerical models with applications to the tectonics of the Himalayan-Tibetan orogen. Journal of Geophysical Research B: Solid Earth **109**: 1–29. doi: 10.1029/2003JB002809.

Beaumont, C., Nguyen, M.H., Jamieson, R.A., and Ellis, S. 2006. Crustal flow modes in large hot orogens. Geological Society, London, Special Publications **268**: 91–145. doi: 10.1144/GSL.SP.2006.268.01.05.

Bethune, K., and Davidson, A. 1997. Grenvillian Metamorphism of the Sudbury Diabase Dyke-Swarm: from Protolith to Two-Pyroxene - Garnet Coronite. The Canadian Mineralogist **35**: 1191–1220.

Card, K.D. 1990. A review of the Superior province of the Canadian Shield, a product of Archean accretion. Precambrian Research **48**: 99–156.

Carr, S.D., Easton, R.M., Jamieson, R.A., and Culshaw, N.G. 2000. Geologic transect across the Grenville orogen of Ontario and New York. Canadian Journal of Earth Sciences **37**: 193–216.

Chandler, F.W., Young, G.M., and Wood, J. 1969. Diaspore in Early Proterozoic quartzites (Lorrain Formation) of Ontario. Canadian Journal of Earth Sciences **6**: 337–340. doi: 10.1139/e69-029.

Chen, Y.D., Krogh, T.E., and Lumbers, S.B. 1995. Neoarchean trondhjemitic and tonalitic orthogneisses identified within the northern Grenville Province in Ontario by precise U-Pb dating and petrologic studies. Precambrian Research **72**: 263–281.

Condie, K. 2013. Preservation and Recycling of Crust during Accretionary and Collisional Phases of Proterozoic Orogens: A Bumpy Road from Nuna to Rodinia. Geosciences **3**: 240–261. doi: 10.3390/geosciences3020240.

Corfu, F. 2003. Atlas of Zircon Textures. Reviews in Mineralogy and Geochemistry **53**: 469–500. doi: 10.2113/0530469.

Corfu, F. 2012. A century of U-Pb geochronology: The long quest towards concordance. Geological Society of America Bulletin **125**: 33–47. doi: 10.1130/B30698.1.

Corfu, F., and Andrews, A.J. 1986. A U- Pb age for mineralized Nipissing diabase, Gowganda, Ontario1. Canadian Journal of Earth Sciences **23**: 107–109. doi: 10.1139/e86-011.

Corfu, F., and Easton, R.M. 2000. U–Pb evidence for polymetamorphic history of Huronian rocks within the Grenville front tectonic zone east of Sudbury, Ontario, Canada. Chemical Geology **172**: 149–171.

Corrigan, D., Culshaw, N.G., and Mortensen, J.K. 1994. Pre-Grenvillian evolution and Grenvillian overprinting of the Parautochthonous Belt in Key Harbour, Ontario: U–Pb and field constraints. Canadian Journal of Earth Sciences **31**: 583–596. doi: 10.1139/e94-051.

Cottle, J.M., Kylander-Clark, A.R., and Vrijmoed, J.C. 2012. U–Th/Pb geochronology of detrital zircon and monazite by single shot laser ablation inductively coupled plasma mass spectrometry (SS-LA-ICPMS). Chemical Geology **332–333**: 136–147. Elsevier B.V. doi: 10.1016/j.chemgeo.2012.09.035.

Craddock, J.P., Rainbird, R.H., Davis, W.J., Davidson, C., Vervoort, J.D., Konstantinou, A., Boerboom, T., Vorhies, S., Kerber, L., and Lundquist, B. 2013. Detrital Zircon Geochronology and Provenance of the Paleoproterozoic Huron (2.4–2.2 Ga) and Animikie (2.2–1.8 Ga) Basins, Southern Superior Province. The Journal of Geology **121**: 623–644. doi: 10.1086/673265.

Culshaw, N., Foster, J., Marsh, J., Slagstad, T., and Gerbi, C. 2016. Kiosk domain, Central Gneiss Belt, Grenville Province, Ontario: A Labradorian palimpsest preserved in the ductile deep crust. Precambrian Research **280**: 249–278. Elsevier B.V. doi: 10.1016/j.precamres.2016.05.002.

Culshaw, N., Gerbi, C., and Marsh, J. 2010. Softening the lower crust: Modes of syn-transport transposition around and adjacent to a deep crustal granulite nappe, Parry Sound domain, Grenville Province, Ontario, Canada. Tectonics **29**: 1–28. doi: 10.1029/2009TC002537.

Culshaw, N.G., Beaumont, C., and Jamieson, R.A. 2006. The orogenic superstructure-infrastructure concept: Revisited, quantified, and revived. Geology **34**: 733–736. doi: 10.1130/G22793.1.

Culshaw, N.G., Corrigan, D., Drage, J., and Wallace, P. 1988. Georgian Bay geological synthesis: Key Harbour to Dillon, Grenville Province of Ontario. Geological Survey of Canada Special Paper **88–1C**: 129–133.

Culshaw, N.G., Jamieson, R.A., Ketchum, J.W.F., Wodicka, N., Corrigan, D., and Reynolds, P.H. 1997. Transect across the northwestern Grenville orogen, Georgian Bay, Ontario: Polystage convergence and extension in te lower orogenic crust. Tectonics **16**: 966–982.

Culshaw, N.G., Van De Kerckhove, S.R., and Jamieson, R.A. 2013a. Reconnaissance Geological Mapping in the Nepewassi Domain, Central Gneiss Belt, Grenville Province. Summary of Field Work and Other Activites, Ontario Geological Survey, Open File Report **6290**: 18-1-5.

Culshaw, N.G., Ketchum, J.W.F., Wodicka, N., and Wallace, P. 1994. Deep crustal ductile extension following thrusting in the southwestern Grenville Province, Ontario. Canadian Journal of Earth Sciences **31**: 160–175.

Culshaw, N.G., Slagstad, T., Raistrick, M., and Dostal, J. 2013b. Geochemical, geochronological and isotopic constraints on the origin of members of the allochthonous Shawanaga and basal Parry Sound domains, Central Gneiss Belt, Grenville Province, Ontario. Precambrian Research **228**: 131–150. Elsevier B.V. doi: 10.1016/j.precamres.2013.01.012.

Davidson, A. 1984. Identification of ductile shear zones in the southwestern Grenville Province of the Canadian Shield. *In* Precambrian tectonics illustrated. *Edited by* A. Kröner and R. Greiling. Stuttgart, Germany. pp. 263–279.

Davidson, A. 1986. Grenville Front relationships near Killarney, Ontario. *In* The Grenville Province, Geological Association of Canada Special Paper 31. pp. 107–117.

Davidson, A. 1998. An overview of Grenville Province geology, Canadian Shield. *In* Geology of the Precambrian Superior and Grenville Provinces and Precambrian Fossils in North America. pp. 205–270.

Davidson, A., and van Breeman, O. 1994. U-Pb ages of granites near the Grenville Front, Ontario. Radiogenic Age and Isotopic Studies: Report 8, Geological Survey of Canada, Current Research **1994–F**: 107–114.

Davidson, A., van Breemen, O., and Sullivan, R.W. 1992. Circa 1.75 Ga ages for plutonic rocks from the Southern Province and adjacent Grenville Province: What is the expression of the Penokean orogeny? Radiogenic Age and Isotopic Studies: Report 6, Geological Survey of Canada Paper **92–2**: 107–118.

Davidson, a., and van Breemen, O. 1988. Baddeleyite-zircon relationships in coronitic metagabbro, Grenville Province, Ontario: implications for geochronology. Contributions to Mineralogy and Petrology **100**: 291–299. doi: 10.1007/BF00379740.

Dickin, A.P. 1998a. Pb isotope mapping of differentially uplifted Archean basement : a case study from the Grenville Province , Ontario. Precambrian Research **91**: 445–454.

Dickin, A.P. 1998b. Nd isotope mapping of a cryptic continental suture, Grenville Province of Ontario. Precambrian Research **91**: 433–444. doi: 10.1016/S0301-9268(98)00062-X.

Dufréchou, G., and Harris, L.B. 2013. Tectonic models for the origin of regional transverse structures in the Grenville Province of SW Quebec interpreted from regional gravity. Journal of Geodynamics **64**: 15–39. Elsevier Ltd. doi: 10.1016/j.jog.2012.12.001.

Dufréchou, G., Harris, L.B., and Corriveau, L. 2014. Tectonic reactivation of transverse basement structures in the Grenville orogen of SW Quebec, Canada: Insights from gravity and aeromagnetic data. Precambrian Research **241**: 61–84. Elsevier B.V. doi: 10.1016/j.precamres.2013.11.014.

Easton, R.M. 1992. The Grenville Province and the Proterozoic history of central and southern Ontario. *In* Geology of Ontario, Ontario Geological Survey, Special Volume 4, Part 2. pp. 714–904.

Easton, R.M. 2001. Geochronology of Ontario. Ontario Geological Survey, Miscellaneous Release—Data **75**: 1 CD-ROM.

Easton, R.M. 2006. Geology and Mineral Potential of the Eastern Tomiko Terrane, Grenville Province. *In* Ontario Geological Survey, Open File Report.

Easton, R.M. 2011. Detrital Zircon Geochronology of the uraniferous Paleoproterozoic Matinenda Formation (Huronian Supergroup), Elliot Lake, Ontario. Geological Society of America Abstracts with Programs **43**: 41.

Easton, R.M. 2014. Geology and Mineral Potential of the Nepewassi Domain, Central Gneiss Belt, Grenville Province. Summary of Field Work and Other Activities 2014, Ontario Geological Survey, Open File Report 6300: 16-1-12.

Easton, R.M., Davidson, A., and Murphy, E.I. 1999. Transects across the Southern–Grenville Province Boundary near Sudbury, Ontario. Traverse C: Wanapitei complex and its tectonic setting. *In* Geological Association of Canada, Sudbury '99 Annual Meeting, Guidebook #A2. p. 52.

Easton, R.M., and Heaman, L.M. 2008. Detrital zircon geochronology of Hurnoian Supergroup sandstones located within the Vernon structure , north of Espanola , Ontario. *In* 54th Institute on Lake Superior Geology. pp. 1–2.

Easton, R.M., and Heaman, L.M. 2011. Detrital zircon geochronology of Matinenda Formation sandstones (Huronian Supergroup) at Elliot Lake , Ontario: Implications for Uranium mineralization. 57th Institute of Lake Superior Geology 57: 31–32.

Ferry, J.M., and Spear, F.S. 1978. Experimental Calibration of the Partitioning of Fe and Mg Between Biotite and Garnet. Contributions to Mineralogy and Petrology 66: 113–117. doi: 10.1007/s00410-011-0686-4.

Fralick, P.W., and Miall, A.D. 1989. Sedimentology of the Lower Huronian Supergroup (Early Proterozoic), Elliot Lake area, Ontario, Canada. Sedimentary Geology 63: 127–153.

Fueten, F., and Redmond, D.J. 1994. Documentation of a 1450 Ma contractional orogeny preserved between the 1850 Ma Sudbury impact structure and the 1 Ga Grenville orogenic front , Ontario. Geological Society Of America Bulletin 109: 268–279.

Gagné, S. 2004. Textural, Chemical and Age variation of monazites of the Paleoproterozoic Longstaff Bluff Formation, Central Baffin Island, Nunavut. Dalhousie University.

Ghent, E.D. 1976. Plagioclase-garnet-Al2SiO5-quartz: a potential geobarometer-geothermometer. American Mineralogist 61: 710–714.

Gower, C.F., and Krogh, T.E. 2002. A U–Pb geochronological review of the Proterozoic history of the eastern Grenville Province. Canadian Journal of Earth Sciences 39: 795–829. doi: 10.1139/e01-090.

Graham, C.M., and Powell, R. 1984. A garnet-hornblende geothermometer: calibration, testing, and application to the Pelona Schist, Southern California. Journal Of Metamorphic Geology 2: 13–31. doi: 10.1111/j.1525-1314.1984.tb00282.x.

Gupta, V.K. 1991. Bouguer gravity of Ontario, southern sheet; Ontario Geological Survey, Map 2595, scale 1:1 000 000.

Gupta, V.K. 1992. Shaded image of vertical gravity gradient of Ontario, southern sheet; Ontario Geological Survey, Map 2599, scale 1:1 000 000.

Halls, H.C., Lovette, A., Hamilton, M., and Soderlund, U. 2015. A paleomagnetic and U-Pb geochronology study of the western end of the Grenville dyke swarm: Rapid changes in paleomagnetic field direction at ca. 585Ma related to polarity reversals? Precambrian Research 257: 137–166. Elsevier B.V. doi: 10.1016/j.precamres.2014.11.029.

Holdaway, M.J. 2000. Application of new experimental and garnet Margules data to the garnet-biotite geothermometer. American Mineralogist **85**: 881–892.

Holdaway, M.J. 2001. Recalibration of the GASP geobarometer in light of recent garnet and plagioclase activity models and versions of the garnet-biotite geothermometer. American Mineralogist **86**: 1117–1129.

Holdaway, M.J. 2004. Optimization of some key geothermobarometers for pelitic metamorphic rocks. Mineralogical Magazine **68**: 1–14. doi: 10.1180/0026461046810167.

Holdaway, M.J., Mukhopadhyay, B., Dyar, M.D., Guidotti, C. V., and Dutrow, B.L. 1997. Garnet-biotite geothermometry revised: New Margules parameters and a natural specimen data set from Maine. American Mineralogist **82**: 582–595.

Hutton, D.H.W. 1979. Tectonic slides: A review and reappraisal. Earth Science Reviews **15**: 151–172.

Hutton, P.F. 1997. Tectonic genealogy of North America. *In* Earth structure: an introduction to structural geology and tectonics. *Edited by* B.A. van der Pluijm and S. Marshak. McGraw-Hill, New York, USA. pp. 459–464.

Hynes, A., Indares, A., Rivers, T., and Gobeil, A. 2000. Lithoprobe line 55: integration of out-of-plane seismic results with surface structure, metamorphism, and geochronology, and the tectonic evolution of the eastern Grenville Province. Canadian Journal of Earth Sciences **37**: 341–358. doi: 10.1139/e99-076.

Hynes, A., and Rivers, T. 2010. Protracted continental collision — evidence from the Grenville Orogen. Canadian Journal of Earth Sciences **47**: 591–620. doi: 10.1139/E10-003.

Jackson, S.E., Pearson, N.J., Griffin, W.L., and Belousova, E.A. 2004. The application of laser ablation-inductively coupled plasma-mass spectrometry to in situ U-Pb zircon geochronology. Chemical Geology **211**: 47–69. doi: 10.1016/j.chemgeo.2004.06.017.

Jaffey, A.H., Flynn, K.F., Glendenin, W.C., Bentley, W.C., and Essling, A.M. 1971. Precision measurements of half-lives and specific activities of 235U and 238U. Physical Reviews C: Nuclear Physics **4**: 1889–1906.

Jamieson, R.A., and Beaumont, C. 2013. On the origin of orogens. Geological Society of America Bulletin **125**: 1671–1702. doi: 10.1130/B30855.1.

Jamieson, R.A., Beaumont, C., Nguyen, M.H., and Culshaw, N.G. 2007. Synconvergent ductile flow in variable-strength continental crust: Numerical models with application to the western Grenville orogen. Tectonics **26**: 1–23. doi: 10.1029/2006TC002036.

Jamieson, R.A., Beaumont, C., Warren, C.J., and Nguyen, M.H. 2010. The Grenville Orogen explained? Applications and limitations of integrating numerical models with geological and geophysical data. Canadian Journal of Earth Sciences **47**: 517–539. doi: 10.1139/E09-070.

Jamieson, R.A., Culshaw, N.G., and Corrigan, D. 1995. North-west propagation of the Grenville orogen: Grenvillian structure and metamorphism near Kev Harbour, Georgian Bay, Ontario , Canada. Journal of Metamorphic Geology **13**: 185–207.

Jamieson, R.A., Culshaw, N.G., Wodicka, N., and Corrigant, D. 1992. Timing and tectonic setting of Grenvillian metamorphism-constraints from a transect along Georgian Bay , Ontario ". Journal of Metamorphic Geology **10**: 321–332.

Kay, S.M. 1977. The origin of antiperthites in anorthosites. American Mineralogist **62**: 905. Available from d:/TEMP/AmMin%5CnTOC1/AmMin%5CnTOC1(6176).pdf:pdf.

Ketchum, J.W. 1994. Extensional shear zones and lithotectonic domains in the Southwest Grenville Orogen: Structure, Metamorphism and U-Pb Geochronology of the Central Gneiss Belt near Pointe-Au-Baril, Ontario. Dalhousie University.

Ketchum, J.W., and Davidson, A. 2000. Crustal architecture and tectonic assembly of the Central Gneiss Belt, southwestern Grenville Province, Canada: a new interpretation. Canadian Journal of Earth Sciences **37**: 217–234.

Ketchum, J.W.F., Heaman, L.M., Krogh, T.E., Culshaw, N.G., and Jamieson, R.A. 1998. Timing and thermal influence of late orogenic extension in the lower crust: a U-Pb geochronological study from southwest Grenville orogen, Canada. Precambrian Research **89**: 25–45.

Ketchum, J.W.F., Jamieson, R.A., Heaman, L.M., Culshaw, N.G., and Krogh, T.E. 1994. 1.45 Ga granulites in the southwestern Grenville province: Geologic setting, P-T conditions, and U-Pb geochronology. Geology **22**: 215–218.

Kirkland, C.L., Whitehouse, M.J., and Slagstad, T. 2009. Fluid-assisted zircon and monazite growth within a shear zone: A case study from Finnmark, Arctic Norway. Contributions to Mineralogy and Petrology **158**: 637–657. doi: 10.1007/s00410-009-0401-x.

Kohn, M.J., and Spear, F.S. 1990. Two new geobarometers for garnet amphibolites, with applications to southeastern Vermont. American Mineralogist **75**: 89–96.

Krogh, T.E. 1989. Terrane Identification in the Grenville Province from detrital and metamorphic zircon ages. *In* The Abitibi–Grenville Lithoprobe Project: 1989 Transect Report and Updated Proposal, Lithoprobe Abitibi–Grenville Project Workshop, June 1989. Lithoprobe Secretariat, University of British Columbia, Vancouver, British Columbia. pp. 63–65.

Krogh, T.E. 1994. Precise U-Pb ages for Grenvillian and pre-Grenvillian thrusting of Proterozoic and Archean metamorphic assemblages in the Grenville Front tectonic zone, Canada. Tectonics **13**: 963–982.

Krogh, T.E., Corfu, F., Davis, D.W., Dunning, G.R., Heaman, L.M., Kamo, S.L., Machado, N., Greenough, J.D., and Nakamura, E. 1987. Precise U-Pb isotopic ages of diabase dykes and mafic to ultramafic rocks using trace amounts of baddeleyite and zircon. H. C. Halls & W. F. Fahrig (Eds.), Mafic Dyke Swarms. Geological Association of Canada Special Paper **34**: 147–152.

Krogh, T.E., and Davis, G.L. 1969. Old isotopic ages in the northwestern Grenville Province, Ontario. Geological Association of Canada Special Paper **5**: 189–192.

Krogh, T.E., and Davis, G.L. 1972. The effect of regional metamorphism on U-Pb systems in zircons and a comparison with Rb-Sr systems in the same whole rock. Carnegie Institution of Washington. Yearbook **71**: 564–571.

Long, D.G.F. 2004. The tectonostatigraphic evolution of the Huronian basement and the subsequent basin fill: geological constraints on impact models of the Sudbury event. Precambrian Research **129**: 203–223. doi: 10.1016/j.precamres.2003.10.003.

Ludden, J., and Hynes, A. 2000. The Lithoprobe Abitibi-Grenville transect: two billion years of crust formation and recycling in the Precambrian Shield of Canada. Canadian Journal of Earth Sciences **37**: 459–476.

Ludwig, K.R. 2008. User â€™ s Manual for Isoplot 3.70. A Geochronological Toolkit for Microsoft Excel. *In* Berkeley Geochronology Center Special Publication No. 4.

Lumbers, S.B. 1971. Geology of the North Bay Area, Districts of Nipissing and Parry Sound. Ontario Geological Survey, Geological Report **94**: 1–112.

Lumbers, S.B. 1974. Burwash, Nipissing, Parry Sound and Sudbury districts; Ontario Division of Mines, Map 2271.

Lumbers, S.B. 1975. Geology of the Burwash Area, Districts of Nipissing, Parry Sound, and Sudbury. Ontario Division Mines, GR116. Accomanied by Map 2271, scale 1 inch to 2 miles: 1–160.

McLelland, J., Daly, J.S., and McLelland, J.M. 1996. The Grenville Orogenic Cycle (ca. 1350-1000 Ma): an Adirondack perspective. Tectonophysics **265**: 1–28. doi: 10.1016/S0040-1951(96)00144-8.

Meert, J.G. 2012. What's in a name? The Columbia (Paleopangaea/Nuna) supercontinent. Gondwana Research **21**: 987–993. International Association for Gondwana Research. doi: 10.1016/j.gr.2011.12.002.

Miall, A.D. 1985. Sedimentation on an early Proterozoic continental margin under glacial influence: the Gowganda Formation (Huronian), Elliot Lake area, Ontario, Canada. Sedimentology **32**: 763–788.

Montel, J., Foret, S., Veschambre, M., Nicollet, C., and Provost, A. 1996. Electron microprobe dating of monazite. Chemical Geology **131**: 37–53.

Myers, J.S. 1978. Formation of banded gneisses by deformation of igneous rocks. Precambrian Research **6**: 43–64.

Ontario Geological Survey. 1991. Bedrock geology of Ontario, southern sheet; Ontario Geological Survey, Map 2544.

Parrish, R.R. 1990. U-Pb dating of monazite and its application to geological problems. Canadian Journal of Earth Sciences **27**: 1431–1450.

Passchier, C., and Trouw, R. 2005. Microtectonics 2nd edition. *In* Tectonophysics. doi: 10.1007/978-3-662-08734-3.

Prevec, S.A. 1992. U-Pb age constraints on Early Proterozoic mafic magmatism from the southern Superior and western Grenville provinces, Ontario. Radiogenic Age and Isotopic Studies, Report 6, Geological Survey of Canada, Paper 92-2: 97–106.

Prevec, S.A. 1993. An isotopic, geochemical and petrographic investigation of the genesis of early Proterozoic mafic intrusions and associated volcanics near Sudbury, Ontario. PhD thesis, University of Alberta, Edmonton, Alberta.

Prevec, S.A. 1995. Sm - Nd isotopic evidence for crustal contamination in the ca. 1750 Ma Wanapitei Complex, western Grenville Province, Ontario. Canadian Journal of Earth Sciences **32**: 486–495.

Prevec, S.A. 2004. Basement tracing using Mid-Proterozoic anorthosites straddling a palaeoterrane boundary, Ontario, Canada. Precambrian Research **129**: 169–184. doi: 10.1016/j.precamres.2003.10.009.

Pyle, J.M., Spear, F.S., Wark, D.A., Daniel, C.G., and Storm, L.C. 2005. Contributions to precision and accuracy of monazite microprobe ages. American Mineralogist **90**: 547–577. doi: 10.2138/am.2005.1340.

Pyle, J.M., Spear, F.S., and Wark, D. a. 2002. Electron Microprobe Analysis of REE in Apatite, Monazite and Xenotime: Protocols and Pitfalls. Reviews in Mineralogy and Geochemistry **48**: 337–362. doi: 10.2138/rmg.2002.48.8.

Quirke, T.T., and Collins, W.H. 1930. The Disappearance of the Huronian. *In* Canada Department of Mines, Geological Survey, Memoir 160.

Raharimahefa, T., Lafrance, B., and Tinkham, D.K. 2014. New structural , metamorphic , and U – Pb geochronological constraints on the Blezardian Orogeny and Yavapai Orogeny in the Southern Province, Sudbury, Canada. Canadian Journal of Earth Sciences **51**: 750–774. doi: dx.doi.org/10.1139/cjes-2014-0025.

Rainbird, R.H., and Davis, W.J. 2006a. Detrital zircon geochronology of the western Huronian basin r. *In* Proceedings of the 52nd ILSG Annual Meeting – Part 1. pp. 55–56.

Rainbird, R.H., and Davis, W.J. 2006b. Sampling Superior: Detrital Zircon Geochronology of the Huronian. Geological Association of Canada-Mineralogical Association of Canada (GAC-MAC) Abstracts **31**: 125. Annual Meeting, Montreal.

Ramsay, J.G. 1967. Folding and fracturing of rocks. McGraw-Hill Book Company, New York, USA.

Regan, P. 2014. Monazite Geochronology of the Nepewassi domain, Ontario. unpublished ERTH 6400 report, Dalhousie University.

Rivers, T. 2009. The Grenville Province as a large hot long-duration collisional orogen - insights from the spatial and thermal evolution of its orogenic fronts. Geological Society, London, Special Publications **327**: 405–444.

Rivers, T. 2012. Upper-crustal orogenic lid and mid-crustal core complexes : signature of a collapsed orogenic plateau in the hinterland of the Grenville Province. Canadian Journal of Earth Sciences **49**: 1–42. doi: 10.1139/E11-014.

Rivers, T., and Corrigan, D. 2000. Convergent margin on southeastern Laurentia during the Mesoproterozoic: tectonic implications. Canadian Journal of Earth Sciences **37**: 359–383.

Rivers, T., Culshaw, N., Hynes, A., Indares, A., Jamieson, R., and Martignole, J. 2012. The Grenville. Orogen — A post-LITHOPROBE perspective. Chapter 3. *In* Tectonic Styles in Canada: The LITHOPROBE Perspective. Edited by J.A. Percival, F.A. Cook, and R.M. Clowes. Geological Association of Canada, Special Paper 49. pp. 97–236.

Rivers, T., Martignole, J., Gower, C.F., and Davidson, A. 1989. New tectonic divisions of the Grenville Province, Southeast Canadian Shield. Tectonics **8**: 63–84. doi: 10.1029/TC008i001p00063.

Rollinson, H.R. 1993. Using Geochemical Data: Evaluation, Presentation, Interpretation. Pearson Education Limited Longman Group UK Limited. doi: 10.1180/minmag.1994.058.392.25.

Rousell, D.H., Petrus, J.A., Easton, R.M., Tinkham, D.K., and Napoli, M.G. 2012. The tectonometamorphic, magmatic and mineralization history of the Wanapitei Complex, Grenville Front tectonic zone, Ontario. 58th Institute on Lake Superior Geology, Proceedings **58**: 75–76.

Sawyer, E.W. 2008. Atlas of Migmatites. *In* National Research Council of Canada Special Publication 9. NRC Research Press, Ottawa, Ontario, Canada.

Schoene, B. 2014. U – Th – Pb Geochronology. *In* Treatise on Geochemistry 2nd Edition. pp. 341–378. doi: 10.1016/B978-0-08-095975-7.00310-7.

Skår, Ø. 2002. U-Pb geochronology and geochemistry of early Proterozoic rocks of the tectonic basement windows in central Nordland, Caledonides of north-central Norway. Precambrian Research **116**: 265–283. doi: 10.1016/S0301-9268(02)00026-8.

Steenkamp, H.M. 2012. A metamorphic history of supracrustal rocks on Haroya and Ninnoya, Nordoyane, Western Gneiss Region, Norway. M.Sc. thesis, Dalhousie University, Halifax, Nova Scotia.

Suzuki, K., Adachi, M., and Kazjizuka, I. 1994. Electron microprobe observations of Pb diffusion in metamorphosed detrital monazites. Earth and Planetary Science Letters **128**: 391–405.

Taylor, S.R., and McLennan, S.M. 1985. The continental crust: its composition and evolution. *In* Blackwell Scientific Publications. Oxford, UK.

Tollo, R.P., Aleinikoff, J.N., Borduas, E.A., Hackley, P.C., and Fanning, C.M. 2004. Petrologic and geochronologic evolution of the Grenville orogen, northern Blue Ridge Province, Virginia. Geological Society of America Memoir **197**: 647–677.

Tyler, S. 2013. Structures and southern boundary zone of the Nepewassi domain, Central Gneiss Belt, Grenville Province, ON. B.Sc. thesis, Dalhousie University, Halifax, Nova Scotia.

Van Achterbergh, E., Ryan, C.G., Jackson, S.E., and Griffin, W.L. 2001. LA-ICP-MS in the Earth Sciences - Appendix 3, data reduction software for LA-ICP-MS. *In* Sylvester, P.J. (ed.): Short Course volume 29: St.John's, Mineralogical Association of Canada. pp. 239–243.

van Breemen, O., Davidson, A., Loveridge, W.D., and Sullivan, R.D. 1986. U- Pb zircon geochronology of Grenvillian tectonites, granulites and igneous precursors, Parry Sound, Ontario. *In* The Grenville Province, Geological Association of Canada Special Paper 31. *Edited by* J.M. Moore and and A.J.B. A. Davidson. pp. 191–207.

Van De Kerckhove, S.R., and Easton, R.M. 2016. Geological, Geochemical and Geophysical Data from the Nepewassi Area, Central Gneiss Belt, Grenville Province. Ontario Geological Survey Miscellaneous Release-Data 338.

Vernon, R.H. 2004. A practical guide to Rock Microstructure. *In* Cambridge University Press. Cambridge, UK.

White, D.J., Forsyth, D. a, Asudeh, I., Carr, S.D., Wu, H., Easton, R.M., and Mereu, R.F. 2000. A seismic-based cross-section of the Grenville Orogen in southern Ontario and western Quebec. Canadian Journal of Earth Sciences **37**: 183–192. doi: 10.1139/e99-094.

Wiedenbeck, M., Allé, P., Corfu, F., Griffin, W.L., Meier, M., Oberli, F., Von Quadt, A., Roddick, J.C., and Spiegel, W. 1995. Three natural zircon standards for U-Th-Pb.Lu-Hf, trace element and REE analyses. Geostandards Newsletter 19: 1–23.

Williams, M.L., and Jercinovic, M.J. 2002. Microprobe monazite geochronology: putting absolute time into microstructural analysis. Journal of Structural Geology **24**: 1013–1028. doi: 10.1016/S0191-8141(01)00088-8.

Williams, M.L., Jercinovic, M.J., Goncalves, P., and Mahan, K. 2006. Format and philosophy for collecting, compiling, and reporting microprobe monazite ages. Chemical Geology **225**: 1–15. doi: 10.1016/j.chemgeo.2005.07.024.

Williams, M.L., Jercinovic, M.J., and Hetherington, C.J. 2007. Microprobe Monazite Geochronology: Understanding Geologic Processes by Integrating Composition and Chronology. Annual Review of Earth and Planetary Sciences **35**: 137–175. doi: 10.1146/annurev.earth.35.031306.140228.

Winter, J.D. 2001. An introduction to igneous and metamorphic petrology. Prentice Hall, Upper Saddle River, NJ.

Wodicka, N., and Card, K.D. 1995. Late Archean history of the Levack gneiss complex, southern Superior Province, Sudbury, Ontario: New evidence from U-Pb geochronology. Precambrian'95, Program with Abstracts: 191.

Wu, C.-M. 2004. Empirical Garnet-Biotite-Plagioclase-Quartz (GBPQ) Geobarometry in Medium- to High-Grade Metapelites. Journal of Petrology **45**: 1907–1921. doi: 10.1093/petrology/egh038.

Wynne-Edwards, H.R. 1972. The Grenville Province. In Variations in tectonic styles in Canada. *In* Geological Association of Canada Special Paper 11. pp. 263–334.

Young, G.M. 2015. Did prolonged two-stage fragmentation of the supercontinent Kenorland lead to arrested orogenesis on the southern margin of the Superior province? Geoscience Frontiers **6**: 419–435. doi: 10.1016/j.gsf.2014.04.003.

Young, G.M., Long, D.G.., Fedo, C.M., and Nesbitt, H.W. 2001. Paleoproterozoic Huronian basin: product of a Wilson cycle punctuated by glaciations and a meteorite impact. Sedimentary Geology **141–142**: 233–254. doi: 10.1016/S0037-0738(01)00076-8.

Zolnai, A.I., Price, R.A., and Helmstaedt, H. 1984. Regional cross section of the Southern Province adjacent to Lake Huron, Ontario: implications for the tectonic significance of the Murray Fault Zone. Canadian Journal of Earth Sciences **21**: 447–456.

543095 E
5131029 N
563964 E
5132724 N
559829 E
5121895 N
554107 E
5112164 N

FIGURE 1

Precambrian Geology of the West Arm of Lake Nipissing, Grenville Province

Scale 1:20 000

500 m 0 0.5 1 km

NTS References: parts of 41 I/1, I/8

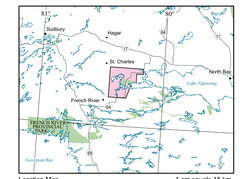

Location Map 1 cm equals 15 km

1:20,000

0 0.5 1 2 3 4 Kilometers

LEGEND

NEOPROTEROZOIC

SMALL MAFIC BODIES

- Nd — Unmetamorphosed nephelinite dike
- Md_2 — Garnet-bearing, amphibolite dikes
- Md_3 — Amphibolite dikes

PALEOPROTEROZOIC TO NEOPROTEROZOIC

SMALL MAFIC BODIES

- Md_1 — Diabase dikes (similar to Sudbury dike swarm)
- Mmd — Dioritic metatexite and diatexite dikes and sills

MAFIC & INTERMEDIATE METAPLUTONIC ROCKS

- QD — Quartz dioritic gneiss
- Mm_1 — Dioritic metatexite and diatexite
- Mm_2 — Dioritic stromatic metatexite
- Mn — Diorite and gabbro gneiss
- GMb — Intrusion breccia; gabbroic xenoliths in syenogranite to monzogranite matrix
- MA — Gneissic to massive leucogabbro, gabbroic anorthosite, anorthositic gabbro, and anorthosite
- UM — Pyroxene hornblendite

FELSIC METAPLUTONIC ROCKS

- Gd — Monzogranite dikes and sills
- Gnm — Quartz monzonitic gneiss and migmatite (West Bay batholith)
- Gn_1 — Leucocratic quartz monzonitic gneiss (West Phase)
- GMn — Undivided leucocratic quartz monzonitic gneiss (Gn1) with Dioritic stromatic metatexite (Mm2), Amphibolite dikes (Md3), and Monzogranite dikes and sills (Gd)
- Gn_2 — Magnetite-bearing leucocratic monzogranitic gneiss
- Gn_3 — Monzonitic gneiss with minor syenite and quartz syenite

GNEISS OF UNCERTAIN PROTOLITH

- Im_1 — Heterogeneous, layered metatexite of multiple compositions
- Im_2 — Heterogeneous, layered garnet, hornblende, biotite, plagioclase, quartz, K-feldspar metatexite
- Bn — Biotite gneiss

PROBABLE SUPRACRUSTAL ROCKS

- Pm — Garnet, biotite, plagioclase migmatite
- Fm — Feldspathic migmatite
- Fn — Feldspathic gneiss
- Im_3 — Layered tonalitic to granodioritic gneiss and metatexite
- InFm — Undivided layered gneiss and minor migmatite (In) and Feldspathic migmatite (Fm) with Monzogranite dikes and sills (Gd), Pelite/semipelite (Sn2), Leucocratic gneiss with probable volcanic protolith (VFn), Dioritic stromatic metatexite (Mm2), and Quartz dioritic gneiss (QD)
- In — Layered gneiss and minor migmatite
- VGMn — Undivided felsic gneiss with probable volcanic protolith (Vfn), Gn2, and Mn1 with minor Monzogranite dikes and sills (Gd), Dioritic metatexite and diatexite dikes and sills (Mmd) and Amphibolite dikes (Md3)
- VFn — Leucocratic gneiss; probable volcanic protolith

SUPRACRUSTAL: METASEDIMENTARY ROCKS

- Sn_1 — Paragneiss: Quartzite
- Sn_2 — Paragneiss: Pelite/semipelite
- Sn_3 — Paragneiss: Psammite

ARCHEAN

TONALITIC GREY GNEISSES

- Tn — Tonalitic and granodioritic gneiss and migmatites

SYMBOLS

- Outcrop
- Geological contact (interpreted, observed)
- Fault; unknown displacement (trend only, interpreted)
- Shear zone
- Fold; antiform, unknown generation (limbs dip in opposite directions, interpreted)
- Fold; synform, unknown generation (limbs dip in opposite directions, interpreted)
- Fold; synform, overturned, unknown generation (limbs dip in the same direction, interpreted)
- Foliation; unknown generation (trend only, inclined, horizontal)
- Compositional layering; unknown generation (trend only, inclined, horizontal)
- Compositional layering and/or parallel tectonic foliation; unknown generation (trend only, inclined, horizontal)
- Compositional layering and/or parallel tectonic foliation; unknown generation; from compiled data (inclined)
- Lineation; unknown generation (with plunge)
- Lineation; mineral, unknown generation (with plunge)
- Lineation; intersection, unknown generation (with plunge)
- Lineation; elongation, unknown generation (with plunge)
- Lineation; unknown asymmetry, unknown generation (with plunge)
- Schistosity; unknown generation (inclined)
- Ductile fault; unknown generation, unknown separation (trend only, inclined)
- Brittle-ductile fault; first generation, unknown vertical displacement (inclined)
- Dike contact (trend only, inclined)
- Igneous contact (trend only, inclined)
- Boundary (administrative)
- Road (primary, secondary)

543095 E
5131609 N
563964 E
5131609 N
559829 E
5121895 N
554107 E
5112164 N
543095 E
5112164 N

West Phase
West Bay batholith
Mashkinonje Island
Mashkinonje Provincial Park
St. Charles-Lavigne Shear Zone
Lavigne
Big Cut
Little Cut
Monetville
North Monetville
Jennings Tp.
Cherriman Tp.
Casimir Tp.
Haddo Tp.
MacPherson Tp.
London Tp.
Martland Tp.
Cosby Tp.
Louden Tp.
Falconer Tp.
Lake Nipissing (West Arm)
Lake Nipissing
Bear Lake
Lily Lake
Jack Lake
Shanty Bay
Warren (Deer) Bay
Monet Lake
Duck Creek
Sucker Creek
Mountain Creek

FIGURE 2

Precambrian Geology of the West Arm of Lake Nipissing, Grenville Province

Scale 1:20 000

500 m 0 0.5 1 km

NTS References: parts of 41 I/1, I/8

Location Map — 1 cm equals 15 km

LEGEND

NEOPROTEROZOIC

SMALL MAFIC BODIES

- Nd — Unmetamorphosed nephelinite dike
- Md_2 — Garnet-bearing, amphibolite dikes
- Md_3 — Amphibolite dikes

PALEOPROTEROZOIC TO NEOPROTEROZOIC

SMALL MAFIC BODIES

- Md — Diabase dikes (similar to Sudbury dike swarm)
- Mmd — Dioritic metatexite and diatexite dikes and sills

MAFIC & INTERMEDIATE METAPLUTONIC ROCKS

- QD — Quartz dioritic gneiss
- Mm — Dioritic metatexite and diatexite
- Mm_2 — Dioritic stromatic metatexite
- Mn — Diorite and gabbro gneiss
- GMb — Intrusion breccia; gabbroic xenoliths in syenogranite to monzogranite matrix
- MA — Gneissic to massive leucogabbro, gabbroic anorthosite, anorthositic gabbro, and anorthosite
- UM — Pyroxene hornblendite

FELSIC METAPLUTONIC ROCKS

- Gd — Monzogranite dikes and sills
- Gnm — Quartz monzonitic gneiss and migmatite (West Bay batholith)
- Gn_1 — Leucocratic quartz monzonitic gneiss (West Phase)
- GMn — Undivided leucocratic quartz monzonitic gneiss (Gn1) with Dioritic stromatic metatexite (Mm2), Amphibolite dikes (Md3), and Monzogranite dikes and sills (Gd)
- Gn_2 — Magnetite-bearing leucocratic monzogranitic gneiss
- Gn_3 — Monzonitic gneiss with minor syenite and quartz syenite

GNEISS OF UNCERTAIN PROTOLITH

- Im_2 — Heterogeneous, layered metatexite of multiple compositions
- Im_1 — Heterogeneous, layered garnet, hornblende, biotite, plagioclase, quartz, K-feldspar metatexite
- Bn — Biotite gneiss

PROBABLE SUPRACRUSTAL ROCKS

- Pm — Garnet, biotite, plagioclase migmatite
- Fm — Feldspathic migmatite
- Fn — Feldspathic gneiss
- Im_3 — Layered tonalitic to granodioritic gneiss and metatexite
- InFm — Undivided layered gneiss and minor migmatite (In) and Feldspathic migmatite (Fm) with Monzogranite dikes and sills (Gd), Pelite/semipelite (Sn2), Leucocratic gneiss with probable volcanic protolith (VFn), Dioritic stromatic metatexite (Mm2), and Quartz dioritic gneiss (QD)
- In — Layered gneiss and minor migmatite
- VGMn — Undivided felsic gneiss with probable volcanic protolith (Vfn), Gn2, and Mn1 with minor Monzogranite dikes and sills (Gd), Dioritic metatexite and diatexite dikes and sills (Mmd) and Amphibolite dikes (Md3)
- VFn — Leucocratic gneiss; probable volcanic protolith

SUPRACRUSTAL: METASEDIMENTARY ROCKS

- Sn_1 — Paragneiss: Quartzite
- Sn_2 — Paragneiss: Pelite/semipelite
- Sn_3 — Paragneiss: Psammite

ARCHEAN

TONALITIC GREY GNEISSES

- Tn — Tonalitic and granodioritic gneiss and migmatites

SYMBOLS

- Outcrop
- Geological contact (interpreted, observed)
- Fault; unknown displacement (trend only, interpreted)
- Shear zone
- Fold; antiform, unknown generation (limbs dip in opposite directions, interpreted)
- Fold; synform, unknown generation (limbs dip in opposite directions, interpreted)
- Fold; synform, overturned, unknown generation (limbs dip in the same direction, interpreted)
- Boundary (administrative, provincial park)
- Road (primary, secondary)

0 0.5 1 2

1:20,000